Lecture Notes in Control and Information Sciences

437

Olivier Sename
Péter Gáspár
József Bokor (Eds.)

Robust Control and Linear Parameter Varying Approaches

Application to Vehicle Dynamics

Lecture Notes in Control and Information Sciences 437

Olivier Sename, Péter Gáspár,
and József Bokor (Eds.)

Robust Control and Linear Parameter Varying Approaches

Application to Vehicle Dynamics

Springer

Editors
Prof. Olivier Sename
GIPSA-lab
UMR CNRS 5216
Department of Control Systems
(Dpt Automatique)
Grenoble INP / ENSE3
Saint Martin d'Hères
Cedex
Grenoble

Prof. Péter Gáspár
Computer and Automation
Research Institute
Hungarian Academy of Sciences
Budapest
Hungary

Prof. József Bokor
Computer and Automation
Research Institute
Hungarian Academy of Sciences
Budapest
Hungary

ISSN 0170-8643
ISBN 978-3-642-36109-8
DOI 10.1007/978-3-642-36110-4
Springer Heidelberg New York Dordrecht London

e-ISSN 1610-7411
e-ISBN 978-3-642-36110-4

Library of Congress Control Number: 2012955946

Printed on acid-free paper

Springer is part of Springer Science+Business Media (www.springer.com)

Preface

This book results from the 32th International Summer School in Automatic that held in Grenoble, France, September, 12-16, 2011. 15 speakers have merged to give presentations, about Linear Parameter Varying methods and vehicle control, to an audience of more than 50 people (researchers and PhD students), from different european contries (Italy, Hungary, Austria, Czech Republic and France). The objective of this school was to provide recent methods (based on robust control and LPV technics) to the control of vehicle dynamics (mainly road vehicles).

Indeed, due to the rapidly changing techniques and technologies for information and communication, the last decade has seen increasing improvements of the performance of active systems for road vehicles. Then embedded control is becoming more prevalent in vehicles (intelligent electric actuators, sensors, etc..). Nevertheless, the possibilities offered by new approaches to improve the safety of passengers and pedestrians, are still largely underused. Furthermore the vehicle systems (nonlinear, multi-variable) become now more complex systems where the abundance of onboard functions should ensure better security.

On the other hand LPV methods whose theoretical developments in the context of robust control are very recent (less than a decade), and are still the topic of an intensive research, have shown their advantage in various applications [1]. They allow the application of linear methods to perform robust control of nonlinear systems and / or time-varying parameters. These methods need to understand some theoretical concepts related to modeling, analysis, observation and control. It is then particularly interesting to evaluate the potential of methods such as LPV ones within the framework of vehicle dynamics. Indeed such a type of LPV methods can help to:

- proposed control-oriented model, complex enough to handle some system non linearities but still simple for control or observer design,
- take into account the adaptability of the vehicle's response to situations encountered (normal, critical, dangerous ...) and under the conditions of operations,
- incorporate a model of actuators whose parameters are adjustable,
- manage interactions between various actuators to optimize the dynamic behavior of vehicles.

The main objective of the book is to demonstrate the value of this approach for controlling the dynamic behavior of vehicles. After some theoretical background and a view on some recent works on LPV approaches (for modelling, analysis, control, observation and diagnosis), the main emphasis is put on road vehicles but some illustrations are concerned with railway, aerospace and underwater vehicles. It presents, in a firm way, background and new results on LPV methods and their application to vehicle dynamics.

The content of the book is as follows, and it is divided in 3 parts.

In the first part some backgrounds on LPV systems are presented. Marco Lovera introduces first the concept of LPV systems in Chapter 1. József Bokor and Zoltán Szabó then presents in Chapter 2 some important features of the geometric approach for LPV systems analysis, and in Chapter 3, they introduce a specific class of LPV systems, namely the bimodal switching systems, where the switch from one mode to the other one depends on the state (closed-loop switching). In Chapter 4, Didier Henrion presents some recent results on LPV systems with positive polynomial matrices. Chapter 5, from Meriem Halimi, Gilles Millerioux and Jamal Daafouz, is dedicated to polytopic observers for LPV discrete-time systems. Chapter 6 tackles the fault diagnosis issue, and David Henry introduces the Fault Detection and Isolation LPV filters with some aerospace application.

The second part concerns the application of LPV methods to road vehicles. First Anh-Lam Do, Charles Poussot-Vassal, Olivier Sename and Luc Dugard present some LPV control approaches in view of comfort improvement of automotive suspensions equipped with MR dampers.In Chapter 8 Péter Gáspár proposes some design methods of integrated control (of suspension, braking and steering actuators) for road vehicles. In Chapter 9, a coordinated control of braking/steering actuators through LPV technics is proposed by Charles Poussot-Vassal, Olivier Sename, Soheib Fergani, Moustapha Doumiati and Luc Dugard. In Chapter 10, John J. Martinez and Sébastien Varrier present some new results on Multisensor Fault-Tolerant Automotive Control in the LPV framework. In Chapter 11, some theory and application to braking control of the Virtual Reference Feedback Tuning approach for LPV systems, are presented by Simone Formentin, Giulio Panzani and Sergio M. Savaresi. This part is concluded by Péter Gáspár and Zoltán Szabó in Chapter 12, with the design of a hierarchical LPV controller of an active suspension system for a full-car vehicle.

The third and final part is an opening to other vehicles such as railway, aerospace and underwater applications, for which the LPV approaches can be very attractive. First Péter Gáspár and Zoltán Szabó present in Chapter 13 an observer-based brake control for railways. Then Jean-Marc Biannic gives, in Chapter 14, a large overview of LPV control strategies for aerospace applications. Finally Chapter 15 by Emilie Roche, Olivier Sename and Daniel Simon, concludes the book with the design of LPV controllers with varying sampling for the altitude control of an AUV (Autonomous Underwater Vehicle), where depth measurements are asynchronously supplied by acoustic sensors.

We also would like to mention that this book is also part of the results of the 3-years bilateral collaboration project between the CNRS and the Hungarian Academy of Sciences: Robust and fault tolerant multivariable control for Automotive Vehicle.

We would like to thank all the contributors for providing very nice and high level chapters in this book.

We hope that this book will interest various researchers and graduate students in control of vehicle dynamics as wall as in robust control and LPV systems.

Reference

1. Mohammadpour, C.S. (ed.): Control of Linear Parameter Varying Systems with Applications. Springer, Heidelberg (2012)

Grenoble (France),
August 2012

Olivier Sename
Péter Gáspár
József Bokor

Acknowledgements

The Editors would like to thank the local organization of the Summer School, which have allowed the school to be a success in particular to Dr. Alexandre Seuret (on leave from CNRS, GIPSA-Lab, Grenoble, France).

Contents

Part II LPV Methods Applied to Road Vehicles

Part I
Some Background on LPV Systems (Modeling, Identification Control, Observation)

Chapter 1
LPV Modelling and Identification: An Overview

Marco Lovera, Marco Bergamasco, and Francesco Casella

Abstract. The current state-of-the-art in the fields of control-oriented LPV modelling and LPV system identification is surveyed and the potential synergies between the two research areas are highlighted and discussed. Indeed, a number of methods and tools for the development of LPV models from nonlinear systems and for the identification of black-box LPV models from input/output data have been derived, in a rather independent way, in different research communities. The relative merits of analytical and experimental methods for the derivation of LPV models, as well as possible combinations of the two approaches, are analysed and eventually evaluated on a case study based on the modelling of a thermo-fluid system.

1.1 Introduction

In the practice of control engineering there is a significant number of applications in which a single control system must be designed to guarantee the satisfactory closed-loop operation of a plant in many operating conditions. The most common control approach used in these applications is gain scheduling, see, e. g., [11, 24, 26, 27, 30, 41, 46, 49, 69]. The gain scheduling approach, which has been common practice in control engineering for decades, can be briefly summarised as follows: find one or more *scheduling variables* which parameterise the operating space of interest for the system to be controlled; define a parametric *family* of linearised models for the plant covering the set of operating points of interest; design a *parametric* controller ensuring that both the desired control objectives in each operating point and an acceptable behaviour during (slow) transients between one operating condition and the other are guaranteed. As is well known, a wide variety of design methods and tools is now available for this problem (see, e. g., the survey papers [32, 53], the

Marco Lovera · Marco Bergamasco · Francesco Casella
Dipartimento di Elettronica e Informazione, Politecnico di Milano
e-mail: {lovera,bergamasco,casella}@elet.polimi.it

O. Sename et al. (Eds.): *Robust Control and LPV Approaches*, LNCIS 437, pp. 3–24.
DOI: 10.1007/978-3-642-36110-4_1

references therein and the recent book [43]), which can be reliably solved, provided that a suitable model in parameter-dependent form has been derived.

This modelling problem can be formulated along many different lines, which lead to a number of different approaches. More precisely, it is possible to identify two broad classes of methods: *analytical* methods based on the availability of (relatively) reliable nonlinear equations for the dynamics of the plant, from which suitable control-oriented representations can be derived (see, again [32, 53] and [39]); *experimental* methods based entirely on identification, i.e., aiming at deriving LPV models for the plant directly from input/output data (see, among many others, [31, 63, 34] and the recent books [61, 33]).

The methods belonging to the first class aim at developing LPV models for the plant to be controlled by resorting to suitable extensions of the familiar notion of linearisation, possibly taking into account off-equilibrium operation of the system.

For the second class, many algorithms have been proposed in the literature in the last ten years or so, aiming at the estimation of the parameters for both input/output and state space models. While most LPV identification techniques are based on the assumption that the identification procedure can rely on one *global* identification experiment in which both the control input and the scheduling variables are (persistently) excited in a simultaneous way, this assumption may not be a reasonable one in many applications, in which it would be desirable to try and derive a parameter-dependent model on the basis of *local* experiments only, i.e., experiments in which the scheduling variable is held constant and only the control input is excited. Such a viewpoint has been considered in, e.g., [58, 47, 34], where numerical procedures for the construction of parametric models for gain scheduling on the basis of local experiments and for the interpolation of local controllers have been proposed.

In spite of the extensive (and increasing) research effort in this area, however, a number of issues are still open, both in terms of the development of suitable methodologies and in terms of proving their actual applicability to real life problems. In this respect, there is a strongly felt need to investigate new approaches for dealing, in a systematic way, with the complexity and the increasingly stringent requirement specifications arising in advanced applications.

In particular, both analytical and experimental methods suffer from some restrictions and limitations, which will be described in the following, and which might be mitigated by combining techniques originating from the former and the latter approach. Surprisingly enough, taking advantage of the potential synergies which might arise from the cross-fertilization of these two research areas seems to be a currently unexplored approach. In this respect, a third approach to LPV model identification has been proposed in a few recent contributions dealing with modelling of mechanical systems ([42]) and corresponds to a *glocal* perspective in which data collected in local experiments are used to estimate system's parameters based on a global parameterisation.

Finally, from the standpoint of application, many real systems exhibit dynamics which can be reasonably described by LPV models (see the recent special issue [35]) and there is an increasing interest for this modelling and identification framework in such diverse areas as, e.g., aeronautics [14, 39, 37, 38, 30], space [45, 28, 40, 18],

automotive [11, 16, 24, 25, 26, 27, 46, 59, 69], mechanics [19], mechatronics [47, 58], robotics [23, 6, 22, 7], bio-engineering [49], semiconductor manufacturing [68] and computing systems [52, 51, 60].

In the light of the above discussion, the aim of this chapter can be summarised in the following points: to provide an overview of the state-of-the art in the neighboring fields of analytical and experimental methods for LPV modelling, with an emphasis on state space modelling; to propose possible combined developments for new techniques which might make the most of analytical and experimental methods; to discuss the relative merits of the two classes of methods with reference to a simple case study.

The chapter is organised as follows. The considered LPV model classes are first defined in Section 1.2, while Sections 1.3, 1.4 provide an overview of analytical and experimental methods for LPV modelling, respectively. Finally, some simulation results related to the control-oriented modelling of a superheated steam generator are presented in Section 1.5.

1.2 Continuous- and Discrete-Time LPV Models

We define LPV systems as finite-dimensional linear time-varying plants whose state space matrices are fixed functions of some vector of varying, measurable parameters. In the following both continuous-time and discrete-time LPV models will be considered. In this Section, the main definitions and the relevant notation are provided. The focus will be on state space representations of LPV systems, see [61] for an in-depth treatment of input-output models and issues in LPV realisation theory.

Continuous-time state space LPV models are usually defined as

$$\begin{bmatrix} \dot{x} \\ y \end{bmatrix} = \begin{bmatrix} A(\rho) & B(\rho) \\ C(\rho) & D(\rho) \end{bmatrix} \begin{bmatrix} x \\ u \end{bmatrix}, \tag{1.1}$$

where ρ is the external scheduling parameter vector. A particular case of the above is the one of *quasi*-LPV (qLPV) systems,

$$\begin{bmatrix} \dot{z} \\ \dot{w} \\ y \end{bmatrix} = \begin{bmatrix} A_{11}(\rho) & A_{12}(\rho) & B_1(\rho) \\ A_{21}(\rho) & A_{22}(\rho) & B_2(\rho) \\ C_1(\rho) & C_2(\rho) & D(\rho) \end{bmatrix} \begin{bmatrix} z \\ w \\ u \end{bmatrix}, \tag{1.2}$$

where the state variables are divided in two separate parts, i.e., z are the scheduling states and w the nonscheduling ones. The scheduling vector ρ is composed, for the sake of generality, of both scheduling states z and exogenous scheduling variables ω, i.e.,

$$\rho = \begin{bmatrix} z \\ \omega \end{bmatrix}. \tag{1.3}$$

Discrete-time state space LPV models, on the other hand, are usually defined as

$$\begin{aligned} x_{k+1} &= A(\delta_k)x_k + B(\delta_k)u_k \\ y_k &= C(\delta_t)x_k + D(\delta_k)u_k, \end{aligned} \tag{1.4}$$

where $\delta \in \mathbb{R}^s$ is the parameter vector and $x \in \mathbb{R}^n$, $u \in \mathbb{R}^m$, $y \in \mathbb{R}^l$. In the LPV identification literature, additional assumptions are usually introduced regarding the way in which δ_k enters the system matrices. The most common assumptions are

1. Affine parameter dependence (LPV-A):

$$A(\delta_k) = A_0 + A_1\delta_{1,k} + \ldots + A_s\delta_{s,k} \tag{1.5}$$

   and similarly for B, C and D, and where by $\delta_{i,k}, i = 1,\ldots,s$ we denote the i-th component of vector δ_k. This form can be immediately generalised to polynomial parameter dependence.
2. Input-affine parameter dependence (LPV-IA): this is a particular case of the LPV-A parameter dependence in which only the B and D matrices are considered as parametrically-varying, while A and C are assumed to be constant: $A = A_0$, $C = C_0$.
3. LFT parameter dependence (LPV-LFT): the plant is constituted by the feedback interconnection of an LTI system

$$\begin{aligned} x_{k+1} &= \mathscr{A}x_k + \mathscr{B}_0 w_k + \mathscr{B}_1 u_k \\ z_k &= \mathscr{C}_0 x_k + \mathscr{D}_{00} w_k + \mathscr{D}_{01} u_k \\ y_k &= \mathscr{C}_1 x_k + \mathscr{D}_{10} w_k + \mathscr{D}_{11} u_k \end{aligned} \tag{1.6}$$

   with a time-varying block which depends on the parameter vector

$$w_k = \Delta_k z_k, \quad \Delta_k = \mathrm{diag}(\delta_{1,k}I_{r_1} \ldots \delta_{s,k}I_{r_s}), \tag{1.7}$$

   and $w, z \in \mathbb{R}^r$, $r = r_1 + \ldots + r_s$. The elements of the system matrices turn out to be first order rational functions of the elements of the parameter vector if $\mathscr{D}_{00} \neq 0$ and linear functions of the parameter vector if $\mathscr{D}_{00} = 0$.

As is well known in the robust control literature and also pointed out in [31] with respect to LPV-IA and LPV-LFT models, affine and linear-fractional representations for LPV systems are related to each other. Focusing, e.g., on discrete-time systems and denoting the composition of the system matrices

$$M(\delta_k) = \begin{bmatrix} A & B(\delta_k) \\ C & D(\delta_k) \end{bmatrix} = M_0 + M_1\delta_{1,k} + \ldots + M_s\delta_{s,k}$$

by expressing each of the $M_i's$ by means of a rank r_i decomposition as $M_i = U_iV_i$ one can write $M(\delta_k)$ as $M(\delta_k) = M_0 + U\Delta_k V$ where

$$U = [U_1 \ldots U_s], V = [V_1^T \ldots V_s^T]^T \tag{1.8}$$

and Δ_k is given by equation (1.7). The obtained form for the system matrices coincides with that of the special case of a linear fractional transformation characterised by having $\mathscr{D}_{00} = 0$, hence the transformation between the two forms.

1.3 Analytical LPV Modelling

In this Section an overview of the available methods for the analytical derivation of LPV models for nonlinear systems is provided. The interested reader is referred to the survey papers [32, 53, 39] for additional details. The underlying assumption for the development of analytical methods is that a nonlinear state-space model for the considered plant is available

$$\dot{x} = f(x,u) \tag{1.9}$$
$$y = g(x,u), \tag{1.10}$$

for which a set of equilibria $(\bar{x},\bar{u})$ is known, and parameterised by a scheduling vector defined as in equation (1.3).

1.3.1 Jacobian Linearisation

The Jacobian linearization approach is the simplest methodology used to obtain LPV models. In terms of applicability, it can be reliably adopted for any nonlinear system which admits a linearisation at its equilibrium points of interest.

The idea is to obtain an LPV system based on a family of linearized models obtained with respect to a set of equilibrium points that represents the operational space of interest for the system. The resulting model is a local approximation to the dynamics of the nonlinear plant around this set of equilibrium points. For practical purposes, the implementation of a Jacobian linearisation for the plant also calls for a suitable interpolation scheme, to be applied both the state space matrices of the system and to the equilibrium curve, if the latter is not available in analytical form. More details on the interpolation problem will be provided in Section 1.4.1.

1.3.2 State Transformation

The state transformation approach is based on the idea of performing a coordinate change in the nonlinear equations of the system, the aim of which is the elimination of all the nonlinear terms which do not depend on the scheduling parameter. This technique can effectively lead to a qLPV representation for the given system, but it is restricted to nonlinear systems in the form

$$\begin{bmatrix} \dot{z} \\ \dot{w} \end{bmatrix} = A(\rho) \begin{bmatrix} z \\ w \end{bmatrix} + B(\rho)u + K(\rho), \tag{1.11}$$

where z are the scheduling states and w the nonscheduling ones, and such that the number of scheduling states equals the number of control inputs u. Assume, further, that there exist continuously differentiable functions $w_{eq}(\rho)$ and $u_{eq}(\rho)$ such that

$$\begin{bmatrix} 0 \\ 0 \end{bmatrix} = \begin{bmatrix} K_1(\rho) \\ K_2(\rho) \end{bmatrix} + \begin{bmatrix} A_{11}(\rho)\ A_{12}(\rho) \\ A_{21}(\rho)\ A_{22}(\rho) \end{bmatrix} \begin{bmatrix} z \\ w_{eq}(\rho) \end{bmatrix} + \begin{bmatrix} B_1(\rho) \\ B_2(\rho) \end{bmatrix} u_{eq}(\rho). \tag{1.12}$$

Subtracting (1.12) from (1.11) and recalling that $\dot{w}_{eq}(\rho) = \frac{\partial w_{eq}(\rho)}{\partial \rho}\dot{z}$ one obtains the qLPV model for the plant, in the form

$$\begin{bmatrix} \dot{z} \\ \dot{w} - \dot{w}_{eq}(\rho) \end{bmatrix} = \begin{bmatrix} 0 & A_{12}(\rho) \\ 0\ A_{22}(\rho) - \frac{\partial w_{eq}(\rho)}{\partial z}|_{\rho} A_{12}(\rho) \end{bmatrix} \times \\ \begin{bmatrix} z \\ w - w_{eq}(\rho) \end{bmatrix} + \begin{bmatrix} B_1(\rho) \\ B_2(\rho) - \frac{\partial w_{eq}(\rho)}{\partial z}|_{\rho} B_1(\rho) \end{bmatrix} (u - u_{eq}(\rho)). \tag{1.13}$$

The application of the Jacobian linearisation and of the state transformation methods to a case study will be considered in Section 1.5.

1.3.3 Function Substitution

In [39] a novel approach to the derivation of qLPV models was proposed, named function substitution. This approach applies to qLPV systems with nonlinearities in the control input and is based on the substitution of a so-called decomposition function by (scheduling parameter-dependent) functions linear in the scheduling vector. The decomposition function is defined as the combination of all the terms of the nonlinear system that are not both, affine with respect to the nonscheduling states and control inputs, and function of the scheduling vector alone (after a coordinate change with respect to a single equilibrium point has been performed). The decomposition is carried out through a minimization procedure, which leads to a series of numerical optimisation problems.

1.4 Experimental LPV Modelling

LPV model identification algorithms can be divided in two classes, according to the assumptions they rely on from the experimental point of view. Global approaches assume that the input/output data are collected in a single experiment in which the parameter is also excited and lead to an LPV model in a single step. Local approaches, on the other hand, rely on multiple experiments performed with constant parameter values and lead to many LTI models which have to be interpolated in order to arrive at the complete LPV representation for the system. Global methods

for LPV identification provide a very general way of dealing with the problem, at the cost of critical requirements on the experimental conditions which might not be easily realisable in many applications. On the other hand, local techniques have the advantage of being much closer to the actual practice of linear time-invariant system identification but suffer from the additional complexity associated with the interpolation of local models. In this Section a brief overview of local and global methods will be provided.

1.4.1 Local Methods

The local approach to LPV model identification can be briefly formalised as follows. Consider the MIMO linear parametrically-varying system given by

$$\dot{x} = A(\rho)x + B(\rho)u \tag{1.14}$$

$$y = C(\rho)x + D(\rho)u \tag{1.15}$$

where $u \in \mathbb{R}^m$, $y \in \mathbb{R}^l$, $x \in \mathbb{R}^n$ and $\rho \in \mathbb{R}^r$ and assume that the results of a number of P identification experiments are available, associated with the operation of the system near P different values of the parameter vector ρ. Then, the aim of the local LPV identification procedure is to determine a set of parameter dependent matrices $\hat{A}(\rho)$, $\hat{B}(\rho)$, $\hat{C}(\rho)$ and $\hat{D}(\rho)$ (usually in affine or LFT form) which can provide a good approximation of the system (1.14)-(1.15) over the considered range of operating points.

Focusing on the algorithm first presented in [34], which is representative of the results currently available in the literature, we have that a typical state space local approach can be summarised in the following steps.

- Linear state-space models are estimated for each operating point (using, e.g., a subspace model identification algorithm).
- The identified models are brought (as close as possible to) a common state space representation (e.g., in [34] the internally balanced form was used).
- Finally, the parameter-dependent model is obtained by direct interpolation of the state-space matrices of the local models.

A few comments for each of the above steps follow.

Local Model Identification

The identification of the local linear time-invariant models can be carried out using any technique for LTI model identification. A convenient choice for the identification of the local models in state space form is to resort to subspace model identification (SMI) algorithms - particularly so when dealing with multivariable problems. The only, well known, downside of the SMI approach to state space model identification is the impossibility to impose a fixed basis to the state space representation. This, in turn, implies that it is hard to impose a parameterisation to

the state space matrices in this framework, and therefore difficulties in recovering physically-motivated models arise. This, to date, prevents the successful application of SMI methods to some specific problems, including, e. g., the initialisation of iterative methods for the identification of structured state space representations and the identification of local models for LPV interpolation.

Consistency of the State Space Basis

Once P local models have been obtained, the problem of recovering the whole parameter-dependent system has to be faced. To this purpose, it is first essential to guarantee that the local state space models are represented in a consistent state space basis, so that the subsequent interpolation can be carried out in a meaningful way.

The problem has been initially addressed in [58], where the canonical controllability form was proposed for the case of SISO systems, while in [34] it was proposed to fix the state space basis of the estimated matrices by using the algorithm first derived in [29] to find a similarity transformation T such that $\left\{T^{-1}\hat{A}T, T^{-1}\hat{B}, \hat{C}T, \hat{D}\right\}$ is in internally balanced form. Balanced realisations have an interesting and relevant property in this framework, i. e., under suitable assumptions (see [29] and [44] for details), the balancing transformation T is essentially unique. This, in turn, implies that if the true LPV system exhibits a smooth dependence from the scheduling parameter δ, then the overall parameter dependent model can be directly reconstructed from the identified local models.

More recently, in [50], the state space identification of a general black-box model of the same order as the physical system is assumed as a starting point and the physical and identified models are related to each other via a similarity transformation. The bilinear equations resulting from the definition of the transformation are then converted into a null-space problem, the solution of which leads to a non-convex optimization problem, for which uniqueness of the solution can be guaranteed by assuming that the user-defined physical state space form is identifiable and the identified black-box model is consistent. Even more recently, in [5] the problem is addressed in a different perspective, with the aim of reducing the complexity of the non-convex optimisation problem to be addressed in order to match the structured and the unstructured state space representations. More precisely, the problem is formulated as an input-output model matching one, in terms of the H_∞ norm of the difference between the two models. The solution of the problem is subsequently computed using recent results in non-smooth optimisation techniques, see [1], which yield effective computational tools (see [17]). The main advantage of this approach is that no explicit construction of the similarity transformation is needed, so the complexity of the non-convex optimisation task remains related to the number of uncertain parameter and is independent of the dimension of the model class. Furthermore, it can be applied to all instances of the problem corresponding to model classes for which the H_∞ norm (or, rather, the L_2 gain) can be computed, as

illustrated in the case of linear time-periodic (LTP) models and linear parameter-varying (LPV) models identified using a periodic scheduling sequence (see also [15]).

Interpolation of the Local Models

The problem of interpolating local models has been studied by many authors in recent years. Indeed, this problem arises not only when interpolating local black-box models but also when dealing with multiple models derived from Jacobian linearisation of a nonlinear simulator. For some recent references on this topic see for example [20, 48]. In the following reference will be made to the interpolation approach used in [4].

Once the elements of the state-space matrices of the system have been estimated following the above steps, and set of N_θ local linear time-invariant state space models has been obtained, a number of options are available as far as the derivation of the actual parameter dependent model is concerned. The first, and simplest, would be to directly fit to the system matrices of the local models using suitable regressors formed from the scheduling parameter $\theta \in \mathbb{R}^{n_p}$. This would directly yield a parameter dependent model in so-called *affine* form, i.e.,

$$\begin{aligned} \dot{x} &= A(\gamma)x + B(\gamma)u \\ y &= C(\gamma)x + D(\gamma)u \end{aligned} \tag{1.16}$$

where $\gamma \in \mathbb{R}^{n_\gamma}$ is the vector of regressors (formed from linear or nonlinear combinations of the elements of θ) such that the parameter dependent matrices can be written as

$$A(\gamma) = A_0 + A_1\gamma_1 + A_2\gamma_2 + \ldots + A_{n_\gamma}\gamma_{n_\gamma}$$

and similarly for $B(\gamma)$, $C(\gamma)$ and $D(\gamma)$. The state space matrices are represented as transfer function

$$G_k(s) = C(\gamma(k))(sI - A(\gamma(k)))^{-1}B(\gamma(k)) + D(\gamma(k)), \quad k = 1, \ldots, N_\theta$$

where k is the scheduling index of the k^{th} identified local model. The matrices are also aggregated in the following form

$$F(\gamma(k)) = \begin{bmatrix} A(\gamma(k)) & B(\gamma(k)) \\ C(\gamma(k)) & D(\gamma(k)) \end{bmatrix}, \; k = 1, \ldots, N_\theta. \tag{1.17}$$

The polynomial interpolation of the elements of the matrix F is performed by solving a least squares problem as $Y = \Phi\Theta$, where Y contains the elements f_{ij} of F, Φ contains the regressors γ, and Θ contains the polynomial coefficients. The root means square error (RMS_e) is defined as

$$RMS_e = \frac{\|Y - \Phi\hat{\Theta}\|_2}{\|Y\|_2}, \tag{1.18}$$

and it expresses the fitting error.

In order to reduce the model complexity, as suggested in [48] and reported here for the sake of completeness, the fitting procedure is divided in two steps: the sensitivity analysis and the polynomial fitting.

The H_∞-norm sensitivity (note that in [48] the ν-gap metric is instead used as a measure of sensitivity) is computed for each element f_{ij} of the matrix $F(\gamma(k))$ and it is defined as

$$S_{ij} = \max_k \frac{\|G_k - G_{k_{ij}}\|_\infty}{\|G_k\|_\infty}, \tag{1.19}$$

where $G_{k_{ij}}$ is equal to G_k except for the element f_{ij} that is substituted with the mean of the N_θ values $f_{ij}(\gamma(k))$. If the influence of an element f_{ij} on the transfer functions is lower than a (user-defined) bound $\underline{S} \in [0,1]$, its mean value is used instead of performing a polynomial fitting. It is also possible to define an upper bound $\overline{S}$ beyond which the maximum polynomial degree is used. If S_{ij} is in the interval $[\underline{S}, \overline{S}]$ a linear function of the influence is considered in order to obtain the most reasonable trade-off between model complexity, i.e., polynomial degree, and fitting error. In other words, the coefficient ζ_{ij} is defined for each (i,j) as a function of the sensitivity S_{ij} as follows

$$\zeta_{ij} = \begin{cases} \infty & S_{ij} < \underline{S} \\ \frac{K_e - 1}{\underline{S} - \overline{S}} S_{ij} + \frac{\underline{S} - K_e \overline{S}}{\underline{S} - \overline{S}} & \underline{S} \le S_{ij} \le \overline{S} \\ 1 & S_{ij} > \overline{S}, \end{cases} \tag{1.20}$$

where $K_e > 1$ is the value of ζ_{ij} when S_{ij} is equal to $\underline{S}$. The value for this parameter suggested in [48] is 2, which corresponds to twice the absolute and the relative tolerances than their original values, and in this way the low sensitivity of the parameter (i,j) is taken into account. The absolute and the relative tolerances of the mean square error are respectively $\zeta_{ij}\varepsilon_a$ and $\zeta_{ij}\varepsilon_r$.

The algorithm increases the polynomial degree of the approximation and computes the new polynomial coefficients by solving the least squares problem until the RMS_e drops below the absolute tolerance $\zeta_{ij}\varepsilon_a$ or the improvement in the RMS_e becomes less than the relative tolerance $\zeta_{ij}\varepsilon_r$.

Finally, it is interesting to point out that a different viewpoint for the local approach has been proposed in a series of papers (see [12, 13] and the references therein), in which the interpolation is carried out at the level of poles and zeros of the identified local models. Clearly, as poles and zeros are invariant with respect to the choice of coordinates in the state space, the issue of the state space basis is circumvented. This benefit however comes with a price, namely that the construction of parametric maps for the singularities of the input-output representations of the local models is a critical process which is hard to carry out in a fully automated way.

1.4.2 Global Methods

Global methods for state space models have been first proposed in [36, 31]. In the first paper the case of measurable state was addressed and a subspace identification

algorithm was first proposed. In the second paper, on the other hand, an iterative maximum-likelihood approach to the identification of LPV models in LFT form has been derived. Indeed, the classical way to perform linear system identification is by minimizing the error between the real output and the predicted output of the model. A similar approach can be used for LPV state-space systems of the form (1.4). Let the system matrices of (1.4) be completely described by a set of parameters θ, then identification can be carried out by minimizing the cost function

$$V_N(\theta) := \sum_{k=1}^{N} ||y_k - \widehat{y}_k(\theta)||_2^2 = E_N^T(\theta) E_N(\theta),$$

with respect to θ, where

$$E_N^T(\theta) = \left[\left(y_1 - \hat{y}_1(\theta) \right)^T \cdots \left(y_N - \hat{y}_N(\theta) \right)^T \right],$$

and y_k denotes the measured output and $\widehat{y}_k(\theta)$ denotes the output of the LPV model to be identified. In general, the minimization of $V_N(\theta)$ is a nonlinear, nonconvex optimization problem. Different algorithms can be used to numerically search for a solution to such an optimization problem; typically, the Levenberg-Marquardt algorithm is employed. An important question that arises is how to choose the parameters θ to describe the system matrices in (1.4), as its choice may give rise to structural identifiability issues. A state space parameterisation in general implies that the minimization of $V_N(\theta)$ does not have a unique solution, because there exist different systems, corresponding to different values of Θ, that have the same input/output behavior. In order to deal with the nonuniqueness of the optimal θ, in [31] a solution has been proposed in which, at each iteration, the directions that do not change the value of the cost function are identified and are projected out of the search direction used in the update rule. This solution can be interpreted as letting the algorithm decide the parameterization that is used at each iteration.

The approach is very effective provided that the available data meet the stringent persistency of excitation requirements, which call for the simultaneous excitation of the control inputs and of the parameters of the system and, furthermore, that a reliable initial estimate for the iterative optimisation procedure is available. To this purpose, in the cited reference it was proposed to start by estimating the parameters of a model in LPV-IA form, as its parameters can be retrieved by using conventional algorithms for LTI systems (such as, e.g., subspace identification algorithms) by suitably extending the input vector. As is well known (see also Section 1.2), LPV-IA models can be converted exactly into LPV-LFT form, so they provide a useful initial guess for iterative methods.

The search for effective means for the initialisation of interative methods such as the above described one led over the last decade to the development of subspace model identification algorithms for LPV systems. Such methods stemmed from research on the identification of bilinear models (see [63, 67] and has since led to the development of relatively mature methods such as the ones in [65, 64, 66, 15, 62].

Finally, an alternative approach leading to successive approximation techniques was developed in a series of paper, again stemming from research work on the identification of bilinear systems, see [54, 55, 56, 57] and the edited book [33].

1.4.3 Glocal Methods

Analytical methods for LPV and qLPV modelling generally provide simple and reliable ways to derive control-oriented representations even for relatively complex nonlinear systems. Apart from the specific requirements of each of the methods available in the literature, however, the general assumption is that a fully determined, reliable set of nonlinear equations for the system is available. This, in particular, leaves open the issue of dealing with the rather frequent situation in which the nonlinear equations include unknown parameters and/or functions of the scheduling variables.

Experimental methods, on the other hand, suffer from a number of limitations. Local methods can only, to their best, provide the same level of performance as the Jacobian linearisation approach. Therefore, from a practical point of view, they may only be considered as a viable alternative in cases in which the additional modelling effort required to derive a nonlinear model for the system is more expensive than the set of experiments needed to apply a black-box identification procedure. When moving from local to global experimental methods the situation becomes even more critical, in view of the very strong requirements such methods have in terms of the informative content of the input/output data to be used in the derivation of the LPV model. Indeed, global methods require very complex persistence of excitation assumption to be fulfilled (see, e.g., [2, 3], where persistency of excitation conditions for LPV model identification were first characterised), which also involve the scheduling variables. As such conditions are rarely realistic in practical applications, it would appear that global methods are restricted to a very limited set of applications (see, for example, [60]) in which it is feasible to apply excitation signals also to the scheduling parameter vector. In this respect, current research is aiming at developing LPV model identification techniques which are less demanding as far as parameter variation is concerned (see, e.g., [15]).

As an example of potential synergies between analytical and experimental methods, consider the case of a nonlinear system in the form (1.11), for which a qLPV representation of the form (1.13) has been derived. Assume now that the state space matrices of the qLPV form are functions of an unknown parameter vector θ, i.e., that letting

$$v = u - u_{eq}(\rho), \quad t = w - w_{eq}(\rho) \tag{1.21}$$

and $\bar{x} = \begin{bmatrix} z & t \end{bmatrix}^T$, equation (1.13) can be equivalently written as

$$\dot{\bar{x}} = F(\rho, \theta)\bar{x} + G(\rho, \theta)v \tag{1.22}$$

$$y = z. \tag{1.23}$$

The problem of estimating the elements of the θ vector from measurements of the input v and the output y can be therefore recast in terms of a local or global model identification problem not unlike the ones discussed in Section 1.4. Similarly, if the uncertainty in the state space matrices of the qLPV form is given by an unknown function $\theta(\rho)$ of the parameter vector, one can reduce the problem to the previous case by defining a suitable parameterisation for the unknown function (such as, e.g., an affine one $\theta(\rho) = \theta_0 + \theta_1\rho_1 + \ldots + \theta_s\rho_s$) and introducing it in the state space qLPV form. Finally, note that this approach to mixed anaytical/experimental LPV modelling can be performed directly in continuous-time by resorting to classical results for state space model identification (see, e.g., [8]).

Inspired by the discussion in [10], the above-described idea has been further developed in [42, 70], where the knowledge available from the study of the non-linear equations governing the system behavior are used to fix the structure of the global LPV model. More precisely, based on local experiments (corresponding to a constant scheduling parameter value), the following procedure yields a global LPV model without requiring an interpolation stage. This basic idea of realizing global functions by local actions is inspired from S. Hara's work dedicated to the design of "glocal controllers" [21]. For this reason, the identification procedure described hereafter will be also called "glocal" in the sequel. This approach is interesting from a theoretical as well as a practical point of view because

- it circumvents the classical problems related to the interpolation of local models;
- the numerical issues which arise if an ill-conditioned parameterization for the model class is chosen (e.g., use of canonical forms with coefficients with large magnitude variations) are avoided;
- the challenge of realizing all the models with respect to the same state variables, which comes into play when interpolating black-box local state-space models is circumvented;
- persistency of excitation of the scheduling parameters is not required. Indeed, persistently exciting the scheduling parameters is sometimes difficult to be satisfied in a number of application domains such as, e.g., in the mechatronics or aeronautics domains.

The activity in this area, however is fairly recent and has not yet lead to mature, general purpose, methods and tools.

1.5 A Case Study

1.5.1 Process Description and Simulation

The above-described techniques are tested using a superheated steam generator as a case study. The plant is composed by a boiler and a steam superheater, feeding a steam turbine. The drum boiler is fed with slightly subcooled water and produces saturated steam at the outlet; the superheater receives the saturated steam at the inlet

and adds more heat to it. The boundary conditions for the system are: a prescribed flow rate and specific enthalpy for the feed water, a multi-stage turbine at the superheater outlet, and a prescribed heat flow entering both the boiler and the superheater, with a fixed ratio. A process simulator, represented in Figure 1.1, has been set up using the Modelica library ThermoPower (see [9]). The lumped-parameter boiler model is based on dynamic mass and energy balances, assuming a uniform temperature for the liquid, the vapour, and the metal wall. The superheater has been split into three finite volumes, accounting for the mass and energy balance of the steam. Additional heat storage in the superheater tube walls is modelled by three lumped thermal capacitances, having the same temperature as the steam in the corresponding volume, which is a reasonable assumption due to the very high heat transfer coefficient between the steam and the tube walls. The thermodynamic properties of water and steam are computed using the accurate standard IF97 model.

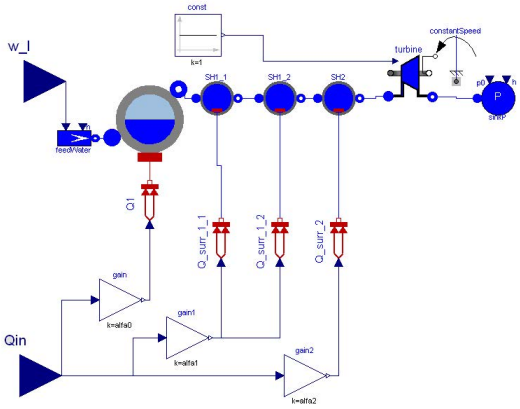

Fig. 1.1 The simulator for the considered plant

1.5.2 Nonlinear Mathematical Model

It is possible to derive a nonlinear mathematical model of the process by introducing the following additional assumptions:

- the mass and energy storage of the steam in the superheater is negligible, compared to the mass and energy storage in the boiler and in the superheater walls;
- the specific heat at constant pressure of the superheated steam is constant;
- the mass flow rate through the turbine is proportional to the inlet pressure;
- the derivative of the mass stored in the boiler mainly depends on the void fraction derivative;
- the derivative of the energy storage in the boiler mainly depends on the pressure derivative.

Under the above assumptions, the mass and energy balance equations in the boiler, and the energy balance equations in the superheaters can be written as

$$\dot{\alpha} = \frac{w_l}{f_1(p)} - \frac{k_v p}{f_1(p)}, \tag{1.24}$$

$$\dot{p} = k_v p \frac{h_l - h_{vs}(p)}{f_2(p,\alpha)} + a_b \frac{Q_{in}}{f_2(p,\alpha)}, \tag{1.25}$$

$$\dot{T}_2 = n\frac{k_v p c_p}{C_m} T_{sat}(p) - n\frac{k_v p c_p}{C_m} T_2 + a_s \frac{Q_{in}}{C_m}, \tag{1.26}$$

$$\dot{T}_3 = n\frac{k_v p c_p}{C_m} T_2 - n\frac{k_v p c_p}{C_m} T_3 + a_s \frac{Q_{in}}{C_m}, \tag{1.27}$$

$$\dot{T}_4 = n\frac{k_v p c_p}{C_m} T_3 - n\frac{k_v p c_p}{C_m} T_4 + a_s \frac{Q_{in}}{C_m}, \tag{1.28}$$

where α is the void fraction in the boiler, p is the boiler pressure, w_l is the feedwater mass flow rate, k_v is the valve flow coefficient, h_l is the feedwater specific enthalpy, h_{vs} is the saturated steam enthalpy, c_p is the heat capacity at constant pressure of the steam, Q_{in} is the total heat flow to the system, a_b and a_s are the fractions of the total heat flow going to the boiler and to the superheater, f_1 and f_2 are suitable functions of the boiler dimensional parameters and of the water/steam saturation properties, T_{sat} is the saturation temperature, T_2, T_3, and T_4 are the temperatures of the superheated steam in the three finite volumes, n is the number of finite volumes, and C_m is the total heat capacitance of the superheater pipe walls.

1.5.3 Analytical LPV Modelling

On the basis of the above equations, suitable LPV representations can be obtained analytically by applying both the Jacobian linearisation and the state transformation methods described in Section 1.3. In particular, the state variables α and p are assumed as scheduling states in the application of the state transformation approach, so that, in terms of the notation adopted in Section 1.3 we have $z = \begin{bmatrix}\alpha & p\end{bmatrix}^T$ and $w = \begin{bmatrix}T_1 & T_2 & T_3\end{bmatrix}^T$. While the explicit expression for the Jacobian linearisation representation of the system is omitted for brevity, it is however interesting to point out that for this specific application the state transformation approach leads to a particularly simple structure. Indeed, note that if the nonlinear mathematical model is rewritten in the form (1.11), it leads to equation (1.29), from which one can see that

$$\begin{bmatrix}\dot{\alpha}\\ \dot{p}\\ \dot{T}_2\\ \dot{T}_3\\ \dot{T}_4\end{bmatrix} = \begin{bmatrix} 0 & \frac{-k_v}{f_1(p)} & 0 & 0 & 0 \\ 0 & \frac{k_v(h_l - h_{vs}(p))}{f_2(p,\alpha)} & 0 & 0 & 0 \\ 0 & \frac{nk_v c_p}{C_m} T_{sat}(p) & -\frac{nk_v c_p}{C_m} p & 0 & 0 \\ 0 & 0 & \frac{nk_v c_p}{C_m} p & -\frac{nk_v c_p}{C_m} p & 0 \\ 0 & 0 & 0 & \frac{nk_v c_p}{C_m} p & -\frac{nk_v c_p}{C_m} p \end{bmatrix} \begin{bmatrix}\alpha\\ p\\ T_2\\ T_3\\ T_4\end{bmatrix} + \begin{bmatrix} \frac{1}{f_1(p)} & 0 \\ 0 & \frac{a_b}{f_2(p,\alpha)} \\ 0 & \frac{a_s}{C_m} \\ 0 & \frac{a_s}{C_m} \\ 0 & \frac{a_s}{C_m} \end{bmatrix} \begin{bmatrix} w_l \\ Q_{in}, \end{bmatrix} \tag{1.29}$$

the $A_{12}(\rho)$ block is zero, so that the eventual LPV model will have a much simpler structure than the general one presented in Section 1.3. Finally, for simulation purposes the actual LPV model must be complemented with an explicit representation of the equilibrium curve along which it has been derived.

1.5.4 Experimental LPV Modelling

For the considered process, five representative operating points have been considered, and the response of the state variables to perturbations applied on the Q_{in} control input have been collected in simulated experiments. The considered input sequence is a sum of Schroeder-phased sinusoids, effectively covering the frequency range from DC to about 10^{-1} rad/s. Five local models have been identified using the approach summarised in Section 1.4 and have been subsequently interpolated using as unique scheduling parameter the pressure p. In the following Figures 1.2-1.4, the non-parametric frequency responses associated with the input/output data obtained in the first of the five local experiments for the α, p and T_4 variables, respectively, are compared with the frequency response of the corresponding local model and of the interpolated LPV model. As can be seen from the Figures, the LPV model constructed from data can match very accurately the local behaviour of the real system; similar results – omitted for brevity – have been obtained for the other operating points of interest.

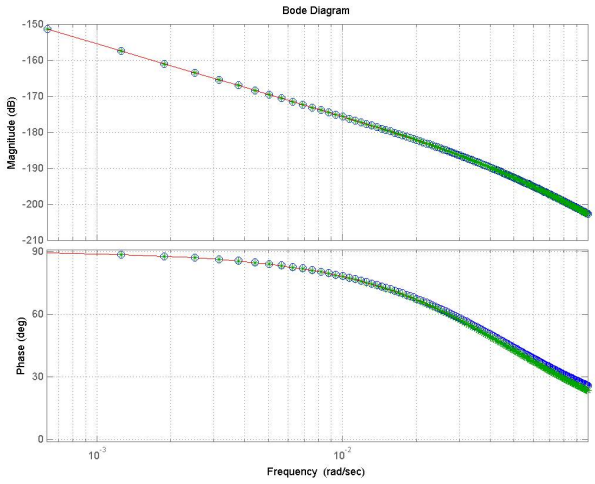

Fig. 1.2 Non-parametric (solid), local (o) and interpolated (*) frequency responses from perturbations to Q_{in} to perturbations to α, near the first operation point

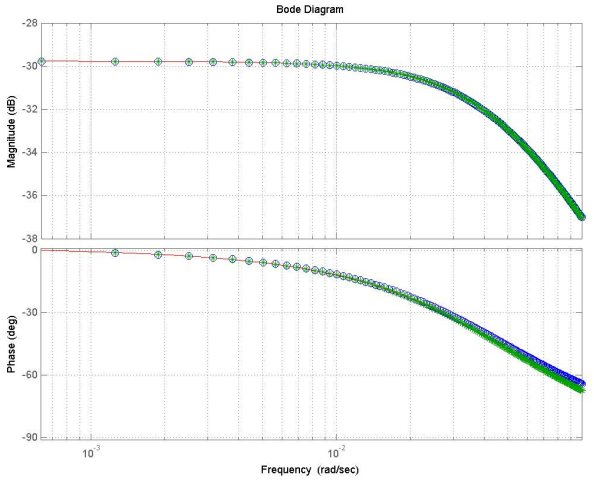

Fig. 1.3 Non-parametric (solid), local (o) and interpolated (*) frequency responses from perturbations to Q_{in} to perturbations to p, near the first operation point

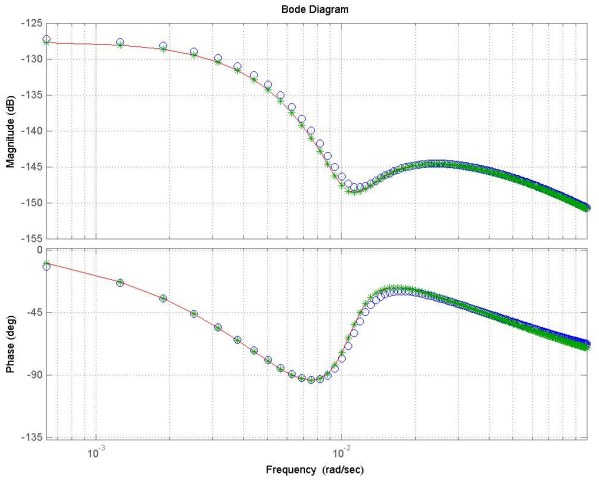

Fig. 1.4 Non-parametric (solid), local (o) and interpolated (*) frequency responses from perturbations to Q_{in} to perturbations to T_4, near the first operation point

1.5.5 Comparison of Results

For this specific application the comparison of analytical and experimental LPV models leads to the following results: as the state transformation method can be

applied exactly, the performance of the obtained model when compared to the "real system" in simulation is clearly very satisfactory. On the other hand, the analytical model obtained from Jacobian linearisation and the experimental one obtained from local identification lead to results of comparable quality both in near-equilibrium operation and during transients. However, in the development of this case study a number of practical issues emerged, which do not seem to have been thoroughly investigated in the literature.

1.6 Conclusions

The problem of deriving MIMO parameter-dependent models for LPV control design from analytical and experimental methods has been considered, the relative merits of the two approaches have been discussed and potential synergies which ought to be further explored have been analysed.

References

1. Apkarian, P., Noll, D.: Nonsmooth H_∞ synthesis. IEEE Transactions on Automatic Control 51(1), 71–86 (1996)
2. Bamieh, B., Giarré, L.: Identification of linear parameter varying models. In: Proceedings of the IEEE Conference on Decision and Control, Phoenix, USA (1999)
3. Bamieh, B., Giarré, L.: Identification of linear parameter varying models. International Journal of Robust and Nonlinear Control 12(9), 841–853 (2002)
4. Bergamasco, M., Lovera, M.: Subspace identification of continuous-time state-space LPV models. In: Linear Parameter-Varying System Identification: New Developments and Trends. Advanced Series in Electrical and Computer Engineering. World Scientific (2012)
5. Bergamasco, M., Lovera, M.: State space model identification: from unstructured to structured models with an h_∞ approach. In: IFAC Symposium on System Structure and Control, Grenoble, France (Submitted, 2013)
6. Boonto, S., Werner, H.: Closed-loop system identification of LPV input-output models: application to an arm-driven inverted pendulum. In: Proceedings of the 47th IEEE Conference on Decision and Control, Cancun, Mexico (2008)
7. Boonto, S., Werner, H.: Closed-loop identification of LPV models using cubic splines with application to an arm-driven inverted pendulum. In: Proceedings of the American Control Conference, Baltimore, MD, USA (2010)
8. Bruls, J., Chou, C., Haverkamp, B., Verhaegen, M.: Linear and non-linear system identification using separable least-squares. European Journal of Control 5(1), 116–128 (1999)
9. Casella, F., Leva, A.: Modelling of thermo-hydraulic power generation processes using Modelica. Mathematical and Computer Modelling of Dynamical Systems 10(1), 19–33 (2006)
10. Casella, F., Lovera, M.: LPV/LFT modelling and identification: Overview, synergies and a case study. In: 2008 IEEE Multi-conference on Systems and Control, San Antonio, USA (2008)

11. Chabaan, R.: H-infinity control and gain scheduling method for electric power assist steering system. US Patent 6651771 (2003)
12. De Caigny, J., Camino, J., Swevers, J.: Interpolating model identification for SISO linear parameter-varying systems. Mechanical Systems and Signal Processing 23, 2395–2417 (2009)
13. De Caigny, J., Camino, J., Swevers, J.: Interpolation-based modeling of MIMO LPV systems. IEEE Transactions on Control Systems Technology 19, 46–63 (2011)
14. Doll, C., Chiappa, C., Biannic, J.M.: LFT modelling of the 2-dof longitudinal nonlinear aircraft behaviour. In: 2008 IEEE Multi-conference on Systems and Control, San Antonio, USA (2008)
15. Felici, F., van Wingerden, J.W., Verhaegen, M.: Subspace identification of MIMO LPV systems using a periodic scheduling sequence. Automatica 43(10), 1684–1697 (2007)
16. Fialho, I.J., Balas, G.: Design of nonlinear controllers for active vehicle suspensions using parameter-varying control synthesis. Vehicle Systems Dynamics 33(5), 351–370 (2000)
17. Gahinet, P., Apkarian, P.: Decentralized and fixed-structure H_∞ control in MATLAB. In: 50th IEEE Conference on Decision and Control and European Control Conference, Orlando, USA (2011)
18. Ghersin, A., Sanchez Pena, R.: LPV control of a 6-DOF vehicle. IEEE Transactions on Control Systems Technology 10(6), 883–887 (2002)
19. Giarré, L., Bauso, D., Falugi, P., Bamieh, B.: LPV model identification for gain scheduling control: An application to rotating stall and surge control problem. Control Engineering Practice 14(4), 351–361 (2006)
20. Groot Wassink, W., van de Wal, M., Scherer, C., Bosgra, O.: LPV control for a wafer stage: beyond the theoretical solution. Control Engineering Practice 13, 231–245 (2005)
21. Hara, S.: Workshop on "glocal control". In: IEEE Multi-Conference on Systems and Control, Yokohama, Japan (2010)
22. Hashemi, S., Abbas, H., Werner, H.: LPV modelling and control of a 2-DOF robotic manipulator using PCA-based parameter set mapping. In: Proceedings of the 48th IEEE Conference on Decision and Control (with the 28th Chinese Control Conference), Shangai, P.R. China (2009)
23. van Helvoort, J., Steinbuch, M., Lambrechts, P., van de Molengraft, R.: Analytical and experimental modelling for gain-scheduling of a double scara robot. In: Proceedings of the 3rd IFAC Symposium on Mechatronic Systems, Sydney, Australia (2004)
24. Henry, R., Applebee, M.: Vehicle suspension system with gain scheduling. US Patent 5497324 (1996)
25. Hingwe, P., Tan, H., Packard, A., Tomizuka, M.: Linear parameter varying controller for automated lane guidance: experimental study on tractor-trailers. IEEE Transactions on Control Systems Technology 10(6), 793–806 (2002)
26. Hong, K., Sohn, H., Hedrick, J.: Modified skyhook control of semi-active suspensions: A new model, gain scheduling, and hardware-in-the-loop tuning. Journal of Dynamic Systems, Measurement, and Control 124(1), 158–167 (2002)
27. Hunt, K., Johansen, T., Kalkkuhl, J., Fritz, H., Gottsche, T.: Speed control design for an experimental vehicle using a generalized gain scheduling approach. IEEE Transactions on Control System Technology 8(3), 381–395 (2000)
28. Kron, A., de Lafontaine, J., Peuvédic, C.L.: Mars entry and aerocapture robust control using static output feedback and LPV techniques. In: 6th International ESA Conference on Guidance, Navigation and Control Systems, Loutraki, Greec (2005)
29. Laub, A., Heath, M., Paige, C., Ward, R.: Computation of system balancing transformations and other applications of simultaneous diagonalization algorithms. IEEE Transactions on Automatic Control 32, 115–122 (1987)

30. Lee, C., Shin, M., Chung, M.: A design of gain-scheduled control for a linear parameter varying system: an application to flight control. Control Engineering Practice 9(1), 11–21 (2001)
31. Lee, L., Poolla, K.: Identification of linear parameter-varying systems using nonlinear programming. ASME Journal of Dynamic Systems, Measurement and Control 121(1), 71–78 (1999)
32. Leith, D.J., Leithead, W.E.: Survey of gain-scheduling analysis and design. International Journal of Control 73(11), 1001–1025 (2000)
33. Lopes Dos Santos, P., Azevedo Perdicoulis, T.P., Novara, C., Ramos, J.A., Rivera, D. (eds.): Linear Parameter-Varying System Identification: New Developments and Trends. Advanced Series in Electrical and Computer Engineering. World Scientific (2012)
34. Lovera, M., Mercere, G.: Identification for gain-scheduling: a balanced subspace approach. In: 2007 American Control Conference, New York, USA (2007)
35. Lovera, M., Novara, C., Lopes Dos Santos, P., Rivera, D.: Guest editorial, special issue on applied LPV modeling and identification. IEEE Transactions on Control Systems Technology 19(1), 1–4 (2011)
36. Lovera, M., Verhaegen, M., Chou, C.T.: State space identification of MIMO linear parameter varying models. In: Proc. of the International Conference on Mathematical Theory of Networks and Systems, Padova, Italy (1996)
37. Lu, B., Wu, F.: Probabilistic robust linear parameter-varying control of an F-16 aircraft. Journal of Guidance, Control and Dynamics 29(6), 1454–1460 (2006)
38. Lu, B., Wu, F., Kim, S.: Switching LPV control of an F-16 aircraft via controller state reset. IEEE Transactions on Control System Technology 14(2), 267–277 (2006)
39. Marcos, A., Balas, G.: Development of linear-parameter-varying models for aircraft. Journal of Guidance, Control and Dynamics 27(2), 218–228 (2004)
40. Marcos, A., Penin, L., Sotto, E.D.: LFT modelling for the analysis of relative motion controllers in eccentric orbits. In: 2008 IEEE Multi-conference on Systems and Control, San Antonio, USA (2008)
41. Matsumura, F., Namerikawa, T., Hagiwara, K., Fujita, M.: Application of gain scheduled h8 robust controllers to a magnetic bearing. IEEE Transactions on Control System Technology 4(5), 484–493 (1996)
42. Mercère, G., Laroche, E., Lovera, M.: Identification of a flexible robot manipulator using a linear parameter-varying descriptor state-space structure. In: IEEE Conference on Decision and Control and European Control Conference, Orlando, USA (2011)
43. Mohammadpour, J., Scherer, C.W. (eds.): Control of Linear Parameter Varying Systems with Applications. Springer (2012)
44. Moore, B.: Principal component analysis in linear systems: controllability, observability and model reduction. IEEE Transactions on Automatic Control 26, 17–32 (1981)
45. Ohara, A., Yamaguchi, Y., Morito, T.: LPV modeling and gain scheduled control of reentry vehicle in approach and landing phase. In: AIAA Guidance, Navigation, and Control Conference and Exhibit, Montreal, Canada (2001)
46. Onat, C., Kucukdemiral, I., Sivrioglu, S., Yuksek, I.: LPV model based gain-scheduling controller for a full vehicle active suspension system. Journal of Vibration and Control 13(11), 1629–1666 (2007)
47. Paijmans, B., Symens, W., Brussel, H.V., Swevers, J.: A gain-scheduling-control technique for mechatronic systems with position-dependent dynamics. In: Proceedings of the 2006 American Control Conference, Minneapolis, USA (2006)
48. Pfifer, H., Hecker, S.: Generation of optimal linear parametric models for LFT-based robust stability analysis and control design. IEEE Transactions on Control Systems Technology 19(1), 118–131 (2011)

49. Previdi, F., Carpanzano, E.: Design of a gain scheduling controller for knee-joint angle control by using functional electrical stimulation. IEEE Transactions on Control System Technology 11(3), 310–324 (2000)
50. Prot, O., Mercere, G., Ramos, J.: Null-space-based technique for the estimation of linear-time invariant structured state-space representations. In: 16th IFAC Symposium on System Identification, Brussels, Belgium (2012)
51. Qin, W., Wang, Q.: An LPV approximation for admission control of an internet web server: identification and control. Control Engineering Practice 15(12), 1457–1467 (2007)
52. Qin, W., Wang, Q.: Modeling and control design for performance management of web servers via an LPV approach. IEEE Transactions on Control Systems Technology 15(2), 259–275 (2007)
53. Rugh, W., Shamma, J.: Research on gain scheduling. Automatica 36(10), 1401–1425 (2000)
54. Lopes dos Santos, P., Ramos, J.A., Martins de Carvalho, J.L.: Identification of bilinear systems using an iterative deterministic-stochastic approach. In: 44th IEEE Conference on Decision and Control and European Control Conference (2005)
55. Lopes dos Santos, P., Ramos, J.A., Martins de Carvalho, J.L.: Identification of linear parameter varying systems using an iterative deterministic-stochastic subspace approach. In: European Control Conference (2007)
56. Lopes dos Santos, P., Ramos, J.A., Martins de Carvalho, J.L.: Identification of LPV systems using successive approximations. In: 44th IEEE Conference on Decision and Control (2008)
57. Lopes dos Santos, P., Ramos, J.A., Martins de Carvalho, J.L.: Identification of bilinear systems with white noise inputs: An iterative deterministic-stochastic subspace approach. IEEE Transactions on Control Systems Technology 17(3), 1145–1153 (2009)
58. Steinbuch, M., van de Molengraft, R., van der Voort, A.: Experimental modelling and LPV control of a motion system. In: Proceedings of the 2003 American Control Conference, Denver, USA (2003)
59. Tan, H.: Estimating vehicle velocities using linear-parameter-varying and gain varying scheduling theories. US Patent 6618651 (2003)
60. Tanelli, M., Ardagna, D., Lovera, M.: LPV model identification for power management of web service systems. In: IEEE International Symposium on CACSD, San Antonio, USA (2008)
61. Tóth, R.: Modeling and Identification of Linear Parameter-Varying Systems. LNCIS, vol. 403. Springer, Heidelberg (2010)
62. van Wingerden, J., Verhaegen, M.: Subspace identification of bilinear and LPV systems for open- and closed-loop data. Automatica 45, 372–381 (2009)
63. Verdult, V.: Nonlinear system identification: a state space approach. Ph.D. thesis, University of Twente (2002)
64. Verdult, V., Lovera, M., Verhaegen, M.: Identification of linear parameter varying state space models with application to helicopter rotor dynamics. International Journal of Control 77, 1149–1159 (2004)
65. Verdult, V., Verhaegen, M.: Subspace identification of multivariable linear parameter varying systems. Automatica 38, 805–814 (2002)
66. Verdult, V., Verhaegen, M.: Kernel methods for subspace identification of multivariable LPV and bilinear systems. Automatica 41, 1557–1565 (2005)

67. Verdult, V., Verhaegen, M., Chou, C., Lovera, M.: Efficient and systematic identification of mimo bilinear state-space models. In: IEEE Conference on Decision and Control, Tampa, USA (1998)
68. Wassink, M.G., van de Wal, M., Scherer, C., Bosgra, O.: LPV control for a wafer stage: beyond the theoretical solution. Control Engineering Practice 13(2), 231–245 (2005)
69. Wei, X., del Re, L.: Gain scheduled h_∞ control for air path systems of diesel engines using LPV techniques. IEEE Transactions on Control Systems Technology 15(3), 406–415 (2007)
70. Xin, T., Tanaka, H., Ohta, Y.: Grey-box modeling of rotary type pendulum system with position-variable load. In: 16th IFAC Symposium on System Identification, Brussels, Belgium (2012)

Chapter 2
System Analysis: A Geometric Approach

József Bokor and Zoltán Szabó

Abstract. The mathematically dual concepts of (A,B) and (C,A)-invariance play an important role in the geometric theory of linear time invariant (LTI) systems. These concepts were used to study some fundamental problems of LTI control theory, such as disturbance decoupling (DDP), unknown input observer design, fault detection (FPRG). The nonlinear version of this geometrical approach is much more complex and deals with certain locally controlled or conditioned invariant distributions and codistributions. The aim of the chapter is to present an extension of these notions for the parameter-varying systems by introducing the notion of *parameter-varying (A,B)-invariant*, *parameter-varying (C,A)-invariant*, controllability and unobservability subspaces, and to give some algorithms to compute these subspaces if certain conditions are fulfilled.

2.1 Introduction

For LTI systems the concept of certain invariant subspaces and the corresponding global decompositions of the state equations induced by these invariant subspaces was one of the main thrusts for the development of geometric methods for solutions to problems of disturbance decoupling or noninteracting control, see [33]. In the so called *geometrical approach* to some fundamental problems of LTI control theory, such as disturbance decoupling, unknown input observer design, fault detection, a central role is played by the (A,B)-invariant and (C,A)-invariant subspaces and certain controllability and unobservability subspaces, [25, 33, 22, 23, 14, 2, 9, 5].

József Bokor · Zoltán Szabó
Computer and Automation Research Institute, Hungarian Academy of Sciences,
Kende u. 13-17, Budapest, H1111 Hungary
e-mail: {bokor,szaboz}@sztaki.hu

O. Sename et al. (Eds.): *Robust Control and LPV Approaches*, LNCIS 437, pp. 25–53.
DOI: 10.1007/978-3-642-36110-4_2

Let us consider the state dynamics of a controlled linear time varying (LTV) system:

$$\dot{x}(t) = A(t)x(t) + B(t)u(t) \tag{2.1}$$

where $x(t) \in \mathscr{X} \subset \mathbb{R}^n$ is the state vector, $u(t) \in \mathbb{R}^m$ is the control input while the initial condition is $x_0 = x(t_0)$. The measured signals are obtained by a linear readout map $y(t) = C(t)x(t)$, with $y \in \mathbb{R}^p$.

Our interest in such models is motivated by the fact that nonlinear dynamics can be often cast as an LTV system

$$\dot{x}(t) = A(\rho(y))x(t) + B(\rho(y))u(t) \tag{2.2}$$

by choosing a suitable set of *scheduling functions* ρ that depend only on measured variables y, i.e., its values are available in operational time. These models are called quasi linear parameter varying (qLPV) systems. A special case is when the dependence from the scheduling variables is affine, i.e.,

$$\begin{aligned} A(\rho(t)) &= A_0 + \rho_1(t)A_1 + \ldots + \rho_N(t)A_N, \\ B(\rho(t)) &= B_0 + \rho_1(t)B_1 + \ldots + \rho_N(t)B_N. \end{aligned} \tag{2.3}$$

For the sake of notational simplicity, in what follows, the time dependency of the matrices will be dropped ($A(\rho) := A(\rho(t))$) where it is possible.

Linear parameter varying (LPV) modeling techniques have gained a lot of interest, especially those related to vehicle and aerospace control, [6, 15, 3, 21]. LPV systems have recently become popular as they provide a systematic means of computing gain-scheduled controllers. In this framework the system dynamics are written as a linear state-space model with the coefficient matrices functions of external scheduling variables. Assuming that these scheduling variables remain in some given range then analytical results can guarantee the level of closed loop performance and robustness. The parameters are not uncertain and can often be measured in real-time during system operation. However, it is generally assumed that the parameters vary slowly in comparison to the dynamics of the system. LPV based gain-scheduling approaches are replacing ad-hoc techniques and are becoming widely used in control design.

A series of control tasks can be solved efficiently by exploiting the inner structure present in the dynamics, i.e., to make use of specific invariant manifolds of the controlled system. Nonlinear systems can be studied using tools from differential geometry, when the central role is played by the concept of *invariant distributions*. From the geometric viewpoint results of the classical linear control can be seen as special cases of more general nonlinear results, for details see [18] and [29]. Due to the computational complexity involved, these nonlinear methods have limited applicability in practice.

Controllability

One of the main questions of system theory is to determine whether the system is controllable and/or is observable. A state x_0 is said to be controllable at time t_0 if there exist a control function $u(t)$ that steers the system into the origin in finite time; a state x_f is said to be reachable if the system can be steered from the origin into x_f in finite time. If the property holds for every state x and every t_0 then the system will be called controllable (reachable). The system (2.1) is called observable on a finite interval $[t_0, T]$ if any initial state x_0 at t_0 can be determined from knowledge of the system output $y(t)$ and input $u(t)$ over the given interval.

The controllability subspace is denoted by $\mathscr{C}$, while the reachability subspace by $\mathscr{R}$, respectively. For linear systems (complete) controllability and reachability are equivalent, i.e., the system is completely controllable if and only if $\mathscr{C} = \mathscr{R} = \mathscr{X}$.

Analogously $\mathscr{U}$ ($\mathscr{O}$) denotes the unobservability (observability) subspace; $\mathscr{U}$ is the set of all initial states that cannot be recognized from the output function. The system is observable if and only if $\mathscr{U} = 0$, i.e., $\mathscr{O} = \mathscr{X}$.

A convenient way to study all solutions of a linear equation on the interval $[\sigma, \tau]$, for all possible initial values simultaneously, is to introduce the corresponding transition matrix $\Phi(\tau, \sigma)$[1]:

$$x(\tau) = \Phi(\tau,\sigma)x(\sigma) + \int_\sigma^\tau \Phi(\tau,t)B(t)u(t)\mathrm{d}t = \Phi(\tau,\sigma)(x_0 + \int_\sigma^\tau \Phi(\sigma,t)B(t)u(t)\mathrm{d}t).$$

Applying the time varying coordinate change $z = \Phi(\sigma,t)x$ in the state space, the dynamic equation transforms into $\dot{z} = \Phi(\sigma,t)B(t)u(t)$. Thus in this new coordinate system controllability reduces to the solvability study of the equation:

$$z_0 = -\int_\sigma^\tau \Phi(\sigma,t)B(t)u(t)\mathrm{d}t$$

for a suitable finite τ. If we denote by $\mathscr{C}_\tau$ the set of states controllable at τ then $\mathscr{C}_\tau$ is a (closed) subspace, moreover $\mathscr{C}_{\tau_1} \subset \mathscr{C}_{\tau_2}$ for $\tau_1 < \tau_2$. Since the image space of the corresponding integral operator is finite dimensional, if the system is controllable there must be a finite $\bar{\tau} > 0$ such that $\mathscr{C}_{\bar{\tau}} = \mathbb{R}^n$. Hence, the controllability problem of an LTV system has been reduced to the question wether the finite rank operator $\mathfrak{L} : \mathscr{L}_2([\sigma,\bar{\tau}],\mathbb{R}^m) \to \mathbb{R}^n$ defined as $\mathfrak{L}u = \int_\sigma^{\bar{\tau}} \Phi(\sigma,t)B(t)u(t)\mathrm{d}t$ is onto. These type of linear operators have a nice theory: it is immediate that the adjoint operator $\mathfrak{L}^* : \mathbb{R}^n \to \mathscr{L}_2^*([\sigma,\bar{\tau}],\mathbb{R}^m)$ can be identified with $\mathfrak{L}^*x = B^*(t)\Phi^*(\sigma,t)x$ and that $\mathfrak{L}$ is onto if and only if $\mathfrak{L}\mathfrak{L}^* > 0$.

So, the fundamental result, see [19], concerning controllability of the LTV system (2.1) can be stated as the equivalence of the following statements:

Proposition 1. *There exist a $\tau > 0$ such that*

1. *the controllability Grammian $W(\sigma,\tau) = \int_\sigma^\tau \Phi(\sigma,s)B(s)B^*(s)\Phi^*(\sigma,s)ds$ is positive definite;*

[1] $\Phi(t,t_0)$ is nonsingular and $\Phi(t,t_0) = X(t)X^{-1}(t_0)$ with $\dot{X}(t) = A(t)X(t)$, $X(t_0) = \mathbb{I}$, $X(t) \in \mathbb{R}^{n\times n}$.

2. *there is no nonzero vector* $p \in \mathbb{R}^n$ *such that* $\langle p, \Phi(\sigma,t)b_i(t)\rangle = 0$, *for* $t \in [\sigma,\tau]$, *and* $i = 1,\cdots,m$.

It is a standard result, [31], that one can derive a rank condition that guarantees controllability while it does not involve integration and it can be obtained directly from the initial data matrices $(A(t),B(t))$:

Proposition 2. *if* (2.1) *is analytic on an interval* I *and* t *is an arbitrary fixed element of* I, *then the system is completely controllable on every nontrivial subinterval of* I *if and only if*

$$rank\left[B_0(t)\ B_1(t)\ \cdots\ B_k(t)\right] = n, \tag{2.4}$$

for some integer k, *where*

$$B_0(t) := B(t), \quad B_{i+1}(t) := A(t)B_i(t) - \frac{d}{dt}B_i(t). \tag{2.5}$$

If the analyticity condition is dropped, then the rank condition is only sufficient.

The problem is that it is hard to compute the rank of a time varying matrix, and we have no information about how to compute the controllability decomposition of the system.

Kalman's controllability result also reveals a structural property of linear systems: namely, by applying a suitable – in general time-varying – state transformation these systems decompose into a controllable an a purely uncontrollable part. To see this, suppose that there are at most r vectors $p_i \in \mathscr{X}$, $\langle p_i, \Phi(\sigma,s)B(s)\rangle = 0$, $s \in [\sigma,\tau]$. Choose them such that $\Pi^*\Pi = \mathbb{I}_r$, where $\Pi = [X^*(\sigma)p_i]$. Consider $n-r$ vectors $\lambda_i \in \mathscr{X}$ orthogonal on p_i, such that $\Lambda^*\Lambda = \mathbb{I}_{n-r}$, where $\Lambda = [X^*(\sigma)\lambda_i]$. Then, the time varying matrix $z = Tx$ with $T(t) = \begin{bmatrix}\Pi^*\\ \Lambda^*\end{bmatrix} X^{-1}(t)$ transforms system (2.1) into the *controllability decomposition* form:

$$\dot{z}_1(t) = 0, \quad \dot{z}_2(t) = \Lambda^* X^{-1}(t)B(t)u. \tag{2.6}$$

with the uncontrollable mode $z_1(t) = \Pi^* X^{-1}(t)x(t)$ and with the completely controllable mode $z_2(t) = \Lambda^* X^{-1}(t)x(t)$. In other words, the reachable set is *invariant* to the action of the controlled dynamics. The notion of invariance met in this context plays a central role in the investigations of geometric systems theory and it has been proven to be very useful in solving a series of control problems.

Controllability of Linear Affine Systems

For affine time dependency $A(t) = \sum_{i=1}^{N} \rho_i(t)A_i$ the fundamental matrix can be given, at least locally, in terms of the *coordinates of second kind*, [32], i.e., the solutions of the Wei–Norman equation:

$$\dot{g}(t) = (\sum_{i=1}^{K} e^{\Gamma_1 g_1} \cdots e^{\Gamma_{i-1} g_{i-1}} E_{ii})^{-1} \rho(t), \quad g(0) = 0. \tag{2.7}$$

Here $\rho(t) = [\rho_1(t), \ldots, \rho_N(t)]^T$ and $\{\hat{A}_1, \ldots, \hat{A}_K\}$ is a basis of the Lie-algebra $\mathscr{L}(A_1, \ldots, A_N)$, the structure matrices $\Gamma_i = [\gamma^l_{i,j}]_{l,j=1,\cdots,K}$ of the algebra are given by $[\hat{A}_i, \hat{A}_j] = \sum_{l=1}^{K} \gamma^l_{i,j} \hat{A}_l$ and E_{ii} is the matrix with a single nonzero unitary entry at the i-th diagonal element.

Locally, the fundamental matrix is given by the expression:

$$\Phi(t) = e^{g_1(t)\hat{A}_1} e^{g_2(t)\hat{A}_2} \cdots e^{g_n(t)\hat{A}_n}, \tag{2.8}$$

and generally it is not available in closed form.

Exploiting the affine structure and using the Peano–Baker formula for the transition matrix one can prove the following result:

Lemma 1. *For affine linear systems the points attainable from the origin are those from the subspace $\mathscr{R}_{(\mathscr{A},\mathscr{B})}$ given by:*

$$\mathscr{R}_{(\mathscr{A},\mathscr{B})} = span\{\prod_{j=1}^{J} A_{l_j}^{i_j} B_k \,|\, J \geq 0, l_j, k \in \{0, \cdots, N\}, i_j \in \{0, \cdots, n-1\}\}, \tag{2.9}$$

i.e., $\mathscr{R} \subset \mathscr{R}_{(\mathscr{A},\mathscr{B})}$.

Moreover, if one consider the finitely generated Lie-algebra $\mathscr{L}(A_0, \ldots, A_N)$ which contains the matrices $A_0, \ldots, A_N$, and a basis $\hat{A}_1, \ldots, \hat{A}_K$ of this algebra, then

$$\mathscr{R}_{(\mathscr{A},\mathscr{B})} = \sum_{l=0}^{N} \sum_{n_1=0}^{n-1} \cdots \sum_{n_K=0}^{n-1} Im(\hat{A}_1^{n_1} \ldots \hat{A}_K^{n_K} B_l).$$

A direct consequence of this fact is that if the inclusion $\mathscr{R}_{\mathscr{A},\mathscr{B}} \subset \mathbb{R}^n$ is strict, i.e, if $\mathscr{R}_{\mathscr{A},\mathscr{B}}$ is a proper subspace, then the system (2.1) cannot be completely controllable.

The main question is that under which condition is the reachability set equal to the Lie algebra, i.e., when we have $\mathscr{R} = \mathscr{R}_{\mathscr{A},\mathscr{B}}$. In what follows, if this property holds, then the system will be called *c-excited*. Characterization of this property by using only the initial data seems to be difficult. However, from condition (2.) of the Kalman's controllability result, one has the following statement:

Proposition 3. *A system is c-exciting if and only if the following implication holds: there exist a nonzero $\xi \in \mathbb{R}^n$ such that*

$$B(t)^* \Phi^*(t_0, t)\xi = 0$$

for all $t \in [t_0, T]$ implies that

$$\mathscr{R}^*_{\mathscr{A},\mathscr{B}} \Phi^*(t_0, t)\xi = 0$$

for all $t \in [t_0, T]$.

It is clear, that for c-excited systems controllability is guaranteed if the relation $\mathscr{R}_{\mathscr{A},\mathscr{B}} = \mathbb{R}^n$, i.e., the *multivaraiable Kalman rank condition*, holds. Moreover, if the rank condition does not hold, for this class of sytems one can construct the controllability decomposition by using a time independent state transformation matrix that depends only on the matrix Lie algebra.

Therefore it would be useful to give a condition that uses the original data only to decide wether a system is c-exciting or not. Unfortunately, such a condition has not been available yet.

The following (negative) example illustrates the importance of the c-excitedness property of the scheduling variables for controllability: let us consider the system

$$\dot{x}_1 = x_1 x_2 + x_2, \quad \dot{x}_2 = u$$

that can be rewritten as $\dot{x} = A_0 + \rho A_1 + Bu$, where $A_0 = \begin{bmatrix} 0 & 1 \\ 0 & 0 \end{bmatrix}$, $A_1 = \begin{bmatrix} 1 & 0 \\ 0 & 0 \end{bmatrix}$, $B = \begin{bmatrix} 0 \\ 1 \end{bmatrix}$ and with $\rho = x_2$.

Since $A_0 B = \begin{bmatrix} 1 \\ 0 \end{bmatrix}$ one has $\dim R_{\mathscr{A},\mathscr{B}} = 2$, i.e., the Kalman rank condition holds.

Applying the Silverman Meadows approach, one has $B_0 = B$ and $B_1 = A_0 B$, i.e., $\operatorname{rank}[B_0\, B_1] = 2$, that shows that the system is controllable for any $\rho(t)$.

Using the Wei–Normann theory, one has $[A_0, A_1] = -A_0$, i.e., $\gamma^0_{01} = -1$, $\gamma^0_{10} = 1$ and the rest of the $\gamma^j_{ij} = 0$. It follows that

$$\Gamma_1 = \begin{bmatrix} 0 & -1 \\ 0 & 0 \end{bmatrix}, \ \Gamma_2 = \begin{bmatrix} 1 & 0 \\ 0 & 0 \end{bmatrix}, \text{ i.e., } \quad e^{\Gamma_1 t} = \begin{bmatrix} 1 & -t \\ 0 & 1 \end{bmatrix}, \ e^{\Gamma_2 t} = \begin{bmatrix} e^t & 0 \\ 0 & 1 \end{bmatrix}.$$

From

$$E_{11} + e^{\Gamma_1 g_1} E_{22} = \begin{bmatrix} 1 & -g_1 \\ 0 & 1 \end{bmatrix},$$

it follows that the Wei–Normann equations are

$$\dot{g}_1 = \rho g_1 + 1, \quad \dot{g}_2 = \rho.$$

The fundamental solution is given by $\Phi(t) = e^{\Gamma_1 A_0} e^{\Gamma_2 A_1}$, i.e., $\Phi(t) = \begin{bmatrix} e^{g_2} & g_1 \\ 0 & 1 \end{bmatrix}$.

If the system is uncontrollable, according to the Kalman condition there should be a nonzero vector ξ such that $B^* \Phi^{-*}(t) \xi = 0$ for all t, i.e., a number ν must exists such that $e^{-g_2} g_1 + \nu = 0$. But such a number does not exists[2], hence the system should be controllable. However, it is immediate that $x_1 = -1$ is an uncontrollable manifold of the system.

The reason why these tests fail relays in the fact that the uncontrollable manifold, i.e., $(-1, x_2)$ is not a subspace, while in the linear case the set of uncontrollable points is always a subspace.

If one shift the system from the equilibria point $(-1,0)$, to $(0,0)$, i.e., apply a (time-varying) change of coordinates $z_1 = x_1 + 1$, $z_2 = x_2$, then one has the

[2] Otherwise $\frac{\mathrm{d}}{\mathrm{d}t}(e^{-g_2} g_1) = 0$, i.e., $-\dot{g}_2 g_1 + \dot{g}_1 = 0$; but the left hand side is 1.

system $\dot{z}_1 = z_1 z_2, \quad \dot{z}_2 = u$, with $\bar{A}(\rho) = \begin{bmatrix} \rho & 0 \\ 0 & 0 \end{bmatrix}$, and $\rho = z_2 = x_2$, that is clearly uncontrollable.

One of the main motivation doing this "tour de force" in this introductory section along a classical topic of linear control theory was to illustrate that the controllability problem cannot be tackled in a mathematical completeness and rigor even for linear systems, if the system is time varying. The situation is even worse if the dynamics is actually nonlinear, but cast as a qLPV system. This stays in contrast to the familiar framework of LTI systems where the answer to the fundamental problem concerning controllability is very accessible and transparent.

The simplicity of the time invariant results might be regained in that of a splitting of the state space in a surely uncontrollable mode and a mode, that might be controllable. Controllability of this mode cannot be inferred, in general, only if some additional conditions on the parameters are fulfilled (c-excitedness). Moreover, the simple example at the end of the chapter warn us on the inherent limitations of the approach when trying to extend it for nonlinear systems.

Concerning the (q)LPV systems (2.3) with affine parameter dependence the main issue is the problem of finding a time independent – and global – state transformation that splits the state space into modes that has specific properties – in these examples potentially controllable/uncontrollable modes. Concentrating on a rigorous proof of the controllability of the potentially uncontrollable mode is futile: not only due to the encountered mathematical difficulty of the computations but also due to the inherent uncertainty present in every practical model used in a nontrivial engineering application.

This fact motivates our desire in finding certain "robust" invariant subspaces that often provides acceptable (sufficient) conditions to obtain an engineering solution for a series of basic control problems. What we apparently miss in these constructions, i.e., the knowledge of controllability/observability, might cause problems at a different (higher) level of the design: namely, in obtaining stable controllers or filters. Lacking of a stable design might be a clear indication that our assumptions on the c-exitedness of the scheduling variables might not hold, or, more likely, our techniques to ensure stability are too conservative. Hence, a different approach should be used.

The proposed geometric framework based on parameter varying invariant subspaces provides an example for a strategy, in which giving up to get the complete mathematical solution of the problem but not sacrificing the mathematical correctness in following a more "rough" route to an acceptable result leads to a useful, engineering design.

2.2 Parameter-Varying Invariant Subspaces

Linear time varying (LTV) case and nonlinear systems can be studied using tools from differential geometry, when the central role is played by the concept of

invariant distributions and much more complex mathematical objects given by the locally controlled or conditioned invariant distribution(or codistribution) algorithms. From a geometric viewpoint results of the classical linear control can be seen as special cases of these more general nonlinear results, for details see, e. g., [18, 29, 11]. Due to the computational complexity involved, these nonlinear methods have limited applicability in practice. The main problem that arises in practical situations is that either one cannot perform the computations or one cannot verify the conditions under the given algorithms provide the desired results.

If certain conditions are fulfilled, e. g., if the parameter functions are differential algebraically independent, then the parameter invariant subspaces, that will be introduced in this chapter, coincide with the corresponding invariant distribution or codistribution, respectively. However, to give sufficient conditions for the solution of certain state feedback and observer filter design problems it is enough that some decompositions of the state equations could be performed. The parameter–varying versions of these invariant spaces are suitable objects to define the required decompositions, therefore they can play the same role in the solution of the fundamental problems, such as disturbance decoupling(DDP), unknown input observer design, fault detection (FPRG), as their counterparts in the time invariant context.

Invariant Subspaces for Time Varying Systems

Before the introduction of the invariance notion that best suits the parameter varying framework let us recall some the corresponding term used in the general nonlinear context: a distribution Δ is said to be *invariant*[3] under a vector field f if for $\tau \in \Delta$ one has $[f,\tau] \in \Delta$, or shortly, $[f,\Delta] \subset \Delta$. Dealing with codistributions, Ω is said to be invariant[4] under the vector field f if for $\omega \in \Omega$ one has $L_f\omega \in \Omega$ or shortly $L_f\Omega \subset \Omega$.

By doing a usual augmentation, see e. g., [17], of the original state space to $\xi := [t,x]^T$, an LPV system can be viewed as an affine nonlinear system:

$$\dot{\xi} = g_0(\xi) + \sum_{i=1}^{m} g_i(\xi)u_i, \quad y = h(\xi)\xi,$$

where $g_0(\xi)$ denotes $\begin{bmatrix} 1 \\ A(\rho)x \end{bmatrix}$, $g_i(\xi)$ is the vector $\begin{bmatrix} 0 \\ B_i(\rho) \end{bmatrix}$ with $B_i(\rho)$ the i^{th} column of $B(\rho)$ and $h(\xi) = [0 \;\; C(\rho)]$.

[3] Let $\Delta_{\mathscr{V}}(x) = \mathscr{V}$ be a constant distribution, where $\mathscr{V}$ is a subspace of $\mathbb{R}^n$ and $f_A(x) = Ax$ be a linear vector field. Since $[f_A, v](x) = -Av$ for all $v \in \mathscr{V}$ and $x \in \mathbb{R}^n$, we get back the usual invariance notion for subspaces, i. e., $A\mathscr{V} \subset \mathscr{V}$.

[4] Now let $\Omega_{\mathscr{W}}(x) = \mathscr{W}_c$ be a constant codistribution, where $\mathscr{W}_c$ is a subspace of $(\mathbb{R}^n)^*$ and the vector field $f_A(x) = Ax$ is linear then we get back the invariance notion of subspaces in $(\mathbb{R}^n)^*$, i. e., $A^T\mathscr{W} \subset \mathscr{W}$. Recall that $\mathscr{W}_c A \subset \mathscr{W}_c$ and we identify $\mathscr{W}_c \subset (\mathbb{R}^n)^*$ with $\mathscr{W} \subset \mathbb{R}^n$ in a usual way, i. e., if $\mathscr{W} = \operatorname{Im} W$ than $\mathscr{W}_c = \operatorname{Im} W^T$.

Restricting the investigations to linear subspaces, as special instances of distributions, i.e., with some subspace $\mathscr{V}$ of $\mathbb{R}^n$ $\Delta(\xi) = \begin{bmatrix} 0 \\ \mathscr{V} \end{bmatrix}$, then Δ will be invariant under the vector fields g_i if and only if $\partial_\xi g_i \Delta(\xi) \subset \Delta(\xi)$, for all i and ξ. Performing the computations one has that Δ is an invariant distribution for the action of the vector fields g_i if and only if $A(\rho)\mathscr{V} \subset \mathscr{V}$ for all $\rho \in \mathscr{P}$. Using a similar argument, one can get the analogous relations for the corresponding codistributions.

These facts motivate the introduction of the following notion:

Definition 1. *A subspace $\mathscr{V}$ is called parameter-varying invariant subspace (or shortly $\mathscr{A}$–invariant subspace) for the family of the linear maps $A(\rho)$ if*

$$A(\rho)\mathscr{V} \subset \mathscr{V} \quad \text{for all } \rho \in \mathscr{P}. \tag{2.10}$$

As for the LTI case an $\mathscr{A}$-invariant subspace $\mathscr{V}$ induces a splitting $x = \bar{x} + \tilde{x}$ of the state space with $\bar{x} = \mathbf{P}_{\mathscr{V}}$ and $\tilde{x} = \mathbf{P}_{\mathscr{V}^\perp}$ such that the system $\dot{x} = A(\rho)x$ will have the form

$$\dot{\bar{x}} = \bar{A}(\rho)\bar{x} + \tilde{A}_1(\rho)\tilde{x}, \quad \dot{\tilde{x}} = \tilde{A}_2(\rho)\tilde{x}. \tag{2.11}$$

where

$$\bar{A}(\rho) = A(\rho)|_{\mathscr{V}}, \tag{2.12}$$

is the restriction of $A(\rho)$ to the subspace $\mathscr{V}$.

The main point here is the fact that the state transform $x = T \begin{bmatrix} \bar{x} \\ \tilde{x} \end{bmatrix}$ defined by $T = \begin{bmatrix} \mathscr{V} & \mathscr{V}^\perp \end{bmatrix}$ leads to the splitting $A \xrightarrow{TAT^{-1}} \begin{bmatrix} \bar{A} & \tilde{A}_1 \\ 0 & \tilde{A}_2 \end{bmatrix} \begin{matrix} \}\mathscr{V} \\ \}\mathscr{V}^\perp \end{matrix}$ and this splitting is independent of the actual values of the parameters ρ, i.e., it can be performed offline. This fact has a great impact on the applicability of the newly introduced concept for design problems.

2.2.1 Controlled Invariance

Let us observe, that if $\mathscr{V}$ is an $\mathscr{A}$-invariant subspace and $\mathrm{Im}B(\rho) \subset \mathscr{V}$ for all $\rho \in \mathscr{P}$ then the system $\dot{x} = A(\rho)x + B(\rho)u$ can be decomposed as

$$\dot{\bar{x}} = \bar{A}(\rho)\bar{x} + \tilde{A}_1(\rho)\tilde{x} + \overline{B}(\rho)u, \quad \dot{\tilde{x}} = \tilde{A}_2(\rho)\tilde{x}, \tag{2.13}$$

An involutive distribution Δ is said to be *controlled invariant* on an open set U if

$$[g_i, \Delta](x) \subset \Delta(x) + G(x), \quad i = 0, 1, \ldots, m,\ x \in U.$$

or shortly $[g_i, \Delta] \subset \Delta + G$, assuming that Δ, G and $\Delta + G$ are nonsingular, where G denotes the distribution $\operatorname{span}\{g_1, \ldots, g_m\}$. For the covectorial version: a codistribution Ω is said to be controlled invariant if $L_{g_i}(\Omega \cap G^{\perp}) \subset \Omega, \quad i = 0, 1, \ldots, m$. If the intersection may fail to be smooth, then L_{g_i} is only defined on the smooth codistributions of the intersection.

Using again the augmented state space and the distribution $\begin{bmatrix} 0 \\ \mathscr{V} \end{bmatrix}$ one can show that when $B(\rho) = \mathscr{B}$ then $\mathscr{V} \subset \mathbb{R}^n$ is controlled invariant subspace (distribution) if and only if $A(\rho)\mathscr{V} \subset \mathscr{V} + \mathscr{B}$ for all $\rho \in \mathscr{P}$.

These facts motivate the introduction of the following notion:

Definition 2. *The subspace $\mathscr{V}$ is called a parameter-varying (A,B)–invariant subspace (or shortly $(\mathscr{A},\mathscr{B})$–invariant subspace) if for all $\rho \in \mathscr{P}$ any of the following equivalent conditions holds :*

$$A(\rho)\mathscr{V} \subset \mathscr{V} + \mathscr{B}(\rho), \tag{2.14}$$

and there exists a mapping (a state feedback) $F \circ \rho : [0,T] \to \mathbb{R}^{m \times n}$ such that:

$$(A(\rho) + B(\rho)F(\rho))\mathscr{V} \subset \mathscr{V}, \tag{2.15}$$

where $\mathscr{B}(\rho)$ denotes $\mathrm{Im}B(\rho)$.

Dealing with parametric uncertainties a similar concept was introduced in [4], called *robust controlled invariant* subspace. If one sets the gain matrix to be constant then the resulting subspace will be more restrictive, this approach was used in [7] and [30], and was termed as *generalized controllability* (A,B)*–invariant subspace*.

It is obvious that the subspace $\mathscr{R}_{(\mathscr{A},\mathscr{B})}$ in (3.3) is $A(\rho)$ invariant, i.e.,

$$A(\rho)\mathscr{R}_{(\mathscr{A},\mathscr{B})} \subseteq \mathscr{R}_{(\mathscr{A},\mathscr{B})}, \quad \text{for all} \quad \rho \in \mathscr{P}, \tag{2.16}$$

moreover, one has that for the induced decomposition $\mathscr{R}_{(\mathscr{A},\mathscr{B})} = \mathscr{R}_{(\bar{\mathscr{A}},\bar{\mathscr{B}})}$. Actually $\mathscr{R}_{(\mathscr{A},\mathscr{B})}$ is the minimal $A(\rho)$ invariant subspace containing $\mathscr{B}$.

The set of all $\mathscr{A}$–invariants containing $\mathscr{B}$ is a nondistributive lattice with respect to the set operations $\subseteq, \cup, \cap$. The supremum of the lattice is the entire state space $\mathscr{X}$, while the infimum is the intersection of all the $\mathscr{A}$–invariants containing $\mathscr{B}$. It will be called, the *minimal $\mathscr{A}$–invariant subspace containing $\mathscr{B}$*, which is also an $(\mathscr{A},\mathscr{B})$–invariant subspace, and it will be denoted by $\langle \mathscr{A} | \mathscr{B} \rangle$.

As for the LTI systems (2.15) guarantees that with a suitable state feedback $u = F(\rho)x + v$ equation (2.13) can be rendered diagonal, i.e.,

$$\dot{x} = A(\rho)x + B(\rho)u \xrightarrow[u=F(\rho)x+v]{TAT^{-1},\, TB} \begin{matrix} \dot{\bar{x}} = \bar{A}(\rho)\bar{x} + & +\overline{B}(\rho)v \\ \dot{\tilde{x}} = & \tilde{A}_2(\rho)\tilde{x}, \end{matrix} \tag{2.17}$$

$\tilde{x}$ being an uncontrollable mode. Controllability of $\bar{x}$ can be asserted only if $\mathscr{V} = \langle \mathscr{A} | \mathscr{B} \rangle$ and the c-persistency property holds.

The set of all $(\mathscr{A},\mathscr{B})$–invariant subspaces contained in a given subspace $\mathscr{K}$, is an upper semilattice with respect to subspace addition. This semilattice admits a maximum which will be denoted by $\mathscr{V}^*$.

As far as the LPV case is concerned it was found that the following definition would be usable for the generalization of the concept of the controllability subspace:

Definition 3. *A subspace $\mathscr{R}$ is called parameter-varying controllability subspace if there exists a constant matrix K and a parameter varying matrix $F:[0,T]\to\mathbb{R}^{m\times n}$ such that $\mathscr{R}=\langle\mathscr{A}+B\mathscr{F}|Im\,BK\rangle$, where the notation $\mathscr{A}+B\mathscr{F}$ stems for the system $A(\rho)+BF(\rho)$ with $Im\,B(\rho)=Im\,B$.*

Properties analogous with the corresponding LTI results hold for the parameter-varying controllability subspace.

2.2.2 Conditioned Invariance

The dual notion of controlled invariance is conditioned invariance which can be defined as follows: a distribution Δ is said to be *conditioned invariant* on an open set U if it satisfies $[g_i,\Delta\cap\mathrm{Ker}\,\mathrm{d}h](x)\subset\Delta(x)$, or shortly $[g_i,\Delta\cap\mathrm{Ker}\,\mathrm{d}h]\subset\Delta$ for $i=0,1,\ldots,m$, $x\in U$. For the covectorial version: a codistribution Ω is said to be conditioned invariant if $L_{g_i}\Omega\subset\Omega+\mathrm{span}\,\mathrm{d}h\}$ for $i=0,1,\ldots,m$.

Considering a subspace $\mathscr{W}$ for affine parameter dependence one hast that for any $w\in\mathscr{W}\cap\mathrm{Ker}\,C$

$$\frac{\partial(A(\rho)x)v}{\partial x}=A(\rho)v+\sum_{i=1}^{N}A_ix\frac{\partial\rho_i}{\partial y}Cv=A(\rho)v,\quad \frac{\partial B_i(\rho)v}{\partial x}=\sum_{i=1}^{N}B_i\frac{\partial\rho_i}{\partial y}Cv=0.$$

Using the augmented state space, the distribution $\begin{bmatrix}0\\ \mathscr{W}\end{bmatrix}$ and considering the case $C(\rho)=C$ it follows that for LPV systems with affine parameter dependence $\mathscr{W}\subset\mathbb{R}^n$ is a conditioned invariant subspace if and only if $A(\rho)(\mathscr{W}\cap\mathrm{Ker}\,C)\subset\mathscr{W}$ for all $\rho\in\mathscr{P}$. This fact leads us to the introduction of the following notion:

Definition 4. *The subspace $\mathscr{W}$ is called a parameter-varying (C,A)–invariant subspace (or shortly $(\mathscr{C},\mathscr{A})$–invariant subspace) if for all $\rho\in\mathscr{P}$ any of the following equivalent conditions holds:*

$$A(\rho)(\mathscr{W}\cap\mathscr{C}(\rho))\subset\mathscr{W} \tag{2.18}$$

and there exists a mapping $G\circ\rho:[0,T]\to\mathbb{R}^{n\times p}$ such that:

$$(A(\rho)+G(\rho)C(\rho))\mathscr{W}\subset\mathscr{W}, \tag{2.19}$$

where $\mathscr{C}(\rho)$ denotes $Ker\,C(\rho)$.

The set of all $\mathscr{A}$–invariants contained in $\mathscr{C}$ is a nondistributive lattice with respect to to the set operations $\subseteq,\cup,\cap$. The infimum of the lattice is clearly $\{0\}$, while the

supremum is the sum of all the $\mathscr{A}$–invariants contained in $\mathscr{C}$. It will be called the *maximal $\mathscr{A}$–invariant contained in $\mathscr{C}$*, which is also a $(\mathscr{C},\mathscr{A})$–invariant subspace, and it will be denoted by $\langle\mathscr{C}|\mathscr{A}\rangle$.

As for the LTI systems (2.18) guarantees that the following splitting holds:

$$\begin{array}{l}\dot{x} = A(\rho)x \\ y = \quad Cx\end{array} \xrightarrow{TAT^{-1},\, CT^{-1}} \begin{array}{l}\dot{\bar{x}} = \quad \bar{A}(\rho)\bar{x} \\ \dot{\tilde{x}} = \tilde{A}_{21}(\rho)\bar{x} + \tilde{A}_{22}(\rho)\tilde{x} \\ y = \quad \bar{C}\bar{x}\end{array} \tag{2.20}$$

$\tilde{x}$ being an unobservable mode. In general, however, observability of $\bar{x}$ can be asserted only if $\mathscr{W} = \langle\mathscr{C}|\mathscr{A}\rangle$ and the c-persistency property holds.

With a suitable output injection $G(\rho)y$ one has $\tilde{A}_{21}(\rho)\bar{x} = G(\rho)y = G(\rho)C\bar{x}$:

$$\dot{\tilde{x}} = \tilde{A}_{22}(\rho)\tilde{x} + G(\rho)y. \tag{2.21}$$

The dual notion of parameter-varying controllability subspace is the following:

Definition 5. *A subspace $\mathscr{S}$ is called parameter-varying unobservability subspace if there exists a constant output mixing matrix H and a parameter varying output injection gain $G : [0,T] \to \mathbb{R}^{n\times p}$ such that $\mathscr{S} = \langle Ker HC|\mathscr{A} + \mathscr{G}C\rangle$, where $\mathscr{A} + \mathscr{G}C$ denotes the system $A(\rho) + G(\rho)C$.*

The family of parameter-varying unobservability subspaces containing a given subspace $\mathscr{L}$ is closed under subspace intersection. The minimal element of this family will be denoted by $\mathscr{S}_*$.

2.2.3 Parameter-Varying Invariant Subspace Algorithms

In [4, 8] an algorithm was given to determine the robust controlled invariant subspace for arbitrary parameter dependence, however, since the number of conditions is not finite, the algorithm, in general is not applicable in practice. Therefore, from a practical point of view it is an important question to characterize these parameter-varying subspaces by a finite number of conditions.

It turns out that this is possible for the class of LPV systems, where the parameter dependency is affine. To impose this requirement is not too restrictive: even the true parameter dependency is more general, e. g., is given by a linear fractional transform, commonly used relaxation techniques that are used to obtain stability will embed it in a finitely generated (polytopic) convex set. But this convexified set can be always associated with an affine parameter dependence.

Affine Parameter Dependency

Assuming an affine parameter dependency of the state matrix, i. e., $A(\rho) = \sum_{i=1}^{N} \rho_i A_i$, it is immediate that if the inclusions hold for all A_i, then they hold also for all $\rho \in \mathscr{P}$. It is not so straightforward under which conditions the reverse implication is true, too.

A sufficient condition that characterizes property can be given as:

Lemma 2. *If ρ_i are linearly independent over $\mathbb{R}$ then $A(\rho)\mathscr{V} \subset \mathscr{W} \ \ \forall \rho \in \mathscr{P}$ if and only if $A_i\mathscr{V} \subset \mathscr{W}$, $i = 0,\ldots,N$.*

In what follows, as otherwise is not stated, an affine parameter dependence is assumed. We are interested in finding supremal $\mathscr{A}$-invariant subspaces in a given subspace $\mathscr{K}$ or containing a given subspace $\mathscr{L}$.

As far as the first purpose is concerned, by applying Lemma 2, one can formulate the $\mathscr{A}$-$\mathscr{I}$nvariant $\mathscr{S}$ubspace $\mathscr{A}$lgorithm over $\mathscr{L}$ as:

$$\mathscr{A}\mathscr{I}\mathscr{S}\mathscr{A}\mathscr{L}: \quad \mathscr{V}_0 = \mathscr{L}, \quad \mathscr{V}_{k+1} = \mathscr{L} + \sum_{i=0}^{N} A_i\mathscr{V}_k, \quad k \geq 0, \tag{2.22}$$

$$\mathscr{V}^* = \lim_{k\to\infty} \mathscr{V}_k. \tag{2.23}$$

Obviously the algorithm will stop after a finite number of steps, i.e., $\mathscr{V}^* = \mathscr{V}_{n-1}$.

Proposition 4. *The subspace $\mathscr{V}^*$ is such that $\mathscr{L} \subset \mathscr{V}^*$, $\mathscr{V}^*$ is $\mathscr{A}$-invariant and assuming that the parameters are c-excited, it is minimal with these properties.*

Similar to the linear case the subspace $\mathscr{V}^*$ is denoted by $\langle \mathscr{A} | \mathscr{L} \rangle$.

By duality, one has the $\mathscr{A}$-$\mathscr{I}$nvariant $\mathscr{S}$ubspace $\mathscr{A}$lgorithm in $\mathscr{K}$, i.e.,

$$\mathscr{A}\mathscr{I}\mathscr{S}\mathscr{A}\mathscr{K}: \quad \mathscr{W}_0 = \mathscr{K}, \quad \mathscr{W}_{k+1} = \mathscr{K} \cap \bigcap_{i=0}^{N} A_i^{-1}\mathscr{W}_k, \quad k \geq 0, \tag{2.24}$$

$$\mathscr{W}^* = \lim_{k\to\infty} \mathscr{W}_k. \tag{2.25}$$

The subspace $\mathscr{W}^*$ will be denoted by $\langle \mathscr{K} | \mathscr{A} \rangle$.

The corresponding version of Proposition 1. follows by duality, and can be stated as:

Proposition 5. *The subspace $\mathscr{W}^*$ is such that $\mathscr{W}^* \subset \mathscr{K}$, $\mathscr{W}^*$ is $\mathscr{A}$-invariant and assuming that the parameters are c-excited, it is maximal with these properties.*

The set of all $(\mathscr{A},\mathscr{B})$-invariant subspaces contained in a given subspace $\mathscr{K}$, is an upper semilattice with respect to subspace addition which admits a maximum that can be computed from the $(\mathscr{A},\mathscr{B})$-$\mathscr{I}$nvariant $\mathscr{S}$ubspace $\mathscr{A}$lgorithm:

$$\mathscr{A}\mathscr{B}\mathscr{I}\mathscr{S}\mathscr{A}: \quad \mathscr{V}_0 = \mathscr{K}, \quad \mathscr{V}_{k+1} = \mathscr{K} \cap \bigcap_{i=0}^{N} A_i^{-1}(\mathscr{V}_k + \mathscr{B}). \tag{2.26}$$

The limit of this algorithm will be denoted by $\mathscr{V}^*$ and its calculation needs at most n steps.

The set of all $(\mathscr{C},\mathscr{A})$-invariant subspaces containing a given subspace $\mathscr{L}$, is a lower semilattice with respect to subspace intersection. This semilattice admits a minimum which can be computed using the $(\mathscr{C},\mathscr{A})$-$\mathscr{I}$nvariant $\mathscr{S}$ubspace $\mathscr{A}$lgorithm (note that $\mathscr{C} = \mathrm{Ker}C$):

$$\mathscr{CAISA}: \quad \mathscr{W}_0 = \mathscr{L}, \quad \mathscr{W}_{k+1} = \mathscr{L} + \sum_{i=0}^{N} A_i(\mathscr{W}_k \cap \mathscr{C}). \tag{2.27}$$

The limit of this algorithm will be denoted by $\mathscr{W}^*$. It takes at most n steps to compute.

The family of unobservability subspaces associated to an LPV system containing a given subspace $\mathscr{L}$ is closed under subspace intersection. The minimal element $\mathscr{S}_*$ of this family is the result of the $\mathscr{U}$nobservability $\mathscr{S}$ubspace $\mathscr{A}$lgorithm:

$$\mathscr{USA}: \quad \mathscr{S}_0 = \mathscr{X}, \ \mathscr{S}_{k+1} = \mathscr{W}^* + \left(\bigcap_{i=0}^{N} A_i^{-1} \mathscr{S}_k \cap \mathscr{C} \right), \ \mathscr{S}_* = \lim_{k \to \infty} \mathscr{S}_k, \tag{2.28}$$

where $\mathscr{W}^*$ is computed by $\mathscr{CAISA}$.

2.3 Applications

2.3.1 Inversion of LPV Systems

There are two aspects concerning dynamical system inversion: *left invertibility*, which is related to unknown input observability – the target application field being fault detection filter design – and *right invertibility*, related to the solution of output tracking control problems. Dynamic inversion based controllers are popular in aerospace control, see, e. g., [26, 20].

This section provides a geometric view of dynamic inversion of LPV systems. In contrast to the pseudo-inversion techniques, in the proposed method the availability of the full state measurements is not assumed, instead, it is supposed that measured outputs, and possibly some of their derivatives are available, for which the resulting system is minimum phase and left (right) invertible. For output tracking a two degree of freedom controller structure is proposed, where the first part is an inversion based controller making the linearization of the plant while the second controller, using an error feedback, achieves the required stability properties.

The General Nonlinear Setting

Let us consider the nonlinear input affine system Σ,

$$\dot{x} = f(x) + \sum_{i=1}^{m} g_i(x) u_i, \quad y = h(x), \tag{2.29}$$

with $y = [y_j]_{j=1,p}$ and $h(x) = [h_j(x)]_{j=1,p}$, respectively. It is reasonable to assume that the rank of $g = [g_i]_{i=1,m}$ is m and that the rank of h is p.

The problem when the outputs – and possible its derivatives – are measured and the unknown input is to be determined involves the notion of the *left invertibility* of the system. We are going to construct another dynamic system

$$\dot{\zeta}(t) = \varphi(\zeta, y, \dot{y}, \ldots, u, \dot{u}, \ldots), \quad u(t) = \omega(\zeta, y, \dot{y}, \ldots, u, \dot{u}, \ldots)$$

with outputs u and inputs $\vartheta = (\tilde{y}, \tilde{u})$ that contains the measurements of the signals u, y and possible their time derivatives.

Let us recall, that the system (2.29) is *(left)invertible* at x_0, if the output functions corresponding to the initial state x_0 and distinct admissible controls u are different. A system is called *strongly invertible* if there exist an open and dense submanifold of the state manifold on which the system is invertible. Left invertibility can be characterized more completely by using algebraic techniques, for more details see, e. g., [34, 10]. However, for practical purposes design algorithms based on a geometrical framework are often more suitable.

A dual problem is to find a suitable input signal that produces a desired behavior of the outputs, i. e., output tracking, is related to the concept of *right invertibility*. A dynamical system is right invertible at x_0 if the rank of its input-output map at this point is p, i. e., the number of outputs (to be tracked), see [27].

A Geometrical Framework

Let us recall, first, some elementary definitions and facts from [18] and [28]. A smooth connected submanifold M which contains the point x_0 is said to be *locally controlled invariant* at x_0 if their is a smooth feedback $u(x)$ and a neighborhood U_0 of x_0 such that the vector field $\tilde{f}(x) = f(x) + g(x)u(x)$ is tangent to M for all $x \in M \cap U_0$, i.e. M is locally invariant under $\tilde{f}$.

An *output zeroing submanifold* of Σ is a smooth connected submanifold M with contains x_0 and satisfy:

1. for all $x \in M$ one has $h(x) = 0$,
2. M is locally controlled invariant at x_0.

This means that for some choice of the feedback control $u(x)$ the trajectories of Σ which start in M stay in M for all t in a neighborhood of $t_0 = 0$ and the corresponding output is identically zero. Such a submanifold Z^* can be determined by a "zero dynamics algorithm", [29].

If in addition

$$\dim \operatorname{span}\{ g_i(x_0) \,|\, i = 1, m\} = m, \tag{2.30}$$

and $\dim \operatorname{span}\{ g_i(x) \,|\, i = 1, m\} \cap T_x Z^*$ is constant for all $x \in Z^*$ then Z^* is a *locally maximal output zeroing submanifold*. Moreover, if

$$\dim \operatorname{span}\{ g_i(x) \,|\, i = 1, m\} \cap T_x Z^* = 0, \tag{2.31}$$

then there is a unique smooth feedback u^* such that $f^*(x) := f(x) + g(x)u^*(x)$ is tangent to Z^*. An algorithm for computing Z^* for a general case can be found in [18] and [28]. In some cases, however, Z^* can be determined relative easily relating it to the maximal controlled invariant distribution Δ^* contained in $\mathrm{Ker}\, \mathrm{d}h$, given by the controlled invariant codistribution algorithm ($\Delta^* = \Omega_*^\perp$), namely $\Delta^*(x) = T_x Z^*$, for details see [18].

An important case when this relation holds is the set of LTI systems and the class of systems that have a vector relative degree. The concept of relative degree plays a key role in several control problems both for linear and nonlinear systems. In particular, the computation of the relative degree and the derivation of consequent normal forms for nonlinear systems, represents key design step in order to solve successfully several control problems, like disturbance decoupling, feedback linearization and system inversion problems.

A multivariable nonlinear system has a vector relative degree $r = \{r_1, \cdots, r_p\}$ at a point x_0 if

i. $L_{g_j} L_f^k h_i(x) = 0$ for $j = 1, \cdots, m, \quad i = 1, \cdots, p$, and $k < r_i - 1$.
ii. the matrix

$$A(x) := \begin{bmatrix} L_{g_1} L_f^{r_1 - 1} h_1(x) & \cdots & L_{g_m} L_f^{r_1 - 1} h_1(x) \\ \cdots & \cdots & \cdots \\ L_{g_1} L_f^{r_p - 1} h_p(x) & \cdots & L_{g_m} L_f^{r_p - 1} h_p(x) \end{bmatrix} \tag{2.32}$$

has rank m for left invertibility (p for right invertibility) at x_0.

For further usage let us denote by

$$B(x) := \begin{bmatrix} L_f^{r_1} h_1(x) \\ \vdots \\ L_f^{r_p} h_p(x) \end{bmatrix}. \tag{2.33}$$

If condition (**ii.**) does not hold but there exist numbers r_i with property (**i.**) then they are called *relative orders* of the system (2.29).

Lemma 3. *Let us suppose that the system* (2.29) *has relative degree. Then the row vectors* $\{dh_1(x_0), \cdots, dL_f^{r_1 - 1} h_1(x_0), \cdots, dh_p(x_0), \cdots, dL_f^{r_p - 1} h_p(x_0)\}$ *are linearly independent.*

Conditions (2.30) and (2.31) can be interpreted as a special property of (left) invertibility of the system Σ. Our interest in the determination of the output zeroing manifold is motivated by the role played by these notions in the question of invertibility and the construction of the reduced inverse of linear and nonlinear controlled systems.

The characterization of right invertibility, related to the number of zeros at infinity, is analogous, for details see [27].

Nonlinear Systems with Vector Relative Degree

If rank$A(x) = m$ then $Z^* = \{x | L_f^k h_i = 0, i = 1, \cdots, p \quad k = 0, \cdots, r_i - 1\}$ and the maximal controlled invariant distribution in Ker dh is $V^* = \text{Ker}\,\text{span}\{dL_f^k h_i, i = 1, \cdots, p \quad k = 0, \cdots, r_i - 1\}$, see also [28]. Moreover the feedback $u^*(x) = \alpha(x)$ is the solution of an equation $A(x)\alpha(x) = B(x)$.

Let us denote by $\xi = (\xi^i)_{i=1,p} = \Xi(x)$ the diffeomorphism defined by $\xi^i = (L_f^k h_i(x))_{k=0,r_i-1}$. It is a standard computation, that $\dot{\xi}^i = A^i \xi^i + B^i y_i^{(r_i)}$, where A^i, B^i are in the Brunowsky form ($\xi_1^i = y_i$).

Let us complete $\Xi(x)$ to a diffeomorphism on X: $\begin{bmatrix} \xi \\ \eta \end{bmatrix} = \Phi(x) := \begin{bmatrix} \Xi(x) \\ \Lambda(x) \end{bmatrix}$. Since $\partial_x \Xi = [\text{d}L_f^k h_i]$, one has $\dot{\xi} = [\text{d}L_f^k h_i] f|_{\Phi^{-1}} + [\text{d}L_f^k h_i] g|_{\Phi^{-1}} u$, i.e., maintaining the nonzero rows: $[\dot{\xi}_{r_i}^i] = B|_{\Phi^{-1}} + A|_{\Phi^{-1}} u$, and $\dot{\eta} = \partial_x \Lambda f|_{\Phi^{-1}} + \partial_x \Lambda g|_{\Phi^{-1}} u$. The zero dynamics[5] can be obtained by $\dot{\eta} = \partial_x \Lambda f|_{\Phi^{-1}} + \partial_x \Lambda g \alpha|_{\Phi^{-1}}$, putting $\xi = 0$.

Finally, the *output equations* of the dynamic inverse are

$$u(t) = A^{-1} \begin{bmatrix} \xi \\ \eta \end{bmatrix} \left(y^{(r)} - L_f^r h \begin{bmatrix} \xi \\ \eta \end{bmatrix} \right)$$

and one can get the (*minimal*) inverse dynamics as $\dot{\eta} = f(\xi, \eta)$, where ξ contains the corresponding output derivatives. Observe that the inverse does not inherit the structure of the original system, i.e., it is not necessarily input affine.

The main difficulty in the construction of the dynamical inverse in this general nonlinear context consists in obtaining and handling the time varying coordinate transform $\Phi(x)$ with its splitting in $\Xi(x)$ and $\Lambda(x)$. This is a state dependent nonlinear transformation, and the construction of the suitable extension requires, in general, solution of partial differential equations, hence, it is necessary to know the full state vector of the system. The linearized system will be a chain of integrators and the actual input of the linearizing controller will be the derivative, with order equal to the relative degree of the system, of the desired output.

Even if all the data required for the implementation of dynamical the inverse is available the method might be useless in practice. Invertibility does not involve the knowledge of the initial condition but for the implementation it plays an implicit role. The zero dynamics should be stable because it cannot be influenced by output injection since it is not observable for the outputs used in the inversion process.

The next section will provide a method for a class of LPV systems when the entire construction can be performed based on a suitable parameter varying conditioned invariant subspace.

Dynamic Inverse of LPV Systems

Let us consider the class of LPV systems (2.2) with m inputs and p outputs, i.e.,:

$$\dot{x}(t) = A(\rho(t))x(t) + B(\rho(t))u(t), \quad y(t) = Cx(t). \tag{2.34}$$

[5] If g is involutive, then one can choose $d\Lambda \subset g^\perp$, and then $\dot{\eta} = \partial_x \Lambda f|_{\Phi^{-1}}$.

It is not hard to figure out that in the LTI case $T_x Z^* = V^*$, where V^* is the maximal (A,B)-invariant subspace contained in $\operatorname{Ker} C$ while for the LPV case if some technical conditions for the parameter functions (persistency) are fulfilled, then $T_x Z^* = \mathscr{V}^*$, where $\mathscr{V}^*$ is the maximal $(\mathscr{A},\mathscr{B})$-invariant subspace contained in $\mathscr{C} = \operatorname{Ker} C$. The minimal $(\mathscr{C},\mathscr{A})$-invariant subspace containing $\mathscr{B} = \operatorname{Im} B$ is denoted by $\mathscr{S}_*$.

Left and right invertibility of LPV system can be characterized in geometric terms as follows:

Proposition 6. *The LPV system (2.34) is left-invertible if*

$$\mathscr{V}^* \cap \mathscr{B} = 0. \tag{2.35}$$

The system is right invertible if

$$\mathscr{S}_* + \mathscr{C} = \mathscr{X}. \tag{2.36}$$

Let us observe, that if conditions (2.35) are fulfilled, one can always choose a coordinate transform of the form $z = Tx$,where $T = \begin{bmatrix} \mathscr{V}^{*\perp} \\ \Lambda \end{bmatrix}$, $\Lambda \subset \mathscr{B}^{\perp}$.

Accordingly, the system will be decomposed into:

$$\begin{aligned} \dot{\xi} &= A_{11}(t)\xi + A_{12}(t)\eta + \bar{B}(t)u \\ \dot{\eta} &= A_{21}(t)\xi + A_{22}(t)\eta, \quad y = \bar{C}\xi. \end{aligned} \tag{2.37}$$

It follows, that applying a suitable feedback

$$u = F_2(t)\eta + v, \tag{2.38}$$

that makes the subspace $\mathscr{V}^*$ be $(\mathscr{A} + \mathscr{B}F, \mathscr{B})$ invariant, one can obtain the system:

$$\dot{\xi} = A_{11}(t)\xi + \bar{B}v, \quad y = \bar{C}\xi. \tag{2.39}$$

Maximality of $\mathscr{V}^*$ ensures that both ξ and v can be expressed as functions of y and its derivatives.

By introducing the notation $\tilde{y} = \mathscr{S}\xi$, $\tilde{y} = \left[y_1, \cdots, y_1^{(r_1-1)}, \cdots, y_p, \cdots, y_p^{(r_p-1)}\right]^T$ one has $v = \bar{B}^{\{-1\}}\mathscr{S}^{-1}(\dot{\tilde{y}} - \dot{\mathscr{S}}\mathscr{S}^{-1}\tilde{y} - \mathscr{S}A_{11}\mathscr{S}^{-1}\tilde{y})$, i.e.,

$$\dot{\eta} = A_{22}\eta + A_{21}\mathscr{S}^{-1}\tilde{y} \tag{2.40}$$

$$u = F_2\eta + \bar{B}^{\{-1\}}\mathscr{S}^{-1}(\dot{\tilde{y}} - \dot{\mathscr{S}}\mathscr{S}^{-1}\tilde{y} - \mathscr{S}A_{11}\mathscr{S}^{-1}\tilde{y}). \tag{2.41}$$

The coordinate transform $\mathscr{S}(t)$ can be obtained by applying the recursive algorithm defined by: $S_i^0(t) = c_i$, $S_i^{k+1}(t) = \dot{S}_i^k(t) + S_i^k(t)A_{11}(t)$, see, e.g., [31].

Remark 1. *It is clear that the method presented above can be also applied for nonlinear dynamics cast as quasi LPV systems with affine parameter dependence. One can observe that to compute the matrix $\mathscr{S}(t)$ one needs certain derivatives of the*

parameter functions $\rho_i(y)$, i.e., certain derivatives of the output y, but the order of these derivatives are bounded by $\max_i r_i$.

Inversion Based Output Tracking Controller

Since condition of right-invertibility is $\mathscr{V}^* + \mathscr{S}_* = \mathscr{X}$, one has the dual result as:

Proposition 7. *If the the LPV system (2.34) has a relative degree and condition (2.36) is fulfilled, the system has a well defined right dynamical inverse of the form (2.40)-(2.41). If the parameter dependence is affine the dynamical inverse, i.e., the output tracking controller can be computed in finite steps.*

The right inverse is realizable in exactly the same way as the (left)inverse system. The input u corresponding to the desired output is not unique, in general. The difference between any two admissible input corresponds to a zero-state motion on $R_{\mathscr{V}^*} = \mathscr{V}^* \cap \mathscr{S}_*$ which does not affect the output. A common solution is to set to zero the input components which, expressed in a suitable basis, correspond to forcing actions belonging to $\mathscr{V}^* \cap \mathscr{B}$.

Applying the dynamic inversion algorithm, one can obtain a system that realizes the tracking if the initial conditions are known. Let us denote the outputs to be tracked by y_d. Due to the effect caused by the unknown initial condition, there will be an error of the estimated state η. Introducing an outer-loop based on error feedback, one can obtain the following structure for the tracking controller:

$$\dot{\bar{\eta}} = A_{22}\bar{\eta} + A_{21}\mathscr{S}^{-1}\tilde{y}_d + \Gamma_1\tilde{e}, \quad \bar{u} = F_2\bar{\eta} + \lambda(\tilde{y}_d) + \Gamma_2\tilde{e}, \tag{2.42}$$

with $\lambda(\tilde{y}_d) = \bar{B}^{\{-1\}}\mathscr{S}^{-1}(\dot{\tilde{y}} - \dot{\mathscr{S}}\mathscr{S}^{-1}\tilde{y} - \mathscr{S}A_{11}\mathscr{S}^{-1}\tilde{y})$, the tracking error $e = \hat{y} - y_d$ and the possibly parameter dependent gain matrices Γ_1 and Γ_2.

Let us denote by $e_\xi = \hat{\xi} - \xi_d$ and $e_\eta = \hat{\eta} - \bar{\eta}$ and recall that $\tilde{e} = \mathscr{S}e_{x_1}$. Then the error dynamics can be expressed as:

$$\dot{e}_\xi = (A_{11} + \bar{B}\Gamma_2\mathscr{S})e_\xi + A_{12}e_\eta, \;\; \dot{e}_\eta = (A_{21} + \Gamma_1\mathscr{S})e_\xi + A_{22}e_\eta, \;\; \tilde{e} = \mathscr{S}e_\xi.$$

Actually the decay rate of e_η cannot be increased – the dynamics determined by A_{22} should be stable – therefore a convenient choice is $\Gamma_1 = -A_{21}\mathscr{S}^{-1}$. The gain Γ_2 is tuned to obtain a desired decay rate for e_ξ, this can be done by solving a suitable set of LMIs.

In implementing the tracking control a problem might be that $\tilde{e}$ is not available for the measurement. If a state observer is available, then the inversion scheme can be replaced by the combination of this observer and the linearization feedback. Such a state observer can be design if additional measured outputs are available, say:

$$z = C_2x = C_{21}\xi + C_{22}\eta, \tag{2.43}$$

that makes the plant fully observable. Then, the inversion is achieved by the following dynamical system:

$$\dot{\bar{w}} = (A - K\bar{C} + BF)\bar{w} + K\bar{y} + B\lambda(\tilde{y}_d) + \Gamma_1\tilde{e}, \quad \bar{u} = F\bar{w} + \lambda(\tilde{y}_d) + \Gamma_2\tilde{e}.$$

where $\bar{C}^T = [C^T\, C_2^T]$ and $\bar{y} = [y\, z]^T$.

The additional degree of freedom can be used to improve the performance properties – estimation time, disturbance rejection – of the unknown input observer or of the output tracking controller, respectively.

Example

As an illustrative example for the LPV inversion scheme let us consider the following linearized parameter varying model:

$$\dot{x}(t) = A(\rho)x(t) + Bv(t), \quad y(t) = Cx(t),$$

where $A(\rho) = A_0 + \rho_1 A_1 + \rho_2 A_2$. The state matrices are:

$$A_0 = \begin{bmatrix} -1 & 0 & 0 & 0 & 0 \\ 0 & -1 & 0 & 0 & 0 \\ 0 & 0 & -1 & 0 & 0 \\ 0 & 0 & 0 & -1 & 0 \\ 0 & 0 & 0 & 0 & -1 \end{bmatrix}, \quad A_1 = \begin{bmatrix} 0 & -1 & 1 & 1 & 0 \\ 0 & 0 & 0 & 0 & 1 \\ 0 & 0 & 0 & 0 & 0 \\ 0 & 0 & 0 & 0 & 0 \\ 1 & 0 & 0 & 0 & 0 \end{bmatrix}, \quad A_2 = \begin{bmatrix} 0 & 0 & 0 & 0 & 0 \\ 0 & 0 & 0 & 0 & 0 \\ 1 & 0 & 0 & 0 & 0 \\ 0 & 0 & 0 & 0 & 0 \\ 0 & 1 & 0 & 0 & 0 \end{bmatrix}, \quad B = \begin{bmatrix} 1 & 0 \\ 0 & 1 \\ 0 & 1 \\ 0 & 0 \\ 0 & 0 \end{bmatrix}, \quad C = \begin{bmatrix} 0 & 0 & 0 & 0 & 1 \\ 0 & 1 & 0 & 0 & 0 \\ 0 & 0 & 0 & 1 & 1 \end{bmatrix}.$$

Applying the $\mathscr{A}\mathscr{B}\mathscr{I}\mathscr{S}\mathscr{A}$ algorithm one has $\mathscr{V}^* = \mathrm{Im}\begin{bmatrix} 0 & 0 & 1 & 0 & 0 \end{bmatrix}^T$ and the corresponding state transform can be chosen as:

$$T = \begin{bmatrix} 1 & 0 & 0 & 0 & 0 \\ 0 & 1 & 0 & 0 & 0 \\ 0 & 0 & 0 & 1 & 0 \\ 0 & 0 & 0 & 0 & 1 \\ 0 & -1 & 1 & 0 & 0 \end{bmatrix}, \quad \text{i.e.,} \quad T^{-1} = \begin{bmatrix} 1 & 0 & 0 & 0 & 0 \\ 0 & 1 & 0 & 0 & 0 \\ 0 & 1 & 0 & 0 & 1 \\ 0 & 0 & 1 & 0 & 0 \\ 0 & 0 & 0 & 1 & 0 \end{bmatrix}.$$

Accordingly the the system splits as

$$\begin{bmatrix} A_{11}^0 & A_{12}^0 \\ A_{21}^0 & A_{22}^0 \end{bmatrix} = \left[\begin{array}{cccc|c} -1 & 0 & 0 & 0 & 0 \\ 0 & -1 & 0 & 0 & 0 \\ 0 & 0 & -1 & 0 & 0 \\ 0 & 0 & 0 & -1 & 0 \\ \hline 0 & 0 & 0 & 0 & -1 \end{array}\right], \quad \begin{bmatrix} A_{11}^1 & A_{12}^1 \\ A_{21}^1 & A_{22}^1 \end{bmatrix} = \left[\begin{array}{cccc|c} 0 & 0 & 1 & 0 & 1 \\ 0 & 0 & 0 & 1 & 0 \\ 0 & 0 & 0 & 0 & 0 \\ 1 & 0 & 0 & 0 & 0 \\ \hline 0 & 0 & 0 & -1 & 0 \end{array}\right],$$

$$\begin{bmatrix} A_{11}^2 & A_{12}^2 \\ A_{21}^2 & A_{22}^2 \end{bmatrix} = \left[\begin{array}{cccc|c} 0 & 0 & 0 & 0 & 0 \\ 0 & 0 & 0 & 0 & 0 \\ 0 & 0 & 0 & 0 & 0 \\ 0 & 1 & 0 & 0 & 0 \\ \hline 1 & 0 & 0 & 0 & 0 \end{array}\right], \quad \begin{bmatrix} \bar{B} \\ 0 \end{bmatrix} = \left[\begin{array}{cc} 1 & 0 \\ 0 & 1 \\ 0 & 0 \\ 0 & 0 \\ \hline 0 & 0 \end{array}\right], \quad \begin{bmatrix} \bar{C} & 0 \end{bmatrix} = \left[\begin{array}{cccc|c} 0 & 0 & 0 & 1 & 0 \\ 0 & 1 & 0 & 0 & 0 \\ 0 & 0 & 1 & 1 & 0 \end{array}\right].$$

The matrix $F(\rho) = F_0 + \rho_1 F_1 + \rho_2 F_2$, is given by

$$F_0 = 0, \quad F_1 = \begin{bmatrix} 0 & 0 & -1 & 0 & 0 \\ 0 & 0 & 0 & 0 & 0 \end{bmatrix}, \quad F_2 = 0.$$

The transformation $\mathscr{S}(\rho) = S_0 + \rho_1 S_1 + \rho_2 S_2$, where

$$S_0 = \begin{bmatrix} 0&0&0&1\\ 0&0&0&-1\\ 0&1&0&0\\ 0&0&1&1 \end{bmatrix}, \quad S_1 = \begin{bmatrix} 0&0&0&0\\ 1&0&0&0\\ 0&0&0&0\\ 0&0&0&0 \end{bmatrix}, \quad S_2 = \begin{bmatrix} 0&0&0&0\\ 0&1&0&0\\ 0&0&0&0\\ 0&0&0&0 \end{bmatrix},$$

maps ξ to $\tilde{y} = \begin{bmatrix} y_1 & \dot{y}_1 & y_2 & y_3 \end{bmatrix}^T$.

One can figure out that

$$\mathscr{S}^{-1}(t) = \begin{bmatrix} \frac{1}{\rho_1} & \frac{1}{\rho_1} & -\frac{\rho_2}{\rho_1} & 0\\ 0 & 0 & 1 & 0\\ -1 & 0 & 0 & 1\\ 1 & 0 & 0 & 0 \end{bmatrix} \quad \text{and} \quad \dot{\mathscr{S}}(t)\mathscr{S}^{-1}(t) = \begin{bmatrix} 0 & 0 & 0 & 0\\ \frac{\dot{\rho}_1}{\rho_1} & \frac{\dot{\rho}_1}{\rho_1} & -\frac{\dot{\rho}_1\rho_2}{\rho_1} + \dot{\rho}_2 & 0\\ 0 & 0 & 0 & 0\\ 0 & 0 & 0 & 0 \end{bmatrix}$$

It follows, that

$$\mathscr{S}A_{11}\mathscr{S}^{-1} = \begin{bmatrix} -1&0&0&0\\ 0&-1&0&0\\ 0&0&-1&0\\ 0&0&0&-1 \end{bmatrix} + \rho_1 \begin{bmatrix} \frac{1}{\rho_1} & \frac{1}{\rho_1} & -\frac{\rho_2}{\rho_1} & 0\\ \rho_2 - \rho_1 - \frac{1}{\rho_1} & -\frac{1}{\rho_1} & \frac{\rho_2}{\rho_1} & 0\\ 1 & 0 & 0 & 0\\ \frac{1}{\rho_1} & \frac{1}{\rho_1} & -\frac{\rho_2}{\rho_1} & 0 \end{bmatrix} + \rho_2 \begin{bmatrix} 0&0&1&0\\ 0&0&-1&0\\ 0&0&0&0\\ 0&0&1&0 \end{bmatrix},$$

$$\bar{B}^{-r}\mathscr{S}^{-1} = \begin{bmatrix} \frac{1}{\rho_1} & \frac{1}{\rho_1} & -\frac{\rho_2}{\rho_1} & 0\\ 0 & 0 & 1 & 0 \end{bmatrix}.$$

Finally, for the unknown input observer, i.e., the left inverse system one has

$$\dot{\eta} = -\eta + (\frac{\rho_2}{\rho_1} - \rho_1)y_1 + \frac{\rho_2}{\rho_1}\dot{y}_1 - \frac{\rho_2^2}{\rho_1}y_2,$$

and

$$\hat{v} = \begin{bmatrix} -\rho_1\\ 0 \end{bmatrix}\eta + \begin{bmatrix} \frac{1}{\rho_1} & \frac{1}{\rho_1} & -\frac{\rho_2}{\rho_1} & 0\\ 0 & 0 & 1 & 0 \end{bmatrix}\Big(\begin{bmatrix} \dot{y}_1\\ \ddot{y}_1\\ \dot{y}_2\\ \dot{y}_3 \end{bmatrix} - \begin{bmatrix} 0 & 1 & 0 & 0\\ \rho_1\rho_2 - \rho_1^2 + \frac{\dot{\rho}_1 - \rho_1}{\rho_1} & \frac{\dot{\rho}_1 - \rho_1}{\rho_1} & \frac{\dot{\rho}_2\rho_1 - \dot{\rho}_1\rho_2}{\rho_1} & \rho_1^2\\ \rho_1 & 0 & -1 & 0\\ 1 & 1 & 0 & -1 \end{bmatrix} \begin{bmatrix} y_1\\ \dot{y}_1\\ y_2\\ y_3 \end{bmatrix} \Big).$$

During the simulation the parameters vary as on Figure 7.10 and some measurement noise was also considered. The applied and reconstructed inputs are depicted on Figure 2.2.

Since $\mathscr{S}_* = \mathrm{Im} \begin{bmatrix} 0&1&0&-1\\ 0&0&1&0\\ 1&0&0&0\\ 0&0&0&0\\ 0&1&0&1 \end{bmatrix}$ one has $\mathscr{S}_* + \mathscr{V}^* \neq \mathscr{X}$, i.e., the right invertibility condition is not fulfilled, as it was expected.

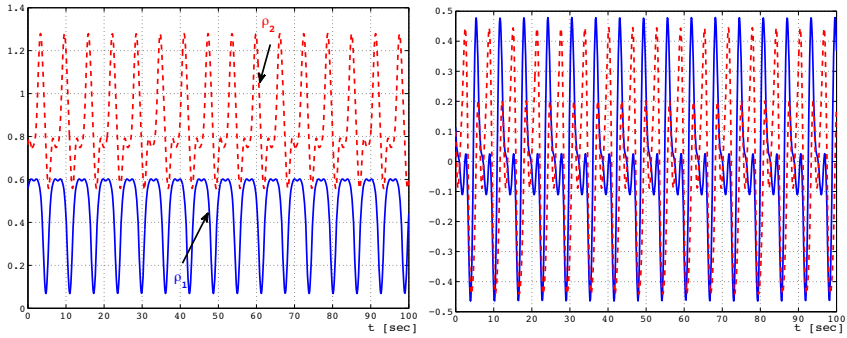

Fig. 2.1 Parameters ρ_1 and ρ_2 (dashed) and its derivatives

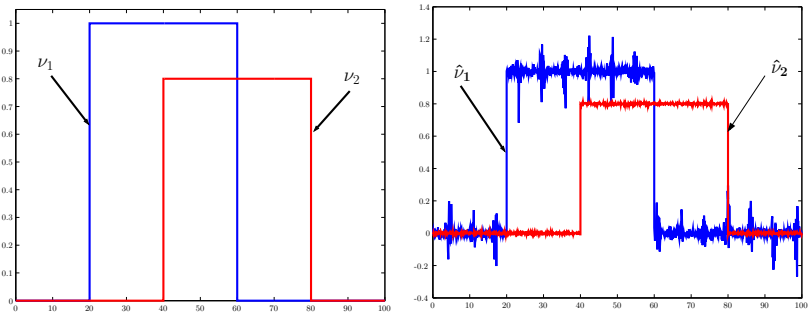

Fig. 2.2 Applied and reconstructed inputs

To make the system right invertible consider the first two outputs only, i.e., $y_t = C_t x$ with $C_t = \begin{bmatrix} 0\,0\,0\,0\,1 \\ 0\,1\,0\,0\,0 \end{bmatrix}$. With this setting one has $\mathscr{V}^* = \mathrm{Im} \begin{bmatrix} 0\,0\,0\,1\,0 \\ 0\,0\,1\,0\,0 \end{bmatrix}^T$ and $\mathscr{S}_* = \mathrm{Im} \begin{bmatrix} 0\,1\,0\,0 \\ 0\,0\,1\,0 \\ 1\,0\,0\,0 \\ 0\,0\,0\,0 \\ 0\,0\,0\,1 \end{bmatrix}$, i.e., $\mathscr{S}_* + \mathscr{V}^* = \mathscr{X}$. The corresponding state transform can be chosen as:

$$T = \begin{bmatrix} 1 & 0 & 0\,0\,0 \\ 0 & 1 & 0\,0\,0 \\ 0 & 0 & 0\,0\,1 \\ 0 & -1 & 1\,1\,0 \\ 0 & 0 & 0\,1\,0 \end{bmatrix}, \quad \text{i.e.,} \quad T^{-1} = \begin{bmatrix} 1\,0\,0\,0 & 0 \\ 0\,1\,0\,0 & 0 \\ 0\,1\,0\,1 & -1 \\ 0\,0\,0\,0 & 1 \\ 0\,0\,1\,0 & 0 \end{bmatrix}.$$

Accordingly the the system splits as

$$\begin{bmatrix} A_{11}^0 & A_{12}^0 \\ A_{21}^0 & A_{22}^0 \end{bmatrix} = \left[\begin{array}{ccc|cc} -1 & 0 & 0 & 0 & 0 \\ 0 & -1 & 0 & 0 & 0 \\ 0 & 0 & -1 & 0 & 0 \\ \hline 0 & 0 & 0 & -1 & 0 \\ 0 & 0 & 0 & 0 & -1 \end{array}\right], \quad \begin{bmatrix} A_{11}^1 & A_{12}^1 \\ A_{21}^1 & A_{22}^1 \end{bmatrix} = \left[\begin{array}{ccc|cc} 0 & 0 & 0 & 1 & 0 \\ 0 & 0 & 1 & 0 & 0 \\ 1 & 0 & 0 & 0 & 0 \\ \hline 0 & 0 & -1 & 0 & 0 \\ 0 & 0 & 0 & 0 & 0 \end{array}\right],$$

$$\begin{bmatrix} A_{11}^2 & A_{12}^2 \\ A_{21}^2 & A_{22}^2 \end{bmatrix} = \left[\begin{array}{ccc|cc} 0 & 0 & 0 & 0 & 0 \\ 0 & 0 & 0 & 0 & 0 \\ 0 & 1 & 0 & 0 & 0 \\ \hline 1 & 0 & 0 & 0 & 0 \\ 0 & 0 & 0 & 0 & 0 \end{array}\right], \quad \begin{bmatrix} \bar{B} \\ 0 \end{bmatrix} = \left[\begin{array}{cc} 1 & 0 \\ 0 & 1 \\ 0 & 0 \\ \hline 0 & 0 \\ 0 & 0 \end{array}\right],$$

$$\begin{bmatrix} \bar{C} & 0 \end{bmatrix} = \left[\begin{array}{ccc|cc} 0 & 0 & 1 & 0 & 0 \\ 0 & 1 & 0 & 0 & 0 \end{array}\right].$$

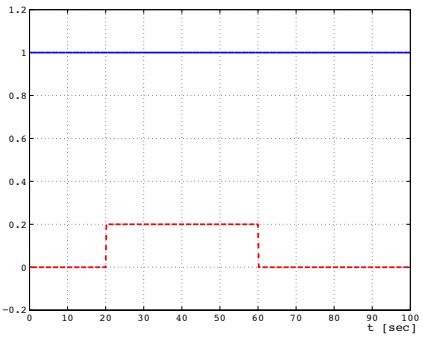

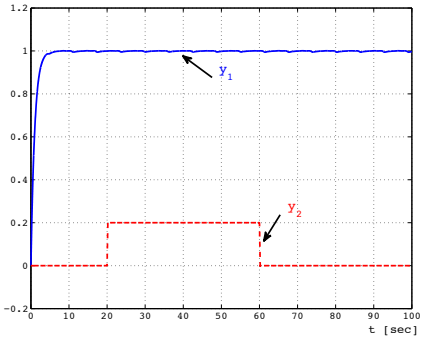

Fig. 2.3 Desired and actual outputs

One has $\mathscr{S}(\rho) = \begin{bmatrix} 0 & 0 & 1 \\ \rho_1 & \rho_2 & -1 \\ 0 & 1 & 0 \end{bmatrix}$ that maps ξ to $\tilde{y} = \begin{bmatrix} y_1 & \dot{y}_1 & y_2 \end{bmatrix}^T$.

One can figure out that

$$S^{-1}(t) = \begin{bmatrix} \frac{1}{\rho_1} & \frac{1}{\rho_1} & -\frac{\rho_2}{\rho_1} \\ 0 & 0 & 1 \\ 1 & 0 & 0 \end{bmatrix} \quad \text{and} \quad \dot{S}(t)S^{-1}(t) = \begin{bmatrix} 0 & 0 & 0 \\ \frac{\dot{\rho}_1}{\rho_1} & \frac{\dot{\rho}_1}{\rho_1} & -\frac{\dot{\rho}_1\rho_2}{\rho_1} + \dot{\rho}_2 \\ 0 & 0 & 0 \end{bmatrix},$$

while

$$\mathscr{S}A_{11}\mathscr{S}^{-1} = \begin{bmatrix} 0 & 1 & 0 \\ \rho_1\rho_2 - 1 & -2 & 0 \\ \rho_1 & 0 & -1 \end{bmatrix}, \quad \bar{B}^{-r}\mathscr{S}^{-1} = \begin{bmatrix} \frac{1}{\rho_1} & \frac{1}{\rho_1} & -\frac{\rho_2}{\rho_1} \\ 0 & 0 & 1 \end{bmatrix}.$$

The output tracking controller has the form:

$$\dot{\zeta} = -\zeta + \left[\begin{array}{ccc} \frac{\rho_2}{\rho_1} - \rho_1 & \frac{\rho_2}{\rho_1} & -\frac{\rho_2\rho_2}{\rho_1} \end{array}\right] \tilde{y}$$

$$u = -\rho_1\zeta + \left[\begin{array}{ccc} \frac{1}{\rho_1} & \frac{1}{\rho_1} & -\frac{\rho_2}{\rho_1} \\ 0 & 0 & 1 \end{array}\right] (\dot{\tilde{y}} - \left[\begin{array}{ccc} 0 & 1 & 0 \\ \rho_1\rho_2 + \frac{\dot{\rho}_1 - \rho_1}{\rho_1} & \frac{\dot{\rho}_1 - 2\rho_1}{\rho_1} & \frac{\dot{\rho}_2\rho_1 - \dot{\rho}_1\rho_2}{\rho_1} \\ \rho_1 & 0 & -1 \end{array}\right] \tilde{y}) + \Gamma\tilde{y},$$

with the gain $\Gamma = \left[\begin{array}{ccc} \frac{-100}{\rho_1} & \frac{-100}{\rho_1} & \frac{100\rho_2}{\rho_1} \\ -\rho_1 & 0 & -50 \end{array}\right]$.

The results of the simulation are depicted on Figure 2.3.

2.3.2 *Fundamental Problem of Residual Generation (FPRG)*

Let us consider the following LTI system, that has two failure events:

$$\dot{x}(t) = Ax(t) + Bu(t) + L_1m_1(t) + L_2m_2(t), \quad y(t) = Cx(t),$$

then the task to design a residual generator that is sensitive to L_1 and insensitive to L_2 is called the fundamental problem of residual generation (FPRG). More precisely, one has to design a residual generator with outputs r such that if $m_1 \neq 0$ then $r \neq 0$ and if $m_1 = 0$ then $\lim_{t\to\infty} ||r(t)|| = 0$, i.e., a stability condition is required.

In the solution of this problem a central role is played by the (C,A)–invariant subspaces and certain unobservability subspaces, [23, 24] or observability codistributions, [11, 12], in the nonlinear version of this problem.

As it is well known, for LTI models, a subspace $\mathscr{W}$ is (C,A)–invariant if $A(\mathscr{W} \cap \mathrm{Ker}C) \subset \mathscr{W}$ that is equivalent with the existence of a matrix G such that $(A+GC)\mathscr{W} \subset \mathscr{W}$. A (C,A)–unobservability subspace $\mathscr{U}$ is a subspace such that there exist matrices G and H with the property that $(A+GC)\mathscr{U} \subset \mathscr{U}$, i.e., $\mathscr{U}$ is (C,A)–invariant, and $\mathscr{U} \subset \mathrm{Ker}HC$. The family of (C,A)–unobservability subspaces containing a given set $\mathscr{L}$ has a minimal element $\mathscr{U}^*$.

Let us denote by $\mathscr{S}^*$ the smallest unobservability subspace containing $\mathscr{L}_2$, where $\mathscr{L}_i = ImL_i$. Then one has the following result, [23]:

Proposition 8. *A FPRG has a solution if and only if $\mathscr{S}^* \cap \mathscr{L}_1 = 0$, moreover, if the problem has a solution, the dynamics of the residual generator can be assigned arbitrary.*

Given the residual generator in the form

$$\dot{w}(t) = Nw(t) - Gy(t) + Fu(t) \tag{2.44}$$

$$r(t) = Mw(t) - Hy(t), \tag{2.45}$$

then H is a solution of $\mathrm{Ker}HC = \mathrm{Ker}C + \mathscr{S}^*$, and M is the unique solution of $MP = HC$, where P is the projection $P : \mathscr{X} \to \mathscr{X}/\mathscr{S}^*$. Let us consider a G_0 such

that $(A+G_0C)\mathscr{S}^* \subset \mathscr{S}^*$ and denote by $A_0 = A+G_0C|_{\mathscr{X}/\mathscr{S}^*}$. Then there is a G_1 such that $N = A_0 + G_1M$ has prescribed eigenvalues. Then set $G = PG_0 + G_1H$ and $F = PB$.

Extending this result to the case with multiple events one has the extension of the fundamental problem of residual generation (EFPRG), that has a solution if and only if $\mathscr{S}_i^* \cap \mathscr{L}_i = 0$, where $\mathscr{S}_i^*$ is the smallest unobservability subspace containing $\overline{\mathscr{L}}_i := \sum_{j\neq i}\mathscr{L}_j$.

These ideas were also applied to nonlinear systems, and a similar condition was obtained for the solvability of the FPRG problem in terms of the observability codistributions, see [16, 13].

In what follows, this result will be extended to the LPV systems where the state matrix depends affinely on the parameter vector and quasi LPV systems, where the parameters depends on measurable outputs.

FPRG for LPV Systems

Let us consider the class of linear parameter–varying systems of which state matrix depends affinely on the parameter vector will be considered. This class of systems can be described as:

$$\dot{x}(t) = A(\rho)x(t) + B(\rho)u(t) + \sum_{j=1}^{m} L_j(\rho)v_j(t), \quad y(t) = Cx(t), \tag{2.46}$$

where v_j are the failures to be detected, C is right invertible,

$$A(\rho) = A_0 + \rho_1 A_1 + \cdots + \rho_N A_N, \tag{2.47}$$
$$B(\rho) = B_0 + \rho_1 B_1 + \cdots + \rho_N B_N, \tag{2.48}$$
$$L_j(\rho) = L_{j,0} + \rho_1 L_{j,1} + \cdots + \rho_N L_{j,N}, \tag{2.49}$$

and ρ_i are time varying parameters. It is assumed that each parameter ρ_i and its derivatives $\dot{\rho}_i$ ranges between known extremal values $\rho_i(t) \in [-\overline{\rho}_i, \overline{\rho}_i]$ and $\dot{\rho}_i(t) \in [-\overline{\dot{\rho}}_i, \overline{\dot{\rho}}_i]$, respectively. Let us denote this parameter set by $\mathscr{P}$.

For LPV systems (2.46) one has the following result:

Proposition 9. *For the LPV systems (2.46) one can design a – not necessarily stable – residual generator of type*

$$\dot{w}(t) = N(\rho)w(t) - G(\rho)y(t) + F(\rho)u(t) \tag{2.50}$$
$$r(t) = Mw(t) - Hy(t), \tag{2.51}$$

if and only if for the smallest (parameter varying) unobservability subspace $\mathscr{U}^*$ containing $\mathscr{L}_2$ one has $\mathscr{U}^* \cap \mathscr{L}_1 = 0$, where $\mathscr{L}_i = \cup_{j=0}^{N} Im\, L_{i,j}$.

Example

As an illustrative example let us consider the following linearized parameter varying model of the longitudinal dynamics of an aircraft:

$$\dot{x}(t) = A(\rho)x(t) + Bu(t) + L_1 v_1(t) + L_2 v_2(t), \quad y(t) = Cx(t),$$

where $A(\rho) = A_0 + \rho_1 A_1 + \rho_2 A_2$. It is assumed that the parameter ρ_1 and ρ_2 vary in the intervals $[-0.3, 0.3]$ and $[-0.6, 0.6]$, respectively, see Figure 2.4.

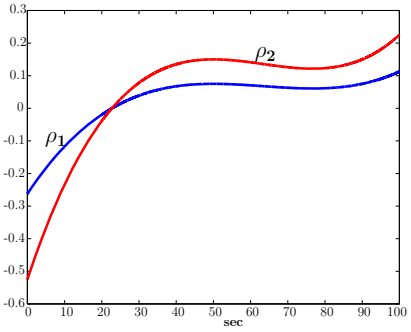

Fig. 2.4 Scheduling variables for the simulation

The state matrices are:

$$A_0 = \begin{bmatrix} -1.05 & -2.55 & 0 & 0 & -169.66 & -0.0091 \\ 2.55 & -1.05 & 0 & 0 & 57.09 & 0.0017 \\ 0 & 0 & -77.53 & 39.57 & 0 & 0 \\ 0 & 0 & 0 & -20.20 & 0 & 0 \\ 0 & 0 & -8.80 & 0 & -20.20 & 0 \\ 0 & 0 & 0 & 0 & 0 & -0.1000 \end{bmatrix}, \quad A_1 = \begin{bmatrix} 0 & 1 & 0 & 0 & 1 & 0 \\ 1 & 0 & 0 & 0 & 1 & 0 \\ 0 & 0 & 0 & 0 & 0 & 0 \\ 0 & 0 & 0 & 0 & 0 & 0 \\ 0 & 0 & 0 & 0 & 0 & 0 \\ 0 & 0 & 0 & 0 & 0 & 0 \end{bmatrix} \quad A_2 = \begin{bmatrix} 1 & 0 & 0 & 0 & 0 & 0 \\ 0 & 1 & 0 & 0 & 0 & 0 \\ 0 & 0 & 0 & 0 & 0 & 0 \\ 0 & 0 & 0 & 0 & 0 & 0 \\ 0 & 0 & 0 & 0 & 0 & 0 \\ 0 & 0 & 0 & 0 & 0 & 0 \end{bmatrix}$$

$$B = \begin{bmatrix} 0 \\ 0 \\ 0 \\ -4.49 \\ 0 \\ 0 \end{bmatrix} \quad L_1 = \begin{bmatrix} 0 \\ 0 \\ 0 \\ 0 \\ 1.00 \\ 0 \end{bmatrix}, L_2 = \begin{bmatrix} 3.55 & 2.41 \\ -0.55 & 8.04 \\ 0 & 0 \\ 0 & 0 \\ -0.02 & 0.56 \\ 0 & 0 \end{bmatrix}, C = \begin{bmatrix} -0.01 & 0.1 & 0.07 & 0 & 0.0 & -0.000 \\ -0.48 & -0.6 & 0.00 & 0 & -49.5 & -0.002 \\ 0.03 & 0.1 & -0.06 & 0 & -0.0 & 0.000 \\ 0.26 & -0.1 & 0.01 & 0 & 0.0 & -0.000 \end{bmatrix}$$

The simulation results are depicted on Figure 2.5.

The Question of Stability

In contrast to the LTI case, when stabilizability is guaranteed by certain pole allocation properties, in the LPV case the problem of stability is more involved. A common stabilization strategy in these schemes is to suppose a Lyapunov function

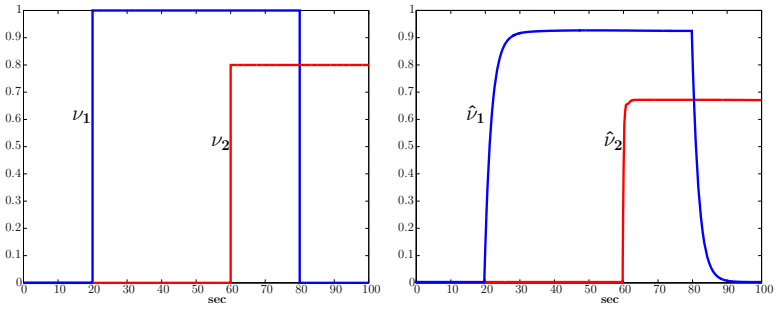

Fig. 2.5 Fault signals and the estimated residuals

of certain type – usually a quadratic Lyapunov function defined by a constant positive definite matrix – and to find the stabilizing feedback gains starting from the corresponding analysis equations.

An (q)LPV system is said to be quadratically stable if there exist a matrix $P = P^T > 0$ such that

$$A(\rho)^T P + PA(\rho) < 0 \tag{2.52}$$

for all the parameters $\rho \in \mathscr{P}$. A necessary and sufficient condition for a system to be quadratically stable is that the condition (2.52) holds for all the corner points of the parameter space, i.e., one can obtain a finite system of LMI's that has to be fulfilled for $A(\rho)$ with a suitable positive definite matrix P, see [1].

In order to obtain a quadratically stable residual generator one can set $N(\rho) = A_0(\rho) + G(\rho)M$ in (2.50), where $G(\rho) = G_0 + \rho_1 G_1 + \cdots \rho_N G_N$ is determined such that the LMI defined in (2.52), i.e.,

$$(A_0(\rho) + G(\rho)M)^T P + P(A_0(\rho) + G(\rho)M) < 0$$

holds for suitable $G(\rho)$ and $P = P^T > 0$. By introducing the auxiliary variable $K(\rho) = G(\rho)P$, one has to solve the following set of LMIs on the corner points of the parameter space:

$$A_0(\rho)^T P + PA_0(\rho) + M^T K(\rho)^T + K(\rho)M < 0.$$

Remark 2. *If $KerC \subset \mathscr{U}^*$ then one can choose $G(\rho)$ such that the matrix $N(\rho)$ be parameter independent with arbitrary eigenvalues, since the equation $G(\rho)CU = UT - A(\rho)U$ has a solution for arbitrary T, where U is the insertion map of $\mathscr{X}/\mathscr{U}^*$.*

This method for quadratic stabilization can be also used for computing the gains Γ_i for the inversion based tracking controller (2.42).

2.4 Conclusions

This work extends the notions of different LTI invariant subspaces to (quasi) parameter-varying systems by introducing the notion of *parameter-varying* $(\mathscr{A},\mathscr{B})$-*invariant* and *parameter-varying* $(\mathscr{C},\mathscr{A})$-*invariant* subspaces. In introducing the various parameter-varying invariant subspaces an important goal was to set notions that lead to computationally tractable algorithms for the case when the parameter dependency of the system matrices is affine. These invariant subspaces provides a viable alternative of the more complex objects such as the corresponding invariant distributions and codistributions of the full nonlinear framework. Efficient algorithms are provided to compute these subspaces.

In general it is a hard task to give an exhaustive characterization for the solution of the fundamental problems such as the disturbance decoupling problem (DDP) or the fundamental problem of residual generation (FPRG) even in the LPV case. However, since the main ingredient in the solution of these problems are certain local decomposition theorems – in observable and unobservable subsystems, for example – using suitable invariant subspaces instead of the distributions or codistributions one can get sufficient conditions for solvability that can be useful in practical engineering applications.

References

1. Apkarian, P., Becker, G.: Self-scheduled $\mathscr{H}_\infty$ control of linear parameter varying systems: a design example. Automatica 31(9), 1251–1261 (1995)
2. Assan, J., Lafay, J.F., Perdon, A.M.: Computation of maximal pre-controllability submodules over a Noetherian ring. Systems and Control Letters 37(3), 153–161 (1999)
3. Barker, J., Balas, G.: Flight control of a tailless aircraft via linear parameter-varying techniques. In: AIAA Guidance, Navigation and Control Conference, Portland (1999)
4. Basile, G.B., Marro, G.: On the robust controlled invariant. Systems Contr. Letters 9, 191–195 (1987)
5. Basile, G.B., Marro, G.: Controlled and Conditioned Invariants in Linear System Theory. Prentice Hall, Englewood Cliffs (2002)
6. Becker, G., Packard, A.: Robust performance of linear, parametrically varying systems using parametrically-dependent linear dynamic feedback. Systems and Control Letters 23, 205–215 (1994)
7. Bhattacharyya, S.P.: Generalized controllability (A,B)-invariant subspaces and parameter invariant control. SIAM J. Alg. Disc. Meth. 4, 529–533 (1983)
8. Conte, G., Perdon, A.M., Marro, G.: Computing the maximum robust controlled invariant subspace. Systems and Control Letters 17(2), 131–135 (1991)
9. Conte, G., Perdon, A.M.: Systems over rings: Geometric theory and applications. Annual Reviews in Control 24, 113–124 (2000)
10. Conte, G., Moog, C., Perdon, A.M.: Algebraic Methods for Nonlinear Control Systems. Springer (2006)
11. De Persis, C., Isidori, A.: On the observability codistributions of a nonlinear system. Systems and Control Letters 40(5), 297–304 (2000)

12. De Persis, C., Isidori, A.: A geometric approach to nonlinear fault detection and isolation. IEEE Transactions on Automatic Control 46(6), 853–865 (2001)
13. De Persis, C., Isidori, A.: On the design of fault detection filters with game-theoretic-optimal sensitivity. International Journal of Robust and Nonlinear Control 12(8), 729–747 (2002)
14. Edelmayer, A., Bokor, J., Szigeti, F., Keviczky, L.: Robust detection filter design in the presence of time varying system perturbations. Automatica 33(3), 471–475 (1997)
15. Fiahlo, I., Balas, G.: Design of nonlinear controllers for active vehicle suspensions using parameter-varying control synthesis. Vehicle Systems Dynamics (1997)
16. Hammouri, H., Kinnaert, M., El Yaagoubi, E.: Observer-based approach to fault detection and isolation for nonlinear systems. IEEE Transactions on Automatic Control 44(10), 1879–1884 (1879)
17. Hermann, R., Krener, A.J.: Nonlinear controllability and observability. IEEE Transactions on Automatic Control AC-22(5), 728–740 (1977)
18. Isidori, A.: Nonlinear Control Systems. Springer (1989)
19. Kalman, R.E.: Contributions to the theory of optimal control. Boletin de la Sociedad Matematica Mexicana 5, 102–119 (1960)
20. Looye, G., Joos, H.G.: Design of robust dynamic inversion control laws using multi-objective optimization. In: AIAA Guidance, Navigation, and Control Conference, Montreal, Canada (2001)
21. Marcos, A., Balas, G.: Linear parameter varying modeling of the Boeing 747-100/200 longitudinal motion. In: AIAA Guidance, Navigation and Control Conference, pp. AIAA–01–4347. American Institute of Aeronautics and Astronautics (2001)
22. Malabre, M.: Generalized linear systems: geometric and structural approaches. Linear Algebra Appl. 122-124, 591–624 (1989)
23. Massoumnia, M.: A geometric approach to the synthesys of failure detection filters. IEEE Transactions on Automatic Control 31, 839–846 (1986)
24. Massoumnia, M., Verghese, G., Willsky, A.: Failure detection and identification. IEEE Transactions on Automatic Control 34, 316–321 (1989)
25. Morse, A.S.: Structural invariants of linear multivariable systems. SIAM J. Control 11, 446–465 (1973)
26. Morton, B., Enns, D., Zhang, B.Y.: Stability of dynamic inversion control laws applied to nonlinear aircraft pitch-axis models. Int. Journal Control 63, 1–26 (1996)
27. Nijmeijer, H.: Right invertibility for a class of nonlinear control systems: a geometric approach. Systems and Control Letters 7, 125–132 (1986)
28. Nijmeijer, H.: Invertibility of affine nonlinear control systems: a geometric approach. Systems and Control Letters 2, 163–168 (1991)
29. Nijmeijer, H., van der Schaft, A.J.: Nonlinear Dynamical Control Systems. Springer (1990)
30. Otsuka, N.: Generalized invariant subspaces and parameter insensitive disturbance-rejection problems with static output feedback. IEEE Transactions on Automatic Control 45, 1691–1697 (2000)
31. Silverman, L.M., Meadows, H.E.: Controllability and observability in time-variable linear systems. SIAM J. Control 5, 64–73 (1967)
32. Wei, J., Norman, E.: On the global representations of the solutions of linear differential equations as a product of exponentials. Proc. of the Amer. Math. Soc. 15, 327–334 (1964)
33. Wonham, W.M.: Linear Multivariable Control - A Geometric Approach, 3rd edn. Springer, New York (1985)
34. Zheng, Y., Cao, L.: Reduced inverse for controlled systems. Mathematics of Control Signals and Systems 6(4), 363–379 (1993)

Chapter 3
Bimodal and Linear Switched Systems

József Bokor and Zoltán Szabó

Abstract. The chapter considers some special topics related to controllability and stabilizability of linear switching systems. While providing a short overview on the most important facts related to the topic it is shown how fundamental role is played by the finite switching property in obtaining the controllability and stabilizability results. The (closed–loop) stabilizability problem of controlled linear switched systems is also revisited. It is shown that the completely controllable sampled switching system can be robustly stabilized (against disturbances and model uncertainties) with suitable linear feedbacks and a periodic switching strategy. A self contained treatment of the bimodal LTI problems is also provided pointing to the relevant structures of the problem. It is shown that for a certain class of bimodal systems controllability in case of closed–loop switching systems is equivalent with controllability of an open–loop switching system using nonnegative controls, i.e., to the controllability of a constrained open–loop switching system.

3.1 Introduction

Motivated by the need of dealing with physical systems that exhibit a more complicated behavior that those normally described by classical continuous and discrete time domains, hybrid systems have become very popular nowadays. In particular, there has been a relevant interest in the analysis and synthesis of so-called *switching systems* intended as the simplest class of hybrid systems.

A switching system is composed of a family of different (smooth) dynamic modes such that the switching pattern gives continuous, piecewise smooth trajectories. Moreover, we assume that one and only one mode is active at each time instant.

József Bokor · Zoltán Szabó
Computer and Automation Research Institute, Hungarian Academy of Sciences,
Kende u. 13-17, Budapest, H1111 Hungary
e-mail: {bokor,szaboz}@sztaki.hu

O. Sename et al. (Eds.): *Robust Control and LPV Approaches*, LNCIS 437, pp. 55–85.
DOI: 10.1007/978-3-642-36110-4_3

Controllability of switching systems has been investigated mostly for the case when arbitrary switching is possible (open–loop switching) and the objective is to design a proper switching sequence to ensure controllability or stability of (usually) piecewise linear systems, see [3], [63], [70], [75], or [57], for recurrent neural networks. In these investigations the control input set for the individual modes is assumed to be unconstrained.

Bimodal systems are special classes of switching systems, where the switch from one mode to the other one depends on the state (closed–loop switching). In the simplest case the switching condition is described by a hypersurface $\mathscr{C}$ in the state space. A fundamental achievement is that for a certain class of bimodal systems controllability question can be reduced to the problem of controllability of sign constrained open–loop switching system.

One of the most elementary constrained controllability problems is that of the single-input-single-output (SISO) linear time invariant (LTI) system, with nonnegative inputs, see [50] for details. The multi-input LTI case, i.e., a special sign constrained switching problem, was solved in [11] and [32], for further insights see [59], [47], [23]. Constrained controllability results for the linear time varying case with continuous right hand side can be found e.g., in [51].

From practical point of view it is important to know if controllability can be performed using a finite number of switchings. It is known that for the unconstrained case and for the constrained case when the small time controllability property holds or the dynamics is continuous the answer is affirmative, [36], [62], [34], moreover in all these cases there exist a bound for the number of switchings.

After recalling some fundamental results from geometrical control theory it is shown that if the system is globally controllable then one can always achieve controllability by applying only a finite number of switchings, moreover, as in the unconstrained situation, the number of necessary switchings is bounded. Despite the fact that linear switched systems are time varying nonlinear systems, their controllability and stabilizability properties can be described entirely in terms of the system matrices by using matrix algebraic manipulations. This property does not hold for general LTV systems.

For LTI systems $\dot{x} = Ax + Bu$ controllability is intimately related to stabilizability in that the former implies the later, moreover stabilizability can be achieved by applying a linear state feedback $u = Kx$, that can be computed relative easily. Similar result, with a suitable set of linear state feedbacks, is valid for the case when the inputs are sign constrained, see [52] and [33].

Stability issues of switched systems, especially switched linear systems, have been of increasing interest in the recent decade, see for example [18], [40], [39], [37], [44], [62]. In the study of the stability of switched systems one may consider switched systems governed by given switching signals or one may try to synthesize stabilizing switching signals for a given collection of dynamical systems. Concerning the first class a lot of papers focus on the asymptotic stability analysis for switched homogeneous linear systems under arbitrary switching (strong stability, robust stabilization), and provide necessary and sufficient conditions, see [8], [1], [45].

The requirement of (robust) stability imposes very strict conditions on the dynamics, e. g., all the subsystems must be stable or stabilizable. Even under this condition, one has, in general, further restrictions on the allowable switching frequency (dwell time), determined by the spectrum of the matrices, [67].

For strongly stabilizable linear controlled switching systems the feedback control always can be chosen as a "patchy", linear variable structure controller, see [8]. The control is defined by a conic partition $\mathbb{R}^n = \bigcup_{k=1}^{N} \mathscr{C}_k$ of the state space while on each cone $\mathscr{C}_k$ the feedback is linear, i. e., it is given by $u = F_k x$.

In the more general situation, when one has unstable modes, more severe conditions on the switching sequence have to be imposed. In this respect one of the most elusive problems is the switched stabilizability problem, i. e., under what condition is it possible to stabilize a switched system by properly designing autonomous (event driven) switching control laws. For autonomous switchings the vector field changes discontinuously when the state hits certain "boundaries". This problem corresponds to the weak asymptotic stability notion of the associated differential inclusions.

Based on the ideas presented in [46] it was proved that the (weak) asymptotic stabilizability of switched autonomous linear systems by means of an event driven switching strategy can be formulated in terms of a conic partition of the state space, see [41], [42]. This result can be seen as a generalization of the corresponding theorem for strong stability. However, in contrast to the strong stability results, the corresponding Lyapunov function is not always convex, see [9].

An extension of the fundamental LTI stabilizability results for the weak stabilizability of the class of completely controllable linear switching systems is given, where the control inputs might also be sign constrained, i. e., it is shown that a completely controllable linear switching system is closed–loop stabilizable, moreover, the stabilization can be performed by using a generalized piecewise linear feedback.

3.2 Linear Switched Systems

A switching system is composed of a family of different (smooth) dynamic modes such that the switching pattern gives continuous, piecewise smooth trajectories. We assume that one and only one mode is active at each time instant. During the last decade there has been a considerably interest in the analysis and synthesis of *linear switched systems*, intended as the simplest class of hybrid systems.

A lot of work has been done to address the fundamental questions of control theory – controllability, observability, stabilizability – that were reported in a series of papers, [38, 21, 73, 15, 44, 63] and monographs like [37, 62], just to list a few of them.

Controllability of switched systems has been investigated mostly for the case when arbitrary switching is possible (open–loop switching) and the objective is to design a proper switching sequence to ensure controllability or stability of

(usually) piecewise linear systems, see [3], [63], [70], [75], or [57] for recurrent neural networks. Usually the input set $\mathfrak{U}$ is assumed to be unconstrained, i.e., $\mathfrak{U} = \mathbb{R}^m$, however for certain systems, e.g., in process engineering applications where the inputs cannot be negative due to physical reasons, the sign constrained case $\mathfrak{U} = \mathbb{R}^m_+$ is more relevant.

For LTI systems the controllability question was entirely solved. Moreover there is a controllability condition that describes both the unconstrained and constrained problems, [32, 20]. It turns out that a condition of the same type can be also formulated for switching systems. The elaboration of the solution to the controllability problem gives an opportunity to revise the main tools applied to the investigation of linear switched systems and to reveal facts and relations that remain hidden in previous works. In the elaboration of the topic advanced techniques like the geometric control theory of [29, 22, 2], nonsmooth analysis and differential inclusions of [5, 68, 19, 53] met the more elementary techniques of [69].

General Considerations

Consider the class of (open-loop) linear switched[1] systems:

$$\dot{x}(t) = A(\sigma(t))x(t) + B(\sigma(t))u(t) \tag{3.1}$$

where $x \in \mathbb{R}^n$ is the state variable and $u \in \mathfrak{U}$ is the input variable. $\sigma : \mathbb{R}^+ \to \mathfrak{S}$ is a measurable switching function mapping the positive real line into $\mathfrak{S} = \{1, \cdots, s\}$, i.e., the matrices $A(\sigma)$ and $B(\sigma)$ are measurable. The input set might be unconstrained $\mathfrak{U} = \mathbb{R}^m$ or constrained $\mathfrak{U} = \mathbb{R}^m_+$.

A solution (Carathéodory) of (3.1) on an interval I is an almost everywhere differentiable function $\varphi(t) : I \to \mathbb{R}^n$ that satisfies (3.1) *a.e.* on I. A state $x \in \mathbb{R}^n$ is *controllable* at time t_0, if there exist a time instant $t_f > t_0$, a (measurable) switching function $\sigma : [t_0, t_f] \to \mathfrak{S}$, and a bounded measurable input function $u : [t_0, t_f] \to \mathfrak{U}$ such that $x(t_f; t_0, x, u, \sigma) = 0$. A state $x \in \mathbb{R}^n$ is *reachable* at time t_0, if there exist a time instant $t_f > t_0$, a switching function $\sigma : [t_0, t_f] \to \mathfrak{S}$, and a bounded measurable input function $u : [t_0, t_f] \to \mathfrak{U}$ such that $x(t_f; t_0, 0, u, \sigma) = x$. We will term as reachability set the set ($\mathscr{R}$) of points reachable from the origin, and as controllability set ($\mathscr{C}$) the set of points from which the origin is reachable.

Following classical lines, (3.1) is said to be *completely controllable*[2] if every point in the state space is reachable from any other point in the state space by using bounded measurable controls and a suitable switching function.

[1] The fact that the switching signal can be chosen and in particular, can be set to be a specific one, motivates that the term *switched* is preferred against *switching*.

[2] In [62] complete observability and reconstructibility are defined along classical lines as dual notions for complete reachability (controllability). Since these notions guarantees the possibility to recover the initial state only for some switching trajectories they does not cover the situation needed in practice. The requirement to reconstruct the state regardless the switching signal implies the complete observability of the individual modes. Therefore in this work we does not investigate problems related to this topic.

A *trajectory* of the switching system (3.1) will be defined as follows: let $x(t)$ be an absolutely continuous function. We say that $x(t)$ is a (admissible) trajectory of the system (3.1) on $[t_0,t_f]$ if there exists a finite subdivision $t_0 < t_1 < \cdots < t_{N-1} < t_N = t_f$ of the interval $[t_0,t_f]$, such that on each subinterval (t_{k-1},t_k) there exists an admissible function u_k such that one has $\dot{x} = A_k x + B_k u_k$.

The set of admissible inputs depends on the specific application: usually it is fixed to be the set of piecewise constant functions, but could be the set of sufficiently smooth functions, too. The notion of the trajectory excludes problematic situations from open– loop switching, like Zeno behavior, that might appear, however in closed–loop switching systems. In practical problems besides the left continuity of the switching signal it is often required that any time interval within which σ is constant is no less than a proper positive scalar $T_\delta > 0$, which is called the *dwell time*. Therefore it is an important issue how complete controllability by trajectories, i.e., using piecewise constant switching, is related to complete controllability by measurable switchings.

Switching Systems and Vector Fields

The concept of *control system* plays a central role in the geometric theory of nonlinear control. A control system is a collection $\mathfrak{F}$ of smooth vector fields depending on independent parameters $w = [w_1, \cdots, w_m] \in \mathfrak{W} \subset \mathbb{R}^m$, called control inputs, such that $w(t)$ belongs to a suitable class of real valued functions, called admissible controls, [2]. Usually it is supposed that the state space M is an n-dimensional real analytic manifold.

Associated with the control system $\mathfrak{F}$ denote by $\mathscr{A}_{\mathfrak{F}}(x,t)$ the set of all elements attainable from x at time t. For each $x \in M$, $\mathscr{A}_{\mathfrak{F}}(x) = \cup_{t\geq 0}\mathscr{A}_{\mathfrak{F}}(x,t)$. To a controlled nonlinear system $\dot{x} = f(x,u)$ can be associated in a natural way the collection of vector fields $V_f = \{f_u \,|\, u \in \mathfrak{U}\}$, that can be used, e. g., in a Lie algebraic treatment, quite suitable for unconstrained problems and small time local controllability problems[3].

An important object of the controllability study of nonlinear systems is the set of (positive) orbits[4] $\Phi^q_{\tau,x_0}(\omega)(T) = e^{f_{u_q}t_q} e^{f_{u_{q-1}}t_{q-1}} \cdots e^{f_{u_2}t_2} e^{f_{u_1}t_1} x_0$, where $e^{f_u t} x_0$ is the solution of the equation $\dot{\xi} = f_u(\xi)$, $\xi(0) = x_0$, and $\tau = (t_1, t_2, \cdots t_q)$, $t_i \geq 0$ with $T = \sum_{j=1}^q t_j$ while $\omega = (u_1, u_2 \cdots u_q) \in \mathfrak{U}^q$, $f_{u_i} \in \mathscr{F}$. Observe that an orbit can be interpreted as a possible trajectory corresponding to a switched system formed by the modes $\dot{x} = f_{u_i}(x)$. Starting from this idea, a switched system can be considered as a nonlinear polysystem of the form $\dot{x} = f(x(t), w(t))$, $x(0) = 0$ where in general, it is assumed that $x \in M$ and $f(.,w)$, $w \in \mathfrak{W}$ is an analytic (smooth) vector field on M. The benefit of this interpretation is that the controllability study of switched systems with unconstrained inputs can be placed in the framework of the nonlinear geometric control theory. The aim of this section is to show that the powerful techniques of

[3] A system is small-time locally controllable from the initial state x_0 if the reachable set from x_0 in time at most $T > 0$ contains x_0 in its interior for each $T > 0$, i.e., $x_0 \in \mathrm{int}\mathscr{A}_{\mathfrak{F}}(x_0,t)$ for all $t > 0$.

[4] For the notation and for additional details see, e. g., [29] and the Appendix.

the general theory provides an elegant and transparent tool which can be applied efficiently in the controllability study of switched systems.

We would like to decide (global) controllability by just examining the vector fields that define a control system without the necessity of obtaining solutions of any kind of the given system. It turns out that it is possible possible to "expand" the available vector fields, e.g., by convexification, without changing the system itself, obtaining equivalent descriptions of the same system.

To introduce more and more redundancy in this description – by enlarging the set of vector fields that describes the system – is very useful in deciding the controllability question. This goal can be achieved by using the procedure of Lie extension, sketched in the next section.

Lie Saturate

The Lie bracket of two vector fields f and g is denoted by $[f,g]$. Under the Lie bracket, and the pointwise addition, the space of all analytic vector fields on M becomes a Lie algebra; $Lie(\mathfrak{F})$ denotes the subalgebra generated by $\mathfrak{F}$. For each $q \in M$, $Lie_q(\mathfrak{F})$ is a subspace of T_qM, the tangent space of M at q. A set of vector fields $\mathfrak{F}$ on a connected smooth manifold M is called *bracket-generating* (full-rank) if $Lie_q\mathfrak{F} = T_qM$ for all $q \in M$.

Families of vector fields $\mathfrak{F}$ and $\mathfrak{G}$ are said to be (strongly) *equivalent* if $Lie(\mathfrak{F}) = Lie(\mathfrak{G})$ and $\overline{\mathscr{A}_{\mathfrak{F}}(q,T)} = \overline{\mathscr{A}_{\mathfrak{G}}(q,T)}$ for all $q \in M$ and for all $T > 0$, where the overbar denotes the closure of the sets. The Lie Saturate $LS(\mathfrak{F})$ of a family of vector fields $\mathfrak{F}$ is the union of families strongly equivalent to $\mathfrak{F}$.

In general it is difficult to construct the Lie saturate explicitly, however one can construct a completely ascending family of compatible vector fields – *Lie extension* – starting from a given set $\mathfrak{F}$ of vector fields. A vector field f is called compatible with the system $\mathfrak{F}$ if $\mathscr{A}_{\mathfrak{F}\cup f}(q) \subset \overline{\mathscr{A}_{\mathfrak{F}}(q)}$ for all $q \in M$. Since $LS(\mathfrak{F})$ is a closed convex positive cone in $Lie(\mathfrak{F})$, a possibility to obtain compatible vector fields is extension by convexification, see [29]: for $f_1, f_2 \in \mathfrak{F}$ and any nonnegative functions $\alpha_1, \alpha_2 \in C^\infty(M)$ the vector fields $\alpha_1 f_1 + \alpha_2 f_2$ is compatible with $\mathfrak{F}$. If $LS(\mathfrak{F})$ contains a vector space $\mathscr{V}$, then $Lie(\mathscr{V}) \subset LS(\mathfrak{F})$.

The importance of Lie extension is given by the following result, [2]:

Proposition 10. *If $\mathscr{F}$ is a bracket-generating system such that the positive convex cone generated by $\mathfrak{F}$, i.e.,*

$$cone(\mathfrak{F}) = \{ \sum_{i=1}^{k} \alpha_i f_i \,|\, f_i \in \mathfrak{F}, \alpha_i \in C^\infty(M), \alpha_i \geq 0, k \in \mathbb{N} \}$$

is symmetric, i.e., $cone(\mathfrak{F}) = cone(-\mathfrak{F})$, then $\mathfrak{F}$ is completely controllable.

Let us apply this result to the unconstrained situation: by constructing the Lie extension of the vector field $\mathfrak{F} = \{A_i x + B_i u \,|\, u \in \mathfrak{U}\}$, one can observe that $B_i u$ is

compatible with $\mathfrak{F}$, i.e., $B_i u \in LS(\mathfrak{F})$. Indeed, $B_i u \in \overline{co(\mathfrak{F})}$, since $B_i u = \lim_{\lambda\to\infty} \frac{1}{\lambda}(A_i x + \lambda B_i u)$. If there is a vector $v \in LS(\mathfrak{F})$ such that $-v \in LS(\mathfrak{F})$, then $\pm A_i v \in LS(\mathfrak{F})$, too, see [29].

Then for the unconstrained case a necessary and sufficient condition for controllability can be formulated as:

Proposition 11. *The unconstrained switching system is controllable if and only if*

$$rank\ \mathscr{R}_{\mathscr{A},\mathscr{B}} = n, \tag{3.2}$$

i.e., the multivariable Kalman rank condition*, holds, where the subspace $\mathscr{R}_{\mathscr{A},\mathscr{B}}$ is defined as*

$$\mathscr{R}_{(\mathscr{A},\mathscr{B})} = span\left\{\prod_{j=1}^{J} A_{l_j}^{i_j} B_k \,|\, k = 1,\cdots,s\right\} \tag{3.3}$$

where $J \geq 0, l_j \in \{0,\cdots,s\}, i_j \in \{0,\cdots,n-1\}$. Moreover, if one considers the finitely generated Lie-algebra $\mathscr{L}(A_0,\ldots,A_s)$ which contains $A_0,\ldots,A_s$, and a basis $\hat{A}_1,\ldots,\hat{A}_K$ of this algebra, then

$$\mathscr{R}_{\mathscr{A},\mathscr{B}} = \sum_{k=0}^{s}\sum_{n_1=0}^{n-1}\cdots\sum_{n_K=0}^{n-1} Im\,(\hat{A}_1^{n_1}\ldots\hat{A}_K^{n_K}B_k). \tag{3.4}$$

Controllability of unconstrained switched systems can be determined based on the system matrices only. As an early contribution of the author to the field this controllability result was derived in [60] by using different, matrix Lie algebraic, techniques. In that context it was also stressed that the subspace $\mathscr{R}_{\mathscr{A},\mathscr{B}}$ is the minimal subspace invariant for all of the A_is containing the subspace $\mathscr{B} = \cup_{i=1}^{s} ImB_i$, see e.g., [6]. Using this fact one can obtain a controllability decomposition analogous to the corresponding LTV result.

Further results on how linear switched systems can be related to linear time varying systems are presented in the next section. It is also stressed that for controllable systems the condition on the finiteness of the switching numbers can be relaxed by admitting merely measurable switching rules. One of the main technical benefit of this fact is that it permits the use of nonsmooth analysis (differential inclusions) without the additional condition of piecewise continuity, required by the concept of trajectory, of the switching rules. This property will be exploited later, in the study of controllability with sign constrained control inputs.

3.2.1 Finite Number of Switchings, Sampling

Let us denote by $F_w^t x_0$ the solution of the equation $\dot{\xi} = f_w(\xi)$, $\xi(0) = x_0$ on the interval $[0,t]$. Then for a given vector field $\mathfrak{F}$ one can consider the associated trajectories (positive orbits), i.e., $\Phi_{\omega,\tau}^{q,T}(x_0) := F_{w_q}^{t_q} F_{w_{q-1}}^{t_{q-1}} \cdots F_{w_2}^{t_2} F_{w_1}^{t_1} x_0$ with $\tau = (t_1, t_2, \cdots t_q)$, $t_i \geq$

0, $T = \sum_{j=1}^{q} t_j$ and $f_{w_i} \in \mathfrak{F}$ corresponding to the sequence of piecewise constant controls $\omega = (w_1, w_2 \cdots w_q) \in \mathfrak{W}^q$.

For a switched linear system $f_{w_i}(x) = A_{s_i}x + B_{s_i}u_i$, with $w_i = (s_i, u_i)$. We will suppress the switching sequence $\sigma = (s_1, s_2, \cdots, s_q)$ from the notation and denote the flow by $\Phi_\tau^q x_0$ for fixed $\mu = (u_1, u_2, \cdots, u_q)$ and by $\Phi_\mu^q x_0$ for fixed τ.

A point $y \in M$ is called *normally reachable* from an $x \in M$ if there exist a flow such that $\Phi_{\bar\tau}^q x = y$ and the mapping $\tau \in \mathbb{R}_+^q \to \Phi_\tau^q(x)$, which is defined in an open neighborhood of $\bar\tau$, has rank $n = \dim M$ at $\bar\tau$. The system is *normally controllable* if y is normally reachable from x for every $x, y \in M$.

Proposition 12. *If the switching system (3.1) is globally controllable than it is also globally controllable by using piecewise constant switching functions, i.e., using only a finite number of switchings.*

Moreover, there exist a bound for the necessary number of switchings, that depends only on the system matrices and $\mathfrak{U}$. There exist a universal (finite) switching sequence σ such that the time varying system $\dot x = A(\sigma)x + B(\sigma)u$ is globally controllable.

Remark 3. *The content of Proposition 12 is that one can concentrate on the global controllability problem in general, i.e., admitting measurable controls, which is a common setting for studying controllability and the existence of nice controls (e.g. piecewise constant, non–Zeno) is automatically guaranteed.*

Note that for a fixed $r > 0$ by taking sufficiently large but fixed inputs it is possible to reach all the points of the ball having radius r by controlling the system only with the individual time length t_i of the switching sequence. Actually all $\mathbb{R}^n$ is reachable by having only a finite set of controls and a periodic application of the sequence σ with suitable time instances τ_k. (It is a sort of a bang–bang property.)

In the definition of normal reachability the control input sequence μ is fixed while the switching times may vary in a certain neighborhood of τ. It turns out that the rank of the analogous map $\mu \in \mathfrak{U}^N \to \Phi_\mu^N(x)$ is also significant and it is closely related to the controllability of the sampled system, in general, for details see [54, 58, 56]. A point $y \in M$ will be called called *full rank reachable* from an $x \in M$ if there exist a flow such that $\Phi_{\bar\mu}^N x = y$ and the mapping $\mu \in \mathfrak{U}^N \to \Phi_\mu^N(x)$, which is defined in an open neighborhood of $\bar\mu$, has rank $n = \dim M$ at $\bar\mu$.

Proposition 13. *For the globally controllable linear switching system (3.1) for arbitrary point pairs (x, y) one has that y is full rank reachable from x. Moreover, every point pair can be joined in a full rank reachable way by using the same sequence (σ and τ fixed).*

The next small example illustrates the difference between the concept of "time topology" related to $\Phi_\tau^q(x)$ and the "input topology" related to $\Phi_\mu^q(x)$ – see [55] for the terminology.

Example: *Let us consider the switched system defined by the modes* $A_1 = \begin{bmatrix} 0 & 1 \\ 0 & 0 \end{bmatrix}$, $b_1 = 0$ *and* $A_2 = 0, b_2 = \begin{bmatrix} 0 \\ 1 \end{bmatrix}$, *respectively.*

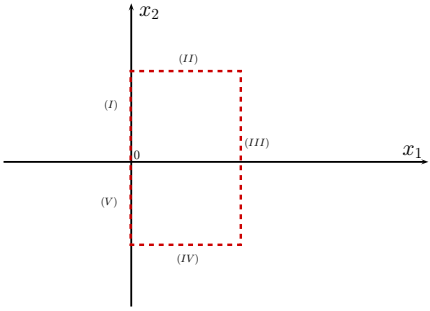

Fig. 3.1 The flow $\Phi_\tau^5(0)$

The corresponding flows are $F_1^t(x) = \begin{bmatrix} 1 & t \\ 0 & 1 \end{bmatrix} x$ *and* $F_{2,u}^t(x) = x + tu \begin{bmatrix} 0 \\ 1 \end{bmatrix}$.

It follows that for any $u > 0$ *and* $t > 0$ *with the switching sequence* $\sigma = (2,1,2,1,2)$*, input sequence* $\mu = (u,0,-2u,0,u)$ *and time sequence* $\bar{\tau} = (t,t,t,t,t)$ *the flow*

$$\Phi_\tau^5(0) = F_{2,u}^{t_5} \circ F_1^{t_4} \circ F_{2,-2u}^{t_3} \circ F_2^{t_2} \circ F_{2,u}^{t_1}(0) = \\ = t_1 u \begin{bmatrix} t_2 + t_4 \\ 1 \end{bmatrix} - 2t_3 u \begin{bmatrix} t_4 \\ 1 \end{bmatrix} + t_5 u \begin{bmatrix} 0 \\ 1 \end{bmatrix}$$

has full rank at $\bar{\tau}$ *with* $\Phi_{\bar{\tau}}^5(0) = 0$.

For any $t > 0$ *with the switching sequence* $\sigma = (2,1,2)$*, input sequence* $\mu = (u_1,0,u_2)$ *and time sequence* $\tau = (t,t,t)$ *the flow*

$$\Phi_\mu^3(x) = F_{2,u_2}^t \circ F_2^t \circ F_{2,u_1}^t(0) = \begin{bmatrix} 1 & t \\ 0 & 1 \end{bmatrix} x + \begin{bmatrix} t^2 & 0 \\ t & t \end{bmatrix} \begin{bmatrix} u_1 \\ u_2 \end{bmatrix}$$

has full rank at any $\bar{\mu}$ *with* $\Phi_{\bar{\mu}}^3(x) = y$ *(*$\bar{\mu} = (0,0)$ *for x=y=0).*

Observe that in the input topology, i.e., for the discretized system, the design problem is linear in the unknown variables. This fact motivates that in the investigations of linear switched systems the usage of this topology is preponderant.

From Proposition 13 it is immediate that for sufficiently small sampling times the sampled system is also completely controllable – which is already known from the general theory – which is quite involved in this respect, see e.g., [54, 48].

In what follows a more constructive proof of Proposition 13 will be presented: actually the result is a consequence of the similar fact that holds for the LTI systems, i.e., for the minimal A invariant set containing $\mathscr{V}$ $(< A, \mathscr{V} >)$ for almost all $t \in \mathbb{R}$ one has

$$< A, \mathscr{V} > = < e^{At}, \mathscr{V} > . \tag{3.5}$$

The content of the assertion is that there is a switching sequence σ and times τ such that one has

$$\prod_{i=1}^{N} \bar{A}_{s_i} x_o + \mathscr{C}_\tau^\sigma u = x_f \tag{3.6}$$

where $u = [u_1^T, \ldots, u_N^T]^T$, the l^{th} column of $\mathscr{C}_\tau^\sigma$ is $\bar{A}_{s_N} \cdots \bar{A}_{s_{l+1}} B_{s_l}$ with $(\bar{A}_i, \bar{B}_i)$ corresponding to the t_i sampled linear system (A_i, B_i) and with $\bar{A}_{s_{N+1}} = \mathbb{I}$ such that the matrix $\mathscr{C}_\tau^\sigma$ is of full rank. Let us denote by $\bar{A}_\sigma = \prod_{i=1}^{N} \bar{A}_{s_i}$.

To obtain the constrained result let us consider a point that is full rank reachable from the origin. Such a point clearly exists, e.g., $z = \mathscr{C}_{\tau_1}^{\sigma_1} e$ from (3.6), the vector e having ones for its components. However, by controllability, the origin can be reached from the point z by using a finite switching sequence, say $(\sigma_2, \tau_2, \tilde{u}^{(2)})$. By joining these two finite sequences one has that an open neighborhood of the origin is full rank reachable from the origin. Since the reachability set $\mathscr{R}_\sigma$ is a pointed cone that contains a ball it follows that $\mathscr{R}_\sigma = \mathbb{R}^n$.

It is instructive to detail these ideas: in the first step one can build a sequence such that $\mathscr{C}_{\tau_1}^{\sigma_1}$ is of full rank and $\bar{A}_{\sigma_2} \mathscr{C}_{\tau_1}^{\sigma_1} e + \mathscr{C}_{\tau_2}^{\sigma_2} \tilde{u}^{(2)} = 0$. Moreover, the equation $\bar{A}_{\sigma_2} \bar{A}_{\sigma_1} x_0 + \bar{A}_{\sigma_2} \mathscr{C}_{\tau_1}^{\sigma_1} u^1 = x_f$ has an unconstrained solution $u^{(1)}$ for arbitrary (x_0, x_f). Then for sufficiently large λ the components of $u_c^1 = u^1 + \lambda e$ are all nonnegative, e.g., for $\lambda = \max\{|u_i^1| \,|\, u_i < 0\}$, hence $\bar{A}_{\sigma_2} \bar{A}_{\sigma_1} x_0 + \bar{A}_{\sigma_2} \mathscr{C}_{\tau_1}^{\sigma_1} u_c^1 + \lambda \mathscr{C}_{\tau_2}^{\sigma_2} \tilde{u}^{(2)} = x_f$. As a consequence, for both cases there is a switching sequence σ and time sequence τ such that one has (3.6) with $u \in \mathfrak{U}^N$.

The construction is illustrated through the following small example:

Example: *Let us consider the switched systems described by the two modes:*

$$A_1 = \begin{bmatrix} 0 & 1 \\ -1 & 0 \end{bmatrix},\ b_1 = 0, \quad \textit{and} \quad A_2 = 0,\ b_2 = \begin{bmatrix} 1 \\ 0 \end{bmatrix}.$$

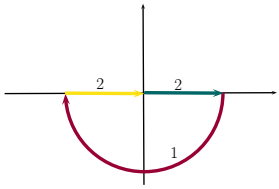

Fig. 3.2 Time topology

The flow corresponding to the time topology is generated by the switching sequence $\sigma = (2,1,2)$ and fix input sequence $w = (u_1, 0, u_2)$, respectively:

$$x_f = \begin{bmatrix} \cos t_2 & \sin t_2 \\ -\sin t_2 & \cos t_2 \end{bmatrix} x_0 + \begin{bmatrix} \cos t_2 & \sin t_2 \\ -\sin t_2 & \cos t_2 \end{bmatrix} \begin{bmatrix} t_1 \\ 0 \end{bmatrix} u_1 + \begin{bmatrix} t_2 \\ 0 \end{bmatrix} u_2$$

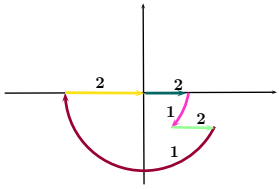

Fig. 3.3 Input topology

The flow corresponding to the input topology is generated by the switching sequence $\sigma = (2,1,2,1,2)$ *and fixed switching time sequence* $\tau = (\sqrt{2}, \frac{\pi}{4}, \sqrt{2}, \pi - \arctan(1/3), \sqrt{10})$*:*

$$x_f = \bar{A}x_0 + \bar{A}\begin{bmatrix} 1 & \sqrt{2} \\ -1 & 0 \end{bmatrix}\begin{bmatrix} u_1 \\ u_2 \end{bmatrix} + \begin{bmatrix} \sqrt{10} \\ 0 \end{bmatrix} u_3,$$

where $\bar{A} = \begin{bmatrix} -0.9487 & 0.3162 \\ -0.3162 & 0.9487 \end{bmatrix}$*. Accordingly, the full rank matrix* $\mathscr{C}_\tau^\sigma$ *is given by*

$$\mathscr{C}_\tau^\sigma = \begin{bmatrix} -1.2649 & -0.9487\sqrt{2} & \sqrt{10} \\ -1.2649 & -0.3162\sqrt{2} & 0 \end{bmatrix}.$$

Thus we obtain a generalization of Theorem 1 from [76] derived for positively controlled discrete LTI systems:

Corollary 1. *The sign constrained linear switching system* (3.1) *is completely controllable if and only if there exist* $\sigma = (\sigma_1, \sigma_2)$ *and* $\tau = (\tau_1, \tau_2)$

- $\mathscr{C}_{\tau_1}^{\sigma_1}$ *has full rank (i.e. the unconstrained linear switching system is completely controllable)*
- *equation* $\bar{A}_{\sigma_2}\mathscr{C}_{\tau_1}^{\sigma_1}u^1 + \mathscr{C}_{\tau_2}^{\sigma_2}u^{(2)} = 0$ *has a solution such that* u^1 *is positive and* u^2 *is nonnegative.*

Corollary 2. *For every completely controllable linear switching system* (3.1) *the sampled discrete–time system is also completely controllable for suitable sampling rates.*

As a consequence one has the following embedding/restriction, see [60] for further details:

Corollary 3. *For every completely controllable linear switching system* (3.1) *one can associate – not necessary a unique – completely controllable periodic linear time varying system* $\dot{x} = A(t)x + B(t)$*.*

One can relate this result with c-exitedness. Linear switched systems are c-excited, i.e., there is a switching sequence and corresponding switching times such that the

resulting time varying system will be c-excited. This fact explains from another point of view why controllability of linear switched systems can be decided by a multivariate rank condition.

The switching sequence of Proposition 13 can be determined relative easily. The non uniqueness comes from the fact that one has more switching sequences σ such that $\mathscr{R}_\sigma = \mathbb{R}^n$. For discrete time systems – with nonsingularA_i matrices – the core of the solution is to determine a sequence $\sigma = (s_1, \ldots, s_N)$ such that the matrix $\mathscr{C}_\sigma$ has rank equal to n where

$$\mathscr{C}_\sigma = \left[A_{s_N} \cdots A_{s_2} B_{s_1} \ \ldots \ A_{s_N} B_{s_{N-1}} \ B_{s_N}\right]. \tag{3.7}$$

For the continuous time case one can use the matrices of the zero-older hold discretized systems instead. Actually this step can be skipped because the algorithms instead of doing a blind search based on (3.7) uses the corresponding invariant subspaces. Different techniques exists to determine such sequences, for details see e.g. [72, 28, 27].

However it is an open question that for a given controllable linear switched system what is the sequence σ containing the minimal number of switches (of minimal length) such that $\operatorname{rank}\mathscr{C}_\sigma = n$. It is obvious that performing a search on a finite, but possible very big, set such a sequence can be obtained. The point is if there exist a characterization of the "optimal" sequence that would facilitate to find it efficiently. To illustrate the idea: for the multi input LTI system (A,B) the controllability indices shows where the switch in the "input" direction (actuator) should be performed; these indices can be determined by a suitable ranking of the vectors $A^k b_j$ and a basis selection procedure, see [69]. Such a transparent algorithm to determine the extended "controllability indices" is missing yet. These problems are significant for the control synthesis problems, e. g., stabilizability, which will be detailed in the next part of the chapter.

Controllability of linear switched systems was an intensively researched area, thus, besides our approach, the multivariable Kalman rank condition was obtained in a series of other papers using algebraic techniques, see e.g. [61, 63, 74, 71]. These papers basically uses the identity formulated in (3.5). The equivalence of the controllability of the continuous time system and the discrete time system obtained by sampling, however, was not realized in these works.

A contribution of the chapter to this topic was to observe and exploit this equivalence which, together with the invariance property of $\mathscr{R}_{\mathscr{A},\mathscr{B}}$, provides a common framework for the study of discrete-time and continuous-time switched systems. This property was intensively used in the stabilizability study of these systems.

Relation (3.4) can be obtained by using the general differential geometric approach, see e.g. [65, 14, 48] or equivalently the geometric control theory of [29]. We do not insist further in this direction. The main reason to abandon the technique based on the vector field description is that it is hard to obtain useful conditions for complete controllability for switched systems with sign constrained inputs, see e.g.

[10] for further details. A result that gives a necessary and sufficient condition for the small time controllability, i.e., controllability in an arbitrary small time, of the constrained switching system and uses Lie algebraic ideas is [66] and [34]. These results are quite restrictive, since small time controllability requires that the convex cone generated by B_i contain a subspace, i.e., $\overline{co}(\cup_{i=1}^{s} B_i) - \overline{co}(\cup_{i=1}^{s} B_i) \neq \emptyset$.

These observations motivates the necessity to search for other methods in order to obtain a useful algorithm that might test controllability in the sign constrained case. This will be done in the next section.

3.3 Linear Switched Systems with Sign Constrained Inputs

In practical applications there are often constrains that are imposed to the control input of the systems. The most widely studied case is when the inputs are constrained to a ball of given radius (bounded inputs). The obstruction caused by this type of constraint to (global) controllability is revealed by the equation (3.6): it is immediate that we always have both (small time) local reachability and (small time) local controllability in a neighborhood of the origin, however, in general it is not possible to extend this property to the entire state space, i.e., the system is not globally controllable, in general.

The case when the inputs are sign constrained is more difficult. It differs from the bounded input constraint in that even (small time) local controllability does not hold, in general, the system might be globally controllable. As an example, consider the switched system with two modes $\dot{x} = u$ and $\dot{x} = -u$, with $u \geq 0$. It is not hard to figure out that the system is globally controllable, see Figure 3.4 – for illustration purposes the points x_0, x_f from the line are slightly misplaced.

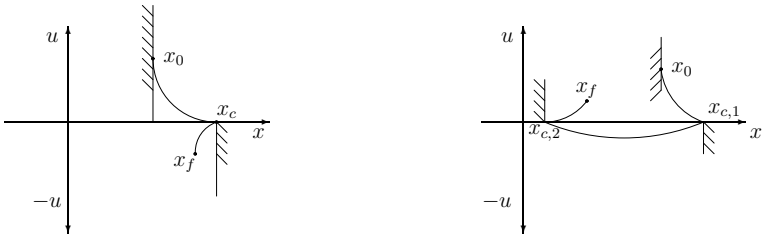

Fig. 3.4 From the given point the shaded area cannot be reached directly

This fact explains why the usual differential-geometric (Lie algebraic) techniques fail in obtaining useful controllability conditions. As in the previous chapter our goal is to decide controllability by just examining the vector fields that define a control system without the necessity of obtaining solutions of any kind of the given system.

Differential Inclusions

By the Filippov–Ważewski relaxation theorem the solution set defined by (3.1) is dense in the set of relaxed solutions, i.e., the solutions of the differential inclusion whose right hand side is the convex hull of the original set valued map, see e.g., [5]. This implies that the corresponding attainable sets coincides. Hence, instead of (3.1) one can consider the controllability problem associated to the convexified differential inclusion $\dot{x} \in \mathscr{A}_c(x)$, where $\mathscr{A}_c(x) = \sum_{i=1}^{s} \alpha_i (A_i x + B_i u)$ and $\alpha_i \geq 0$ and $\sum_{i=1}^{s} \alpha_i = 1$.

Generalization of the LTI systems, which maintains some fundamental properties of the class, is the concept of convex processes. A closed convex process A is a set-valued map whose graph is a closed convex cone and that it is strict if its domain is the whole space. With a strict closed convex process A one can associate the Cauchy problem for the differential inclusion: $\dot{x}(t) \in A(x(t)),\ x(0) = 0$, for details see [5]. In this framework the class of LTI systems with sign (cone) constrained inputs: $\dot{x} \in \mathscr{A}(x) = \{Ax + \mathfrak{C}\}$, with $\mathfrak{C} = \mathbb{R}^m_+$ can be naturally cast and a fundamental controllability result was obtained, [20], that contains result of Kalman, [30], for the unconstrained case and also the results reported in [11] and [32] for the constrained input case.

Let us consider the differential inclusion $\dot{x} \in F(x), x(0) = \xi$ and the corresponding reachable set $\mathscr{R}^T(\xi) = \{x(T) \,|\, x(0) = \xi, x \text{is a solution}\}$. If F has nonempty, compact, convex values and is locally Lipschitz then by using the Euler discretization of the inclusion one has $\mathscr{R}^T(\xi) = \lim_{N\to\infty}(I + \frac{T}{N}F)^N(\xi) := [ExpF](T\xi)$, where the limit is in the sense of Kuratowski, for definitions and details see [68].

Extending this result, Proposition 2 of [12] shows that for a positively homogeneous inclusion, $(F(\alpha) = \alpha F(x),\ \alpha > 0)$, one has

$$[ExpF](t\xi) = \xi + \sum_{k=1}^{\infty} \frac{t^k}{k!} F^k(\xi), \tag{3.8}$$

where $F^k = F \circ F \circ \cdots \circ F$. This exponentiation formula was the main tool in obtaining the controllability result of sign constrained linear switched systems that will be detailed in the next section.

3.3.1 Controllability Analysis

Even the differential inclusion related to a linear switched system (3.1) does not define a convex process, a controllability result of the same type still remains valid:

Proposition 14. *The following conditions are equivalent:*

a) the switching system $\dot{x} = A_i x + B_i u, i \in \{1, \cdots, s\}, \quad u \in \mathfrak{U}$ *is controllable,*
b) for the associated differential inclusion $\dot{x} \in A_c(x)$ *one has* $A_c^k(0) = (-A)_c^k(0) = \mathbb{R}^n$ *for some* $k \geq 1$.

Introducing the notation $\mathbf{co}\{V_j\}$ for the convex hull of the subsets $V_j \subset \mathbb{R}^n$, then the sets $A_p^k := A_c^k(0)$ and $A_m^k := (-A)_c^k(0)$ can be computed using the following algorithm:

General Controllability Algorithm (GCA):

$$\mathbf{U} = \mathbf{co}\{B_i\mathfrak{U} \,|\, i = 1, \cdots, s\} \tag{3.9}$$

$$A_p^1 = \mathbf{U}, \quad A_m^1 = -\mathbf{U}, \tag{3.10}$$

$$A_p^{k+1} = \mathbf{co}\{A_i A_p^k + B_i\mathfrak{U} \,|\, i = 1, \cdots, s\}, \tag{3.11}$$

$$A_m^{k+1} = \mathbf{co}\{-A_i A_m^k - B_i\mathfrak{U} \,|\, i = 1, \cdots, s\}. \tag{3.12}$$

Example 1. *To illustrate the results let us consider the system*

$$A_1 = 0, B_1 = \begin{bmatrix} 0 \\ 1 \\ 1 \end{bmatrix}, \quad A_2 = \begin{bmatrix} 0 & 1 & 0 \\ -1 & 0 & 0 \\ 0 & 0 & 0 \end{bmatrix}, B_2 = 0, \quad A_3 = \begin{bmatrix} 0 & 1 & 0 \\ 0 & 0 & 0 \\ -1 & 0 & 0 \end{bmatrix}, B_3 = 0.$$

Applying the algorithm one can find that $A_p^k = A_m^k$ with $k = 4$, i.e., the system is globally controllable.

3.4 Stabilizability of Completely Controllable Linear Switched Systems

The concept of stabilizability is related to the property that there exists a state dependent control law (closed-loop) which, starting from any initial state, asymptotically drives the system into the equilibrium (the origin). This concept expresses the requirements imposed by practical applications to an automatic control solution and it is a corner-stone of every control design algorithm.

For controlled LTI and LTV systems controllability is intimately related to stabilizability in that the former implies the later, moreover stabilizability can be achieved by applying a linear state feedback. Similar result, with a suitable set of linear state feedbacks, is valid for LTI systems when the inputs are sign constrained, see [52] and [33].

For general nonlinear systems, however, there is no such result. Controllability ensures that from every initial state the system can be driven to the origin in finite time by using a suitable control. It is not known, in general, whether among these controls there exists at least one which is uniformly bounded by the norm of the initial condition. If this property holds, the system is called *asymptotically controllable*, and despite its name the concept is related to stabilizability rather than controllability, see [17]. Moreover, it turns out that asymptotic controllability is not only equivalent to stabilizability but also guarantees – under fairly mild conditions – the existence of a not too pathological feedback and control Lyapunov function, see [4], [31], [49].

Unfortunately, these results are hard to be applied in practice to construct directly the required feedback, i.e., to obtain the closed–loop switching strategy and necessary control inputs or even to infer that the control inputs are given by linear feedbacks. Concerning linear switched systems, they are essentially nonlinear, even the individual dynamics are linear. This fact makes the stabilizability problem of linear switched systems nontrivial.

Asymptotic Controllability and Weak Stabilizability

The zero solution of the differential inclusion $\dot{x} \in A_c(x)$ is called asymptotically weakly stable if there exists a solution $x(t)$ such that for any $\varepsilon > 0$ there is a $\delta > 0$ and $\Delta > 0$ such that if $||x(0)|| < \delta$ then $||x(t)|| < \varepsilon$ holds for all $t \geq 0$ and if $||x(0)|| < \Delta$ then $\lim_{t\to\infty} x(t) = 0$ holds.

In order to prove stabilizability of completely controllable linear switching systems it is sufficient to show that they are globally asymptotically controllable.

Lemma 4. *A completely controllable linear switching system is globally asymptotically controllable.*

Proposition 15. *The completely controllable linear switching system (3.1) is closed–loop stabilizable.*

3.4.1 Stabilizability by Generalized Piecewise Linear Feedback

Given an autonomous linear switching system

$$\dot{x} = A_i x, \quad i \in S$$

it is a nontrivial task to decide if the system is (weakly) stabilizable or not, in general. There are only a few sufficient conditions that guarantee stabilizability and provide a relatively simple closed-loop switching strategy. One such situation is when the convex hull of the system matrices contains a stable (Hurwitz) matrix, i.e., when there are $\alpha_i > 0$, $\sum_{i=1}^{s} \alpha_i = 1$ such that $\sum_{i=1}^{s} \alpha_i A_i$ is stable.

For the non-autonomous case with unconstrained inputs it is known that if the sum of the individual controllability subspaces gives the whole state space, then there are linear state feedbacks $u = K_i x$ such that the resulting linear switching system

$$\dot{x} = (A_i + B_i K_i)x, \quad i \in S$$

is stable with a suitable closed–loop switching strategy, see [62]. It is not hard to figure out that the required condition is sufficient to guarantee that for any convex combination $\alpha_i > 0$, $\sum_{i=1}^{s} \alpha_i = 1$ there exist feedbacks K_i such that $\sum_{i=1}^{s} \alpha_i (A_i + B_i K_i)$ is stable.

As it can be concluded through simple examples, see [62], there are completely controllable switching systems that are not stabilizable by merely applying a single linear state feedback for the individual subsystems. However, as it will be shown in this Section, if the number of linear feedbacks is increased, one can obtain a set of autonomous linear systems that are (weakly) stabilizable.

For a given set of non–autonomous (controlled) linear switched systems (3.1) we call *Generalized Piecewise Linear Feedback Stabilizability* (GPLFS) the problem of finding a closed-loop switching strategy with

- suitable linear feedbacks $u_i = K_{l_i} x, \quad i \in S$
- a switching law $\kappa(x) \in S, x \in \mathbb{R}^n$

that (weakly)stabilizes the system.

The reasoning behind introducing the concept of generalized piecewise linear feedback stabilizability is to separate the task of finding a suitable switching strategy and that of finding suitable control inputs with low complexity that stabilizes the system in closed–loop.

The main idea is to substitute the original stabilizable non-autonomous system by a stabilizable autonomous linear switched system that might contain more modes then the original one, by applying as control inputs a number of suitable static linear control feedbacks.

Proposition 16. *The completely controllable linear switching system* (3.1) *is generalized piecewise linear feedback stabilizable.*

Remark 4. *Complete controllability of the vector field $\mathscr{F}$ has a very intuitive geometrical background. Since the solutions of a linear autonomous differential equations realizes some rotations and dilations/compressions in $\mathbb{R}^n$, it means that for a given point pair (y,z) it is possible to select a finite set of feedbacks such that the resulting set of autonomous systems transform the point y into z for a suitable (finite) switching sequence.*

Concerning the switching strategy the existence of the suitable closed–loop switching rule is guaranteed by the general results for nonlinear globally asymptotically controllable systems, [49]. However, for nonautonomous switching systems with unconstrained controls slightly more can be asserted.

In [43] it was shown that the existence of an asymptotically stabilizing switching strategy (without sliding motion) of an autonomous linear switched system implies the existence of a conic partition based switching law which globally asymptotically stabilizes the closed–loop switching system. The control is defined by a conic partition $\mathbb{R}^n = \bigcup_{l=1}^{L} \mathscr{C}_l$ of the state space while on each cone $\mathscr{C}_l$ the system defined by $A_{i_l} + B_{i_l} K_l$ with $i_l \in S$ is active.

Remark 5. *Since for linear autonomous switching systems asymptotical stability and exponential stability are equivalent, see [62], Proposition 15 shows that completely controllable linear switching systems with (unconstrained input) are exponentially stabilizable.*

The sign constrained case is more delicate. The resulting autonomous systems correspond to certain regions of the state space, i.e., the resulting switching system is an autonomous state constrained linear switching system. Therefore the result from [62] is not applicable directly and the case needs further investigation.

Remark 6. *Proposition 16 guarantees the generalized piecewise linear feedback stabilizability but does not give a method to compute such feedbacks. However – for the unconstrained input case – the property of complete controllability is feedback invariant. It is known that any controllable unconstrained multi–input linear switching system can be changed into a controllable single–input system via suitable non–regular state feedbacks, see [62]. Moreover, the controllable single–input system can be put into the form* $(A_1, b_1), A_2, \cdots, A_s$. *Proposition 15 guarantees that by these transformations not only controllability but also stabilizability is preserved. Hence one can obtain a switching system with a reduced complexity for which one might find suitable stabilizing feedbacks more easily, e.g. the resulting BMI or LMI equations in finding suitable piecewise quadratic Lyapunov functions will be simpler.*

Besides the fact that stabilization schemes with state depending switching rules are hard to construct these schemes might not be robust against the quantization errors introduced by a sampled implementation.

From a more general perspective the difficulties encountered at the feedback stabilization of switching systems are not surprising. For continuous–time control systems the existence of smooth Lyapunov functions implies that the differential inclusion satisfy a certain covering condition – an extension of Brockett's "covering condition" from continuous feedback stabilization theory, [16]. However, robustness of the feedback scheme and the existence of a smooth control Lyapunov function are closely related, see [35]. Moreover, in general, stabilizable switched linear systems does not have a convex Lyapunov function, see [9].

In contrast to the pure continuous–time approach, discrete–time asymptotic controllability implies smooth control Lyapunov function. Moreover, robustness can be induced via a sample–and–hold control. For details see [31].

The results of the previous section gives an opportunity to verify these claims for the class of unconstrained linear switching systems (3.1).

By choosing a nonsingular Schur-stable matrix A_d, one can explicitly construct the inputs that stabilize the time–varying systems obtained by a periodic repetition of the sequence σ defined in Proposition 13 by choosing the sequence of inputs as follows:

$$u^{x_0} = (\mathscr{C}_\tau^\sigma)^\dagger (A_d - \bar{A}_\sigma) x_0, \tag{3.13}$$

where $M^\dagger$ denotes a generalized inverse of M. Considering linear feedbacks, i.e., the closed-loop matrix $A_c = \prod_{i=1}^{N} (\bar{A}_{s_i} + \bar{B}_{s_i} K_i)$, one has $A_d = A_c$ provided that the system

$$\tilde{K}_i = K_i \prod_{j=1}^{i-1} (\bar{A}_{s_i} + \bar{B}_{s_i} K_i) \tag{3.14}$$

is solvable for $\tilde{K}_i = P_i(\mathscr{C}_\tau^\sigma)^\dagger (A_d - \bar{A}_\sigma)$ with P_i the projection that gives the i^{th} input from (3.13). This is equivalent with the assertion that the resulting feedback sequence is such that $\bar{A}_{s_i} + \bar{B}_{s_i} K_i$ is nonsingular. It is not true, in general, that for an arbitrary nonsingular A_d (3.14) always has a solution. Despite this fact there always exist feedback gains such that A_c is a (nonsingular) Schur matrix.

Observe that the number of modes needed for the stabilization is bounded by the length of the switching sequence σ. This fact motivates the interest in finding efficiently the shortest sequence.

An LMI condition can be given for the synthesis of the stabilizing feedback gains of unconstrained controllable discrete–time linear switching systems. Moreover, this result can be directly applied for the stabilization of sampled unconstrained controllable linear switching systems.

This section will be concluded by a slightly extended version of the result, by setting LMIs that provide robust stabilization for uncertain systems.

Proposition 17. *Suppose that the uncertain discrete–time switching system* $x_{k+1} = A_i(\Delta)x_k + B_i(\Delta)u_k$, $u_k \in \mathbb{R}^m$ *is controllable and suppose that there exist a switching sequence* $\sigma = (s_1, \cdots, s_M)$ *such that* $\mathscr{R}_\sigma = \mathbb{R}^n$ *independently of* Δ.

Then there exist a positive definite matrix S, nonsingular matrices V_i *and matrices* F_i *such that the following LMI is feasible.*

$$\begin{bmatrix} S & A_{s_M}V_M + B_{s_M}F_M & \dots & 0 & 0 \\ (\bullet)^T & V_M + V_M^T & \dots & 0 & 0 \\ \vdots & \vdots & \vdots & \vdots & \vdots \\ 0 & 0 & \dots & V_2 + V_2^T & A_{s_1}V_M + B_{s_1}F_1 \\ 0 & 0 & \dots & (\bullet)^T & V_1 + V_1^T - S \end{bmatrix} > 0$$

The system can be stabilized with the periodic switching signal defined by σ *and the state feedback gains given by* $K_i = F_i V_i^{-1}$, $i = 1, \cdots, M$.

Remark 7. *Having a polytopic uncertainty, i. e.,* $A(\Delta) = A_0 + \delta_1 A_1 + \cdots + \delta_k A_K$, *the LMIs of Proposition 17 form a finite set of conditions that can be easily solved.*

Proposition 18. *Completely controllable linear switched systems can be piecewise linear feedback stabilized using a periodic switching sequence.*

Example

This chapter will be concluded by an illustrative example, which is based on a problem setting borrowed from the book of [62].

Let us consider the controlled linear switching system $\dot{x} = A_i x + B_i u$, $i \in \{1, 2\}$ defined by

$$A_1 = \begin{bmatrix} 0 & 0 & 0 \\ 1 & 1 & 0 \\ 0 & 0 & 1 \end{bmatrix} B_1 = \begin{bmatrix} 1 \\ 0 \\ 0 \end{bmatrix}, \quad A_2 = \begin{bmatrix} 0 & 0 & 0 \\ 0 & 1 & 0 \\ 1 & 0 & 1 \end{bmatrix},$$

which was exposed in [62] as a system which is globally controllable but that is not trivial to stabilize since $< A_1, B_1 > + < A_2, B_2 > \neq \mathbb{R}^3$ and the individual dynamics have a common unstable mode. By applying the methods presented in this chapter, however, it is possible to construct a homogeneous linear switched system by applying suitable linear state feedbacks. Moreover, this switched system can be stabilized by applying a periodic switching law.

One can figure out that $\mathscr{R}_\sigma = \mathbb{R}^3$ for the switching sequence $\sigma = (1,1,1,2,1)$.

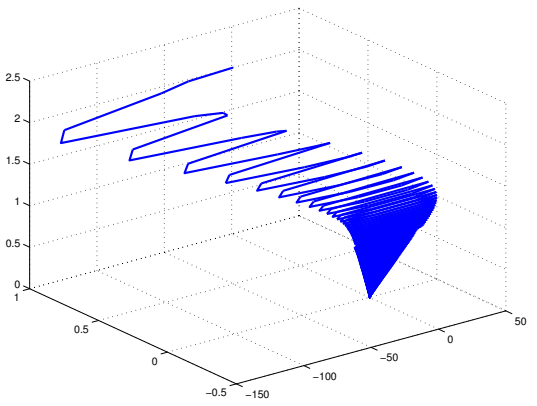

Fig. 3.5 GPLF stabilizability

Solving the LMIs the stabilizing feedback gains are:

$$k_1 = 10^4 \begin{bmatrix} -0.1086 & -8.6083 & 1.4443 \end{bmatrix}$$
$$k_2 = 10^5 \begin{bmatrix} -0.0112 & -1.2846 & 0.2099 \end{bmatrix}$$
$$k_3 = 10^4 \begin{bmatrix} -0.1081 & -6.6929 & -7.1136 \end{bmatrix}$$
$$k_4 = 10^3 \begin{bmatrix} -1.0000 & 0.0000 & -0.0000 \end{bmatrix}$$

The feedbacks were designed for the Euler discretization corresponding to the sampled time of $\tau = 0.001$ sec, while the simulation was started from the initial point $x_0 = [1\,1\,2]$.

The overshoots are due to the unstability present in the individual modes that acts as a performance barrier in these type of problems. Even some preliminary results concerning the LQ control of discrete–time switched systems are reported recently in [77] and [78], there are no reliable design algorithms for feedback stabilization, in general. The stabilizability result presented here makes possible to extend the discrete–time results to continuous–time design problems.

It is a subject of further research to investigate the optimal performance level achievable by certain configurations and to determine how it can be imposed additional performance requirements in the design process.

3.5 Bimodal Systems

Bimodal systems are special classes of switched systems governed by event-driven switchings, where the switch from one mode to the other is performed in closed-loop, i.e., in the simplest case the switching condition is described by a hypersurface in the state space. The controllability study of event-driven switched systems is very involved, since, in general, not even the well-posedness of the system, i.e., the existence and uniqueness of the solutions starting from any initial condition, is guaranteed.

The study of bimodal systems was motivated by an application representing a true emerging technology, related to the linearized longitudinal motion of a high speed supercavitating vehicle. There are more common examples, however, for a bimodal behavior, e.g., the dynamics of a hydraulic actuator in an active suspension system. The research revealed that for a wide class of bimodal systems the controllability can be cast in terms of the behavior of an associated open-loop switch system that has sign constrained control inputs, i.e., the controllability conditions can be tested in practice by using matrix algebraic tools. In this study the geometric view and the tools concerning robust invariant subspaces have been proven to be very useful. In what follows a detailed presentation of the results is provided.

Problem Formulation

Consider a *bimodal piecewise linear system*, i.e., a division of the state space by a hyperplane $\mathscr{C}$. The dynamics valid within each region is

$$\dot{x}(t) = \begin{cases} A_1 x(t) + B_1 u(t) & \text{if } x \in \mathscr{C}_-, \\ A_2 x(t) + B_2 u(t) & \text{if } x \in \mathscr{C}_+, \end{cases} \tag{3.15}$$

where $x(t) \in \mathbb{R}^n$ is the state vector and $u(t) \in \mathscr{U} \subset \mathbb{R}^m$ is the input vector[5].

The initial state of the system at time t_0 is determined by the initial state $x_0 = x(t_0)$ and the initial mode $s_0 \in \{1,2\}$ in which the system is found at t_0. $\mathscr{C}$ denotes the hyperplane $\mathrm{Ker} C = \{x | Cx = 0\}$ and let $\mathscr{C}_\pm$ denote the half spaces $\mathscr{C}_+ = \{x | Cx \geq 0\}$ and $\mathscr{C}_- = \{x | Cx \leq 0\}$. The state matrices are constant and of compatible dimensions, B_1, B_2 having full column rank. $y_s = Cx$ defines the decision vector.

[5] One can consider a number of different inputs for each mode. For sake of simplicity we chose $m_1 = m_2 = m$ but this does not affect the generality of the results.

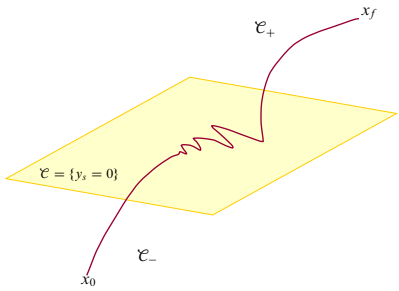

Fig. 3.6 Bimodal system

Let us suppose that the *relative degree* corresponding to the output y_s and the ith mode is r_i, i.e., $y_s^{(k)} = CA_i^k x$, $k < r_i$ and $y_s^{(r_i)} = CA_i^{r_i} x + CA_i^{r_i-1} B_i u$ with $CA_i^{r_i-1} B_i \neq 0$, see [26]. It is reasonable to assume that $r_i < n$, otherwise it would follows that y_s fulfills a homogeneous differential equation, defined by the characteristic polynomial of A_i. In this case the i^{th} mode would not be able to leave the points of the hypersurface $\mathscr{C}$, characterized by $y_s = 0$, i.e., such a system would not be well–posed nor completely controllable.

If $r_i < n$ then the system is *right invertible*. Right invertibility denotes the possibility of imposing any sufficiently smooth output function by a suitable input function, starting at the zero state. It turns out that this property is related to $\mathscr{S}_{i,*}$, i.e., the minimal $(C_i, A_i)-$invariant subspace containing $Im B_i$. On the other hand *left invertibility*, i.e., the property that for every admissible y_s corresponds uniquely an input u, is closely related to the subspace $\mathscr{V}_i^*$, the maximal $(A_i, B_i)-$invariant subspace contained in $\mathscr{C}$.

For linear systems the points of $\mathscr{V}_i^*$ are not visible by the output. Only the orthogonal projection of the state on the subspace $\mathscr{V}_i^{*,\perp}$ can be deduced from the output and its derivatives, moreover this is the largest subspace where the orthogonal projection of the state can be recognized solely from the output. If the state is known, the orthogonal projection of the input can be determined modulo $B_i^{-1,T} \mathscr{V}_i^*$, see [7].

Having a single output, in order to remove the ambiguity in the right inverse, one can always redefine the inputs of the system. Indeed, define an input transformation $M_i u = \begin{bmatrix} \tilde{u}_i \\ w_i \end{bmatrix}$ such that $B_i M_i^{-1} = \begin{bmatrix} \tilde{B}_i & b_i \end{bmatrix}$ with $CA_i^{r_i-1} \tilde{B}_i = 0$ and $CA_i^{r_i-1} b_i = 1$, e.g., by considering the basis $\{b_i, \tilde{b}_{i,j} = b_{i,j} - CA_i^{r_i-1} b_{i,j} b_i,\ j = 2, \cdots, m\}$ in $\operatorname{Im} B_i$. Then the single input single output (SISO) subsystem (A_i, b_i, C) is left and right invertible, i.e., $\tilde{\mathscr{V}}_i^* \cap \tilde{\mathscr{S}}_{i,*} = 0$ and $\tilde{\mathscr{V}}_i^* + \tilde{\mathscr{S}}_{i,*} = \mathbb{R}^n$, where the invariant subspaces correspond to the SISO system, while the remaining subsystem $(A_i, \tilde{B}_i, C)$ is not invertible.

The invariant subspace $\mathscr{V}_i^*$ produces a decomposition of the state corresponding to the i^{th}, i.e., the system can be transformed into:

$$\begin{bmatrix}\dot{\eta}_i\\ \dot{\xi}_i\end{bmatrix} = \begin{bmatrix}P_i\eta_i + R_i y_s + Q_i\tilde{u}_i\\ A_{r_i}\xi_i + B_{r_i}v_i\end{bmatrix}, \quad y_s = C_{r_i}\xi_i,$$

where $\eta_i \in \mathscr{V}_i^*$ and the subsystem for ξ_i is a chain of integrators with $B_{r_i} = [1\,0\cdots 0]^T$ and $C_i = [0\cdots 0\,1]$. The inputs v_i and w_i are related as $v_i = CA_i^r x + w_i$.

Since y_s is common for both systems, if $r_1 = r_2 = r$ then $\xi_1 = \xi_2 = \xi$. Recall that the components of ξ are formed by y_s and its derivatives up to order $r-1$. It follows that the complementer subspaces (zero dynamics) have the same dimension, i.e., there exist a basis transformation T such that $\eta_2 = T\eta_1 = T\eta$. In this case the bimodal system can be written as

$$\dot{\eta} = \begin{cases}P_1\eta + R_1 y_s + Q_1\tilde{u}_1 & \text{if} \quad y_s \geq 0\\ P_2\eta + R_2 y_s + Q_2\tilde{u}_2 & \text{if} \quad y_s \leq 0\end{cases} \tag{3.16}$$

$$\dot{\xi} = \begin{cases}A_r\xi + B_r v_1 & \text{if} \quad y_s \geq 0\\ A_r\xi + B_r v_2 & \text{if} \quad y_s \leq 0\end{cases} \tag{3.17}$$

Remark 8. *Observe that the required transformation can be performed by the same change of base in the state space. e.g.,* $\begin{bmatrix}\eta\\ \xi\end{bmatrix} = Tx$*, where for the last rows of* T *are chosen the vectors* CA_2^j*,* $j = 0,\cdots,r-1$*. However the feedback to obtain the desired structure might differ. The input transformations are also different, in general; this difference is reflected in the notation* u_1, u_2 *and* v_1, v_2*, respectively.*

Since the decomposition – i.e., the transformation T *– depends only on* C, A *and* r*, the choice of the input transformation does not play any role in the validity of the controllability results.*

In the case when $r_1 \neq r_2$ such a splitting is not possible but the system can be transformed into (suppose that $r_1 < r_2$):

$$\dot{\eta} = \begin{cases}P_1\eta + R_1 y_s + Q_1\tilde{u}_1 & \text{if} \quad y_s \geq 0\\ P_2\eta + R_2 y_s + Q_2\tilde{u}_2 + Q_3 v_2 & \text{if} \quad y_s \leq 0\end{cases} \tag{3.18}$$

$$\dot{\xi} = \begin{cases}A_r\xi + B_r v_1 & \text{if} \quad y_s \geq 0\\ A_r\xi + B_r\bar{\eta} & \text{if} \quad y_s \leq 0,\end{cases} \tag{3.19}$$

where $\bar{\eta}$ denotes the last component of η.

In contrast to the previous situation, in this case the subsystem ξ, hence the decision variable y_s, cannot be controlled independently from the subsystem η in both modes. Moreover, in the first mode the only way to control the higher order derivatives of y_s is through the inputs $\tilde{u}_1$. This fact makes the study of the controllability problem for these systems, in general, more difficult.

Here it is addressed the case when $r_i = r$, for which the system is always well posed, see [25]. For sake of simplicity the results will be presented for the case when $r = 1$, i.e.,

$$\dot{\eta} = \begin{cases} P_1\eta + R_1 y_s + Q_1 u & \text{if} \quad y_s \geq 0 \\ P_2\eta + R_2 y_s + Q_2 u & \text{if} \quad y_s \leq 0 \end{cases}. \tag{3.20}$$

$$\dot{y}_s = v, \tag{3.21}$$

but the assertions remain valid for the general case.

3.5.1 The Controllability Result

The controllability question of the bimodal system can be reduced to the question of controllability/reachability of the origin through the closed-loop switchings allowed by the switching surface $\mathscr{C}$. Due to the fact that the bimodal system is not a linear system, the affirmative answer given on this question is not completely trivial.

The reference [66] deals directly with problems described by (3.20) and (3.21), while [13] assumes only single input left and right–invertible systems whose dynamics are smooth, i.e., continuous along the trajectories. In this case one has $A_1x + B_1u = A_2x + B_2u$, for all $x \in \mathscr{C}, u \in \mathscr{U}$. It follows that $A_2 = A_1 - KC$ and $B_1 = B_2 = B$ for a suitable matrix K, i.e., one has $P_1 = P_2 = P$ and $Q_1 = Q_2 = 0$ in (3.20).

Note, that in Proposition 11 the subspace $\mathscr{R}_{\mathscr{A},\mathscr{B}}$ is the minimal subspace invariant for all of the A_is containing $\mathscr{B} = \sum_{i=0}^{s} \mathrm{Im} B_i$. Thus the bimodal system can be transformed, via a state transform and suitable feedbacks, to

$$\dot{\eta}_1 = \begin{cases} P_{1,1}\eta_1 + \tilde{R}_1 y_s + \tilde{Q}_1 u_1 & \text{if} \quad y_s \geq 0 \\ P_{2,1}\eta_1 + \tilde{R}_2 y_s + \tilde{Q}_2 u_2 & \text{if} \quad y_s \leq 0 \end{cases}, \tag{3.22}$$

$$\dot{\eta}_2 = \begin{cases} P_{1,2}\eta_2 + R_1 y_s & \text{if} \quad y_s \geq 0 \\ P_{2,2}\eta_2 + R_2 y_s & \text{if} \quad y_s \leq 0 \end{cases}, \tag{3.23}$$

$$\dot{y}_s = v, \tag{3.24}$$

where, by Proposition 11, subsystem (3.22) is controllable on $\mathscr{C}$ using open–loop switchings. It follows that this decomposition can be viewed as a controllability decomposition of the bimodal LTI system where the study of the controllability of the original bimodal system reduces to controllability of the bimodal system formed by (3.23) and (3.24).

Remark 9. *When $y_s = 0$, i.e., on $\mathscr{C}$, subsystems (3.22) does not contain y_s and the switching law must be defined externally. However for linear switching systems there exist a universal switching sequence that provides complete controllability, hence the switching sequence is fixed and a fundamental solution of (3.22) (as a linear time varying system) is well defined. Therefore, by linearity, the controllability of (3.22) is not affected by the values of y_s.*

Lemma 5. *The bimodal system (3.20), (3.21) is completely controllable if and only if the subsystem defined by (3.23), (3.24) is completely controllable.*

Having the decomposition (3.23),(3.24) for a bimodal system it is immediate that if the system is controllable then the input constrained open–loop switching system of the type

$$\dot{\eta} = P_i\eta + \bar{R}_i w, \quad i \in \{ 1,2 \}, \quad w \geq 0 \tag{3.25}$$

with $\bar{R}_i = (-1)^{i+1}R_i$ is also controllable. Consulting the result of [13], i.e., the case $P_1 = P_2$, it is apparent that the controllability condition of the bimodal system is equivalent to the input constrained controllability condition of the corresponding open–loop system given by (3.25). It is less apparent, but this consequence also holds for the case presented in [66].

A Separation Theorem

The bimodal system (3.23), (3.24) can be seen as a dynamic extension[6] of

$$\dot{\eta}_2 = P_{i,2}\eta_2 + \bar{R}_{i,2} w, \quad i \in \{ 1,2 \}, \quad w \geq 0. \tag{3.26}$$

Controllability of the dynamically extended system, provided that the original system was controllable, is by far non–trivial issue though for smooth vector fields it was proved in [64, 57]. For linear systems it is straightforward for unconstrained input case. This can be verified by checking the Kalman rank condition of the extended system, however this result cannot be directly applied here, since the input is signed constrained.

Lemma 6. *If the points η_0 and η_f can be connected by a trajectory of the linear system $\dot{\eta} = P\eta + Rw$ using nonnegative control $w \geq 0$ then, for a given r, they can be also connected using a smooth nonnegative control $\omega \geq 0$ with prescribed end points, i.e., $\omega^{(k)}(0) = \omega_{0,k}$ and $\omega^{(k)}(T_f) = \omega_{T_f,k}$ for $k = 0, 1, \cdots, r$.*

Using this lemma the main controllability result for the given bimodal system can be formulated as:

Proposition 19. *The bimodal system given by (3.23) and (3.24) is controllable if and only if the input constrained open–loop switching system (3.26) is controllable.*

Using this result controllability can be decided by using the result of Proposition 14 and the signed constraint Controllability Algorithm.

Remark 10. *The assertion of Proposition 19 remains valid for qLPV systems, too, and if the dynamics depends affinely on the scheduling variables, the reduction of the bimodal systems to the form given by (3.22), (3.23), (3.24) can be performed effectively.*

This section is concluded by an example to illustrate the content of the controllability result an the role of the separation lemma in the construction.

[6] See [26] for details.

Example 2. *Let us consider the system:*

$$\dot{x} = \begin{cases} P_1 x + R_1 y_s \ \textit{if} & y_s \geq 0 \\ P_2 x + R_2 y_s \ \textit{if} & y_s \leq 0 \end{cases}, \quad \dot{y}_s = u,$$

where $P_1 = \begin{bmatrix} 0 & 1 \\ 0 & 0 \end{bmatrix}$ $R_1 = \begin{bmatrix} 0 \\ 1 \end{bmatrix}$, $P_2 = \begin{bmatrix} 1 & 0 \\ 0 & 1 \end{bmatrix}$ $R_2 = \begin{bmatrix} 0 \\ 1 \end{bmatrix}$.

According to Proposition 19 controllability of the original system is equivalent to controllability of the sign constraint switched system:

$$\dot{\eta} = P_i \eta + \bar{R}_i w. \quad w \geq 0 \tag{3.27}$$

It is not hard to figure out that the coordinates corresponding to trajectories of the individual subsystems can be obtained as:

$$\eta_{1,1}(t) = \eta_{1,1}(t_0) + \eta_{1,2}(t_0)t + \int_0^t \int_0^\tau w(\sigma) d\sigma d\tau, \quad \eta_{1,2}(t) = \eta_{1,2}(t_0) + \int_0^t w(\tau) d\tau,$$

and

$$\eta_{2,1}(t) = e^t \eta_{2,1}(t_0), \quad \eta_{2,2}(t) = e^t \eta_{2,2}(t_0) - e^t \int_0^t v(\tau) d\tau,$$

with $w(\tau) = e^\tau v(\tau)$.

Let us apply the following control strategy: fix $t_1 > 0$ *and steer the second subsystem with constant control* $v \geq 0$ *then apply the first subsystem for a time* t_2 *with constant control* $w \geq 0$.

One has the following system of equations:

$$\eta_{2,1}(t_1) = e^{t_1} \eta_{2,1}(t_0), \quad \eta_{2,2}(t_1) = e^{t_1} \eta_{2,2}(t_0) - t_1 e^{t_1} v,$$
$$\eta_{1,1}(t_2) - \eta_{2,1}(t_1) = \eta_{2,2}(t_1) + \frac{1}{2} w t_2^2, \quad \eta_{1,2}(t_2) - \eta_{2,2}(t_1) = w t_2.$$

One has

$$t_2 = 2 \frac{\eta_{1,1}(t_2) - \eta_{2,1}(t_1)}{\eta_{1,2}(t_2) + \eta_{2,2}(t_1)}, \quad w = \frac{\eta_{1,2}^2(t_2) - \eta_{2,2}^2(t_1)}{2(\eta_{1,1}(t_2) - \eta_{2,1}(t_1))},$$

i.e.,

$$\tilde{\eta}_1^f - \eta_1^0 - \eta_2^0 = \frac{1}{2} \tilde{w} t_2, \ \ \eta_{2,2}(t_1) = e^{t_1} \eta_{2,2}(t_0) - t_1 e^{t_1} v, \ \ \tilde{\eta}_2^f - \eta_2^0 = \tilde{w} - t_1 e^{t_1} v,$$

with $\tilde{\eta}_i^f = e^{-t_1} \eta f_i$ *and* $\tilde{w} = e^{-t_1} w t_2$. *This equation can be solved satisfying the non-negativity constraint for a suitable choice of* t_1 *and* v *for any* η_0 *and* η_f. *Therefore the input constrained open–loop switching system (3.27) is controllable.*

In order to prove complete controllability for the original bimodal system, we have to ensure that (3.27) can be controlled with inputs that has arbitrarily

prescribed end conditions. By linearity it is sufficient to ensure null end conditions for the input w.

By replacing the piecewise constant inputs by $w \to w\varphi_t(\tau)$ *and* $v \to v\varphi_t(\tau)$ *where the function defined as* $\varphi_t(\tau) = \frac{6}{t^2}\tau(t-\tau)$ *is nonnegative on* $[0,t]$ *and fulfills the end–point conditions* $\varphi_t(0) = \varphi_t(t) = 0$ *and has* $\int_0^t \varphi_t(\tau)d\tau = t$, $\int_0^t \int_0^\tau \varphi_t(\sigma)d\sigma d\tau = \frac{t^2}{2}$, *one obtain the same equations for* t_1, t_2, v, w, *i. e., it follows that the bimodal system is also controllable.*

3.5.2 Stabilizability of Bimodal Systems

The bimodal system (3.15) is said to be stabilizable if any initial state can be asymptotically steered to the origin by a suitable admissible input u, i.e., for all $x_0 \in \mathbb{R}^n$ there exist a solution $x(t)$ of the bimodal system such that $\lim_{t\to\infty} x(t) = 0$.

Let us first examine bimodal systems with continuous dynamics. In view of Proposition 19 these systems are equivalent with an LTI system with two sign constrained inputs. Starting from this observation one has the following result:

Proposition 20. *If the bimodal system has continuous dynamics, i. e.,* $P_1 = P_2 = P$, *then the bimodal system* (3.23), (3.24) *is stabilizable if and only if the corresponding sign constrained open–loop switching system is stabilizable.*

In [24] one can find the following characterization of the stabilizability of a sign constrained LTI system:

Proposition 21. *The system* $\dot{x} = Px + Rw$, $w \in \mathbb{R}^2_+$ *is stabilizable if and only if*

- *the unconstrained system is stabilizable and*
- *all real eigenvectors v of* P^T *corresponding to a nonnegative eigenvalue of* P^T *have the property that* $R^T v$ *has both positive and negative components.*

The general case is more difficult. We conclude this section with a result that provides a sufficient condition for stabilizability:

Proposition 22. *If the bimodal system* (3.23), (3.24) *is globally controllable, then it is asymptotically stabilizable.*

3.6 Conclusions

The target of the research presented by this chapter is placed at the forefront of modern control theory. The work extends the formulation of basic properties of LTI control systems originated from R.E. Kalman, such as controllabiliy and stabilizability, to a special class of switched systems, the bimodal systems. A main result of the research states that controllability of bimodal systems is equivalent to controllability of a corresponding open-loop switched system having sign constraint control

inputs. Moreover, using geometric tools an algebraic condition that describes controllability and extends the Kalman rank test was given.

Since the basic topics of control theory, such as controllability, geometrical system theory, are revisited, the provided theoretical methods and practical algorithms can be used through the educational activity. The results demonstrate directly the applicability and impact of theoretical concepts to the solution of practical, engineering problems.

There are still a lot of open problems related to this relatively narrow field, motivated by real world applications, to solve. Considering a quadratic performance criteria for controlled linear switched systems is a relatively new topic, where only a few preliminary results for discrete time switched systems are available. An extension of the bimodal class, the cone-wise systems, i.e., systems with a state space having a conic partition and on each of the individual partitions the dynamics being linear, is also a recent topic with some early results for the planar setting.

References

1. Agrachev, A., Liberzon, D.: Lie-algebraic conditions for exponential stability of switched systems. In: Proceedings of the 38th IEEE Conference on Decision and Control, vol. 3, pp. 2679–2684 (1999)
2. Agrachev, A.A., Sachkov, Y.L.: Control Theory from the Geometric Viewpoint. Encyclopaedia of Mathematical Sciences, vol. 87. Springer (2004)
3. Altafini, C.: The reachable set of a linear endogenous switching system. Systems and Control Letters 47(4), 343–353 (2002)
4. Ancona, F., Bressan, A.: Patchy vector fields and asymptotic stabilization. ESAIM-Control, Optimization and Calculus of Variations 4, 445–471 (1999)
5. Aubin, J., Cellina, A.: Differential Inclusions. Springer, Berlin (1984)
6. Balas, G., Bokor, J., Szabo, Z.: Invariant subspaces for LPV systems and their applications. IEEE Transactions on Automatic Control 48(11), 2065–2069 (2003)
7. Basile, G.B., Marro, G.: A new characterization of some structural properties of linear systems: unknown-input observability, invertability and functional controllability. Int. Journal on Control 17, 931–943 (1973)
8. Blanchini, F.: Nonquadratic Lyapunov functions for robust control. Automatica 31, 451–461 (1995)
9. Blanchini, F., Savorgnan, C.: Stabilizability of switched linear systems does not imply the existence of convex lyapunov functions. In: Proc. of the 45th IEEE Conference on Decision and Control, San Diego, pp. 119–124 (2006)
10. Bokor, J., Szabó, Z., Szigeti, F.: Controllability of LTI switching systems using non-negative inputs. In: Proc. of the European Control Conference, ECC 2007, Kos, Greece (2007)
11. Brammer, R.F.: Controllability in linear autonomous systems with positive controllers 10(2), 329–353 (1972)
12. Cabot, A., Seeger, A.: Multivalued exponentiation analysis. part I: Maclaurin exponentials. Set-Valued Analysis 14(4), 347–379 (2006)
13. Çamlıbel, M.K., Heemels, W.P.M.H., Schumacher, J.M.: On the Controllability of Bimodal Piecewise Linear Systems. In: Alur, R., Pappas, G.J. (eds.) HSCC 2004. LNCS, vol. 2993, pp. 250–264. Springer, Heidelberg (2004)

14. Cheng, D.: Controllability of switched bilinear systems. IEEE Transactions on Automatic Control 50(4), 511–515 (2005)
15. Cheng, D., Chen, H.F.: Accessibility of switched linear systems. In: Proceedings. 42nd IEEE Conference on Decision and Control, vol. 6, pp. 5759–5764 (2003)
16. Clarke, F., Ledyaev, Y., Stern, R.: Asymptotic stability and smooth Lyapunov functions. Journal of Differential Equations 149, 69–114 (1998)
17. Clarke, F.H., Ledyaev, Y., Sontag, E., Subbotin, A.: Asymptotic controllability implies feedback stabilization. IEEE Trans. Automat. Control 42(10), 1394–1407 (1997)
18. Dayawansa, W., Martin, C.: Dynamical systems which undergo switching. IEEE Transactions on Automatic Control 44(4), 751–760 (1999)
19. Dontchev, A.L., Lempio, F.: Difference methods for differential inclusions: a survey. SIAM Review 34(2), 263–294 (1992)
20. Frankowska, H., Olech, C., Aubin, J.P.: Controllability of convex processes 24(6), 1192–1211 (1986)
21. Ge, S., Sun, Z., Lee, T.: Reachability and controllability of switched linear systems. In: Proceedings of the American Control Conference, vol. 3, pp. 1898–1903 (2001)
22. Grasse, K.A., Sussmann, H.J.: Global controllability by nice controls. In: Nonlinear Controllability and Optimal Control, pp. 33–79. Dekker, New York (1990)
23. Hajek, O., Loparo, K., Fashoro, M.: Controllability properties of constrained linear systems. Journal of Opt. Th. and Appl. 73(2), 329–347 (1992)
24. Heemels, W., van Eijndhoven, S., Stoorvogel, A.: Linear quadratic regulator problem with positive controls. Int. Journal on Control 70(4), 551–578 (1998)
25. Imura, J.: Well-posedness analysis of switch-driven hybrid systems. IEEE Transactions on Automatic Control 48(11), 1926–1935 (2003)
26. Isidori, A.: Nonlinear Control Systems. Springer (1989)
27. Ji, Z., Wang, L., Guo, X.: Design of switching sequences for controllability realization of switched linear systems. Automatica 43(4), 662–668 (2007)
28. Jia, Z., Fengb, G., Guoc, X.: A constructive approach to reachability realization of discrete-time switched linear systems. Systems and Control Letters 56(11-12), 669–677 (2007)
29. Jurdjevic, V.: Geometric Control Theory. Cambridge University Press (1997)
30. Kalman, R.E.: Contributions to the theory of optimal control. Boletin de la Sociedad Matematica Mexicana 5, 102–119 (1960)
31. Kellett, C., Teel, A.: Discrete–time asymptotic controllability implies smooth control–Lyapunov function. Systems and Control Letters 52, 349–359 (2004)
32. Korobov, V.I.: A geometric criterion of local controllability of dynamical systems in the presence of constraints on the control. Differential Equations 15, 1136–1142 (1980)
33. Krastanov, M., Veliov, V.: On the Stabilizability of Control Constrained Linear Systems. In: Dimov, I.T., Lirkov, I., Margenov, S., Zlatev, Z. (eds.) NMA 2002. LNCS, vol. 2542, pp. 238–245. Springer, Heidelberg (2003)
34. Krastanov, M., Veliov, V.: On the controllability of switching linear systems. Automatica 41(4), 663–668 (2005)
35. Ledyaev, Y., Sontag, E.: A Lyapunov characterization of robust stabilization. Nonlinear Anal. 37(7, Ser. A: Theory Methods), 813–840 (1999)
36. Lee, E., Markus, L.: Foundation of Optimal Control Theory. Jhon Wiley, New York (1967)
37. Liberzon, D.: Switching in Systems and Control. Birkhäuser, Basel (2003)
38. Liberzon, D., Agrachev, A.: Lie-algebraic stability criteria for switched systems 40(1), 253–269 (2001)

39. Liberzon, D., Hespanha, J.P., Morse, A.S.: Stability of switched systems: a Lie-algebraic condition. Systems and Control Letters 37, 117–122 (1999)
40. Liberzon, D., Morse, A.S.: Basic problems in stability and design of switched systems. IEEE Control Systems Magazine 19(5), 59–70 (1999)
41. Lin, H., Antsaklis, P.: A necessary and sufficient condition for robust asymptotic stabilizability of continuous-time uncertain switched linear systems. In: Proc. of the 43rd IEEE Conference on Decision and Control, Bahamas, vol. 4, pp. 3690–3695 (2004)
42. Lin, H., Antsaklis, P.: A converse Lyapunov theorem for uncertain switched linear systems. In: Proc. of the European Control Conference. CDC-ECC 2005, Sevilla, pp. 3291–3296 (2005)
43. Lin, H., Antsaklis, P.: Switching stabilizability for continuous–time uncertain switched linear systems. IEEE Trans. Autom. Contr. 52(4), 633–646 (2007)
44. Lin, H., Antsaklis, P.J.: Stability and stabilizability of switched linear systems: A short survey of recent results. In: Proc. of the 13th IEEE Mediterranean Conference on Control and Automation, Limassol, pp. 24–29 (2005)
45. Liu, D., Molchanov, A.: Criteria for robust absolute stability of time-varying nonlinear continuous-time systems. Automatica 38(4), 627–637 (2002)
46. Molchanov, A.P., Pyatnitskiy, Y.S.: Criteria of asymptotic stability of differential and difference inclusions encountered in control theory. Systems Control Lett. 13(1), 59–64 (1989)
47. Pachter, M., Jacobson, D.: Control with a conic constraint set. Journal of Opt. Th. and Appl. 25(2), 117–123 (1978)
48. Petreczky, M.: Reachability of linear switched systems: differential geometric approach. Systems and Control Letters 565, 112–118 (2006)
49. Rifford, L.: Semiconcave control-Lyapunov functions and stabilizing feedbacks. SIAM J. Contr. Optim. 41(3), 659–681 (2002)
50. Saperstone, S.H.: Global controllability of linear systems using positive controls 11(3), 417–423 (1973)
51. Schmitendorf, W.E., Barmish, B.: Null controllability of linear systems with constrained controls 18(4), 327–345 (1980)
52. Smirnov, G.V.: Stabilization by constrained controls 34(5), 1616–1649 (1996)
53. Smirnov, G.V.: Introduction to the theory of differential inclusions. Graduate Studies in Mathematics, vol. 41. American Mathematical Society, Providence (2002)
54. Sontag, E.: Remarks on the preservation of various controllability properties under sampling. In: Mathematical Tools and Models for Control, Systems Analysis and Signal Processing. Travaux Rech. Coop. Programme 567, vol. 3, pp. 623–637. CNRS, Paris (1983)
55. Sontag, E.: An approximation theorem in nonlinear sampling. In: Fuhrmann, P.A. (ed.) Mathematical Theory of Networks and Systems. LNCIS, vol. 58, pp. 806–812. Springer, London (1984)
56. Sontag, E.: Orbit theorems and sampling. In: Algebraic and Geometric Methods in Nonlinear Control Theory. Math. Appl., vol. 29, pp. 441–483. Reidel, Dordrecht (1986)
57. Sontag, E., Qiao, Y.: Further results on controllability of recurrent neural networks. Systems and Control Letters 36, 121–129 (1999)
58. Sontag, E., Sussmann, H.: Accessibility under sampling. In: Proc. IEEE Conf. Dec. and Control, Orlando (December 1982)
59. Stern, M., Heymann, R.: Controllability of linear systems with positive controls: Geometric considerations. Journal of Math. Anal. and Appl. 52, 36–41 (1975)
60. Stikkel, G., Bokor, J., Szabó, Z.: Necessary and sufficient condition for the controllability of switching linear hybrid systems. Automatica 40(6), 1093–1098 (2004)

61. Sun, Z., Ge, S.: Sampling and control of switched linear systems. In: Proceedings of the 41st IEEE Conference on Decision and Control, vol. 4, pp. 4413–4418 (2002)
62. Sun, Z., Ge, S.S.: Switched Linear Systems. Control and Design. Springer (2005)
63. Sun, Z., Ge, S.S., Lee, T.H.: Controllability and reachability criteria for switched linear systems. Automatica 38(5), 775–786 (2003)
64. Sussmann, H.J.: Local controllability and motion planning for some classes of systems with drift. In: Proceedings of 30th IEEE CDC, Brighton, England, pp. 1110–1114 (1991)
65. Szigeti, F.: A differential algebraic condition for controllability and observability of time varying linear systems. In: Proc. of the 31st IEEE Conf. on Decision and Control, Tucson, USA, pp. 3088–3090 (1992)
66. Veliov, V., Krastanov, M.: Controllability of piecewise linear systems. Systems and Control Letters 7, 335–341 (1986)
67. Wirth, F.: A converse Lyapunov theorem for linear parameter-varying and linear switching systems 44(1), 210–239 (2005)
68. Wolenski, P.R.: The exponential formula for the reachable set of a Lipschitz differential inclusion 28(5), 1148–1161 (1990)
69. Wonham, W.M.: Linear Multivariable Control - A Geometric Approach, 3rd edn. Springer, New York (1985)
70. Xie, G., Wang, L.: Necessary and sufficient conditions for controllability of switched linear systems. In: Proceedings of the 2002 American Control Conference, vol. 3, pp. 1897–1902 (2002)
71. Xie, G., Wang, L.: Equivalence of some controllability notions for linear switched systems and their geometric criteria. In: Proc. of the Am. Contr. Conf., Denver, Colorado, pp. 5158–5190 (2003)
72. Xie, G., Wang, L.: Reachability realization and stabilizability of switched linear discrete-time systems. Journal of Mathematical Analysis and Applications 280(2), 209–220 (2003)
73. Xie, G., Zheng, D., Wang, L.: Controllability of switched linear systems. IEEE Trans. Automat. Contr. 47(8), 1401–1405 (2002)
74. Xie, G., Zheng, D., Wang, L.: Controllability of switched linear systems. IEEE Transactions on Automatic Control 47(8), 1401–1405 (2002)
75. Yang, Z.: An algebraic approach towards the controllability of controlled switching linear hybrid systems. Automatica 38, 1221–1228 (2002)
76. Yoshida, H., Tanaka, T., Yunokuchi, K.: Positive reachability of discrete-time linear systems. In: Proc. of European Control Conference, Cambridge, United Kingdom (2003)
77. Zhang, W., Abate, A., Vitus, M.P., Hu, J.: On piecewise quadratic control-Lyapunov functions for switched linear systems. In: Proc. of the IEEE Conference on Decision and Control, Shanghai, China (2009)
78. Zhang, W., Hu, J., Abate, A.: On the value functions of the discrete-time switchedLQR problems. IEEE Transaction on Automatic Control 54(11), 2669–2674 (2009)

Chapter 4
Positive Polynomial Matrices for LPV Controller Synthesis

Didier Henrion

Abstract. Positive polynomial matrices and linear matrix inequalities (LMI) can be used to design linear parameter varying (LPV) controllers depending polynomially on the scheduling parameters, and robust to polynomial parametric uncertainty. The salient features of the approach are (a) the ability to design a controller of order and structure fixed a priori; (b) the use of a transfer function, or polynomial modeling framework that bypasses difficulties typically encountered with canonical state-space representations of LPV controllers; (c) the existence of a user-friendly Matlab interface to model this class of LMI problems. The main limitation of the approach is the choice of a nominal, or central characteristic polynomial around which the design is carried out.

4.1 Introduction

The purpose of this contribution is to survey some achievements of the last decade in the use of polynomial and linear matrix inequality (LMI) methods for designing linear parameter varying (LPV) controllers. No new results are reported here, but various technical statements scattered in the literature are gathered and presented in a hopefully unified fashion. These results are the outcome of eight-year long collaboration (2001-2008) between LAAS-CNRS, an academic research laboratory, and Safran-Snecma, a company dedicated to design, development and production of engines for civil aircrafts, military aircrafts, launch vehicles and satellites. This collaboration resulted in the defense of two PhD theses [20, 8] and several engineering projects and scientific productions, see e.g. [21, 23], culminating with the paper [9].

Didier Henrion
CNRS, LAAS, 7 avenue du colonel Roche, F-31400 Toulouse, France;
Université de Toulouse, LAAS, F-31400 Toulouse, France;
Faculty of Electrical Engineering, Czech Technical University in Prague, Technická 2,
CZ-16626 Prague, Czech Republic
e-mail: henrion@laas.fr

O. Sename et al. (Eds.): *Robust Control and LPV Approaches*, LNCIS 437, pp. 87–96.
DOI: 10.1007/978-3-642-36110-4_4

The main objective of the project was the development of computer-aided control system design tools for designing LPV controllers for aircraft turbofan engines. Some of these tools have been integrated into the ATOL framework used by Safran-Snecma to design new engines and improve control laws of existing engines [23]. The main requisites for controller design were as follows:

- both open-loop plant and controller are given in the form of multi-input multi-output (MIMO) transfer functions, i.e. ratios of numerator and denominator polynomials;
- open-loop plant data (i.e. polynomial coefficients) depend polynomially on the real parametric uncertainty affecting the system; uncertain parameters are confined to a given compact basic semialgebraic set (e.g. a ball, a box);
- controller data (i.e. polynomial coefficients) depend polynomially on the real scheduling parameters; scheduling parameters are confined to a given compact basic semialgebraic set (e.g. a ball, a box);
- controller order and structure are fixed from the outset (e.g. PID controller depending quadratically on two scheduling parameters) independently of the open-loop system order.

In our opinion, the originality of our approach lies in the choice of polynomials and rational transfer functions as modeling objects. This bypasses the standard complications arising from the use of canonical state-space representations in interpolated scheduling control laws and LPV design, see e.g. [24].

The price one has to pay for the ability of designing controllers of fixed complexity is the use of potentially conservative convex linear matrix inequality (LMI) conditions. The main tuning parameter of the approach, which results in a convexification of the design problem, has however the physical interpretation of being a reference, or nominal, or central closed-loop system around which the design is carried out. Mathematically, a convex LMI inner approximation of the nonconvex stability domain is built, in coefficient parameter space, around a so-called central polynomial. Typically, engineering insight yields a reasonable choice of central polynomial around which LPV controller design is achieved.

In this contribution, we outline the whole approach, starting from sufficient LMI conditions for stability of polynomial matrices, and concluding with LMI conditions for robust polynomial LPV controller design. For confidentiality reasons we cannot reproduce the examples of LPV control laws designed for the Safran-Snecma aircraft turbofan engine project.

4.2 Stability of Polynomial Matrices

The minimum requirement for a feedback control law is closed-loop system stability. Since we follow a polynomial modeling framework, stability amounts to location of the roots of the characteristic polynomial in a specific region of the complex plane.

We consider regions

$$\mathscr{S} = \{s \in \mathbb{C} : \begin{bmatrix} 1 \\ s \end{bmatrix}^* \underbrace{\begin{bmatrix} s_{11} & s_{21}^* \\ s_{21} & s_{22} \end{bmatrix}}_{S} \begin{bmatrix} 1 \\ s \end{bmatrix} < 0\}$$

obtained by a conformal mapping of the open unit disk, parametrized by three complex scalars s_{11}, s_{21}, s_{22} gathered into a 2-by-2 Hermitian matrix S. As above and throughout the text, the star denotes transpose conjugation. The case $s_{11} = 0$, $s_{21} = 1$, $s_{22} = 0$ corresponds to the open left half-plane (continuous-time systems), whereas $s_{11} = -1$, $s_{21} = 0$, $s_{22} = 1$ models the open unit disk (discrete-time systems). We can also consider intersections of several such stability regions, and hence model damping cones or more complicated frequency-domain specifications, see e.g. [11].

A MIMO rational matrix transfer function can be expressed as a left matrix fraction $D^{-1}(s)N(s)$ where $D(s)$ and $N(s)$ are polynomial matrices of the operator s (the Laplace variable for continuous-time systems, the shift variable for discrete-time systems) of appropriate dimensions. In the (generic) absence of pole-zero cancellations, stability of the transfer function amounts to location of the roots of the determinant of $D(s)$ into region $\mathscr{S}$.

Given a polynomial matrix $D(s) = D_0 + D_1 s + D_2 s^2 + \cdots + D_d s^d$ of degree d, let us denote by

$$D = \begin{bmatrix} D_0 & D_1 & D_2 & \cdots & D_d \end{bmatrix}$$

the constant matrix obtained by appending columnwise matrix coefficients of increasing powers of indeterminate s. Let us define

$$\Pi_1 = \begin{bmatrix} 0 & I & & \\ \vdots & & \ddots & \\ 0 & & & I \end{bmatrix}, \quad \Pi_2 = \begin{bmatrix} I & & & 0 \\ & \ddots & & \vdots \\ & & I & 0 \end{bmatrix}$$

two matrices of size dn-by-$(d+1)n$ with I denoting the identify matrix of size n. Finally, given a 2-by-2 Hermitian stability matrix S as above, let us define the linear mapping

$$F(P) = s_{11}\Pi_1^* P \Pi_1 + s_{21}\Pi_2^* P \Pi_1 + s_{21}^* \Pi_1^* P \Pi_2 + s_{22}\Pi_2^* P \Pi_2$$

transforming a Hermitian matrix of size dn into a Hermitian matrix of size $(d+1)n$.

The following theorem gives a necessary and sufficient condition for stability of polynomial matrix $D(s)$, that is, for inclusion of the roots of $\det D(s)$ into region $\mathscr{S}$. The notation $X \succeq 0$ means that X is Hermitian positive semidefinite, i.e. all the eigenvalues of X are real nonnegative.

Theorem 4.1. *Polynomial matrix $D(s)$ is stable if and only if there exists a stable polynomial matrix $C(s)$ and a Hermitian matrix P such that*

$$C^* D + D^* C - F(P) \succeq 0. \tag{4.1}$$

Proof. It can be traced back to [10, 11], see also [13, Lemma 2] and [9, Theorem 1] for alternative proofs. In particular, it must be emphasized that P plays the role of the Hessian matrix of a quadratic Lyapunov function of the linear system with transfer function $D^{-1}(s)C(s)$. □

Polynomial matrix $C(s)$ is called the central polynomial. Once it is fixed, inequality (4.1) becomes linear in D and P. This joint linearity is a key characteristic of the LMI conditions of Theorem 4.1, shared e.g. with the discrete-time stability conditions of [4]. In particular, if $D(s)$ depends linearly on the controller parameters, controller design boils down to solving a convex LMI problem. The whole conservatism of the approach is therefore captured by the choice of central polynomial $C(s)$. Even though this is not developed here, LMI condition (4.1) can also be used for robustness analysis, see [13, 12].

Geometrically, the condition of Theorem 4.1 can be interpreted as follows. In the space of polynomial matrix coefficients, a convex region is built around C. It is modeled as a projection of an affine section of the cone of positive semidefinite matrices. The operation of projection corresponds to elimination of the variable P. This class of convex regions is called semidefinite representable, cf. [1]. It is a very broad class of convex regions. Currently it is not known how versatile it is exactly, but it is conjectured that all convex semialgebraic sets (i.e. convex sets described by polynomial inequalities) can be modelled like that [19], and international research programmes are currently carried out to further investigate these questions at the boarder between convex analysis, real algebraic geometry and mathematical programming.

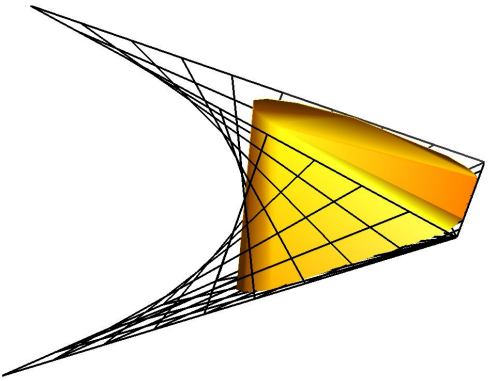

Fig. 4.1 Convex LMI inner approximation of the nonconvex stability region for a third-degree discrete-time polynomial

For illustration, on Figure 4.1 we represent a convex LMI inner approximation of the nonconvex stability region in the case of scalar $(n = 1)$ discrete-time $(s_{11} = -1,$ $s_{21} = 0,$ $s_{22} = 1)$ third degree $(d = 3)$ monic $(D_3 = 1)$ polynomials with real coefficients, for the choice of stable central polynomial $C(s) = s^3$. The exact stability

domain in the coefficient space $x = (D_0, D_1, D_2) \in \mathbb{R}^3$ is a nonconvex region delimited by two triangles and a parabolic hyperboloid. The LMI approximation (4.1) is given by

$$\{x \in \mathbb{R}^3 : \exists p \in \mathbb{R}^6 : \begin{bmatrix} p_0 & & & \\ p_1 & p_3 - p_0 & & \\ p_2 & p_4 - p_1 & p_5 - p_3 & \\ x_0 & x_1 - p_2 & x_2 - p_4 & 2 - p_5 \end{bmatrix} \succeq 0\}$$

where symmetric entries are not reproduced, and vector p of additional variables, or liftings, correspond to the 6 linearly independent entries of the 3-by-3 symmetric matrix P.

4.3 Fixed-Order Robust Controller Design

Based on Theorem 4.1, fixed-order robust controller design boils down to convex LMI optimization, and the main tuning parameter, capturing all degrees of freedom as well as all the conservatism of the approach, is the central polynomial. The use of the LMI conditions of Theorem 4.1 for fixed-order controller design was proposed in [12], and it was used e.g. in [6, 16].

4.3.1 H_∞ Performance

In addition to locating the closed-loop poles into a region $\mathscr{S}$ of complex plane, we may want a control law to ensure some performance requirements. In the case of H_∞ performance, we can readily exploit well-known links with robust stability of systems with unstructured uncertainty. We assume now that polynomial matrix is affected by an additive norm-bounded uncertainty

$$D_\delta(s) = D(s) + \delta N(s), \quad \|\delta\|_\infty \leq \gamma^{-1}$$

where δ is an unknown real (or complex) valued matrix whose maximum singular value does not exceed a given positive threshold γ^{-1}. Using the small-gain theorem [26, Theorem 9.1], robust stability of matrix $D_\delta(s)$ is equivalent to the H_∞ performance constraint

$$\|D^{-1}(s)N(s)\|_\infty \leq \gamma$$

where the infinity norm denotes the maximum singular value achieved for s along the boundary of open set $\mathscr{S}$.

The following result, proved e.g. in [25, Corollary 1] or [9, Theorem 2], is an extension of Theorem 4.1 to H_∞ performance.

Lemma 4.1. *Given a stable polynomial matrix $C(s)$, rational matrix $D^{-1}(s)N(s)$ is stable with H_∞ norm less than or equal to γ if there exists a Hermitian matrix P and a real scalar λ such that*

$$\begin{bmatrix} C^*D + D^*C - F(P) - \lambda C^*C & N^* \\ N & \lambda\gamma^2 I \end{bmatrix} \succeq 0. \tag{4.2}$$

In particular, in H_∞ LMI (4.2) we retrieve the stability LMI (4.1) in the upper-left block for the choice $\lambda = 0$. For examples of lower-order controller design using Lemma 4.1, see [14, 25].

4.3.2 H_2 Performance

The extension of Theorem 4.1 to H_2 performance was carried out in [8], but since this document is not publicly available, we reproduce the main result below.

If u denotes the input signal, y the output signal, and G the transfer function of a linear plant, the H_∞ norm of G can be defined as an energy to energy norm $\|G\|_\infty = \sup \|y\|_2/\|u\|_2$. Similarly, the H_2 norm can be defined as an energy to peak norm $\|G\|_2 = \sup \|y\|_\infty/\|u\|_2$.

Lemma 4.2. *Given a stable polynomial matrix $C(s)$, rational matrix $D^{-1}(s)N(s)$ is stable with H_2 norm less than or equal to γ if there exists a Hermitian matrix P such that*

$$C^*D + D^*C - C^*C - F(P) \succeq 0, \quad \begin{bmatrix} P & N^* \\ N & \gamma^2 I \end{bmatrix} \succeq 0. \tag{4.3}$$

4.3.3 Robustness

For notational simplicity, in stability LMI (4.1), H_∞ LMI (4.2) or H_2 LMI (4.3), let us gather plant (or controller) parameters N, D into a vector k.

Let us assume that plant parameters are uncertain, that is, coefficients of polynomial matrices $N(s)$ and $D(s)$ depend on parameters δ which belong to a given compact set Δ but which are otherwise unknown. If the dependence of N and D on δ is polynomial, LMI (4.1) or (4.2) or (4.3) becomes a so-called parametrized, or uncertain LMI

$$L_\delta(k,P) \succeq 0, \quad \forall \delta \in \Delta \tag{4.4}$$

which must be solved for k and P uniformly for all possible values of $\delta \in \Delta$. If Δ is not discrete, then LMI (4.4) is semi-infinite, in the sense that an infinite number of constraints (one for each value of δ in Δ) must be solved for a finite number of variables (in k and P). Such robust LMIs are extensively studied in [2] and [22].

In many cases of interest, an equivalent robust LMI condition

$$L(k,P) \succeq 0 \tag{4.5}$$

can be derived to remove dependence on uncertain parameter δ, in the sense that there is a solution to uncertain LMI (4.4) if and only if there is a solution to robust LMI (4.5). Depending on the class of uncertainty set Δ, robust LMI (4.5) can be significantly larger than uncertain LMI (4.4), but this is the price to pay to convert a

semi-infinite LMI into a finite LMI. The simplest example is when N and D depend affinely on δ and Δ is a polytope, the so-called polytopic uncertain model [7, 3]. Robust LMI (4.5) then corresponds to all the instances of uncertain LMI (4.4) at vertices of Δ. In the next section, in the context of LPV controller design, we describe a general technique to deal with parametrized LMIs when the dependence on the parameters is polynomial.

4.4 LPV Controller Design

In this section we assume that numerator and denominator polynomial matrices now depend on a vector of parameters

$$\begin{aligned} N(s,\theta) &= N_0(\theta) + N_1(\theta)s + N_2(\theta)s^2 + \cdots + N_d(\theta)s^d \\ D(s,\theta) &= D_0(\theta) + D_1(\theta)s + D_2(\theta)s^2 + \cdots + D_d(\theta)s^d \end{aligned}$$

which is assumed to belong to a given set

$$\theta \in \Theta.$$

Such a parameter depends on the operation condition of the open-loop system, and it can be measured on-line by the controller. For simplicity, we assume first that parameter θ does not vary in time, even though at the end of the section we will indicate how to relax this assumption. In this context, the objective of linear parameter varying (LPV) controller design is to find a controller depending explicitly on θ and that ensures closed-loop stability and performance.

4.4.1 A Hierarchy of LMI Problems

Following the approach described in the previous section, the designer comes up with a parametrized LMI

$$L_\theta(k,P) \succeq 0, \quad \forall \theta \in \Theta \tag{4.6}$$

to be solved for controller coefficients k and Lyapunov coefficients P, where L_θ is one of the LMI mapping (4.1), (4.2) or (4.3) with an additional explicit dependence of N and D on θ.

If the dependence on θ is polynomial, i.e.

$$\begin{aligned} N(s,\theta) &= \textstyle\sum_{\alpha\in\mathbb{N}^q} N_\alpha(s)\theta^\alpha \\ D(s,\theta) &= \textstyle\sum_{\alpha\in\mathbb{N}^q} D_\alpha(s)\theta^\alpha \end{aligned}$$

where in the above sums $\alpha \in \mathbb{N}^q$ is a vector of indices, $\theta^\alpha = \theta_1^{\alpha_1}\theta_2^{\alpha_2}\cdots\theta_q^{\alpha_q}$, and if set Θ is basic semi-algebraic, i.e. if it is modeled as

$$\Theta = \{\theta \in \mathbb{R}^q : g_i(\theta) \geq 0, i = 1, \ldots, r\}$$

for explicitly given polynomials $g_i(\theta)$, then we can use recent results on positive polynomials [17] to solve parametrized LMI (4.6) via a hierarchy of robust LMIs.

In particular, we can use Putinar's Positivstellensatz under the non-restrictive assumption that the semialgebraic set Θ is compact and that it is included in a ball of radius ρ centered around the origin. For example, this is ensured if $g_i(\theta) = \rho^2 - \theta^*\theta$ for some i.

Lemma 4.3. *There exists k and P such that $L_\theta(k,P) \succ 0$ for all $\theta \in \Theta$ if and only if there exists sum-of-squares matrix polynomials $M_i(\theta)$ such that $L_\theta(k,P) = M_0(\theta) + \sum_{i=1}^r g_i(\theta)M_i(\theta)$.*

Proof. See [22, Theorem 24] and [17, Theorem 2.22], an extension to the matrix case of scalar result by Putinar used for polynomial optimization. □

Practically speaking, the discrepancy between the strict inequality in Lemma 4.3 and the non-strict inequality in (4.6) is not relevant. In terms of implementation, the constraint that $L_\theta(k,P)$ is a linear combination of sum-of-squares (SOS) matrix polynomials can be expressed as an LMI, as soon as the degree of the SOS multipliers is fixed. The decision variables are then k and P, but also the Gram matrices of the SOS multipliers, see [17, Chapter 2]. By increasing the degree of the SOS multipliers, we obtain a hierarchy of robust LMI problems of increasing size whose solution is guaranteed to be equivalent, asymptotically, to the solution of the polynomially parametrized LMI (4.6). The Matlab modeling environment YALMIP [18] allows to model matrix SOS problems and generate the corresponding LMI problems in a user-friendly way. The LMI problems can then be solved by any semidefinite programming solver (e.g. SeDuMi, PENSDP, SDPT3, SDPA, CSDP).

4.4.2 Parameter-Dependent Lyapunov Functions

So far we have considered a polynomially parametrized LMI (4.6) which is an instance of stabilization LMI (4.1), H_∞ LMI (4.2) or H_2 LMI (4.3) in which decision variable P is the Hessian matrix of a Lyapunov function certifying stability and performance. The Lyapunov function does not depend on scheduling parameter θ, hence we are assessing quadratic stability of the LPV system, i.e. stability for all possible time variations of θ, including jumps or discontinuities. If we have some information of the time variation of θ (e.g. bounds on the rate of variation), or if θ is assumed to be constant, but otherwise unknown, this information can be incorporated in parametrized LMI (4.6) by allowing Lyapunov matrix P to depend on θ. We can use the same robust LMI as in Lemma 4.3 as soon as the dependence of P on θ is polynomial. The trade-off to be found is between the complexity (degree) of the dependence of P on θ and the size of LMI problems in the hierarchy.

Finally, we can additionally assume as in paragraph 4.3.3 that the open-loop plant parameters are uncertain, depending polynomially on a vector or matrix δ of uncertain parameters assumed to belong to a compact basic semialgebraic set Δ. We can

use the same hierarchy of LMI problems as in Lemma 4.3, the only difference being that the controller is not allowed to depend polynomially on δ (uncertain parameters are not measurable). In contrast, Lyapunov matrix P can depend simultaneously on scheduling parameter θ and uncertain parameter δ.

4.5 Conclusion

We have described in a unified framework the application of recent positive polynomial and LMI techniques to the design of fixed-order robust LPV controllers for linear systems described by input-output transfer functions whose coefficients depend polynomially on scheduling parameters and uncertain parameters. The main tuning parameter of the approach is the central polynomial, a reference closed-loop system around which design is carried out. Once the central polynomial is fixed, design boils down to solving a hierarchy of LMI problems. These problems can be modeled easily under Matlab with the YALMIP interface, and they can be solved with any semidefinite programming solver. These techniques have been succesfully applied within the scope of a eight-year industrial project with the French aerospace engine manufacturer Safran-Snecma. Outcomes have been the defense of two PhD theses [20, 8] and an industrial software environment to assist engineers when developing advanced control laws for new aircraft engine prototypes [23].

Acknowledgements. This work resulted from a collaboration with Jacques Bernussou, David Boyer, Wilfried Gilbert, Luc Reberga and Florian Vary. It was funded by research contracts between LAAS-CNRS and the Safran-Snecma company. The research of Didier Henrion on positive polynomials was also funded in part by project no. 103/10/0628 of the Grant Agency of the Czech Republic.

References

1. Ben-Tal, A., Nemirovski, A.: Lectures on modern convex optimization. SIAM, Philadelphia (2001)
2. Ben-Tal, A., Nemirovski, A., El Ghaoui, L.: Robustness. In: Wolkowicz, H., Saigal, R., Vandenberghe, L. (eds.) Handbook of Semidefinite Programming. Kluwer Academic Publishers, Dordrecht (2000)
3. Boyd, S., El Ghaoui, L., Feron, E., Balakrishnan, V.: Linear matrix inequalities in system and control Theory. SIAM, Philadelphia (1994)
4. de Oliviera, M.C., Bernussou, J., Geromel, J.C.: A new discrete-time robust stability condition. Syst. Control Lett. 37(4), 261–265 (1999)
5. Doyle, J.C., Francis, B.A., Tannenbaum, A.R.: Feedback control theory. MacMillan, New York (1992)
6. Dumitrescu, B.: Positive trigonometric polynomials and signal processing applications. Springer, Berlin (2007)

7. Geromel, J.C., Peres, P.L.D., Bernussou, J.: On a convex parameter space method for linear control design of uncertain systems. SIAM J. Control Optim. 29, 381–402 (1991)
8. Gilbert, W.: Synthèse LPV polynomiale appliquée à la commande de turboréacteurs. PhD thesis, INSA Toulouse, LAAS-CNRS and Safran-Snecma (not publicly available) (November 2008)
9. Gilbert, W., Henrion, D., Bernussou, J., Boyer, D.: Polynomial LPV synthesis applied to turbofan engines. Control Eng. Practice 18, 1077–1083 (2010)
10. Henrion, D., Arzelier, D., Peaucelle, D., Šebek, M.: An LMI condition for robust stability of polynomial matrix polytopes. Automatica 37(3), 461–468 (2001)
11. Henrion, D., Bachelier, O., Šebek, M.: D-stability of polynomial matrices. Int. J. Control 74(8), 845–856 (2001)
12. Henrion, D., Šebek, M., Kučera, V.: Positive polynomials and robust stabilization with fixed-order controllers. IEEE Trans. Autom. Control 48(7), 1178–1186 (2003)
13. Henrion, D., Arzelier, D., Peaucelle, D.: Positive polynomial matrices and improved LMI robustness conditions. Automatica 39, 1479–1485 (2003)
14. Henrion, D., Ghildiyal, P.: Optimization with polynomials and fixed-order robust controllers: a design example. Views-and-News letter of the SIAM Activity Group on Optimization 15(2), 15–17 (2004)
15. Henrion, D., Lasserre, J.-B.: Convergent relaxations of polynomial matrix inequalities and static output feedback. IEEE Trans. Autom. Control 51(2), 192–202 (2006)
16. Karimi, A., Khatibi, H., Longchamp, R.: Robust control of polytopic systems by convex optimization. Automatica 43(8), 1395–1402 (2007)
17. Lasserre, J.-B.: Moments, positive polynomials and their applications. Imperial College Press, London (2009)
18. Löfberg, J.: YALMIP: a toolbox for modeling and optimization in Matlab. In: Proc. IEEE CACSD Symposium, Taipei, Taiwan (2004)
19. Nemirovski, A.: Advances in convex optimization: conic programming. In: Proc. Int. Congress Math., Madrid (August 2006)
20. Reberga, L.: Commande robuste multivariable des turboréacteurs. PhD thesis, INSA Toulouse, LAAS-CNRS and Safran-Snecma (not publicly available) (September 2005)
21. Reberga, L., Henrion, D., Bernussou, J., Vary, F.: LPV modeling of a turbofan engine. In: Proc. IFAC World Congress on Automatic Control, Prague, Czech Rep. (July 2005)
22. Scherer, C.W.: LMI relaxations in robust control. Europ. J. Control 12(1), 3–29 (2006)
23. Vary, F., Reberga, L.: Programming and computing tools for jet engine control design. In: Proc. IFAC World Congress on Automatic Control, Prague, Czech Rep. (July 2005)
24. Wassink, M.G., van de Wal, M., Scherer, C.W., Bosgra, O.: LPV control for a wafer stage: beyond the theoretical solution. Control Eng. Practice 13(2), 231–245 (2005)
25. Yang, F., Gani, M., Henrion, D.: Fixed-order robust H-infinity controller design with regional pole assignment. IEEE Trans. Autom. Control 52(10), 1959–1963 (2007)
26. Zhou, K., Doyle, J.C., Glover, K.: Robust and optimal control. Prentice-Hall, Upper Saddle River (1996)

Chapter 5
Polytopic Observers for LPV Discrete-Time Systems

Meriem Halimi, Gilles Millerioux, and Jamal Daafouz

Abstract. The main goal of this work is to give a general treatment on observer synthesis for LPV systems in the framework of Linear Matrix Inequalities. A special Parameter Dependent Lyapunov Function, called poly-quadratic Lyapunov function, is considered. It incorporates the parameter variations for LPV systems with polytopic parameter dependence and allows to guarantee a so-called poly-quadratic stability which is sufficient to ensure Global Asymptotic Stability. The concept of polytopic observers is introduced. A LMI-based method for the synthesis of this type of observers is proposed. The case when LPV systems are subjected to disturbances or when the parameter is known with a bounded level of uncertainty is further addressed. Conditions to guarantee performances like Input-to-State Stability (ISS), bounded peak-to-peak gain and L2 gain are given. The design of polytopic Unknown Input Observers both in the deterministic and in the noisy or uncertain cases is also presented. Finally, two illustrative examples dealing with polytopic observers for chaos synchronization and air path management of a turbocharged Spark Ignition engine are detailed.

5.1 Introduction

Linear Parameter Varying (LPV) systems are linear models whose state representation depends on a parameter vector which can vary in time. Since several years these systems give rise to more and more attention, both in control [2] [32] [24] [38] [23] [16] and in observation and filtering [4] [20] [40] [37]. Contrarily to systems with parametric uncertainties, in this case the current values of the parameters are assumed to be known. The variation of the parameters within a bounded set might be arbitrarily fast or restricted by a certain rate of variation. This LPV modeling techniques have gained a lot of interest as they provide a systematic procedure to design

Meriem Halimi · Gilles Millerioux · Jamal Daafouz
Université de Lorraine,
CRAN Centre de Recherche en Automatique de Nancy (UMR CNRS 7039),
Campus Sciences, BP 70239, 54506 VANDOEUVRE Cedex

O. Sename et al. (Eds.): *Robust Control and LPV Approaches*, LNCIS 437, pp. 97–124.
DOI: 10.1007/978-3-642-36110-4_5

gain-scheduled controllers, especially those related to aerospace control [36]. The main goal of this work is to give a general treatment on observer synthesis for LPV systems in the framework of Linear Matrix Inequalities [22].

A key stage for the synthesis of observer is the search for an adequate Lyapunov function. A usual approach is to call for a single quadratic Lyapunov function [5][22]. This approach suffers from conservatism since it does not take into account the parameter variations of the LPV system. In some cases, it may cause the problem to be infeasible, meaning that quadratic stabilization cannot be achieved. A significant improvement can be obtained by considering Parameter Dependent Lyapunov Functions (PDLF) which incorporate the parameter variations. A special parameter dependence is the affine one [18][17] and can be extended to a polynomial one [6]. Unfortunately, affine parameter dependent Lyapunov functions lead to an infinite number of constraints because all the values of the parameters which continuously vary in some prescribed range have to be considered. Thus, one must discretize the range of all admissible values in order to obtain a finite set of constraints. Another usual dependence is the polytopic one which allows to overpass the discretization and to turn the problem into the resolution of a finite set of constraints by only considering the vertices of the polytope. This is precisely the option which is chosen in the present treatment. A suitable Parameter Dependent Lyapunov function associated to the polytopic description is the so-called poly-quadratic Lyapunov function [11]. It allows to guarantee the so-called poly-quadratic stability which is sufficient to ensure Global Asymptotic Stability.

The layout of the paper is the following. In Section 5.2, some basic definitions are recalled including the notions of Global Asymptotical Stability and Input-to-State Stability (ISS). Section 5.3 is devoted to LPV models with special emphasis on the polytopic one. In Section 5.4 is introduced the concept of polytopic observers. A LMI-based method for the synthesis of this type of observers is proposed. It is based on the notion of poly-quadratic stability. Section 5.5 addresses the case when the LPV system is subjected to disturbances or when the parameter is known with a bounded level of uncertainty. Conditions to guarantee performances like ISS, bounded peak-to-peak gain and $\mathscr{L}_2$ gain are given. Section 5.6 deals with the design of polytopic Unknown Input Observers both in the deterministic and in the noisy or uncertain cases. Finally, illustrative examples are detailed in Section 5.7.

Notation

$\mathbb{R}$, $\mathbb{R}_+$ and $\mathbb{N}$: the field of real numbers, the set of non-negative real numbers and the set of non-negative integers, respectively.

$z^{(i)}$: the ith component of a real vector z. z^T: the transpose for the vector z. $\|z\| = \sqrt{z^T z}$: the Euclidean norm of z. $\|z\|_\infty$: the infinity norm of z given by $\max_i |z^{(i)}|$. $\{z\}$: a sequence of samples $z_k, z_{k+1}, \ldots$ without explicit initial and final discrete-time $k \in \mathbb{N}$. $\{z\}_{k_1}^{k_2}$: a sequence of samples $z_{k_1}, \ldots, z_{k_2}$. $\|z\|_2 = \sqrt{\sum_{k=0}^{\infty} z_k^T z_k}$: the Euclidean norm for a sequence $\{z\}$. $\|z\|_\infty$: the supremum norm given by $\|z\|_\infty = sup_{k\in\mathbb{N}} \|z_k\|$ for a sequence $\{z\}$.

$\mathbf{1}$: the identity matrix of appropriate dimension. $\mathbf{0}$: the zero matrix of appropriate dimension. X^T: the transpose for the matrix X. $X > 0$ $(X < 0)$: a positive definite

(negative definite) matrix X. $X \geq 0$ $(X \leq 0)$: a semi-positive definite (semi-negative definite) matrix X. $\|X\| = \sqrt{\lambda_{max}(X^T X)}$: the spectral norm of the matrix X, where λ_{max} is the largest eigenvalues of $X^T X$. $X^\dagger$: the generalized inverse (Moore-Penrose) of X satisfying $X^\dagger X$ symmetric, $XX^\dagger$ symmetric, $XX^\dagger X = X$ and $X^\dagger XX^\dagger = X^\dagger$. If X is nonsingular then $X^\dagger = X^{-1}$. $(\bullet)$: the blocks of a matrix induced by symmetry.

5.2 Preliminaries

Definition 5.1. A function $\varphi : \mathbb{R}_+ \to \mathbb{R}_+$ belongs to class $\mathscr{K}$ if it is continuous, strictly increasing and $\varphi(0) = 0$, and to class $\mathscr{L}_\infty$ if additionally $\varphi(s) \to \infty$ as $s \to \infty$

Definition 5.2. A function $\beta : \mathbb{R}_+ \times \mathbb{R}_+ \to \mathbb{R}_+$ belongs to class $\mathscr{K}\mathscr{L}$ if for each fixed $k \in \mathbb{R}_+$, $\beta(.,k) \in \mathscr{K}$ and for each fixed $s \in \mathbb{R}_+$, $\beta(s,.)$ is decreasing and $lim_{k\to\infty}\beta(s,k) = 0$.

Consider the discrete-time nonlinear systems

$$x_{k+1} = f(x_k) \tag{5.1}$$
$$x_{k+1} = f_w(x_k, w_k) \tag{5.2}$$

with $x_k \in \mathbb{R}^n$ is the state vector, $w_k \in \mathbb{R}^{d_w}$ is an unknown disturbance input.

Definition 5.3. The system (5.1) is called Globally Asymptotically Stable (GAS) if there exists a $\mathscr{K}\mathscr{L}$-function β such that, for each $x_0 \in \mathbb{R}^n$, it holds that the corresponding state trajectory satisfies for all $k \in \mathbb{N}$

$$\|x_k\| \leq \beta(\|x_0\|, k)$$

Definition 5.4. The system (5.2) is said to be Input-to-State Stable (ISS) with respect to w_k if there exist a $\mathscr{K}\mathscr{L}$ function β and a $\mathscr{K}$ function γ such that, for all input sequences $\{w\}$, for each $x_0 \in \mathbb{R}^n$, it holds that the corresponding state trajectory satisfies for all $k \in \mathbb{N}$

$$\|x_k\| \leq \beta(\|x_0\|, k) + \gamma(\|w\|_\infty) \tag{5.3}$$

If β can be taken of the form $\beta(s,k) = ds\zeta^k$ for some $d \geq 0$ and $0 < \zeta < 1$, ζ is the decay factor for (5.1) and the function γ is an ISS gain for (5.2).

5.3 LPV Models

We investigate LPV systems given by the following form:

$$\begin{cases} x_{k+1} = A(\rho_k)x_k + Bu_k \\ y_k = Cx_k + Du_k \end{cases} \tag{5.4}$$

where $x_k \in \mathbb{R}^n$ is the state vector, $u_k \in \mathbb{R}^m$ is the control input, $y_k \in \mathbb{R}^p$ is the output vector, $A \in \mathbb{R}^{n\times n}$ is the dynamical matrix depending on the possibly time varying parameter vector $\rho_k = \left[\rho_k^{(1)}, \rho_k^{(2)}, ..., \rho_k^{(L)}\right] \in \mathbb{R}^L$, $C \in \mathbb{R}^{p\times n}$ is the output matrix, $B \in \mathbb{R}^{n\times m}$ is the input matrix.

For obvious practical considerations and as usual in the framework of LPV systems, we assume that each component $\rho^{(i)}$ $(i = 1, \ldots, L)$ of ρ_k lies in a bounded range $[\rho_{min}^{(i)}, \rho_{max}^{(i)}]$. As a result, ρ_k lies in a bounded set $\Omega_\rho \subset \mathbb{R}^L$. The dependence of $A(\rho_k)$ with respect to ρ_k can take many forms. However, some of them are of special importance when it comes to analysis and synthesis. We focus here on two specific decompositions, namely, affine and polytopic.

The affine decomposition refers to an affine dependency of $A(\rho_k)$ with respect to ρ_k. $A(\rho_k)$ is thereby of class C^1 with respect to ρ_k and so, can be rewritten as

$$A(\rho_k) = \bar{A_0} + \sum_{j=1}^{L} \rho_k^{(j)} \bar{A_j} \tag{5.5}$$

where $\bar{A_0}$ and $\bar{A_j}$ are constant matrices obtained by separating constant terms and terms depending on $\rho_k^{(j)}$.

The polytopic decomposition refers to a dependence on ρ_k of $A(\rho_k)$ which reads

$$A(\rho_k) = \sum_{i=1}^{N} \xi_k^{(i)}(\rho_k) A_i \tag{5.6}$$

where ξ_k belongs to the compact set S

$$S = \left\{ \mu_k \in \mathbb{R}^N, \mu_k = \left[\mu_k^{(1)}, \ldots, \mu_k^{(N)}\right], \mu_k^{(i)} \geq 0 \; \forall \, i \text{ and } \Sigma_{i=1}^N \; \mu_k^{(i)} = 1 \right\}$$

Owing to the convexity of S, the set of matrices $\{A_1, \ldots, A_N\}$ defines a polytope denoted D_A and the matrices A_i correspond to the vertices of D_A. Hereafter, for the sake of simplicity and whenever possible, the parameter dependency on ρ_k of $\xi_k^{(i)}$ will be omitted, that is the notation $\xi_k^{(i)}$ will be used instead of $\xi_k^{(i)}(\rho_k)$.

It is noteworthy to mention that the affine decomposition (5.5) can be rewritten in the polytopic form (5.6). Indeed, since ρ_k belongs to a bounded set Ω_ρ, it can be embedded in a polytope D_ρ with vertices $\theta_i, \ldots, \theta_N \in \mathbb{R}^L$, such that

$$\rho_k = \sum_{i=1}^{N} \xi_k^{(i)} \theta_i, \; \xi_k \in S \tag{5.7}$$

Substituting (5.7) into (5.5) yields:

$$A(\rho_k) = \bar{A_0} + \sum_{j=1}^{L} (\sum_{i=1}^{N} \xi_k^{(i)} \theta_i^{(j)}) \bar{A_j}, \; \xi_k \in S \tag{5.8}$$

Since $\sum_{i=1}^{N} \xi_k^{(i)} = 1$ and A_0 is a constant matrix, it follows that $A_0 = \sum_{i=1}^{N} \xi_k^{(i)} A_0$ and therefore (5.8) turns into:

$$A(\rho_k) = \sum_{i=1}^{N} \xi_k^{(i)} (\bar{A}_0 + \sum_{j=1}^{L} \theta_i^{(j)} \bar{A}_j), \ \xi_k \in S \tag{5.9}$$

Identifying (5.6) and (5.9) yields

$$A_i = \bar{A}_0 + \sum_{j=1}^{L} \theta_i^{(j)} \bar{A}_j \tag{5.10}$$

The constraint "$\xi_k \in S$" is equivalent to "$\rho_k \in D_\rho$". Since $\Omega_\rho \subseteq D_\rho$, it should be pointed out that the polytopic description (5.6) may describe a broader class of systems than the original one, leading thereby to some conservatism. However, when the components $\rho_k^{(j)}$ $(j = 1, \ldots, L)$ of (5.5) are independent, Ω_ρ turns into a specific polytope D_ρ called hypercube with $N = 2^L$ vertices and in this case $\Omega_\rho = D_\rho$.

5.3.1 Minimal Polytope

It may happen that obtaining analytically the polytope D_ρ is either a hard task or even is not possible. Moreover, we should be concerned, for the sake of conservatism, to get a minimal polytope. Let us assume that we can get, by simulation or experimentally, a sufficient number of vectors ρ_k, collected in a finite set Γ_ρ of cardinality N_ρ, to describe the set Ω_ρ with proper accuracy. The minimal polytope D_ρ^* wherein Ω_ρ is embedded can thereby be considered as the convex hull of the set of points Γ_ρ. We recall that an element of a finite set of points is an extreme point if it is not a convex combination of other points in this set. Hence, finding out D_ρ^* amounts to finding out the extreme points of Γ_ρ. It turns out that the computation can be performed by standard methods. They are briefly recalled below while a detailed review is provided in [25].

The computation of the convex hull for the dimension $L = 2$ has been extensively studied and several efficient algorithms are available. The most popular is the Graham Scan [19]. It is based on the consideration that the angle between two consecutive faces (formed by three consecutive vertices) of the convex hull is lower than π. The complexity of the algorithm is $O(N_\rho log N_\rho)$. This algorithm has a main drawback in that it cannot be extended to dimensions greater than 2. Another efficient algorithm called Quick hull is based on the "divide and conquer" approach. It has been introduced in slightly different forms by [15] and [35]. Such an algorithm uses the property which stipulates that given a triangle of three points of the original set, the points strictly inside this triangle do not belong to the convex hull. Hence, they can be discarded. The complexity of this algorithm is also $O(N_\rho log N_\rho)$. Moreover it can be easily extended to any dimension (see [1] for the dimension $L = 3$).

However, the complexity grows up rapidly and becomes redhibitory for large dimensions. The algorithm Quick hull is incorporated into the built-in function *convhull* of the software Matlab. The algorithm Random Sampling presented in [9] is based on iterative projections on hyperplanes randomly chosen. Finally, a linear program approach is proposed in [33] which calls for solving an optimization problem.

5.3.2 On Line Polytopic Decomposition

In this subsection, we are concerned with a way of working out on-line the vector $\xi_k = \left[\xi_k^{(1)} \cdots \xi_k^{(N)}\right]^T$ involved in the polytopic decomposition (5.7) of ρ_k and (5.6) of $A(\rho_k)$. The vector ξ_k is solution of

$$\begin{array}{c} W_k = Z \;\; \xi_k \\ s.t \; \xi_k^{(i)} \geq 0, \;\; i = 1, \ldots, N \end{array} \tag{5.11}$$

where

$$W_k = [\rho_k^{(1)} \cdots \rho_k^{(L)} \; 1]^T \quad \text{and} \quad Z = \begin{bmatrix} \theta_1^{(1)} & \cdots & \theta_N^{(1)} \\ \vdots & \cdots & \vdots \\ \theta_1^{(L)} & & \theta_N^{(L)} \\ 1 & \ldots & 1 \end{bmatrix}$$

and where the entries θ_i are given, the matrix Z of dimension $(L+1) \times N$ being thereby constant and known. Indeed, it is assumed that ρ_k is on-line available, as usual in the framework of LPV systems. The matrix Z may be of large dimension and is likely to be not amenable for an efficient on-line computation of ξ_k. A method has been proposed in [25] to circumvent this problem.

5.3.3 LPV Models for the Description of Nonlinear Systems

LPV systems can model nonlinear systems under certain conditions. Standard procedures call for interpolation of linearized systems but the resulting LPV model is only an approximation of the actual nonlinear system. As a result, concluding on stability and performances of the nonlinear system based on the LPV approximation may be misleading [24]. Hence, we should rather be interested in an exact description. Such a purpose has been investigated in the works reported in [7] or in the paper [25].

Consider the nonlinear system

$$x_{k+1} = g(x_k, u_k) \tag{5.12}$$

where $x_k \in X \subseteq \mathbb{R}^n$ is the state vector and $u_k \in \mathbb{R}^m$ is the control input.

Proposition 1. *If the following conditions are fulfilled*

- *there exists a function* $\rho : \mathbb{R}^n \to \mathbb{R}^L$ *such that* $A(\rho(x_k))x_k + Bu_k = g(x_k, u_k)$
- $\rho(x_k)$ *depends only on measured signals*
- $\rho(x_k)$ *is bounded when* x_k *lies in the admissible set* $X \subseteq \mathbb{R}^n$

then the nonlinear system (5.12) admits an exact LPV description in the form of the first equation of (5.4) with $\rho_k = \rho(x_k)$.

It is worth pointing out that, most often, the LPV description is not unique and multiple functions ρ can be candidates. Furthermore, the resulting LPV model describes a larger class of systems than the original nonlinear one. Indeed, a trajectory of the nonlinear system is also a trajectory of the LPV model, among an infinite number of possibilities, but the converse is not true. More formally, an LPV system is a linear differential inclusion parameterized in the vector ρ_k. And yet, there is no unique linear differential inclusion of a nonlinear system. The choice can be guided by the objective of reducing the conservatism of the stability conditions or enhancing their tractability both for analysis of synthesis issues. It can also be interesting to select an appropriate function ρ so as the domains of attraction of both models are as most coincident as possible.

In the rest of this work, it will be assumed that the matrix $A(\rho_k)$ in (5.4) is rewritten in the polytopic form (5.6).

The extension to LPV systems with time varying matrices B, C and D is possible. A first option is to merely consider an augmented vector $\bar{\rho}_k$ which involves all the parameter vectors associated to the respective matrices A, B, C and D and to get a polytopic description of the matrix

$$\begin{bmatrix} A(\bar{\rho}_k) & B(\bar{\rho}_k) \\ C(\bar{\rho}_k) & D(\bar{\rho}_k) \end{bmatrix} = \sum_{i=1}^{N} \xi_k^{(i)} \begin{bmatrix} A_i & B_i \\ C_i & D_i \end{bmatrix}, \quad \xi_k \in S$$

Another alternative would follow the same line of reasoning as the one provided in Theorem 1 of [31].

5.4 Polytopic Observers in a Noise-Free Context

5.4.1 Observability and Detectability

5.4.1.1 Observability

As far as the observability of LPV systems is concerned, the following theorem, borrowed from [40] holds.

Theorem 5.1. *System (5.4) is completely observable if* $rank(\mathcal{O}_n(\rho_{k:k+n-1})) = n$ *for all* $k \in \mathbb{Z}$.

where $\mathscr{O}_n(\rho_{k:k+n-1})$ is the so-called parameter varying state-observability matrix of (5.4) defined, for $n > 1$, as

$$\mathscr{O}_n(\rho_{k:k+n-1}) = \begin{bmatrix} C \\ CA(\rho_k) \\ \vdots \\ C\prod_{l=0}^{n-2} A(\rho_{k+n-2-l}) \end{bmatrix} \tag{5.13}$$

and $\rho_{k:k+n-1} = [\rho_k, \cdots, \rho_{k+n-1}]$. For $n = 1$, $\mathscr{O}_n(\rho_{k:k+n-1})$ reduces to $\mathscr{O}_1(\rho_{k:k}) = C$.

In other words, the concept of observability is defined similarly to the linear case when considering all possible trajectories of the parameter $\rho_k \in \Omega_\rho$. Actually, Theorem 5.1 is a straightforward extension of the condition of observability stated in [34] which deals with linear time-varying systems. Hence, in Theorem 5.1, the constraint "for all $k \in \mathbb{Z}$" can be reinterpreted in the case of LPV systems as "for all $\rho_k \in \Omega_\rho$".

The problem lies in that the conditions are much less tractable for LPV systems than for linear systems since, in the general case, the number of trajectories of $\rho_k \in \Omega_\rho$, and so the number of vectors $\rho_{k:k+n-1}$ is infinite. And yet, unfortunately, the observability of the pairs (C, A_i) assigned to the vertices of the polytope D_A does not necessarily induce the observability for all the pairs $(C, A(\rho_k))$. As an example, let us consider the system obeying the form (5.4) with

$$A(\rho_k) = \begin{bmatrix} 0.6+\rho_k & 1 \\ 1 & 0 \end{bmatrix} \quad \text{and} \quad C = \begin{bmatrix} 1 & 0.5 \end{bmatrix}$$

The parameter ρ_k belongs to the range $[0\ 1]$.

The observability matrix is given by

$$\mathscr{O}_2([\rho_k, \rho_{k+1}]) = \begin{bmatrix} 1 & 0.5 \\ \rho_k + 1.1 & 1 \end{bmatrix}$$

The observability matrix for the respective pairs (C, A_1) and (C, A_2), with $A_1 = A(0)$ and $A_2 = A(1)$ numerically reads

$$\mathscr{O}_2([0, *]) = \begin{bmatrix} 1 & 0.5 \\ 1.1 & 1 \end{bmatrix} \quad \text{and} \quad \mathscr{O}_2([1, *]) = \begin{bmatrix} 1 & 0.5 \\ 2.1 & 1 \end{bmatrix}$$

where * stands for an arbitrary value of ρ_{k+1}, the observability matrix depending exclusively on ρ_k.

It is clear that $rank(\mathscr{O}_2([0, *])) = rank(\mathscr{O}_2([1, *])) = 2$. However, for $\rho_k = 0.9$, the observability matrix numerically reads

$$\mathscr{O}_2([0.9, *]) = \begin{bmatrix} 1 & 0.5 \\ 2 & 1 \end{bmatrix}$$

and so $rank(\mathscr{O}_2([0.9,*])) = 1$. As a result, the two pairs (C,A_1) and (C,A_2) are observable whereas the observability is not satisfied inside the polytope D_A when $\rho_k = 0.9$.

A reduction of the computational cost for testing the observability rank condition of Theorem 5.1 is most often either a hard task or merely infeasible.

5.4.1.2 Detectability

The notion of detectability relies on the notion of stability of the unobservable subspace. And yet, similarly to general nonlinear systems, stability of LPV systems can match different definitions. Hence, despite the resulting conservatism, we must resort to specific ones. For instance in [41], detectability is defined analogously to quadratic stability, that is

Theorem 5.2. *The LPV system (5.4) is quadratically detectable, if there exists a matrix $P = P^T > 0$ and a matrix function $L(\rho_k)$ such that*

$$(A(\rho_k) + L(\rho_k)C)^T P + P(A(\rho_k) + L(\rho_k)C) < 0 \;\; \forall \rho_k \in \Omega_\rho$$

It turns out that checking for the conditions of Theorem 5.2 is equally computationally demanding as the actual observer synthesis. Let us also notice that the computation of related invariant subspaces associated to the notion of detectability is not trivial (see however a special treatment in [3] for example).

As a conclusion of this section, the practical use of observability and detectability is often of limited interest and these notions do not deserve in general extensive investigation.

5.4.2 Synthesis

Let us recall that it is assumed that the matrix $A(\rho_k)$ in (5.4) is rewritten in the polytopic form (5.6).

A polytopic observer for (5.4) obeys the following state space description

$$\begin{cases} \hat{x}_{k+1} = A(\rho_k)\hat{x}_k + Bu_k + L(\rho_k)(y_k - \hat{y}_k) \\ \hat{y}_k = C\hat{x}_k + Du_k \end{cases} \tag{5.14}$$

where L is a time varying gain matrix depending on ρ_k which reads

$$L(\rho_k) = \sum_{i=1}^{N} \xi_k^{(i)}(\rho_k) L_i, \;\; \xi_k \in S \tag{5.15}$$

and where the $\xi_k^{(i)}(\rho_k)$ in (5.15) coincide, for every discrete time k, with the ones involved in the polytopic decomposition (5.6) of $A(\rho_k)$.

It's a simple matter to see that, from (5.4) and (5.14), the reconstruction error $e_k = x_k - \hat{x}_k$ is governed by the dynamics

$$e_{k+1} = (A(\rho_k) - L(\rho_k)C)\, e_k \tag{5.16}$$

The dynamics of the state reconstruction is nonlinear since A and L depend on ρ_k. However, (5.16) can be viewed as an autonomous LPV polytopic system with state vector $e_k \in \mathbb{R}^n$. Indeed, from (5.6) and (5.15), and taking into account the coincidence between the $\xi_k^{(i)}$s involved in (5.15) and (5.6), we get that

$$e_{k+1} = \sum_{i=1}^{N} \xi_k^{(i)} (A_i - L_i C) e_k, \quad \xi_k \in S \tag{5.17}$$

Global Asymptotical Stability around the equilibrium point $e^* = 0$ can be ensured by a suitable choice of the gains L_i $(i = 1, \ldots, N)$ involved in (5.15). To this end, the following theorem is central.

Theorem 5.3. *If there exist symmetric matrices P_i, matrices G_i and matrices F_i fulfilling, $\forall (i,j) \in \{1...N\} \times \{1...N\}$, the Linear Matrix Inequalities*

$$\begin{bmatrix} P_i & (\bullet)^T \\ G_i A_i - F_i C & G_i^T + G_i - P_j \end{bmatrix} > 0 \tag{5.18}$$

then the polytopic observer (5.14) with gain $L(\rho_k) = \sum_{i=1}^{N} \xi_k^{(i)}(\rho_k) L_i$ and $L_i = G_i^{-1} F_i$ ensures that the system (5.16) is GAS.

Proof 1. *The detailed proof is given in [12]. It is shown that (5.18) ensures the existence of a Lyapunov function $V : \mathbb{R}^n \times \mathbb{R}^L \to \mathbb{R}_+$ defined by $V(e_k, \rho_k) = e_k^T P(\rho_k) e_k$ with $P(\rho_k) = \sum_{i=1}^{N} \xi_k^{(i)}(\rho_k) P_i$ and $\xi_k \in S$, called poly-quadratic Lyapunov function, fulfilling for all $e_k \in \mathbb{R}^n$, for all $\xi_k \in S$*

$$V(e_{k+1}, \rho_{k+1}) - V(e_k, \rho_k) < 0 \tag{5.19}$$

Such a function ensures the poly-quadratic stability of (5.16) which is sufficient for Global Asymptotical Stability.

5.4.3 Decay Rate

We should be concerned with monitoring the rate of convergence towards $e^* = 0$. In this respect, the decay rate is well suited. The global asymptotical convergence of (5.16) towards $e^* = 0$ with decay rate $\alpha > 1$ is formalized as follows:

$$\forall e_0 \in \mathbb{R}^n, \quad \lim_{k \to \infty} \alpha^k \|e_k\| = 0 \tag{5.20}$$

In other words, $\|e_k\|$ decreases faster than α^{-k}. A sufficient condition for the global convergence of (5.16) towards $e^* = 0$ with decay rate α is given by the following theorem.

Theorem 5.4. *If there exist symmetric matrices P_i, matrices F_i and G_i fulfilling, for a prescribed scalar κ, $\forall (i,j) \in \{1,\cdots,N\} \times \{1,\cdots,N\}$, the Linear Matrix Inequalities*

$$\begin{bmatrix} \kappa P_i & (\bullet)^T \\ G_i A_i - F_i C & G_i^T + G_i - P_j \end{bmatrix} > 0 \tag{5.21}$$

then the polytopic observer (5.14) with gain $L(\rho_k) = \sum_{i=1}^{N} \xi_k^{(i)}(\rho_k) L_i$ and $L_i = G_i^{-1} F_i$ ensures the global convergence of (5.16) with decay rate α no less than $\kappa^{-\frac{1}{2}}$ $(0 < \kappa < 1)$.

Proof 2. *The proof is detailled in [26]. It is shown that (5.21) ensures the existence of a Lyapunov function $V : \mathbb{R}^n \times \mathbb{R}^L \to \mathbb{R}_+$, defined by $V(e_k, \rho_k) = e_k^T P(\rho_k) e_k$ with $P(\rho_k) = \sum_{i=1}^{N} \xi_k^{(i)}(\rho_k) P_i$ and $\xi_k \in S$, called poly-quadratic Lyapunov function, fulfilling for all $e_k \in \mathbb{R}^n$, for all $\xi_k \in S$*

$$V(e_{k+1}, \rho_{k+1}) - \kappa V(e_k, \rho_k) < 0 \tag{5.22}$$

which is sufficient to obtain (5.20) with $\alpha \geq \kappa^{-\frac{1}{2}}$.

5.5 Polytopic Observers in a Noisy or Uncertain Context

In this section, we are concerned with the situation when the system (5.4) is subjected to disturbances and obeys

$$\begin{cases} x_{k+1} = A(\rho_k) x_k + B u_k + E w_k^d \\ y_k = C x_k + D u_k + H w_k^o \end{cases} \tag{5.23}$$

where $w_k^d \in \mathbb{R}^{d_{w^d}}$ is the disturbance acting on the dynamics through E while $w_k^o \in \mathbb{R}^{d_{w^o}}$ is the disturbance acting on the output through H.

In such a case, Equation (5.16) of the state reconstruction error $e_k = x_k - \hat{x}_k$ turns into

$$e_{k+1} = (A(\rho_k) - L(\rho_k) C) e_k + v_k \tag{5.24}$$

with $v_k = E w_k^d - L(\rho_k) H w_k^o$.

Besides, we can also be concerned with the case when ρ_k is not available but only an estimated parameter $\hat{\rho}_k \in \Omega_{\hat{\rho}}$ is available. The uncertainty level Δ satisfies $\|\rho_k - \hat{\rho}_k\|_\infty < \Delta$. Then, the polytopic observer (5.14) can take the form

$$\begin{cases} \hat{x}_{k+1} = A(\hat{\rho}_k) \hat{x}_k + B u_k + L(\hat{\rho}_k)(y_k - \hat{y}_k) \\ \hat{y}_k = C \hat{x}_k + D u_k \end{cases} \tag{5.25}$$

with

$$L(\hat{\rho}_k) = \sum_{i=1}^{N} \hat{\xi}_k^{(i)}(\hat{\rho}_k) L_i \tag{5.26}$$

In such a case, (5.24) still holds provided that ρ_k is replaced by $\hat{\rho}_k$ and that $v_k = \Delta A(\rho_k, \hat{\rho}_k)x_k$ with $\Delta A(\rho_k, \hat{\rho}_k) = A(\rho_k) - A(\hat{\rho}_k)$.

5.5.1 Input-to-State-Stability (ISS)

Many approaches to derive sufficient conditions to guarantee the ISS are based on the notion of ISS Lyapunov functions.

Definition 5.5. Let $d_1, d_2 \in \mathbb{R}_+$, let $a, b, c, l \in \mathbb{R}_+$ with $a \leq b$ and let $\alpha_1(s) = as^l, \alpha_2(s) = bs^l, \alpha_3(s) = cs^l$ and $\tau \in \mathscr{K}$. A function $V : \mathbb{R}^n \times \mathbb{R}^L \to \mathbb{R}_+$ which satisfies

$$\alpha_1(\|e_k\|) \leq V(e_k, \rho_k) \leq \alpha_2(\|e_k\|) \tag{5.27}$$

$$V(e_{k+1}, \rho_{k+1}) - V(e_k, \rho_k) \leq -\alpha_3(\|e_k\|) + \tau(\|v_k\|) \tag{5.28}$$

for all $e_k \in \mathbb{R}^n$, all $v_k \in \mathbb{R}^n$ and all $\rho_k \in \Omega_\rho$ is called an ISS Lyapunov Function for (5.24).

Theorem 5.5. *If the system (5.24) admits an ISS Lyapunov function, then (5.24) is ISS with respect to v_k, that is there exist a $\mathscr{K}\mathscr{L}$ function β and a $\mathscr{K}$ function γ such that, for all sequences $\{v\}$, for each $e_0 \in \mathbb{R}^n$, it holds that, for all $k \in \mathbb{N}$*

$$\|e_k\| \leq \beta(\|e_0\|, k) + \gamma(\|v\|_\infty) \tag{5.29}$$

5.5.1.1 Link between Poly-Quadratic Stability and ISS

Theorem 5.6. *If the LMIs (5.18) are feasible, then the system (5.24) is ISS with respect to v_k and*

$$\|e_k\| \leq \sqrt{\frac{c_2}{c_1}} \left(1 - \frac{c_3 - \delta}{c_2}\right)^{k/2} \|e_0\| + \sqrt{\frac{c_2 + \delta^{-1}c_4^2}{c_1} \cdot \frac{c_2}{c_3 - \delta}} \cdot \|v\|_\infty \tag{5.30}$$

c_1, c_2, c_3, c_4 and δ are some scalars depending on the eigenvalues of the matrices derived from the solution of (5.18). The quantity $(1 - \frac{c_3 - \delta}{c_2})^{1/2}$ is called the decay factor.

In other words, the polytopic observer (5.14) with gain $L(\rho_k)$ given by (5.15) and derived from the solution of (5.18), built from the matrices of the noise-free system (5.4) and from the assumption that ρ_k is perfectly known, ensures the poly-quadratic stability of (5.16), also guarantees the ISS of (5.24), that is of the state reconstruction error derived from the system (5.23) which describes the system (5.4) subjected to disturbances or/and bounded uncertainties on ρ_k.

Proof 3. *The proof is detailed in [30]. It is shown that (5.18) ensures the existence of an ISS Lyapunov function $V : \mathbb{R}^n \times \mathbb{R}^L \to \mathbb{R}_+$ with $P(\rho_k) = \sum_{i=1}^N \xi_k^{(i)}(\rho_k) P_i$ and $\xi_k \in S$, which is sufficient to derive (5.30).*

5.5.1.2 Minimization of the ISS Gain: A LMI Formulation

The point is that both the decay factor and the ISS gain in (5.30) cannot be prescribed beforehand. The following theorem is an attempt to handle this problem.

Theorem 5.7. *If there exist symmetric matrices P_i, matrices G_i, matrices F_i, fulfilling, for a prescribed scalar $\sigma_{ev} \geq 1$, $\forall (i,j) \in (1,\ldots,N) \times (1,\ldots,N)$, the Linear Matrix Inequalities*

$$\begin{bmatrix} G_i^T + G_i - P_j & \mathbf{0} & G_iA_i - F_iC & G_i \\ (\bullet)^T & \mathbf{1} & \mathbf{1} & \mathbf{0} \\ (\bullet)^T & (\bullet)^T & P_i & \mathbf{0} \\ (\bullet)^T & (\bullet)^T & (\bullet)^T & \sigma_{ev}\mathbf{1} \end{bmatrix} > 0 \tag{5.31}$$

then the polytopic observer (5.14) with gain $L(\rho_k) = \sum_{i=1}^{N} \xi_k^{(i)}(\rho_k) L_i$ and $L_i = G_i^{-1} F_i$, ensures that the system (5.24) is ISS with respect to v_k and

$$\|e_k\| \leq \sqrt{\sigma_{ev}} \left(1 - \frac{1}{\sigma_{ev}}\right)^{k/2} \|e_0\| + \sigma_{ev} \|v\|_\infty \tag{5.32}$$

Proof 4. *The detailed proof is provided in [13] [20]. It is shown that (5.31) ensures the existence of an ISS Lyapunov function $V : \mathbb{R}^n \times \mathbb{R}^L \to \mathbb{R}_+$ with $P(\rho_k) = \sum_{i=1}^{N} \xi_k^{(i)}(\rho_k) P_i$ and $\xi_k \in S$ which verifies for all $e_k \in \mathbb{R}^n$, all $v_k \in \mathbb{R}^n$ and all $\xi_k \in S$ of (5.24), the following conditions*

$$\|e_k\|^2 \leq V(e_k, \rho_k) \leq \sigma_{ev} \|e_k\|^2 \tag{5.33}$$

$$V(e_{k+1}, \rho_{k+1}) - V(e_k, \rho_k) \leq -\|e_k\|^2 + \sigma_{ev} \|v_k\|^2 \tag{5.34}$$

And yet, the existence of V is sufficient to obtain (5.32).

Moreover, we should be interested in optimizing the ISS gain by minimizing σ_{ev} in (5.32). Insofar as σ_{ev} appears in a linear way in the Matrix Inequalities (5.31), the problem

$$\begin{array}{l} min \quad \sigma_{ev} \\ s.t \ (5.31) \end{array} \tag{5.35}$$

is still a convex problem.

5.5.1.3 Decoupling of the Decay Rate and the ISS Gain

It is worth pointing out that, in the previous formulation and in particular when considering (5.32), the quantity σ_{ev} is both involved in the decay factor and in the ISS gain. We should be interested in monitoring independently both of them. This is the purpose of the following theorem.

Theorem 5.8. *If there exist symmetric matrices P_i, matrices G_i, matrices F_i and two real numbers $\mu > 0$ and ν fulfilling, for a prescribed $\lambda \in]0\ 1[$, $\forall (i,j) \in \{1 \cdots N\} \times \{1 \cdots N\}$, the Linear Matrix Inequalities*

$$\begin{bmatrix} (1-\lambda)P_i & (\bullet)^T & (\bullet)^T \\ \boldsymbol{0} & \mu\boldsymbol{1} & (\bullet)^T \\ G_iA_i - F_iC & G_i & G_i^T + G_i - P_j \end{bmatrix} > 0 \tag{5.36}$$

and

$$\begin{bmatrix} \lambda P_i & (\bullet)^T & (\bullet)^T \\ \boldsymbol{0} & (\nu-\mu)\boldsymbol{1} & (\bullet)^T \\ \boldsymbol{1} & \boldsymbol{0} & \nu\boldsymbol{1} \end{bmatrix} > 0 \tag{5.37}$$

then the polytopic observer (5.14) with gain $L(\rho_k) = \sum_{i=1}^{N} \xi_k^{(i)}(\rho_k) L_i$ *and* $L_i = G_i^{-1}F_i$*, ensures that the system (5.24) is ISS with respect to* v_k *and*

$$\|e_k\| \leq \sqrt{\nu\lambda\mu}(1-\lambda)^{k/2} \|e_0\| + \nu \|v\|_\infty \tag{5.38}$$

Proof 5. *The proof follows the same lines of reasoning that the ones provided in [28]. It is shown that (5.36)-(5.37) ensures the existence of an ISS Lyapunov function* $V : \mathbb{R}^n \times \mathbb{R}^L \to \mathbb{R}_+$ *with* $P(\rho_k) = \sum_{i=1}^{N} \xi_k^{(i)}(\rho_k) P_i$ *and* $\xi_k \in S$ *which verifies for all* $e_k \in \mathbb{R}^n$*, all* $v_k \in \mathbb{R}^n$ *and all* $\xi_k \in S$*, the following conditions*

$$\frac{1}{\nu\lambda} \|e_k\|^2 \leq V(e_k, \rho_k) \leq \mu \|e_k\|^2 \tag{5.39}$$

$$V(e_{k+1}, \rho_{k+1}) - V(e_k, \rho_k) \leq -\frac{1}{\nu} \|e_k\|^2 + \mu \|v_k\|^2 \tag{5.40}$$

And yet, the existence of V *is sufficient to obtain (5.38).*

Remark 1. *It can be shown that the conditions (5.36)-(5.37) are less conservative than (5.31) and that (5.31) is a special case of (5.36)-(5.37) when* $\nu = \sigma_{ev}, \lambda = \frac{1}{\sigma_{ev}}$ *and* $\mu = \sigma_{ev}$ *as well.*

Remark 2. *The Matrix Inequalities (5.36)-(5.37) are not linear because of the products* λP_i *in (5.36). Actually, they turn into LMIs if* λ *is fixed. Hence, they can be easily solved due to the fact that* λ *is a scalar and that the range of* λ *is bounded since* $\lambda \in]0, 1[$*. As a result, a simple line search can be performed and* $\lambda = \frac{1}{\sigma_{ev}}$*, that is the solution of (5.31), may be used as an admissible initial starting value.*

Moreover, we should be interested in optimizing the ISS gain by minimizing ν in (5.38). Insofar as ν appears in a linear way in the Matrix Inequalities (5.37), for a prescribed $\lambda \in]0\ 1[$, the problem

$$\begin{array}{c} min \quad \nu \\ s.t \ (5.36) - (5.37) \end{array} \tag{5.41}$$

is still a convex problem.

5.5.2 Peak-to-Peak Gain

The peak-to-peak gain of the state error equation (5.24) is defined as the ratio

$$\sup_{0<\|v\|_\infty<\infty,\ \rho_k\in\Omega_\rho} \frac{\|e\|_\infty}{\|v\|_\infty} \tag{5.42}$$

The peak-to-peak gain is defined in the same way as in the linear case, except that, in addition, all possible trajectories $\rho_k \in \Omega_\rho$ have to be considered.

The following theorem holds.

Theorem 5.9. *If the Linear Matrix Inequalities (5.31) (resp. (5.36)-(5.37)) are fulfilled, then the polytopic observer (5.14) with gain $L(\rho_k) = \sum_{i=1}^{N} \xi_k^{(i)}(\rho_k) L_i$ and $L_i = G_i^{-1} F_i$, ensures that the error e_k of (5.24) admits a peak-to-peak gain smaller than σ_{ev} (resp. smaller than ν). One gets respectively*

$$\sup_{0<\|v\|_\infty<\infty,\ \rho_k\in D_\rho} \frac{\|e\|_\infty}{\|v\|_\infty} < \sigma_{ev} \tag{5.43}$$

$$\sup_{0<\|v\|_\infty<\infty,\ \rho_k\in D_\rho} \frac{\|e\|_\infty}{\|v\|_\infty} < \nu \tag{5.44}$$

Proof 6. *The result can be directly inferred from the inequality (5.32) (resp. (5.38)) by taking the limit of k to infinity and assuming that $\|e_0\| = 0$.*

Let us notice that (5.31) or (5.36)-(5.37) guarantees that the peak-to-peak gain is bounded for all possible trajectories ρ_k in $D_\rho \supseteq \Omega_\rho$ and not in Ω_ρ.

The minimization of the peak-to-peak gain can be performed through (5.35) or (5.41).

5.5.3 $\mathscr{L}_2$ Gain

Let $z_k = \tilde{H} e_k$ be a linear combination of the state reconstruction error e_k obeying the dynamics (5.24).

Definition 5.6. The $\mathscr{L}_2$ gain of the state error equation (5.24) is defined as

$$\sup_{\|v\|_2\neq 0,\ \rho_k\in\Omega_\rho} \frac{\|z\|_2}{\|v\|_2} \tag{5.45}$$

Similarly to the peak-to-peak gain, the $\mathscr{L}_2$ gain is defined in the same way as in the linear case, except that, in addition, all possible trajectories $\rho_k \in \Omega_\rho$ have to be considered.

Theorem 5.10. *If there exist symmetric matrices P_i, matrices G_i and matrices F_i, fulfilling, for a prescribed real number σ_2, $\forall (i,j) \in \{1 \cdots N\} \times \{1 \cdots N\}$, the Linear Matrix Inequalities*

$$\begin{bmatrix} P_i & (\bullet)^T & (\bullet)^T & (\bullet)^T \\ \mathbf{0} & \sigma_2 \mathbf{1} & (\bullet)^T & (\bullet)^T \\ G_i A_i - F_i C & G_i E - F_i H & G_i^T + G_i - P_j & (\bullet)^T \\ \tilde{H} & \mathbf{0} & \mathbf{0} & \sigma_2 \mathbf{1} \end{bmatrix} > 0 \tag{5.46}$$

then the polytopic observer (5.14) with gain $L(\rho_k) = \sum_{i=1}^{N} \xi_k^{(i)}(\rho_k) L_i$ *and* $L_i = G_i^{-1} F_i$*, ensures that the error* e_k *of (5.24) admits a* $\mathscr{L}_2$ *gain smaller than* σ_2*.*

Proof 7. *The proof follows the same lines of reasoning than the ones provided in [27]. It is shown that (5.46) ensures the existence of a Lyapunov function* $V : \mathbb{R}^n \times \mathbb{R}^L \to \mathbb{R}_+$ *defined by* $V(e_k, \rho_k) = e_k^T P(\rho_k) e_k$ *with* $P(\rho_k) = \sum_{i=1}^{N} \xi_k^{(i)}(\rho_k) P_i$ *and* $\xi_k \in S$*, fulfilling for all* $e_k \in \mathbb{R}^n$*, all* $\xi_k \in S$

$$V(e_{k+1}, \rho_{k+1}) - V(e_k, \rho_k) + \sigma_2^{-1} (\tilde{C} e_k)^T (\tilde{C} e_k) - \sigma_2 v_k^T v_k < 0$$

which is sufficient to obtain

$$\sup_{\|v\|_2 \neq 0,\ \rho_k \in D_\rho} \frac{\|z\|_2}{\|v\|_2} < \sigma_2$$

Since σ_2 appears in a linear way in (5.46), the minimization problem

$$\begin{array}{ll} min & \sigma_2 \\ s.t & (5.46) \end{array} \tag{5.47}$$

is still a convex problem.

Let us notice that (5.46) guarantees that the $\mathscr{L}_2$ gain is bounded for all possible trajectories ρ_k in $D_\rho \supseteq \Omega_\rho$ and not in Ω_ρ.

5.6 Unknown Input Observers

This section is devoted to the design of polytopic Unknown Input Observers for LPV systems. State reconstruction error dynamics and its analysis are investigated both in the deterministic case (consideration of Equation 5.4)) and in the case when the system (5.4) is subjected to disturbances (consideration of Equation (5.23)).

5.6.1 Notation and Definitions

In the deterministic case (consideration of Equation (5.4)), when the system (5.4) is driven by an input sequence $\{u\}_0^\infty$, the output y_{k+i} of (5.4) $(i = 0, \cdots, \infty)$ reads

$$y_{k+i} = C(\rho_{k+i}) A_{\rho_k}^{\rho_{k+i-1}} x_k + \sum_{j=0}^{i} \mathscr{T}_{i,j}(\rho_k) u_{k+j} \tag{5.48}$$

with

$$\mathscr{T}_{i,j}(\rho_k) = C(\rho_{k+i})A_{\rho_{k+j+1}}^{\rho_{k+i-1}}B(\rho_{k+j}) \text{ if } j \leq i-1, \;\; \mathscr{T}_{i,i}(\rho_k) = D(\rho_{k+i})$$

Stacking up the outputs (5.48) yields

$$\underline{y}_k^i = \mathscr{O}^i(\rho_k)x_k + M^i(\rho_k)\underline{u}_k^i \tag{5.49}$$

with

$$\mathscr{O}^i(\rho_k) = \begin{bmatrix} C(\rho_k) \\ C(\rho_{k+1})A(\rho_k) \\ \vdots \\ C(\rho_{k+i})A_{\rho_k}^{\rho_{k+i-1}} \end{bmatrix} \tag{5.50}$$

$$\underline{u}_k^i = \begin{bmatrix} u_k \\ u_{k+1} \\ \vdots \\ u_{k+i} \end{bmatrix} \tag{5.51}$$

$$\underline{y}_k^i = \begin{bmatrix} y_k \\ y_{k+1} \\ \vdots \\ y_{k+i} \end{bmatrix} \tag{5.52}$$

and the Toeplitz-like matrix $M^i(\rho_k)$ defined as the following.

$$\text{For } i<0 \;\; M^i(\rho_k) = \mathbf{0}, \text{ for } i=0 \;\; M^0(\rho_k) = D(\rho_k) \;\; \text{and for } i>0,$$

$$M^i(\rho_k) =$$

$$\begin{bmatrix} D(\rho_k) & \mathbf{0}_{p\times m} & \cdots & \cdots & \cdots \\ C(\rho_{k+1})B(\rho_k) & D(\rho_{k+1}) & \mathbf{0}_{p\times m} & \cdots & \cdots \\ \vdots & \vdots & \ddots & \ddots & \ddots \\ \vdots & \vdots & \ddots & \ddots & \ddots \\ C(\rho_{k+i})A_{\rho_{k+1}}^{\rho_{k+i-1}}B(\rho_k) & C(\rho_{k+i})A_{\rho_{k+2}}^{\rho_{k+i-1}}B(\rho_{k+1}) & \cdots & C(\rho_{k+i})B(\rho_{k+i-1}) & D(\rho_{k+i}) \end{bmatrix} \tag{5.53}$$

where

$$\begin{aligned} A_{\rho_{k_0}}^{\rho_{k_1}} &= A(\rho_{k_1})A(\rho_{k_1-1})\ldots A(\rho_{k_0}) \text{ if } \; k_1 \geq k_0 \\ &= \mathbf{1}_n \;\; \text{if} \;\; k_1 < k_0 \end{aligned}$$

is the transition matrix.

In the case when the system (5.4) is subjected to disturbances (consideration of Equation (5.23), when the system (5.23) is driven by an input sequence $\{u\}_0^\infty$, the output y_{k+i} of (5.23) $(i = 0, \cdots, \infty)$ reads

$$y_{k+i} = C(\rho_{k+i})A_{\rho_k}^{\rho_{k+i-1}} x_k + \sum_{j=0}^{i} \mathscr{T}_{i,j}(\rho_k) u_{k+j} + \sum_{j=0}^{i} \mathscr{S}_{i,j}(\rho_k) w_{k+j}^d + H w_{k+i}^o \quad (5.54)$$

with

$$\mathscr{T}_{i,j}(\rho_k) = C(\rho_{k+i})A_{\rho_{k+j+1}}^{\rho_{k+i-1}} B(\rho_{k+j}) \text{ if } j \leq i-1, \;\; \mathscr{T}_{i,i}(\rho_k) = D(\rho_{k+i})$$

$$\mathscr{S}_{i,j}(\rho_k) = C(\rho_{k+i})A_{\rho_{k+j+1}}^{\rho_{k+i-1}} E \text{ if } j \leq i-1, \;\; \mathscr{S}_{i,i}(\rho_k) = \mathbf{0}$$

Stacking up the outputs (5.54) yields

$$\underline{y}_k^i = \mathscr{O}^i(\rho_k) x_k + M^i(\rho_k)\underline{u}_k^i + F^i(\rho_k)\underline{w}_k^{di} + N^i \, \underline{w}_k^{oi} \quad (5.55)$$

with

$$\underline{w}_k^{di} = \begin{bmatrix} w_k^d \\ w_{k+1}^d \\ \vdots \\ w_{k+i}^d \end{bmatrix} \quad (5.56)$$

$$\underline{w}_k^{oi} = \begin{bmatrix} w_k^o \\ w_{k+1}^o \\ \vdots \\ w_{k+i}^o \end{bmatrix} \quad (5.57)$$

The matrix N^i is defined as the following.

$$N^0 = \mathbf{0}, \quad N^1 = \begin{bmatrix} H & \mathbf{0}_{p\times d_{w^o}} \\ \mathbf{0}_{p\times d_{w^o}} & H \end{bmatrix} \quad (5.58)$$

and for $i > 1$, N^i is recursively defined as

$$N^{i+1} = \begin{bmatrix} N^i & \mathbf{0}_{(i+1)\cdot p\times d_{w^o}} \\ \mathbf{0}_{p\times d_{w^o}\cdot(i+1)} & H \end{bmatrix} \quad (5.59)$$

The matrix $F^i(\rho_k)$ is defined as the following.

For $i \leq 0$ $F^i(\rho_k) = \mathbf{0}$ and for $i > 0$,

$$F^i(\rho_k) = \begin{bmatrix} \mathbf{0}_{p\times d_{w^d}} & \mathbf{0}_{p\times d_{w^d}} & \cdots & \cdots & \cdots \\ C(\rho_{k+1})E & \mathbf{0}_{p\times d_{w^d}} & \mathbf{0}_{p\times d_{w^d}} & \cdots & \cdots \\ \vdots & \vdots & \ddots & \ddots & \ddots \\ \vdots & \vdots & \ddots & \ddots & \ddots \\ C(\rho_{k+i})A_{\rho_{k+1}}^{\rho_{k+i-1}}E & C(\rho_{k+i})A_{\rho_{k+2}}^{\rho_{k+i-1}}E & \cdots & C(\rho_{k+i})E & \mathbf{0}_{p\times d_{w^d}} \end{bmatrix} \quad (5.60)$$

Central notions for the design of UIO are left invertibility and inherent delay.

Definition 5.7. The LPV system (5.4) is *left invertible* if it is possible to recover the input u_0 from a finite number of $r+1$ measurements y_i $(i=0,\ldots,r)$, the state vector x_0 at time $k=0$ and the sequence $\{\rho\}_0^r$ of the parameter ρ_k being known. The least integer r for which (5.4) is left invertible is called the *left inherent delay*.

Definition 5.7 is an extension of the notion introduced in [39] for linear MIMO systems. Let us point out that the inherent delay generalizes the notion of relative degree which only holds for SISO systems.

Theorem 5.11. *The LPV system* (5.4) *is* left invertible *if there exists a nonnegative integer* $r<\infty$ *such that for all* $\rho_k \in \Omega_\rho$,

$$rank\, M^r(\rho_k) - rank\, M^{r-1}(\rho_{k+1}) = m \tag{5.61}$$

Proof 8. *The proof follows the same lines of reasoning than the ones provided in [29].*

5.6.2 Deterministic Case

A polytopic unknown input observer for (5.4) obeys the following equations

$$\begin{cases} \hat{x}_{k+r+1} = \bar{P}^r(\rho_k)\hat{x}_{k+r} + \bar{Q}^r(\rho_k)\underline{y}_k^r + L(\rho_k)(y_k - \hat{y}_{k+r}) \\ \hat{y}_{k+r} \quad\quad = C(\rho_k)\hat{x}_{k+r} \end{cases} \tag{5.62}$$

with $\bar{Q}^r(\rho_k)$ obeying

$$\bar{Q}^r(\rho_k) = B(\rho_k)\bar{I}_m M^{r^\dagger}(\rho_k) + Y(\rho_k)(\mathbf{1}_{p(r+1)} - M^r(\rho_k)M^{r^\dagger}(\rho_k)) \tag{5.63}$$

with

$$\bar{I}_m = (\mathbf{1}_m\ \mathbf{0}_{m\times(m\cdot r)}) \tag{5.64}$$

and

$$\bar{P}^r(\rho_k) = A(\rho_k) - \bar{Q}^r(\rho_k)\mathscr{O}^r(\rho_k) \tag{5.65}$$

Let $e_k = x_k - \hat{x}_{k+r}$ be the state error reconstruction. Assuming that Theorem 5.11 is fulfilled, it can be shown, from (5.4) and (5.62)-(5.65) that

$$\begin{aligned} e_{k+1} = &(A(\rho_k) - B(\rho_k)\bar{I}_m M^{r^\dagger}(\rho_k)\mathscr{O}^r(\rho_k) \\ &-Y(\rho_k)(\mathbf{1}_{p(r+1)} - M^r(\rho_k)M^{r^\dagger}(\rho_k))\mathscr{O}^r(\rho_k) \\ &-L(\rho_k)C(\rho_k))e_k \end{aligned} \tag{5.66}$$

The matrix $Y(\rho_k)$ is an arbitrary matrix which plays the role of a parameterization. However, it is worth stressing that in some special cases, an arbitrary choice of $Y(\rho_k)$ may not be suitable for state reconstruction purposes (see [14] in the linear case). To overcome this problem, the computation of $Y(\rho_k)$ should be included in the design procedure. From this perspective, we proceed to the change

of variable $\tilde{A}(\rho_k) = A(\rho_k) - B(\rho_k)\bar{I}_m M^{r^\dagger}(\rho_k)\mathscr{O}^r(\rho_k)$, $\tilde{L}(\rho_k) = [Y(\rho_k) \;\; L(\rho_k)]$ and $\tilde{C}(\rho_k) = \begin{bmatrix} (\mathbf{1}_{p(r+1)} - M^r(\rho_k)M^{r^\dagger}(\rho_k))\mathscr{O}^r(\rho_k) \\ C(\rho_k) \end{bmatrix}$.
Consequently, (5.66) turns into:

$$e_{k+1} = (\tilde{A}(\rho_k) - \tilde{L}(\rho_k)\tilde{C}(\rho_k))e_k \tag{5.67}$$

The problem of guaranteeing the Global Asymptotical Stability of (5.67) around $e^* = 0$ can be tackled in a similar way than in the previous sections devoted to polytopic observers, that is resorting to poly-quadratic stability.

5.6.3 Noisy Case

Likewise in Section 5.5 when the inputs were supposed to be known, we are concerned with the situation when the system (5.4) is subjected to disturbances and obeys (5.23).

Assuming that Theorem 5.11 is fulfilled, it can be shown from (5.4) and the polytopic UIO (5.62) that, after some heavy but quite basic manipulations, the reconstruction error $e_k = x_k - \hat{x}_{k+r}$ obeys

$$\begin{aligned} e_{k+1} = \; & (\bar{P}^r(\rho_k) - L(\rho_k)C(\rho_k))e_k + (Ew_k^d - L(\rho_k)Hw_k^o) \\ & -\bar{Q}^r(\rho_k)(F^r(\rho_k)\underline{w}_k^{dr} + N^r\underline{w}_k^{or}) \end{aligned} \tag{5.68}$$

Replacing the expression (5.63) of $\bar{Q}^r(\rho_k)$ into $\bar{P}^r(\rho_k)$ yields

$$\begin{aligned} e_{k+1} = \; & (A(\rho_k) - B(\rho_k)\bar{I}_m M^{r^\dagger}(\rho_k)\mathscr{O}^r(\rho_k) \\ & -Y(\rho_k)(\mathbf{1}_{p(r+1)} - M^r(\rho_k)M^{r^\dagger}(\rho_k))\mathscr{O}^r(\rho_k) \\ & -L(\rho_k)C(\rho_k))e_k + Ew_k^d - L(\rho_k)Hw_k^o \\ & -(B(\rho_k)\bar{I}_m M^{r^\dagger}(\rho_k) + Y(\rho_k)(\mathbf{1}_{p(r+1)} - M^r(\rho_k)M^{r^\dagger}(\rho_k))) \\ & (F^r(\rho_k)\underline{w}_k^{dr} + N^r\underline{w}_k^{or}) \end{aligned} \tag{5.69}$$

Similarly to the previous case, $Y(\rho_k)$ is an arbitrary matrix which plays the role of a parameterization and we should proceed to the change of variable $\tilde{A}(\rho_k) = A(\rho_k) - B(\rho_k)\bar{I}_m M^{r^\dagger}(\rho_k)\mathscr{O}^r(\rho_k)$, $\tilde{L}(\rho_k) = [Y(\rho_k) \;\; L(\rho_k)]$,
$\tilde{C}(\rho_k) = \begin{bmatrix} (\mathbf{1}_{p(r+1)} - M^r(\rho_k)M^{r^\dagger}(\rho_k))\mathscr{O}^r(\rho_k) \\ C(\rho_k) \end{bmatrix}$.
Consequently, (5.69) turns into:

$$e_{k+1} = (\tilde{A}(\rho_k) - \tilde{L}(\rho_k)\tilde{C}(\rho_k))e_k + v_k \tag{5.70}$$

with:

$$\begin{aligned} v_k = \; & Ew_k^d - L(\rho_k)Hw_k^o \\ & -(B(\rho_k)\bar{I}_m M^{r^\dagger}(\rho_k) + Y(\rho_k)(\mathbf{1}_{p(r+1)} - M^r(\rho_k)M^{r^\dagger}(\rho_k))) \\ & (F^r(\rho_k)\underline{w}_k^{dr} + N^r\underline{w}_k^{or}) \end{aligned}$$

Again, the problem of polytopic unknown input observer design for guaranteeing performances of the convergence behavior around $e^* = 0$ of (5.70) can be tackled in a similar way than in the previous sections devoted to polytopic observers, that is resorting to poly-quadratic stability.

5.7 Illustrative Examples

5.7.1 Example 1

The purpose of this example is to illustrate both an LPV polytopic description of a nonlinear system and the search for the minimal polytope D_ρ^* wherein the set Ω_ρ is embedded. Let us consider the map, with state vector $x_k = [x_k^{(1)} \;\; x_k^{(2)} \;\; x_k^{(3)} \;\; x_k^{(4)}]^T$, given by

$$\begin{cases} x_{k+1}^{(1)} &= (x_k^{(1)})^2 - (x_k^{(2)})^2 + a x_k^{(1)} + b x_k^{(2)} \\ x_{k+1}^{(2)} &= 2 x_k^{(1)} x_k^{(2)} + c x_k^{(1)} + d x_k^{(2)} \\ x_{k+1}^{(3)} &= 0.1 b x_k^{(2)} - 0.1 (x_k^{(2)})^2 + 0.1 x_k^{(3)} \\ x_{k+1}^{(4)} &= 0.5 x_k^{(1)} + 0.1 x_k^{(2)} + 0.3 x_k^{(4)} \\ y_k^{(1)} &= x_k^{(1)} \\ y_k^{(2)} &= x_k^{(2)} \end{cases} \tag{5.71}$$

with $a = 0.9$, $b = -0.6013$, $c = 2$, and $d = 0.5$. For this typical parameters setting, the system exhibits a chaotic motion. A projection of the corresponding chaotic attractor in the 3-dimensional space $(x_k^{(1)}, x_k^{(2)}, x_k^{(3)})$ is depicted in Figure 5.1. We aim at rewriting (5.71) into the LPV form (5.4). To this end, let us choose ρ_k as a parameter vector obeying

$$\begin{aligned} \rho_k^{(1)} &= a + x_k^{(1)} \\ \rho_k^{(2)} &= b - x_k^{(2)} \end{aligned} \tag{5.72}$$

Then, (5.71) can be written as an LPV system of the form (5.4) with

$$A(\rho_k) = \begin{bmatrix} \rho_k^{(1)} & \rho_k^{(2)} & 0 & 0 \\ c & d + 2(\rho_k^{(1)} - a) & 0 & 0 \\ 0 & 0.1\rho_k^{(2)} & 0.1 & 0 \\ 0.5 & 0.1 & 0 & 0.3 \end{bmatrix}$$

and

$$C = \begin{bmatrix} 1 & 0 & 0 & 0 \\ 0 & 1 & 0 & 0 \end{bmatrix}$$

while B and D are zero since the system (5.71) is autonomous.

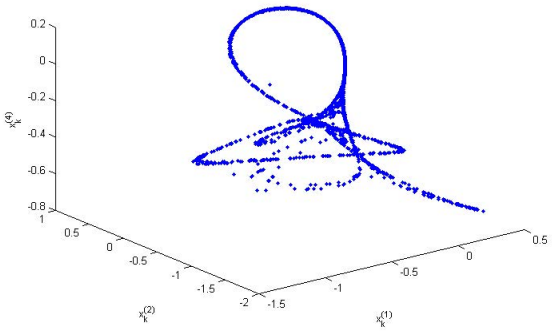

Fig. 5.1 Chaotic attractor in the 3-dimensional space $(x_k^{(1)}, x_k^{(2)}, x_k^{(3)})$

Let us point out that such a choice for ρ_k matches the conditions of the Proposition 1 provided in Subsection 5.3.3. In particular, ρ_k is accessible from the output y_k. Indeed, $\rho_k^{(1)} = a + y_k^{(1)}$ and $\rho_k^{(2)} = b - y_k^{(2)}$.

Now, by simulating (5.71) from an initial condition $x_0 = [-0.72 \ \ -0.64 \ \ 0.1 \ \ 0]^T$ which belongs to the chaotic attractor, we collect 2000 vectors ρ_k in order to build up the set Γ_ρ. Then, the Quick hull approach, implemented in the built-in function *convhull* of the software Matlab, is performed to find out the minimal polytope D_ρ^*. It turns out that 108 vertices θ_i have been found. Both the set Ω_ρ and the minimal polytope D_ρ^* are depicted in Figure 2(a). It should be noted that if the number of the vertices of the polytope is very large, it can be more interesting to minimize the number of vertices in order to enhance the tractability of the LMIs. This is what has precisely been done, as shown in Figure 2(b). The number of the vertices has been reduced to 5 vertices. Let us point out however that the LMIs become more conservative than the ones derived from the minimal polytope.

5.7.2 Example 2

This section illustrates the synthesis of a polytopic observer both in a noise-free as well as in a noisy context. The system under consideration is borrowed from [10] and is called "turbocharged SI engines". Actually, only a part of the system is investigated here. It is briefly described and motivated.

From the perspective of reducing fuel consumption and pollutant emissions of Spark Ignition (SI) engines, new air path management systems have to be proposed. Hence, efficient control of the air actuators is required. For any set point of the torque intended to move the engine, the ratio between the air mass m_{air} and the fuel quantity trapped in the cylinder must be kept constant in order to minimize the pollutant emissions. To this end, the air mass m_{air} trapped in the cylinder must be

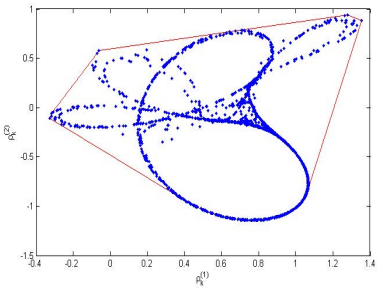

(a)

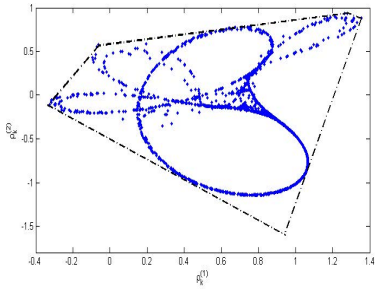

(b)

Fig. 5.2 Set Ω_ρ and polytopes D_ρ^* (a) and D_ρ (b)

known with optimal accuracy in order to predict the quantity of fuel to be injected. It turns out that m_{air} is directly linked to the air flow Q_{cyl} captured in the cylinder.

Actually, a compressor produces a flow from the ambient air. The resulting air flow Q_{th} enters a manifold of which volume is V_{man} and is characterized by a pressure p_{man} and temperature T_{man}. Then, two flows leave the manifold: the first flow which is captured in the cylinder Q_{cyl} and the flow Q_{sc} scavenged from the intake to the exhaust. Unlike Q_{sc}, Q_{th} and p_{man} which are accessible quantities, Q_{cyl} must be estimated from an open loop model of the in-cylinder air mass which delivers $\hat{Q}_{cyl}$. As a result, $Q_{cyl} = \hat{Q}_{cyl} + \Delta Q_{cyl}$ and the error ΔQ_{cyl} can be assumed to be constant because slowly time-varying regarding the overall dynamics. The flow balance in the manifold reads

$$\dot{p}_{man} = \frac{rT_{man}}{V_{man}}(Q_{th} - \hat{Q}_{cyl} - \Delta Q_{cyl} - Q_{sc})$$

As a conclusion, we must estimate ΔQ_{cyl}. However, a direct estimation from the flow balance equation cannot be directly done since it requires the derivative $\dot{p}_{man}$ of p_{man}. Thus, the flow balance equation is written in a state space form where the state vector is composed of p_{man} and ΔQ_{cyl}, the input are the accessible variables, namely, Q_{th}, $\hat{Q}_{cyl}$ and Q_{sc} and finally, the output is p_{man}. An observer is designed to

reconstruct both p_{man} and ΔQ_{cyl}. For implementation reasons, we must discretize the equations. After discretization, one obtains

$$\begin{cases} x_{k+1} = A_d(\rho_k)x_k + B_d(\rho_k)u_k \\ y_k = C_d x_k + D_d u_k \end{cases} \tag{5.73}$$

with:

$$x_k = \begin{bmatrix} p_{man}(k) \\ \Delta Q_{cyl}(k) \end{bmatrix}, \quad u_k = \begin{bmatrix} Q_{th}(k) \\ Q_{cyl}(k) \\ Q_{sc}(k) \end{bmatrix}, \quad y_k = p_{man}(k)$$

$$A_d(\rho_k) = \begin{bmatrix} 1 & \rho_k \\ 0 & 1 \end{bmatrix}, \; B_d = \begin{bmatrix} -\rho_k & \rho_k & \rho_k \\ 0 & 0 & 0 \end{bmatrix}, \; C_d = [1 \quad 0], \; D_d = 0$$

and

$$\rho_k = -r\frac{T_{man}(k)}{V_{man}} t_{tdc}(k)$$

The scalar r is the ideal gas constant and t_{tdc} is the sampling period which is actually time-varying because it depends on the engine speed. After normalization, ρ_k lies in the range $[\rho_{min} \;\; \rho_{max}] = [-3.3453 \;\; -0.0174]$.

We get typically an LPV system which admits a simple polytopic description since D_ρ has clearly only two vertices $\theta_1 = \rho_{min} = -3.3453$ and $\theta_2 = \rho_{max} = -0.0174$. The corresponding matrices A_1 and A_2 are computed according to (5.10) with $L = 2$:

$$A_1 = \begin{bmatrix} 1 & \rho_{min} \\ 0 & 1 \end{bmatrix} \text{ and } A_2 = \begin{bmatrix} 1 & \rho_{max} \\ 0 & 1 \end{bmatrix}$$

In our present case, the matrix B is also parameter dependent. Since it also depends on ρ_k in a similar way, it admits the same polytopic decomposition with vertices

$$B_1 = \begin{bmatrix} -\rho_{min} & \rho_{min} & \rho_{min} \\ 0 & 0 & 0 \end{bmatrix} \text{ and } B_2 = \begin{bmatrix} -\rho_{max} & \rho_{max} & \rho_{max} \\ 0 & 0 & 0 \end{bmatrix}$$

For the state reconstruction of x_k, we resort to a polytopic observer of the form (5.14). The toolbow *Yalmip* of Matlab is used to solve the LMIs required to derive the gain $L(\rho_k)$ of the observer.

Results

Poly-Quadratic stability

It turns out that the LMIs (5.18) are feasible. The resulting gains are respectively $L_1 = [1.9623 \;\; -0.2877]^T, L_2 = [1.0056 \;\; -0.2977]^T$ and ensure the Global Asymptotical convergence of the observer.

Performances in a noisy context: ISS

We solve the problem (5.35) involving the LMIs (5.31) in order to minimize σ_{ev} in the ISS gain of (5.32). The optimal solution is given by $\sigma^*_{ev} = 1.3401\ 10^4$ with observer gains $L_1 = [2.8856 \;\; -0.5637]^T$ and $L_2 = [1.0101 \;\; -0.5779]^T$. Next, in order to minimize ν in the ISS gain of (5.38), we solve the problem (5.41) involving the LMIs (5.36)-(5.37) for different values of λ within the admissible range

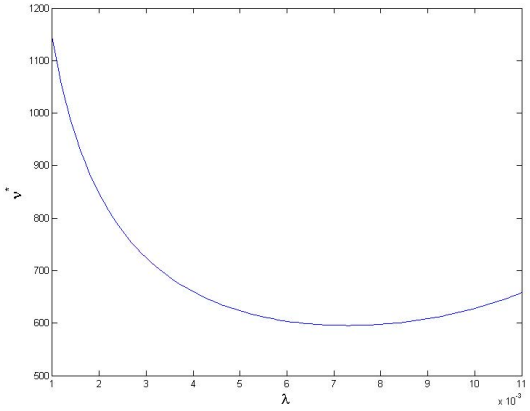

Fig. 5.3 variation of ν^* with respect to λ

$[0.0001 \quad -0.9999]$. The variation of the optimal solution ν^* with respect to λ is plotted in Figure 5.3. As we can see, this variation is convex. The best ISS gain corresponds to $\nu^* = 596.2197$, $\lambda^* = 7.2\ 10^{-3}$ and $\mu^* = 595.9576$. The gains are given by $L_1 = [2.3882 \quad -0.4150]^T$ and $L_2 = [1.0073 \quad -0.4195]^T$. As expected, one has $\sigma_{ev}^* > \nu^*$ since the LMIs (5.31) are more conservative than (5.36)-(5.37).

It can also be interesting to compare the decay factor obtained respectively from (5.31) and (5.36)-(5.37) for the same ISS gain. Let us check the conditions for $\nu = \sigma_{ev}^* = 13401$, that is, for the optimal value of σ_{ev} when considering (5.31). On one hand, the decay factor is given by: $\sqrt{1 - \frac{1}{\sigma_{ev}^*}} = 0.99996$. On the other hand, the solution of (5.36)-(5.37) for $\nu = \sigma_{ev}^* = 13401$ gives $\mu^* = 12207.0353$ and $\lambda^* = 0.0202$ and so a decay factor $\sqrt{1-\lambda^*} = 0.98985$. The corresponding gains are $L_1 = [2.7256 - 0.5158]^T$ and $L_2 = [1.0103 - 0.5891]^T$. As expected by the consideration on the conservatism, for a same ISS gain, we can also get a better decay rate when considering the LMIs (5.36)-(5.37) instead of (5.31).

5.8 Conclusion

Observer design for LPV systems has been discussed. It has been shown that a polytopic approach can be used to take into account not only the classical situation where the parameters can be perfectly measured but also the more realistic situation when the measured parameters are affected by a bounded uncertainty and/or when the system is subjected to disturbances. Both stability of the observation error and performance (ISS, bounded peak-to-peak gain and $\mathscr{L}_2$ gain) have been considered. The theoretical developements end up with the design of polytopic unknown input observers both in the deterministic and in the noisy or uncertain cases. These results

can be extended to take into account constraints related to the parameter rate of variation. Indeed, motivated by practical issues, taking into account the bounds on the rate of variation of the parameters has already been discussed for control design (see [8, 21] and references therein). And yet, it turns out that such a consideration makes sense for observer design as well. Finally, polytopic LPV observers discussed here can be used for both control and diagnosis. As an example, a solution based on polytopic observers for output feedback observer based controllers for LPV systems with inexact parameter measurement is proposed in [20].

References

1. Allison, D.C.S., Noga, M.T.: Computing the three-dimensional convex hull. Computer Physics Communications 103(1), 74–82 (1997)
2. Apkarian, P., Gahinet, P., Becker, G.: A convex characterization of gain-scheduled H_∞ Controllers. IEEE Transactions on Automatic Control 40(5), 853–864 (1995)
3. Balas, G., Bokor, J., Szabo, Z.: Invariant subspaces for lpv systems and their applications. IEEE Trans. on Automatic Control 48(11), 2065–2069 (2003)
4. Bara, G.I., Daafouz, J., Kratz, F., Ragot, J.: Parameter-dependent state observer design for affine LPV systems. International Journal of Control 74(16), 1601–1611 (2001)
5. Becker, G., Packard, A., Philbrick, D., Balas, G.: Control of parametrically-dependent linear systems: a single quadratic lyapunov approach. In: Proc. of American Control Conference, San Fransisco (June 1993)
6. Bliman, P.-A.: Nonconservative lmi approach to robust stability for systems with uncertain scalar parameters. In: Proceeding of 41st IEEE Control and Decision Conference, Las Vegas, USA (December 2002)
7. Bruzelius, F.: Linear Parameter-Varying Systems: an approach to gain scheduling. PhD thesis, Department of Signals and Systems, Chalmers University of Technology, Goteborg, Sweden (2004)
8. Casavola, A., Famularo, D., Franze, G.: A feedback min-max mpc algorithm for lpv systems subject to bounded rates of change of parameters. IEEE Transactions on Automatic Control 47(7) (2002)
9. Chatterjee, S., Chatterjee, S.: A note of finding extreme points in multivariable space. Computational Statistics and Data Analysis 10(1), 87–92 (1990)
10. Colin, G., Bloch, G., Chamaillard, Y., Anstett, F.: Two air path observers for turbocharged SI engines with VCT. Control Engineering Practice 17(5), 571–578 (2009)
11. Daafouz, J., Bernussou, J.: Parameter dependent lyapunov functions for discrete time systems with time varying parametric uncertainties. Systems and Control Letters 43, 355–359 (2001)
12. Daafouz, J., Millérioux, G., Iung, C.: A poly-quadratic stability based approach for switched systems. International Journal of Control 75, 1302–1310 (2002)
13. Daafouz, J., Millérioux, G., Rosier, L.: Observer design with guaranteed bound for lpv systems. In: Proc. of the 16th IFAC World Congress, Prague, Czech Republic, July 4-8 (2005)
14. Darouach, M., Zazadinski, M., Xu, S.J.: Full-order observers for linear systems with unknown inputs. IEEE Trans. on Automatic Control 39(3), 606–609 (1994)
15. Eddy, W.F.: A new convex hull algorithm for planar sets. ACM Transactions on Mathematical Software 3, 398–403 (1977)

16. Farhood, M., Dullerud, G.E.: Control of nonstationary LPV systems. Automatica 44, 2108–2119 (2010)
17. Feron, E., Apkarian, P., Gahinet, P.: Analysis and synthesis of robust control systems via parameter-dependent lyapunov functions. IEEE Trans. on Automatic Control 41, 1041–1046 (1996)
18. Gahinet, P., Apkarian, P., Chilali, M.: Parameter-dependent lyapunov functions for real parametric uncertainty. IEEE Trans. on Automatic Control 41(3), 436–442 (1996)
19. Graham, R.L.: An efficient algorithm for determining the convex hull of a finite planar set. Information Processing Letters 2(1), 132–133 (1973)
20. Heemels, M., Daafouz, J., Millérioux, G.: Observer-based control of discrete-time lpv systems with uncertain parameters. IEEE Trans. on Automatic Control 55(9), 2130–2135 (2010)
21. Jungers, M., Oliveira, R., Peres, P.: Mpc for lpv systems with bounded parameter variations. International Journal of Control 84(1) (2011)
22. El Ghaoui, L., Niculescu, S.-I. (eds.): Advances in Linear Matrix Inequality Methods in Control. SIAM's Advances in Design and Control (2000)
23. Lee, S.M., Park, J.H.: Output feedback model predictive control for LPV systems using parameter-dependent Lyapunov-function. Applied Mathematics and Computation 190, 671–676 (2007)
24. Leith, D.J., Leithead, W.E.: Survey of gain scheduling analysis and design. International Journal of Control 73, 1001–1025 (2000)
25. Millerioux, G., Anstett, F., Bloch, G.: Considering the attractor structure of chaotic maps for observer-based synchronization problems. Mathematics and Computers in Simulation 68(1), 67–85 (2005)
26. Millérioux, G., Daafouz, J.: Global chaos synchronization and robust filtering in noisy context. IEEE Trans. on Circuits and Systems I: Fundamental Theory and Applications 48(10), 1170–1176 (2001)
27. Millérioux, G., Daafouz, J.: Performances of unknown input observers for chaotic lpv maps in a stochastic context. In: Proc. of 12th International IEEE Workshop on Nonlinear Dynamics of Electronic Systems, NDES 2004, Evora, Portugal (May 2004)
28. Millérioux, G., Daafouz, J.: Performances of unknown input observers for chaotic lpv maps in a stochastic context. Nonlinear Dynamics 44, 205–212 (2006)
29. Millérioux, G., Daafouz, J.: Flatness of switched linear discrete-time systems. IEEE Trans. on Automatic Control 54(3), 615–619 (2009)
30. Millérioux, G., Rosier, L., Bloch, G., Daafouz, J.: Bounded state reconstruction error for lpv systems with estimated parameters. IEEE Trans. on Automatic Control 49(8), 1385–1389 (2004)
31. Montagner, V.F., Oliveira, R., Leite, V., Peres, P.: Gain scheduled state feedback control of discrete-time systems with time-varying uncertainties: an lmi approach. In: Procc. of the 44th IEEE Conf. on Deciion and Control (CDC 2005), Seville, Spain (December 2005)
32. Packard, A., Balas, G.: Theory and application of linear parameter-varying control techniques. In: Proceedings of the American Control Conference, Tutorial Workshop (1997)
33. Pardalos, P.M., Li, Y., Hager, W.W.: Linear programming approaches to the convex hull problem in $\mathbb{R}^m$. Computers and Mathematics with Applications 29(7), 23–29 (1995)
34. Park, B.P., Verriest, E.I.: Canonical forms for linear time-varying multivariable discrete systems. In: Proceedings. 28th Annual Allerton Conf. on Communication, Control and Computers, Urbana, USA (1990)
35. Preparata, F.P., Shamos, M.I.: Computational Geometry. Springer (1985)

36. Rugh, W., Shamma, J.: Research on gain scheduling. Automatica 36, 1401–1425 (2000)
37. Sato, M.: Filter design for lpv systems using quadratically parameter-dependent lyapunov functions. Automatica 42, 2017–2023 (2006)
38. Scherer, C.: LPV control and full block multipliers. Automatica 37, 361–375 (2001)
39. Silverman, L.M.: Inversion of multivariable linear systems. IEEE Trans. Automatic Control 14(3), 270–276 (1969)
40. Toth, R., Felici, F., Heuberger, P.S.C., Van den Hof, P.M.J.: Discrete time lpv i/o and state-space representations, differences of behavior and pitfalls of interpolation. In: Proc. of the European Control Conference (ECC 2007), Kos, Greece (2007)
41. Wu: Control of Linear Parameter Varying Systems. PhD thesis, University of Carlifonia at Berkeley, Mechanical Engineering (1995)

Chapter 6
Design of Norm Based Fault Detection and Isolation LPV Filters

David Henry

Abstract. This chapter investigates the design of robust[1] fault detection and isolation (FDI) filters for linear parameter varying (LPV) systems. The goal is to obtain structured fault detection filters with enhanced fault transmission H_- gain and large H_∞ nuisance attenuation. Both the so-called polytopic and Linear Fractional Representation (LFR) approaches are considered. With respect to the polytopic approach, a sufficient condition is established to guarantee sensitivity performance of the residual signal vector to faults. Robustness constraints against model perturbations and disturbances are also taken into account in the design method. A key feature of the proposed method is that the residual structuring matrices are optimized as an integral part of the design, together with the dynamic part (i.e. the filter). The design problem is formulated as a convex optimization problem and solved using LMI (Linear Matrix Inequalities) techniques. With regards to the LFR approach, it is shown by means of the scaling matrices technique that the synthesis of the residual structuring and the filter state space matrices can be performed simultaneously using LMI techniques. Computational aspects are discussed and it is shown that the proposed solution is structurally well-defined. Academic examples are considered and discussed all along the chapter. A benchmark from the European FP7 funded ADDSAFE (Advanced Fault Diagnosis for Sustainable Flight Guidance and Control) project is finally considered to demonstrate the potential of the proposed approaches. The goal is to propose new fault detection and fault diagnosis techniques that could significantly help developing environmentally-friendlier aircraft. A LPV)model-based fault detection scheme is presented for robust and early

David Henry
Bordeaux 1 University - IMS-LAPS (UMR CNRS n.5218), 351 cours de la libération, 33405 Talence Cedex
e-mail: david.henry@u-bordeaux1.fr
http://extranet.ims-bordeaux.fr/IMS/pages/pageAccueilPerso.php?email=david.henry

[1] All along the chapter and as classically used in the H_∞/μ fault detection problems, robustness refers to approximate decoupling.

O. Sename et al. (Eds.): *Robust Control and LPV Approaches*, LNCIS 437, pp. 125–180.
DOI: 10.1007/978-3-642-36110-4_6

detection of faults in aircraft control surfaces servo-loop. A complete MonteCarlo campaign from a "high-fidelity" simulator provided by AIRBUS, demonstrates the potential of the proposed technique. It is shown that the proposed fault detection scheme can be embedded within the structure of in-service monitoring systems as a part of the Flight Control Computer (FCC) software.

6.1 Introduction

The problem of Fault Detection and Diagnosis (FDD)[2] has received considerable attention world–wide and been theoretically and experimentally investigated with different types of approaches, as can be seen from the general survey works [1, 2, 3, 4, 5, 6, 7, 8, 9]. This development has been mainly stimulated by the trend in automation toward systems with increasing complexity and the growing demands for fault tolerance, cost efficiency, reliability, and safety which constitute fundamental design features in modern control systems, specially in the aeronautic and aerospace fields. Thus, hardware and software (analytical) redundancy schemes have been investigated over the last thirty years [2, 6]. Analytical redundancy makes use of a mathematical model of the monitored process and is therefore often referred to as the model–based approach to FDI/FDD [1, 2, 10, 11, 6, 7].

A model–based FDI/FDD scheme is normally implemented as a computer software algorithm. The main problem of the model–based approach regards the real complex systems, where modeling uncertainty arises inevitably, because of process noise, parameter variations and modeling errors. The FDI/FDD of incipient faults represents a challenge to model–based FDI/FDD techniques due to inseparable mixture between fault effects and modeling uncertainty [6, 2].

To carry out such FDI/FDD objectives, two main approaches have been developed in last years: the fault estimation techniques and the residual–based methods.

The fault estimation approaches focus on seeking the fault indicating signal to be an optimal estimate, in some criteria sense, of the fault. This can be a parameter estimate or an unknown input signal estimate. It follows that any estimation technique can be used on an adequate formulated problem, one of the most famous being the kalman-based techniques [12], see for instance the Extended Kalman Filter (EKF) technique and its improved versions such as the Unscented Kalman Filter (UKF) proposed in [13] and further investigated in [14, 15], the Divided Difference Filter (DDF) initially proposed by [16] (the DDF uses divided-difference approximations of derivatives based on the Stirling's interpolation formula) and the particle filtering approaches, a technique belonging to the class of Monte–Carlo methods for nonlinear systems with non–gaussian noises [17, 18, 19, 20, 21].

[2] The term Fault Detection and Diagnosis (FDD) is a development of the term Fault Detection and Isolation (FDI). Generally speaking, FDD goes slightly further than FDI by including the possibility of estimating the effect of the fault and/or diagnosing the effect or severity of the fault.

Residual generation is different from fault estimation because it does not only require the disturbances and model perturbations attenuation. The residual has to remain sensitive to faults while guaranteeing robustness against unknown inputs. A number of researchers have developed residual–based methods for dynamic systems such as (to name a few):

- the parity space approach [22, 23, 24, 25, 26, 27, 28, 29, 30, 31, 32, 33].
- the observer based approach through the so-called Unknown Input Observers (UIO) approaches and the eigenstructure assignment (EA) technique [34, 24, 25, 35, 36, 37, 38, 38, 39, 40, 41, 42, 43].
- the so-called norm-based approaches sometimes referred as the approximate decoupling approach. These approaches can be further classified according to the previous discussion as fault-estimation approaches [44, 45, 46, 47, 48, 49, 50, 51, 52] and residual generation approaches [43, 53, 54, 55, 56, 57, 58, 52, 59, 60, 9].

A crucial issue with any FDI/FDD scheme is its robustness to modelling uncertainty. The robustness problem in FDD is defined as the maximisation of the detectability and isolability of faults together with the minimisation of the effects of uncertainty and disturbances on the FDD procedure [2, 6]. A number of FDD techniques have been mainly developed for linear systems as it is mentioned above. However, practical models of real-world systems are mostly nonlinear. Hence, viable procedures for practical application of FDI/FDD techniques must take into account model-reality mismatches and hence modelling uncertainty.

To carry out such FDI/FDD objectives, the geometrical concepts for FDI/FDD initially proposed by [61], were successfully extended in theoretical work to nonlinear systems [62, 63]. Nonlinear geometric approaches can also be found in [64, 65], in which the fault estimation method relies on the successive derivatives of input/output signals. A drawback of these strategies is a high sensitivity to measurement noise and uncertainty due to dynamical system structure. In [66], an interesting FDD application of an UIO strategy for Lipschitz-bounded nonlinear systems is presented. This approach is applicable to a wide class of non-linear systems without requiring a non-linear geometrical approach. A further approach to FDI/FDD has been based on state estimation using non-linear stochastic methods such EKF-DDF and particle filtering as mentioned above. Adaptive methods for fault estimation and FDI/FDD are applicable to a wide class of nonlinear systems and are becoming popular as they blend well with fault tolerant Control (FTC) or fault detection, isolation and recovery (FDIR).

Even if there exist some proofs of optimality and robustness, such advanced techniques have not been used so far in on-board computers, specially for aeronautic and space missions. One of the main reasons is related to the fact that any new technique should provide a solution having well-defined real-time characteristics and well-defined error-rates, and many published works fail to address this important issue. The selection of an advanced FDI/FDD solution at a local or global level, necessarily includes a trade-off between the best adequacy of the technique and its implementation level for covering an expected fault profile, as well as its industrialization process with support tools for its design/tuning and validation. Very attractive advanced

FDI/FDD solutions would not be accepted without such industrial framework capability. A classical FDI/FDD approach could there be preferred despite its smaller fault coverage, because well industrially mastered and well characterized, without risk of false alarm. It follows that a good balance between physical redundancy and model-based techniques appears to be the right solution, leading to more efficient health monitoring systems based on less redundant elements [8, 9].

As an alternative to nonlinear approaches, one can consider linear parameter varying (LPV) methods because

- the LPV theory offers an efficient paradigm to model nonlinear systems with on-line measurable state depending parameters, see for instance [67, 68] and the surveys [69, 70],
- it provides stability and performance guarantee over wide range of changing parameters, see [71, 72, 73, 74, 75, 76, 77].
- it fundamentally relies on linear theory which is very attractive for an on-board implementation point of view, see the previous discussion.

The goal of this chapter is to address our recent work on robust model-based FDI/FDD. The considered techniques can be seen as a nice and practically relevant framework in which various design goals and trades-off are formulated and managed. It is shown that the design problem can be formulated as an optimization problem that can be solved by numerically powerful LMI-based techniques. The output of the design is a filter for Fault Detection, or a bank of filters for Fault Detection and Isolation. The presented approaches have been developed by the author at IMS/LAPS, Bordeaux, see the reference section. The developed techniques have been successfully applied to a number of aeronautic and space applications through different projects, both at national and European levels, e.g. generic aircrafts from AIRBUS, satellite, atmospheric re-entry and rendezvous missions.

The chapter is organized as follows.

Section 6.2 is dedicated to some mathematical developments and definitions. Section 6.3 states the model-based FDD/FDI filter design problem. Two general approaches are presented to design robust FDI filters for LPV systems under feedback control: the so-called "polytopic" and "LFR" approaches. The methods are a generalization to the fault detection generators design problem for LPV systems of the H_∞/H_- method initially proposed in [57] and further considered in [58, 52, 60, 78, 9]. The approach consists in designing an optimal FDI filter that maximizes fault sensitivity performance (in the H_-–norm sense), and simultaneously minimizes the influence of unknown inputs (in the H_∞–norm sense). The design problem is formulated so that all free parameters are optimized via Linear Matrix Inequality techniques. Section 6.4 is dedicated to the polytopic approach whereas section 6.5 is dedicated to the LFR approach. Academic examples are presented to outline the different steps of the methods. Finally, section 6.7 is dedicated to an industrial (AIRBUS) problem from the aeronautic domain. The work is undertaken within the European FP7 funded ADDSAFE (Advanced Fault Diagnosis for Sustainable Flight Guidance and Control) project. The goal is to propose new

fault diagnosis techniques that could significantly help developing environmentally-friendlier aircraft, by optimizing structural load design objectives.

6.2 Preliminaries

Throughout the chapter, the following notations are used: $\mathbb{R}$ and $\mathbb{C}$ denote the real and complex sets respectively. A^T, $A > 0$ means the transpose and the definite positiveness of A, respectively. $A \geq (>) B$ means $A - B$ is positive semi-definite (positive definite). $\overline{\sigma}(A)/\underline{\sigma}(A)$ denote the maximum/minimum singular values of the matrix A. $\|w\|_2$ is used to denote the L_2-norm of the signal w. $P(s)$ or simply P, is assumed to be in $\mathbb{R}H_\infty$, real rational function with ($||P||_\infty$ is also the largest gain of P)

$$||P||_\infty = \sup_\omega \overline{\sigma}(P(j\omega)) < \infty \tag{6.1}$$

Referring to a LPV model $P(\theta)$ so that $z(s) = P(s,\theta)w(s)$ (simply denoted $z = P(\theta)w$), the H_∞-norm is defined according to:

$$||P(\theta)||_\infty = \sup_{\substack{\forall\theta \\ ||w||_2 \neq 0}} \frac{||z||_2}{||w||_2} \tag{6.2}$$

In accordance with the induced norm, $||P||_-$ is used to denote the smallest gain of a transfer matrix P. However, this is not a norm. Despite there exist clear definitions and notations of the H_∞ norm, there exists some confusing notations for the H_- gain. For example, the H_- gain for LTI systems is defined on a finite frequency range in [43, 47, 57] whereas it is defined on an infinite frequency horizon in [79, 80]. The purpose of the following developments is to clearly define the H_--gain for both LTI and LPV systems. In contrast with other definitions reported in the literature, it is shown how our definition is related to the L_2-norm of signals.

The smallest gain of $P(s)$ is defined according to $\inf_\omega \underline{\sigma}(P(j\omega))$. It can be verified that for some P, e.g. strict proper P, $\inf_\omega \underline{\sigma}(P(j\omega)) = 0$ since the frequency range of interest is infinite. This motivates the introduction of the **non-zero smallest** gain of P, i.e. the H_- index, as the restriction of $\inf_\omega \underline{\sigma}(P(j\omega))$ to a finite frequency domain Ω, i.e.

$$||P||_- = \inf_{\omega\in\Omega} \underline{\sigma}(P(j\omega)) < \infty \tag{6.3}$$

However, it is not a norm since it does not verify the Schwartz inequality. This H_- index[3] is used in the FDI community (and therefore throughout the chapter) as a criteria for fault sensitivity performance.

[3] Note that the H_--index is often called by some authors the H_--norm, even if it is not a norm, see for instance [43]

In [81, 53], a signal evaluation function $||w||_e$, which is a restriction of the L_2 signal norm to a finite frequency domain, is defined according to (the time domain counterpart was too considered by the authors):

$$||w||_e = \left(\frac{1}{2\pi} \int_{\omega_1}^{\omega_2} ||w(j\omega)||_2^2 d\omega \right)^{1/2} \tag{6.4}$$

Then, given a transfer P so that $z = Pw$, it can be verified that the following relations yields

$$||Pw||_e^2 = \frac{1}{2\pi} \int_{\omega_1}^{\omega_2} ||P(j\omega)w(j\omega)||_2^2 d\omega \tag{6.5}$$

$$= \frac{1}{2\pi} \int_{\omega_1}^{\omega_2} \left\| P(j\omega) \frac{w(j\omega)}{||w||_2} \right\|_2^2 ||w||_2^2 d\omega \tag{6.6}$$

$$\geq ||P||_-^2 ||w||_e^2 \tag{6.7}$$

and, then that:

$$||P||_- = \inf_{\omega \in \Omega} \underline{\sigma}(P(j\omega)) \leq \inf_{||w||_e=1} ||Pw||_e \leq ||P||_\infty \tag{6.8}$$

It follows that the quantity $\inf_{||w||_e=1} ||Pw||_e$ takes sense of the minimum value over a finite frequency range of a singular value of $P(j\omega)$ and thus that

$$||P||_- = \inf_{||w||_e=1} ||Pw||_e = \inf_{\omega \in \Omega} \underline{\sigma}(P(j\omega)) \tag{6.9}$$

yields only if $\dim(w) = 1$ and/or $\dim(Pw) = 1$.

In the context of residual generators design, this means that $\inf_{\omega \in \Omega} \underline{\sigma}(P(j\omega)) = \inf_{||f||_e=1} ||r||_e = \inf_{||f||_e=1} ||T_{rf} f||_e$ if $\dim(r) = 1$, where T_{rf} denotes the transfer between the residuals and faults vectors. In others words, the minimum singular value based definition and the signal L_2-norm based definition of the H_- gain coincide. Thus, similarly to the definition of the H_∞-norm for LPV systems given by (6.2), the following evaluation criteria which is the generalization of the LTI H_- gain to LPV case, is considered. Given $r(s) = P(s,\theta) f(s) : \dim(r) = 1$, the H_- gain for LPV systems is defined according to:

$$||P(\theta)||_- = \inf_{\substack{\forall \theta \\ ||u||_e \neq 0}} \frac{||r||_e}{||f||_e} \tag{6.10}$$

Note that the definition of the H_{sens} criteria proposed in [82] is strictly equivalent to the H_- gain when $\dim(r) = 1$, but it consists of an upper bound for $\dim(r) \neq 1$.

Linear Fractional Representation (LFR) are extensively used in the paper. For appropriately dimensioned matrices N and $M = \begin{pmatrix} M_{11} & M_{12} \\ M_{21} & M_{22} \end{pmatrix}$, the lower LFR is defined according to $F_l(M,N) = M_{11} + M_{12} N (I - M_{22} N)^{-1} M_{21}$ and the upper LFR

according to $F_u(M,N) = M_{22} + M_{21}N(I - M_{11}N)^{-1}M_{12}$, under the assumption that the involved matrix inverses exist. This assumption is discussed in the paper when it is judged necessary. Otherwise, it is assumed to be satisfied.

6.3 Problem Statement

In this chapter, two general approaches are presented to design robust FDI filters for LPV systems under feedback control. The method is a generalization to the fault detection generators design problem for LPV systems of the H_∞/H_- method initially proposed in [57] and further considered in [58, 52, 60, 78, 9]. The approach consists in designing an optimal FDI filter that maximizes fault sensitivity performance (in the H_-–norm sense), and simultaneously minimizes the influence of unknown inputs (in the H_∞–norm sense). The design problem is formulated so that all free parameters are optimized via Linear Matrix Inequality techniques.

Consider a LPV dynamical system subject to q_f simultaneous faults $f_i(t), i = 1...q_f$ entering the system via corresponding fault injection matrices $K_{1|i}(\theta)$ and $K_{2|i}(\theta)$, where $\theta(t) \in \mathbb{R}^q$ is a time varying parameter vector. It is assumed that all parameters $\theta_i(t), i = 1,...,q$ are bounded so that $\theta_i \in [\underline{\theta}_i, \overline{\theta}_i], i = 1,...,q$, and that $\theta(t)$ is a time–varying parameter vector so that all parameters $\theta_i(t), i = 1...q$ are bounded, measurable (or estimated if the estimation error can be guaranteed to be bounded). The fault model $\left[K_{1|1}(\theta)f_1(t) + ... + K_{1|q_f}(\theta)f_{q_f}(t)\right] = K_1(\theta)f(t)$ refers to actuator and component faults, whereas $\left[K_{2|1}(\theta)f_1(t) + ... + K_{2|q_f}(\theta)f_{q_f}(t)\right] = K_2(\theta)f(t)$ refers to sensor faults, see for instance [83, 4, 84, 5, 85].

To focus on the effect of a specific set of faults, say the ith, f is splited into two parts: f_i and $\overline{f}_i$. Then the robust fault detection and isolation (FDI) problem concerns the detection of $f_i \neq 0$ while rejecting $\overline{f}_i$ and guaranteeing some robustness performance level to disturbances and model perturbations.

To formulate this problem, consider the effect of the faults f_i and $\overline{f}_i$, the process and the measurement noises. Then, the dynamical system can be modeled as follows:

$$\begin{cases} \dot{x}(t) = A(\theta)x(t) + B(\theta)u(t) + E_w(\theta)w(t) + K_{1|i}(\theta)f_i(t) + \overline{K}_{1|i}(\theta)\overline{f}_i(t) \\ y(t) = C(\theta)x(t) + D(\theta)u(t) + E_v(\theta)v(t) + K_{2|i}(\theta)f_i(t) + \overline{K}_{2|i}(\theta)\overline{f}_i(t) \end{cases} \quad (6.11)$$

In this formulation, $x \in \mathbb{R}^n$,$u \in \mathbb{R}^p$, $y \in \mathbb{R}^m$ denote the state, the input and the output vectors, respectively and $w \in \mathbb{R}^{q_w}$ and $v \in \mathbb{R}^{q_v}$ also refer to the state and measurement noise vectors, respectively. $A, B, C, D, E_w, E_v, K_{1|i}, K_{2|i}, \overline{K}_{1|i}$ and $\overline{K}_{2|i}$ are known matrices of adequate dimension that depend on $\theta(t)$. For clarity and without loss of generality, the following developments are done assuming that $dim(f_i) = 1$. Thus, in (6.16),

$$\overline{K}_{1|i}(\theta) = \left[K_{1|1}(\theta),...,K_{1|i-1}(\theta),K_{1|i+1}(\theta),...,K_{1|q_f}(\theta)\right] \in \mathbb{R}^{n\times(q_f-1)} \quad (6.12)$$

$$\overline{K}_{2|i}(\theta) = \left[K_{2|1}(\theta), ..., K_{2|i-1}(\theta), K_{2|i+1}(\theta), ..., K_{2|q_f}(\theta)\right] \in \mathbb{R}^{m\times(q_f-1)} \quad (6.13)$$

and

$$\overline{f}_i(t) = \left[f_1(t), ..., f_{i-1}(t), f_{i+1}(t), ..., f_{q_f}(t)\right]^T \in \mathbb{R}^{q_f-1} \quad (6.14)$$

It follows that the FDI problem concerns the detection of $f_i(t) \neq 0$ while rejecting $w(t), v(t)$ and $\overline{f}_i(t)$.

In order to make the problem well-posed, we assume that:

- (A.1) The system that admits the model (6.11) is detectable and stabilizable;
- (A.2) For any i, $K_{1|i}(\theta)$ satisfies $C(\theta)K_{1|i}(\theta) \neq 0$;
- (A.3) For any i, $K_{1|i}(\theta)$ is monic $\forall\theta$, viz. $f_i(t) \neq 0 \Rightarrow K_{1|i}(\theta)f_i(t) \neq 0\ \forall\theta$;
- (A.4) $rank\left(C(\theta)[K_{1|1}, ..., K_{1|q_f}]\right) = q_f$.

Condition (A.1) is required for the existence of a controller able to robustly stabilize the system (6.11). This assumption is done since we consider in the following developments that the system operates in a closed-loop configuration, see later. Conditions (A.2) and (A.3) assume that the fault f_i is observable from the output y, which is a prior condition for the fault f_i to be detected. Condition (A.4) guarantees that the fault f_i can be isolated from the remaining ones, see [86, 87] for more details.

With some abuse of notations, let us denote f the fault f_i to be detected and let d be the augmented vector defined according to:

$$d = \left(w^T \ v^T \ \overline{f}_i^T\right)^T \in \mathbb{R}^{q_w+q_v+q_f-1} \quad (6.15)$$

Then, introducing adequate matrices $E_1(\theta), E_2(\theta), K_1(\theta)$ and $K_2(\theta)$, it follows from (6.11) that the general state-space model of the system can be written:

$$\begin{cases} \dot{x}(t) = A(\theta)x(t) + B(\theta)u(t) + E_1(\theta)d(t) + K_1(\theta)f(t) \\ y(t) = C(\theta)x(t) + D(\theta)u(t) + E_2(\theta)d(t) + K_2(\theta)f(t) \end{cases} \quad (6.16)$$

Now let us consider $K(\theta)$ a LPV (or LTI, i.e. K) controller that robustly stabilizes the system (6.16) for all parameter trajectories $\theta_i(t), i = 1, ..., q$ taken their values in the considered range.

The FDI filter design problem we are interested is formulated as follows:

Problem 6.1. Assume that assumptions (A-1)-(A-4) yield. The goal is to find the (stable) filter realization matrices $A_F(\theta) \in \mathbb{R}^{n_F\times n_F}$, $B_F(\theta) \in \mathbb{R}^{n_F\times(p+m)}$, $C_F(\theta) \in \mathbb{R}^{q_r\times n_F}$ and $D_F(\theta) \in \mathbb{R}^{q_r\times(p+m)}$ and the matrices $M_y(\theta) \in \mathbb{R}^{q_r\times p}$ and $M_u(\theta) \in \mathbb{R}^{q_r\times m}$, such that the residual signal r defined by

$$r(s) = M_y(\theta)y(s) + M_u(\theta)u(s) - \hat{z}(s), \quad r \in \mathbb{R}^{q_r} \quad (6.17)$$

$$\hat{z}(s) = F(s,\theta)\begin{pmatrix} y(s) \\ u(s) \end{pmatrix}, \quad F(s,\theta) = C_F(\theta)\left(sI - A_F(\theta)\right)B_F(\theta) + D_F(\theta) \quad (6.18)$$

$$u(s) = K(s,\theta)y(s) \quad (6.19)$$

meets the following specifications:

- (S.1) $||T_{rd}(\theta)||_\infty < \gamma_1$, for all parameter trajectories $\theta(t)$ where $T_{rd}(\theta)$ denotes the closed-loop transfer between r and d.
- (S.2) $||T_{rf}(\theta)||_- > \gamma_2$ over a specified frequency range Ω, for all parameter trajectories $\theta(t)$. $T_{rf}(\theta)$ denotes the closed-loop transfer between r and f, and Ω is the frequency range where the energy of the faults is likely to be concentrated.

In (6.17)-(6.18), $\hat{z}$ is an estimation of $z = M_y(\theta)y + M_u(\theta)u$, a subset of available input/output signals. $M_y(\theta)$ and $M_u(\theta)$ are two (static) matrices that are known in the FDI community as the structuring matrices. The role of $M_y(\theta)$ and $M_u(\theta)$ is to merge optimally the available measurement and control signals to build the residual r. The performance index γ_1 guarantees a minimum nuisances attenuation H_∞–gain, whereas the performance index γ_2 guarantees a maximum faults amplification H_-–gain, see the preliminary section for the definition of the H_∞ and H_- gains. Of course the smaller γ_1 and the bigger γ_2 will be, the better the FDI performance will be.

Problem 6.1 could also be interpreted as a multiobjective optimization problem whereby the choice of γ_1 and γ_2 is guided by the Pareto optimal points, see [88] for a discussion on solving Pareto multi-criteria optimization problems. However, in practice, γ_1 and γ_2 are better considered as parameters to be selected by the designer since finding "optimal" values is highly related to the system under consideration, see for instance [52, 89, 60, 78].

In the following sections, two solutions to problem 6.1 are proposed depending on the manner (6.16) is modeled:

- the first one is developed within the so-called polytopic setting. In this case, it is assumed that all parameters $\theta_i(t), i = 1...q$ take their values in the domain Θ which is assumed to be a polytope.
- the second one is developed within the so-called LFR (Linear Fractional Representation) setting [90, 91, 92, 93, 94], i.e. all parameters $\theta_i(t), i = 1, ..., q$ entering in equation (6.16) are "pulled out" so that the model appears as a LTI (Linear Time Invariant) nominal model $P(s)$ subject to a time-varying bounded artificial feedback $\Theta(t)$.

Remark 6.1. The majority of methods reported in the literature involves the use of an open-loop model of the monitored system, in spite of that the FDI scheme is placed in a feedback loop. In such situations, it is well known that faults may be covered by control actions and the early detection of them, is clearly more difficult. This motivates the so-called integrated design of control and diagnosis schemes where robust controllers and fault detectors are designed together by optimizing a set of mixed control and fault detection objectives [95, 96, 97, 98, 99, 100]. However, this solution is judged questionable from a practical point of view, since the already in place controller is validated and certified and, then, can't be removed. This motivates the problem formulation previously stated.

6.4 The Polytopic Approach

In this section, a solution to the problem 6.1 is provided within the so-called polytopic setting. A core element of the following developments is that all free parameters (i.e. the filter state space matrices $A_F(\theta), B_F(\theta), C_F(\theta), D_F(\theta)$ and the structuring matrices $M_y(\theta)$ and $M_u(\theta)$) are directly optimized via LMI techniques in order to reach residual optimality. In fact, despite the used formalism seems to be complex, the idea behind the theory is very simple: using the convex property of the polytopic models (more precisely, the so–called vertex property), one can reproduce the LTI approach proposed in [57, 58, 52, 60, 78, 9] by considering the problem at each vertex of the polytope describing the model set with a common Lyapunov function, using the definition of the H_∞ and H_- norms for LPV systems stated in preliminaries. This, of course, may bring some conservativeness of the solution with respect to a parameter-dependent Lyapunov function and that's why this is called the quadratic H_∞ approach.

To proceed, consider the state space model (6.16) that we denote in a compact form $M(\theta) = \left(\begin{array}{c|ccc} A(\theta) & B(\theta) & E_1(\theta) & K_1(\theta) \\ \hline C(\theta) & D(\theta) & E_2(\theta) & K_2(\theta) \end{array}\right)$. It is assumed that $\theta(t)$ takes their values in the domain Θ, so that Θ is a convex polytope.

The LPV system (6.16) admits then a polytopic model if it is possible to determine a set of matrices $M_i, i = 1,...,N$, constituting the vertices of a polytope defined by

$$Co\{\beta_1,...,\beta_N\} = \left\{ \sum_{i=1}^{N} \beta_i M(\Pi_i), \beta_i \geq 0, \sum_{i=1}^{N} \beta_i = 1 \right\} \tag{6.20}$$

and such that it corresponds to the image by $M(\theta)$ of the domain Θ, i.e.

$$\{M(\theta), \theta \in \Theta\} \equiv Co\{M(\Pi_1),...,M(\Pi_N)\} \tag{6.21}$$

Then, $\beta_i, i = 1,...,N$ define the barycentric coordinates of Θ and the following convex decomposition yields:

$$\theta = \beta_1\Pi_1 + ... + \beta_N\Pi_N = (\beta_1 \ ... \ \beta_N) \begin{pmatrix} \Pi_1 \\ \vdots \\ \Pi_N \end{pmatrix}, \quad \beta_i \geq 0, \sum_{i=1}^{N} \beta_i = 1 \tag{6.22}$$

which offers a numerical procedure to compute $\theta(t)$ at each time t by means of linear algebra.

Note that the establishment of a non-conservative polytopic model is of major importance since it directly influences the performance of the FDI scheme. For instance, the Tensor Product (TP) model transformation approach proposed in [101, 102] is capable of establishing polytopic forms of LPV dynamic models, both in a theoretical and algorithmic context. Using the TP model transformation, different optimization and convexity constraints can be considered, and transformations can be executed without any analytical interactions, within a reasonable amount of

time (irrespective of whether the model is given in the form of analytical equations resulting from physical considerations, as an outcome of soft computing based identification techniques such as neural networks or fuzzy logic based methods, or as a result of a black-box identification). The interested reader can refer to [101, 102] for more details.

6.4.1 The Quasi-standard Form

In this section, a solution is provided to compute simultaneously $M_y(\theta), M_u(\theta)$ and $F(\theta)$ so that the requirements (S.1) and (S.2) are satisfied. It is straightforward to verify that the major difficulty in this problem is related to the fault sensitivity requirement (S.2) since (S.1) can be solved using the techniques developed in the robust control community. To overcome this problem, a sufficient condition is established in terms of a fictitious H_∞ problem. It is then shown in the following that a solution to this fictitious problem is a solution of the original one.

For clarity, it is assumed in the following developments that the structuring matrices $M_y(\theta)$ and $M_u(\theta)$ do not depend on θ. If this assumption vanishes, it can be verified that the following theoretical developments still yields. The only difference in such a case is that, if we consider $M_y(\theta)$ and $M_u(\theta)$ in the design problem, a set of structuring matrices $M_y(\Pi_i)$ and $M_u(\Pi_i)$ for each vertex of the polytope Θ would be obtained rather than constant matrices.

To proceed, consider the state space model (6.16) and the controller $K(\theta)$: $u(s) = K(s,\theta)y(s)$. Including $K(\theta)$ into the state space equations (6.16) leads to a new model $P(\theta)$ that can be deduced from the linear fractional representation $F_l(M(\theta), K(\theta))$ so that (see figure 6.1 for easy reference)

$$\begin{pmatrix} y(s) \\ u(s) \end{pmatrix} = P(s,\theta) \begin{pmatrix} d(s) \\ f(s) \end{pmatrix} \tag{6.23}$$

Then the problem 6.1 turns out to be the design of the triplet $(M_y, M_u, F(s,\theta))$ so that the robustness requirements (S.1) and the fault sensitivity specifications (S.2) are satisfied.

With some abuse of notations, let $P(\theta) = \left(\begin{array}{c|cc} A(\theta) & B_d(\theta) & B_f(\theta) \\ \hline C(\theta) & D_d(\theta) & D_f(\theta) \end{array}\right)$ with $A(\theta) \in \mathbb{R}^{n\times n}$, $B_d(\theta) \in \mathbb{R}^{n\times q_d}, B_f(\theta) \in \mathbb{R}^{n\times q_f}$ and $C(\theta) \in \mathbb{R}^{(p+m)\times n}$. Using some algebra manipulations, the filter design problem illustrated on figure 6.1 can be recasted into the setup depicted in the figure 6.2, where $\overline{P}(\theta, M_y, M_u)$ is deduced from $P(\theta), M_y$ and M_u according to:

$$\overline{P}(\theta, M_y, M_u) = \left(\begin{array}{c|ccc} A(\theta) & B_d(\theta) & B_f(\theta) & 0_{n\times q_r} \\ \hline \mathbb{M}C(\theta) & \mathbb{M}D_d(\theta) & \mathbb{M}D_f(\theta) & -I_{q_r} \\ C(\theta) & D_d(\theta) & D_f(\theta) & 0_{(p+m)\times q_r} \end{array}\right) \tag{6.24}$$

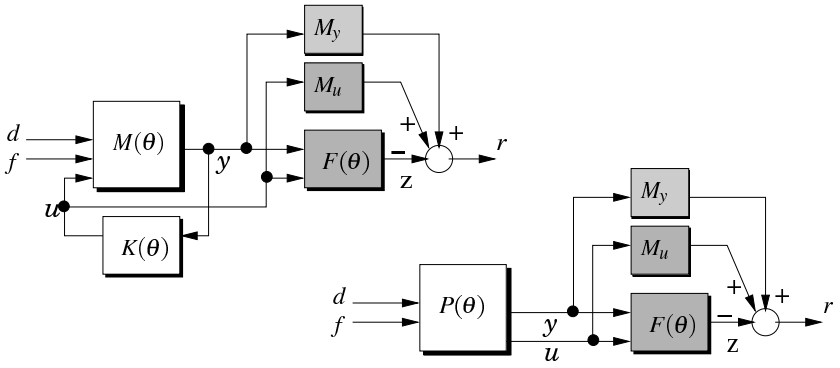

Fig. 6.1 The FDI filter design problem

In this equation $\mathbb{M} = (M_y \; M_u)$ and I_{q_r} and $0_{i\times j}$ denote respectively the identity matrix of dimension q_r and the null matrix of dimension $i \times j$.

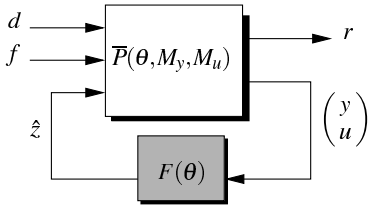

Fig. 6.2 The equivalent form of the FDI filter design problem

The requirements (S.1) and (S.2) are then expressed in terms of loop shapes, i.e. of desired gain responses for the appropriate closed-loop transfers. These shaping objectives are then turned into uniform bounds by means of shaping filters. To proceed, define two shaping filters W_d and W_f such that

$$||W_d||_\infty \leq \gamma_1 \quad ||W_f||_- \geq \gamma_2 \tag{6.25}$$

Assume that W_d and W_f are invertible (this can be done without loss of generality because it is always possible to add zeros in W_d and W_f to make them invertible). W_d and W_f are also defined in order to tune the gain responses for, respectively, $T_{rd}(\theta)$ and $T_{rf}(\theta)$. Then, if the condition

$$||T_{rd}(\theta)W_d^{-1}||_\infty < 1 \Leftrightarrow ||T_{r\tilde{d}}(\theta)||_\infty < 1 \tag{6.26}$$

is satisfied, the robustness design specification (S.1) yields. In (6.26), $\tilde{d} \in \mathbb{R}^{q_{\tilde{d}}}$ is a fictitious signal generating d through W_d and $T_{r\tilde{d}}(\theta)$ denotes the looped transfer between r and $\tilde{d}$.

Now, we need the following lemma to transform the fault sensitivity specification (S.2) into a H_∞ constraint.

Lemma 6.1. *Consider the robust fault sensitivity specification (S.2) and the shaping-filter W_f defined by (6.25). Introduce W_F, a right invertible transfer matrix so that $||W_f||_- = \frac{\gamma_2}{\lambda}||W_F||_-$ and $||W_F||_- > \lambda$, where $\lambda = 1+\gamma_2$. Define the signal $\tilde{r}$ such that $\tilde{r}(s) = r(s) - W_F(s)f(s)$. Then a sufficient condition for the specification (S.2) to hold, is*

$$||T_{rf}(\theta) - W_F||_\infty < 1 \Leftrightarrow ||T_{\tilde{r}f}(\theta)||_\infty < 1 \tag{6.27}$$

Proof

Consider the closed-loop transfer $T_{rf}(\theta)$ and let W_F be any LTI transfer matrix. Due to the definition of the H_- gain for LTI and LPV systems (see the preliminaries if necessary), it can be verified that the following relation yields:

$$||T_{rf}(\theta)||_- \geq ||W_F||_- - ||T_{rf}(\theta) - W_F||_\infty \tag{6.28}$$

Now, let us consider a fictitious signal $\tilde{r}$ such that $\tilde{r}(s) = r(s) - W_F(s)f(s)$, it can be verified that (6.28) can be re-written according to:

$$||T_{rf}(\theta)||_- \geq ||W_F||_- - ||T_{\tilde{r}f}(\theta)||_\infty \tag{6.29}$$

Now consider the weighting function W_F and assume that it is invertible. Then, we get

$$\frac{1}{||W_F||_-} = ||W_F^+||_{\infty\Omega} \tag{6.30}$$

where $||W_F^+||_{\infty\Omega} = \sup_{\omega\in\Omega} \overline{\sigma}\left(W_F^+(j\omega)\right)$. W_F^+ denotes the inverse of W_F which always exists by assumption (see lemma 6.1). Then, factorizing the right term of (6.29) by $||W_F||_-$ gives

$$||T_{rf}(\theta)||_- \geq \left(1 - \frac{||T_{\tilde{r}f}(\theta)||_\infty}{||W_F||_-}\right)||W_F||_- \tag{6.31}$$

that can be done since, by definition, $||W_F||_- \neq 0$. With (6.30), it follows that

$$||T_{rf}(\theta)||_- \geq \left(1 - ||T_{\tilde{r}f}(\theta)||_\infty ||W_F^+||_{\infty\Omega}\right)||W_F||_- \tag{6.32}$$

Now, since by construction $||W_F||_- > \lambda$, it is straightforward to verify that the following relation yields:

$$||W_F^+||_{\infty\Omega} < \frac{1}{\lambda} \tag{6.33}$$

Suppose now that the inequality $||T_{\tilde{r}f}(\theta)||_\infty < 1$ yields. From (6.33), it follows that

$$||T_{\tilde{r}f}(\theta)||_\infty ||W_F^+||_{\infty\Omega} < \frac{1}{\lambda} \tag{6.34}$$

and with (6.32), we get

$$||T_{rf}(\theta)||_- > \frac{\lambda - 1}{\lambda}||W_F||_- \tag{6.35}$$

Thus, if $||W_f||_- = \frac{\gamma_2}{\lambda}||W_F||_-$ with $\lambda = 1 + \gamma_2$, then (6.35) implies that

$$||T_{rf}(\theta)||_- > ||W_f||_- \tag{6.36}$$

which terminates the proof □

Following equations (6.26) and (6.27), the design problem can be re-casted according to the setup depicted in the figure 6.3 a, where $\tilde{d}$ and $\tilde{r}$ are two signals, so that $\tilde{d} = W_d d$ and $\tilde{r} = r - W_F f$. Then including W_d^{-1} and W_F into $\overline{P}(\theta, M_y, M_u)$ leads to the equivalent block diagram of figure 6.3 b, where the transfer matrix $\tilde{P}(\theta, M_y, M_u)$ is deduced from W_d^{-1}, W_F and $\overline{P}(\theta, M_y, M_u)$ using some linear algebra manipulations.

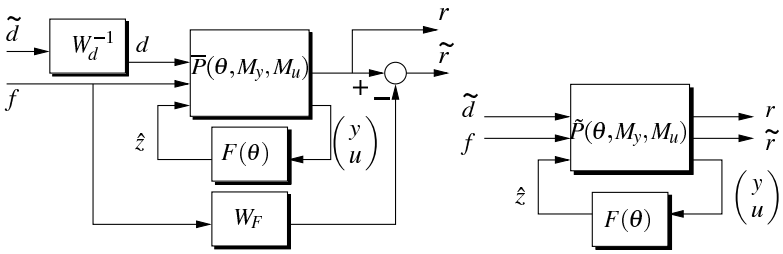

Figure 6.3 a Figure 6.3 b

Fig. 6.3 The equivalent forms of the filter design problem

The residual generation problem can now be formulated in a standard LPV H_∞ framework, by combining both requirements (6.26) and (6.27) into a single H_∞ constraint: a sufficient condition for (6.26) and (6.27) to hold for all parameter trajectories $\theta(t)$ in the polytope Θ is

$$\left\| F_l(\tilde{P}(\theta, M_y, M_u), F(\theta)) \right\|_\infty < 1 \tag{6.37}$$

This equation seems to be similar to a standard H_∞ LPV problem. In fact, this is not the case since the transfer $\tilde{P}(\theta, M_y, M_u)$ depends on M_y and M_u that are unknown. In the following section, a procedure is given to overcome this problem.

Remark 6.2. Coming back to the above developments, it is clear that a key feature in the proposed formulation is the *a-priori* choice of the shaping filters W_d and W_f. From a practical point of view, it is required that the residuals r are as "big" and as "fast" as possible, when a fault occurs. Then, if the considered faults manifest themselves, e.g., in low frequencies, this leads to select W_f as a low pass filter with the static gain and the cutting frequency, the highest possible. With regards to the

robustness objectives, it is required that the effects of the disturbances on the residuals are as "small" as possible. This implies to choose the gain of W_d as small as possible in the frequency range where the energy content of the disturbances is located. In other words, it is required a high attenuation level of the disturbances on the residuals in the appropriate frequencies. However, both sensitivity to faults and robustness against disturbances might be not achieved in some cases. Faults having similar frequency characteristics as those of disturbances might go undetected. In such cases, the proposed formulation provides a framework to find a good balance between fault sensitivity and robustness via the construction of the shaping filters W_d and W_f, see for instance [52, 89, 60, 78] where practical cases are considered. Furthermore, since the relation

$$\max\{||T_{rd}(\theta)W_d^{-1}||_\infty, ||T_{\tilde{r}f}(\theta)||_\infty\} \leq ||F_l\left(\tilde{P}(\theta, M_y, M_u), F(\theta)\right)||_\infty \quad (6.38)$$

yields, the combination of (6.26) and (6.27) into the single H_∞ constraint (6.37) might be conservative in some cases. As it is explained, the goal is to minimize only two channels (see equations (6.26) and (6.27)) from the whole objective. Thus, the selection of proper weights W_d and W_f for such a MIMO objective plays an important role. Similarly to the so-called "mixed sensitivity" approach from the H_∞ control community, W_d and W_f should be selected at least, as diagonal transfer functions.

6.4.2 The LMI Solution

In the following developments, a numerical tractable solution to (6.37) is derived in terms of a SDP (Semi Definite Programming) problem. To proceed, let $W_d^{-1}(s) = C_{wd}\left(sI - A_{wd}\right)^{-1}B_{wd} + D_{wd}$ and $W_F(s) = C_{wF}\left(sI - A_{wF}\right)^{-1}B_{wF} + D_{wF}$ be the state-space representations of $W_d - 1$ and W_F respectively, and denote n_{wd} and n_{wF} the associated order, i.e. $A_{wd} \in \mathbb{R}^{n_{wd}\times n_{wd}}$ and $A_{wF} \in \mathbb{R}^{n_{wF}\times n_{wF}}$. Using some linear algebra manipulations, it can be verified from (6.24) that the matrices $\tilde{A}(\theta), \tilde{B}(\theta), \tilde{C}(\theta)$ and $\tilde{A}(\theta)$ of the state-space representation of $\tilde{P}(\theta, M_y, M_u)$ are defined according to :

$$\tilde{A}(\theta) = \begin{pmatrix} A(\theta) & B_d(\theta)C_{wd} & 0 \\ 0 & A_{wd} & 0 \\ 0 & 0 & A_{wF} \end{pmatrix} \quad \tilde{A}(\theta) \in \mathbb{R}^{(n+n_{wd}+n_{wF})\times(n+n_{wd}+n_{wF})} \quad (6.39)$$

$$\tilde{B}(\theta) = \left(\tilde{B}_1(\theta)\middle|\tilde{B}_2\right) = \left(\begin{array}{cc|c} B_d(\theta)D_{wd} & B_f(\theta) & 0 \\ B_{wd} & 0 & 0 \\ 0 & B_{wF} & 0 \end{array}\right) \quad \tilde{B}(\theta) \in \mathbb{R}^{(n+n_{wd}+n_{wF})\times(q_{\tilde{d}}+q_f+q_r)} \quad (6.40)$$

$$\tilde{C}(\theta) = \begin{pmatrix} \tilde{C}_1(\theta) \\ \hline \tilde{C}_2(\theta) \end{pmatrix} = \left(\begin{array}{ccc} \mathbb{M}C(\theta) & \mathbb{M}D_d(\theta)C_{wd} & 0 \\ \mathbb{M}C(\theta) & \mathbb{M}D_d(\theta)C_{wd} & -C_{wF} \\ \hline C(\theta) & D_d(\theta)C_{wd} & 0 \end{array}\right) \quad (6.41)$$

$$\tilde{C}(\theta) \in \mathbb{R}^{(2q_r+m+p)\times(n+n_{wd}+n_{wF})}$$

$$\tilde{D}(\theta)=\left(\begin{array}{c|c}\tilde{D}_{11}(\theta)&\tilde{D}_{12}\\\hline\tilde{D}_{21}(\theta)&\tilde{D}_{22}\end{array}\right)=\left(\begin{array}{cc|c}\mathbb{M}D_d(\theta)D_{wd}&\mathbb{M}D_f(\theta)&-I_{q_r}\\\mathbb{M}D_d(\theta)D_{wd}&\mathbb{M}D_f(\theta)-D_{wF}&-I_{q_r}\\\hline D_d(\theta)D_{wd}&D_f(\theta)&0\end{array}\right)\quad(6.42)$$
$$\tilde{D}(\theta)\in\mathbb{R}^{(2q_r+m+p)\times(q_{\tilde{d}}+q_f+q_r)}$$

Note that by construction, $\tilde{B}_2=0$ and $\tilde{D}_{22}=0$ which illustrates that the filter $F(\theta)$ is in open-loop versus the monitored system.

Having in mind the definition of (6.39)-(6.42), it can be noted that the H_∞ optimization problem formulated by (6.37) is non-convex since it involves simultaneously the residual structuring matrices M_u and M_y and the filter state-space matrices $A_F(\theta),B_F(\theta),C_F(\theta),D_F(\theta)$. A solution may then consist in choosing heuristically the residual structuring matrices. However, as it is well known, there is no guarantee to the optimal solution. The following proposition gives the solution to this problem.

Proposition 6.1. *Consider the realization of the transfer $\tilde{P}(\theta,M_y,M_u)$ given by equations (6.39) - (6.42) and let $\tilde{A}(\Pi_i),\tilde{B}(\Pi_i),\tilde{C}(\Pi_i),\tilde{D}(\Pi_i)\ \forall i=1,...,N$ be the evaluation of $\tilde{A}(\theta),\tilde{B}(\theta),\tilde{C}(\theta),\tilde{D}(\theta)$ at each vertex $\Pi_i, i=1,...N$ of the polytope Θ. Assume that the parameter dependency in $\tilde{C}_2(\theta)$ and $\tilde{D}_{21}(\theta)$ can be removed (this can be done without loss of generality, see the following discussion) and let $W=(\tilde{C}_2\quad\tilde{D}_{21})^\perp$. Then there exists a solution of (6.37) if there exist a matrix $H\in\mathbb{R}^{q_r\times 1}$, $\gamma<1$ and $\mathbb{M}\in\mathbb{R}^{q_r\times(m+p)}$ and two symmetric matrices $R,S\in\mathbb{R}^{(n+n_{wd}+n_{wF})\times(n+n_{wd}+n_{wF})}$ solving the following SDP problem involving $2N+1$ LMI constraints*

$$\min\gamma\quad s.t.:$$

$$\left(\begin{pmatrix}I_{n+n_{wd}+n_{wF}}&0\\0&H\\0&-H\end{pmatrix}\begin{matrix}0\\0\end{matrix}\right)^T\begin{pmatrix}\tilde{A}(\Pi_i)R+R\tilde{A}^T(\Pi_i)&R\tilde{C}_1^T(\Pi_i)&\tilde{B}_1(\Pi_i)\\\tilde{C}_1(\Pi_i)R&-\gamma I&\tilde{D}_{11}(\Pi_i)\\\tilde{B}_1^T(\Pi_i)&\tilde{D}_{11}^T(\Pi_i)&-\gamma I\end{pmatrix}...$$
$$...\left(\begin{pmatrix}I_{n+n_{wd}+n_{wF}}&0\\0&H\\0&-H\end{pmatrix}\begin{matrix}0\\0\end{matrix}\right)<0\quad i=1,...,N\quad(6.43)$$

$$\begin{pmatrix}W&0\\0&I\end{pmatrix}^T\begin{pmatrix}\tilde{A}^T(\Pi_i)S+S\tilde{A}(\Pi_i)&S\tilde{B}_1(\Pi_i)&\tilde{C}_1^T(\Pi_i)\\\tilde{B}_1^T(\Pi_i)S&-\gamma I&\tilde{D}_{11}^T(\Pi_i)\\\tilde{C}_1(\Pi_i)&\tilde{D}_{11}(\Pi_i)&-\gamma I\end{pmatrix}\begin{pmatrix}W&0\\0&I\end{pmatrix}<0\quad i=1,...,N\quad(6.44)$$

$$\begin{pmatrix}R&I\\I&S\end{pmatrix}\geq 0\quad(6.45)$$

Moreover, $F(\theta)$ is of full-order, i.e. $n_F=n+n_{wd}+n_{wF}$. The state space realization of the LPV filter $F(\theta)$ is then computed using the barycentric coordinates of Θ given by (6.22), so that:

$$\begin{pmatrix}A_F(\theta)&B_F(\theta)\\C_F(\theta)&D_F(\theta)\end{pmatrix}=\sum_{i=1}^{N}\beta_i\begin{pmatrix}A_F(\Pi_i)&B_F(\Pi_i)\\C_F(\Pi_i)&D_F(\Pi_i)\end{pmatrix}\quad(6.46)$$

In this equation, $A_F(\Pi_i), B_F(\Pi_i), C_F(\Pi_i)$ and $D_F(\Pi_i)$ $i = 1,...,N$ are the state space matrices of the N LTI filters $F(\Pi_i), i = 1,...,N$ that are deduced from the unique solution $H, R, S, M_y, M_u, \gamma$ of the SDP problem (6.43)-(6.45), see the following proof for details. □

Proof

We first state that, by virtue of the scaled-bounded real lemma [72], $(M_y, M_u, F(\theta))$ satisfies the H_∞-norm constraint (6.37) (and $F(\theta)$ is stable $\forall\theta$) if there exists a $\gamma < 1$, $\mathbb{M} \in \mathbb{R}^{q_r \times (m+p)}$ and a (unique) Lyapunov matrix $X_{cl} = X_{cl}^T > 0$ such that

$$\begin{pmatrix} A_{cl}^T(\theta)X_{cl} + X_{cl}A_{cl}(\theta) & X_{cl}B_{cl}(\theta) & C_{cl}^T(\theta) \\ B_{cl}^T(\theta)X_{cl} & -\gamma I & D_{cl}^T(\theta) \\ C_{cl}(\theta) & D_{cl}(\theta) & -\gamma I \end{pmatrix} < 0 \tag{6.47}$$

where $F_l(\tilde{P}(\theta, M_y, M_u), F(\theta)) = C_{cl}(\theta)(sI - A_{cl}(\theta))^{-1}B_{cl}(\theta) + D_{cl}(\theta)$. Moreover $F(\theta)$ is a full-order filter if $n_F = n + n_{wd} + n_{wF}$. Because of the unique Lyapunov matrix, the FDI filter $(M_y, M_u, F(\theta))$ verifies only quadratic performance.

Secondly, we restrict the parameter-dependent inequality (6.47) to a finite set of inequalities using the so-called vertex property, i.e. (6.47) is satisfied if and only if there exists a $\gamma < 1$, $\mathbb{M} \in \mathbb{R}^{q_r \times (m+p)}$ and a (unique) Lyapunov matrix $X_{cl} = X_{cl}^T > 0$ such that

$$\begin{pmatrix} A_{cl}^T(\Pi_i)X_{cl} + X_{cl}A_{cl}(\Pi_i) & X_{cl}B_{cl}(\Pi_i) & C_{cl}^T(\Pi_i) \\ B_{cl}^T(\Pi_i)X_{cl} & -\gamma I & D_{cl}^T(\Pi_i) \\ C_{cl}(\Pi_i) & D_{cl}(\Pi_i) & -\gamma I \end{pmatrix} < 0 \quad i = 1,...,N \tag{6.48}$$

Let $\mathscr{F}_i = \begin{pmatrix} A_F(\Pi_i) & B_F(\Pi_i) \\ C_F(\Pi_i) & D_F(\Pi_i) \end{pmatrix} \in \mathbb{R}^{(n_F+q_r)\times(n_F+p+m)}$. Then, it can be verified using some linear matrix algebra manipulations, that (6.48) can be written as

$$\Psi(\mathbb{M}, \Pi_i) + Q^T(\Pi_i)\mathscr{F}_i^T P(\Pi_i) + P^T(\Pi_i)\mathscr{F}_i Q(\Pi_i) < 0 \quad i = 1,...,N \tag{6.49}$$

where the matrices $P(\Pi_i)$ and $Q(\Pi_i)$ depend only on X_{cl} and known matrices and where $\Psi(\mathbb{M}, \Pi_i)$ depends on X_{cl} and $\mathbb{M}$.

Now consider the case of full-order FDI filter, i.e. $n_F = n + n_{wd} + n_{wF}$. Using the projection lemma [103], it is possible to eliminate $\mathscr{F}_i$ in (6.49). To proceed, consider the realization of the transfer $\tilde{P}(\Pi_i, M_y, M_u)$ given by equations (6.39) - (6.42) and assume that the parameter dependency in $\tilde{C}_2(\theta)$ and $\tilde{D}_{21}(\theta)$ can be removed. Let $\mathscr{W}$ and W denote orthonormal bases of the null spaces of $(\tilde{B}_2^T \quad \tilde{D}_{12}^T)$ and $(\tilde{C}_2 \quad \tilde{D}_{21})$ respectively and let X_{cl} and X_{cl}^{-1} be partitioned as follows

$$X_{cl} = \left(\begin{array}{c|c} S & N \\ \hline N^T & X_1 \end{array}\right), \quad X_{cl}^{-1} = \left(\begin{array}{c|c} R & M \\ \hline M^T & X_2 \end{array}\right), \quad R, S, M, N \in \mathbb{R}^{(n+n_{wd}+n_{wF})\times(n+n_{wd}+n_{wF})} \tag{6.50}$$

where R and S are two symmetric matrices of adequate dimension. By construction, the following relation yields

$$MN^T = I - RS \tag{6.51}$$

By virtue of the projection lemma, there exists a solution of (6.49) if and only if R and S solves the following system of inequalities [72]

$$\left(\begin{array}{c|c} \mathscr{W} & 0 \\ \hline 0 & I \end{array}\right)^T \left(\begin{array}{cc|c} \tilde{A}(\Pi_i)R + R\tilde{A}^T(\Pi_i) & R\tilde{C}_1^T(\Pi_i) & \tilde{B}_1(\Pi_i) \\ \tilde{C}_1(\Pi_i)R & -\gamma I & \tilde{D}_{11}(\Pi_i) \\ \hline \tilde{B}_1^T(\Pi_i) & \tilde{D}_{11}^T(\Pi_i) & -\gamma I \end{array}\right) \left(\begin{array}{c|c} \mathscr{W} & 0 \\ \hline 0 & I \end{array}\right) < 0 \quad i = 1,...,N \tag{6.52}$$

$$\left(\begin{array}{c|c} W & 0 \\ \hline 0 & I \end{array}\right)^T \left(\begin{array}{cc|c} \tilde{A}^T(\Pi_i)S + S\tilde{A}(\Pi_i) & S\tilde{B}_1(\Pi_i) & \tilde{C}_1^T(\Pi_i) \\ \tilde{B}_1^T(\Pi_i)S & -\gamma I & \tilde{D}_{11}^T(\Pi_i) \\ \hline \tilde{C}_1(\Pi_i) & \tilde{D}_{11}(\Pi_i) & -\gamma I \end{array}\right) \left(\begin{array}{c|c} W & 0 \\ \hline 0 & I \end{array}\right) < 0 \quad i = 1,...,N \tag{6.53}$$

$$\left(\begin{array}{cc} R & I \\ I & S \end{array}\right) \geq 0 \tag{6.54}$$

Because $\mathbb{M}$ enters in the terms $\tilde{C}_1(\Pi_i)R$ and $R\tilde{C}_1^T(\Pi_i)$ in (6.52), the inequality (6.52) is not jointly affine in R and $\mathbb{M}$. Hence solving this system of inequalities is not an LMI problem. To overcome this problem, consider the expression of $\tilde{B}_2$ and $\tilde{D}_{12}$ given by (6.40) and (6.42). It follows that bases of the null space of $(\tilde{B}_2^T \quad \tilde{D}_{12}^T)$ are of the form

$$\mathscr{W} = \left(\begin{array}{cc} I_{n+n_{wd}+n_{wF}} & 0 \\ 0 & H \\ 0 & -H \end{array}\right) \quad H \in \mathbb{R}^{q_r \times 1} \tag{6.55}$$

With this expression of $\mathscr{W}$, it can be verified that the system of inequalities (6.52)-(6.54) can be written as (6.43)-(6.45) which, for a given H, is now jointly affine in $\gamma, \mathbb{M}, R$ and S, and therefore is now a LMI problem. □

Coming back to the statement of the proposition 6.1, it is required that $\tilde{C}_2$ and $\tilde{D}_{21}$ do not depend on θ. From the above proof, it can be verified that this assumption is also done for the basis $\mathscr{W}$ to be computed. If, by construction, such an assumption is not verified, the solution may consist in post-filtering $(y^T \; u^T)^T$ by a LTI filter with a high cutting frequency. This solution has already been proposed in [72].

Furthermore, it is clear that the LPV FDI filter is not unique since many feasible solutions γ, H, R, S, M_y and M_u satisfying (6.43)-(6.45) exist. It is possible to characterize the family of the solutions and therefore the family of robust FDI filters corresponding to a γ. However, since γ enters linearly in (6.43) and (6.44), it can be directly minimized by LMI optimization techniques. So the procedure allows to find the smallest achievable H_∞-norm and to determine the optimal solution $M_y, M_u, F(\theta)$, which is unique for a given matrix H.

Finally, note that $H = 0$ can be a viable solution for the LMI problem (6.43)-(6.45). Thus, from a practical point of view, it could be more efficient to derive the FDI filter from the following proposition:

Proposition 6.2. *Consider the realization of the transfer $\tilde{P}(\theta, M_y, M_u)$ given by equations (6.39) - (6.42) and let $\tilde{A}(\Pi_i), \tilde{B}(\Pi_i), \tilde{C}(\Pi_i), \tilde{D}(\Pi_i)$ $\forall i = 1,...,N$ be the evaluation of $\tilde{A}(\theta), \tilde{B}(\theta), \tilde{C}(\theta), \tilde{D}(\theta)$ at each vertex Π_i, $i = 1,...N$ of the polytope Θ. Assume that the parameter dependency in $\tilde{C}_2(\theta)$ and $\tilde{D}_{21}(\theta)$ can be removed*

and let $W = (\tilde{C}_2 \quad \tilde{D}_{21})^{\perp}$. *Then there exists a solution of* (6.37) *if there exist* $\gamma < 1$ *and* $\mathbb{M} \in \mathbb{R}^{q_r \times (m+p)}$ *and two symmetric matrices* $R, S \in \mathbb{R}^{(n+n_{wd}+n_{wF}) \times (n+n_{wd}+n_{wF})}$ *solving the following SDP problem involving* $2N+1$ *LMI constraints*

$$\min \gamma \quad s.t.:$$

$$\begin{pmatrix} \tilde{A}(\Pi_i)R + R\tilde{A}^T(\Pi_i) & \tilde{B}_1(\Pi_i) \\ \tilde{B}_1^T(\Pi_i) & -\gamma I \end{pmatrix} < 0 \quad i = 1, ..., N \tag{6.56}$$

$$\begin{pmatrix} W & 0 \\ 0 & I \end{pmatrix}^T \begin{pmatrix} \tilde{A}^T(\Pi_i)S + S\tilde{A}(\Pi_i) & S\tilde{B}_1(\Pi_i) & \tilde{C}_1^T(\Pi_i) \\ \tilde{B}_1^T(\Pi_i)S & -\gamma I & \tilde{D}_{11}^T(\Pi_i) \\ \tilde{C}_1(\Pi_i) & \tilde{D}_{11}(\Pi_i) & -\gamma I \end{pmatrix} \begin{pmatrix} W & 0 \\ 0 & I \end{pmatrix} < 0 \quad i = 1, ..., N \tag{6.57}$$

$$\begin{pmatrix} R & I \\ I & S \end{pmatrix} \geq 0 \tag{6.58}$$

6.4.3 Computational Issues

To derive a numerical solution from proposition 6.1 or 6.2, a computational procedure is now considered. The computation of $M_y, M_u, A_F(\Pi_i), B_F(\Pi_i)$, $C_F(\Pi_i)$ and $D_F(\Pi_i)$ can be made using the following procedure:

- First solve the system of LMIs (6.43)-(6.45) minimizing γ to get the optimal matrices $R, S, \mathbb{M} = (M_y \quad M_u)$.
- Second compute the bounded real lemma matrix X_{cl}. Inspecting the proof, it can be seen that X_{cl} is uniquely determined by (6.50) (remember that X_{cl} do not depend on θ by assumption). Specially, X_{cl} is the unique solution of the linear equation $X_{cl} \begin{pmatrix} R & I \\ M^T & 0 \end{pmatrix} = \begin{pmatrix} I & S \\ 0 & N^T \end{pmatrix}$ where $M, N \in \mathbb{R}^{(n+n_wd+n_{wF}) \times (n+n_{wd}+n_{wF})}$ are two matrices satisfying $MN^T = I - RS$
- Once X_{cl}, M_y and M_u have been determined, it is straightforward to verify that (6.48) is now a LMI problem in $A_F(\Pi_i), B_F(\Pi_i), C_F(\Pi_i)$ and $D_F(\Pi_i)$ with dimensions $A_F \in \mathbb{R}^{(n+n_{wd}+n_{wF}) \times (n+n_{wd}+n_{wF})}$, $B_F \in \mathbb{R}^{(n+n_{wd}+n_{wF}) \times (p+m)}$, $C_F \in \mathbb{R}^{q_r \times (n+n_{wd}+n_{wF})}$ and $D_F \in \mathbb{R}^{q_r \times (p+m)}$. Thus, the FDI filter matrices can be deduced from any solution of (6.48). LMI optimization algorithms can be used to derive such numerical solution. This option is most appropriate when additional constraints restrict the admissible $A_F(\Pi_i), B_F(\Pi_i), C_F(\Pi_i)$ and $D_F(\Pi_i)$ (e.g. filter poles can be restricted in a LMI region). However, as it has been outlined in [103], when these restrictions are immaterial, a solution can be computed more efficiently via elementary linear algebra.

Furthermore, because of the need of the computation of $MN^T = I - RS$, one should keep in mind that $I - RS$ ought to be well conditioned. Unfortunately, $I - RS$ will be nearly singular if the constraint $\begin{pmatrix} R & I \\ I & S \end{pmatrix} \geq 0$ is satured at the optimum. To avoid

such difficulties, the idea consists in maximizing the minimal eigenvalue of RS, and hence, to push them away from "1" such that $I-RS$ are expected to be well conditioned. This can be done, by e.g., changing the SDP optimization problem in proposition 6.1 according to:

$$\begin{array}{l} \min \gamma + \varepsilon\rho \quad s.t \\ (6.43) \text{ and } (6.44) \quad (\text{ or } (6.56) \text{ and } (6.57)) \\ \begin{pmatrix} R & \rho I \\ \rho I & S \end{pmatrix} \geq 0 \end{array} \tag{6.59}$$

where ε is a negative scalar.

6.4.4 Application to an Academic System

To illustrate the potential of the proposed approach, an illustrative example of academic nature is considered. Consider the following system definition (see eq. (6.16))

$$\begin{cases} \dot{x}(t) = A(\theta)x(t) + B(\theta)u(t) + E_1(\theta)d(t) + K_1(\theta)f(t) \\ y(t) = C(\theta)x(t) + D(\theta)u(t) + E_2(\theta)d(t) + K_2(\theta)f(t) \end{cases} \tag{6.60}$$

where

$$A(\theta) = \begin{pmatrix} 0 & \theta_2(t) \\ -0.1\theta_1(t) & -\theta_3(t) \end{pmatrix}, \quad B = \begin{pmatrix} 0 \\ 0.1 \end{pmatrix}, \quad E_1 = \begin{pmatrix} 1 & 0 \\ 1 & 0 \end{pmatrix} \tag{6.61}$$

$$K_1 = \begin{pmatrix} 1 \\ 1 \end{pmatrix}, \quad C = I_2, \quad D = 0_{2\times 1}, \quad E_2 = \begin{pmatrix} 0 & 1 \\ 0 & 1 \end{pmatrix}, \quad K_2 = 0_{2\times 1} \tag{6.62}$$

The problem dimensions are as follows:

$$m = 2, \quad p = 1, \quad q_d = 2, \quad q_f = 1$$

We assume that the energy content of the state noise (i.e. the term $E_1 d(t)$) is located close to $0.1 rd/s$ and that the energy content of the measurement noise (i.e. the term $E_2 d(t)$) is located at high frequencies. With regards to the faults (the term $f(t)$), we assume that they manifest themselves in low frequencies. The time-varying parameter vector is assumed to belongs to the polytope Θ of 8 vertices as illustrated in figure 6.4, so that

$$\Theta = \{\theta(t) : 5 \leq \theta_1(t) \leq 8; 0 \leq \theta_2(t) \leq 4; 2 \leq \theta_3(t) \leq 4; \dot{\theta} \not< \infty\} \tag{6.63}$$

We assume that the system operates in a closed loop under a controller K so that for all parameter trajectories, the closed-loop system is stable in both fault-free and faulty situations (a LQ–based controller was designed for this purpose).

Following the theoretical developments presented in section 6.4, the design problem is put into the so-called quasi-standard form. This boils down to the following definition of $\overline{P}(\theta, M_y, M_u)$:

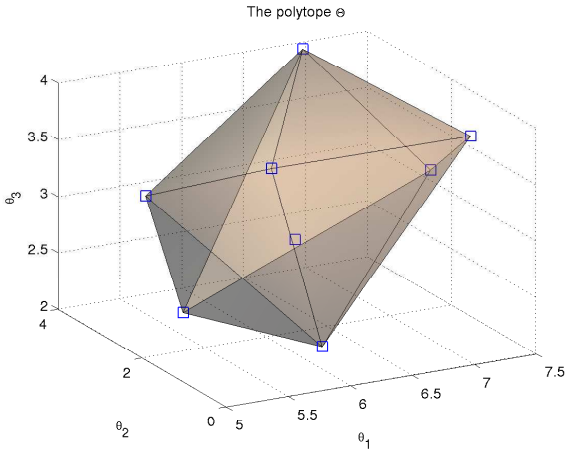

Fig. 6.4 The polytope Θ with $N = 8$ vertices

$$\overline{P}(\theta, M_y, M_u) = \left(\begin{array}{c|ccc} A(\theta)+BK & E_1 & K_1 & 0 \\ \hline M_y(C+DK)+M_uK & M_yE_2 & M_yK_2 & -1 \\ C+DK & E_2 & K_2 & 0 \\ K & 0 & 0 & 0 \end{array}\right) \tag{6.64}$$

Note that here, we are only interesting in the fault detection problem. Thus, only one filter is designed with $q_r = 1$.

Due to the definition of d, it is natural to choose the shaping filter W_d that manage the robustness requirements according to

$$W_d = diag(W_w, W_n) \tag{6.65}$$

W_w and W_n allow to formulate the robustness objectives against the state and measurement noises, respectively. Because we suppose that the energy content of the state noise is located close to $0.1rd/s$ rad/s, W_w is fixed as a selective band-pass filter at the frequency $0.1rd/s$ with static gain γ_w. i.e,

$$W_w = \gamma_w \frac{\frac{2z}{\omega_0}s(1+0.01s)}{s^2+\frac{2z}{\omega_0}s+\frac{1}{\omega_0^2}} \quad z = 0.5, \omega_0 = 0.1rd/s \tag{6.66}$$

In others words, it is desired to have a rejecting behavior of $T_{wr}(\theta, j\omega)$ in a frequency range close to 0.1 rad/s.

With regards to the measurement noise, because we suppose that the energy content of the measurement noise is located in the high frequency range, W_n is fixed as a low pass filter with static gain γ_n. i.e,

$$W_n = \gamma_n \frac{1+10s}{1+0.01s} \tag{6.67}$$

In others words, it is desired to have a rejecting behavior of $T_{nr}(\theta, j\omega)$ at high frequencies. In the definition of W_w, W_n the parameters γ_w and γ_n have been introduced in order to manage the robustness level of the fault detection scheme against w and n separately. The high frequency zero in W_w is introduced to make W_w invertible.

For the purpose of the fault sensitivity objective, we consider that all faults we are focused on manifest themselves in low frequencies. This boils down to considering W_f as a low-pass filter defined according to

$$W_f = \gamma_2 \frac{1}{1+10s} \tag{6.68}$$

where γ_2 is introduced in order to manage the fault sensitivity level of the fault detection scheme.

The computation of $M_y, M_u, F(\Pi_i), i = 1, ..., 8$ is next performed using lemma 6.1 and proposition 6.2. The SDP optimization problem is solved using the SDPT3 solver. The parameters γ_w, γ_n and γ_2 have been (iteratively) tuned in order to obtain the best robustness and fault sensitivity performance. This boils down to the following results

$$M_y \approx (0.005 \quad 0.01), \quad M_u \approx -1.3451, \quad \gamma_2 = 5, \quad \gamma_w = 0.1, \quad \gamma_n = 2 \tag{6.69}$$

Figure 6.5 illustrates the frequency behavior of $F(\Pi_i), i = 1, ..., 8$, i.e. the frequency behavior of $F(\theta)$ evaluated at each vertex of the polytope Θ. As it can be seen, the frequency behavior of $F(\theta)$ is, say, scheduled by $\theta(t)$.

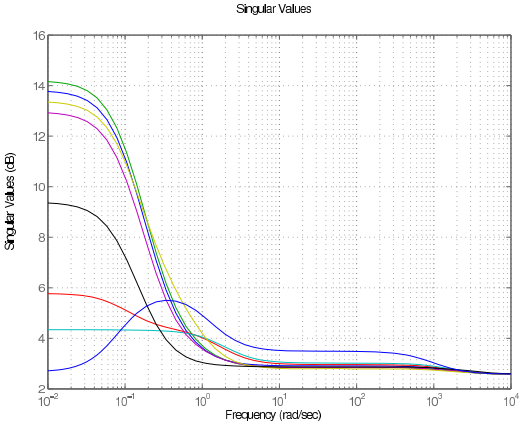

Fig. 6.5 Behavior of $F(\Pi_i, j\omega), i = 1, ..., 8$

The FDI unit is next implemented within the simulator of the system. $F(\theta)$ is also deduced from $F(\Pi_i), i = 1, ..., 8$ by means of the barycentric coordinates of Θ, see figure 6.4 if necessary. The simulations are carried out for $150s$. A fault occurs

at $t = 50s$. The simulated fault corresponds to a step of magnitude 1. Figure 6.6-left illustrates the time behavior of $\theta_1(t)$ used for the simulation (the same behavior is chosen for $\theta_2(t)$ and $\theta_3(t)$). A zoom is too presented to appreciate the behavior of $\theta_i(t), i = 1,..,N$. Figure 6.6-right illustrates the time behavior of the residual $r(t)$: $r(s) = M_y y(s) + M_u u(s) - F(s,\theta)\begin{pmatrix} y(s) \\ u(s) \end{pmatrix}$ for both fault-free and faulty situations. Note that, as expected, the (static) amplification of the fault $f(t)$ on $r(t)$ is higher than $\gamma_2 = 5$.

As it can be seen, the fault can be easily diagnosed from $r(t)$, e.g. using a simple threshold–based decision making approach.

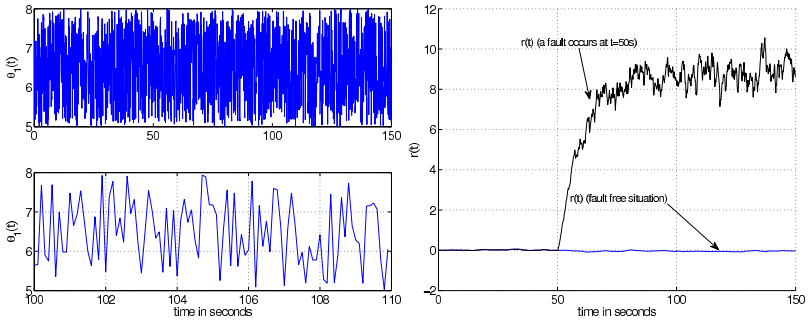

Fig. 6.6 Behavior of $\theta_1(t)$ (left) - $r(t)$ (right)

6.5 The LFR Approach

The second approach that is presented in this chapter is developed within the so-called LFR (Linear Fractional Representation) setting [90, 91, 92, 93, 94]. In this approach, all parameters $\theta_i(t), i = 1,...,q$ entering in equation (6.16) are "pulled out" so that the model appears as a LTI (Linear Time Invariant) nominal model $P(s)$ subject to a time-varying bounded artificial feedback $\Theta(t)$ (see figure 6.7 for easy reference):

$$y(s) = F_u(P(s),\Theta)\begin{pmatrix} d(s) \\ f(s) \\ u(s) \end{pmatrix}, \quad u(s) = K(s)y(s) \tag{6.70}$$

Here, P denotes a LTI model and Θ is a block diagonal time-varying operator specifying how θ enters P, so that

$$\Theta = blockdiag\left(\theta_1 I_{k_1},....,\theta_q I_{k_q}\right) \tag{6.71}$$

where $k_i > 1$ whenever the parameter θ_i is repeated. In this formalism, $|\theta_i(t)| \leq 1, \forall t \Leftrightarrow ||\Theta||_\infty \leq 1$. This can be assumed without loss of generality since the model P can always be scaled.

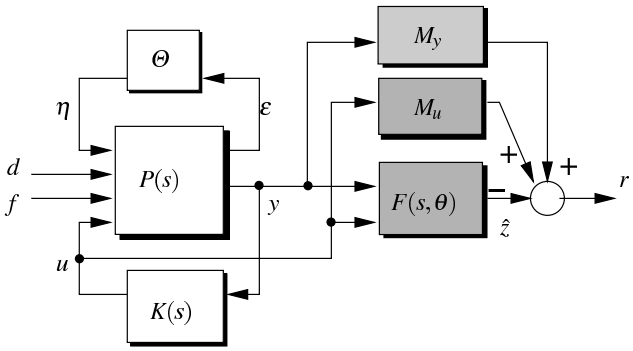

Fig. 6.7 The FDI filter design problem

Now, let us consider the following general form of a residual vector given by (6.17)-(6.19), that is (see figure 6.7 for easy reference):

$$r(s) = M_y y(s) + M_u u(s) - \hat{z}(s), \quad \hat{z}(s) = F(s,\theta)\begin{pmatrix} y(s) \\ u(s) \end{pmatrix}, \quad r \in \mathbb{R}^{q_r} \tag{6.72}$$

Then problem 6.1 can be formulated in a LFR manner as follows:

Problem 6.2. Let f entering in (6.70) be detectable faults. Consider the residual vector r defined by equation (6.72) and let the dynamical LPV filter $F(\theta)$ be put into a LFT-form so that $F(\theta) = F_l(\mathbb{F}, \Theta)$ where the LTI filter $\mathbb{F}$ admits the following representation:

$$\mathbb{F}(s) = \begin{pmatrix} C_{F1} \\ C_{F\theta} \end{pmatrix} (sI - A_F)^{-1} \begin{pmatrix} B_{F1} & B_{F\theta} \end{pmatrix} + \begin{pmatrix} D_{F11} & D_{F1\theta} \\ D_{F\theta 1} & D_{F\theta\theta} \end{pmatrix} \tag{6.73}$$

Our aim is to derive simultaneously M_y, M_u and the state space matrices of the LTI filter $\mathbb{F}$ that solve the following optimisation problem:

$$\begin{aligned} &\min_{M_y, M_u, F(\theta)} \ \gamma_1 \\ &s.t. \ ||T_{d\to r}(\theta)||_\infty < \gamma_1 \end{aligned} \tag{6.74}$$

$$\begin{aligned} &\max_{M_y, M_u, F(\theta)} \ \gamma_2 \\ &s.t. \ ||T_{f\to r}(\theta)||_- > \gamma_2 \end{aligned} \tag{6.75}$$

$T_{d\to r}(\theta)$ and $T_{f\to r}(\theta)$ denote the LPV transfers between d and r, and f and r respectively. γ_1 and γ_2 are respectively the robustness and the fault sensitivity performance indexes for the residual vector (6.72). θ playing the role of a scheduling variable, $F(\theta) = F_l(\mathbb{F}, \Theta)$ gives the rule for updating the FDI filter state-space matrices (6.73) based on the measurements of θ. The problem dimensions are $M_y \in \mathbb{R}^{q_r \times m}$, $M_u \in \mathbb{R}^{q_r \times p}$, $A_F \in \mathbb{R}^{n_F \times n_F}$, $D_{F11} \in \mathbb{R}^{q_r \times (m+p)}$, $D_{F\theta\theta} \in \mathbb{R}^{q_\Theta \times q_\Theta}$, where $q_\Theta = dim(\Theta)$. Note that if θ enters linearly in (6.16), then $q_\Theta = q$. □

Remark 6.3. In problem 6.2, it is assumed that the residual structuring matrices M_y and M_u do not depend on θ. This assumption will be justified later, see section 6.5.2.

6.5.1 Solution to the Problem

In this section, a solution is provided to compute simultaneously M_y, M_u and the state-space matrices of the dynamical LTI filter $\mathbb{F}$. Similarly to the developments presented in section 6.4, a sufficient condition is established in terms of a fictitious H_∞ LPV problem. It is then shown that a solution to this fictitious problem is a solution of the original one. Unfortunately, as it will be seen later, this formulation leads to a non-convex problem since it involves simultaneously the residual structuring matrices M_y, M_u and the filter state-space matrices (6.73). To solve this problem, a solution is derived by means of the small gain theory. It is then shown that the design problem can be formulated in a Semi Definite Programming (SDP) optimization problem. Computational issues are investigated and it is shown that the proposed solution is structurally well-defined.

6.5.1.1 The Quasi-standard Setup

To solve problem 6.2, the design objectives are formulated in terms of loop shapes, i.e. desired gain responses for the appropriate closed-loop transfers. The shaping objectives are then turned into uniform bounds by means of the shaping filters.

To proceed, consider the setup illustrated on figure 6.7. Including K into P leads to a new model P_K as illustrated on figure 6.8.a . Now let $W_d : ||W_d||_\infty \leq \gamma_1$ and $W_f : ||W_f||_- \geq \gamma_2$ be the shaping filters associated to $T_{d\to r}(\theta)$ and $T_{f\to r}(\theta)$ respectively. It is assumed that W_d is invertible. This can be done without loss of generality since it is always possible to add zeros in W_d to make it invertible. Then, there exists a solution to (6.74) iff :

$$\exists M_y, M_u, F(s) : \left\| T_{d\to r}(\theta) W_d^{-1} \right\|_\infty < 1 \tag{6.76}$$

or, equivalently,

$$\exists M_y, M_u, F(s) : \left\| T_{\tilde{d}\to r}(\theta) \right\|_\infty < 1 \tag{6.77}$$

where $\tilde{d}$ is a fictitious signal generating d through W_d^{-1} (see figure 6.8.a for easy reference).

The following lemma allows the sensitivity constraint (6.75) to be formulated in terms of a fictitious H_∞ one.

Lemma 6.2. *Let W_F be an invertible LTI transfer matrix defined such that $||W_f||_- = \gamma_2/\lambda ||W_F||_-$ and $||W_F||_- > \lambda$ where $\lambda = 1+\gamma_2$. Define the (fictitious) signal $\tilde{r}$ such that $\tilde{r}(s) = r(s) - W_F(s) f(s)$ (see figure 6.8.a for easy reference). Then a sufficient condition for (6.75) to hold is*

$$\exists M_y, M_u, F(s) : \left\| T_{f\to\tilde{r}}(\theta) \right\|_\infty < 1 \tag{6.78}$$

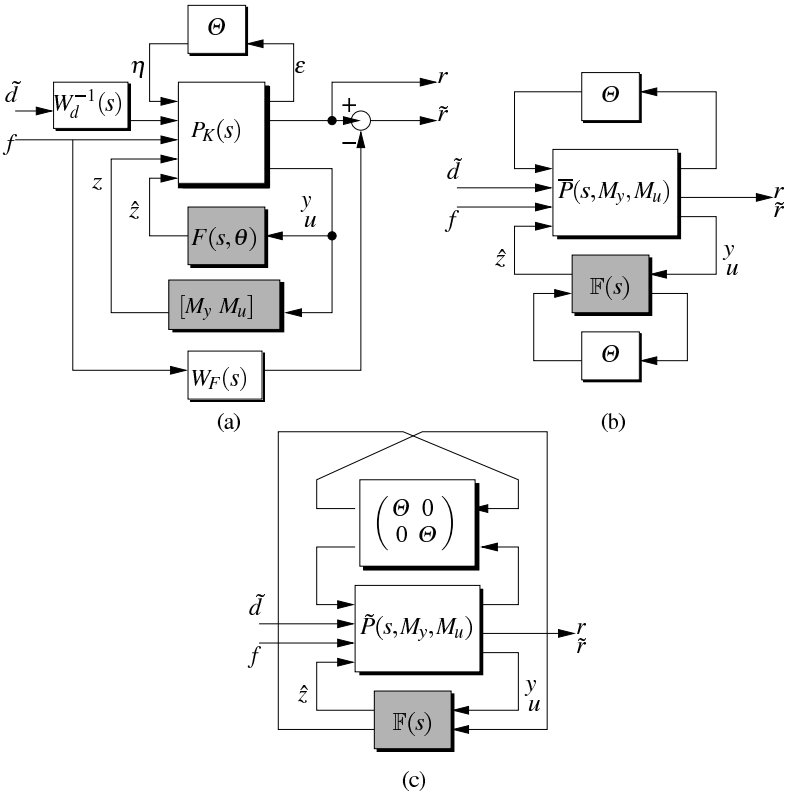

Fig. 6.8 (a): The weighted design problem, (b) The LPV filter structure, (c) the "quasi-standard" structure

Proof: The proof is similar to those of lemma 6.1. □

Following the above developments, the design problem can be re-casted in a framework which looks like a standard H_∞ problem for LPV systems, by combining both requirements (6.77) and (6.78) into a single constraint: a sufficient condition for M_y, M_u and $\mathbb{F}$ to solve problem 6.2 is

$$\left\| T_{(\tilde{d}^T f^T)^T \to (r^T \tilde{r}^T)^T}(\theta) \right\|_\infty < 1 \tag{6.79}$$

where $T_{(\tilde{d}^T f^T)^T \to (r^T \tilde{r}^T)^T}(\theta)$ denotes the transfer between $(\tilde{d}^T f^T)^T$ and $(r^T \tilde{r}^T)^T$ that depends on P_K, $\mathbb{F}$, M_y, M_u, W_d and W_F, see figure 6.8.a. This equation shows that the original problem can be viewed as a gain-scheduling H_∞ performance problem, where the time varying parameter vector θ enters both the plant and the dynamical filter $\mathbb{F}$. However, a particularity of this problem is that the transfer $T_{(\tilde{d}^T f^T)^T \to (r^T \tilde{r}^T)^T}(\theta)$ depend on the residual structuring matrices M_y and M_u that are unknown.

To apprehend this problem with the small gain theory, all parameter-dependent components must be put into a single uncertainty block. To proceed, let us consider the diagram depicted on figure 6.8.a. Including M_y, M_u, W_d^{-1} and W_F into P_K leads to a new model $\overline{P}(M_y, M_u)$ that depends on the matrix M_y and M_u (the mathematical details about this manipulation is omitted here for clarity). Introducing the augmented plant

$$\tilde{P}(s, M_y, M_u) = \begin{pmatrix} 0 & 0 & I_{q_\Theta} \\ 0 & \overline{P}(s, M_y, M_u) & 0 \\ I_{q_\Theta} & 0 & 0 \end{pmatrix} \tag{6.80}$$

it can be verified that the closed-loop mapping from exogenous inputs $(\tilde{d}^T \; f^T)^T$ to output signals $(r^T \; \tilde{r}^T)^T$ can be expressed as:

$$\begin{pmatrix} r \\ \tilde{r} \end{pmatrix} = F_u \left(F_l \left(\tilde{P}(M_y, M_u), \mathbb{F} \right), \begin{pmatrix} \Theta & 0 \\ 0 & \Theta \end{pmatrix} \right) \begin{pmatrix} \tilde{d} \\ f \end{pmatrix} \tag{6.81}$$

This expression amounts to redrawing the diagram illustrated in figure 6.8.b as in figure 6.8.c. It follows with (6.79) that a sufficient condition for M_y, M_u and $\mathbb{F}$ to solve problem 6.2 is:

$$\left\| F_u \left(F_l \left(\tilde{P}(M_y, M_u), \mathbb{F} \right), \begin{pmatrix} \Theta & 0 \\ 0 & \Theta \end{pmatrix} \right) \right\|_\infty < 1 \tag{6.82}$$

This equation shows that the original problem can be viewed as a gain-scheduling H_∞ performance problem, where the time varying parameters θ enter both the plant and the filter $\mathbb{F}$. In other words, the FDI filter design problem seems to be a standard LPV H_∞ performance problem for the LTI plant $\tilde{P}(M_y, M_u)$ in the face of the norm-bounded block-repeated uncertainty $\begin{pmatrix} \Theta & 0 \\ 0 & \Theta \end{pmatrix}$. As already mentioned, this is not the case since the transfer $\tilde{P}(M_y, M_u)$ depends on the structuring residual matrix M_y, M_u that is a part of the FDI filter we are looking for. However, sufficient conditions for solvability can be provided by means of the small gain theory using adequate commutable scaling matrices and the projection lemma using a judiciously chosen basis. This is the purpose of the next section.

6.5.1.2 The SDP Formulation

With some abuse of notation, let us denote the state-space realization of $\overline{P}(M_y, M_u)$ according to

$$\overline{P}(s, M_y, M_u) = \begin{pmatrix} C_\theta \\ C_1 \\ C_2 \end{pmatrix} (sI - A)^{-1} \begin{pmatrix} B_\theta & B_1 & B_2 \end{pmatrix} + \begin{pmatrix} D_{\theta\theta} & D_{\theta 1} & D_{\theta 2} \\ D_{1\theta} & D_{11} & D_{12} \\ D_{2\theta} & D_{21} & D_{22} \end{pmatrix} \tag{6.83}$$

The problem dimensions are $A \in \mathbb{R}^{n \times n}, D_{\theta\theta} \in \mathbb{R}^{q_\Theta \times q_\Theta}, D_{11} \in \mathbb{R}^{p_1 \times m_1}, D_{22} \in \mathbb{R}^{p_2 \times m_2}$.

From the above section, it can be verified that:

- $B_2, D_{\theta 2}, D_{22}$ are null matrices. This shows that the FDI filter does not affect neither the state, nor the measurements of the system, i.e. the FDI filter operates *obviously* in open loop with regard to the system. The interested reader can refer to [57] where details on the computation of $B_2, D_{\theta 2}, D_{22}$ are given for a very similar problem.
- $C_1, D_{1\theta}$ and D_{11} depend on M_y, M_u.
- $m_1 = q_d + q_f$, $p_1 = 2q_r$, $m_2 = q_r$ and $p_2 = m + p$.

The following assumption, that greatly simplifies the following developments, is made:

Assumption 1. *We assume that D_{11} is a square matrix. This can be always fulfilled by augmenting the problem with columns/rows of zeros.* □

This assumption will be justified later, see theorem 6.2.

Now, let Δ denote the structure set associated with Θ defined by (6.71) and L_Δ be the set of commutable scaling matrices defined so that

$$L_\Delta = \{L > 0 : L\Theta = \Theta L, \forall \Theta \in \Delta\} \subset \mathbb{R}^{q_\Theta \times q_\Theta} \tag{6.84}$$

The following theorem allows to formulate the design problem in terms of a SDP optimization one:

Theorem 6.1. *Consider Δ, L_Δ and the state-space realization of $\overline{P}(M_y, M_u)$ defined by (6.83). Let W be any matrix whose columns form a basis of the null space of $(C_2\ D_{2\theta}\ D_{21})$ and consider a matrix $X \neq 0 : X \in \mathbb{R}^{m_2 \times m_2}$. The H_∞ requirement (6.82) is satisfied and $F(\theta)$ is internally stable and of full-order (i.e. $n_F = n$) if there exist $\gamma < 1, M = [M_y\ M_u] \in \mathbb{R}^{m_2 \times p_2}$ and pairs of symmetric positive definite matrices $(R, S) \in \mathbb{R}^{n \times n}$ and $(L_3, J_3) \in L_\Delta$ solving the following SDP problem:*

$$\min \gamma \quad \text{subject to:}$$

$$\begin{pmatrix} AR + RA^T & RC_\theta^T & RC_1^T H^T & B_\theta J_3 & B_1 \\ C_\theta R & -J_3 & 0 & D_{\theta\theta} J_3 & D_{\theta 1} \\ HC_1 R & 0 & -\gamma diag\left(2X^T X, I_j\right) & HD_{1\theta} J_3 & HD_{11} \\ J_3 B_\theta^T & J_3 D_{\theta\theta}^T & J_3 D_{1\theta}^T H^T & -J_3 & 0 \\ B_1^T & D_{\theta 1}^T & D_{11}^T H^T & 0 & -\gamma I \end{pmatrix} < 0 \tag{6.85}$$

$$\left(\begin{array}{c|c} W & 0 \\ 0 & I \end{array}\right)^T \left(\begin{array}{ccc|cc} A^T S + SA & SB_\theta & SB_1 & C_\theta^T L_3 & C_1^T \\ B_\theta^T S & -L_3 & 0 & D_{\theta\theta}^T L_3 & D_{1\theta}^T \\ B_1^T S & 0 & -\gamma I & D_{\theta 1}^T L_3 & D_{11}^T \\ \hline L_3 C_\theta & L_3 D_{\theta\theta} & L_3 D_{\theta 1} & -L_3 & 0 \\ C_1 & D_{1\theta} & D_{11} & 0 & -\gamma I \end{array}\right) \left(\begin{array}{c|c} W & 0 \\ 0 & I \end{array}\right) < 0 \tag{6.86}$$

$$\begin{pmatrix} R & I \\ I & S \end{pmatrix} \geq 0, \quad \begin{pmatrix} L_3 & I \\ I & J_3 \end{pmatrix} \geq 0, \quad H = diag\left(\begin{bmatrix} X^T & -X^T \end{bmatrix}, I_j\right) \tag{6.87}$$

where "j" denotes the number of rows added to D_{11} in order to verify assumption 1, i.e. if no rows are added to D_{11} or if only columns are added, then $H = \begin{bmatrix} X^T & -X^T \end{bmatrix}$. □

Proof: Consider the structure Δ and the associated set of commutable matrices L_Δ defined in (6.84). It follows that the block-repeated $\begin{pmatrix} \Theta & 0 \\ 0 & \Theta \end{pmatrix}$ admits the following set of commutable scalings:

$$L_{\Delta\oplus\Delta} = \left\{ \begin{pmatrix} L_1 & L_2 \\ L_2^T & L_3 \end{pmatrix} > 0 : L_1, L_3 \in L_\Delta,\ L_2\Theta = \Theta L_2, \forall \Theta \in \Delta \right\} \subset \mathbb{R}^{2q_\Theta \times 2q_\Theta} \tag{6.88}$$

Then, from the small gain theory, the following statement yields:

Theorem 6.2. *Let $L_{\mathscr{D}}$ be the set of commutable scaling matrices defined so that*

$$L_{\mathscr{D}} = \left\{ \mathscr{D} > 0 : \mathscr{D}\tilde{\Delta} = \tilde{\Delta}\mathscr{D},\ \forall \tilde{\Delta} \right\} \subset \mathbb{R}^{m_1 \times p_1} \tag{6.89}$$

where $\tilde{\Delta}$ is an uncertainty block introduced to close the loop between $(\tilde{d}^T\ f^T)^T$ and $(r^T\ \tilde{r}^T)^T$. If there exist $\gamma < 1$, M_y, M_u, scaling matrices $\mathscr{L} \in L_{\Delta\oplus\Delta}$, $\mathscr{D} \in L_{\mathscr{D}}$ and a LTI filter $\mathbb{F}$ that satisfies

$$\left\| \begin{pmatrix} \mathscr{L}^{1/2} & 0 \\ 0 & \frac{1}{\sqrt{\gamma}}\mathscr{D} \end{pmatrix} F_l\left(\tilde{P}(M_y, M_u), \mathbb{F}\right) \begin{pmatrix} \mathscr{L}^{-1/2} & 0 \\ 0 & \frac{1}{\sqrt{\gamma}}\mathscr{D}^{-1} \end{pmatrix} \right\|_\infty < 1 \tag{6.90}$$

then $F_l(\mathbb{F}, \Theta)$ is internally stable and the H_∞ performance (6.82) is satisfied. □

Proof: The proof is a straightforward application of the small gain theory to the particular structure of $\overline{P}(M_y, M_u)$, and specially taking into account the fact that the FDI filter operates in open loop versus the system. Thus internal stability of the closed loop ensures internal stability of $F(\Theta) = F_l(\mathbb{F}, \Theta)$. Note that since D_{11} is a square matrix, then $\tilde{\Delta}$ reduces to a single square block. This greatly simplifies the definition of $L_{\mathscr{D}}$. Specially, $\mathscr{D}$ is a square matrix and this allows numerical facilities, see [74].

Now, by virtue of the bounded real lemma [104] and the projection lemma [103], the following theorem can be established:

Theorem 6.3. *Consider the scaling matrix $\mathscr{L}$ introduced in theorem 6.2 and let $\mathscr{J} = \begin{pmatrix} J_1 & J_2 \\ J_2^T & J_3 \end{pmatrix} \in L_{\Delta\oplus\Delta} : \mathscr{L}\mathscr{J} = I$. Consider the state-space realization of $\overline{P}(M_y, M_u)$ defined in (6.83) and let N_R and N_S be any matrices whose columns form bases of the null spaces of $(B_2^T\ D_{\theta 2}^T\ D_{12}^T\ 0)$ and $(C_2\ D_{2\theta}\ D_{21}\ 0)$ respectively. Then, there exists a solution to (6.90) iff there exist symmetric matrices $(R, S) > 0 \in \mathbb{R}^{n\times n}$ and $M = [M_y\ M_u] \in \mathbb{R}^{m_2 \times p_2}$ such that*

$$N_R^T \begin{pmatrix} AR+RA^T & RC_\theta^T & RC_1^T & B_\theta J_3 & B_1 \\ C_\theta R & -J_3 & 0 & D_{\theta\theta} J_3 & D_{\theta 1} \\ C_1 R & 0 & -\gamma I & D_{1\theta} J_3 & D_{11} \\ J_3 B_\theta^T & J_3 D_{\theta\theta}^T & J_3 D_{1\theta}^T & -J_3 & 0 \\ B_1^T & D_{\theta 1}^T & D_{11}^T & 0 & -\gamma I \end{pmatrix} N_R < 0 \tag{6.91}$$

$$N_S^T \begin{pmatrix} A^T S+SA & SB_\theta & SB_1 & C_\theta^T L_3 & C_1^T \\ B_\theta^T S & -L_3 & 0 & D_{\theta\theta}^T L_3 & D_{1\theta}^T \\ B_1^T S & 0 & -\gamma I & D_{\theta 1}^T L_3 & D_{11}^T \\ L_3 C_\theta & L_3 D_{\theta\theta} & L_3 D_{\theta 1} & -L_3 & 0 \\ C_1 & D_{1\theta} & D_{11} & 0 & -\gamma I \end{pmatrix} N_S < 0 \tag{6.92}$$

$$\begin{pmatrix} R & I \\ I & S \end{pmatrix} \geq 0, \quad \begin{pmatrix} L_3 & I \\ I & J_3 \end{pmatrix} \geq 0, \quad n_F = n \tag{6.93}$$

Proof: The proof is an immediate application of the results presented in [105].

Because $C_1, D_{1\theta}$ and D_{11} depend on M_y, M_u, it is readily verified that the inequality (6.91) is not jointly affine in R, M_y and M_u and thus do not define a LMI problem. In fact, a deeper investigation into the expression (6.91) reveals a BMI problem. To overcome this problem, consider the matrices $B_2, D_{\theta 2}$ and D_{12}. As already outlined, a particularity of our problem is that the matrices B_2 and $D_{\theta 2}$ are null matrices. Furthermore, it can be verified that $D_{12} = -\begin{pmatrix} I_{m_2} \\ I_{m_2} \\ O_j \end{pmatrix}$, where "$j$" denotes the number of added rows in D_{11} to make it square. It follows that bases N_R and N_S of the null spaces of $(B_2^T \; D_{\theta 2}^T \; D_{12}^T \; 0)$ and $(C_2 \; D_{2\theta} \; D_{21} \; 0)$ are respectively of the form

$$N_R = diag\left(I_{n+q_\Theta}, \begin{bmatrix} X \\ -X \end{bmatrix}, I_{j+q_\Theta+m_1}\right), \quad X \neq 0 \tag{6.94}$$

$$N_S = diag\left(W, I_{j+q_\Theta+p_1}\right) \tag{6.95}$$

where W denotes a matrix whose columns form a basis of the null spaces of $(C_2 \; D_{2\theta} \; D_{21})$. $X \in \mathbb{R}^{m_2 \times m_2}$ also denotes an arbitrary chosen matrix.

Taking into account these expressions of N_R and N_S, it can be verified that the inequalities (6.91)-(6.92) can be written as (6.85)-(6.86). This latest set of inequalities is now jointly affine in M_y, M_u, R, S, L_3 and J_3, and therefore is now a LMI problem. Finally, noting that γ enters linearly in (6.91)-(6.92) leads to the SDP formulation stated in theorem 6.1, which terminates the proof. □

Remark 6.4. Coming back to the statement of theorem 6.1, it can be noted that X is a user-defined matrix and this may induce some conservativeness. Coming back to the above developments, it can be verified that any X of full column rank leads N_R to be a basis for $(B_2^T \; D_{\theta 2}^T \; D_{12}^T \; 0)$. It follows that the choice of X is only guided by numerical aspects, see section 6.5.3 where an example is discussed.

6.5.1.3 Computational Issues

Theorem 6.1 provides sufficient conditions for the existence of M_y, M_u and the LTI filter $\mathbb{F}$. However, it does not offer a procedure to compute the state-space matrices defined by (6.73). To derive these state-space matrices from the unique solution (γ, R, S, L_3, J_3) the method discussed in [73, 105] is used. The proposed method also parallels the algorithm proposed in section 6.4 and thus will not be described here.

However, some computational aspects need to be discussed. Because $\mathscr{L}\mathscr{J} = I$ (see theorem 6.3), it can be verified that

$$I - L_3 J_3 = L_2^T J_2 \tag{6.96}$$

Then, one should keep in mind that $I - L_3 J_3$ ought to be well conditioned in order to allow the computation of L_2, J_2. Unfortunately, $I - L_3 J_3$ will be nearly singular if the constraint $\begin{pmatrix} L_3 & I \\ I & J_3 \end{pmatrix} \geq 0$ is satured at the optimum. The same remark yields for $I - RS$.

To avoid such difficulties, the idea consists in maximizing the minimal eigenvalue of RS and $L_3 J_3$, and hence, to push them away from "1" such that $I - RS$ and $I - L_3 J_3$ are expected to be well conditioned. This can be done, by e.g., changing the SDP optimisation problem in theorem 6.1 according to:

$$\begin{array}{l} \min \gamma + \varepsilon \rho \quad s.t \\ (6.85) \text{ and } (6.86) \\ \begin{pmatrix} R & \rho I \\ \rho I & S \end{pmatrix} \geq 0, \quad \begin{pmatrix} L_3 & \rho I \\ \rho I & J_3 \end{pmatrix} \geq 0 \end{array}$$

where ε is a negative scalar.

Furthermore, since the computation of the residual vector r involves the computation of $F(\theta) = F_l(\mathbb{F}, \Theta)$, it is natural to ask about the existence of this lower LFR for all admissible values $\theta(t)$. Taking into account the state-space matrices defined by (6.73), $F_l(\mathbb{F}, \Theta)$ exists iff the matrix

$$I - D_{F\theta\theta}\Theta \tag{6.97}$$

is invertible $\forall \Theta, ||\Theta||_\infty \leq 1$. Coming back to the developments given in the previous section, and specially the small gain theorem used to state (6.90), it is guaranteed that $F_u\left(F_l\left(\tilde{P}(M_y, M_u), \mathbb{F}\right), \begin{pmatrix} \Theta & 0 \\ 0 & \Theta \end{pmatrix}\right)$ exists $\forall \Theta, ||\Theta||_\infty \leq 1$. It follows that the inversion of the matrix

$$I - \begin{pmatrix} D_{F\theta\theta} & D_{F\theta 1} D_{2\theta} \\ D_{\theta 2} D_{F1\theta} & D_{\theta\theta} + D_{\theta 2} D_{F11} D_{2\theta} \end{pmatrix} \begin{pmatrix} \Theta & 0 \\ 0 & \Theta \end{pmatrix} \tag{6.98}$$

is guaranteed $\forall \Theta : ||\Theta||_\infty \leq 1$. Since, by construction $D_{\theta 2} = 0$, if follows that the inversion of (6.98) implies that of (6.97). In other words, the existence of $F(\theta) = F_l(\mathbb{F}, \Theta)$ is guaranteed for all parameter trajectories.

Finally, it should be outlined that, because the proposed procedure optimizes M_y, M_u and $\mathbb{F}$ simultaneously, there may exist no unique solution for the part of the fault detection filter consisting of $M = [M_y\, M_u]$ and the static part of $\mathbb{F}$, as the final residual filter includes the subtraction of these two parts, see equation (6.72). More precisely, this problem is concerned by D_{F11}, see eq (6.73). A solution to this problem consists in adding constraints on M to the LMIs (6.91)-(6.93) and/or to add an optimization objective on some functional of M. For instance, one useful constraint consist of the normalization constraint

$$\sum_j M_{ij} = 1,\ \forall i \tag{6.99}$$

restricting the set of admissible solutions. However we argue that this problem is not so crucial since γ entering in the SDP optimization problem (6.91)-(6.93) is minimized, i.e., the fault detection performance are optimized that is fundamentally the problem we want to solve. Note that in some cases, D_{F11} may be found to be zero, thus vanishing the need of additional constraints on M. This fact has already been observed in e.g., [52, 89, 60, 78]. Note that the same remark yields for the polytopic approach presented in the section 6.4.

6.5.2 The Case of Parameter-Dependent Residual Structuring Matrices

Consider now the case of parameter-dependent residual structuring matrices defined so that:

$$r(s) = M_y(\theta)y(s) + M_u(\theta)u(s) - \hat{z}(s), \quad \hat{z}(s) = F(s,\theta)\begin{pmatrix} y(s) \\ u(s) \end{pmatrix}, \quad r \in \mathbb{R}^{q_r} \tag{6.100}$$

Our aim is to derive simultaneously $M_y(\theta)$, $M_u(\theta)$ and the state space matrices of the LTI filter F defined by (6.73), that solve the optimization problem defined by equations (6.74)-(6.75).

A particularity of this formulation is that the time varying parameters enter now both the structuring matrices and the filter $F(\theta) = F_l(\mathbb{F}, \Theta)$. To apprehend this problem with the small gain theory, we must first gather all parameter-dependent components into a single uncertainty block. To proceed, let $M(\theta) = \begin{pmatrix} M_y(\theta)\ M_u(\theta) \end{pmatrix}$ be put into a LFT-form so that:

$$M(\theta) = F_l(\mathbb{M}, \Theta), \quad \mathbb{M} = \begin{pmatrix} M_{11}\ M_{1\theta} \\ M_{\theta 1}\ M_{\theta\theta} \end{pmatrix}, \quad M_{11} \in \mathbb{R}^{q_r \times (m+p)}, \quad M_{\theta\theta} \in \mathbb{R}^{q_\Theta \times q_\Theta} \tag{6.101}$$

θ playing the role of a scheduling variable, equation (6.101) gives the rule for updating $M_y(\theta)$ and $M_u(\theta)$ based on the measurements of θ.

Following the same developments than those presented in the previous sections, it can be verified that a sufficient condition for $\mathbb{M}$ and $\mathbb{F}$ to solve the FDI filter design problem is (see figures 6.9 for easy references):

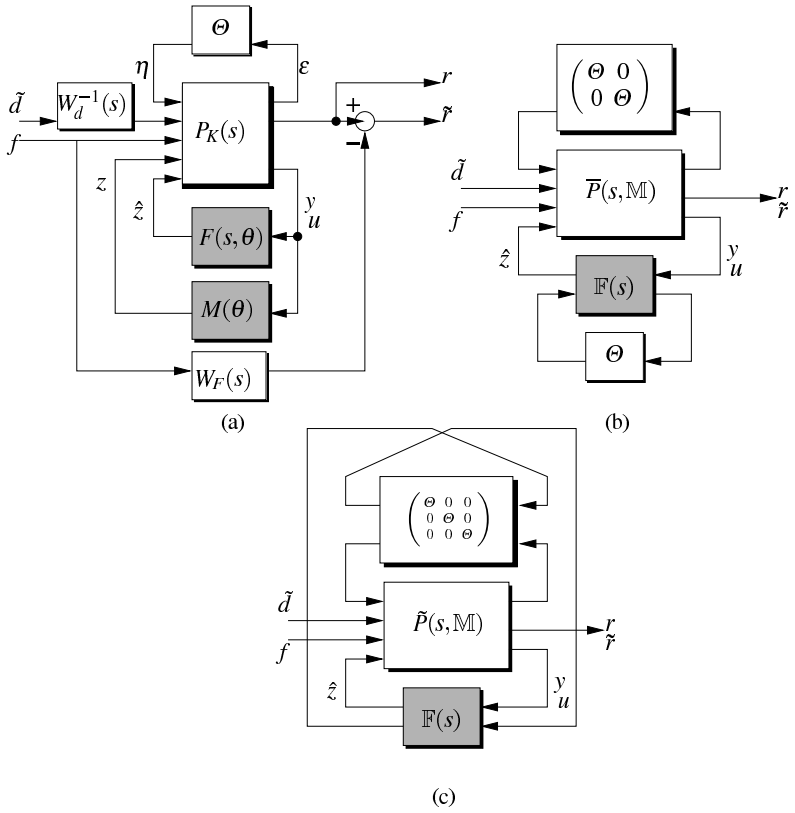

Fig. 6.9 (a): The weighted design problem, (b) The LPV filter structure, (c) the "quasi-standard" structure

$$\left\| F_u\left(F_l\left(\tilde{P}(\mathbb{M}),\mathbb{F}\right), diag(\Theta,\Theta,\Theta)\right)\right\|_\infty < 1 \tag{6.102}$$

This equation shows that the original problem can be viewed as a gain-scheduling H_∞ performance problem in the face of the norm-bounded block-repeated uncertainty $diag(\Theta,\Theta,\Theta)$.

Applying the small gain theory to the setup illustrated in figure 6.9.b leads to the set of commutable scaling matrices L_Δ defined according to $L_\Delta = \{L > 0 : L\Theta = \Theta L, \forall \Theta \in \Delta\} \subset \mathbb{R}^{2q_\Theta \times 2q_\Theta}$. Clearly, the dimension of this new set L_Δ is twice bigger than those defined for constant residual structuring matrices and this drives to conservative solutions. The same argument yields for the set $L_{\Delta\oplus\Delta} \subset \mathbb{R}^{3q_\Theta \times 3q_\Theta}$. Thus, it is preferred constant residual structuring matrices at this stage. Note that some solutions to this problem may exist by using e.g. the full-block multipliers-based approach proposed in [75] or the parameter-dependent quadratic Lyapunov function technique presented in [106].

Finally, as the final residual filter includes the subtraction of $M_y(\theta)y + M_u(\theta)u$ and $F_l(\mathbb{F},\Theta)$, another solution to this problem may consist in including $M_{11}, M_{1\theta}$, $M_{\theta 1}$, $M_{\theta\theta}$ into $D_{F11}, D_{F1\theta}, D_{F\theta 1}, D_{F\theta\theta}$ respectively. Even if this leads to the same

level of fault detection performance (see the discussion in section 6.5.1.3), it could be verified that in this case, it is impossible to separate $M_{11}, M_{1\theta}, M_{\theta 1}, M_{\theta\theta}$ from $D_{F11}, D_{F1\theta}, D_{F\theta 1}, D_{F\theta\theta}$ and thus to determine the expression of $M_y(\theta)$ and $M_u(\theta)$; This is thought to be an important aspect of the proposed technique from a practical point of view since these latest matrices address the structuration of the residual generator. Note that the same remark yields for the polytopic approach presented in the section 6.4, but it is less crucial in terms of conservativeness.

6.5.3 Illustrative Example

To illustrate the potential of the proposed approach, an illustrative example of academic nature is considered. Consider the following system:

$$G(\theta): \begin{cases} \dot{x} = A(\delta)x + Bu + K_1 f \\ y = Cx + n \end{cases} \tag{6.103}$$

$$A(\delta) = \begin{pmatrix} 0 & \delta_2 \\ -0.1\delta_1 & -\delta_3 \end{pmatrix}, B = \begin{pmatrix} 0 \\ 0.1 \end{pmatrix}, K_1 = \begin{pmatrix} 1 \\ 1 \end{pmatrix}, C = I_2 \tag{6.104}$$

f denotes the fault to be detected and n is the measurement noise which is assumed to be high frequency signals located in the frequency range $[100rd/s, +\infty[$. $\delta_i(t), i = 1,2,3$ are assumed to vary in the following bounds

$$5 \leq \delta_1(t) \leq 8, \quad -2 \leq \delta_2(t) \leq -1, \quad 2 \leq \delta_3(t) \leq 4$$

with arbitrary time variations. It is assumed that the system operates in a feedback control loop so that the closed loop is internally stable (a LQ controller has been designed for this purpose).

Following the above presented developments (see section 3), the system is put into a LFR form according to the setup illustrated in figure 6.8.c. This boils down to the block diagonal time-varying operator Θ defined according to $\Theta = diag(\theta_1, \theta_2, \theta_3)$ which has been normalized so that $|\theta_i| \leq 1, i = 1,2,3$. The problem dimension are $q = q_\Theta = 3$, $q_r = 1$, $q_d = 1$, $q_f = 1$, $m = 2$, $p = 1$.

The shaping filters W_d and W_f that allow to specify the robustness and the sensitivity objectives have been fixed according to:

$$W_d = 10\frac{1 + 10^{-2}s}{1 + 10s} I_2, \quad W_f = 0.1\frac{1}{1 + 2s} \tag{6.105}$$

By this choice, it is required:

- S.1) an attenuation factor of, at least, $40dB$ of $n(t)$ on the residual $r(t)$ $\forall\theta(t)$ and,
- S.2) an amplification factor of, at least, $-20dB$ of $f(t)$ on $r(t)$ in the frequencies $\Omega = [0rd/s, 0.5rd/s]$ $\forall\theta(t)$.

Lemma 6.2 and theorem 6.1 are then used to derive M_y, M_u, $F(\theta)$. Since $q_r = 1$, $q_d = 2$ and $q_f = 1$, one row of zeros is added to $C_1, D_{1\theta}, D_{11}$ and D_{12} in order

to satisfy assumption 1. For the purpose of the SDP optimisation problem (6.85)-(6.87), the SDPT3 solver is used.

Five different values of X are considered for numerical aspects, see remark 6.4. The obtained results are listed in table 6.1. From this table, it is observed that X does not influence the optimal value of γ. Furthermore, it is observed that four cases are ill-conditioned. The cases $X = 1, 10, 20$ reveal that, due to numerical difficulties in the SDP solver, the negative definite constraints for some LMIs can not be numerically guaranteed. The case $X = 500$ is concerned by the constraint $\mathscr{L}\mathscr{J} = I$ which is tested *a posteriori*, i.e., when the optimization procedure has succeeded. Specially, it is observed that $L_1J_2 + L_2J_3 = 0$ is not fulfilled.

Table 6.1 Numerical aspects of the optimization problem (6.85)-(6.87)

X	γ_{opt}	Numerical difficulties
1	0.9911	constraint $\Psi + P'\Omega Q + Q'\Omega P < 0$ beyond the solver precision ($\lambda_i \approx -8,4.10^{-13}$)
10	0.9909	constraint eq. (6.86) beyond the solver precision
15	0.9918	no problem detected
20	0.9908	constraint $\Psi + P'\Omega Q + Q'\Omega P < 0$ beyond the solver precision($\lambda_i \approx -1,15.10^{-12}$)
500	0.9890	$L_1J_2 + L_2J_3 = 0$ not fulfilled

Finally, it is observed from table 6.1 that $X = 15$ yields a better conditioned problem. The found computed solution is given according to:

$$M_u = 1.7151 \quad M_y = [-0.3494 \ -0.3657]$$

$$A_F = \begin{pmatrix} -4.3425 & -2.3359 & 4.2194 & 3.5534 & -7.0176 \\ -2.5577 & -2.3404 & 2.9579 & 3.1445 & -9.3983 \\ -0.8242 & -0.2675 & -0.1067 & -0.7127 & 5.0677 \\ -0.0250 & -0.3128 & 0.0101 & -0.7254 & 0.4713 \\ -0.0077 & -0.0092 & 0.0932 & 2.5985 & -12.0599 \end{pmatrix}$$

$$\left(B_{F1} \middle| B_{F\theta}\right) = \left(\begin{array}{ccc|ccc} -0.0765 & -0.1433 & -0.0316 & 206.8172 & 401.1529 & 608.1251 \\ -0.5659 & -1.0620 & -0.0147 & 135.0142 & -151.9848 & 396.9957 \\ -0.3733 & -0.7007 & 0.0028 & -55.8217 & 51.6555 & -164.1381 \\ 0.0020 & 0.0038 & 0.0003 & 2.7347 & -1.0040 & 8.0410 \\ -0.0003 & -0.0005 & 0.0000 & -0.0150 & 0.0068 & -0.0442 \end{array}\right)$$

$$\left(\frac{C_{F1}}{C_{F\theta}}\right) = \left(\begin{array}{ccccc} 0.0000 & 0.0000 & -0.0000 & -0.0025 & -1.8635 \\ \hline -0.0001 & 0.0002 & -0.0002 & -0.0031 & 0.0152 \\ 0.0017 & 0.0030 & -0.0049 & -0.0302 & 0.1374 \\ -0.0003 & 0.0004 & -0.0005 & -0.0071 & 0.0344 \end{array}\right)$$

$$\left(\begin{array}{c|c} D_{F11} & D_{F1\theta} \\ \hline D_{F\theta 1} & D_{F\theta\theta} \end{array}\right) = \left(\begin{array}{ccc|ccc} -0.2218 & -0.4337 & 1.7144 & 0 & 0 & 0 \\ \hline 0 & 0 & 0 & 0 & 0 & 0 \\ 0 & 0 & 0 & 0 & 0 & 0 \end{array}\right)$$

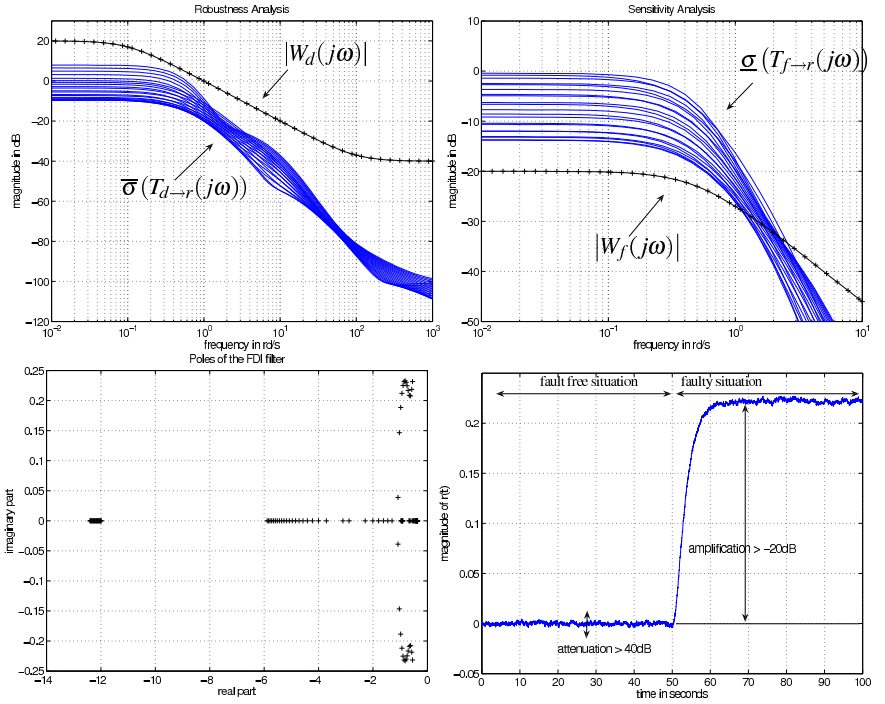

Fig. 6.10 The principal gains $\overline{\sigma}(T_{d\to r}(j\omega))$ / $\underline{\sigma}\left(T_{f\to r}(j\omega)\right)$, the objectives $|W_d(j\omega)|$ / $\left|W_f(j\omega)\right|$ and the poles of $F(\Theta)$ for some fixed values of $\theta_i(t), i = 1,2,3$ - Behaviour of $r(t)$

To provide a deeper insight into the solution, the principal gains $\overline{\sigma}(T_{d\to r}(j\omega))$ and $\underline{\sigma}\left(T_{f\to r}(j\omega)\right)$ are plotted versus the required objectives $|W_d(j\omega)|$ and $\left|W_f(j\omega)\right|$ for some arbitrary fixed values of $\theta_i(t), i = 1,2,3$, see Figure 6.10. Note that these plots only offer necessary conditions since the time-varying aspect of $\theta_i(t), i = 1,2,3$ is not considered. However, it can be argued that the required objectives specified by S.1) and S.2) are met since $\overline{\sigma}(T_{d\to r}(j\omega)) < |W_d(j\omega)|$ and $\underline{\sigma}\left(T_{f\to r}(j\omega)\right) > \left|W_f(j\omega)\right| \ \forall \omega \in \Omega$ for all fixed $\theta_i(t), i = 1,2,3$. Furthermore, the small gap between the gains and the weighting functions illustrates a not too conservative solution. Following the statements in the theorem 6.1, we can claim that these conclusions still yield for all $\theta_i(t), i = 1,2,3$, since the optimal value of γ is found to be ≈ 0.9918. Finally, the poles of $F(\Theta) = F_l(F,\Theta)$ are plotted for some arbitrary fixed values of $\theta_i(t), i = 1,2,3$, see Figure 6.10. As it can be seen, the poles of $F(\Theta)$ lie in the left-half complex plan for the considered values of $\theta_i(t), i = 1,2,3$ and, again, following the statements in the theorem 6.1, we know that it still holds for all $\theta_i(t), i = 1,2,3$ with arbitrary time variations.

The behavior of $r(t)$ is illustrated in Figure 6.10. Arbitrary time varying signals have been considered for the simulation of $\delta_i(t), i = 1,2,3$. For the purpose of the fault simulation, a step of magnitude "1" is considered between $50s \leq t \leq 100s$. As it can be seen, the required objectives specified by S.1) and S.2) are met. The fault can be detected using, e.g., a threshold-based decision making algorithm.

6.6 The Case of Non-measured Parameters

In this section, we would like to come back to the assumption about measured parameters $\theta_i(t), i = 1,...,q$. The aim is to provide "good" solutions in the case of non-measured parameters.

In the case when θ contains non-measured components (say θ_1 as opposed to θ_2 that is assumed to be measured), it is possible to use the computed solution $F(s,\theta) \equiv F(s,\theta_1,\theta_2)$ to obtain a suitable approximation $\overline{F}(s,\theta_2)$ depending only of θ_2. There are several possibilities to *robustly* fit $\overline{F}(s,\theta_2)$ to $F(s,\theta_1,\theta_2)$:

- The first solution aims at preserving the structure of $F(s,\theta_1,\theta_2)$. This involves finding a value $\overline{\theta}_1$ of θ_1 which produces the best approximation $\overline{F}(s,\theta_2) \equiv F(s,\overline{\theta_1},\theta_2)$ by solving the following optimization problem

$$\overline{\theta}_1 = \arg \min_{\rho \in \Theta_\rho} \max_{\theta \in \Theta} \|F(s,\theta_1,\theta_2) - F(s,\rho,\theta_2)\| \tag{6.106}$$

  where $||.||$ is a measure of the quality of the approximated solution, e.g., the H_2 or H_∞ norms can be used for this problem.
- The second solution assumes for $\overline{F}(s,\theta_2)$ a certain parametric form $\tilde{F}(s,\theta_2)$ (e.g. affine, polynomial, rational..etc..) and fit the free parameters ρ by solving the following optimization problem

$$\overline{\rho} = \arg \min_{\rho \in \Theta_\rho} \max_{\theta \in \Theta} \left\|F(s,\theta_1,\theta_2) - \tilde{F}(s,\rho,\theta_2)\right\| \tag{6.107}$$

- The third solution consists in fitting by globally minimizing a suitable worst-case (weighted) system norm, that is:

$$\max_{\theta \in \Theta} \left\| \left(F(s,\theta_1,\theta_2) - \overline{F}(s,\theta_2)\right) W(s,\theta)\right\| \tag{6.108}$$

  where $W(s,\theta)$ is a weighting function.

When using standard optimization tools to solve the above min-max parameter fitting problems, the evaluation of the above criteria involves performing a worst-case optimization-based search. Thus, function evaluations are potentially expensive, and therefore an alternative is to replace the semi-infinite optimization problems by computationally tractable finite dimensional optimization problems. A frequently used

approximation method is to use instead the continuous domain Θ only a discrete set of points $\Theta_N = \{\theta^{(1)}, \theta^{(2)}, ..., \theta^{(N)})\}$ obtained, for example, by parameter griding. By using a sufficiently dense grid of points, it is expected to obtain a satisfactory approximation of the continuous-case worst-case. One advantage of the gridding based approach is the possibility to perform in parallel all function evaluations necessary for the determination of worst-case maximum.

6.7 Application for Early Fault Detection in Aircraft Control Surfaces Servo-Loops

The work presented in this section is undertaken within the European FP7 funded ADDSAFE[4] project. The goal is to propose new fault diagnosis techniques that could significantly help developing environmentally-friendlier aircraft, by optimizing structural load design objectives. A Linear Parameter Varying (LPV) model-based fault detection scheme is proposed for robust and early detection of faults in aircraft control surfaces servo-loop. The proposed methodology is based on the H_∞/H_- LPV technique proposed in the above section for LPV systems modeled in a linear fractional representation (LFR) fashion.

The state-of-practice applied worldwide by all aircraft manufacturers to diagnose Electrical Flight Control System (EFCS, a.k.a. Fly-By-Wire (FBW)) faults and obtain full flight envelope protection at all times, consists mainly of hardware redundancy in order to perform consistency tests, cross checks, voting mechanisms and built in test techniques of varying sophistication [107]. This hardware-redundancy fault diagnosis approach fits also into current aircraft certification processes for ensuring the highest level of safety standards. Nevertheless, for the envisioned "sustainable" aircraft of the future (i.e. more affordable, cleaner and quieter as stated by the European Commission Vision 2020 objectives), the applicability of the current state of practice is becoming increasingly problematic.

Highlighting the link between aircraft sustainability and fault detection, it can be demonstrated that improving the performance of fault diagnosis in EFCS allows to optimize the aircraft structural design (weight saving) and then to improve the aircraft performance and *de facto* to decrease its environmental footprint (e.g. less fuel consumption and noise). EFCS failure cases that may affect structural loads are for example oscillatory failure cases [108, 109]. Similarly for the specific case of control surface runaway (a.k.a. hard-over) [110, 111, 112] or jamming [112], the reaction of the aircraft is a deflection of other control surfaces to compensate the aircraft attitude leading to an increase of drag proportional to the amplitude and to the origin of the failure. For instance, for the case of control surface jamming, if this dissymmetry remains during a significant time it could generate fuel overconsumption. The stake is the ability to correctly achieve the flight mission: if the overconsumption remains undetected there is risk to not be compliant with regulations like the ETOPS (an acronym for Extended-range Twin-engine Operational

[4] Advanced Fault Diagnosis for Sustainable Flight Guidance and Control.

Performance Standards, a regulation permitting twin-engined commercial air transporters to fly routes that, at some points, are farther than a given distance flying time from an emergency or diversion airport with one engine inoperative).

Towards this goal, a consortium of 2 industrial partners (AIRBUS and DEIMOS SPACE), 6 research establishments and Universities (DLR, SZTAKI, CNRS-IMS, Univ. of Leicester, Univ. of Hull and Delft University of Technology) has been established with funding from the European Union $7th$ Framework Program (FP7). The aim of the project, named Advanced Fault Diagnosis for Sustainable Flight Guidance and Control (ADDSAFE), is to research and develop advanced model-based fault diagnosis methods for aircraft flight control systems faults, predominantly sensor and actuator malfunctions. The aircraft model used in the project has been provided by AIRBUS. It is equipped by 2 engine throttles, 4 ailerons (2 inboards and 2 outboards), 12 spoilers, 2 elevators, 1 rudder and 1 trimmable horizontal stabilizer.

The work presented in this section is undertaken within this project. The goal is to propose a model-based fault diagnosis scheme for control surface servo-loops. The failure scenarios concern an abnormal aircraft behavior caused by an actuator or sensor failure in control surface servo-loops. More precisely, we investigate the cases of control surface jamming or being disconnected from its actuator on the roll axis, i.e. an aileron is stuck at a small deflection or disconnected from its actuator.

The conventional monitoring technique for such faults is industrially well mastered and well characterized (high level of robustness and good performance). The technique is validated and certified for implementation in the on board Flight Control Computer (FCC). It follows that any modification to this technique should provide, first of all, a viable technological solution ensuring good performance while guaranteeing the same level of robustness. Moreover, the selection of any advanced model-based monitoring solution necessarily includes a trade-off between the best adequacy of the technique and its implementation level for covering an expected fault profile, as well as its industrialization process with support tools for its design/tuning and validation. Very attractive advanced detection algorithmic solutions would not be accepted without such industrial framework capability. A classical monitoring technique may be preferred despite its smaller fault coverage thanks to its simplicity and robustness, without risk of false alarm. On the other hand, for future programs it could be necessary to detect earlier faults in control surfaces, which means e.g. that the control surface has reached a smaller deflection when the detection is confirmed. It follows that a good balance between conventional and in-service monitoring solutions and model based techniques could be the right solution to anticipate the more and more stringent requirements which would come in force for future environmentally-friendlier programs.

The work presented in this paper should be understood in this context. The objective is to design a reliable FDI (Fault Detection and Isolation) scheme to diagnose aileron jamming and disconnections.

Among a large number of possible model-based solutions, we focus on candidate methods which offer a reasonable computational burden while offering also the possibility of reuse (or building around it) with adequate design and tuning

engineering tools. We believe that the H_∞/H_- LPV technique proposed in section 6.5 could provide such a framework since:

- it offers an efficient paradigm to model nonlinear systems with on-line measurable state depending parameters,
- it provides stability and performance guarantees over a wide range of changing parameters,
- it offers tunable design parameters through the so-called weighting functions that allow the designer to specify the fault detection performance and thus to manage the trade-offs.

6.7.1 Modeling the Aileron Servo-Loop

One of the benchmark problem considered in ADDSAFE is a scenario involving abnormal aircraft behaviors that lead to the degradation of the aircraft performance. In this section, we focus on ailerons. Such abnormal configurations are caused by an actuator or a sensor failure in the control loop of a control surface, between the Flight Control Computer (FCC) and the moving surface, including these two elements.

The control surface (CS) servo-loop modeling, from the FCC to the CS, including these 2 elements, is illustrated on figure 6.11. Referring to figure 6.11, x_{ref} (in *degree*) is the position order delivered by the FCC and y (in *mm*) is the measured actuator position. n refers to the measurement noise. V_0 is the opening of the valve (which further controls the pressure and flow through the nonlinear dynamics) which is considered here to be the control u computed according to a proportional law denoted K_c. K_{iv} refers to the valve model so that $V_0 = K_{iv}i$ (with i in mA). $\Phi(x_{ref})$ also refers to the (nonlinear) conversion $degree \rightarrow mm$. It is assumed that the only available signals are x_{ref} (coming from the FCC) and y (a Linear Variable Differential Transducer (LVDT) is used to measure y).

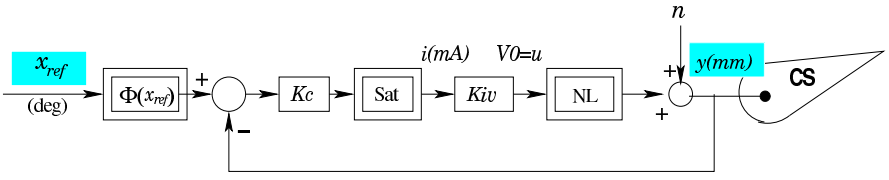

Fig. 6.11 The setup of the aileron servo-loop

The nonlinear model of the actuator (denoted "NL" in figure 6.11) is derived from physical consideration, i.e. the rod speed is a function of the hydraulic pressure delivered to the actuator and the forces applying on the control surface and reacted by the actuator. The two main contributors are aerodynamic forces and the servo-control load in damping mode of the passive actuator in the case of two actuators per CS. This results in the following nonlinear state-space model:

$$\dot{x} = -u\sqrt{\frac{\Delta P - \frac{F_{aero}}{S} sign(u)}{\Delta P_{ref} + \frac{Ka}{S}u^2}} \tag{6.109}$$

$$y = x \tag{6.110}$$

x is the rod position and F_{aero} represents the above mentioned aerodynamic forces. S is the actuator piston surface area, ΔP is the hydraulic supply pressure really delivered to the actuator, ΔP_{ref} is a reference differential pressure, at which the maximum rod speed performances are computed and Ka refers to the actuator damping coefficient (in case of two actuators per control surface in an active/passive scheme). The minus sign in (6.109) is introduced for simplicity in the following developments with the convention that K_{iv} is negative definite. The dimensions are $x \in \mathbb{R}^1, y \in \mathbb{R}^1, u \in \mathbb{R}^1$.

6.7.1.1 Nonlinear Parameter Varying (NLPV) Model

Following the results presented in [109], the main difficulty in eq. (6.109) comes from the term F_{aero}, so it was proposed in this paper to neglect F_{aero}. In fact and to be more precise, a complex model with identified aerodynamic databases is known from AIRBUS, but for computational burden limitation and because of the required monitoring performances, neglecting F_{aero} was judged acceptable. Here, such an assumption is not made and it is chosen to schedule F_{aero} by means of the dynamic pressure P_d, the angle of attack α, the Mach number $Mach$, the roll velocity p and the rod position of the actuator x so that:

$$F_{aero} = \frac{P_d(b_0 + b_1.(\alpha - \alpha_k p) + b_2 x)}{1 + a_1 x + a_2 x^2 + a_3 x^3} \tag{6.111}$$

with

$$b_0(Mach) = \begin{cases} Cte \text{ if } Mach < 0.7 \\ \sum_{i=0}^{4} b_{0i} Mach^i \text{ otherwise} \end{cases} \tag{6.112}$$

$$b_1(Mach) = \sum_{i=0}^{3} b_{1i} Mach^i, \quad \alpha_k(Mach) = \frac{k}{Mach} \tag{6.113}$$

$$b_2(Mach) = \begin{cases} Cte \text{ if } Mach < 0.82 \\ \sum_{i=0}^{2} b_{2i} Mach^i \text{ otherwise} \end{cases} \tag{6.114}$$

To derive a suitable expression of F_{aero}, the coefficients $b_{0i}, b_{1i}, b_{2i}, k$ of the polynomial functions $b_0(Mach)$, $b_1(Mach), b_2(Mach)$ and $\alpha_k(Mach)$ have been estimated using the data coming from the nonlinear high fidelity simulator provided by AIRBUS for different types of maneuvers, by means of a quadratic optimization procedure. Then from (6.109),(6.110) and (6.111), it follows that the overall model of the actuator can be written according to

$$\begin{cases} \dot{x} = -u.g(x,u,\theta) \\ y = x \end{cases} \tag{6.115}$$

which results in a NLPV model scheduled by the parameter vector θ defined according to:

$$\theta = (P_d \ \alpha \ Mach \ p \ sign(u))^T, \quad \underline{\theta_i} \leq \theta_i \leq \overline{\theta}_i, i = 1,..,5 \tag{6.116}$$

Note that due to its definition, θ is bounded and measured in real time since the Air Data Inertial Reference Units (ADIRUs) supply the measurement of $P_d, \alpha, Mach$ and p. u can be easily computed according to

$$u = K_{iv}.K_c.(\Phi(x_{ref}).x_{ref} - y) \tag{6.117}$$

x_{ref} and y being measured, see above.

6.7.1.2 Modeling the Faults

With regards to the faults and following the ADDSAFE benchmark problem definition, three main fault profiles are considered:

i) "liquid" faults: the liquid failure adds to the normal signal;
ii) "solid" faults: the solid failure substitutes the normal signal.
iii)"disconnection" faults: the control surface is disconnected from its actuator.

The disconnection can be interpreted as the cancellation of the term F_{aero} in (6.109) since the control surface is no more connected to the rod, i.e. the disconnection of the aileron vanishes the contribution of the aileron aerodynamic forces in (6.109). Such an effect can be modeled according to

$$\dot{x} = -u\sqrt{\frac{\Delta P - \frac{(F_{aero}+\phi_1(t))}{S} sign(u)}{\Delta P_{ref} + \frac{Ka}{S}u^2}} \tag{6.118}$$

where $\phi_1(t) = -F_{aero}$ in case of disconnection and $\phi_1(t) = 0$ in fault free situations. Liquid and solid jamming faults can be modeled as an abnormal variation of the rod position, i.e.

$$y(t) = x(t) + \phi_2(t) \tag{6.119}$$

where $\phi_2(t)$ is an exogenous signal for liquid fault types and $\phi_2(t) = -x(t) + \chi(t)$ with $\chi(t)$ being the fault signal that substitutes the normal signal. Of course, $\phi_2(t) = 0$ in fault free situations. Using an approximation of the fault models in terms of an additive fault type one, it follows from (6.115), (6.118) and (6.119) that the NLPV model of the actuator can be written as

$$\begin{cases} \dot{x} = -u.g(x,u,\theta) + \sum_{i=1}^{2} K_{1i} f_i \\ y = x + \sum_{i=1}^{2} K_{2i} f_i \end{cases} \quad f = (f_1 \ f_2)^T \tag{6.120}$$

where $(K_{1i}f_i, K_{2i}f_i)\, i = 1,2$ is the ith fault signature associated to the ith fault mode ϕ_i. Note that by definition, $K_{12} = K_{21} = 0$. This approximation makes sense as long as the control law of the aileron servo-loop (see figure 6.11) keeps stability in faulty

situations. The interested reader can refer to [113, 84] for a discussion of such an approximation.

6.7.1.3 Towards a LPV Formulation

To formulate the model (6.120) in a fashion that is convenient for the H_∞/H_- LPV paradigm described in section 6.5, the nonlinear equations (6.120) are approximated by means of a first-order Taylor series expansion around the time varying reference position point $(x^*(t), u^*(t))$. This boils down to the following LPV model:

$$\begin{cases} \dot{x} = A(\theta)x + B(\theta)u + \sum_{i=1}^{2} K_{1i} f_i \\ y = x + \sum_{i=1}^{2} K_{2i} f_i \end{cases} \tag{6.121}$$

where the expressions of $A(\theta)$ and $B(\theta)$ are given by (6.122)-(6.123). In these expressions, $\phi(x) = 1 + a_1 x + a_2 x^2 + a_3 x^3$, $\theta = (P_d \ \alpha \ Mach \ p \ x^* \ u^* \ \theta_u)^T$ is the scheduling parameters vector with $\theta_u = sign(u^*)$.

$$A(\theta) = -\frac{1}{2} u^* \frac{P_d.\theta_u}{\phi(x^*).S} \frac{\left(\frac{b_2(Mach)}{\Phi(x_{ref})} + F_{aero}(\theta) \left. \frac{\delta\phi(x)}{\delta x} \right|_{x^*} \right)}{\sqrt{\left(\Delta P - \frac{F_{aero}(\theta)}{S}.\theta_u \right) . \left(\Delta P_{ref} + \frac{Ka}{S} u^{*2} \right)}} \tag{6.122}$$

$$B(\theta) = -\sqrt{\frac{\Delta P - \frac{F_{aero}(\theta)}{S}.\theta_u}{\Delta P_{ref} + \frac{Ka}{S} u^{*2}}} + \frac{Ka}{S} u^{*2} \frac{\left(\Delta P - \frac{F_{aero}(\theta)}{S}.\theta_u \right)}{\sqrt{\frac{\Delta P - \frac{F_{aero}(\theta)}{S}.\theta_u}{\Delta P_{ref} + \frac{Ka}{S} u^{*2}}} . \left(\Delta P_{ref} + \frac{Ka}{S} u^{*2} \right)^2} \tag{6.123}$$

Then, the model defined by equations (6.121), (6.122) and (6.123) can put into a Linear Fractionnal Representation (LFR) such that:

$$y(s) = F_u(P(s), \Theta)(f^T(s) \ u(s))^T \tag{6.124}$$

$$\text{with } \Theta(t) = blockdiag\left(\theta_i(t) I_{k_i}\right) \ i = \overline{1,7} \tag{6.125}$$

In other words, all parameters θ_i, $i = \overline{1,7}$ entering in (6.122) and (6.123) are "pulled out" so that equations (6.121) appear as a LTI nominal model P subject to an artificial block diagonal time-varying operator $\Theta(t) = blockdiag\left(\theta_1(t) I_{k_1}, ..., \theta_7(t) I_{k_7}\right)$ specifying how each $\theta_i(t)$, $i = \overline{1,7}$ enters P where $k_i > 1$ whenever the parameter $\theta_i(t)$ is repeated, see the developments presented in section 6.5.

Unfortunately, it can be verified that θ_i, $i = \overline{1,7}$ enter $A(\theta)$ and $B(\theta)$ in a nonlinear manner. More precisely, the nonlinearities come from the polynomial functions introduced to model F_{aero} and the square root function. Despite recent developments on LFRs allow to consider the polynomial and rational dependencies in θ_i, $i = \overline{1,7}$, there is no available technique able to derive from (6.122) and (6.123) an exact LFR for the model (6.121). Thus, a solution to this problem results in the introduction of hyper-parameters, leading obviously to a conservative LFR.

To proceed, let us introduce the following hyper-parameters

$$\psi_1(t) = A(\theta), \quad \psi_2(t) = B(\theta) \tag{6.126}$$

This choice is guided by the fact that $dim(x) = 1$ and thus, that the conservativeness introduced by this choice is thought not so important. Then, it could be verified that (6.121) admits the following LPV LFR which is convenient for the LPV H_∞/H_- technique presented in section 6.5.

$$y(s) = F_u(P(s), \Psi(t))(f^T(s)\ u(s)\ n(s))^T \tag{6.127}$$

$$\text{with } \Psi(t) = blockdiag\,(\psi_1, \psi_2) \tag{6.128}$$

In this formulation, n denotes the measurement noise (those related to the LVDT sensor).

To validate the LPV model of the actuator, equation (6.127) is implemented in the AIRBUS nonlinear simulator and simulations are performed for 29 different flight maneuvers. The estimated position $\hat{y} = \hat{x}$ is plotted on figure 6.12 superposed with the LVDT measurement, for a fault free situation. The (non normalized) behavior

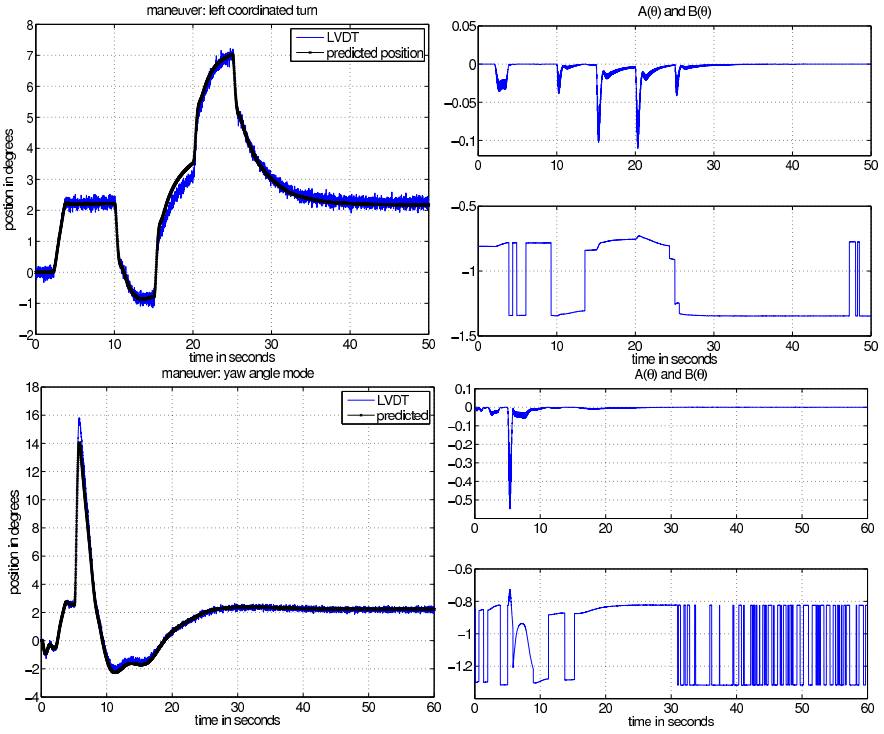

Fig. 6.12 left: The estimated position $\hat{y} = \hat{x}$ (black) and the LVDT measurement (blue) in degrees - right: $A(\theta)$ and $B(\theta)$ - Coordinated turn (top) and Yaw angle mode maneuver (bottom)

of $A(\theta)$ and $B(\theta)$ are too presented on figure 6.12. To save place, figure 6.12 only presents the results obtained for flying maneuvers that correspond to a left coordinated turn maneuver (top) and a "yaw angle mode" maneuver (bottom), the flying conditions corresponding to a nominal configuration.

Clearly, as it can be seen from figure 6.12, the LPV assumption takes all its sense and the LPV model (6.127) successfully approximates the nonlinear behavior of the actuator.

6.7.2 Design of the LPV H_∞/H_- Filter

The fault detection strategy that is proposed to detect liquid, solid and disconnection faults in control surface servo-loops consists of a slightly modification of the fault detection scheme presented in section 6.5. It consists of a LPV H_∞/H_- filter that generates a residual signal r robust against the measurement noise n and the reference actuator position x_{ref} delivered by the FCC while remaining sensitive to the faults $f_i, i = 1,2$, so that (see figure 6.13 for easy reference):

$$r(s) = \mathscr{F}(s,\Psi)\begin{pmatrix} \varepsilon(s) \\ x_{ref}(s) \end{pmatrix}, i = 1,2 \tag{6.129}$$

In other words, we do not consider the residual matrices M_y and M_u since $dim(x_{ref}) = dim(\varepsilon) = dim(r) = 1$ and thus that there is no need to look for a combination of any kind of signals.

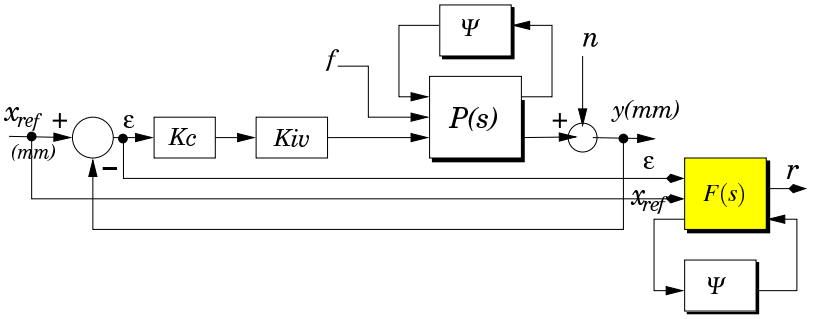

Fig. 6.13 Formulation of the H_∞/H_- problem (6.129)

Then, following the method described in section 6.5, the robustness and fault sensitivity requirements are expressed in terms of loop shapes, i.e. of desired gain responses W_d and W_f for the appropriate closed-loop transfers. These shaping objectives are then turned into uniform bounds by means of the shaping filters.

Because it is required robustness against the position order x_{ref} and the measurement noise n, it is natural to choose W_d according to $W_d = diag\,(W_x, W_n)$. W_x allows to specify robustness requirements against x_{ref} and W_n allows to formulate robustness objectives against n. An investigation of the energy content of x_{ref} for

different flight maneuvers reveals that it is located in low frequencies. So W_x is fixed to a low pass filter with low cutting frequency ω_x and static gain γ_x. With regard to W_n, because we assume that the energy content of the measurement noise is located in high frequencies, W_n is fixed to a low pass filter with cutting frequency ω_n and static gain γ_n. In other words, it is desired to reject the measurement noise n at high frequencies.

For the fault sensitivity objectives and due to the definition of f, see equation (6.120), it is natural to define the shaping filter W_f as $W_f = diag(W_{f1}, W_{f2})$. Furthermore, because it is required to enforce fault sensitivity in low frequencies, W_{fi} are chosen as low pass filters with cutting frequencies ω_{fi} and static gain $\gamma_{fi}, i = 1,2$.

The positive constants $\gamma_x, \gamma_n, \gamma_{fi}, i = 1,2$ and $\omega_x, \omega_n, \omega_{fi}, i = 1,2$ are introduced to manage the gain and the frequency behavior of W_x, W_n and $W_{fi}, i = 1,2$. By this parametrization, proper weights W_d and W_f can be adequately tuned in order to obtain the best achievable robustness and fault sensitivity performance.

The LPV fault detector (6.129) is then computed following Lemma 6.2 and Theorem 6.1. The parameters $\gamma_x, \gamma_n, \gamma_{fi}, i = 1,2$ and $\omega_x, \omega_n, \omega_{fi}, i = 1,2$ are optimized by performing an iterative refinement. Because the goal is to minimize the effects of x_{ref} and n on the residual r while maximizing the effects of the faults $f_i, i = 1,2$, a trade-off between $\gamma_x, \gamma_n, \gamma_{fi}, i = 1,2$ and $\omega_x, \omega_n, \omega_{fi}, i = 1,2$ is necessary. Specially, W_{f_2} and W_n should be carefully designed since it could be verified that these two weights address the same transfer. Fortunately, since the frequency characteristics of f_2 differ from those of n, the proposed parametrization provides a framework to find a good balance between robustness against n and sensitivity against f_2. After some iterations, the obtained numerical values are found to be:

$$\begin{gathered} \gamma_x \approx 1,\ \gamma_n \approx 1,\ \gamma_{f1} \approx 0.045\ \gamma_{f2} \approx 0.013 \\ \omega_x \approx 10rd/s,\ \omega_n \approx 10rd/s,\ \omega_{f1} \approx 1rd/s,\ \omega_{f2} \approx 1rd/s \end{gathered} \tag{6.130}$$

6.7.3 The Decision Making Algorithm

The final stage of the fault diagnosis scheme is concerned by the decision making stage. The use of a simple thresholding strategy will give rise to many of false alarms if the threshold is set too low, or increased missed detections if the threshold is set too high. This section describes a solution to this problem. A time-dependent threshold function is developed that exploits the additional information assumed about the system.

Considering the definition of the residual r given by (6.129), it can be partitioned as

$$r(s) = \mathscr{F}_1(s,\Psi)\varepsilon(s) + \mathscr{F}_2(s,\Psi)x_{ref}(s) \tag{6.131}$$

It follows that r can be written in fault free situation as (the Laplace variable is omitted for clarity)

$$r = \frac{\mathscr{F}_1(\psi) + \mathscr{F}_2(\psi)\left(1 + K_c K_{iv} F_u(P_u,\Psi)\right)}{1 + K_c K_{iv} F_u(P_u,\Psi)} x_{ref} - \frac{\mathscr{F}_1(\psi)}{1 + K_c K_{iv} F_u(P_u,\Psi)} n \tag{6.132}$$

where P_u refers to P considering $f = 0$. Direct application of the H_∞-norm definition for LPV systems gives

$$\exists \overline{\psi} : ||r||_2^2 \leq \left\| \frac{\mathscr{F}_1(\overline{\psi}) + \mathscr{F}_2(\overline{\psi})\,(1 + K_c K_{iv} F_u(P_u, \overline{\psi}))}{1 + K_c K_{iv} F_u(P_u, \overline{\psi})} \right\|_\infty^2 \ldots ||x_{ref}||_2^2 + \left\| \frac{\mathscr{F}_1(\overline{\psi})}{1 + K_c K_{iv} F_u(P_u, \overline{\psi})} \right\|_\infty^2 ||n||_2^2 \tag{6.133}$$

that is, there exists a parameter combination $\overline{\psi}$ that leads to the maximum amplification of the reference signal x_{ref} and the measurement noise n on the residual r in terms of energy.

Because the preceding H_∞ norms are constant and under the condition of energy bounded measurement noise, condition (6.133) can be rewritten as

$$||r||_2^2 \leq \kappa_1^2 ||x_{ref}||_2^2 + \tau^2 . \kappa_2^2 \tag{6.134}$$

where $\kappa_1 = \left\| \frac{\mathscr{F}_1(\overline{\psi}) + \mathscr{F}_2(\overline{\psi})(1 + K_c K_{iv} F_u(P_u, \overline{\psi}))}{1 + K_c K_{iv} F_u(P_u, \overline{\psi})} \right\|_\infty$ and $\kappa_2 = \left\| \frac{\mathscr{F}_1(\overline{\psi})}{1 + K_c K_{iv} F_u(P_u, \overline{\psi})} \right\|_\infty$, τ being an upper bound of $||n||_2$.

Equation (6.134) can then be used for fault detection in real-time. Indeed, we can compute the threshold signal

$$\mathscr{G}(t) = \kappa_1^2 ||x_{ref}||_2^2 + \tau^2 . \kappa_2^2 \tag{6.135}$$

for each time t and declare a fault if $||r||_2^2 > \mathscr{G}(t)$ at some time t. However, the use of the triangular inequality and the norm-bounding properties make condition (6.134) a sufficient, but far from necessary for equation (6.132). Therefore, condition (6.134) must be relaxed to make the decision strategy useful in practice. In addition to bridging the gap between equations (6.132) and (6.134), there are other reasons that motivate the modification of the threshold function (6.135). One reason is that the fault detection filter $\mathscr{F}(s, \psi)$ and the threshold function $\mathscr{G}(t)$ are ill suited (because H_∞ is part of a worst-case criteria) for the critical fault detector design task of trading off false alarm and missed detection rates. Thus, based on the structure given by equation (6.135), the following reference-dependent threshold upper and lower functions are computed for each time t in an attempt to compensate for these difficulties:

$$\begin{aligned} \mathscr{G}_u(t) &= \kappa_1 x_{ref}(t - \varphi) + \kappa_2^u, \\ \mathscr{G}_l(t) &= \kappa_1 x_{ref}(t - \varphi) + \kappa_2^l \end{aligned} \tag{6.136}$$

A fault is then declared if $r(t) > \mathscr{G}_u(t)$ or $r(t) < \mathscr{G}_l(t)$. In (6.136), $\varphi, \kappa_1, \kappa_2^u, \kappa_2^l$ are user-defined parameters that are tuned by analyzing $[r(t)\ x_{ref}(t)]^T$ data records coming from the simulator provided by AIRBUS, under a large flying conditions.

6.7.4 Nonlinear Simulation Results

The LPV filter $\mathscr{F}(s,\psi)$ is next converted to discrete-time using a Tustin approximation and implemented within the nonlinear simulator provided by AIRBUS. To make a final decision about the fault, the reference-dependent threshold functions $\mathscr{G}_u(t)$ and $\mathscr{G}_l(t)$ are too implemented.

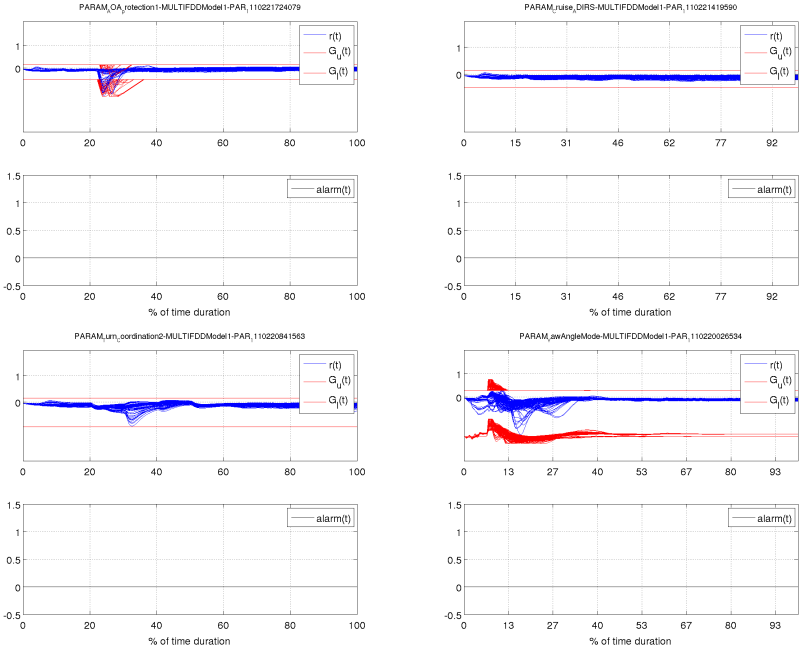

Fig. 6.14 Behavior of $r(kT_s)$, $\mathscr{G}_u(kT_s)$ and $\mathscr{G}_l(kT_s)$ - Fault free situations. From top left to bottom right: *i*) a maneuver with engaged angle of attack protection, *ii*) a cruise flight, *iii*) a left coordinated turn, *iv*) a yaw angle mode maneuver.

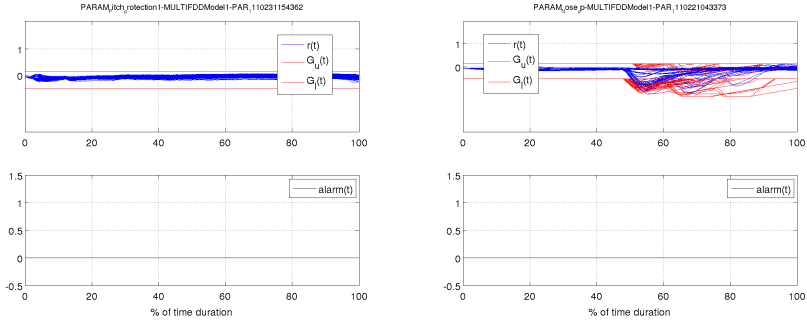

Fig. 6.15 Behavior of $r(kT_s)$, $\mathscr{G}_u(kT_s)$ and $\mathscr{G}_l(kT_s)$ - Fault free situations. pitch maneuver with engaged protection (left) and nose up maneuver (right).

Figures 6.14-6.16[5] illustrate the behavior of the residual $r(kT_s)$ (T_s being the sampling period) and the decision test for a Monte-Carlo campaign of 2400 runs. The operation range considered in the simulations corresponds to variations of mass, altitude, position of center of gravity and Mach number defined by AIRBUS[6]. Figures 6.14-6.15 illustrate the behavior of the residual $r(kT_s)$, the reference-dependent threshold functions $\mathscr{G}_u(kT_s)$ and $\mathscr{G}_l(kT_s)$ and the behavior of the decision test for some fault free situations. The flight maneuvers done by the aircraft correspond to:

i) a maneuver with engaged angle of attack protection,
ii) a cruise flight,
iii) a left coordinated turn,
iv) a yaw angle mode maneuver,
v) a pitch maneuver with engaged protection and
vi) a nose up maneuver.

Figures 6.16 are concerned by the faulty cases, i.e. disconnection, liquid and solid faults occur during the flight. A zoom is presented to better appreciate the detection delay. As it can be seen, the proposed method is able to successfully diagnose the considered faults with a very small detection delay.

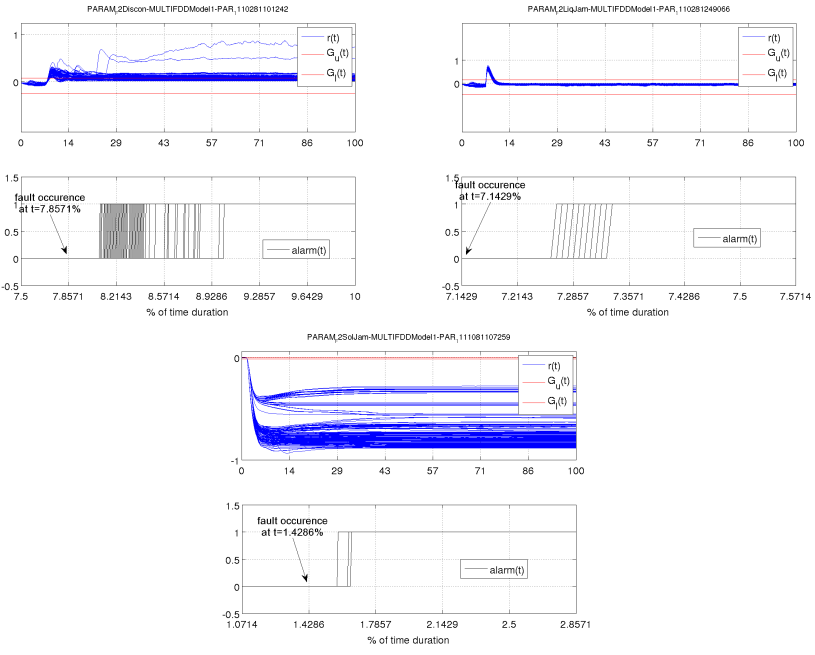

Fig. 6.16 Behavior of $r(kT_s)$, $\mathscr{G}_u(kT_s)$ and $\mathscr{G}_l(kT_s)$ - Faulty situations. From top left to bottom: disconnection, liquid and solid faults

[5] For confidential reasons, the plots have been normalized.

[6] For confidential reasons, the numerical values of these variations are not given.

6.8 Conclusion

This chapter investigated the problem of model–based Fault Detection and Isolation (FDI). A model–based FDI/FDD scheme is normally implemented as a computer software algorithm. The main problem of the model–based approach regards the real complex systems, where modeling uncertainty arises inevitably because of process noise, parameter variations and modeling errors. The FDI/FDD of incipient faults represents a challenge to model–based FDI/FDD techniques due to inseparable mixture between fault effects and modeling uncertainty.

To carry out such FDI/FDD objectives, a general framework to design robust FDD/FDI filters for LPV systems has been proposed. The procedure aims to generate a structured residual vector with guaranteed robustness and fault sensitivity performance. The robustness objectives are expressed in terms of a minimization problem using the H_∞ norm for LPV systems, and the sensitivity requirement is formulated in terms of a maximization constraint using the H_- index for LPV systems.

Two solutions have been proposed depending on the manner the LPV system is modeled:

- The first one is developed within the so-called polytopic setting. In this case, it is assumed that all parameters $\theta_i(t), i = 1...q$ take their values in the domain Θ which is assumed to be a convex polytope. Using jointly the vertex property (convexity of the parametric polytope and its image by the system model state-space matrices), the bounded real lemma and the projection lemma, a sufficient condition is established in terms of a LMI optimization problem.
- The second approach is developed within the so-called LFR (Linear Fractional Representation) setting [90, 91, 92, 93, 94], i.e. all parameters $\theta_i(t), i = 1,...,q$ entering in equation (6.16) are "pulled out" so that the model appears as a LTI (Linear Time Invariant) nominal model $P(s)$ subject to a time-varying bounded artificial feedback $\Theta(t)$. Using jointly the small gain theory, the bounded real lemma and the projection lemma, a sufficient condition is established in terms of a LMI optimization problem. Computational aspects are discussed and it is shown that the proposed solution is well-defined.

It is shown that the proposed methods offer a reasonable computational burden while offering also the possibility of reuse (or building around it) with adequate design and tuning engineering tools, since:

- it offers an efficient paradigm to model nonlinear systems with on-line measurable state depending parameters,
- it provides stability and performance guarantees over a wide range of changing parameters,
- it offers tunable design parameters through the so-called weighting functions that allow the designer to specify the fault detection performance and thus to manage the trade-offs.

Both academic examples and simulated results coming from the high-fidelity simulator provided by industrials demonstrate the benefit of the proposed approach.

It should be pointed out that the proposed methods are based on a parameter-independent Lyapunov matrix. The solution may then be conservative in some cases. A solution to this problem may consist in using the full-block multipliers-based approach proposed in [75]. Another approach may consist in using the parameter-dependent quadratic Lyapunov function (PDQLF) technique presented in [106].

Finally, we would like to come back to the combination of (6.26) and (6.27) and (6.77) and (6.78) into a single H_∞ constraint. As explained, the proposed formulation may yield conservative solutions since the minimized performance objective includes two other channels (i.e. $T_{\tilde{d}\to\tilde{r}}(\theta)$ and $T_{f\to r}(\theta)$) that are disturbing. A solution to this problem may consist in establishing two sets of LMIs for each constraints using similar developments than those presented. This boils down to a set of 2×3 LMIs, each set of 3 LMIs being dedicated to a H_∞ constraint. Basically, this means that two Lyapunov matrices (say X_∞ and X_-) are involved in the overall optimization problem. We have already performed some designs using this philosophy but, unfortunately, for LMI feasibility reasons, it is required to fix $X_\infty = X_-$. This obviously leads to conservative solutions and the overall gain in terms of fault detection performance is not so clear and well defined. Following our experience, we argue that it is preferred to carefully select the design objectives W_d and W_f for a given fault detection problem.

References

1. Gertler, J.: Fault Detection and Diagnosis in Engineering Systems. Marcel Dekker, New York (1998)
2. Chen, J., Patton, R.J.: Robust Model–Based Fault Diagnosis for Dynamic Systems. Kluwer Academic Publishers (1999)
3. Frank, P., Ding, S., Köppen-Seliger, B.: Current developments in the theory of fdi. In: Proceedings of SAFEPROCESS 2000, Budapest, pp. 16–27. IFAC (2000)
4. Venkatasubramanian, V., Rengaswamy, R., Yin, K., Kavuri, S.: A review of process fault detection and diagnosis. part 1: Quantitative model-based methods. Computer and Chemical Engineering 27(3), 293–311 (2003)
5. Blanke, M., Kinnaert, M., Lunze, M., Staroswiecki, M.: Diagnosis and fault tolerant control. Springer, New York (2003)
6. Isermann, R.: Fault–Diagnosis Systems: An Introduction from Fault Detection to Fault Tolerance, 1st edn. Springer (November 28, 2005) ISBN: 3540241124
7. Ding, S.X.: Model–based Fault Diagnosis Techniques: Design Schemes, Algorithms, and Tools, 1st edn. Springer, Heidelberg (2008) ISBN: 978–3540763031
8. Henry, D., Simani, S., Patton, R.: Fault Detection and Diagnosis for Aeronautic and Aerospace Missions in 'Fault Tolerant Flight Control: A Benchmark Challenge'. Springer (2010)
9. Henry, D.: A norm-based point of view for fault diagnosis: Application to aerospace missions. Automatic Control in Aerospace 4(1), online journal (2011)
10. Marcos, A., Ganguli, S., Balas, G.J.: An application of H_∞ fault detection and isolation to a transport aircraft. Control Engineering Practice 13, 105–119 (2005)

11. Amato, F., Cosentino, C., Mattei, M., Paviglianiti, G.: A direct/functional redundancy scheme for fault detection and isolation on an aircraft. Aerospace Science and Technology 10, 338–345 (2006)
12. Kalman, R., Bucy, R.: New results in linear filtering and prediction theory. Journal of Basic Engineering, 95–108 (1997)
13. Julier, S., Uhlmann, J.: A new extension of the kalman filter to nonlinear systems. In: Proc. of AeroSense: The 11th Int. Symp. on Aerospace/Defence Sensing, Simulation and Controls (1997)
14. Wan, E., Merwe, R.V.D.: The Unscented Kalman Filter. S. Haykin, ch. 7. John Wiley & Sons, New York (2001)
15. Julier, S., Uhlmann, J.: Unscented filtering and nonlinear estimation. Proceedings of the IEEE 92(3), 401–422 (2004)
16. Norgaard, M., Poulsen, N., Ravn, O.: New developments in state estimation for nonlinear systems. Automatica 36, 1627–1638 (2000)
17. Verma, V., Langford, J., Simmons, R.: Non-parametric fault identification for space rovers. In: Piedboeuf, J.-C. (ed.) International Symposium on Artificial Intelligence and Robotics in Space (iSAIRAS) (June 2001)
18. DeFreitas, N.: Rao-blackwellised particle filtering for fault diagnosis. In: Aerospace Conference, pp. 1767–1772. IEEE (2001)
19. Hutter, F., Dearden, R.: Efficient on-line fault diagnosis for non-linear systems. In: International Symposium on Artificial Intelligence, Robotics and Automation in Space (iSAIRAS), Nara, Japan, May 19-23 (2003)
20. Dearden, R., Willeke, T., Simmons, R., Verma, V., Hutter, F., Thrun, S.: Real-time fault detection and situational awareness for rovers: report on the mars technology program task. In: Aerospace, March 6-13, pp. 826–840. IEEE (2004)
21. Zhang, Q., Campillo, F., Legland, F.: Nonlinear system fault detection and isolation based on bootstrap particle filters. In: Proc. of 44th IEEE CDC-ECC, Seville, Spain, pp. 3821–3826 (December 2005)
22. Chow, E.: Failure detection system design methodology. PhD thesis, Lab. Information and Decision system, University of Cambrige (1980)
23. Chow, E., Willsky, A.: Analytical redundancy and the design of robust failure detection systems. IEEE Transactions on Automatic Control 29(7), 603–614 (1984)
24. Frank, P.: Fault diagnosis in dynamic systems using analytical and knowledge-based reduncancy - a survey. Automatica 26(3), 459–474 (1990)
25. Patton, R., Chen, J.: A review of parity space approaches to fault diagnosis. In: Proceedings of SAFEPROCESS 1991, Baden Baden, Germany, pp. 239–255. IFAC-IMACS (1991)
26. Delmaire, G., Cassar, J., Staroswiecki, M.: Comparaison of generalized least square identification and parity space techniques for fdi purpose in siso systems. In: Proceedings of 3rd European Control Conference, Rome, Italy, pp. 2011–2016. IFAC (1995)
27. Patton, R., Chen, J.: Observer-based fault detection and isolation: Robustness and applications. Control Eng. Practice 5(5), 671–682 (1997)
28. Höfling, T., Isermann, R.: Adaptive parity equations and advanced parameter estimation for fault detection and diagnosis. In: Proceedings of the 13th Triennial World Congress, San Francisco, USA, pp. 55–60. IFAC (1996)
29. Gertler, J.: Fault detection and isolation using parity relations. Control Eng. Practice 5(5), 653–661 (1997)
30. Gertler, J.: Fault detection and diagnosis in Engineering System. Marcel Dekker Inc. (1998)

31. Staroswiecki, M., Comtet-Varga, G.: Fault detectability and isolability in algebraic dynamic systems. In: European Control Conference ECC 1999, Karlsruhe, Germany, Paper F 0452 (1999)
32. Staroswiecki, M., Comtet-Varga, G.: Analytical redundancy relations for fault detection and isolation in algebraic dynamic systems. Automatica 37(5), 687–699 (2001)
33. Gertler, J., Staroswiecki, M., Shen, M.: Direct design of structured residuals for fault diagnosis in linear systems. In: Proceedings of ACC 2002, Anchorage (2002)
34. Wuennenberg, J.: Observer based fault detection in dynamic systems. PhD thesis, University of Duisburg (1990)
35. Patton, R., Chen, J.: Optimal selection of unknwon input distribution matrix in the design of robust observers for fault diagnosis. In: Proceedings of SAFEPROCESS 1991, Baden Baden, Germany, pp. 221–226. IFAC-IMACS (1991)
36. Patton, R., Chen, J.: Optimal unknown input distribution matrix selection in robust fault diagnosis. Automatica 29(4), 837–841 (1993)
37. Gaddouna, B., Maquin, D., Ragot, J.: Fault detection observers for systems with unknwon inputs. In: Proceedings of SAFEPROCESS 1994, Espoo, Finland, pp. 69–74 (1994)
38. Patton, R.: Robust model-based fault diagnosis: The state of the art. In: Proceedings of SAFEPROCESS 1994, Espoo, Finland, pp. 1–24 (1994)
39. Koenig, D., Nowakowski, S., Cecchin, T.: A comparative study of unknown input observers design methods applied for fault detection, isolation and correction. In: Proceedings of CESA 1996, Lille, France, pp. 665–671 (1996)
40. Isermann, R.: Supervision, fault detection and fault diagnosis methods - an introduction. Control Eng. Practice 5(5), 639–652 (1997)
41. Koenig, D., Nowakowski, S., Cecchin, T.: An original approach for actuator and component fault detection and isolation. In: Proceedings of SAFEPROCESS 1997, Hull, England, pp. 95–105. IFAC (1997)
42. Duan, G., Patton, R.: Robust fault detection in linear systems using luenberger observers. In: Proceedings of CONTROL 1998, Swansea, England, pp. 1468–1473 (1998)
43. Chen, J., Patton, R.: Robust model-based fault diagnosis for dynamic systems. Kluwer Academic Publishers (1999)
44. Mangoubi, R., Appelby, B., Farrell, J.: Robust estimation in fault detection. In: Proceedings of the 31st Conference on Decision and Control, Tucson, Arizona, USA, pp. 2317–2322. IEEE (1992)
45. Edelmayer, A., Bokor, J., Keviczky, L.: H_∞ detection filter design for linear systems: Comparison of two approaches. In: Proceedings of the 13th IFAC World Congres, San Francisco, USA, pp. 37–42 (1996)
46. Mangoubi, R.: Robust estimation and failure detection: A concise treatment. Springer (1998)
47. Rank, M., Niemann, H.: Norm based design of fault detectors. International Journal of Control 72(9), 773–783 (1999)
48. Collins, E., Song, T.: Robust H_∞ estimation and fault detection of uncertain dynamic systems. Journal of Guidance, Control and Dynamics 23(5), 857–864 (2000)
49. Stoustrup, J., Niemann, H.: Fault estimation-a standard problem approach. International Journal of Robust and Nonlinear Control 12(8), 649–673 (2002)
50. Stoorvogel, A., Niemann, H., Saberi, A., Sannuti, P.: Optimal fault signal estimation. International Journal of Robust and Nonlinear Control 12(8), 697–727 (2002)
51. Marcos, A., Ganguli, S., Balas, G.: An application of h_∞ fault detection and isolation to a transport aircraft. Control Engineering Practice 13, 105–119 (2005)
52. Henry, D., Zolghadri, A.: Norm-based design of robust fdi schemes for uncertain systems under feedback control: Comparison of two approaches. Control Engineering Practice 14(9), 1081–1097 (2006)

53. Ding, S., Jeinsch, T., Frank, P., Ding, E.: A unified approach to the optimization of fault detection systems. International Journal of Adaptive Control and Signal Processing 14, 725–745 (2000)
54. Rambeaux, F., Hamelin, F., Sauter, D.: Optimal thresholding for robust fault detection of uncertain systems. International Journal of Robust and Nonlinear Control 10, 1155–1173 (2000)
55. Hamelin, F., Sauter, D.: Robust fault detection in uncertain dynamic systems. Automatica 36(11), 1747–1754 (2000)
56. Zhong, M., Ding, S., Lam, J., Wang, H.: An LMI approach to design robust fault detection filter for uncertain lti systems. Automatica 39(2), 543–550 (2003)
57. Henry, D., Zolghadri, A.: Design and analysis of robust residual generators for systems under feedback control. Automatica 41, 251–264 (2005)
58. Henry, D., Zolghadri, A.: Design of fault diagnosis filters: A multi-objective approach. Journal of Franklin Institute 342(4), 421–446 (2005)
59. Jaimoukha, I., Li, Z., Papakos, V.: A matrix factorization solution to the H_-/H_∞ fault detection problem. Automatica 42, 1907–1912 (2006)
60. Henry, D.: Fault diagnosis of the MICROSCOPE satellite actuators using H_∞/H_- filters. AIAA Journal of Guidance, Control, and Dynamics 31(3), 699–711 (2008)
61. Massoumnia, M.A.: A geometric appoach to failure detection and identification in linear systems. PhD thesis, Massachusetts Institute of Technology, Massachusetts, USA (1986)
62. Hammouri, H., Kinnaert, M., El Yaagoubi, E.: Observer–based approach to fault detection and isolation for nonlinear systems. IEEE Transactions on Automatic Control 44, 1879–1884 (1999)
63. De Persis, C., Isidori, A.: A geometric approach to non–linear fault detection and isolation. IEEE Transactions on Automatic Control 45, 853–865 (2001)
64. Kaboré, P., Othman, S., McKenna, T., Hammouri, H.: An observer-based fault diagnosis for a class of nonlinear systems – application to a free radical copolymerization reaction. International Journal of Control 73, 787–803 (2000)
65. Kaboré, P., Wang, H.: Design of fault diagnosis filters and fault tolerant control for a class of nonlinear systems. IEEE Trans. on Automatic Control 46(11), 1805–1810 (2001)
66. Pertew, A., Marquez, H., Zhao, Q.: LMI–based sensor fault diagnosis for nonlinear Lipschitz systems. Automatica 43(8), 1464–1469 (2007)
67. Bruzelius, E., Petterson, S., Breitholtz, C.: Linear parameter-varying descriptions of nonlinear systems. In: Proceedings of the American Control Conference, Boston, USA, pp. 1374–1379 (2004)
68. Papageorgiou, C., Glover, K.: Robustness analysis of nonlinear flight controllers. AIAA Journal of Guidance, Control and Dynamics 28(4), 639–648 (2005)
69. Leith, D., Leithead, W.: Survey if gain-scheduling analysis and design. International Journal of Control 73(11), 1001–1025 (2000)
70. Rugh, W.J., Shamma, J.S.: Research on gain scheduling. Automatica 36(10), 1401–1425 (2000)
71. Packard, A.: Gain scheduling via linear fractionnal transformations. Systems and Control Letters 22(2), 79–92 (1994)
72. Apkarian, P., Gahinet, P., Becker, G.: Self-scheduled H_∞ control in linear parameter-varying systems: a design example. Automatica 31(9), 1251–1261 (1995)
73. Apkarian, P., Gahinet, P.: A convex characterization of gain-scheduled H_∞ controllers. IEEE Transactions on Automatic Control 40(5), 853–864 (1995)
74. Biannic, J., Apkarian, P., Garrard, W.: Parameter varying control of a high-performance aircraft. AIAA Journal of Guidance, Control and Dynamics 20(2), 225–231 (1997)
75. Scherer, C.: LPV control and full block multipliers. Automatica 37(3), 361–375 (2001)

76. Sato, M.: Filter design for LPV systems using quadratically parameter-dependent lyapunov functions. Automatica 42, 2017–2023 (2006)
77. Bokor, J.: Geometric theory and control of linear parameter varying systems. In: Proceedings of the 4th International Symposium on Applied Computational Intelligence and Informatics, Timisoara, Romania, pp. 163–170, Art. n. 4262505 (2007)
78. Falcoz, A., Henry, D., Zolghadri, A.: Robust fault diagnosis for atmospheric re-entry vehicles: a case study. IEEE Tr. on Systems, Man and Cybernetics - Part A: Systems & Humans 40(5), 886–899 (2010)
79. Liu, J., Wang, J., Yang, G.: An LMI approach to minimum sensitivity analysis with application to fault detection. Automatica 41, 1995–2004 (2005)
80. Wei, X., Verhaegen, M.: Mixed H_-/H_∞ fault detection observer design for LPV systems. In: Proceedings of the 47th Conference on Decision and Control, Cancun, Mexico, pp. 1073–1078 (2008)
81. Ding, X., Guo, L.: Observer based optimal fault detector. In: Proceedings of the 13th IFAC World Congress, San Francisco, USA, pp. 187–192. IFAC (1996)
82. Grenaille, S., Henry, D., Zolghadri, A.: A method for designing fault diagnosis filters for LPV polytopic systems. Journal of Control Science and Engineering - Robustness Issues in Fault Diagnosis and Fault Tolerant Control 2008, Article n.1 (January 2008)
83. Patton, R., Frank, P., Clark, R.: Issues of fault diagnosis for dynamic systems. Springer, London (2000) ISBN: 3-540-19968-3
84. Isermann, R.: Model-based fault detection and diagnosis - status and applications. Annual Reviews in Control 29, 71–85 (2005)
85. Ding, S.: Model-based Fault Diagnosis Techniques - Design schemes, Algorithms and Tools. Springer, New York (2008)
86. Massoumnia, M., Verghese, G., Willsky, A.: Failure detection and identification. IEEE Transactions on Automatic Control 34(3), 316–221 (1989)
87. Chung, W., Speyer, J.: A game theoretic fault detection filter. IEEE Transactions on Automatic Control 43(2), 143–161 (1998)
88. Das, I., Dennis, J.: A closer look at drawbacks of minimizing weighted sums of objective for pareto set generation in multicriteria optimization problems. Structural Optimization 14(1), 63–69 (1997)
89. Falcoz, A., Henry, D., Zolghadri, A., Bornschleg, E., Ganet, M.: On-board model-based robust fdir strategy for reusable launch vehicles (rlv). In: 7th International ESA Conference on Guidance, Navigation and Control Systems, County Kerry, Ireland (2008)
90. Beck, C., Doyle, J., Glover, K.: Model reduction of multidimensional and uncertain systems. IEEE Transactions on Automatic Control 41(10), 1466–1477 (1996)
91. Cockburn, J., Morton, B.: Linear fractional representations of uncertain systems. Automatica 33(7), 1263–1271 (1997)
92. Varga, A., Looye, G., Moormann, D., Griibel, G.: Automated generation of LFT-based parametric uncertainty descriptions from generic aircraft models. Mathematical Modelling of Dynamical Systems 4, 249–274 (1998)
93. Beck, C., Doyle, J.: A necessary and sufficient minimality condition for uncertain systems. IEEE Transactions on Automatic Control 44(10), 1802–1813 (1999)
94. Hecker, S., Varga, A., Magni, J.: Enhanced LFR-toolbox for matlab. Aerospace Science and Technology 9, 173–180 (2005)
95. Nett, C., Jacobson, C., Miller, A.: An integrated approach to controls and diagnostics: The 4-parameter conntroller. In: Proceedings of ACC, Dayton (1988)
96. Murad, G., Postlethwaite, I., Gu, D.-W.: A robust design approach to integrated controls and diagnostics. In: Proceedings of the 13th Triennial World Congress, San Francisco, USA, pp. 199–204. IFAC (1996)

97. Stoustrup, J., Grimble, M.: Integrating control and fault diagnosis: A separation result. In: Proceedings of SAFEPROCESS 1997, Hull, England, pp. 323–328. IFAC (1997)
98. Stoustrup, J., Grimble, M., Niemann, H.: Design of integrated systems for the control and detection of actuator/sensor faults. Sensor Review 17(2), 138–149 (1997)
99. Khosrowjerdi, M., Nikoukhah, R., Safari-Shad, N.: A mixed H_2/H_∞ approach to simultaneous fault detection and control. Automatica 40(2), 261–267 (2004)
100. Marcos, A., Balas, G.: A robust integrated controller/diagnosis aircraft application. International Journal of Robust and Nonlinear Control 15, 531–551 (2005)
101. Lathauwer, L.D., Moor, B.D., Vandewalle, J.: A multilinear singular value decomposition. SIAM Journal on Matrix Analysis and Applications 21(4), 1253–1278 (2000)
102. László, Baranyi, P., Petres, Z., Várlaki, P.: Proceedings of 3rd International Symposium on Computational Intelligence and Intelligent Informatics, ISCIII 2007, Agadir, Marocco, March 28-30, pp. 111–116 (2007)
103. Gahinet, P., Apkarian, P.: A linear matrix inequality approach to H_∞ control. Int. Journal Robust Nonlinear Control 4, 421–428 (1994)
104. Boyd, S., El Ghaoui, L., Feron, E., Balakrishnan, V.: Linear Matrix Inequalities in System and Control Theory. Studies in Applied Mathematics (1994)
105. Biannic, J.: Commande robuste des systèmes à paramètres variables - Application en aéronautique. PhD thesis, Centre d'études et de recherche de Toulouse - Département DERA (1996)
106. Wu, F., Dong, K.: Gain-scheduling control of LFT systems using parameter-dependent lyapunov functions. Automatica 42, 39–50 (2006)
107. Goupil, P.: Airbus state of the art and practices on fdi and ftc in flight control system. Control Engineering Practice 19, 524–539 (2011)
108. Goupil, P.: Oscillatory failure case detection in the a380 electrical flight control system by analytical redundancy. Control Engineering Practice 18(9), 1110–1119 (2010)
109. Alcorta-Garcia, E., Zolghadri, A., Goupil, P.: A nonlinear observer-based strategy for aircraft oscillatory failure detection: A380 case study. IEEE Transactions on Aerospace and Electronic Systems 47(4), 2792–2806 (2011)
110. Caglayan, A., Rahnamai, K., Allen, S.: Detection, identification and estimation of surface damage/actuator failure for high performance aircraft. In: Proceedings of the American Control Conference, pp. 2206–2212 (1988)
111. Zolghadri, A., Gheorghe, A., Cieslak, J., Henry, D., Goupil, P., Dayre, R., LeBerre, H.: Model-based solution to robust and early detection of control surface runaways. SAE International Journal of Aerospace (November 2011)
112. Gheorghe, A., Zolghadri, A., Cieslak, J., Henry, D., Goupil, P., Dayre, R., Le-Berre, H.: Early detection of aircraft control surface faults by dedicated kalman filtering: runaways and jammings. In: Workshop on Advanced Control and Diagnosis (ACD 2011), Budapest, Hungary, pp. 17–18 (November 2011)
113. Frank, P., Alcorta-Garcia, E., Köppen-Seliger, B.: Modelling for fault detection and isolation versus modelling for control. Mathematical and Computer Modelling of Dynamical Systems 7(1), 1–46 (2001)

Part II
LPV Methods Applied to Road Vehicles

Chapter 7
LPV Control Approaches in View of Comfort Improvement of Automotive Suspensions Equipped with MR Dampers

Anh-Lam Do, Charles Poussot-Vassal, Olivier Sename, and Luc Dugard

Abstract. Many studies have shown the importance of automotive suspension systems in vehicle dynamics, see for instance [10], [26], [33] and references therein. Except for passive suspensions whose characteristics are invariant, the semi-active and active suspensions can change their properties by using controlled external signals (voltage, current...). This is why the latter suspensions have been studied intensively in recent years. However, up to now, only the semi-active suspensions are used widely in automotive industry. Indeed, compared with fully active suspensions, semi-active ones can achieve the main performance objectives (see [17], [27]) while they are smaller in weight and volume, cheaper in price, more robust and less energy consuming (see also [9], [10], [16], [19]).

So far, the control problem for semi-active suspensions has been tackled with many approaches during the last three decades. One of the first comfort-oriented control methods, successfully applied in commercial vehicles, is the Skyhook control proposed by Karnopp *et al.* [18]. Then, optimal control [12], [34], clipped optimal control [24], [36], [11], H_∞ control [30], [31] or Model Predictive Control [4], [28] have been considered. Recently, two new control design methods for semi-active suspensions using the LPV techniques have been presented. The first one, proposed in [29], can be applied for all kinds of semi-active dampers where only the bounds on damping coefficients and on the damper forces are necessary for the controller design. In the other one, proposed in [7], the nonlinearities of the

Anh-Lam Do · Olivier Sename · Luc Dugard
GIPSA-Lab, Control Systems Dept., CNRS-Grenoble INP, ENSE3, BP 46,
F-38402 St Martin d'Hères cedex, France
e-mail: {anh-lam.do,olivier.sename}@gipsa-lab.grenoble-inp.fr,
luc.dugard@gipsa-lab.grenoble-inp.fr

Charles Poussot-Vassal
Onera - The French Aerospace Lab, F-31055 Toulouse, France
e-mail: Charles.Poussot-Vassal@onera.fr

O. Sename et al. (Eds.): *Robust Control and LPV Approaches*, LNCIS 437, pp. 183–212.
DOI: 10.1007/978-3-642-36110-4_7

semi-active damper (the bi-viscosity and the hysteresis) are taken into consideration. The comparison of these two recent LPV-based techniques on a nonlinear Magneto-Rheological (MR) damper model is proposed this chapter.

The chapter is organized as follows: In section I, a brief bibliography concerning the modelling of semi-active dampers is given and two specific control-oriented models are detailed and will be used for the synthesis of the LPV controllers. In section II, the control problem of automotive suspension control is formulated in a common way so that the methods proposed in [29] (section III) and [7] (section IV) can be applied. Section V is devoted to numerical simulations on a nonlinear quarter car model. Some remarks and conclusions end this chapter.

7.1 Control-Oriented Models of MR Dampers

Recently, the Magneto-Rheological (MR) dampers have appeared to be one of the most investigated devices in both industrial and academic studies on semi-active suspension control. They use MR fluids whose characteristics can be changed through the application of a magnetic field. Compared with other kinds of semi-active dampers (like ER, friction dampers), they have great advantages like fast time response as well as a stable hysteretic behavior over a broad range of temperature, and a low battery voltage consumption. They represent a new generation of semi-active dampers and are used in many applications like shock absorbers and damping devices, clutches, breaks, actuators or artificial joints, operational earthquake dampers to reduce motion in buildings and of course in automotive systems. Fig. 7.1 shows the schematic layout of an MR damper.

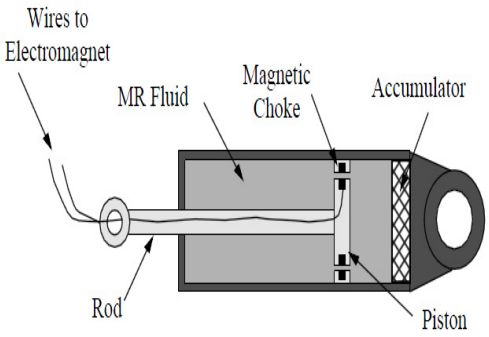

Fig. 7.1 Schematic layout of an MR damper

7.1.1 Damper Modeling

The modeling of semi-active dampers is a challenging problem because of their highly nonlinear behavior such as the bi-viscosity, the temperature dependency and specially the hysteresis. Many modeling methods have been proposed and generally they can be classified into two kinds: static model and dynamic model. Let us denote F_{damper} the damper force $[N]$, x_{mr} the damper deflection $[m]$ and $\dot{x}_{mr}$ the damper deflection velocity $[m/s]$, I is the current $[A]$. In the following, some well-known damper models are briefly introduced.

- Dynamic Bouc-Wen model [3], [37]

$$\begin{cases} F_{damper} = c_0\dot{x}_{mr} + k_0(x_{mr} - x_{mr}0) + \gamma z \\ \dot{z} = -\beta|\dot{x}_{mr}|z|z|^{n-1} - \delta\dot{x}_{mr}|z|^n + A\dot{x}_{mr} \end{cases} \tag{7.1}$$

  where c_0, k_0, A, γ, β, δ, n are the model parameters, $x0_{mr}$ is the critical deflection and z is the internal state that introduces some dynamics in the model and accounts for the hysteresis phenomenon.
- Static model with Coulomb friction [33]:

$$F_{damper} = c\dot{x}_{mr} - c^{sym}|\dot{x}_{mr}| + c^{nl}\sqrt{|\dot{x}_{mr}|}sgn(\dot{x}_{mr}) \tag{7.2}$$

  where c, c^{sym} and c^{nl} are the model parameters. This model describes the presence of the static friction as a constant term, function of the deflection speed sign.
- Static Guo model [15]
  The behavior of the semi-active damper is represented by the following nonlinear equation:

$$F_{damper} = a_2\left(\dot{x}_{mr} + \frac{v_0}{x_0}x_{mr}\right) + a_1\tanh\left(a_3\left(\dot{x}_{mr} + \frac{v_0}{x_0}x_{mr}\right)\right) \tag{7.3}$$

  where a_1 is the dynamic yield force of the MR fluid, a_2 and a_3 are related to the post-yield and pre-yield viscous damping coefficients, v_0 and x_0 denote the absolute value of hysteretic critical velocity $\dot{x}_0$ and hysteretic critical deflection x_0, where $\dot{x}_0$ and x_0 are defined as the velocity and deflection when the MR damper force is zero. The model is of semi-phenomenological type and based on a tangent hyperbolic function that models the hysteresis and bi-viscous characteristic of a damper.
- Non-linear black-box model (static or dynamic) [32]:
  This kind of description is not based on a physical description of the device, but aims at representing the non-linear input-output dynamical relationship. An example of black box model for an electronic shock absorber is the following:

$$F_{damper} = f(x_{mr};\dot{x}_{mr};\ddot{x}_{mr};...;x_{mr}^{(k)};I;\dot{I};\ddot{I};...;I^{(k)}) \tag{7.4}$$

  where $x_{mr}^{(k)}$ is the k^{th} derivative of x_{mr} and $I^{(i)}$ is the i^{th} derivative of I.

Remark 7.1. Note that, due to the high nonlinearity, one of the main difficulties is to obtain accurate parameter identification results. Usually, the model validation will require that all (or part of) the model parameters are current dependent.

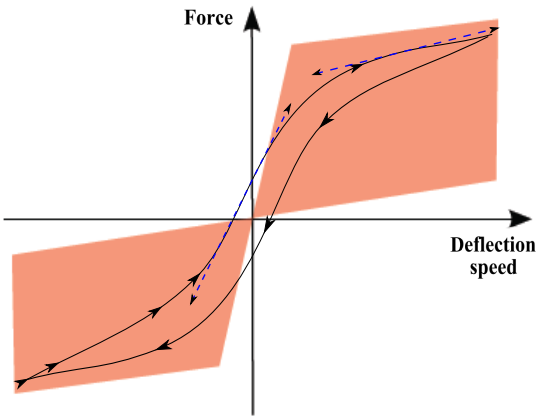

Fig. 7.2 Realistic MR damper force with bi-viscosity (pre-yield and post-yield viscous damping) and hysteresis

Among these models presented above, the one (7.3) proposed by Guo is of interest. Not only it fits with real dampers' behaviors, but it has also a simple and elegant formulation which can be extended for controller design purposes.

In [23], the authors have shown that if each coefficient in (7.3) is defined as a polynomial function of the electric current, the obtained model will better approach the real data. Below and in this chapter, a simpler version that includes only one current dependent parameter, is considered as follows:

$$F_{damper} = C_1 \tanh(C_2 \dot{x}_{mr} + C_3 x_{mr}) + C_4 \dot{x}_{mr} + C_5 x_{mr} + C_6 \ddot{x}_{mr} + C_7 I \tanh(C_8 \dot{x}_{mr} + C_9 x_{mr}) \tag{7.5}$$

The parameters of the model (7.5) have been identified (see [21] and [22]) on the test-rig at *Metalsa* [1] and are given in Tab. 7.1. It is worth noticing that the coefficients in compression ($\dot{x}_{mr} < 0$) and extension ($\dot{x}_{mr} \geq 0$) modes are different to better model the non-symmetric characteristics.

With the presence of the current I in the MR damper force's formulation, the model (7.5) can be obviously used for controller design. However, the complexity of this model is still high and can cause difficulties for the control problem. This is why, in the following, two simpler formulations which have been used in the controller design, are introduced.

[1] www.metalsa.com.mx

Table 7.1 Parameter values of MR damper (Model 7.5 - for simulation)

Parameter	$\dot{x}_{mr} \geq 0$	$\dot{x}_{mr} < 0$	Unit
C_1	128.5	-128.6	$[Ns/m]$
C_2	412.2	-489	$[N/m]$
C_3	83.5	-204	$[N]$
C_4	608.8	611.5	$[N]$
C_5	5457.6	-2855.4	$[s/m]$
C_6	3.9	4.2	$[1/m]$
C_7	484.3	484.3	$[1/m]$
C_8	6.5	6.5	$[1/m]$
C_9	3.4	3.4	$[1/m]$

7.1.2 Controlled-Oriented Model 1

Though the nonlinearity of the damper should be taken into account in the controller design, many studies have been based on a linear model of the damper:

$$F_{damper} = c\dot{z}_{def} \tag{7.6}$$

where c is the varying damping coefficient and limited by $[c_{min}, c_{max}]$. Moreover, the damper force must be limited by a maximal value, i.e $|F_{damper}| \leq F_{max}$ where $F_{max} > 0$.

The great advantage of the model is that it is very good for preliminary designs. It means that many control methods can be used, many complex (multi-objective, constrained...) problems can be formulated from this simple model and the design performance optimality can be obtained (this point is interesting in terms of comparisons among different design methods, even though the optimal performances may be not guaranteed in the implementation step).

In Tab. 7.2, the parameters of the semi-active damper used in this method are given. The values c_{min}, c_{max} and F_{max} are identified from the bounds of the real MR damper used in *Metalsa*.

Table 7.2 Parameter values of damper

Parameter	Value	Unit
c_{min}	881	$[Ns/m]$
c_{max}	7282	$[Ns/m]$
F_{max}	1400	$[N]$

7.1.3 Controlled-Oriented Model 2

As mentioned previously, the model (7.5) approaches very well the behavior of a real MR damper, in particular the hysteresis and the non-symmetric characteristics (in compression and extension modes) are very well modeled. But it is unnecessarily complex for control design. In [6] and [8], a simpler control-oriented model where a single parameter depends on the input signal has been proposed and first studied. According to the authors, a control-oriented model for semi-active damper can be given by

$$F_{damper} = c_0\dot{x}_{mr} + k_0 x_{mr} + f_I \tanh\left(c_1\dot{x}_{mr} + k_1 x_{mr}\right) \tag{7.7}$$

where f_I is the controllable force coefficient which varies according to the electrical current I in the coil ($0 \leq f_{Imin} < f_I \leq f_{Imax}$). In general, f_I can be any positive and invertible function of I. In the reference [5], f_I is simply the described by

$$f_I = y_{mr} I \tag{7.8}$$

where y_{mr} is also a constant parameter.

Compared with the model (7.3) whose characteristics are static and uncontrollable, the model (7.7) reflects the realistic behavior of an MR damper and approaches better the realistic MR damper model (7.5). This model (7.7) allows to fulfill the passivity constraint of the semi-active damper and introduces a control input f_I (or I). Fig. 7.3 presents the dependency of the damper force to the input current. Changing the current in the coil of an MR damper changes its characteristics. Here, the bi-viscous and the hysteresis characteristics are clearly observed.

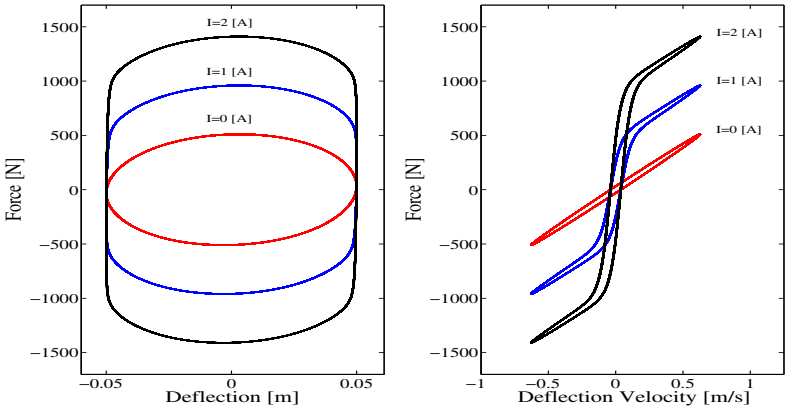

Fig. 7.3 MR damper characteristics with different current values I: Force vs Deflection (Left) and Force vs Velocity (Right) (Model 7.7)

Table 7.3 Parameter values of an MR damper (Model 7.7 - for controller synthesis)

Parameter	Value	Unit
c_0	810.78	$[Ns/m]$
k_0	620.79	$[N/m]$
f_{Imin}	0	$[N]$
f_{Imax}	800	$[N]$
c_1	13.76	$[s/m]$
k_1	10.54	$[1/m]$
y_{mr}	457.04	$[N/A]$

The parameters of the model (7.7) are given in Tab. 7.3 (see [5]).

In what follows, two control methods will be proposed according to the considered model (7.6) or (7.7). The validation of the control method will then be assessed in simulation using the realistic nonlinear model (7.5).

7.2 Control Problem: Application in Automotive Suspension Systems

7.2.1 Quarter Car Model and Performance Criteria

One of the most well-known applications of semi-active dampers in industry is the automotive suspension system. To study the vertical dynamics of a car, i.e comfort and road holding, the simple quarter vehicle, depicted in Fig. 7.4, is considered.

The model is simple and suitable for a preliminary design. It represents a single corner of a vehicle. In this model, the quarter vehicle body is represented by the

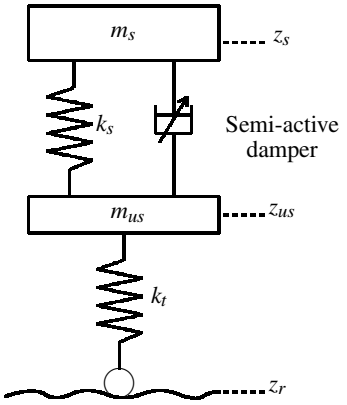

Fig. 7.4 Model of quarter vehicle with a semi-active damper

sprung mass (m_s) and the wheel and tire are represented by the unsprung mass (m_{us}). They are connected by a spring with the stiffness coefficient k_s and a semi-active damper. The tire is modeled by a spring with the constant stiffness coefficient k_t. As seen in the figure, z_s (respectively z_{us}) is the vertical displacement around the equilibrium point of m_s (respectively m_{us}) and z_r is the variation of the road profile. It is assumed that the wheel-road contact is ensured.

By applying the second law of Newton, the dynamical equations of a quarter vehicle are given by

$$\begin{cases} m_s \ddot{z}_s &= -F_{spring} - F_{damper} \\ m_{us} \ddot{z}_{us} &= F_{spring} + F_{damper} - F_{tire} \end{cases} \tag{7.9}$$

where F_{spring} is the dynamical spring force, $F_{tire} = k_t(z_{us} - z_r)$ is the dynamical tire force and F_{damper} is the damper force. Let us denote $z_{def} = z_s - z_{us}$ the damper deflection, $\dot{z}_{def} = \dot{z}_s - \dot{z}_{us}$ the damper deflection velocity.

In this study, the model parameters correspond to the 1/4 Renault Mégane Coupé (1/4 RMC) test car available in MIPS Laboratory (Mulhouse, France) (see in [39]), as given in Tab. 7.4. It is important to notice that two spring models will be used:

- For controller design, the spring force is given by

$$F_{spring} = k_s z_{def} \tag{7.10}$$

- For simulation, the spring has a nonlinear characteristic (see Fig. 7.5).

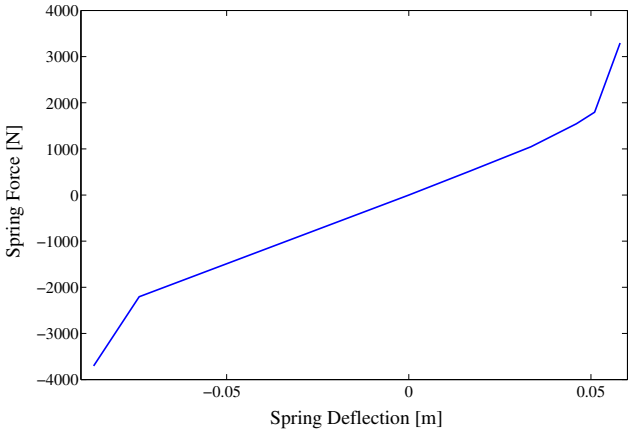

Fig. 7.5 Nonlinear RMC Spring

In the following, the criteria used to evaluate the performances of the semi-active suspension systems are given. By abuse of language, let denote $\ddot{z}_s/z_r$ (respectively $(z_{us} - z_r)/z_r$)) the "frequency response" from the road disturbance z_r to the vehicle

Table 7.4 Parameter values of the Renault Mégane Coupé quarter car model

Parameter	$m_s\ [kg]$	$m_{us}\ [kg]$	$k_t\ [N/m]$	$k_s\ [N/m]$
Value	315	37.5	29500	210000

body acceleration $\ddot{z}_s$ (respectively the dynamic tire deflection $z_{us} - z_r$), i.e. the gain of the transfer function for LTI systems or the gain computed using the "variance gain" algorithm in [34] for nonlinear systems.

In general, the vehicle body acceleration between 0-20 Hz should be filtered to guarantee a good ride comfort, although it is worth noting again that the human is the most sensible to vertical acceleration around 4-8 Hz (ISO 2631). Besides, to maintain the road-wheel contact, it is necessary that the dynamic tire force is smaller than $g(m_s + m_{us})$ (where g is the gravity). Hence, for the road holding improvement, the dynamic tire force $k_t(z_{us} - z_r)$, in other words the dynamic tire deflection $z_{us} - z_r$, should be small in the frequency range 0-30 Hz. Note also that the road holding is improved by limiting the up and down bouncing of the wheel z_{us} around its resonance 10-20 Hz. With these remarks, the performance criteria in the frequency domain are explicitly described as follows

- Comfort

$$J_{CF} = \min \int_0^{20} \ddot{z}_s / z_r(f) df \tag{7.11}$$

- Road holding

$$J_{RH} = \min \int_0^{30} (z_{us} - z_r) / z_r(f) df \tag{7.12}$$

The objectives of the control design are to minimize the two criteria that are consistent with the ones given in [31] and [33].

7.2.2 H_∞ Problem

In this chapter, both proposed control methodologies in Sections 7.3 and 7.4 will be designed in the H_∞ framework for polytopic systems. Indeed some scheduling parameters will be used later, representing, in some sense, the damper nonlinearities. In order to allow for the comparison of these approaches, the same control configuration is used, i.e corresponding to a set of measurements and controlled outputs.

The control configuration for semi-active suspensions is given in Fig. 7.6. The controlled outputs are the vehicle body acceleration $\ddot{z}_s$ (for the ride comfort improvement) and the wheel displacement z_{us} (for the road holding improvement) (see the performance criteria (7.11) and (7.12)). The measurement outputs are the

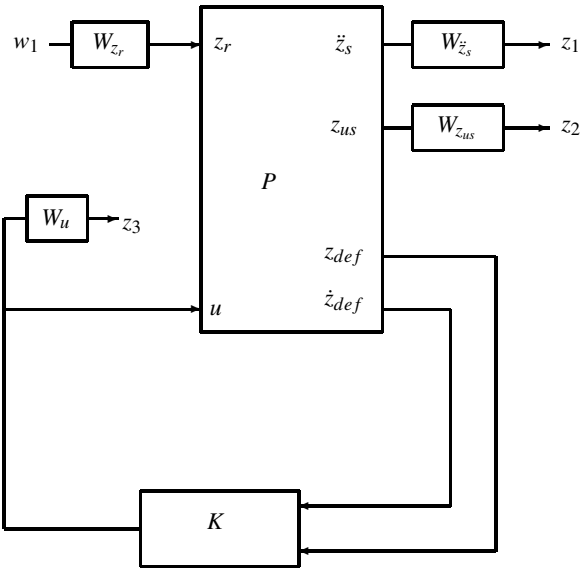

Fig. 7.6 LPV control scheme

suspension deflection z_{def} and suspension deflection velocity $\dot{z}_{def}$. To obtain the desired closed-loop performances, the weighting functions on controlled outputs $\{W_{\ddot{z}_s}, W_{z_{us}}\}$ and disturbance input W_{z_r} are used.

In order to optimize the weighting functions presented in the next section, W_{z_r} is kept constant and the weighting functions on the controlled outputs are second order transfer functions:

$$W_{z_r} = 3 \times 10^{-2} \tag{7.13}$$

$$W_{\ddot{z}_s} = k_{\ddot{z}_s} \frac{s2 + 2\xi_{11}\Omega_{11}s + \Omega_{11}2}{s2 + 2\xi_{12}\Omega_{12}s + \Omega_{12}2} \tag{7.14}$$

$$W_{z_{us}} = k_{z_{us}} \frac{s2 + 2\xi_{21}\Omega_{21}s + \Omega_{21}2}{s2 + 2\xi_{22}\Omega_{22}s + \Omega_{22}2} \tag{7.15}$$

Let us define the set of parameters

$$\nu = [\,\Omega_f\ \Omega_{11}\ \Omega_{12}\ \xi_{11}\ \xi_{12}\ k_{\ddot{z}_s}\ \Omega_{21}\ \Omega_{22}\ \xi_{21}\ \xi_{22}\ k_{z_{us}}\,]^T \tag{7.16}$$

which, in the sense of the optimization problem, is the decision vector.

Consider the generalized plant made of the quarter vehicle model (supposed to be formulated in the LPV framework, as explained later in Sections 7.3 and 7.4) and of the weighting functions, represented as:

$$\begin{aligned}\dot{\xi} &= \mathscr{A}^{\nu}(\rho)\xi + \mathscr{B}_1^{\nu}(\rho)\bar{w} + \mathscr{B}_2^{\nu}u \\ \bar{z} &= \mathscr{C}_1^{\nu}(\rho)\xi + \mathscr{D}_{11}^{\nu}(\rho)\bar{w} + \mathscr{D}_{12}^{\nu}u \\ y &= \mathscr{C}_2\xi + \mathscr{D}_{21}\bar{w}\end{aligned} \tag{7.17}$$

where $\xi = \begin{pmatrix} x^T & {x_w}^T \end{pmatrix}^T$ with x the state of the quarter vehicle model and x_w the state vector of the weighting functions, ρ the vector of scheduling parameters, $\bar{w}$ is the vector of input disturbances, $\bar{z}$ is the vector of controlled outputs. The *LPV* controller is defined as follows

$$K(\bar{\rho}) : \begin{pmatrix} \dot{x}_c \\ u \end{pmatrix} = \begin{pmatrix} A_c^{\nu}(\rho) & B_c^{\nu}(\rho) \\ C_c^{\nu}(\rho) & D_c^{\nu}(\rho) \end{pmatrix} \begin{pmatrix} x_c \\ y \end{pmatrix} \tag{7.18}$$

where x_c, y and u are respectively the state, the input and output of the controller associated with the system (7.17). All matrices have appropriate dimensions.

Remark 7.2. Since ν represents the vector of the weighting function parameters, it is used as an exponent in the notation of equations (7.17)-(7.18) to emphasize the dependence of the generalized plant, and then of the controller, on the parameters of the weighting functions.

H_∞/LPV problem - The objective of the synthesis is to find an LPV controller $K(\rho)$ of the form (7.18) such that the closed-loop system is quadratically stable and that, for a given vector of weighting function parameters ν, a given positive real γ, the L_2-induced norm of the operator mapping $\bar{w}$ into $\bar{z}$ is bounded by γ i.e

$$\forall \bar{\rho} \in \Theta, \quad \frac{\|\bar{z}\|_2}{\|\bar{w}\|_2} \leq \gamma \tag{7.19}$$

Here the polytopic approach with a quadratic Lyapunov function is used. It is stated that for known weighting functions and a suitable pre-defined real positive scalar γ, the sufficient condition that solves the H_∞/LPV problem is given by Eq. (7.20)-(7.21) where the decision variables are X, Y, $\hat{A}$, $\hat{B}$, $\hat{C}$ and $\hat{D}$ (see the detail of the solution in [41]). Note that the weighting function parameter set ν appears in the LMIs problem to optimize the controller.

$$\begin{bmatrix} M_{11}^{\nu}(\rho_i) & * & * & * \\ M_{21}^{\nu}(\rho_i) & M_{22}^{\nu}(\rho_i) & * & * \\ M_{31}^{\nu}(\rho_i) & M_{32}^{\nu}(\rho_i) & -\gamma I_m & * \\ M_{41}^{\nu}(\rho_i) & M_{42}^{\nu}(\rho_i) & M_{43}^{\nu}(\rho_i) & -\gamma I_p \end{bmatrix} \prec 0 \tag{7.20}$$

$$\begin{bmatrix} X & I \\ I & Y \end{bmatrix} \succ 0 \tag{7.21}$$

$$\text{for } \mathrm{i} = 1:4$$

where

$$
\begin{aligned}
M_{11}^{v}(\rho_i) &= \mathscr{A}^{v}(\rho_i)X + X\mathscr{A}^{v}(\rho_i)^T + \mathscr{B}_2\hat{C}(\rho_i) + \hat{C}(\rho_i)^T\mathscr{B}_2^T \\
M_{21}^{v}(\rho_i) &= \hat{A}(\rho_i) + \mathscr{A}^{v}(\rho_i)^T + \mathscr{C}_2^T\hat{D}(\rho_i)^T\mathscr{B}_2^T \\
M_{22}^{v}(\rho_i) &= Y\mathscr{A}^{v}(\rho_i) + \mathscr{A}^{v}(\rho_i)^T Y + \hat{B}(\rho_i)\mathscr{C}_2 + \mathscr{C}_2^T\hat{B}(\rho_i)^T \\
M_{31}^{v}(\rho_i) &= \mathscr{B}_1^{v}(\rho_i)^T + \mathscr{D}_{21}^T\hat{D}(\rho_i)^T\mathscr{B}_2^T \\
M_{32}^{v}(\rho_i) &= \mathscr{B}_1^{v}(\rho_i)^T Y + \mathscr{D}_{21}^T\hat{B}(\rho_i)^T \\
M_{41}^{v}(\rho_i) &= \mathscr{C}_1^{v}(\rho_i)X + \mathscr{D}_{12}\hat{C}(\rho_i) \\
M_{42}^{v}(\rho_i) &= \mathscr{C}_1^{v}(\rho_i) + \mathscr{D}_{12}\hat{D}(\rho_i)C_2 \\
M_{43}^{v}(\rho_i) &= \mathscr{D}_{11}^{v}(\rho_i) + \mathscr{D}_{12}\hat{D}(\rho_i)\mathscr{D}_{21}
\end{aligned}
$$

The controller K_{c_i} at vertex i is then reconstructed as

$$
\begin{aligned}
D_c^{v}(\rho_i) &= \hat{D}(\rho_i) \\
C_c^{v}(\rho_i) &= \left(\hat{C}(\rho_i) - D_c^{v}(\rho_i)C_2X\right)M^{-T} \\
B_c^{v}(\rho_i) &= N^{-1}\left(\hat{B}(\rho_i) - YB_2D_c^{v}(\rho_i)\right) \\
A_c^{v}(\rho_i) &= N^{-1}\left(\hat{A}(\rho_i) - YA(\rho_i)X - YB_2D_c^{v}(\rho_i)C_2X\right)M^{-T} \\
&\quad - B_c^{v}(\rho_i)C_2XM^{-T} - N^{-1}YB_2C_c^{v}(\rho_i)
\end{aligned}
\tag{7.22}
$$

where M, N are defined such that $MN^T = I_n - XY$ which can be solved through a singular value decomposition and a Cholesky factorization. The global H_∞/LPV controller is then the convex combination of these local controllers.

7.2.3 Controller Optimization for Semi-active Suspensions

It is well-known that the key step of the H_∞ control design depends on the selection of the weighting functions, which is linked to the engineer skill and experience. In this section, one applies the optimization procedure for the H_∞/LPV controller optimization of the semi-active suspension control presented in [7]. Let us remark that the control objective is to minimize the frequency-dependent performance criteria (7.11)-(7.12) for closed-loop suspension systems, rather than to minimize its induced $\mathscr{L}_2$-$\mathscr{L}_2$ gain. For this reason, in the following, an LPV controller is sought that solves the following problem:

$$
\begin{aligned}
&\text{minimize} && \mathrm{J^D} \\
&\text{subject to} && \text{LMIs (7.20)-(7.21)}
\end{aligned}
\tag{7.23}
$$

where

$$
J^D = \begin{bmatrix} J^D_{\text{Comfort}} \\ J^D_{\text{RoadHolding}} \end{bmatrix}
\tag{7.24}
$$

$$J^D_{\text{Comfort}} = \sum_{i=1}^{N_v} \alpha_i \int_0^{12} (\ddot{z}_s / z_r(f)_i) df \tag{7.25}$$

$$J^D_{\text{RoadHolding}} = \sum_{i=1}^{N_v} \alpha_i \int_{10}^{20} (z_{us} / z_r(f)_i) df \tag{7.26}$$

Note that the bounds of the integrals are chosen to emphasize the frequency ranges where the comfort and road holding are the most significant. Note also that, in the equations above, “D" is used to differentiate these design objective functions with the ones in Section 7.2.1 and the index “i" stands for the i^{th} vertex of the polytope Θ (see Fig. 7.10). The number of elements in each sum is N_v the number of vertices of the considered polytope of the LPV system (7.17) (supposed that the polytopic approach is used). The scalars α_i are weighting parameters satisfying $\alpha_i \geq 0$ and $\sum_{i=1}^{N_v} \alpha_i = 1$.

It can be seen that the cost function (7.24) is not convex, so (7.23) is a nonconvex optimization problem. Following [7], the purpose is to get the set of parameters v (described in Eq. 7.16) by using the genetic algorithms (GAs) such that J^D is minimized.

Remark 7.3. In many cases, to preserve the performance of the closed-loop system in the presence of input saturation and nonlinearities (for e.g in this study, in the simulation step, the nonlinear quarter vehicle model will be used), a stable stabilizing controller is required. Other advantages for the use of stable controllers concern the practical aspects. The stable controllers are better implemented than the unstable ones and the closed-loop system (provided that the open-loop system is already stable, e.g open-loop semi-active suspension systems) remains stable even when the feedback sensors fail. In this study, the theoretical solution for the existence of a stable *LPV* controller is not given. However, a stable *LPV* controller can be obtained by eliminating the “unstable solutions" corresponding to at least, one unstable local controller during the synthesis. It can be accomplished with genetic algorithms (GAs) by simply choosing $J^D = \infty$ for “unstable solutions". Due t o the “survival of the fittest" property, these “unstable solutions" will disappear after some generations.

To conclude, the optimization procedure in this section is summarized in Fig. 7.7. The next two sections present two recent control design methods for nonlinear semi-active suspensions using the LPV technique. The methodology in [29] can be applied for all kinds of semi-active dampers where only the bounds on damping coefficients and the damper forces are necessary for the controller design. In the other one [6], the nonlinearities of the semi-active damper, i.e the bi-viscous and hysteretic behaviors, have been taken into consideration. It is worth noticing that the optimization procedure above will be applied in each case in order to enhance the controller performances of these two design methods.

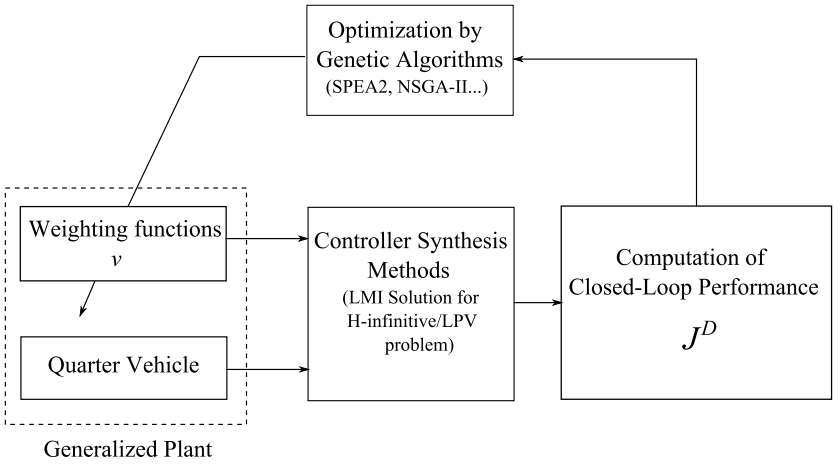

Fig. 7.7 Main idea for controller optimization for semi-active suspension systems using Genetic Optimization

7.3 LPV Controller Design: Method 1

As in [29], the linear model of damper (7.6) is used for the controller design. First, the damper force (7.6) is decomposed as follows

$$F_{damper} = c^0 \dot{z}_{def} + F_d \tag{7.27}$$

where c^0 is the nominal damping coefficient, e.g $c^0 = (c_{min} + c_{max})/2$ and F_d is the additional force. With this decomposition, the control design will be based on the following quarter car model, denoted as (Σ_c),

$$\Sigma_c(c0) := \begin{cases} m_s \ddot{z}_s = -k_s(z_s - z_{us}) - c0(\dot{z}_s - \dot{z}_{us}) - F_d \\ m_{us}\ddot{z}_{us} = k(z_s - z_{us}) + c0(\dot{z}_s - \dot{z}_{us}) + F_d - k_t(z_{us} - z_r) \\ \dot{F}_d = 2\pi\beta(F_{d_{in}} - F_d) \end{cases} \tag{7.28}$$

where β represents the bandwidth of the damper. In the next section, the H_∞ control method will be used, which means that

$$F_{d_{in}} = u^{\mathscr{H}_\infty} \tag{7.29}$$

where $u^{\mathscr{H}_\infty}$ is the additional force provided by an H_∞ controller. Before presenting the method to get the H_∞ controller, let us consider the following definition.

Definition 7.1. Clipping function
Due to the controlled damper limitations (i.e. the effective force provided by the damper F_{damper} should lie in the dissipative domain $\mathscr{D}$), the following Clipping function $\mathscr{D}(F_{damper}, \dot{z}_{def})$ is defined (see also illustration in Fig. 7.8) as:

$$\mathscr{D}(F_{damper},\dot{z}_{def}) \mapsto F_{damper} = \begin{cases} F_{damper} \text{ if } F_{damper} \in \mathscr{D} \\ F^{\perp}_{damper} \text{ if } F_{damper} \notin \mathscr{D} \end{cases} \tag{7.30}$$

where F_{damper} is the required force (given by the controller) and $F^{\perp}_{damper}$ is the orthogonal projection of F_{damper} on $\mathscr{D}$.

This definition will inspire the form of the considered scheduling parameter used in the LPV control.

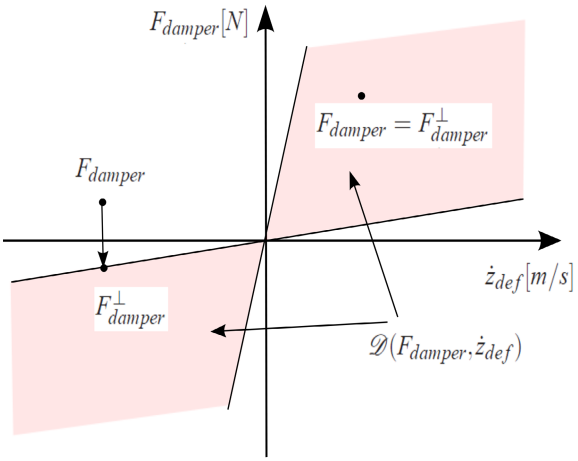

Fig. 7.8 Clipping function illustration

7.3.1 Generalized LPV Plant

The $\mathscr{H}_\infty$ control method for the semi-active suspension system (7.28) referred to as *Method 1*, is given as in Fig. 7.9. This is a particular case of the control scheme given in Fig. 7.6. Besides, due to the fact that the damper force F_{damper} must be limited in the dissipative domain $\mathscr{D}$ (see Definition 7.1), the amplitude of F_d or u^{H_∞} must be limited as well. To deal with this problem, a weighting function $W_u(\rho)$ on the controller output signal u^{H_∞} is introduced:

$$W_u(\rho) = \rho W_u \tag{7.31}$$

where $\rho \in [\underline{\rho};\overline{\rho}] \subseteq \mathbb{R}^+$ and W_u is a strictly proper LTI filter. The scheduling parameter ρ is used here to mitigate the semi-activeness violation of the damper force (i.e the damper force must be limited in $\mathscr{D}$). The next section is dedicated to designing ρ.

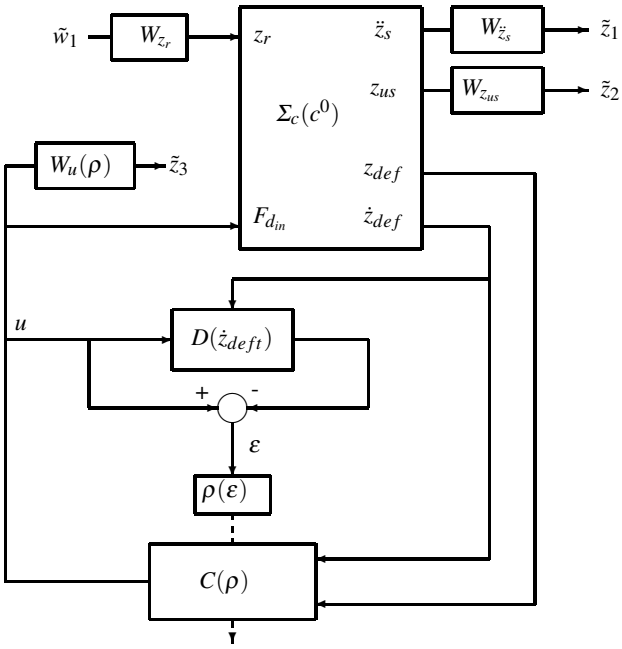

Fig. 7.9 Block diagram for semi-active suspension control: Method 1

7.3.2 Scheduling Strategy for the Parameter ρ

The underlying idea of the "LPV semi-active" control design is to increase the control gain $F_{d_{in}} = u^{\mathscr{H}_\infty}$ when the required force belongs to the allowed dissipative domain $\mathscr{D}$, and otherwise to rely on the nominal damping when the forces are outside the allowable space. To satisfy the dissipative damper constraints (see next subsection), the ρ parameter is adjusted in a particular way:

- when ρ is high, $W_u(\rho)$ is large, then, it tends to attenuate the $u^{\mathscr{H}_\infty}$ signal.
- when ρ is low, $W_u(\rho)$ is small, then, it does not attenuate the $u^{\mathscr{H}_\infty}$ signal.

Therefore, from a general point of view, ρ may be viewed as an anti-windup signal, computed on the actuator model (controlled damper model), and is similar to a variable saturation. For that purpose, the following scheduling strategy $\rho(\varepsilon)$ is introduced:

$$\rho(\varepsilon) := \begin{cases} \underline{\rho} & \text{if } \varepsilon < \mu \\ \underline{\rho} + \frac{\overline{\rho}-\underline{\rho}}{\mu}(\varepsilon - \mu) & \text{if } \mu \leq \varepsilon \leq 2\mu \\ \overline{\rho} & \text{if } \varepsilon > 2\mu \end{cases} \tag{7.32}$$

$$\varepsilon = ||F_{damper} - F^{\perp}_{damper}||_2 \tag{7.33}$$

where ε is the distance between the required force and the force projected on domain $\mathscr{D}$ (according to the function $\mathscr{D}(F_{damper}, \dot{z}_{def})$). μ is a design parameter that modifies the dead-zone of the $\rho(\varepsilon)$ function.

Remark 3 (About the scheduling parameters $\rho(\varepsilon)$)

- *In (7.32), $\rho(\varepsilon)$ belongs to a closed set $[\underline{\rho}, \overline{\rho}]$ which is essential in the LPV framework.*
- *$\varepsilon \neq 0 (\Leftrightarrow F_{damper} \neq F^{\perp}_{damper})$ means that the required force is outside the allowed range. Conversely, $\varepsilon = 0 (\Leftrightarrow F_{damper} = F^{\perp}_{damper})$ means that the force required by the controller is reachable for the considered semi-active actuator.*
- *Note that the scheduling parameter is very similar to what is done in the anti-windup compensator synthesis literature, i.e. it represents the saturation as a dead-zone function. Here, since the saturation depends on the system states, the dead-zone is time varying.*

7.3.3 Design Configuration

The controller design and optimization procedure presented in Section 7.2.3 can be established for *Method 1* with the following parameter specifications:

- $W_u = \frac{2\pi 50}{s+2\pi 50}$
- $\beta = 100\pi$
- $\underline{\rho} = 0.1, \overline{\rho} = 1, \mu = 100$
- $\alpha_1 = 0$ (corresponding to the vertex $\rho = \underline{\rho}$) and $\alpha_2 = 1$ (corresponding to the vertex $\rho = \overline{\rho}$). This means that only the performance of the closed-loop system associated with the more active controller (W_u is small) is taken into account in the performance objective. This is coherent with the idea that the more active controller (W_u is small) provides a better performance (in terms of comfort) than the more passive one (W_u is small).

7.4 Model-Based Controller Design: Method 2

In this section, the LPV formulation and the controller synthesis based on the model (7.7) presented in [6] and [7] are recalled.

7.4.1 LPV Model for Semi-active Suspension Control

Let consider the 1/4 Renault Mégane Coupé (1/4 RMC) depicted in Fig. 7.4. As mentioned previously, the control-oriented model of the MR damper given in (7.7) is used for controller synthesis. The dynamical equations are then written as follows

$$\begin{cases} m_s\ddot{z}_s &= -k_s(z_s - z_{us}) - c_0(\dot{z}_s - \dot{z}_{us}) - k_0(z_s - z_{us}) \\ &\quad - f_I \tanh(c_1(\dot{z}_s - \dot{z}_{us}) + k_1(z_s - z_{us})) \\ m_{us}\ddot{z}_{us} &= k_s(z_s - z_{us}) + c_0(\dot{z}_s - \dot{z}_{us}) + k_0(z_s - z_{us}) \\ &\quad + f_I \tanh(c_1(\dot{z}_s - \dot{z}_{us}) + k_1(z_s - z_{us})) - k_t(z_{us} - z_r) \end{cases} \tag{7.34}$$

With the system and the performance objectives defined in the previous section, a control oriented LPV model is formulated for further analysis and control in the sequel. Denote:

- $c_p = c_0$
- $k_p = k_s + k_0$
- $z_{def} = z_s - z_{us}$
- $\dot{z}_{def} = \dot{z}_s - \dot{z}_{us}$
- $\hat{\rho} = \tanh(c_0(\dot{z}_s - \dot{z}_{us}) + k_0(z_s - z_{us}))$

The state-space representation of the quarter vehicle model can be deduced from (7.34) as follows:

$$\begin{cases} \dot{x}_s = A_s x_s + B_s \hat{\rho} f_I + B_{sw} w \\ z = C_{sz} x_s + D_{sz} \hat{\rho} f_I \\ y = C_s x_s \end{cases} \tag{7.35}$$

where $x_s=(z_s,\ \dot{z}_s,\ z_{us},\ \dot{z}_{us})^T$, $w=z_r$, $y = (z_s - z_{us},\ \dot{z}_s - \dot{z}_{us})^T$, $z = (\ddot{z}_s\ \ z_{us})^T$.

$$A_s = \begin{pmatrix} 0 & 1 & 0 & 0 \\ -\frac{k_p}{m_s} & -\frac{c_p}{m_s} & \frac{k_p}{m_s} & \frac{c_p}{m_s} \\ 0 & 0 & 0 & 1 \\ \frac{k_p}{m_{us}} & \frac{c_p}{m_{us}} & -\frac{k_p+k_t}{m_{us}} & -\frac{c_p}{m_{us}} \end{pmatrix}, B_s = \begin{pmatrix} 0 \\ -\frac{1}{m_s} \\ 0 \\ \frac{1}{m_{us}} \end{pmatrix}, B_{sw} = \begin{pmatrix} 0 \\ 0 \\ 0 \\ \frac{k_t}{m_{us}} \end{pmatrix},$$

$$C_s = \begin{pmatrix} 1 & 0 & -1 & 0 \\ 0 & 1 & 0 & -1 \end{pmatrix}^T C_{sz} = \begin{pmatrix} \frac{-k_p}{m_s} & \frac{-c_p}{m_s} & \frac{k_p}{m_s} & \frac{c_p}{m_s} \\ 0 & 0 & 1 & 0 \end{pmatrix}, D_{sz} = \begin{pmatrix} \frac{-1}{m_s} \\ 0 \end{pmatrix}$$

Remark 7.4. The considered measurement outputs are the suspension deflection and suspension deflection velocity, which allows to state that $\hat{\rho}$ can be known in real-time.

To satisfy the passivity constraint of a semi-active damper, f_I must be constrained by

$$0 < f_{Imin} < f_I \leq f_{Imax} \tag{7.36}$$

This positivity constraint on the control input f_I is in fact very difficult to handle. By defining

$$u_I = f_I - f_0 \tag{7.37}$$

where $f_0 = (f_{Imin} + f_{Imax})/2$, the dissipativity constraint on f_I is recast as a saturation constraint on u_I, i.e.

$$-\bar{u} \leq u_I \leq \bar{u} \tag{7.38}$$

where $\bar{u} = (f_{Imax} - f_{Imin})/2$.

With this modification, the state-space representation of the quarter vehicle is given as follows:

$$P:\begin{cases}\dot{x}_s=(A_s+B_{s1}\frac{\hat{\rho}}{C_{s1}x_s}C_{s1})x_s+B_s\hat{\rho}u_I+B_{sw}w\\ z=(C_{sz}+D_{s1}\frac{\hat{\rho}}{C_{s1}x_s}C_{s1})x_s+D_{sz}\hat{\rho}u_I\\ y=C_sx_s\end{cases}\tag{7.39}$$

where $B_{s1}=\begin{pmatrix}0 & -\frac{f_0}{m_s} & 0 & \frac{f_0}{m_{us}}\end{pmatrix}^T$, $C_{s1}=\begin{pmatrix}k_1 & c_1 & -k_1 & -c_1\end{pmatrix}$, $D_{s1}=\begin{pmatrix}\frac{-f_0}{m_s} & 0\end{pmatrix}^T$.

In this study, the LPV model (7.39) can be used to design an LPV controller. However, such a controller may not ensure the closed-loop stability and performances since the saturation constraint (i.e the dissipativity constraint) is not accounted for during the design. A possible method is to add, in the closed-loop system, an AWBT (Anti Wind-up Bumpless Transfer) compensation to minimize the adverse effects of the control input saturation on the closed-loop performance [13], [14], [20], [25]. In the next section, a simple method is presented to solve the problem by considering the input saturation as a scheduling parameter. This approach is related to that of [38].

Define the saturation function $sat()$ as follows

$$sat(u_I)=\begin{cases}\bar{u} & \text{if} \quad u_I>\bar{u}\\ u_I & \text{if} \quad -\bar{u}\le u_I\le\bar{u}\\ -\bar{u} & \text{if} \quad u_I<-\bar{u}\end{cases}\tag{7.40}$$

The state-space representation of the system (7.39) subject to the input saturation constraint (7.38) is rewritten as

$$P:\begin{cases}\dot{x}_s=(A_s+B_{s1}\frac{\hat{\rho}}{C_{s1}x_s}C_{s1})x_s+B_s\hat{\rho}\frac{sat(u_I)}{u_I}u_I+B_{sw}w\\ z=(C_{sz}+D_{s1}\frac{\hat{\rho}}{C_{s1}x_s}C_{s1})x_s+D_{sz}\hat{\rho}\frac{sat(u_I)}{u_I}u_I\\ y=C_sx_s\end{cases}\tag{7.41}$$

Denote $\rho_1=\hat{\rho}\frac{sat(u_I)}{u_I}$ and $\rho_2=\frac{\hat{\rho}}{C_{s1}x_s}$. From (7.41), the following LPV system is now obtained

$$P:\begin{cases}\dot{x}_s=(A_s+B_{s1}C_{s1}\rho_2)x_s+B_s\rho_1u_I+B_{sw}w\\ z=(C_{sz}+D_{s1}C_{s1}\rho_2)x_s+D_{sz}\rho_1u_I\\ y=C_sx_s\end{cases}\tag{7.42}$$

In (7.42) the control input matrix $B_s\rho_1$ is parameter dependent, which is not consistent with the solution of the H_∞ design problem for polytopic systems [5]. This problem can be overcome by adding the following filter into (7.42) to make the control input matrix independent of the scheduling parameter:

$$W_f:\begin{pmatrix}\dot{x}_f\\ u_I\end{pmatrix}=\begin{pmatrix}A_f & B_f\\ C_f & 0\end{pmatrix}\begin{pmatrix}x_f\\ u\end{pmatrix}\tag{7.43}$$

with

$$\|W_f\|_\infty\le 1\tag{7.44}$$

where A_f, B_f, C_f are constant matrices.

Remark 7.5. The condition (7.44) ensures that the saturation constraint on u_I is kept for the new control input u. It means that the following implies (7.38)

$$-\bar{u} \leq u \leq \bar{u} \tag{7.45}$$

From Eq. (7.42) and Eq. (7.43), the control oriented model is now represented by an LPV system with two scheduling parameters ρ_1 and ρ_2:

$$\begin{cases} \dot{x} = A(\rho_1, \rho_2)x + Bu + B_1 w \\ z = C_z(\rho_1, \rho_2)x \\ y = Cx \end{cases} \tag{7.46}$$

where

$$x = \begin{pmatrix} x_s{}^T & x_f{}^T \end{pmatrix}^T$$

$$A(\rho_1, \rho_2) = \begin{pmatrix} A_s + \rho_2 B_{s1} C_{s1} & \rho_1 B_s C_f \\ 0 & A_f \end{pmatrix}, B = \begin{pmatrix} 0 \\ B_f \end{pmatrix}, B_1 = \begin{pmatrix} B_{s1} \\ 0 \end{pmatrix},$$

$$C = \begin{pmatrix} C_s \\ 0 \end{pmatrix}^T, C_z(\rho_1, \rho_2) = \begin{pmatrix} C_{sz} + \rho_2 D_{s1} C_{s1} & \rho_1 D_{sz} C_f \end{pmatrix}$$

$$\rho_1 = \tanh(C_{s1} x_s) \frac{sat(c_f x_f)}{c_f x_f}, \rho_2 = \frac{\tanh(C_{s1} x_s)}{C_{s1} x_s}$$

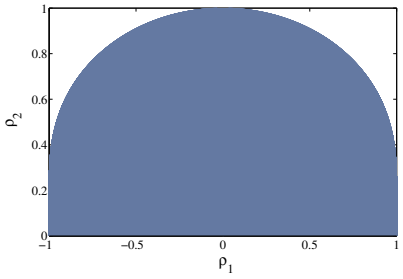

Fig. 7.10 Set of scheduling parameters (ρ_1, ρ_2) (shaded area)

The control configuration for semi-active suspensions is given in Fig. 7.11. This configuration is very similar to the one used by *Method 1* (in this case W_u is set to 0).

7.4.2 Design Configuration

The controller design and optimization procedure presented in Section 7.2.3 is once again applied for *Method 2*. The complete results for *Method 2* are given in [7]. Notice that, due to the self-dependence between ρ_1 and ρ_2, the set of all $\bar{\rho} = (\rho_1, \rho_2)$ is not a polytope, as seen in Fig. 7.10. In this study, a polytopic approach is developed for the LPV control design (which leads to some conservatism). As a consequence, ρ_1 and ρ_2 are considered as independent parameters and $\bar{\rho}$ belongs to a polytope Θ whose vertices are $\bar{\rho}_1 = (-1, 0)$, $\bar{\rho}_2 = (1, 0)$, $\bar{\rho}_3 = (1, 1)$, $\bar{\rho}_4 = (-1, 1)$.

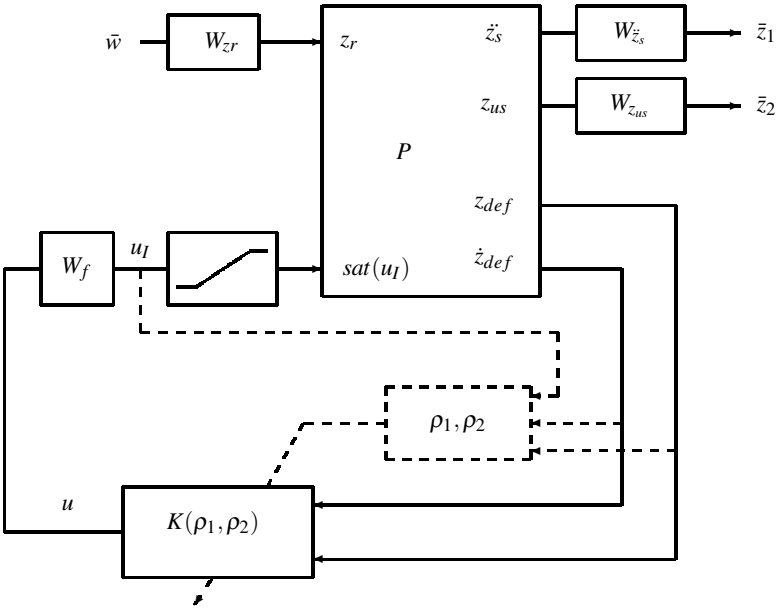

Fig. 7.11 Block diagram for semi-active suspension control: Method 2

7.5 Numerical Analysis and Results

In this part, some design analysis and some simulation results are presented to emphasize the interest and the possible limitations of both methodologies. Following the optimization method previously presented, the solution of the multi-objective problem (7.23) is given by a Pareto front in Fig. 7.12 for *Method 1* and in Fig. 7.13 for *Method 2*. The conflicting relation between comfort and road holding criteria can be observed clearly from the figure. In this chapter, for simplification, the analysis will concern only the best comfort-oriented controller of each method. The road-holding comparison can be done similarly (see also the performance analysis in [7]). The best comfort-oriented controller can be chosen by comparing the performances (see the performance analysis in the sequel) among some solutions which are close to the Y-axis. Here they are the ones closest to the Y-axis in the Fig. 7.12 and Fig. 7.13.

Let us recall that the nonlinear Renault Mégane Coupé (RMC) model used in simulation incorporates the nonlinear spring (see Fig. 7.5) and the nonlinear MR damper whose force is of the form (7.5). The implementation scheme is depicted in Fig. 7.14. As seen in this figure, there is a *Signal converter* block. This block is needed since the current is the control input signal of the damper while the outputs

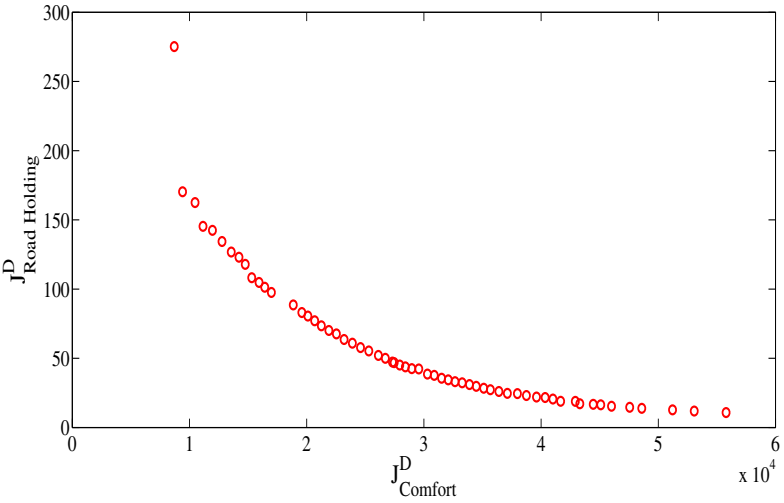

Fig. 7.12 Pareto front obtained for Method 1

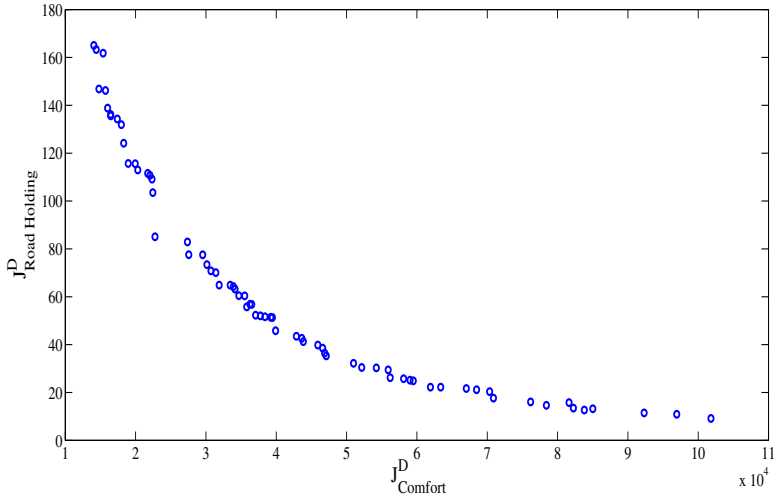

Fig. 7.13 Pareto front obtained for Method 2

of the controllers obtained in *Method 1* and *Method 2* are forces. In the following, the desired current I is reconstructed for each method:

- Method 1: Since the damper model is not included in the controller design, an inverse damper model is needed to regenerate the input current. In this study, with the good approximation to real data, the model (7.7) is used as the inverse model, i.e the input current will be recovered by the following equation:

$$I = \frac{u^{H_\infty} + c0\dot{z}_{def} - c_0\dot{z}_{def} - k_0 z_{def}}{y_{mr}\tanh\left(c_1\dot{z}_{def} + k_1 z_{def}\right)} \tag{7.47}$$

- Method 2: Since the damper model is taken into consideration in the controller design, the input current is simply computed from the controller output u_I by using the equations (7.8) and (7.37):

$$I = \frac{u_I + F_0}{y_{mr}} \tag{7.48}$$

Remark 7.6. Note that the input current must be limited in $[0, f_{Imax}/y_{mr}]$ (see Section 7.1.3).

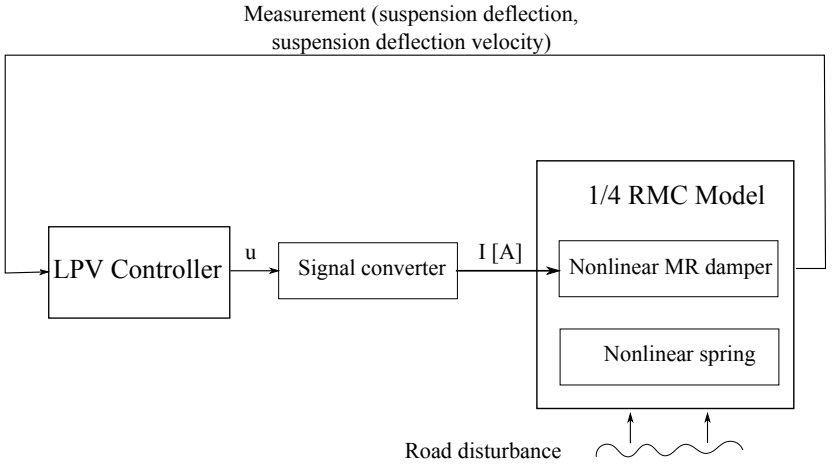

Fig. 7.14 Implementation scheme

In the remaining parts, both comfort-oriented controllers obtained with *Method 1* and *Method 2* are compared to the following passive MR dampers:

- Soft MR damper where the controllable input $f_I = f_{Imin}$
- Hard MR damper where the controllable input $f_I = f_{Imax}$
- Nominal MR damper where the controllable input $f_I = (f_{Imin} + f_{Imax})/2$ (i.e. when the controller output is equal to zero)

7.5.1 Frequency Domain Analysis

In this section, the evaluation in the frequency domain is performed via the nonlinear frequency response of $\ddot{z}_s$ that is computed by the "Variance Gain" algorithm [32] (where the input z_r is chosen to be a sinusoidal signal with magnitude of 1.5 *cm* and frequency varying in [0.1-30] *Hz*). This algorithm is simple and provides a good approximation to the nonlinear frequency response.

Some general remarks can be drawn for passive MR dampers (see [7]):

- Between $0-2\ Hz$, the Hard MRD is the best strategy for ride comfort.
- Between $2-30\ Hz$, the Soft MRD is the best strategy for ride comfort.

As seen in Fig. 7.15, both LPV controllers largely improve the passenger comfort w.r.t passive cases. When compared between each other, the LPV *Method 1* is slightly better in medium frequencies and lightly worse in high frequencies and low frequencies than the LPV *Method 2*.

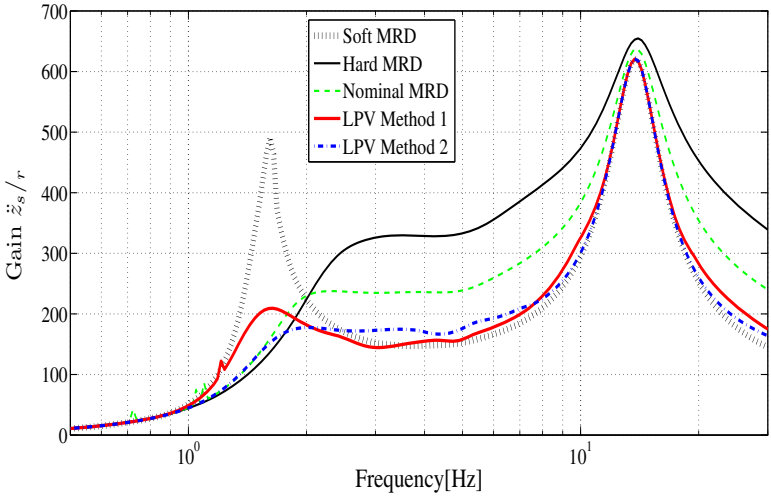

Fig. 7.15 Frequency responses comparison

7.5.2 Time Domain Analysis

Test 1: Step road profile

In this test, the road profile is a step signal (the amplitude is 10 *cm* and the starting time is $t_0 = 1\ s$) filtered beyond 30 Hz. The car body acceleration responses are depicted in Fig. 7.16. The results are coherent with the frequency responses analysis presented previously:

- The peak values around the starting time (1s) are small for the cases of *Soft MRD*, *Method 1* and *Method 2* while they are larger for *Nominal MRD* and *Hard MRD*. This phenomenon corresponds to the responses in high frequencies $[2-20]\ Hz$ (see also Fig. 7.15).
- The damping behavior (the convergence to zero) is the best in the case of *Hard MRD*. The *Method 2* and *Nominal MRD* provide a good damping behavior as well. The *Method 1* is a little worse compared to the *Method 2* and the Soft MRD give the worst damping capacity. This is linked to the frequency responses of all strategies in low frequencies $[0-2]\ Hz$.

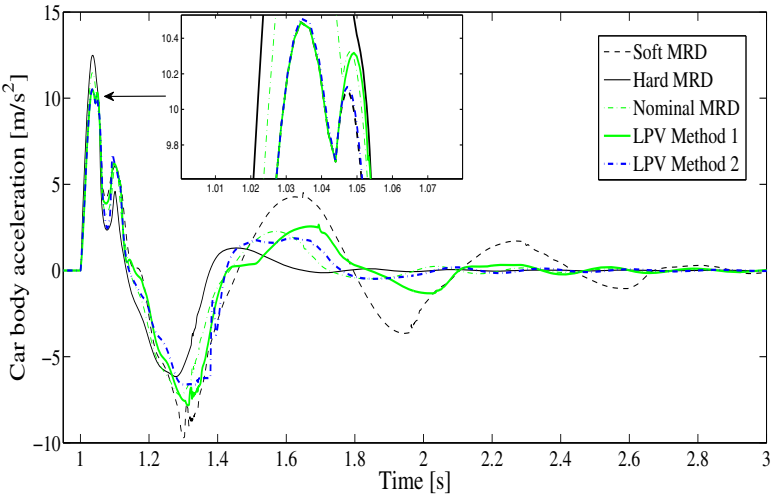

Fig. 7.16 Step responses comparison

The results obtained with a step road profile are summarized in Tab. 7.5. The use of LPV controllers reduce the peak values as well as the RMS values of the car body acceleration. They provide a better comfort improvement w.r.t passive dampers.

Table 7.5 RMS and peak values of car body acceleration obtained in a test with step road profile

Methods	Peak value $[m/s2]$	RMS value $[m/s2]$
Soft Damper	10.4893	2.0158
Hard Damper	12.4847	1.4584
Nominal Damper	11.4790	1.5875
LPV Method 1	10.4893	1.6365
LPV Method 2	10.5118	1.5664

Test 2: Random road profile
The road profile can also be viewed as a random signal, because it is not predicted by the vehicle. However, in practice, its bandwidth is limited. In this test, a road profile is represented by an integrated white noise, band-limited within the frequency range [0-30] Hz (see Fig. 7.17).

In what follows, the comfort is evaluated using the RMS value of the car body acceleration $\ddot{z}_s$:

$$RMS_{\text{Comfort}} = \sqrt{\frac{\int_0^T \ddot{z}_s 2(t)dt}{T}} \tag{7.49}$$

where T is the simulation time $[s]$.

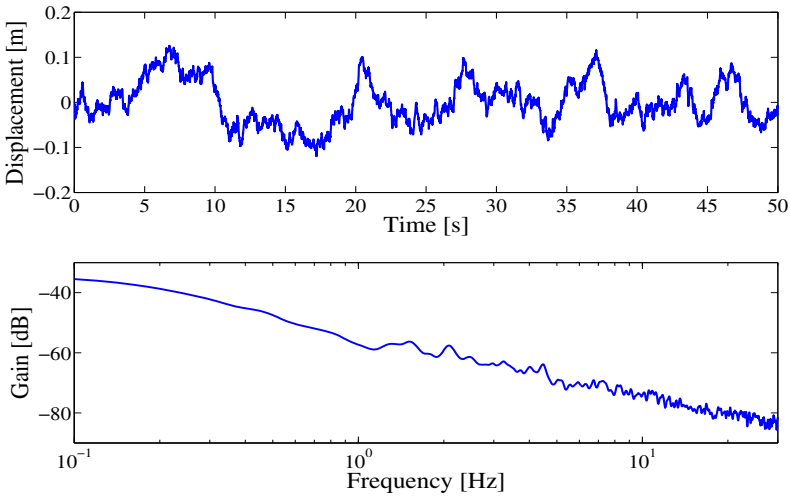

Fig. 7.17 Road profile z_r

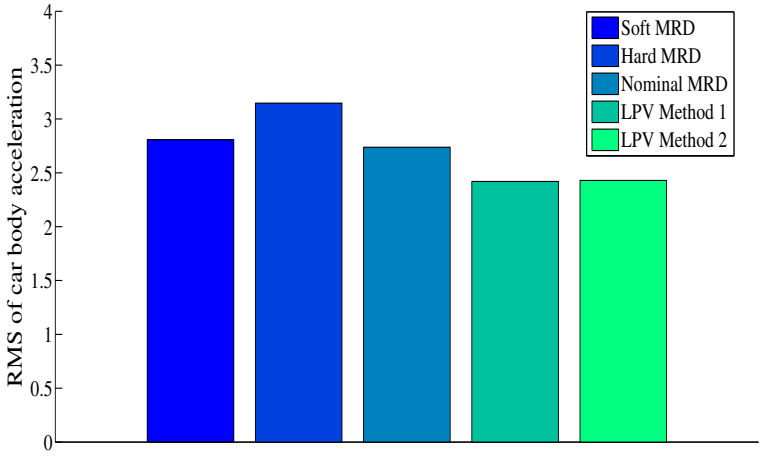

Fig. 7.18 RMS values of car body acceleration $\ddot{z}_s$

The comparison of the RMS values is depicted in Fig. 7.18. It confirms again the efficiency of the LPV approaches to improve the comfort of automotive suspension systems equipped with an MR damper. In this case, the LPV controllers give the same results. This is interesting and coherent with all previous analyses: the controller obtained with *Method 1* behaves slightly better in medium frequencies but slightly worse in low and high frequencies than the one obtained with *Method 2*.

7.6 Conclusion

In this chapter, the comparison of two LPV control methods for automotive suspension systems equipped with MR dampers has been done. The three main contributions of the chapter may be summarized as follows:

- The proposed control schemes are homogenous to ensure a fair comparison between two methods.
- The application (synthesis and implementation) of the LPV approach proposed by [29] on nonlinear MR dampers.
- A multi-objective optimization procedure for the LPV semi-active controller optimization proposed by [7] has been also applied to the control algorithm [29]. The results showed again the efficiency of this optimization procedure in semi-active suspension control.

From a design point of view, both methods are general for other semi-active actuation technologies. With *Method 1*, only the bounds of the dissipative domain (i.e c_{min}, c_{max} and F_{max}) are needed. With *Method 2*, the design is based on the MR damper model (7.7) which can be extended for other semi-active dampers (i.e for ER damper, the current dependent control signal f_I can be replaced by the voltage dependent one, f_V).

From a practical point of view, the two LPV control methods are simple and easy to implement: a single relative displacement sensor to measure the suspension deflection (the deflection velocity can be deduced numerically from the deflection) is needed and the LPV controllers are stable.

The simulations on the nonlinear quarter vehicle model equipped with a validated MR damper (in both frequency and time domains) have shown that similar results have been obtained with the two methods. It is seen that, in terms of design, compared to *Method 2*, *Method 1* is preferred because only the bounds on the damping capacity of a damper is needed. However, the practical implementation of *Method 1* needs further discussions. Indeed, while with *Method 2* the current (needed by a real MR damper) is easy to get by dividing the controller output by a scalar, it is more difficult to obtain with *Method 1*. A simple solution is to convert the controller output of *Method 1* in current using the equation (7.47). However, this model is actually not numerically good because some problem could arise when $c_1\dot{z}_{def} + k_1 z_{def}$ approaches zero and when the measurements of z_{def} and $\dot{z}_{def}$ are nois y. Further work could then concern the design of a local controller of the damper force in order to avoid to use such an inverse model (as proposed in the PhD thesis [2]).

Acknowledgements. This work was supported by the French national project INOVE/ ANR 2010 BLAN 0308. We would like to thank the co-authors of the referenced papers, specially Jorge de Jesus Lozoya-Santos, Ricardo Ambrocio Ramirez-Mendoza, Ruben Morales-Menendez (TEC Monterrey, Mexico) who have worked with us on the modelling and control of MR dampers.

References

1. Apkarian, P., Gahinet, P.: A convex characterization of gain scheduled $\mathscr{H}_\infty$ controllers. IEEE Transaction on Automatic Control 40(5), 853–864 (1995)
2. Aubouet, S.: Modélisation et commande de suspensions semi-actives soben. PhD thesis, INPG, GIPSA-lab, Grenoble, France (2010) (in English)
3. Bouc, R.: Forced vibration of mechanical systems with hysteresis. In: Proceedings of the Fourth Conference on Nonlinear Oscillation, Prague, Czechoslovakia, p. 315 (1967)
4. Canale, M., Milanese, M., Novara, C.: Semi-active suspension control using fast model-predictive techniques. IEEE Transaction on Control System Technology 14(6), 1034–1046 (2006)
5. Do, A.L., Lozoya-Santos, J., Sename, O., Dugard, L., Ramirez-Mendoza, R.A., Morales-Menendez, R.: Modélisation et commande LPV d'un amortisseur magnéto-rhéologique. In: Proceedings de la Conference Internationale Francophone d'Automatique, Nancy, France (2010)
6. Do, A.L., Sename, O., Dugard, L.: An LPV control approach for semi-active suspension control with actuator constraints. In: Proceedings of the IEEE American Control Conference (ACC), Baltimore, Maryland, USA (2010)
7. Do, A.L., Sename, O., Dugard, L.: LPV modelling and control of semi-active dampers in automotive systems. In: Mohammadpour, C.S. (ed.) Control of Linear Parameter Varying Systems with Applications, ch. 15. Springer (2012)
8. Do, A.L., Spelta, C., Savaresi, S., Sename, O., Dugard, L., Delvecchio, D.: An LPV control approach for comfort and suspension travel improvements of semi-active suspension systems. In: Proceedings of the 49th IEEE Conference on Decision and Control (CDC), Atlanta, GA, pp. 5660–5665 (2010)
9. Fialho, I., Balas, G.: Road adaptive active suspension design using linear parameter varying gain scheduling. IEEE Transaction on Control System Technology 10(1), 43–54 (2002)
10. Gillespie, T.D.: Fundamentals of Vehicle Dynamics. Society of Automotive Engineers Inc. (1992)
11. Giorgetti, N., Bemporad, A., Tseng, H., Hrovat, D.: Hybrid model predictive control application toward optimal semi-active suspension. International Journal of Robust and Nonlinear Control 79(5), 521–533 (2006)
12. Giua, A., Melas, M., Seatzu, C., Usai, G.: Design of a predictive semiactive suspension system. Vehicle System Dynamics 41(4), 277–300 (2004)
13. Gomes da Silva Jr., J.M., Limon, D., Alamo, T., Camacho, E.F.: Dynamic output feedback for discrete-time systems under amplitude and rate actuator constraints. IEEE Transaction on Automatic Control 53(10), 2367–2372 (2008)
14. Grimm, G., Hatfield, J., Postlethwaite, I., Teel, A., Turner, M., Zaccarian, L.: Antiwindup for stable linear systems with input saturation: An LMI-based synthesis. IEEE Transaction on Automatic Control 48(9), 1509–1525 (2003)
15. Guo, S., Yang, S., Pan, C.: Dynamic modeling of magnetorheological damper behaviors. Journal of Intelligent Material Systems and Structures 17, 3–14 (2006)
16. Hrovat, D.: Survey of advanced suspension developments and related optimal control application. Automatica 33(10), 1781–1817 (1997)
17. Ivers, D.E., Miller, L.R.: Experimental comparison of passive, semi-active on-off, and semi-active continuous suspensions. SAE Technical Paper 892484 (1989)

18. Karnopp, D., Crosby, M., Harwood, R.: Vibration control using semi-active force generators. Journal of Engineering for Industry 96, 619–626 (1974)
19. Kiencke, U., Nielsen, L.: Automotive Control Systems for Engine, Driveline, and Vehicle. Springer (2000)
20. Kothare, M.V., Campo, P.J., Morari, M., Nett, C.N.: A unified framework for the study of anti-windup designs. Automatica 30, 1869–1883 (1994)
21. Lozoya-Santos, J.J., Aubouet, S., Morales-Menendez, R., Sename, O., Ramirez-Mendoza, R.A., Dugard, L.: Simulation performance of a quarter of vehicle including an MR damper model with hysteresis. In: 7th Eurosim Congress on Modelling and Identification, Prague, Czech Republic (2010)
22. Lozoya-Santos, J.J., Morales-Menendez, R., Ramirez-Mendoza, R.A., Nino-Juarez, E.: Frequency and current effects in an MR damper. Int. J. Vehicle Autonomous Systems 7(3/4), 121–140 (2009)
23. Lozoya-Santos, J.J., Ruiz-Cabrera, J.A., Morales-Menéndez, R., Ramírez-Mendoza, R., Diaz-Salas, V.: Building training patterns for modelling MR dampers. In: ICINCO-SPSMC, pp. 156–161 (2009)
24. Lu, J., DePoyster, M.: Multiobjective optimal suspension control to achieve integrated ride and handling performance. IEEE Transaction on Control System Technology 10(6), 807–821 (2002)
25. Mulder, E.F., Tiwari, P.Y., Kothare, M.V.: Simultaneous linear and anti-windup controller synthesis using multiobjective convex optimization. Automatica 45, 805–811 (2009)
26. Pacejka, H.: Tyre and Vehicle Dynamics. Butterworth Heinemann (2005)
27. Patten, W.N., He, Q., Kuo, C.C., Liu, L., Sack, R.L.: Suppression of vehicle induced bridge vibration via hydraulic semi-active vibration dampers. In: Proceeding of the 1st World Conference on Structural Control, vol. 3, pp. 30–38 (1994)
28. Poussot-Vassal, C., Savaresi, S.M., Spelta, C., Sename, O., Dugard, L.: A methodology for optimal semi-active suspension systems performance evaluation. In: 2010 49th IEEE Conference on Decision and Control (CDC), pp. 2892–2897 (2010)
29. Poussot-Vassal, C., Sename, O., Dugard, L., Gáspár, P., Szabó, Z., Bokor, J.: New semi-active suspension control strategy through LPV technique. Control Engineering Practice 16(12), 1519–1534 (2008)
30. Rossi, C., Lucente, G.: $\mathscr{H}_\infty$ control of automotive semi-active suspensions. In: Proceedings of the 1st IFAC Symposium on Advances in Automotive Control (AAC), Salerno, Italy (2004)
31. Sammier, D., Sename, O., Dugard, L.: Skyhook and $\mathscr{H}_\infty$ control of active vehicle suspensions: some practical aspects. Vehicle System Dynamics 39(4), 279–308 (2003)
32. Savaresi, S., Bittanti, S., Montiglio, M.: Identification of semi-physical and black-box models: the case of MR-dampers for vehicles control. Automatica 41, 113–117 (2005)
33. Savaresi, S., Poussot-Vassal, C., Spelta, C., Sename, O., Dugard, L.: Semi-Active Suspension Control for Vehicles. Elsevier, London (2010) 978-0-08-096678-6
34. Savaresi, S., Silani, E., Bittanti, S.: Acceleration driven damper (ADD): an optimal control algorithm for comfort oriented semi-active suspensions. ASME Transactions: Journal of Dynamic Systems, Measurements and Control 127(2), 218–229 (2005)
35. Scherer, C., Gahinet, P., Chilali, M.: Multiobjective output-feedback control via LMI optimization. IEEE Transaction on Automatic Control 42(7), 896–911 (1997)
36. Tseng, H., Hedrick, J.: Semi-active control laws - optimal and sub-optimal. Vehicle System Dynamics 23(1), 545–569 (1994)

37. Wen, T.: Method for random vibration of hysteretic systems. Journal of Engineering Mechanics, ASCE 102(EM2), 249–263 (1976)
38. Wu, F., Grigoriadis, K.M., Packard, A.: Anti-windup controller design using linear parameter-varying control methods. International Journal of Control 73(12), 1104–1114 (2000)
39. Zin, A.: Robust automotive suspension control toward global chassis control. PhD thesis, INPG, Laboratoire d'Automatique de Grenoble (new GIPSA-lab), Grenoble, France (2005) (in French)

Chapter 8
Design of Integrated Control for Road Vehicles

Péter Gáspár

Abstract. This chapter presents a model-based control design for an integrated vehicle system in which several active components are operated simultaneously. In control-oriented modeling vehicle dynamics is augmented with the performance specifications. The performance specifications must be formulated in such a way that the performance demands are guaranteed, conflicts between performances are achieved and a priority between different actuators is created and various fault information is taken into consideration. A supervisory decentralized control structure is also proposed. The performance specifications are guaranteed by the local controllers, while the coordination of these components is provided by the supervisor. Monitoring components provide the supervisor with information needed to make decisions about the necessary interventions into the vehicle motion and guarantee the robust operation of the vehicle. The operation of the integrated system is illustrated through simulation examples.

Keywords: integrated vehicle control, reconfigurable, performance specifications, robust control, distributed control.

8.1 Introduction and Motivation

Conventionally, the control systems of vehicle functions to be controlled are designed separately by the suppliers and the vehicle companies. One of the problems of independent design is that the performance demands, which are met by independent controllers, are sometimes in conflict with each other in terms of the full vehicle. The braking action affects the longitudinal dynamics of the vehicle, the

Péter Gáspár
Systems and Control Laboratory, Computer and Automation Research Institute,
Hungarian Academy of Sciences, Hungary
e-mail: gaspar@sztaki.hu

O. Sename et al. (Eds.): *Robust Control and LPV Approaches*, LNCIS 437, pp. 213–235.
DOI: 10.1007/978-3-642-36110-4_8

velocity and the pitch angle. However, due to the geometry of the vehicle, the braking action causes changes in both the yaw and roll dynamics, see Figure 8.1. Similarly, the steering angle also modifies the yaw angle of the vehicle. Since the center of gravity is high the consequence of the steering maneuver is that the roll angle and the pitch angle of the sprung mass will also change. Moreover, the second problem in the independent control design is that control hardware can be grouped into discrete subsets with sensor information and control demands operating in parallel processes and these solutions can lead to unnecessary hardware redundancy.

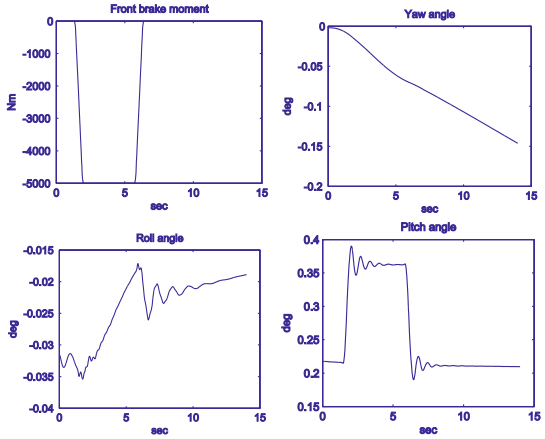

Fig. 8.1 The effect of braking on vehicle dynamics

The purpose of the integrated vehicle control is to combine and supervise all controllable subsystems affecting vehicle dynamic responses. In more details it means that multiple-objective performance from available actuators must be improved, sensors must be used in several control tasks, the number of independent control systems must be reduced, at the same time the flexibility of control systems must be enhanced. An integrated control system is designed in such a way that the effects of a control system on other vehicle functions are taken into consideration in the design process by selecting the various performance specifications. In line with the requirements of the vehicle industry several performance specifications are in the focus of the research, e.g. improving road holding, enhancing passenger comfort and improving roll and pitch stability, proposing fault-tolerant solutions, see e.g. [4, 29].

The demand for vehicle control methodologies including several control components arises at several research centers and automotive suppliers. Here are a few examples for illustration. A vehicle control with four-wheel-distributed steering and four-wheel-distributed traction/braking systems is proposed by [18]. A process to design the control strategy for a vehicle with throttle control and automatic transmission is proposed by [13]. A yaw stability control system in which an active torque distribution and differential braking systems are used is proposed by [30]. An

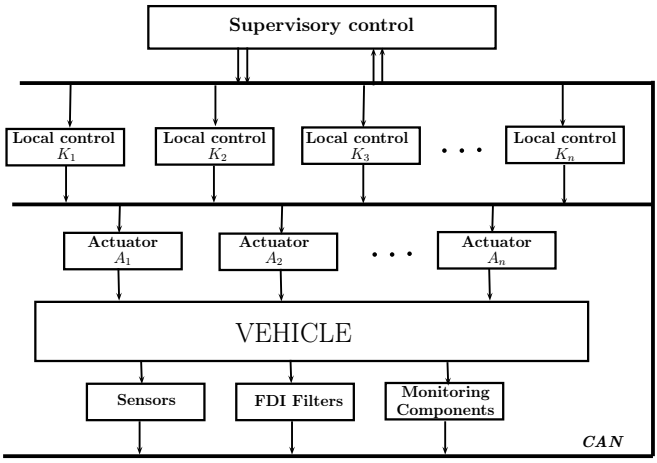

Fig. 8.2 The architecture of integrated vehicle control

integrated control that involves both four-wheel steering and yaw moment control is proposed by [10, 25]. Active steering and suspension controllers are also integrated to improve yaw and roll stability [16]. A global chassis control involving an active suspension and ABS is proposed by [22, 31]. The driveline system and the brake are integrated in [23]. An important solution to the roll stability control is based on the ESC brake control, see [15, 21]. A possible integration of the brake, steering and suspension system is presented by [2, 8, 24].

A centralized controller has several advantages: the designed controller guarantees performance specifications and robustness against uncertainties; the solution reduces the number of necessary sensors; it improves the flexibility of the actuators and avoids unnecessary duplications. The high-complexity control problem, however, is often difficult to handle, i.e. the more complex the vehicle model is the more numerical problems must be handled. Moreover, this centralized approach is not suitable for the partial design tasks carried out by vehicle component suppliers. Furthermore, if a new component is added to the system the entire system must be re-designed.

Thus, decentralized controllers which operate simultaneously are applied for the vehicle. The advantage of this architecture is that the complexity of the vehicle model can be divided into several parts. In this decentralized control structure there is a logical relationship between the supervisor and the local control components. The communication within local controls is performed by using the CAN bus. The role of the supervisor is to meet performance specifications, create a cooperation between components and prevent the interference and conflict between them. The supervisor has information about the current operational mode of the vehicle, i.e., the various vehicle maneuvers or the different fault operations gathered from monitoring components and fault-detection and identification (FDI) filters. The supervisor

is able to make decisions about the necessary interventions into the vehicle components and guarantee the reconfigurable and fault-tolerant operation of the vehicle. These decisions are propagated to the lower layers through predefined interfaces encoded as suitable scheduling signals. As some examples for the topic of fault detection methods in industrial mechatronic products, see [3, 11, 17].

The structure of the chapter is as follows. In Section 8.2 the control-oriented modeling of vehicle dynamics is constructed and the performance specifications in a closed-loop interconnection structure are formulated. In Section 8.3 the design principles of the brake, the steering, the suspension system and the actuator selection method are presented and, moreover, the fault information is also discussed. In Section 8.4 the global stability and performances of the reconfigurable control are discussed. In Section 8.5 the reconfigurable integrated control is demonstrated through simulation examples. Finally, Section 8.6 contains some concluding remarks.

8.2 Control-Oriented Modeling of Vehicle Dynamics

8.2.1 Vehicle Modeling

The vehicle has six degrees of freedom, translations in the x, y, and z directions, as well as rotations round each of these axes. Rotation round the z-axis is called roll ϕ, rotation about the y-axis is pitch θ, and rotation about the z-axis is yaw ψ. Since the driver inputs considered in this analysis are the braking and steering, two force types are considered, i.e. the longitudinal forces F_x and lateral forces F_y. The vehicle is steered by the front tires and the steering angle δ_f. The vehicle motions also result in vertical accelerations, which cause the suspension springs and dampers to generate reaction forces.The forces generated by the active suspension are denoted by F_{zij}.

The chassis vertical (z_s), longitudinal (x), lateral (y), roll, pitch and yaw dynamics are given by the following equations. Here v_x and v_y are the velocities of the chassis in x and y-directions, z_s and z_u are the displacement of the sprung mass and the unsprung masses in z-direction. Using the local coordinate system the following force and moment relations are defined, see e.g.,[12].

$$m\dot{v}_x = -F_{xf}\cos\delta_f - F_{xr} - F_{yf}\sin\delta_f - m\dot{\psi}v_y, \tag{8.1a}$$

$$m\dot{v}_y = -F_{xf}\sin\delta_f + F_{yr} + F_{yf}\cos\delta_f + m\dot{\psi}v_x, \tag{8.1b}$$

$$m_s\ddot{z}_s = -F_{zf} - F_{zr} - F_{dz}, \tag{8.1c}$$

$$m_{usij}\ddot{z}_{usij} = F_{zij} - F_{tzij}, \tag{8.1d}$$

$$I_x\ddot{\theta} = t_r(F_{zrl} - F_{zrr}) + t_f(F_{zfl} - F_{zfr}) + mh\dot{v}_y, \tag{8.1e}$$

$$I_y\ddot{\phi} = \ell_f F_{zf} - \ell_r F_{zr} - mh\dot{v}_x, \tag{8.1f}$$

$$\begin{aligned} I_z\ddot{\psi} = {} & \ell_f(-F_{xf}\sin\delta_f + F_{yf}cos\delta_f) - \ell_r F_{yr} + \\ & + t_f(F_{xfr} - F_{xfl})\cos\delta_f - t_r(F_{xrr} - F_{xrl}) + M_{dz}. \end{aligned} \tag{8.1g}$$

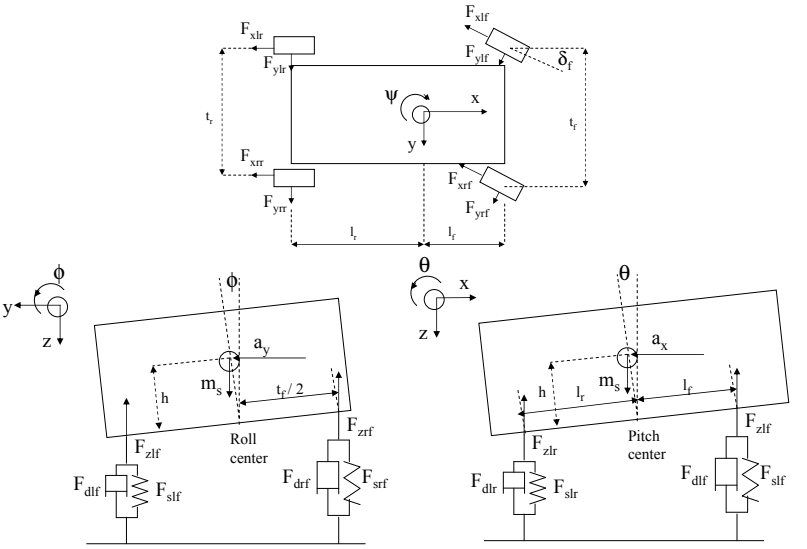

Fig. 8.3 Vehicle body for yaw, roll and pitch motions

The relationship between the yaw dynamics $\dot{\psi}$ and the dynamics of the side slip angle of the center of gravity $\dot{\beta}$ is $\dot{\beta} = \dot{\psi} + F_{tyf}/v_x/m + F_{tyr}/v_x/m$. Using small steering angle the following approximations are applied: $\sin\delta_f = \delta_f$ and $\cos\delta_f = 1$.

The objective of the control design is to track a predefined path, guarantee road holding and increase yaw, roll and pitch stability. Several control components are applied in the system: the active brake, steering and the suspension system. The tracking problem is solved by using active steering. In this system the control input is the steering angle: $u_d = \delta_f$. Road holding and passenger comfort are improved by applying an active suspension system. The suspension system is also able to improve pitch and roll stability by generating pitch moment during abrupt braking and roll moments during emergency maneuver. The control inputs are generated by the suspension actuators: $u_s = \left[f_{fl}, f_{fr}, f_{rl}, f_{rr}\right]^T$. In the control system the brake is able to modify the yaw angle of the vehicle during a cornering and reduce the effect of lateral acceleration. When a rollover is imminent and this emergency persists the brake system is activated to reduce the rollover risk. It is also able to generate unilateral brake forces at the front and the rear wheels at either of the two sides $u_b = \Delta F_b$.

The local controllers are designed based on vehicle models with different complexity. Figure 8.3 illustrates a multi-body vehicle system with its the longitudinal, lateral and vertical dynamics. Their design is based on state space representation form

$$\dot{x} = A(\rho)x + B_1(\rho)w + B_2(\rho)u, \tag{8.2}$$

where x, w and u are the state, disturbance and input, respectively, vector ρ includes the scheduling variables and $A(\rho) = A_0 + \sum_{i=1}^{n} \rho_i A_i$, $B_1(\rho) = B_{10} + \sum_{i=1}^{n} \rho_i B_{1i}$, $B_2(\rho) = B_{20} + \sum_{i=1}^{n} \rho_i B_{2i}$, in which n is the number of the scheduling variables ρ_i. First the state equation is defined and then the performances and measured output are selected considering the control tasks.

The nonlinear effects of the forward velocity v, the adhesion coefficient of the vehicle in the lateral direction μ or the nonlinear characteristics in the suspension damper components ρ_{bij} are taken into consideration $\rho = [v, \mu, \rho_{bij}]^T$ in the design.For example the adhesion coefficients depend on the type of road surface. It is difficult to accurately quantify and measure the effect of all of the external factors on μ, which is a nonlinear and time varying function. An adaptive observer-based grey-box identification method has been proposed for its estimation, [7]. It is assumed that with suitably-selected scheduling variables ρ these nonlinear components can be transformed into affine parameter-dependent forms. Then the nonlinear models are transformed into LPV models in which nonlinear terms are hidden with suitably selected scheduling variables.

8.2.2 *Performance Specifications and the Control Design*

The local components also include units for monitoring vehicle operations. These components are able to detect emergency vehicle operations, various fault operations or performance degradations in controllers. They also send messages to the supervisor. In the reconfigurable and fault-tolerant control of the local controller several signals must be monitored and scheduling variables are added to the scheduling vector in order to improve the safety of the vehicle, e.g., variables are needed to encode the rollover risk, represent the harmful effects of abrupt braking and take a detected failure of an active component into consideration.

The efficient operation of the supervisor and the local controllers require reliable and highly accurate signals from the system. To meet this requirement redundant sensors, diverse calculations and fault detection filters are needed. To achieve the efficient and optimal intervention the detections of faulty sensors are important since they must be substituted for in operations based on these sensors. Low cost solutions are preferred in the vehicle industry, thus simple sensors and software-based redundancy must be applied.

The closed-loop system applied in the design of a local control includes the feedback structure of the model $G(\rho)$, the compensator and elements associated with the performance objectives:

$$z = C(\rho)x + D_1(\rho)w + D_2(\rho)u, \tag{8.3}$$

where $w = [d \ n]^T$ includes both the external disturbances and the sensor noise. A typical interconnection structure is shown in Figure 8.4. These elements define the parameter dependent augmented plant $P(\rho)$. Using the controller K the closed-loop system $M(\rho)$ is given by a LFT (Linear Fractional Transformation) structure.

In this framework performance requirements z are imposed by a suitable choice of the weighting functions W_p. Usually the purpose of weighting functions W_p is to define penalty functions, i.e., weights should be large where small signals are desired and small where large performance outputs can be tolerated. The proposed approach realizes the reconfiguration of the performance objectives by an appropriate scheduling of these weighting functions. Δ_m block contains the uncertainties of the system, such as unmodelled dynamics and parameter uncertainty. In this augmented plant unmodelled dynamics is represented by a weighting function W_r and a block Δ_m. The purpose of the weighting functions W_d and W_n is to reflect the disturbance and sensor noises.

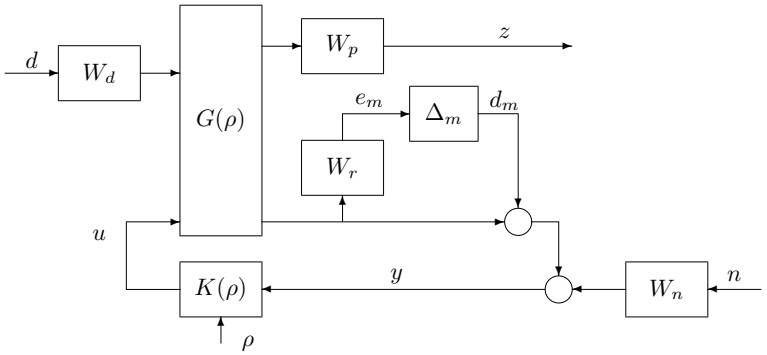

Fig. 8.4 The closed-loop interconnection structure

In the proposed solution the design of local control components is based on LPV methods. LPV methods are well elaborated and successfully applied to various industrial problems. The LPV approaches allow us to take into consideration the highly nonlinear effects in the state space description, [1, 20]. The main point of the approach is that in the control design of the local components scheduling variables received from the supervisor are used as a key of integration. In this way the operation of a local controller can be extended to reconfigurable and fault-tolerant functions.

If parameter-dependent Lyapunov functions are used, the designed controller depends explicitly on $\dot{\rho}$. Thus, in order to construct a parameter-dependent controller, both ρ and $\dot{\rho}$ must be measured or available. When $\dot{\rho}$ is not measured in practice, a suitable extrapolation algorithm must be used to achieve an estimation of the parameter $\dot{\rho}$. To remove $\dot{\rho}$ dependence a ρ-dependent change of variables was proposed in [20].

The quadratic LPV performance problem is to choose the parameter-varying controller $K(\rho)$ in such a way that the resultant closed-loop system $M(\rho)$ is quadratically stable and the induced $\mathscr{L}_2$ norm from w to z is less than γ, i.e.,

$$\|M(\rho)\|_\infty = \inf_K \sup_\Delta \sup_{\|w\|_2 \neq 0, w \in L_2} \frac{\|z\|_2}{\|w\|_2}. \tag{8.4}$$

By assuming an unstructured uncertainty and by applying a weighted small gain approach the existence of a controller that solves the quadratic LPV γ-performance problem can be expressed as the feasibility of a set of LMIs, which can be solved numerically, see [27].

The existence of a controller that solves the quadratic LPV γ-performance problem can be expressed as the feasibility of a set of Linear Matrix Inequalities (LMIs), which can be solved numerically. Stability and performance are guaranteed by the design procedure, see [20, 28]. When the LPV controller has been synthesized, the relation between the state, or output, and the parameter $\rho = \sigma(x)$ is used in the LPV controller, such that a nonlinear controller is obtained.

8.3 Design of the Local and Reconfigurable Control Systems

8.3.1 Design of the Brake System

Roll stability is achieved by limiting the lateral load transfers on both axles to below the levels for wheel lift-off during various vehicle maneuvers. The lateral load transfers are calculated at both axles: $\Delta F_{z,i} = C_i \phi_{t,i}$. The tire contact force is guaranteed if $\frac{mg}{2} \pm \Delta F_z > 0$ for both sides of the vehicle. The normalized values of the lateral load transfers are the ratio of $\Delta F_{z,i}$ and the masses of the vehicle on the axles: $\rho_R = \Delta F_{z,i}/m_i g$. The aim of the control design is to reduce the maximum value of the normalized lateral load transfer if it exceeds a predefined critical value.

In the design of the brake system the command signal is the difference in brake forces while the performance signal is the lateral acceleration: $z_b = \left[a_y, u_r\right]^T$. The weighting function of the lateral acceleration is selected as:

$$W_{p,ay} = \gamma_a \frac{T_{b1}s + 1}{T_{b2}s + 1}. \tag{8.5}$$

where T_{bi} are time constants. Here γ_a is a gain, which reflects the relative importance of the lateral acceleration and it is chosen to be parameter-dependent, i.e., the function of ρ_R.

$$\gamma_a = \begin{cases} 1 & \text{if} \quad |\rho_R| > R_b \\ \frac{|\rho_R| - R_a}{R_b - R_a} & \text{if} \quad R_a \leq |\rho_R| \leq R_b \\ 0 & \text{if} \quad |\rho_R| < R_a \end{cases}$$

When ρ_R is small ($|\rho_R| < R_b$), i.e., when the vehicle is not in an emergency, γ_a is small, indicating that the LPV control should not focus on minimizing acceleration. When ρ_R is approaching the critical value, i.e., when $|\rho_R| \geqq R_b$, γ_a is large, it

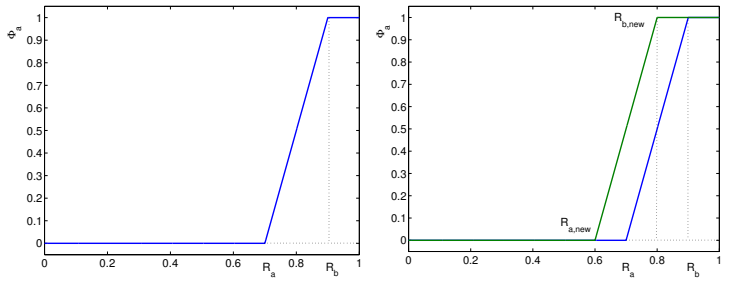

(a) Normal case (b) Fault case

Fig. 8.5 Parameter-dependent gain in the brake control

indicates that the control should focus on preventing the rollover. Here R_b defines the critical status when the vehicle is close to the rollover. Note that the weights used in the chapter are proportional-differential components. Their time constants and gains reflect the required steady state and transient behavior of the different signals that describe the performance specifications.

Remark 11. *If a fault concerning roll stability is detected in the suspension system its role is substituted for by the brake system. The brake system is activated at a smaller critical value than in a fault-free case, i.e., when* $|\rho_{Da}| > 0$. *Consequently, the brake is activated in a modified way and the brake moment is able to assume the role of the suspension actuator in which the fault has occurred. The modified critical value is*

$$R_{a,new} = R_a - \alpha \cdot \rho_{Da}, \tag{8.6}$$

where α *is a predefined constant factor.*

8.3.2 Design of the Steering System

Yaw stability is achieved by limiting the effects of the lateral load transfers. The purpose of the control design is to minimize the lateral acceleration, which is monitored by a performance signal: $z_a = a_y$. Unilateral braking is one of the solutions, in which brake forces are generated in order to achieve a stabilizing yaw moment. In the second solution additional steering angle is generated in order to reduce the effect of the lateral loads. These solutions, however, require active driver intervention into the motion of the vehicle to keep the vehicle on the road.

Another control task is to follow a road by using a predefined yaw rate (angle). In this case the current yaw rate must be monitored and the difference between the reference and the current yaw rate is calculated. The purpose of the control is to minimize the tracking error: $z_\psi = \dot{\psi}_{cmd} - \dot{\psi}_{ref}$.

In order to solve the yaw rate tracking problem in the design of the steering system, the command signal must be fed forward to the controller ($\dot{\psi}_{\text{cmd}}$). The command signal is a pre-defined reference displacement and the performance signal is the tracking error: $z_{\dot{\psi}} = e_{\dot{\psi}}$, which is the difference between the actual yaw rate and the yaw rate command. The weighting function of the tracking error is selected as:

$$W_{pe} = \gamma_e \frac{T_{d1}s + 1}{T_{d2}s + 1}, \tag{8.7}$$

where T_{di} are time constants. Here, it is required that the steady state value of the tracking error should be below $1/\gamma_e$ in steady-state.

Remark 12. *If a fault is detected in the steering system ($|\rho_{Ds}| > 0$), the brake must focus on yaw dynamics in order to reduce the tracking error. Thus, in the control design of the brake the performance specification concerning the steering system is also built in:*

$$W_{pe} = \gamma_{be} \frac{T_{b3}s + 1}{T_{b4}s + 1}, \tag{8.8}$$

where γ_{be} depends on $|\rho_{Ds}|$

$$\gamma_{be} = \begin{cases} 1 & \text{if} \quad |\rho_{Ds}| > \rho_{crit} \\ \frac{|\rho_R| - \rho_{tol}}{\rho_{crit} - \rho_{tol}} & \text{if} \quad \rho_{tol} \leq |\rho_{Ds}| \leq \rho_{crit} \\ 0 & \text{if} \quad |\rho_{Ds}| < \rho_{tol} \end{cases}$$

In this weighting the critical value of the brake intervention is used together with a tolerance value.

Remark 13. *When there is a performance degradation in the operation of the brake system, it is not able to create sufficient yaw moment to improve roll stability. In this sense the brake system is substituted for by the steering system. The steering system receives the fault message from the supervisor and it modifies its operation in such a way that the effects of the lateral loads are also reduced. The difficulty in this solution is that a performance degradation concerning the tracking task also occurs, since the steering system must create a balance between tracking and roll stability.*

8.3.3 Design of the Suspension System

Road holding is achieved by reducing the normalized suspension deflections ρ_k between the sprung and unsprung masses at the four corner points of the vehicle. Since increasing road holding reduces the passenger comfort in the design of the suspension system its desired level is subject to a design decision.

The performance signals in the suspension design are: $z_s = \begin{bmatrix} a_z & s_d & t_d & u_s \end{bmatrix}^T$. The goals are to keep the heave accelerations $a_z = \ddot{q}$, suspension deflections $s_d = x_{1ij} - x_{2ij}$, wheel travels $t_d = x_{2ij} - w_{ij}$, and control inputs small over the desired operation range. The performance weighting functions for heave acceleration, suspension deflections and tire deflections are selected as

$$W_{p,az} = \gamma_{az} \frac{T_{s1}s + 1}{T_{s2}s + 1}, \tag{8.9a}$$

$$W_{p,sd} = \gamma_{sd} \frac{T_{s3}s + 1}{T_{s4}s + 1}, \tag{8.9b}$$

$$W_{p,td} = \gamma_{td} \frac{T_{s5}s + 1}{T_{s6}s + 1}, \tag{8.9c}$$

where T_{si} are time constants while γ_{td} are parameter dependent gains, which depend on the suspension deflection ρ_{kij}.

In normal cruising the suspension system focuses on the conventional performances based on the parameter-dependent gain, which is a function of the suspension deflection ρ_{kij}. The trade-off between passenger comfort and suspension deflection is due to the fact that it is not possible to guarantee them together simultaneously. A large gain γ_{az} and a small gain γ_{sd} correspond to a design that emphasizes passenger comfort while choosing γ_{az} small and γ_{sd} large corresponds to a design that focuses on suspension deflection. The parameter dependence of the gains, which is illustrated in Figure 8.6, is characterized by the constants ρ_1 and ρ_2 in the following way:

$$\gamma_{az} = \begin{cases} 1 & \text{if} \quad |\rho_{kij}| < \rho_1, \\ \frac{|\rho_{kij}| - \rho_2}{\rho_1 - \rho_2} & \text{if} \quad \rho_1 \le |\rho_{kij}| \le \rho_2, \\ 0 & \text{if} \quad R \ge R_s \text{ or } |\rho_{kij}| > \rho_2. \end{cases}$$

$$\gamma_{sd} = \begin{cases} 0 & \text{if} \quad |\rho_{kij}| < \rho_1, \\ \frac{|\rho_{kij}| - \rho_1}{\rho_2 - \rho_1} & \text{if} \quad \rho_1 \le |\rho_{kij}| \le \rho_2, \\ 1 & \text{if} \quad R \ge R_s \text{ or } |\rho_{kij}| > \rho_2. \end{cases}$$

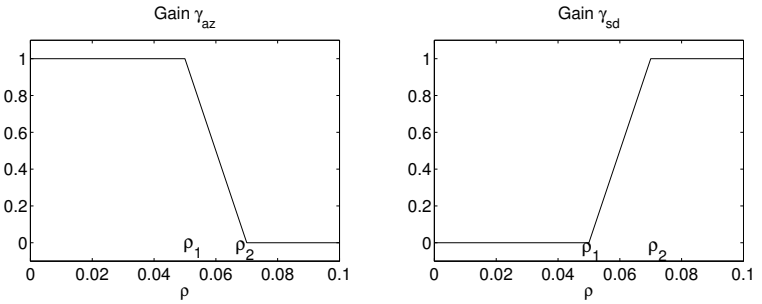

Fig. 8.6 Parameter-dependent gains in the suspension control

Remark 14. *The idea of the reconfigurable suspension system is based on the fact that active suspension systems are used not only to eliminate the effects of road irregularities but also to generate roll moments to improve roll stability or generate pitch moment to improve pitch stability.*

$$W_{p,\theta} = \gamma_P \frac{T_{s7}s+1}{T_{s8}s+1},$$
$$W_{p,\gamma} = \gamma_R \frac{T_{s9}s+1}{T_{s2}s+10}.$$

For a reconfigurable suspension system the parameter-dependent gains are selected as functions of the normalized lateral load transfer ρ_R and the normalized value of the pitch angle ρ_P. If ρ_P exceeds a predefined critical value, i.e., when $|\rho_P| \geqq R_P$, the controller must focus on pitch stability. In an emergency, however, i.e., when $|\rho_R| \geq R_s$, the suspension system must reduce the rollover risk and guaranteeing passenger comfort (and pitch angle) is no longer a priority.

8.3.4 Actuator Selection Procedure

In the control design the distribution of the wheel forces must also be taken into consideration. In a front-wheel-driven vehicle the traction force is distributed between the front wheels by using a differential gear. The steering angle is limited by construction (δ_{crit}), therefore when the maximal steering angle is reached the desired lateral dynamics of the vehicle must be achieved by the brake moment. During braking the load of wheels is modified due to the pitch dynamics of the vehicle. The braking of the front wheels must be stronger while the braking of the rear wheels must be reduced. The wheel forces must be monitored in view of the momentary friction margin of the tire. It requires the estimation of friction coefficient μ, which is also necessary for the determination of maximal cornering velocity, see [5, 26].

The maximal longitudinal force of the wheels ($F_{i,max}$) is calculated and compared to the momentary longitudinal wheel forces (F_i). Note that the maximum longitudinal force depends on the maximum adhesion coefficient and the static and dynamic components of the vertical force at the wheel, i.e., the lateral and pitch dynamics.

$$F_{i,max} = \mu_{max}\{F_{z,stat} \pm m a_y h/2/L \pm m\dot{\psi} v h/b\}.$$

This calculation must be performed at all wheels and the highest rate of $\nu = F_i/F_{i,max}$ is selected. If a skidding incident is imminent the actuation of the brake moment must be reduced and it is replaced by the actuation of front wheel steering. The variable $\nu = max\{F_i/F_{i,max}\}$ is the maximal value between the force ratios considering all the wheels and ν_{crit} is a design parameter.

It is also necessary to consider that the actuations of the different components have energy requirement. By using differential braking the velocity of the vehicle is decreased, which must be compensated for by the driveline with additional energy. Therefore the use of differential braking must be avoided during acceleration

and front-wheel steering is preferred. During deceleration the brake is already being used, thus the lateral dynamics is handled by the braking for practical reasons. Thus differential braking is preferred, but close to the limit of skidding, front-wheel steering must also be generated. The actuation of differential braking causes increased strain on the tyres. When the vehicle moves in the lateral direction the position of each tyre is longitudinal. It also shows that using front-wheel steering is more efficient.

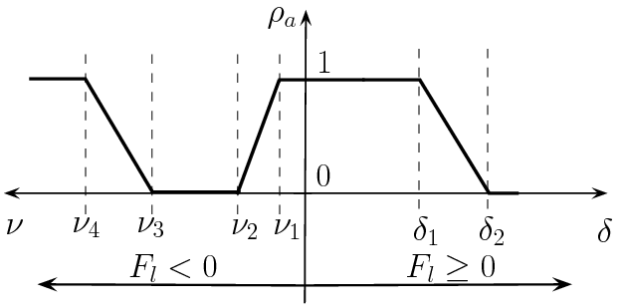

Fig. 8.7 Illustration of the actuator selection

A weighting factor ρ_a, which depends on the vehicle operation and the variables δ and v is shown in Figure 8.7. In case of traction the front wheel steering angle δ determines factor ρ_a. The value is reduced between δ_1 and δ_2, which represents the constructional criterion of the steering system. In the case of braking the variable v affects the factor ρ_a. In this interval differential braking is preferred for practical reasons. It requires an interval to reduce tire skidding and it also requires an interval to prevent chattering between steering and differential braking. Therefore four parameters are designed: v_1 and v_2 are used to prevent chattering and v_3 and v_4 are applied to prevent the skidding of tires. This factor may depend on other parameters such as forward velocity, lateral loads, maneuvers to a certain degree.

Example 1. *The generation of the different actuators is based on the following weighting strategy. The weighting for the front wheel steering and for the brake yaw-moment are*

$$W_{act,\delta} = (1 - \rho_a)/\delta_{max}, \tag{8.10a}$$

$$W_{act,Mbr} = \rho_a / M_{brmax}, \tag{8.10b}$$

where δ_{max} is determined by the constructional maximum steering angle and M_{brmax} is the maximum of brake yaw-moment. Weighting factor ρ_a is chosen according to the relationship between the brake yaw-moment and the front steering angle. This weighting factor must be chosen according to the the examined criteria.

8.3.5 Fault Information in the Decentralized Control

The fault-tolerant local controllers also require components for monitoring fault information. Here the normalized fault information provided by an FDI filter is given by

$$\rho_D = \frac{f_{act}}{f_{max}}, \tag{8.11}$$

where f_{act} is an estimation of the failure (output of the FDI filter) and f_{max} is an estimation of the maximum value of the potential failure (fatal error). The estimated value f_{act} means the measure of the performance degradation of an active component.

The interconnection structure includes the vehicle model $G(\rho)$, the FDI filter $F(\rho)$, and elements associated with performance objectives, see Figure 8.8. The weight W_{p_f} reflects the relative importance of the fault signal. This weight should be large when small errors are desired and small when large errors can be tolerated. The weight W_{f_a} defines the size of the possible fault in the actuator channel. The weight W_{f_s} defines the size of the possible fault in the sensor channel.

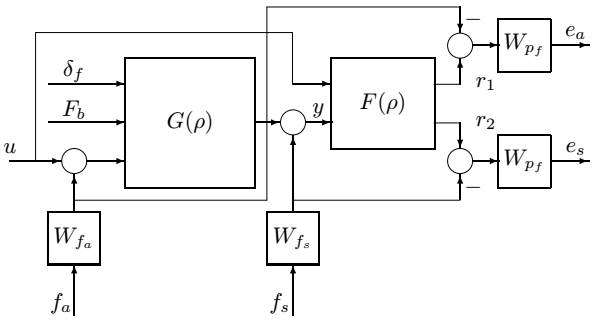

Fig. 8.8 Design of an FDI filter

The design requirement for H_∞ residual generation is to maximize the effect of the fault (f) on the residual and simultaneously minimize the effect of exogenous signals (d, u) on the residual.

$$||T_{rd}||_\infty = \sup_{||f||_2=1, \rho \in \mathscr{P}} ||r||_2, \tag{8.12}$$

wher the residual can be expressed as $r = T_{ru}u + T_{rd}d + T_{rf}f$. The FDI filter designed in the open-loop system can be implemented in the closed-loop system. The filter receives the measured outputs, the control inputs and the filter provides the fault residuals. For more details on the main steps of the FDI filter design see [9].

The fault-tolerant control requires fault information in order to guarantee performances and modify its operation. Thus, FDI filters are also designed for the operation of the actuators. As an example the fault information provided by a fault detection filter is given by $\rho_D = f_{act}/f_{max}$, where f_{act} is an estimation of the failure (output of the FDI filter) and f_{max} is an estimation of the maximum value of the potential failure (fatal error). The value of a possible fault is normalized into the interval $\rho_D = [0, 1]$. The estimated value f_{act} means the rate of the performance degradation of an active component.

The detection of a sensor failure as accurately as possible is crucial since the controller may generate fault actuator intervention as a result of fault sensor information. Sensor failures may also prevent certain actuators from being used; then handling the sensor failure leads to an actuator reconfiguration problem. Thus complex vehicle systems require various FDI filters both for actuator and sensor failures.

8.4 Towards Supervisory Integrated Control

8.4.1 Global Performances

In the entire system three controllers are used simultaneously. It is necessary to guarantee the stability and performances of the entire closed-loop system. This section focuses on the stability and the performances of the entire system. The open-loop LPV system considered for control synthesis has the following state space representation form:

$$\dot{x}_p = A(\rho)x_p + B_1(\rho)w + \sum B_{2i}(\rho)u_i \tag{8.13a}$$

$$z = C_1(\rho)x_p + D_{11}(\rho)w + \sum D_{12i}u_i \tag{8.13b}$$

$$y = C_2(\rho)x_p + D_{21}w \tag{8.13c}$$

where the control signal u is generated by the controllers and some of the matrices depend affinely on the vector ρ with the scheduling variables. The i^{th} controller is considered in LPV form:

$$\dot{x}_i = A_{ci}(\rho)x_i + B_{ci}(\rho)y_i \tag{8.14a}$$

$$u_i = C_{ci}(\rho)x_i + D_{ci}(\rho)y_i \tag{8.14b}$$

where $y_i = C_{2i}x$. Then the closed-loop LPV system in the state space can be obtained in the following form:

$$\dot{x} = A_{cl}(\rho)x + B_{cl}(\rho)w \tag{8.15a}$$

$$z = C_{cl}(\rho)x + D_{cl}w \tag{8.15b}$$

where

$$\left[\begin{array}{c|c} A_{cl} & B_{cl} \\ \hline C_{cl} & D_{cl} \end{array}\right] = \left[\begin{array}{cccc|c} A+\sum B_{2i}D_{ci}C_{2i} & B_{21}C_{c1} & B_{22}C_{c2} & B_{23}C_{c3} & B_1 \\ B_{c1}C_{21} & A_{c1} & 0 & 0 & \\ B_{c2}C_{22} & 0 & A_{c2} & 0 & 0 \\ B_{c3}C_{23} & 0 & 0 & A_{c3} & 0 \\ \hline C_1+\sum D_{12i}D_{ci}C_{2i} & D_{121}C_{c1} & D_{122}C_{c2} & D_{123}C_{c3} & D_{11} \end{array}\right].$$

In the supervisory decentralized method the necessary coupling between control components is realized through a set of well-defined monitoring signals provided by the supervisor to the subsystem. The controller modifies its normal operation if a special condition changes or a fault occurs. On a design level the controller should change its behavior according to these signals, i.e., the control design method should enable the incorporation of this type of information in the performance specification. Thus, in the control design the monitoring components are taken into consideration as scheduling variables in the performance signals.

In order to provide a formal verification of the achieved control performance on a global level, the problem must be formulated globally. Only on this extended level are the performance variables which are relevant for the whole vehicle available. Once the local controllers have been designed, however, it is possible to perform an analysis step in the same robust control framework on a global level, for details see [14]. This might be a highly computation-intensive procedure. Moreover the presence of competing multi-objective criteria deny the applicability of this global approach. E.g., in emergency events certain performance components gain absolute priority over others, thus requiring a given performance level for the ignored performance components is not justified. On the other hand the local design guarantees the prescribed performance level for the critical components. Therefore in practice the formal global verification is often omitted and the quality of the overall control scheme is assessed through simulation experiments.

The relationship between the supervisor and the local controllers guarantee that the system meets the specified performances. Applying parameter-dependent weighting a balance between different controllers is achieved. In different critical cases related to extreme maneuvers or performance degradations/faults in sensors or actuators the controllers reconfigure their operations. However, situations in which different critical performances must be achieved simultaneously may occur.

Example 2. *For example in a high-speed cornering maneuver the risk of a rollover increases significantly. The performances are in contradiction: deviating from the lane might cause the vehicle to run off the road while increasing roll dynamics might lead to rollover. This maneuver requires an intensive cooperation between the steering and the brake. The supervisor sends critical signals to the controllers and consequently these control systems are activated. However, reducing the rollover risk the yaw dynamics is modified and the deviation from the predefined path may increase. In contrast reducing the difference from the path might increase the rollover risk. Since both interventions are critical the supervisor is not able to resolve the problem, thus the performances are handled by the actuators with performance degradation.*

8.4.2 Idea of Plug-and-Play Methods

In the decentralized supervisory control the concept of the plug-and-play method plays and important role. If a new control component is added, an old control is replaced by a new one, or an old component is removed, the structure of the system (or the control) changes. In these cases the conventional control should be redesigned, which is expensive and takes a long time. In the supervisory control concept the supervisory logic must be modified on the highest level. When an old actuator is replaced by a new one only the actuator control must be redesigned. The goal is to provide a design method for a plug-and-play control architecture, i.e., the possibility to use sensors and actuators provided by different vendors interchangeably on a core system by guaranteeing a performance level and leaving the global controller intact.

In the integrated control systems the characteristics of the drivers' behavior should be taken into consideration in the control. The chapter proposes control solutions which create a balance between driving (or road holding) and comfort and guarantee safety all the time. The principle of the compromise leads to solutions which may not be suitable for all the drivers. The control solutions in practice are based on the drivers' behavior, which is learnt by the system during travelling. In the other solutions a switching between different modes is ensured, e.g. comfort and sport modes.

8.4.3 Driver Model in the Closed-Loop System

In the integrated control systems the characteristics of the drivers' behavior should be taken into consideration in the control. The control solutions create a balance between driving (or road holding) and comfort and guarantee safety all the time. This balance often leads to compromise between vehicle functions, which may not be suitable for all the drivers. For example a driver who wants to minimize the length of the trajectory in the bend selects the curvature radius as small as possible, while the driver who requires comfort select a larger curvature radius. At the same time, however, the selection of different curvature radiuses is also related to the possible speed selection, e.g. the larger radius allows the driver to select larger speed. The control solutions in practice are based on the drivers' behavior, which is learnt by the system during travelling.

Example 3. *As an example a driver model is combined with the vehicle model as Figure 8.9 shows. In the trajectory tracking control the lateral dynamics must be taken into consideration and the vehicle must follow the reference yaw-rate signal. The control inputs of the vehicle model are the front steering angle and the brake yaw moment, while its outputs are the measured yaw rate and the realized path. The input of the driver model is the lateral error e_y, while its output is the steering angle of the driver δ_d.*

During maneuvers the difference between the lateral position of the vehicle and the reference lateral position is minimized by the driver. Based on δ_d the yaw rate $\dot{\psi}_{ref}$ is calculated by using a first order proportional transfer function, see [19]:

$$G_{\psi} = \frac{v}{l_1 + l_2 + \frac{\eta}{g} v^2} \cdot \frac{1}{\tau s + 1} \tag{8.16}$$

with an understeer gradient η, the time constant τ, geometric parameters l_1, l_2 are geometric and velocity v. Since $\dot{\psi}_{ref}$ is generated by the driver, this signal is considered as a reference. This signal is used in the design of the steering system and the braking system. Also note that in the closed-loop interconnection structure $\dot{\psi}_{ref}$ is used instead of δ_d, which is compared to the measured yaw rate $\dot{\psi}$. In the trajectory tracking control the lateral dynamics must be taken into consideration and the vehicle must follow the reference yaw-rate signal. This concept was shown in more details in [6].

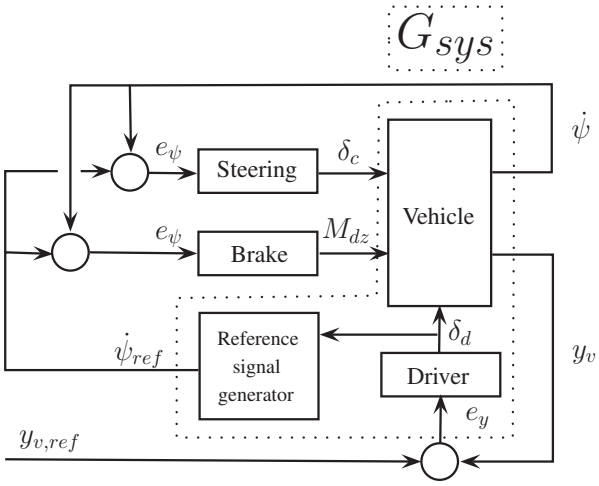

Fig. 8.9 Architecture of the vehicle/driver systemÈ

8.5 Simulation Examples

8.5.1 Illustration of the Fault-Tolerant Control

In the first simulation example the risk of rollover is reduced by using an active brake and the active suspension system, while passenger comfort and road holding are guaranteed by the suspension actuators. The cornering maneuver starts at the 1^{st} second and at the 4^{th} second a 10 cm high bump disturbs the motion of the vehicle. The steering angle is generated with a ramp signal with 3.5 degrees maximum value and 4 rad/s filtering, which represents the finite bandwidth of the driver. The velocity of the vehicle is 70 km/h. Figure 8.10 shows that as the lateral acceleration increases in the cornering, the normalized load transfers also increase. The effect of bump disturbs the heave acceleration at the 4^{th} second. Dashed line illustrates

the operation of the conventional suspension system while the solid line illustrates the operation of the reconfigured suspension system. In the latter case the control system exploits the ability of the suspension system that it is able to generate roll moments to improve roll stability.

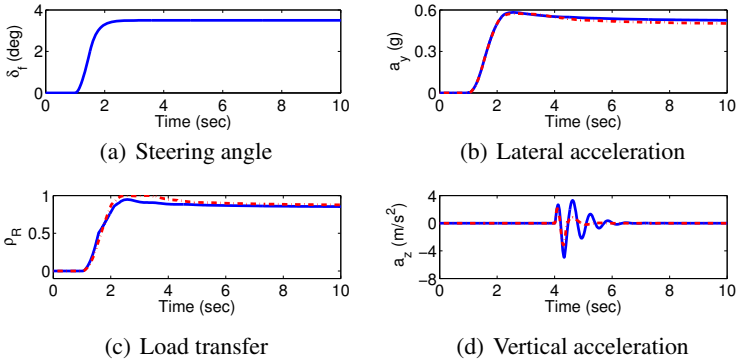

(a) Steering angle (b) Lateral acceleration

(c) Load transfer (d) Vertical acceleration

Fig. 8.10 Time responses of the cornering maneuver

In the example the operation of a reconfigurable suspension system is compared with a fault-tolerant suspension system. Figure 8.11 shows the operation of the actuators, i.e., the braking force and the suspension forces. In the cornering maneuver the active suspension system is not sufficient to reduce the rollover risk of the vehicle. Consequently, the normalized lateral load transfers reach the critical value R_a during the cornering maneuver so the brake control is activated. The brake generates a unilateral braking force (5 *kN*) at 2 *sec* to reduce the rollover risk. As a result the normalized lateral load transfers are below the critical value 1. The brake force figure also shows that the brake is activated earlier and its duration is longer (1.5 *sec*) in the faulty cases than in the absence of a fault.

8.5.2 Illustration of a Driver Assistance System

In the final example the efficiency of the integrated control is compared to the individual actuated control systems. A typical E-Class automobile is traveling along a predefined road, while the suspension system supports the driver to guarantee trajectory tracking, see Figure 8.12(a). The purpose of the control is to track the centerline of the road. The velocity of the vehicle changes along its route as Figure 8.12(b) shows. Note that the uncontrolled vehicle is not able to track the trajectory, i.e., the driver is not able to keep the vehicle on the track without a driver assistance system. At the same time the vehicle which uses supervisory control achieves trajectory tracking with an acceptable threshold.

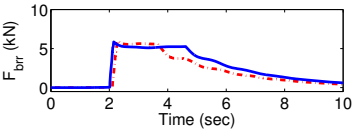

(a) Braking force at the rear

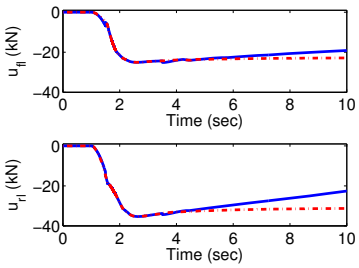

(b) Control forces at the left side

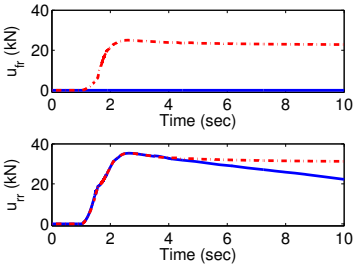

(c) Control forces at the right side

Fig. 8.11 Control forces of the fault-tolerant control system

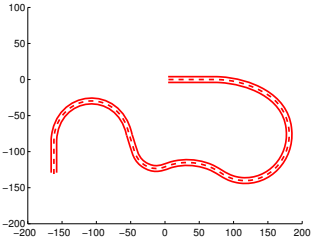

(a) Road course

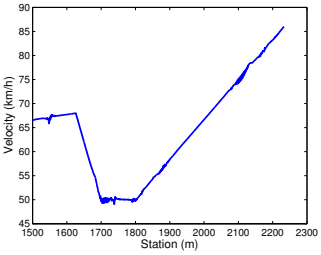

(b) Velocity of the vehicle

Fig. 8.12 Trajectories of vehicles

In the simulation example the supervisory control is compared to systems which use only one controller, i.e., only an active brake system or only an active steering system.

When a steering system is used only, it is not able to guarantee trajectory tracking in the first critical curve. The individual steering actuator is not able to prevent the skidding of the vehicle on the road. Figure 8.13(a) shows that at the beginning of the course the lateral error of the individual steering actuator is not acceptable. Note that the supervisory control ensures trajectory tracking with an acceptable threshold. Figure 8.13(c) shows the difference between the front-wheel steering angles at the pure steering and the integrated case. When a steering system is used only, the

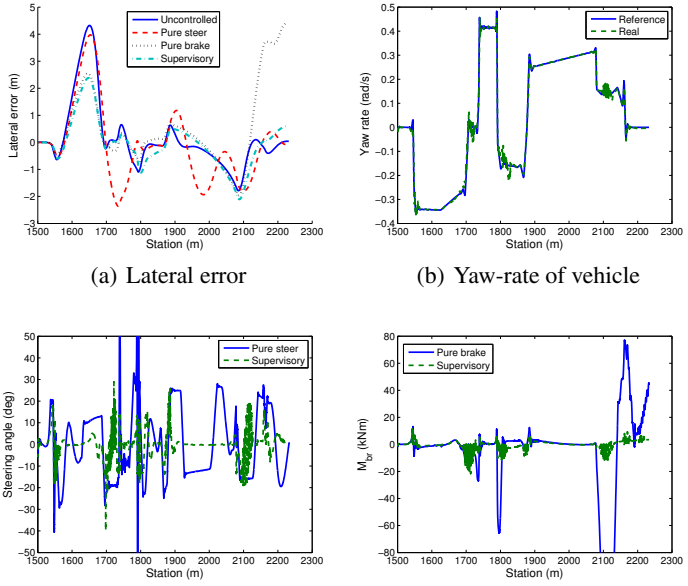

(a) Lateral error (b) Yaw-rate of vehicle

(c) Front wheel steering angle (d) Braking torque M_{br}

Fig. 8.13 Operation of the supervisory control

steering angle is significantly larger than in the integrated system, since the the turning of the steering-wheel affects the front steering angles.

When a brake system is used only, it generates increased braking pressures to keep the vehicle in the centerline. However, during braking the slip of the rear tires increases, which leads to loss of stability in the second critical curve. Figure 8.13(a) shows that in the last section during the travelling the lateral error increases significantly when a brake is used only. Note that the supervisory control is able to consider the slips of tires and avoid the saturation of the differential braking. Although the integrated control also uses a suspension system its activation does not affect the main feature of the vehicle operation. Figure 8.13(d) shows that when a brake system is used only, the differential braking torque is larger than in the integrated system. Note that at the second critical maneuver the torque M_{br} sharply increases because of the skidding effect. When a brake system is used only the longitudinal slip of rear right wheel exceeds -1, which leads to skidding. In the integrated case the longitudinal slip does not exceed -1.

The supervisory integrated control gives the smallest lateral error during the operation. In Figure 8.13(b) the yaw-rate tracking of the supervisory integrated control is shown. Thus, the integrated control provides an acceptable z_1 performance. The simulation example shows that the integration of control components improves the yaw stability and reduces the lateral error of trajectory tracking.

8.6 Conclusions

In the chapter a supervisory decentralized control structure has been proposed. The performance specifications are guaranteed by the local controllers, while the coordination of these components is provided by the supervisor. In the control-oriented modeling the vehicle dynamics is augmented with the performance specifications by applying monitoring components. Monitoring components provide the supervisor with information needed to make decisions about the necessary interventions into the vehicle motion and guarantee the robust operation of the vehicle. In the control design performance specifications must be formulated in such a way that the performance demands are guaranteed, conflicts between performances are handled, priority between different actuators is created and the various fault information is taken into consideration.

References

1. Bokor, J., Balas, G.: Linear parameter varying systems: A geometric theory and applications. In: 16th IFAC World Congress, Prague, pp. 1–11 (2005)
2. Burgio, G., Zegelaar, P.: Integrated vehicle control using steering and brakes. International Journal of Control 79, 534–541 (2006)
3. Fischer, D., Isermann, R.: Mechatronic semi-active and active vehicle suspensions. Control Engineering Practice 12(11), 1353–1367 (2004)
4. Gordon, T., Howell, M., Brandao, F.: Integrated control methodologies for road vehicles. Vehicle System Dynamics 40, 157–190 (2003)
5. Gustafsson, F.: Slip-based tire-road friction estimation. Automatica 33(6), 1087–1099 (1997)
6. Gáspár, P., Németh, Z., Bokor, J.: Design of integrated vehicle control using driver models. In: IFAC Symposium on Robust Control Design, Aalbord, Denmark, pp. 1–6 (2012)
7. Gáspár, P., Szabó, Z., Bokor, J.: Estimation of the friction coefficient for road vehicles. In: American Control Conference, pp. 1–6 (2005)
8. Gáspár, P., Szabó, Z., Bokor, J., Sename, O., Dugard, L.: Design of a reconfigurable global chassis control. In: FISITA Congress, Budapest, pp. 1–6 (2010)
9. Gáspár, P., Szászi, I., Bokor, J.: Reconfigurable control structure to prevent the rollover of heavy vehicles. Control Engineering Practice 13(6), 699–711 (2005)
10. Jianyong, W., Houjun, T., Shaoyuan, L., Wan, F.: Improvement of vehicle handling and stability by integrated control of four wheel steering and direct yaw moment. In: Proc. 26th Chinese Control Conference, Zhangjiajie, pp. 1–6 (2007)
11. Kanev, S., Verhaegen, M.: Controller reconfiguration for non-linear systems. Control Engineering Practice 8, 1223–1235 (2000)
12. Kiencke, U., Nielsen, L.: Automotive control systems. for engine, driveline and vehicle. Springer (2000)
13. Kim, D., Peng, H., Bai, S., Maguire, J.: Control of integrated powertrain with electronic throttle and automatic transmission. IEEE Trans. Control Systems Technology 15(3), 474–482 (2007)

14. Langbort, C., Chandra, R.S., D'Andrea, R.: Distributed control design for systems interconnected over an arbitrary graph. IEEE Transactions on Automatic Control 49(9), 1502–1519 (2004)
15. Lu, J., Messih, D., Salib, A., Harmison, D.: An enhancement to an electronic stability control system to include a rollover control function. SAE Transactions 2007-01-0809 116, 303–313 (2007)
16. Mastinu, G., Babbel, E., Lugner, P., Margolis, D.: Integrated controls of lateral vehicle dynamics. Vehicle System Dynamics 23, 358–377 (1994)
17. Muenchhof, M., Beck, M., Isermann, R.: Fault-tolerant actuators and drives structures, fault detection principles and applications. Annual Reviews in Control 33, 136–148 (2009)
18. Ono, E., Hattori, Y., Muragishi, Y., Koibuchi, K.: Vehicle dynamics integrated control for four-wheel-distributed steering and four-wheel-distributed traction/braking systems. Vehicle System Dynamics 44(2) (2006)
19. Pacejka, H.B.: Tyre and vehicle dynamics. Elsevier Butterworth-Heinemann, Oxford (2004)
20. Packard, A., Balas, G.: Theory and application of linear parameter varying control techniques. In: Proc. of the American Control Conference, Albuquerque, New Mexico (1997)
21. Palkovics, L., Fries, A.: Intelligent electronic systems in commercial vehicles for enhanced traffic safety. Vehicle System Dynamics 35, 227–289 (2001)
22. Poussot-Vassal, C., Sename, O., Dugard, L., Gáspár, P., Szabó, Z., Bokor, J.: Attitude and handling improvements trough gain-scheduled suspensions and brakes control. Control Engineering Practice 19, 252–263 (2011)
23. Rajamani, R., Tan, H., Law, B., Zhang, W.: Demonstration of integrated longitudinal and lateral control for the operation of automated vehicles in platoons. IEEE Transactions on Control Systems Technology 8, 695–708 (2000)
24. Trachtler, A.: Integrated vehicle dynamics control using active brake, steering and suspension systems. International Journal of Vehicle Design 36, 1–12 (2004)
25. Wang, Y., Nagai, M.: Integrated control of four-wheel-steer and yaw moment to improve dynamic stability margin. In: Proc. 35th Conference on Decision and Control, Kobe, pp. 1–6 (1996)
26. de Wit, C.C., Tsiotras, P., Claeys, X., Yi, J., Horowitz, R.: Friction tire/road modelling, estimation and optimal braking control. In: Johansson, Rantzer (eds.) Nonlinear and Hybrid Systems in Automotive Control, pp. 125–146 (2003)
27. Wu, F.: A generalized LPV system analysis and control synthesis framework. International Journal of Control 74, 745–759 (2001)
28. Wu, F., Yang, X., Packard, A., Becker, G.: Induced L_2 norm controller for LPV systems with bounded parameter variation rates. International Journal of Robust and Nonlinear Control 6, 983–988 (1996)
29. Yu, F., Li, D., Crolla, D.: Integrated vehicle dynamics control: State-of-the art review. In: IEEE Vehicle Power and Propulsion Conference, Harbin, China, pp. 1–6 (2008)
30. Zhang, S., Zhang, T., Zhou, S.: Vehicle stability control strategy based on active torque distribution and differential braking. In: Int. Conference on Measuring Technology and Mechatronics Automation, pp. 1–6 (2009)
31. Zin, A., Sename, O., Gáspár, P., Szabó, Z., Dugard, L., Bokor, J.: An LPV/Hinf active suspension control for global chassis technology: Design and performance analysis. Vehicle System Dynamics 46, 889–912 (2008)

Chapter 9
Global Chassis Control Using Coordinated Control of Braking/Steering Actuators

Charles Poussot-Vassal, Olivier Sename, Soheib Fergani,
Moustapha Doumiati, and Luc Dugard

Abstract. Automotive light vehicles are complex systems involving many different dynamics. On one side, vertical, roll and pitch behaviours are often related to comfort performances (indeed, roll is also linked to safety characteristics [23]). On the other hand, safety performances are mainly characterized by the longitudinal, lateral and yaw dynamics [38, 14]. In practice, these two behaviours are often treated in a decoupled may (the first dynamics are often related to suspensions systems while the second one to steering and braking systems). This chapter focuses on the safety problem, and more specifically, on lateral and yaw dynamics. It presents two close techniques to design robust gain-scheduled $\mathscr{H}_\infty$ MIMO VDSC (Vehicle Dynamic Stability Controller), involving both steering and rear braking actuators. Both approaches aim at restoring the yaw rate of the vehicle as close as possible to the nominal motion expected by the driver. The specific framework of each of that approaches is given below.

- First, a methodology allowing to synthesize such a controller while taking into account *the braking actuator limitations and involving the steering actuator only if it is necessary*, is presented. The proposed solution is coupled with a local ABS strategy to guarantee slip stability and make the solution complete. The originality relies on the LPV formulation of the *saturation-like* function of the allowable braking force directly during the synthesis step.

Charles Poussot-Vassal
Onera - The French Aerospace Lab, F-31055 Toulouse, France
e-mail: Charles.Poussot-Vassal@onera.fr

Olivier Sename · Soheib Fergani · Luc Dugard
GIPSA-Lab, Control Systems Dept, CNRS-Grenoble INP, ENSE3, BP 46,
F-38402 St Martin d'Hères cedex, France
e-mail: olivier.sename@gipsa-lab.grenoble-inp.fr

Moustapha Doumiati
Fahad Bin Sultan University, Department of Electrical Engineering,
Tabuk, Kingdom of Saudi Arabia

O. Sename et al. (Eds.): *Robust Control and LPV Approaches*, LNCIS 437, pp. 237–265.
DOI: 10.1007/978-3-642-36110-4_9

- Secondly, the control design methodology aims at using the steering action to control the yaw rate and at limiting the use of the braking actuator only when the vehicle goes toward instability. Judging the vehicle stability region is done from the phase-plane of the side-slip angle and its time derivative, which is used to monitor the car dynamical behaviour.

These controllers are both treated in an original way by the synthesis of a parameter dependent controller built in the LPV framework and by the solution of an LMI problem. Nonlinear time and frequency domain simulations, performed on a complex full vehicle model (which has been validated on a real car), subject to critical driving situations, show the efficiency and robustness of the proposed solutions.

9.1 Introduction

A trend in modern vehicles is the application of active safety systems to improve vehicle handling, stability and comfort. Nowadays, many advanced active chassis control systems have been developed and brought into the market: *e.g.*, *ABS* (Anti-lock Braking System) prevents wheel lock-up, and *ESC* (Electronic Stability Control) enhances vehicle lateral stability. The development of chassis control systems is still the object of intense research activities from both industrial and academic sides. The various vehicle dynamics control systems can be classified into two areas: *(i)* on one side, vertical, roll and pitch behaviours are often related to comfort performances (indeed, roll is also linked to safety characteristics [23]), *(ii)* on the other hand, safety performances are mainly characterized by the longitudinal, lateral and yaw dynamics. In practice, these two behaviours are often treated in a decoupled may (the first dynamics are often related to suspensions systems while the second one to steering and braking systems). This chapter focuses on the safety problem, and more specifically, on lateral and yaw dynamics.

Longitudinal vehicle behaviours have been and still are widely studied trough the rotational wheel and slip dynamic control, leading to the development of ABS strategies [13, 29, 40, 44]; concerning the lateral and yaw behaviours, related to handling and safety performances, many papers involve steering control [2, 17, 47, 27, 32, 39] or braking control [10, 22]. Since the last decade, the tendency is now to use both actuators [1]. Indeed, collaborative control of different kind of actuators is an issue in global chassis control and safety improvements [24, 11, 21].

More specifically, in [7, 38], authors show that the join use of the braking and steering systems highly enhances lateral performances and ground vehicles safety properties. In this joint perspective, recent developments mostly involve MPC [18, 17, 10] or nonlinear [3] techniques which often result to be highly demanding from a computational point of view. Within the linear framework, the following limitations are rarely considered during the synthesis step:

- Braking system, which can only deliver positive torque, is usually treated as a differential braking system, and thus requires a torque dedicated braking force repartition. This point, among others, is more specifically treated in the first approach (**Method 1**).

- Even if the braking system greatly enhances the vehicle dynamical behaviour, it is unlikely for the driver, and quite inefficient due to the induced loss of energy (*i.e.* deceleration). As a consequence, braking actuator should act only in emergency cases [16, 14]. This point, among others, is treated in the second approach (**Method 2**).
- Additionally, in order to not reduce the impact of the steering action of the driver feelings, this actuator should act only over a given frequency range (see [27]). This point is handled in both approaches (**Method 1** and **Method 2**)

This chapter aims to cope with these requirements, introducing two original LPV formulations, based on very recent results (see [38, 14]). The interest of both proposed VDSC, including controller and monitors, is that they provide a hierarchy to the local controllers and actuators. Indeed, the VDSC is to be used as a higher level controller to provide references to local controllers (as illustrated in Figure 9.1).

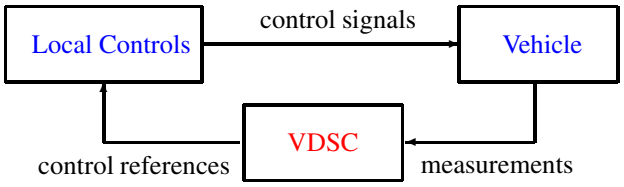

Fig. 9.1 Simplified control scheme

Throughout the chapter, the following standard notations will be adopted: $A+\star^T$ stands for $A+A^T$, the LPV induced $\mathscr{L}_2$ to $\mathscr{L}_2$ norm will be denoted, with a slight abuse, as the $\mathscr{H}_\infty$ norm. The index $i=\{f,r\}$ and $j=\{l,r\}$ are used to identify vehicle front, rear and left, right vehicle corner positions, respectively. Table 9.1

Table 9.1 Linear bicycle Renault Mégane Coupé parameters

Symbol	Value	Unit	Meaning
m	1535	kg	vehicle mass
m_r	648.3	kg	vehicle rear mass
I_z	2149	$kg.m^2$	vehicle yaw inertia
C_f	40000	N/rd	linear lateral tire front cornering stiffness
C_r	40000	N/rd	linear lateral tire rear cornering stiffness
l_f	1.4	m	distance COG - front axle
l_r	1	m	distance COG - rear axle
t_r	1.4	m	rear axle length
R	0.3	m	tire radius
$T_{b_{max}}$	1200	Nm	maximal braking value
g	9.81	m/s^2	gravitational constant
μ	$[2/5;1]$	–	tire/road contact friction interval
v	$[50;120]$	km/h	vehicle velocity interval

summarizes the notations and values used to define the linear bicycle model. Parameters and full description of the complete full nonlinear model are given in [35].

9.2 Simulation Model: Full Vehicle

In this chapter, the full vehicle model presented in [35] is used for simulation and validation purpose. This model and its parameters have been validated on a real Renault Mégane vehicle[1]. For sake of space limitations, the complete model is not given here but the dynamics are simply recalled. Interested reader should refer to [35, 16] for more details on parameters and model validation using real experiments.

It is to be kept in mind that the main interest in using the full nonlinear vehicle model is that is allows to take into consideration load transfer, fast dynamics entering in the tire force description, and consequently, in the global chassis dynamics, in a nonlinear fashion. These considerations are of particular interest, especially when dangerous driving situations are simulated.

This full vehicle model reproduces the longitudinal (x_s), lateral (y_s), vertical (z_s), roll (θ), pitch (ϕ) and yaw (ψ) dynamics of the chassis. It also models the vertical and rotational motions of the wheels ($z_{us_{ij}}$ and ω_{ij}, respectively), the slip ratios (λ_{ij}) and the centre of gravity side slip angle (β) dynamics as a function of the nonlinear tires and suspensions forces. Then, $T_{b_{rj}}$ ($j = \{l, r\}$ left, right), M_{dx}, M_{dy}, M_{dz}, F_{dx}, F_{dy} and F_{dz} are the rear braking torques input, the roll, pitch and yaw moments, longitudinal, lateral and vertical load disturbances respectively. Figure 9.2 recalls theses dynamics.

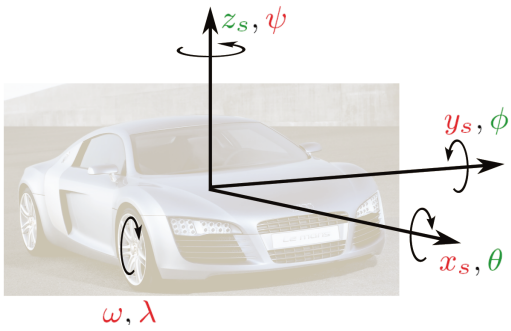

Fig. 9.2 Full vehicle dynamics

9.3 Synthesis Model: Bicycle and Actuators

The previous model will be used later in Section 9.8 to evaluate the controller performances on a faithful model of the vehicle. In this Section, the model used for both

[1] Thanks to M. Basset, G. Pouly and C. Lamy, from the MIAM research team for their kind help in the validation phase.

different control synthesis is presented together with the considered actuators. This model is a modified version of the bicycle model (as the one described in [2, 32]).

9.3.1 Extended Bicycle Model

Since the method presented in this chapter aims at improving vehicle safety properties in critical situations in order to avoid loss of manoeuvrability, the main nonlinear dynamics under interest are the vehicle side-slip (β) and yaw (ψ) dynamics, governed by the following equations:

$$\begin{cases} mv\dot{\beta} = F_{ty_f} + F_{ty_r} + mv\dot{\psi} \\ I_z\ddot{\psi} = l_f\big(-F_{tx_f}\sin(\delta) + F_{ty_f}\cos(\delta)\big) - l_rF_{ty_r} - \Delta F_{tx_r}t_r + M_{dz} \end{cases} \tag{9.1}$$

where $F_{ty_f} = F_{ty_{fl}} + F_{ty_{fr}}$, $F_{ty_r} = F_{ty_{rl}} + F_{ty_{rr}}$ and $\Delta F_{tx_r} = F_{tx_{rl}} - F_{tx_{rr}}$ are the front, rear tire lateral forces and longitudinal rear differential forces, respectively. In the real case, these forces are highly nonlinear and depend, among other, on the side-slip angle (β) and the slip ratio (λ) dynamics. $v = \sqrt{\dot{x}_s^2 + \dot{y}_s^2}$ denotes the longitudinal vehicle speed, m, the vehicle total mass and I_z, the vehicle inertia along the z-axis. ΔF_{tx_r}, the differential rear braking force, depends on the rear braking torques $T_{b_{rj}}$. δ and M_{dz} denote the steering angle and the yaw moment disturbance, respectively. More specifically, $\delta = \delta^d + \delta^+$, where δ^d is the angle provided by the driver and δ^+, the additive steering angle provided by the controller (to be designed). Assuming that low slip value are preserved[2], ΔF_{tx_r} may be rewritten as,

$$\Delta F_{tx_r} = F_{tx_{rl}} - F_{tx_{rr}} = \frac{\mu R m_r g}{2}(T_{b_{rl}} - T_{b_{rr}}) \tag{9.2}$$

where m_r is the rear vehicle mass and g is the gravitational constant. Consequently, (9.1) can be rewritten as follows,

$$\begin{cases} mv\dot{\beta} = F_{ty_f} + F_{ty_r} + mv\dot{\psi} \\ I_z\ddot{\psi} = l_f\big(-F_{tx_f}\sin(\delta) + F_{ty_f}\cos(\delta)\big) - l_rF_{ty_r} - \dfrac{\mu R m_r g}{2}(T_{b_{rl}} - T_{b_{rr}})t_r + M_{dz} \end{cases} \tag{9.3}$$

As long as the proposed design is achieved in the linear control framework, the linear bicycle model (9.4), denoted Σ, obtained from linearization of (9.3) for nominal velocity and assuming,

- low sideslip angles: $|\beta| < 7\text{deg}$
- low longitudinal slip ratios: $|\lambda| < 0.1$
- low steering angles: $\cos(\delta) \simeq 1$

is given as follows:

[2] This assumption is consistent when the vehicle is controlled since the objective is to keep, as much as possible, the vehicle in the linear stability region.

$$\begin{bmatrix}\dot{\beta}\\ \ddot{\psi}\end{bmatrix}=\begin{bmatrix}\mu\dfrac{-C_f-C_r}{mv} & 1+\mu\dfrac{l_rC_r-l_fC_f}{mv^2}\\ \mu\dfrac{l_rC_r-l_fC_f}{I_z} & \mu\dfrac{-l_f^2C_f-l_r^2C_r}{I_zv}\end{bmatrix}\begin{bmatrix}\beta\\ \dot{\psi}\end{bmatrix}+\begin{bmatrix}\dfrac{C_f}{mv} & 0 & 0 & 0\\ \dfrac{l_fC_f}{I_z} & \dfrac{1}{I_z} & -\dfrac{\mu m_r g R t_r}{2I_z} & \dfrac{\mu m_r g R t_r}{2I_z}\end{bmatrix}\begin{bmatrix}\delta\\ M_{dz}\\ T_{b_{rl}}\\ T_{b_{rr}}\end{bmatrix} \tag{9.4}$$

For synthesis purpose, $v = 30$m/s and $\mu = 1$. In the validation section, other conditions will be considered to show that performances are maintained and emphasize the inherent robustness of the control schemes.

9.3.2 Actuator Models

In this chapter, two kinds of actuators are considered:

- As braking system, EMB actuators, providing a continuously variable braking torque, are considered. The corresponding model is given by:

$$\dot{T}_{b_{rj}} = 2\pi\varpi(\widetilde{T^*_{b_{rj}}} - T_{b_{rj}}) \tag{9.5}$$

$$\mathcal{T}_b \subseteq \{T_b \in \mathbb{R} : 0 \leq T_b \leq T_{b_{max}}\} \tag{9.6}$$

  where, $\varpi = 10$Hz is the actuator cut-off frequency, $\widetilde{T^*_{b_{rj}}}$ and $T_{b_{ij}}$ are the local braking controller and actuator outputs, respectively. $T_{b_{max}}$ is the maximal torque allowed by the considered braking actuator. The first relation defines the actuator linear dynamics while the second one defines the brake nonlinear limitations (saturation).
- As active steering system (AS), an active actuator providing an additional steering angle is considered. Such actuator is modeled as:

$$\dot{\delta}^+ = 2\pi\kappa(\delta^* - \delta^+) \tag{9.7}$$

  where, $\kappa = 10$Hz is the actuator cut-off frequency, δ^* and δ^+ are the steering controller and actuator outputs respectively.

9.4 Proposed VDSC Overview and Generalized Plants

9.4.1 Global Control Architecture

In this Section, the problem formulation of the VDSC synthesis of this chapter is presented. First, the performance objectives and the global control scheme (architecture of the control structure) are given, then, the generalized control scheme together with the particular controller structure are described. Following the requirements presented in the introduction section, the general control structure shown in Figure 9.3 aims at:

1. reducing the yaw rate error w.r.t. a reference provided by a reference model (which is a bicycle model where parameters may be adjusted in order to obtain comfort or sport driving performances), without using the side-slip measurement (practically badly known),
2. ensuring that the braking control signal can always be achieved by the considered actuators,
3. enhancing the system performances in critical situation (low road adhesion) or in actuator failure cases,

Note that this scheme will be used later for nonlinear validations in Section 9.8.

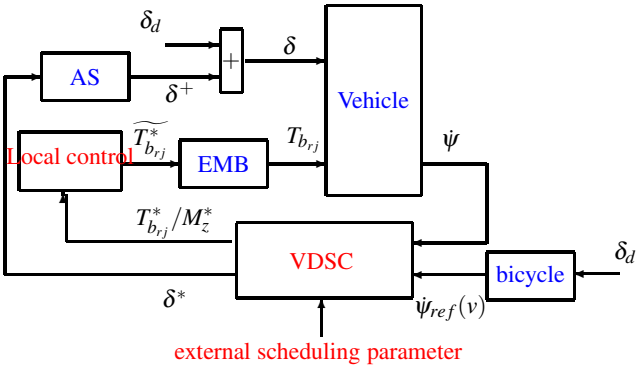

Fig. 9.3 Global control scheme

With reference to Figure 9.3 the proposed global control structure includes the following blocks:

- **Vehicle** is the full nonlinear vehicle (see Section 9.2).
- **Bicycle & Actuators (AS & EMB)** are the nonlinear bicycle and actuator models (see Section 9.3).
- **VDSC** is the proposed braking and steering controller, synthesized either with Method 1 or 2, providing the desired braking torque $T^*_{b_{rj}}$ (when Method 1) or a stabilizing moment $M^*_{d_z}$ (when Method 2) and the additive steering angle δ^*. It is fed by $e_{\dot{\psi}} = \dot{\psi}_{ref}(v) - \dot{\psi}$ and scheduled by:
  - (Method 1) ρ_1, the steering monitoring parameter, and ρ_2, a braking torque parameter which is calculated based on $e_{\dot{\psi}}$ measurement, ensuring the braking torque saturation (i.e. positivity of the torque).
  - (Method 2) ρ, a braking activation parameter, which allows to activate the braking system only in emergency situations.

  $\dot{\psi}_{ref}(v)$ is obtained by a simple bicycle model similar to the one presented in Section 9.3, equation (9.3), function of the vehicle velocity, and parametrized as a neutral vehicle.

- **ABS** is the local ABS control, implemented on each of the rear wheels, that is activated to avoid slipping, providing $\widetilde{T^*_{b_{rj}}}$, the braking torque, according to the set point $T^*_{b_{rj}}$ given by the VDSC controller (this design is based on recently published results, see [44]).

9.4.2 Generalized Control Schemes Σ_g^1 and Σ_g^2

To synthesize the so called gain-scheduled VDSC, the $\mathscr{H}_\infty$ tuning approach is used. Figure 9.4 presents in a schematic way the generalized plants Σ_g^1 and Σ_g^2, used for the synthesis of the gain-scheduled controllers $K_1(\rho_1,\rho_2)$ and $K_2(\rho)$, respectively. Indeed, in this section, two different generalized plants are presented to achieve the stability performances.

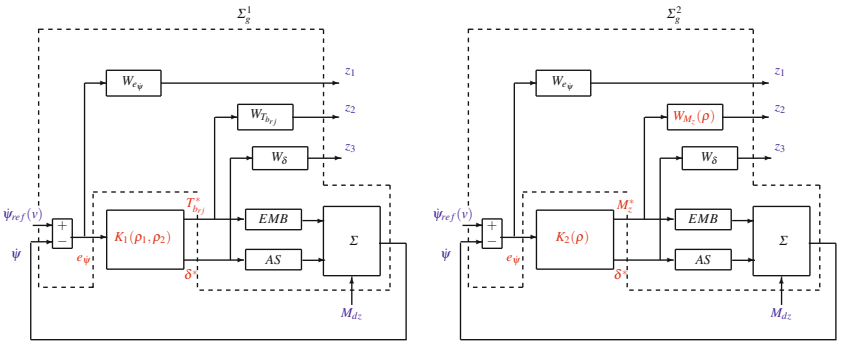

Fig. 9.4 Generalized plant models (left: Method 1, right: Method 2)

According to the standard problem depicted in Figure 9.4 the following systems and signals are defined, characterizing the performance objectives and actuator frequency limitations:

- Σ, EMB and AS stand for the extended bicycle (9.4), braking (9.5) and steering (9.7) actuators models, respectively.
- $K_1(\rho_1,\rho_2)$ (left, Method 1) and $K_2(\rho)$ (left, Method 2) are the gain-scheduled controller to be synthesized (see next subsection).
- z_1, yaw rate error exogenous output signal, is the output of the tracking error performance, weighted by:

$$W_{e_\psi} = \frac{1}{2G_e}\frac{sG_e/2\pi f_1 + 1}{s/2\pi f_1 + 1} \tag{9.8}$$

where $f_1 = 1$Hz is the cut-off frequency of the high pass filter. $G_e = 0.1$ is the attenuation level for low frequencies ($f < f_1$); in this case 0.1 means that the static tracking error should be lower than 10%.

- z_2, the exogenous braking (or moment) control signal attenuation, is the output of the braking control, weighted by:

$$\begin{aligned} W_{T_{b_{rj}}} &= G_T \frac{s/2\pi f_2 + 1}{s/\alpha 2\pi f_2 + 1} \quad (Method1) \\ W_{M_z}(\rho) &= \rho \frac{s/(2\pi f_2) + 1}{s/(\alpha 2\pi f_2) + 1} \quad (Method2) \end{aligned} \tag{9.9}$$

  where $f_2 = 10$Hz and $\alpha = 100$ are the braking actuator bandwidth and the roll-off parameters, respectively. These parameters are chosen to handle the dynamical braking actuator limitations. $G_T = 10^{-4}$ is the allowed amplification gain of the control input which is given to avoid high variations in the control signal. $W_{M_z}(\rho)$ is linearly parametrized by the considered varying parameter $\rho(.)$, where $\rho \in \left\{ \underline{\rho} \leq \rho \leq \overline{\rho} \right\}$ (with $\underline{\rho} = 10^{-5}$ and $\overline{\rho} = 10^{-3}$). Then, when $\rho = \overline{\rho}$, the braking input is penalized, on the contrary, when $\rho = \underline{\rho}$, the braking control signal is relaxed.

  Remark 9.1. This is one of the main differences between both methods, since the braking action will be used, in the case of Method 2, only to handle critical situations.

- z_3, the exogenous steering control signal attenuation, is the output of the steering control performance, weighted by:

$$\begin{aligned} W_\delta &= G_\delta^0 \frac{(s/2\pi f_3 + 1)(s/2\pi f_4 + 1)}{(s/\alpha 2\pi f_4 + 1)^2} \\ G_\delta^0 &= G_\delta \frac{(\Delta_f/\alpha 2\pi f_4 + 1)^2}{(\Delta_f/2\pi f_3 + 1)(\Delta_f/2\pi f_4 + 1)} \\ \Delta_f &= 2\pi(f_4 + f_3)/2 \end{aligned} \tag{9.10}$$

  where $f_4 = 10$Hz is the steering actuator bandwidth and $f_3 = 1$Hz is lower limit of the actuator intervention. This filter is designed in order to allow the steering system to act only in $[f_3 \ f_4]$ frequency range. Outside of this frequency range, the filter rolls off. Between these frequencies, and more specifically, at $\Delta_f/2$, the steering action is allowed and gain amplification is bounded by $G_\delta = 5.10^{-3}$. The interest of such a "complex" filter is to limit the steering system action in a frequency range where the driver cannot act, while handling the actuator limitations. This filter design is inspired from [27, 26] where a filter (Q) of the same shape was used to limit the steering bandwidth action. But in the latter results, the filter is added *a posteriori* and the control law only involves the steering actuator. Here the filter is directly included in the control design problem formulation.

Remark 9.2. Note that in the generalized scheme Σ_g^1 (Method 1), the control torque is controlled, while in Σ_g^2 (Method 2), the yaw moment is directly controlled. Therefore Method 2 includes a lower-level controller that distributes the torque between left/right (see section 9.7.2.2). In the former one, the rear torques are directly controlled, and saturations are handled at the synthesis step.

9.4.2.1 Method 1: Σ_g^1 and Rear Braking Saturation-Handling - Active Front Steering Controller

As rooted in the left frame of Figure 9.4, the generalized plant Σ_g^1 obtained is thus given by:

$$\Sigma_g^1 : \begin{cases} \dot{\xi}(t) = A\xi(t) + B_1 w(t) + B_2 u(t) \\ z(t) = C_1\xi(t) + D_{11} w(t) + D_{12} u(t) \\ y(t) = C_2\xi(t) + D_{21} w(t) \end{cases} \tag{9.11}$$

$$\begin{array}{rll} w(t) = [\dot{\psi}_{ref}(v)(t), M_{dz}(t)] & \text{are the exogenous input signals} \\ u(t) = [\delta^*(t), T^*_{b_{rl}}(t), T^*_{b_{rr}}(t)] & \text{are the control input signals} \\ y(t) = e_{\dot{\psi}}(t) & \text{are the signal measurement} \\ z(t) = [z_1(t), z_2(t), z_3(t)] & \text{are the controlled outputs signals} \end{array} \tag{9.12}$$

where $\xi(t)$ is the concatenation of the linearized vehicle model, actuators and weighting function state variables, which takes its values in $\Xi \in \mathbb{R}^n$, $z(t)$ the performance output which takes its values in $Z \in \mathbb{R}^{n_z}$, $w(t)$ the weighted input which takes its values in $W \in \mathbb{R}^{n_w}$, $y(t)$ the measured signal which takes its values in $Y \in \mathbb{R}^{n_y}$, $u(t)$ the control signal which takes its values in $U \in \mathbb{R}^{n_u}$. Then, $A \in \mathbb{R}^{n\times n}$, $B_1 \in \mathbb{R}^{n\times n_w}$, $B_2 \in \mathbb{R}^{n\times n_u}$, $C_1 \in \mathbb{R}^{n_z\times n}$, $D_{11} \in \mathbb{R}^{n_z\times n_w}$, $D_{12} \in \mathbb{R}^{n_z\times n_u}$, $C_2 \in \mathbb{R}^{n_y\times n}$ and $D_{21} \in \mathbb{R}^{n_y\times n_w}$ are known matrices. In this case, $n = 8$, $n_w = 2$, $n_u = 3$, $n_z = 3$ and $n_y = 1$.

Based on the generalized system Σ_g^1, let us now describe the associated specific controller structure. Usually, when lateral stability control is considered, the controller is built to get linear closed-loop performances without taking into account the fact that the braking torque must be positive. It results in a controller which may provide a negative torque (equivalent to an acceleration), which is practically impossible (except with other actuators such a motor-in-the-wheel). Therefore the braking signal is often saturated and performances are validated afterwards. Unfortunately, as illustrated in Section 9.8, this kind of design may lead to high forces and to undesirable vehicle behavior. Moreover, the steering actuator collaboration would not be appropriately used. To handle these constraints, a particular LPV controller structure is considered, as follows.

$$K(\rho_1,\rho_2) : \begin{cases} \dot{x}_c(t) = A_c(\rho_1,\rho_2)x_c(t) + B_c(\rho_1,\rho_2)e_{\dot{\psi}}(t) \\ \begin{bmatrix} \delta^*(t) \\ T^*_{b_{rl}}(t) \\ T^*_{b_{rr}}(t) \end{bmatrix} = \underbrace{\begin{bmatrix} \rho_1 & 0 & 0 \\ 0 & \rho_2 & 0 \\ 0 & 0 & 1-\rho_2 \end{bmatrix} C_c^0(\rho_1,\rho_2)}_{C_c(\rho_1,\rho_2)} x_c(t) \end{cases} \tag{9.13}$$

where $x_c(t)$, the controller state, takes its values in $\Xi_c \in \mathbb{R}^n$, $u(t) = \left[\delta^*(t)\ T^*_{b_{rl}}(t)\ T^*_{b_{rr}}(t)\right]^T$ and $y(t) = e_{\dot{\psi}}(t)$. Parameter $\rho_1 \in [0\ 1]$ is used to activate the steering action and parameter $\rho_2 \in \{0; 1\}$ aims at ensuring positive braking torque.

Remark 9.3. The specificity of this controller is that the structure is fixed, but a parameter dependency on the control output matrix is introduced. The matrix,

$$U(\rho) = \begin{bmatrix} \rho_1 & 0 & 0 \\ 0 & \rho_2 & 0 \\ 0 & 0 & 1-\rho_2 \end{bmatrix}$$

that allows for actuator distribution, is in fact connected to the 'generalized' plant (9.11) to get an LPV generalized plant that copes with the design of a polytopic controller.

9.4.2.2 Method 2: Σ_g^2 and Coordination of Rear Braking and Active Front Steering Control

As rooted right frame of Figure 9.4, the generalized plant Σ_g^2 obtained is thus given by:

$$\Sigma_g^2 : \begin{cases} \dot{\xi}(t) = A\xi(t) + B_1 w(t) + B_2(\rho)u(t) \\ z(t) = C_1(\rho)\xi(t) + D_{11}w(t) + D_{12}(\rho)u(t) \\ y(t) = C_2\xi(t) + D_{21}w(t) \end{cases} \tag{9.14}$$

$$\begin{array}{rll} w(t) = [\dot{\psi}_{ref}(v)(t), M_{dz}(t)] & \text{are the exogenous input signals} \\ u(t) = [\delta^*(t), M_z^*(t)] & \text{are the control input signals} \\ y(t) = e_{\dot{\psi}}(t) & \text{is the signal measurement} \\ z(t) = [z_1(t), z_2(t), z_3(t)] & \text{are the controlled outputs signals} \end{array} \tag{9.15}$$

where $\xi(t)$ is the concatenation of the linearized vehicle model, actuators and parameter dependent weighting function state variables, which takes its values in $\Xi \in \mathbb{R}^n$, $z(t)$ the performance output which takes its values in $Z \in \mathbb{R}^{n_z}$, $w(t)$ the weighted input which takes its values in $W \in \mathbb{R}^{n_w}$, $y(t)$ the measured signal which takes its values in $Y \in \mathbb{R}^{n_y}$, $u(t)$ the control signal which takes its values in $U \in \mathbb{R}^{n_u}$. Then, $A \in \mathbb{R}^{n\times n}$, $B_1 \in \mathbb{R}^{n\times n_w}$, $B_2 \in \mathbb{R}^{n\times n_u}$, $C_1 \in \mathbb{R}^{n_z\times n}$, $D_{11} \in \mathbb{R}^{n_z\times n_w}$, $D_{12} \in \mathbb{R}^{n_z\times n_u}$, $C_2 \in \mathbb{R}^{n_y\times n}$ and $D_{21} \in \mathbb{R}^{n_y\times n_w}$ are known matrices. In this case, $n = 8$, $n_w = 2$, $n_u = 2$, $n_z = 3$ and $n_y = 1$.

Remark 9.4. Note that matrices B_2, C_1 and D_{12} depend on ρ, which is not compatible with the requirements of the $\mathscr{H}_\infty$ synthesis for polytopic systems. However, as mentioned in [35], this assumption can be relaxed using some filter on the control input, which has been done here.

The LPV controller will be obtained in the following state space representation

$$K_z(\rho) : \begin{cases} \dot{x}_c(t) = A_c(\rho)x_c(t) + B_c(\rho)e_{\dot{\psi}}(t) \\ \begin{bmatrix} \delta^*(t) \\ M_z^*(t) \end{bmatrix} = C_c^0(\rho)x_c(t) \end{cases} \tag{9.16}$$

where $x_c(t)$, the controller state, takes its values in $\Xi_c \in \mathbb{R}^n$, $u(t) = \begin{bmatrix} \delta^*(t) \\ M_z^*(t) \end{bmatrix}$ and $y(t) = e_\psi(t)$.

Remark 9.5. It is also notable that Σ_g^1 (Method 1) is LTI (even if the actual generalized plant is LPV due to the controller distribution $U(\rho)$), while Σ_g^2 is, because of the $W_{M_{d_z}}(\rho)$ parameter dependent weighting function, LPV.

9.5 LMI-Based Polytopic $\mathscr{H}_\infty$ Controller Design

The LMI-based $\mathscr{H}_\infty$ controller design step is briefly recalled in this section. The $\mathscr{H}_\infty$ control synthesis is a disturbance attenuation problem which consists in finding a stabilizing controller that minimizes the impact of the input disturbances $w(t)$ on the controlled output $z(t)$. In the case of the LPV $\mathscr{H}_\infty$ control synthesis, this impact is measured thanks to the induced $\mathscr{L}_2$-$\mathscr{L}_2$ norm [5, 41, 20, 8].

- In Method 1, the generalized system Σ_g^1 is LPV due to the controller structure $K(\rho_1, \rho_2)$.
- In Method 2, the generalized plant is itself LPV.

To find a stabilizing controller, ensuring $\mathscr{H}_\infty$ performances, the following proposition has to be satisfied. Note that the propositions are given for the Method 1, but similar procedure can be applied to Method 2 (with $\rho_1 = \rho_2 = \rho$).

Proposition 9.1 (Feasibility - (ρ_1, ρ_2)-$\mathscr{H}_\infty$ LMI problem). *Let consider the system interconnection on Figure 9.4, where Σ_g is defined by the state space representation given in (9.11) and $\{\rho_1, \rho_2\} \in [\underline{\rho_1}\ \overline{\rho_1}] \times [\underline{\rho_2}\ \overline{\rho_2}]$. There exists a full order gain-scheduled dynamical output feedback controller ($K(\rho_1, \rho_2)$) of the form (9.13), that minimizes the LPV polytopic $\mathscr{L}_2$-$\mathscr{L}_2$ induced norm if there exist symmetric matrices $X, Y \in \mathbb{R}^{n \times n}$, full matrices*

$$\begin{array}{l} \widetilde{\boldsymbol{A}}(\underline{\rho_1}, \underline{\rho_2}), \widetilde{\boldsymbol{A}}(\overline{\rho_1}, \underline{\rho_2}), \widetilde{\boldsymbol{A}}(\underline{\rho_1}, \overline{\rho_2}), \widetilde{\boldsymbol{A}}(\overline{\rho_1}, \overline{\rho_2}) \in \mathbb{R}^{n \times n} \\ \widetilde{\boldsymbol{B}}(\underline{\rho_1}, \underline{\rho_2}), \widetilde{\boldsymbol{B}}(\overline{\rho_1}, \underline{\rho_2}), \widetilde{\boldsymbol{B}}(\underline{\rho_1}, \overline{\rho_2}), \widetilde{\boldsymbol{B}}(\overline{\rho_1}, \overline{\rho_2}) \in \mathbb{R}^{n \times n_y} \\ \widetilde{\boldsymbol{C}}(\underline{\rho_1}, \underline{\rho_2}), \widetilde{\boldsymbol{C}}(\overline{\rho_1}, \underline{\rho_2}), \widetilde{\boldsymbol{C}}(\underline{\rho_1}, \overline{\rho_2}), \widetilde{\boldsymbol{C}}(\overline{\rho_1}, \overline{\rho_2}) \in \mathbb{R}^{n_u \times n} \end{array} \tag{9.17}$$

and $\gamma \in \mathbb{R}^{+*}$ solving the following problem:

$$\begin{array}{rl} \gamma^* = \min\ \gamma & \\ \quad s.t.\ (9.19)\ |_{\underline{\rho_1}, \underline{\rho_2}} & \\ \quad s.t.\ (9.19)\ |_{\underline{\rho_1}, \overline{\rho_2}} & \\ \quad s.t.\ (9.19)\ |_{\overline{\rho_1}, \underline{\rho_2}} & \\ \quad s.t.\ (9.19)\ |_{\overline{\rho_1}, \overline{\rho_2}} & \end{array} \tag{9.18}$$

$$\begin{bmatrix} \boldsymbol{AX}+B_2\widetilde{\boldsymbol{C}}(\rho_1,\rho_2)+(\star)^T & (\star)^T & (\star)^T & (\star)^T \\ \widetilde{\boldsymbol{A}}(\rho_1,\rho_2)+A^T & \boldsymbol{YA}+\widetilde{\boldsymbol{B}}(\rho_1,\rho_2)C_2+(\star)^T & (\star)^T & (\star)^T \\ B_1^T & B_1^T\boldsymbol{Y}+D_{21}^T\widetilde{\boldsymbol{B}}(\rho_1,\rho_2)^T & -\gamma I & (\star)^T \\ C_1\boldsymbol{X}+D_{12}\widetilde{\boldsymbol{C}}(\rho_1,\rho_2) & C_1 & D_{11} & -\gamma I \end{bmatrix} \prec 0 \qquad \begin{bmatrix} \boldsymbol{X} & I \\ I & \boldsymbol{Y} \end{bmatrix} \succ 0 \tag{9.19}$$

Proposition 9.2 (Reconstruction - (ρ_1,ρ_2)-$\mathscr{H}_\infty$ LMI problem). *If Proposition 9.1 is fulfilled, $K(\rho_1,\rho_2)$ exists (Feasibility Proposition 9.1), then, the controller reconstruction is obtained by solving the following system of equations at each vertex of the polytope,* i.e.*:*

$$\begin{array}{r} \textit{solve } (9.21)\,|_{\underline{\rho_1},\underline{\rho_2}} \\ (9.21)\,|_{\underline{\rho_1},\overline{\rho_2}} \\ (9.21)\,|_{\overline{\rho_1},\underline{\rho_2}} \\ (9.21)\,|_{\overline{\rho_1},\overline{\rho_2}} \end{array} \tag{9.20}$$

$$\begin{cases} C_c(\rho_1,\rho_2) = \widetilde{C}(\rho_1,\rho_2)M^{-T} \\ B_c(\rho_1,\rho_2) = N^{-1}\widetilde{B}(\rho_1,\rho_2) \\ A_c(\rho_1,\rho_2) = N^{-1}\big(\widetilde{A}(\rho_1,\rho_2) - YAX - NB_c(\rho_1,\rho_2)C_2X \\ \qquad\qquad - YB_2C_c(\rho_1,\rho_2)M^T\big)M^{-T} \end{cases} \tag{9.21}$$

where M and N are defined such that $MN^T = I - XY$ which may be chosen by applying a singular value decomposition and a Cholesky factorization.

For further details, see the contributive work of [6, 20, 41, 42]. Note that proofs, numerical issues to improve matrix conditioning are also provided in [35].

Remark 9.6. In the case of a single parameter i.e. for Method 1, the propositions are similar, but the number of LMI sets to solve is in that case, divided by two.

9.6 Definition of the Scheduling Parameters

9.6.1 Method 1

The controller parameter used is as follows:

- $\rho_1 \in [0\ 1]$ allows to continuously (de)activates the steering action. This parameter aims at scheduling the VDSC in order to activate the steering system when required. More specifically:
  - when $\rho_1 = 0$, the $\delta^*(t)$ signal is set to zero (no steering action).
  - when $\rho_1 = 1$, the $\delta^*(t)$ signal is activated (steering action is allowed).
  - in-between values provide an intermediate steering activation. As a consequence, the steering system may be smoothly activated through this parameter.

The activating rule is not treated here, but many mechanisms may be used: e.g. a braking system fault detection (see e.g. [36]), a critical situation monitor (see e.g. [23]) or vehicle dynamics monitoring (see e.g. [19]).

- $\rho_2 \in \{0;1\}$ selects the activated braking actuator. Indeed the controller output will change according to its value (either 0 or 1). More specifically:
  - when $\rho_2 = 1$, the $T^*_{b_{rr}}(t)$ signal is set to zero (*i.e.* deactivated)
  - when $\rho_2 = 0$, the $T^*_{b_{rl}}(t)$ signal is set to zero (*i.e.* deactivated)

  To cope with the yaw rate tracking performance, the braking selection parameter ρ_2 is chosen as:

$$\rho_2(t) = \mathbf{sat}_{[0\ 1]}[\mathbf{sign}(e_{\dot{\psi}}(t))] \tag{9.22}$$

  Hence,

$$\begin{array}{l} e_{\dot{\psi}}(t) > 0 \Rightarrow \rho_2 = 1 \text{ (rear left brake is activated)} \\ e_{\dot{\psi}}(t) \leq 0 \Rightarrow \rho_2 = 0 \text{ (rear right brake is activated)} \end{array} \tag{9.23}$$

  As a matter of fact, computing ρ_2 with the rule (9.22) always ensure a positive braking signal, which is consistent with reality. This is due to the specific controller structure (9.13).

On table 9.2, the activated controller output according to the $\{\rho_1, \rho_2\}$ values is summarized.

Table 9.2 $\{\rho_1, \rho_2\}$-parameter configurations and actuators activation

ρ_1	ρ_2	Actuators activated
0	0 ($e_{\dot{\psi}}(t) \leq 0$)	$T^*_{b_{rr}}(t)$
	1 ($e_{\dot{\psi}}(t) > 0$)	$T^*_{b_{rl}}(t)$
1	0 ($e_{\dot{\psi}}(t) \leq 0$)	$\delta^*(t)$ and $T^*_{b_{rr}}(t)$
	1 ($e_{\dot{\psi}}(t) > 0$)	$\delta^*(t)$ and $T^*_{b_{rl}}(t)$

Remark 9.7. The interest of this specific LPV structure is that, at the synthesis step, the controller "knows" that only a single brake is available at each time and that the steering actuator is not always available, which allows to manage the actuator activation while guaranteeing robustness.

9.6.2 Method 2

Monitor: coordination *LPV* strategy of steering and braking actions.

As the brake-based DYC technique is not desirable in normal driving situations because of its direct influence on the longitudinal dynamics, the aim of the monitor is to minimize the use of the braking. Consequently, the braking actuators must be used only when the vehicle goes toward instability. Since vehicle stability is directly related to the sideslip motion of the vehicle, judging the vehicle stability region is derived from the phase-plane ($\beta - \dot{\beta}$) method. A stability bound defined in [28] is used here, and is formulated as:

$$\chi < 1, \tag{9.24}$$

where $\chi = \left|2.49\dot{\beta} + 9.55\beta\right|$ is the "Stability Index". Therefore, when the vehicle states move beyond the control boundaries and enter the unstable region, braking actuators will be involved to generate an additive corrective yaw moment, pulling the vehicle back into the stable region. According to [28], one of the significant benefits of this stability index is that the reference region defined in (9.24) is largely independent of the road surface conditions and hence, the accurate estimation of the road surface coefficient of friction is not required.

Remember that the control task is also supposed to provide a seamless application of the direct yaw moment control when it is required. Hence, the scheduling parameter $\rho(\chi)$ can be defined as:

$$\rho := \begin{cases} \overline{\rho} & \text{if } \chi \leq \underline{\chi} \text{ (steering control-steerability control task)} \\ \frac{\overline{\chi} - \chi}{\overline{\chi} - \underline{\chi}}\overline{\rho} + \frac{\chi - \underline{\chi}}{\overline{\chi} - \underline{\chi}}\underline{\rho} & \text{if } \underline{\chi} < \chi < \overline{\chi} \text{ (steering+braking)} \\ \underline{\rho} & \text{if } \chi \geq \overline{\chi} \text{ (steering+full braking-stability control task)} \end{cases} \tag{9.25}$$

where $\underline{\chi} = 0.8$ (user defined) and $\overline{\chi} = 1$. The control task selection is illustrated in Figure 9.5.

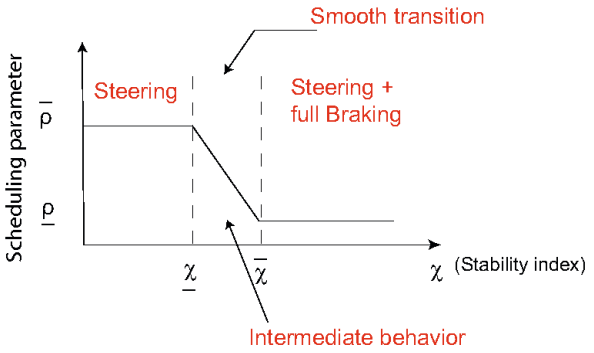

Fig. 9.5 Control task selection according to the stability index variation

Remark 9.8. To calculate the actual stability index χ defined in the previous subsection, a side-slip dynamics observer is used, to evaluate $\dot{\beta}$ and β in real-time:

- $\dot{\beta}$ can be reconstructed using available sensors, according to the following relationship:

$$\dot{\beta} = \frac{a_y}{v_x} - \dot{\psi}, \tag{9.26}$$

where a_y is the lateral acceleration and v_x is the forward vehicle speed that can be approximated by the mean of the rear wheel velocities.

- β is not available using standard sensors, and thus, it must be estimated. The "β-estimation" is widely discussed in the literature, and many papers are concerned with that topic (see [34, 30, 25, 33]). Here, the observer developed in [16, 15] has been used, which is suitable for real-time implementation.

9.7 Frequency-Domain Analysis

9.7.1 Method 1: Rear Braking Saturation-Handling and Active Front Steering Controller

In all what follows the LTI controller is referred to as the controller designed by solving the same $\mathscr{H}_\infty$ problem but choosing a linear constant controller structure, i.e $U = I_3$ for Method 1. In that case the generalized plant is LTI, therefore the control is LTI, and no specific rule is considered to schedule the use of the actuators.

9.7.1.1 Upper-Level Controller (LPV/$\mathscr{H}_\infty$ Controller Synthesis Results)

Applying Proposition 9.1 and 9.2, for $\{\rho_1, \rho_2\} = [\underline{\rho_1}\ \overline{\rho_1}] \times [\underline{\rho_2}\ \overline{\rho_2}] = [0\ 1] \times [0\ 1]$, with YALMIP parser [12] and SeDuMi solver [28] leads to the following sensitivity functions (Figures 9.6) for the LTI and LPV problem (for the LTI controller: $\gamma^* = 0.5945$, and for the LPV controller: $\gamma^* = 0.6820$).

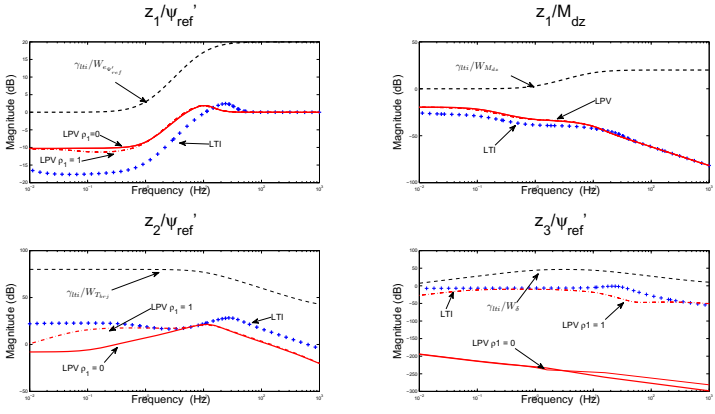

Fig. 9.6 LTI (blue dotted), LPV with $\rho_1 = 0$ (red solid) and LPV with $\rho_1 = 1$ (red dash-dotted) synthesis results. Weighting functions (black dashed)

On these Bode diagrams it is interesting to make the following remarks:

- $z_1/\dot{\psi}_{ref}$: the yaw rate error signal for both the LTI and LPV controllers is well attenuated and a small yaw rate error is guaranteed in low frequencies. Moreover the maximum peak frequency is well attenuated.
- $z_2/\dot{\psi}_{ref}$: the braking control signal rolls off after frequencies higher than f_2 (actuator bandwidth). Consequently the actuator is preserved from high frequencies.
- $z_3/\dot{\psi}_{ref}$: the steering output signal z_3 of the LPV controller is drastically varying for $\rho_1 = 0$ or $\rho_1 = 1$ configurations. Remember that when $\rho_1 = 1$ the steering system is used, while $\rho_1 = 0$ means that the steering action is forbidden. As a consequence, when $\rho_1 = 0$, the steering signal is not used. Nevertheless, when $\rho_1 = 1$, the z_3 signal of the LPV controller is very similar to the LTI one, which is also consistent with the considered performance objective.
- z_1/M_{dz}: the effects of a moment disturbance around the z axis are mitigated, ensuring the vehicle stability in critical situations (over and understeering).
- The output performance signals z_1 and z_2 are very similar between the LTI and LPV design. This remark shows that the proposed LPV design does not introduce too much conservatism (the attenuation level for the LTI controller is: $\gamma^* = 0.5945$ while the LPV controller one is: $\gamma^* = 0.6820$).
- For both LTI and LPV (when $\rho_1 = 1$) control strategies, the steering control (z_3, Figure 9.6) acts in the specified frequency range (between f_3 and f_4) in order to avoid driver unlikely interaction and preserve the actuator bandwidth.

As long as the polytopic design has been used for synthesis, the controller is implemented in the following form:

$$\begin{aligned}\left[\,\delta^*\ T^*_{b_{rl}}\ T^*_{b_{rr}}\,\right]^T &= \rho_1\rho_2 K(\overline{\rho_1},\overline{\rho_2}) + (1-\rho_1)\rho_2 K(\underline{\rho_1},\overline{\rho_2}) \\ &+ \rho_1(1-\rho_2)K(\overline{\rho_1},\underline{\rho_2}) + (1-\rho_1)(1-\rho_2)K(\underline{\rho_1},\underline{\rho_2})\end{aligned} \tag{9.27}$$

where $K(\rho_1,\rho_2)$ are the solutions of the polytopic problem (Proposition 9.1 and 9.2) evaluated at each vertex. Note that the resulting gain-scheduled controller is a convex combination of four LTI controllers of dimension $n = 8$. For implementation purpose, the discretization of the LPV controller should be applied using specific technique (see very interesting work of [46]).

9.7.1.2 Lower-Level Controller: Local ABS

Since the previous controller handles the fact that the braking torque must be positive and the actuator dynamical limits are preserved, it still does not guarantee that the slip ratio is kept low (to avoid wheel locking, leading to loss of manoeuvrability). To propose a complete solution, the local ABS strategy proposed by [40, 44] is also implemented.

This local ABS control law provides a braking torque $\widetilde{T^{ABS}_{b_{rj}}}$ ensuring the slip stability (based on sliding mode techniques). To be integrated to the proposed VDSC structure, this control law is slightly modified as:

$$\widetilde{T^*_{b_{rj}}} = \min(T^*_{b_{rj}}, \widetilde{T^{ABS}_{b_{rj}}}) \tag{9.28}$$

i.e., the braking torque reference given to the actuator is the one provided by the VDSC in all situations and the ABS one when $T^*_{b_{rj}}$ becomes too high.

9.7.2 Method 2: Coordination of Rear Braking and Active Front Steering Control

The yaw controller is designed so that the vehicle follows the reference yaw rate by driving the tracking error between the actual and desired yaw rate to zero. The control involves 2 layers:

1. The *upper-level controller* defines the amount of the active steer angle δ^*, and the corrective yaw moment M^*_z, needed to achieve a good tracking of the yaw-rate set-point.

   Note that when the vehicle operates within the “linear" region, the controller ensures steerability and only steering is used to follow the desired response. However, when the vehicle reaches the handling limits, steering and braking act together to maintain the vehicle stability.
2. The *lower-level controller* converts the stabilizing yaw moment generated by the upper-level controller into an effective braking torque, and decides which wheel must be braked to counteract the undesired yaw motion.

Remark 9.9. Notice that the main contribution is in the synthesis of the LPV upper-level controller which ensures the actuator coordination through the use of a parameter ρ depending on a stability index of the vehicle. The lower-level controller chosen here is simple and distributes efficiently the braking torque at a single wheel. However, since the yaw moment is a control input, this lower-lever controller could be replaced by more advanced strategies including control allocation [45], or some other structures such as differential braking, could be considered as proposed for instance in [12, 10, 9].

9.7.2.1 Upper-Level Controller (LPV/$\mathscr{H}_\infty$ Controller Synthesis Results)

The first step in a control design consists in defining of the control objectives. The proposed integrated control system is designed to achieve the following goals:

- Improvement of the vehicle handling and stability by:
  - making the yaw rate tracking the desired value (given in terms of the response of a bicycle model with linear tire properties);
  - making the side-slip angle small for stability.
- Coordination of Steering/braking control in order to minimize the use of braking actuators.

- Activation of steering control in a frequency band where the driver cannot act (driver comfort as in [38]).
- Rejection of yaw moment disturbances.

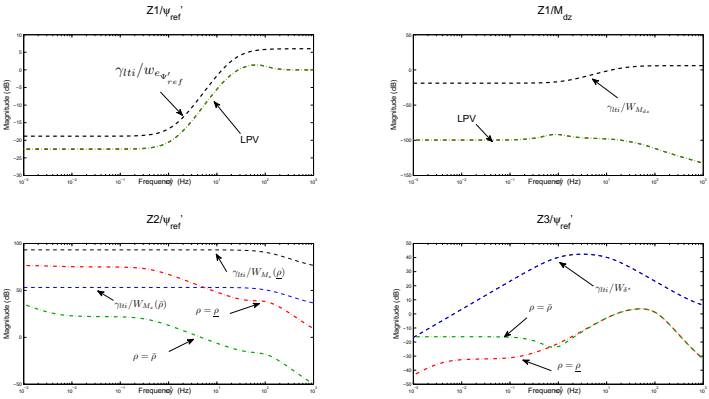

Fig. 9.7 LPV design (frozen values for $\rho = \underline{\rho}$ and $\rho = \underline{\rho}$. Weighting functions in black.

Considering the sensitivity functions Bode diagrams given in Figure 9.7 leads to the following comments:

- $z_1/\dot{\psi}_{ref}$: the yaw rate error signal, $e_{\dot{\psi}}$, is well attenuated.
- $z_2/\dot{\psi}_{ref}$: the braking control is activated for $\rho = \underline{\rho}$ and limited for $\rho = \overline{\rho}$. Note that intermediate values of $\rho \in [\underline{\rho}\ \overline{\rho}]$ give intermediate behaviours.
- $z_3/\dot{\psi}_{ref}$: the steering control is activated especially in the specified frequency range $[1\ 10]Hz$ where the driver cannot act.

9.7.2.2 Lower-Level Controller: Braking Scheme

The desired yaw moment command, M_z^*, produced by the upper-level controller can be generated by applying a torque difference between the two sides of the vehicle.

For simplicity, the quasi-static rotational dynamics of the wheel, at position $\{i, j\}$, is employed and given as:

$$T_{b,ij} = R_w F_{xij}, \tag{9.29}$$

where R_w is the effective tire radius and F_{xij}, the longitudinal tire force.

Assuming a symmetric vehicle mass distribution, the corrective yaw moment demanded by the controller can be expressed as:

$$M_z^* = \frac{t_r \Delta F_x}{2} \tag{9.30}$$

where t_r is the vehicle's rear axle length, ΔF_x is the longitudinal force between the left and right driving wheels of the same axle. Thus, the corresponding torque difference, between the left and right sides, can be expressed in terms of M_z^* and takes the form:

$$\Delta T = T_{left} - T_{right} = \frac{2M_z^* R_w}{t_r}. \tag{9.31}$$

In the following, the control law will be designed in order to select the most effective wheel to apply the brake torque, according to both following situations:

- **Understeer condition:** the absolute value of the vehicle yaw rate, $\dot{\psi}$, is always smaller than the absolute value of the desired vehicle yaw rate, $\dot{\psi}_d$. Therefore, the inner wheels will be chosen to generate a pro-cornering yaw moment.
- **Oversteer condition:** the absolute value of the vehicle yaw rate, $\dot{\psi}$, is always greater than the absolute value of desired vehicle yaw rate, $\dot{\psi}_d$. Hence, the outer wheels will be selected to generate a contra-cornering yaw moment.

In both dynamic conditions, either both wheels or one wheel (on one side) can be braked to generate M_z^*. However, from an optimal control point of view, it is recommended to use one wheel only to generate the control moment [4]. Another advantage of the scheme to apply the brake torque only at one wheel at a time, is that the vehicle is not as much decelerated as when brake torque is applied at more than one wheel to generate the same amount of yaw moment. In this study, to avoid overlapping with front steering actuators, only rear wheels are involved in the control law. Based on the above analysis and assuming counterclockwise positive, the lower-level controller law is described as follows:

$$\begin{cases} \dot{\psi} > 0, \xi > 0 \rightarrow \text{Brake rear left wheel:} & T_{brl}^* = \frac{2RM_z^*}{t_r} \\ \dot{\psi} < 0, \xi > 0 \rightarrow \text{Brake rear right wheel:} & T_{brr}^* = \frac{-2RM_z^*}{t_r} \\ \dot{\psi} > 0, \xi < 0 \rightarrow \text{Brake rear right wheel:} & T_{brr}^* = \frac{-2RM_z^*}{t_r} \\ \dot{\psi} > 0, \xi < 0 \rightarrow \text{Brake rear left wheel:} & T_{brl}^* = \frac{2RM_z^*}{t_r} \end{cases} \tag{9.32}$$

where $\xi = |\dot{\psi}_d| - |\dot{\psi}|$.

Remark 9.10. It is worth noticing that this lower level controller can be completed by the previously considered local ABS strategy.

9.8 Non Linear Simulation Results

In this section, the proposed gain-scheduled VDSC controller performances are evaluated and compared through simulations using the full vehicle nonlinear model presented in Section 9.2.

All simulations are performed on the complete nonlinear vehicle model presented in Section 9.2 and in details in [35, 16]. The implementation scheme, given on Figure 9.3, includes the ABS controller.

The scenario is the following: the vehicle runs at 90km/h on a WET road surface and the driver performs a line change manoeuvre (cf figure 9.8).

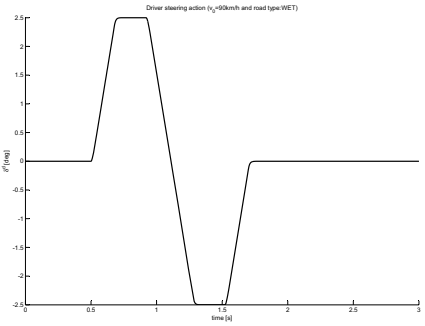

Fig. 9.8 Driver steering input signal (avoidance manoeuvre)

9.8.1 Method 1

In that case, we have chosen to compare the LPV case with $\rho_1 = 1$ (the steering actuator is active) versus the LTI one (using braking and steering actuators without coordination).

The vehicle trajectories for both simulations are given on Figure 9.9, showing that the line change is satisfactory in the LPV case, but less efficient in the LTI one.

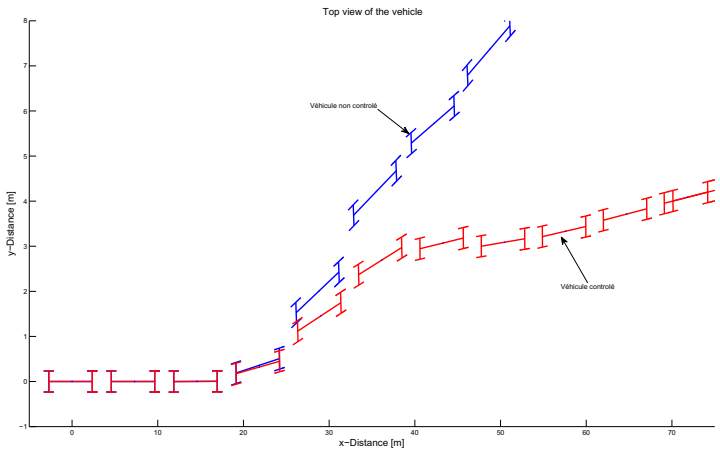

Fig. 9.9 Vehicle trajectory: Uncontrolled 'Mégane' (black), 'VDSC with steer' (red)

In Figure 9.10 it can be seen that the gain-scheduled VDSC controller shows to highly reduce the yaw rate tracking error, even more than the LTI controller.

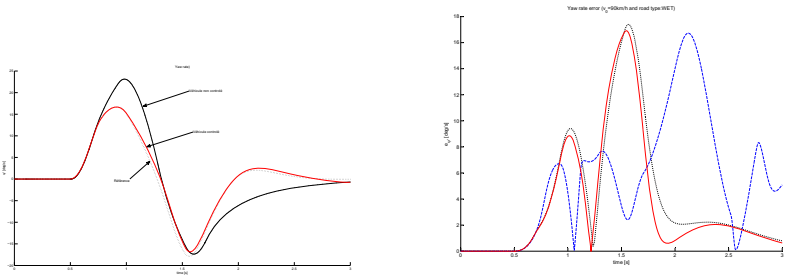

Fig. 9.10 Yaw rate and yaw rate error ($e_{\dot{\psi}}$). For the uncontrolled 'Mégane' (black pointed thin), 'LTI VDSC' (blue dashed thick), 'LPV VDSC with $\rho_1 = 1$' (red solid thick)

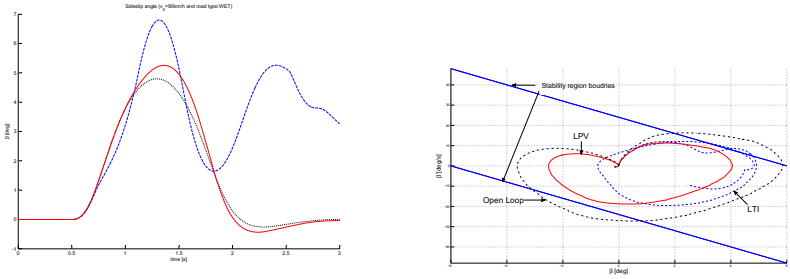

Fig. 9.11 Side slip and Evolutions of the LPV and LTI vehicle in the phase-plane $\beta - \dot{\beta}$. For the uncontrolled 'Mégane' (black pointed thin), 'LTI VDSC' (blue dashed thick), 'LPV VDSC with $\rho_1 = 1$' (red solid thick).

It is clear that the vehicle with the integrated control operates in the safety envelope defined in equation (9.24) during the whole test, while the LTI vehicle enters the critical unsafe zone.

Since the main contribution of this work concerns the controller structure which handles the brakes limitations (*i.e.* the brake saturation), the control signals are more deeply analysed. Figure 9.11 shows the ρ_2 parameter illustrating the switching mechanism, the additive steering signal (generated by the controller and provided by the actuator) as well as the braking torque signals provided by the controller.

It is also interesting to remark that the gain-scheduled VDSC left and right control torques are always positive (while the ones provided by the LTI controller do not satisfy this constraint as shown in [38]). Therefore, the LPV braking actuators are not always saturating, resulting then in an improved efficiency and avoiding a classical trial and error approach to validate the control design.

The authors stress that results founded in the literature handle this problem through a differential mechanism, while here the proposed approach is original

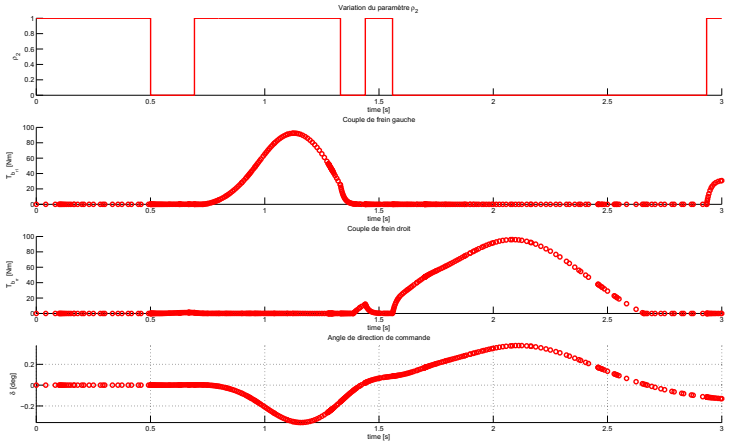

Fig. 9.12 ρ_2 parameter variation (used to ensure braking torque constraints). Control inputs δ^+, $T_{b_{rl}}^+$, $T_{b_{rr}}^+$: LPV (red), LTI (blue dotted).

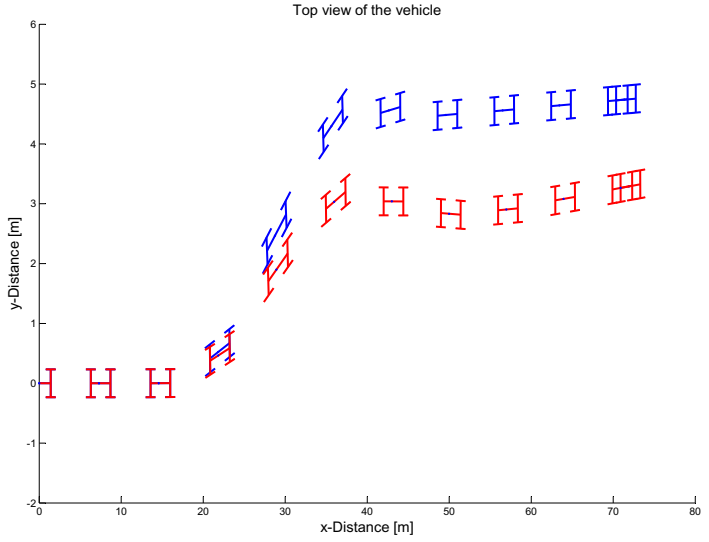

Fig. 9.13 Vehicle trajectory: LTI (blue), 'LPV VDSC' (red)

in the sense that the brakes are treated independently and the saturation effect is tackled with an original LPV design; this is a real contribution with respect to previous works, allowing different left / right brake control in complex situations.

9.8.2 Method 2

The vehicle trajectories for both simulations are given on Figure 9.13, showing that the line change is satisfactory in the LPV case, but less efficient in the LTI one.

It can be deduced that the uncontrolled vehicle becomes rather unstable as the amplitude of the steering input becomes larger. Moreover, the controlled output of the yaw rate is nearly converging to the output of the desired linear model. These results are confirmed by Figure 9.14, where the yaw rate of the uncontrolled vehicle significantly lags the desired yaw rate, while the controlled vehicle closely tracks the desired yaw response.

Comparisons between the side-slip angles and the lateral accelerations of the uncontrolled and controlled vehicles are illustrated in Figure 9.15 (left). The vehicle with integrated control achieves lower peaks for the lateral acceleration and sideslip angle in response to the steer input, compared to the uncontrolled vehicle. Consequently, the handling performances are much improved by the proposed controller. The side-slip dynamic variation is reported in the phase-plane ($\beta - \dot{\beta}$) illustrated in Figure 9.15 (right). It is clear that the vehicle with the integrated control operates in the safety envelope defined in equation (9.24) during the whole test, while the

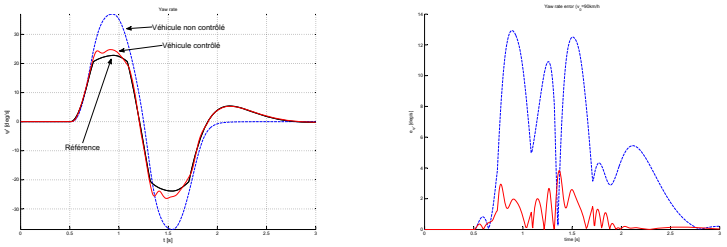

Fig. 9.14 Yaw rate and yaw rate error ($e_{\dot{\psi}}$). For the uncontrolled 'Mégane' (black pointed thin), 'LTI VDSC' (blue dashed thick), 'LPV VDSC with $\rho_1 = 1$' (red solid thick).

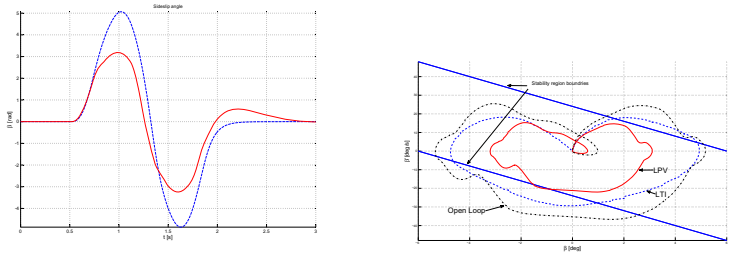

Fig. 9.15 Side slip and Evolutions of the LPV and LTI vehicle in the phase-plane $\beta - \dot{\beta}$. For the uncontrolled 'Mégane' (black pointed thin), 'LTI VDSC' (blue dashed thick), 'LPV VDSC with $\rho_1 = 1$' (red solid thick).

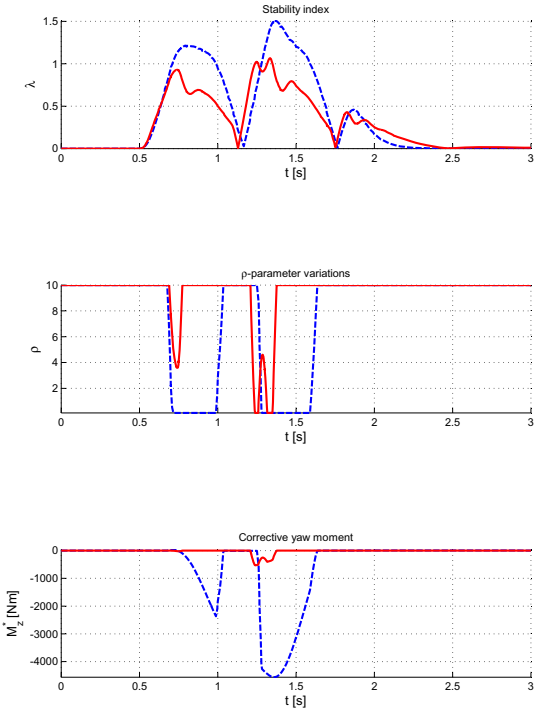

Fig. 9.16 Parameter Variation ρ as function of ξ: LPV (red), LTI (blue dotted)

passive vehicle enters the critical unsafe zone. The controlled car is then brought back to a normal driving situation.

The Figures (9.16-9.17) illustrates the *LPV* integrated control action on the vehicle behaviour. Figure 9.16 illustrates how the stability index, the dependency parameter ρ and the generated corrective yaw moment M_z^* evolve according to the driving situations. As stated before, when the stability index, χ, is below 0.8, only steering control is involved to enhance the handling performances. Indeed ρ in that case equals $\overline{\rho}$ and the corrective yaw moment is penalized and nearly zero. Conversely, when χ exceeds 0.8, the braking system acts in addition to the active steering in order to keep the vehicle stable.

Figure 9.17 shows the generated corrective steering angle and the brake torques to enhance the lateral vehicle control. It is worth noting that, despite the toughness of this test, actuators are far from saturation which may lead to instability. Also as said previously, the simple lower-level control strategy that activates the right or left braking torques could be replaced by more advanced ones since the second controller output is the yaw moment M_z^*.

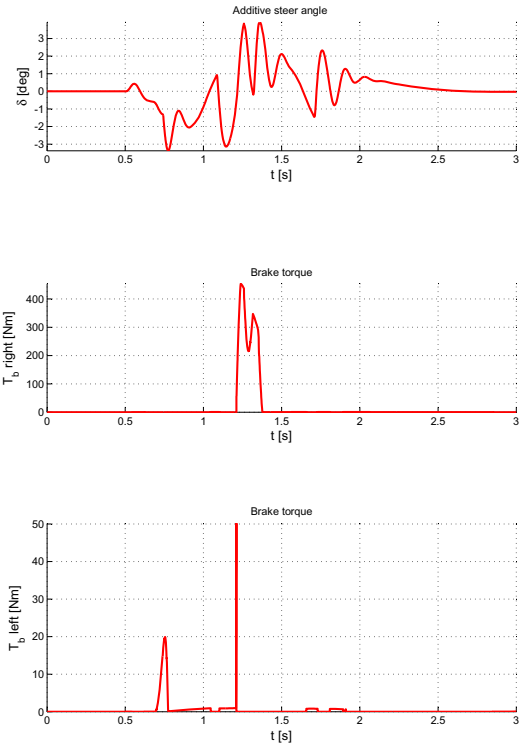

Fig. 9.17 Control signals

9.9 Conclusions and Discussions

This chapter has addressed the problem of yaw vehicle dynamical stability control, which is one of the most critical problems for light vehicles. The proposed MIMO gain-scheduled VDSC solutions involve an active steering and rear braking actuators. The main contribution and innovation are to propose two different methodologies to design controllers tacking into consideration actuator limitations and varying performance requirements, i.e.:

- The steering control only acts over a given frequency range corresponding to an action non achievable by a normal driver (frequencies > 1Hz), and limited by the steering actuator bandwidth. Additionally, while Method 2 considers a permanent use of the steering action, it can be, in the case of Method 1 smoothly activated by a simple parameter adjustment (ρ_1) in order to be used only in emergency situations (if a critical situation is detected).
- In the case of Method 1, the braking torque control signal is guaranteed to be always positive thanks to the ρ_2 parameter, adjusted according to the sign of the yaw rate error and a specific controller structure. This approach avoids, in an

original way, the usual differential braking solution used in the literature. In the case of Method 2, the considered control input is the (braking) yaw moment, and is distributed to the left/right rear wheels according to an oversteer/understeer situation. Moreover this control action is used only during temporary critical situations, evaluated thanks to a classical stability index.

The proposed design methods have been validated in simulation using a complex nonlinear vehicle model, with values identified and validated on a real vehicle, over various driving situations (with both time and frequency domain experiments). The results show the efficiency of the control approaches and also the interesting robustness properties to low road adherence and vehicle velocity variations.

References

1. Acarman, T.: Nonlinear optimal integrated vehicle control using individual braking torque and steering angle with on-line control allocation by using state-dependent Riccati equation technique. Vehicle System Dynamics 47(2), 155–177 (2009)
2. Ackermann, J., Bunte, T.: Yaw disturbance attenuation by robust decoupling of car steering. In: Proceedings of the 13th IFAC World Congress (WC), San Francisco, California, pp. 1–6 (1996)
3. Andreasson, J., Bunte, T.: Global chassis control based on inverse vehicle dynamics models. Vehicle System Dynamics 44(suppl.), 321–328 (2006)
4. Anwar, S.: Yaw stability control of an automotive vehicle via generalized predictive algorith. In: American Control Conference, Portland, USA (2005)
5. Apkarian, P., Gahinet, P.: A convex characterization of gain scheduled $\mathscr{H}_\infty$ controllers. IEEE Transaction on Automatic Control 40(5), 853–864 (1995)
6. Apkarian, P., Gahinet, P., Beker, G.: Self-scheduled $\mathscr{H}_\infty$ control of linear parameter-varying systems: A design example. Automatica 31(9), 1251–1262 (1995)
7. Baslamisli, S., Köse, I., Anlas, G.: Gain scheduled integrated active steering and active differential control for vehicle handling improvement. Vehicle System Dynamics 41(1), 99–119 (2009)
8. Bruzelius, F., Pettersson, S., Breitholz, C.: Linear parameter varying descriptions of nonlinear systems. In: Proceedings of the IEEE American Control Conference (ACC), Boston, Massachusetts, pp. 1374–1379 (2004)
9. Canale, M., Fagiano, L., Ferrora, A., Vecchio, C.: Vehicle yaw control via second order sliding mode technique. IEEE Industrial Electronics 55(11), 3908–3916 (2008)
10. Canale, M., Fagiano, L., Milanese, M., Borodani, P.: Robust vehicle yaw control using an active differential and IMC techniques. Control Engineering Practice 15(8), 923–941 (2007)
11. Chou, H., d'Andréa Novel, B.: Global vehicle control using differential braking torques and active suspension forces. Vehicle System Dynamics 43(4), 261–284 (2005)
12. Corno, M., Tanelli, M., Boniolo, I., Savaresi, S.: Advanced yaw control of four-wheeled vehicles via rear active differential brakin. In: 48th IEEE Conference on Decision and Control, Shanghai, China, pp. 5176–5181 (2009)
13. Denny, M.: The dynamics of antilock brake systems. European Journal of Physics 26, 1007–1016 (2005)

14. Doumiati, M., Sename, O., Dugard, L., Martinez-Molina, J.J., Gaspar, P., Szabo, Z.: Integrated vehicle dynamics control via coordination of active front steering and rear braking. To appear in European Journal of Control (2012)
15. Doumiati, M., Victorino, A., Charara, A., Lechner, D.: On board real-time estimation of vehicle lateral tire-forces and sideslip angle. IEEE Transactions on Mechatronics 16(4), 601–614 (2011)
16. Doumiati, M., Victorino, A., Lechner, D., Baffet, G., Charara, A.: Observers for vehicle tyre/road forces estimations: experimental validation. Vehicle System Dynamics 48(11), 1345–1378 (2010)
17. Falcone, P., Borrelli, F., Asgari, J., Tseng, H., Hrovat, D.: Predictive active steering control for autonomous vehicle systems. IEEE Transaction on Control System Technology 15(3), 566–580 (2007)
18. Falcone, P., Borrelli, F., Tseng, H., Asgari, J., Hrovat, D.: Integrated braking and steering model predictive control approach in autonomous vehicles. In: Proceedings of the 5th IFAC Symposium on Advances on Automotive Control (AAC), Aptos, California (2007)
19. Fisher, D., Borner, M., Schmitt, J., Isermann, R.: Fault detection for lateral vertical vehicle dynamics. Control Engineering Practice 15, 315–324 (2007)
20. Gahinet, P., Apkarian, P., Chilali, M.: Affine parameter-dependent Lyapunov functions and real parametric uncertainty. IEEE Transaction on Automatic Control 41(3), 436–442 (1996)
21. Gáspár, P., Szabó, Z., Bokor, J.: The design of an integrated control system in heavy vehicles based on an LPV method. In: Proceedings of the 44th IEEE Conference on Decision and Control (CDC), Seville, Spain, pp. 6722–6727 (2005)
22. Gáspár, P., Szabó, Z., Bokor, J.: Side force coefficient estimation for the design of an active brake. In: Proceedings of the IEEE American Control Conference (ACC), Mineapolis, Minesota, pp. 2927–2932 (2006)
23. Gáspár, P., Szabó, Z., Bokor, J., Poussot-Vassal, C., Sename, O., Dugard, L.: Toward Global Chassis Control by Integrating the Brake and Suspension Systems. In: Proceedings of the 5th IFAC Symposium on Advances in Automotive Control, Aptos, California, USA (2007)
24. Gáspár, P., Szaszi, I., Bokor, J.: Rollover stability control for heavy vehicles by using LPV model. In: Proceedings of the 1st IFAC Symposium on Advances in Automotive Control (AAC), Salerno, Italy (2004)
25. Grip, H., Imsland, L., Johansen, T., Fossen, T.: Nonlinear vehicle sideslip estimation with friction adaptation. Automatica 44(3), 611–622 (2008)
26. Guvenç, B., Guvenç, L., Karaman, S.: Robust yaw stability and hardware-in-the-loop testing for a road vehicle. IEEE Transaction on Control System Technology 58(2), 555–571 (2009)
27. Güvenç, B., Bünte, T., Odenthal, D., Güvenç, L.: Robust two degree-of-freedom vehicle steering controller design. IEEE Transactions on Control System Technology 12(4), 627–636 (2004)
28. He, J., Crolla, D., Levesley, M., Manning, W.: Coordination of active steering, driveline, and braking for integrated vehicle dynamics control. Proc. Inst. Mech Engineers, PartD: Automobile Engineering 220(10), 1401–1420 (2006)
29. Johansen, T., Petersen, I., Kalkkuhl, J., Ludemann, J.: Gain-scheduled wheel slip control in automotive brake systems. IEEE Transaction on Control System Technology 11(6), 799–811 (2003)
30. Lin-Hui, Z., Zhi-Yuan, L., Hong, C.: Design of a nonlinear observer for vehicle velocity estimation and experiments. IEEE Transactions on Control Systems Technology 19(3), 664–672 (2011)

31. Lofberg, J.: YALMIP: A toolbox for modeling and optimization in MATLAB. In: Proceedings of the CACSD Conference, Taipei, Taiwan (2004), http://control.ee.ethz.ch/~joloef/yalmip.php
32. Mammar, S., Koenig, D.: Vehicle handling improvement by active steering. Vehicle System Dynamics 38(3), 211–242 (2002)
33. Panzani, G., Corno, M., Tanelli, M., Zappavigna, A., Savaresi, S., Fortina, A., Campo, S.: Designing on-demand four-wheel-drive vehicles via active control of the central transfer case. IEEE Transactions on Intelligent Transportation Systems 11(4), 931–941 (2010)
34. Piyabongkarn, D., Rajamani, R., Grogg, J., Lew, J.: Development and experimental evaluation of a slip angle estimator for vehicle stability control. IEEE Transactions on Control Systems Technology 17(1), 78–88 (2009)
35. Poussot-Vassal, C.: Robust Multivariable Linear Parameter Varying Automotive Global Chassis Control. PhD thesis, Grenoble INP, GIPSA-lab, Control System dpt., Grenoble, France (2008)
36. Poussot-Vassal, C., Sename, O., Dugard, L.: A Global Chassis Controller for Handling Improvements Involving Braking and Steering Systems. In: Proceedings of the 47th IEEE Conference on Decision and Control, Cancun, Mexico, pp. 5366–5371 (2008)
37. Poussot-Vassal, C., Sename, O., Dugard, L., Gáspár, P., Szabó, Z., Bokor, J.: Attitude and handling improvements through gain-scheduled suspensions and brakes control. Control Engineering Practice 19(3), 252–263 (2011)
38. Poussot-Vassal, C., Sename, O., Dugard, L., Savaresi, S.M.: Vehicle dynamic stability improvements through gain-scheduled steering and braking control. Vehicle System Dynamics 49(10), 1597–1621 (2010)
39. Rossetter, E., Gerdes, J.: A study of lateral vehicle control under a virtual force framework. In: Proceedings of the International Symposium on Advanced Vehicle Control, Hiroshima, Japan (2002)
40. Savaresi, S., Tanelli, M., Cantoni, C.: Mixed slip-deceleration control in automotive braking systems. ASME Transactions: Journal of Dynamic Systems, Measurement and Control 129(1), 20–31 (2007)
41. Scherer, C., Gahinet, P., Chilali, M.: Multiobjective output-feedback control via LMI optimization. IEEE Transaction on Automatic Control 42(7), 896–911 (1997)
42. Shamma, J., Athans, M.: Guaranteed properties of linear parameter varying gain scheduled control systems. Automatica 27(3), 559–564 (1991)
43. Sturm, J.F.: Using SeDuMi 1.02, a MATLAB toolbox for optimization over symmetric cones. Optim. Methods Softw. 11/12(1-4), 625–653 (1999); Interior point methods
44. Tanelli, M., Sartori, R., Savaresi, S.: Combining slip and deceleration control for brake-by-wire control systems: a sliding-mode approach. European Journal of Control 13(6), 593–611 (2007)
45. Tjonnas, J., Johansen, T.: Stabilization of automotive vehicles using active steering and adaptive brake control allocation. IEEE Transactions on Control Systems Technology 18(3), 545–558 (2010)
46. Toth, R., Felici, F., Heuberger, P., der Hof, P.V.: Crutial aspects of zero-order hold LPV state-space system discretization. In: Proceedings of the 17th IFAC World Congress (WC), Seoul, South Korea (2008)
47. Villagra, J., d'Andréa Novel, B., Mounier, H., Pengov, M.: Flatness-based vehicle steering control strategy with SDRE feedback gains tuned via a sensitivity approach. IEEE Transaction on Control System Technology 15(3), 554–565 (2007)

Chapter 10
Multisensor Fault-Tolerant Automotive Control

John J. Martinez and Sébastien Varrier

Abstract. This chapter deals with the problem of obtaining fault-tolerant guarantees of a multi-sensor switching strategy for automotive control. It is assumed that each sensor (or a family of sensors) has an associated observer that performs a good estimation under normal operation conditions. In presence of sensor failures the related observer provides an estimation that is biased by signals (that often depend of the references). Since the automotive vehicle is modeled as a linear parameter varying (LPV) system by taken the vehicle speed as a scheduling parameter, the main problem concerns the computation of robustly positively invariant-sets for the state trajectories of the controlled system during fault-free operation. These invariant-sets could be used as bounds and/or thresholds for the residuals (here the tracking error estimations for instance) allowing to detect a sensor failure even in presence of nominal disturbances. The invariant-sets provide a support for fast fault-detection avoiding selecting faulty-sensors. Then, these invariant-sets together with a sensor switching mechanism allows to obtain fault-tolerant guarantees of the controlled system. Here, the proposed approach is applied for a vehicle lateral dynamics control.

10.1 Introduction

Modern automotive control applications require multiple redundance sensors to keep the driver safety. However, a sensor could fail or operate outside its specified operating conditions. In longitudinal or lateral dynamics vehicle control the sensors could be affected by traffic spray, fog, rain and/or a simple dirt on the cover. A laser scanners, for instance, can miss the object when the vehicle is pitching.

John J. Martinez · Sébastien Varrier
GRENOBLE-INP, GIPSA-lab, Département Automatique. 11 rue des Mathématiques, Grenoble Campus BP46, F-38402 Saint Martin d'Hères - Cedex France
e-mail: firstname.surname@grenoble-inp.fr

O. Sename et al. (Eds.): *Robust Control and LPV Approaches*, LNCIS 437, pp. 267–287.
DOI: 10.1007/978-3-642-36110-4_10

In heavy rain, standard laser scanners loose measurements because of raindrops even though the laser beam hits objects behind the rain curtain. Sensors works well into certain regions and environmental conditions [23]. Using faulty sensors for feedback-control, even during a few seconds, could be dangerous and the stability of the faulty system is not guaranteed. Hence, during an abrupt sensor failure, it is then very important to perform a fast Fault Detection and Isolation (FDI) and control-reconfiguration actions. The concept of virtual actuators and virtual sensors (or fault-hiding approach) require a fast reconfiguration mechanism in such a way that the fault is hidden from the nominal controller and, the fault effects are compensated [20]. In [19] the concept of virtual actuators and virtual sensors is extended from linear to PWA systems on the basis of the fault-hiding principle. These approaches suggest that a multisensor switching mechanism, as proposed in [12, 21], could be more suitable for fault-tolerant control (FTC) schemes.

Most of works in the literature solve the FDI problem by considering additive faults. However, FTC problems require more accurate faults models. In these terms, severe faults such as component failure is better represented by multiplicative models. Additive faults, when considered as pure exogenous signals, can never destabilise a stable linear closed-loop system, whereas actuator or sensor failures can very well destabilise the control-loop. This consideration shows that additive fault models do not capture the entire nature of severe faults (see for instance [14] and [19] for more details).

Recent advances in sensor technology have generated substantial research interest in developing strategies for multisensor fusion, which aim at combining data supplied by different sensors to provide more accurate and reliable information. When compared with a system employing a single sensor, a multisensor system has enhanced properties such as improved reliability and robustness, extended coverage, increased confidence, faster responses and better resolution [24]. Numerous strategies for multisensor fusion have been proposed in the literature; see, e.g. [4, 8, 10, 11, 22, 24, 25].

The use of sensor fusion estimates in feedback control systems has largely relied on ad-hoc techniques, whereby a multisensor fusion system and a controller are designed independently prior to their assembling within a feedback loop. Recent examples of this type of assembly technique have been reported for automotive applications. For instance, [7] combine a mixture Kalman filter having fault detection capabilities with an arbitrarily designed stabilising controller in a multisensor strategy for vehicle lateral control. The resulting scheme does not have pre-checkable fault tolerance guarantees but it performs well in simulations. Because the vehicle model are often written in terms of the vehicle speed (this is the case when using the classical bicycle vehicle model), LPV modeling and switched systems theory seems to be well adapted to tackle the problem of fault-tolerant control under sensors failures for automotive control applications.

This chapter deals with the problem of obtaining fault-tolerant guarantees of a multi-sensor switching strategy for automotive control. It is assumed that each sensor (or a family of sensors) has an associated observer that performs a good

estimation under normal operation conditions. In presence of sensor failures the related observer provides an estimation that is biased by signals (that often depend of the references). Since the automotive vehicle is modeled as a Linear Parameter Varying (LPV) system by taken the vehicle speed as a scheduling parameter, the main problem concerns the computation of invariant-sets for the state trajectories of the controlled system during fault-free operation. These invariant-sets could be used as bounds and/or thresholds for the residuals (here the tracking error estimations for instance) allowing to detect a sensor failure even in presence of nominal disturbances. The invariant-sets approach provides a support for fast fault-detection avoiding selecting faulty-sensors. Then, these invariant-sets together with a sensor switching mechanism allows to obtain fault-tolerant guarantees of the controlled system. Here, the proposed approach is applied for a vehicle lateral dynamics control.

10.2 Preliminaries

Consider an LPV model given by :

$$\Sigma_{LPV} : \begin{cases} x^+ = A_l(\rho)x + B_l(\rho)u \\ y = C_l(\rho)x + D_l(\rho)u \end{cases} \tag{10.1}$$

where $\rho = \begin{bmatrix} \rho_1 & \rho_2 & \cdots & \rho_n \end{bmatrix}$ stands for the scheduling parameters and where $x \in \mathbb{R}^n$ and $x^+ \in \mathbb{R}^n$ are, respectively, the current and successor system states. The system is supposed to be stable and controllable, whatever the combination of ρ.

10.2.1 Polytopic Modeling

An LPV system as given in (10.1) can be rewritten as a polytopic one in the form :

$$\Sigma_{pol} : \begin{cases} x^+ = A(\alpha)x + B(\alpha)u \\ y = C(\alpha)x + D(\alpha)u \end{cases} \tag{10.2}$$

where $X(\alpha) = \sum_{i=1}^{N} \alpha_i X(\omega_i) = \sum_{i=1}^{N} \alpha_i X_i$, ω_i representing the polytope vertices and $N = 2^n$. Moreover, it is required the further conditions :

$$\begin{aligned} \alpha_i &\geq 0 \\ \sum_{i=1}^{N} \alpha_i &= 1 \end{aligned} \tag{10.3}$$

In this case, there are N vertex systems, defined by constant matrices $(A(\omega_i), B(\omega_i), C(\omega_i), D(\omega_i))$. Polytopic coordinates α_i are enough to describe the whole system in (10.1).

The state of the system in (10.2) can be developed as :

$$x^+ = \left[\alpha_1 A_1 + \alpha_2 A_2 + \cdots + \alpha_N A_N\right] x + B(\rho)u \tag{10.4}$$

From this expression, the system can be viewed as the linear combination of LTI subsystems with one input u affecting each dynamics in matrices A_i. Notice that, even if the the global system is stable, each LTI subsystem is not necessary stable.

10.2.2 Stabilization of LTI Subsystems

In the case where the polytopic system (10.2) is not stable, we can stabilize each subsystem via the input u. Hence, the input u could be considered in the following form :

$$u = u_{stab} + w \tag{10.5}$$

where the input u_{stab} aims to stabilize each subsystems and w is the new control input of the system. It is considered the following structure for the stabilizing input u_{stab} :

$$u_{stab} = \sum_{i=1}^{N} \alpha_i \tilde{A}_i x \tag{10.6}$$

Thus, the equation (10.4) becomes :

$$\begin{aligned}
x^+ &= \sum_{i=1}^{N} \alpha_i A_i x + B(\rho)u \\
&= \sum_{i=1}^{N} \alpha_i A_i x + B(\rho)\left(u_{stab} + w\right) \\
&= \sum_{i=1}^{N} \alpha_i A_i x + B(\rho)\sum_{i=1}^{N} \alpha_i \tilde{A}_i x + B(\rho)w \\
&= \sum_{i=1}^{N} \alpha_i \underbrace{\left[A_i + B(\rho)\tilde{A}_i\right]}_{\bar{A}_i} x + B(\rho)w \\
&= \sum_{i=1}^{N} \alpha_i \bar{A}_i x + B(\rho)w
\end{aligned} \tag{10.7}$$

where each matrices $\bar{A}_i \triangleq A_i + B(\rho)\tilde{A}_i$ is stable.

From equation (10.3), as each polytopic coordinates α_i is positive and its sum is lower than 1, each coordinate is almost lower than 1. It yields that each subsystems defined via the matrix $\bar{A}_i$ is always stable whatever the parameter is. The stabilizing input u_{stab} expressed in (10.6) is computed from the polytopic formulation of the system. It can be afterward rewritten in an LPV form as:

$$u_{stab} = \sum_{i=1}^{N} \alpha_i \tilde{A}_i x$$
$$u_{stab} = \tilde{A}_i(\rho) x \tag{10.8}$$

to ease its implementation.

10.2.3 Perturbed Polytopic LPV System

In the sequel, the following stable polytopic LPV system will be considered :

$$x^+ = A(\alpha)x + B(\alpha)w \tag{10.9}$$

with

$$\begin{aligned} A(\alpha) &= \alpha_1 A_1 + \alpha_2 A_2 + \cdots + \alpha_N A_N \\ B(\alpha) &= \alpha_1 B_1 + \alpha_2 B_2 + \cdots + \alpha_N B_N \end{aligned} \tag{10.10}$$

where $\alpha_1 + \alpha_2 + \cdots + \alpha_N = 1$ and all $\alpha_i \geq 0$, $i = 1, \cdots, N$. We assume that $w \in \Delta$ is a bounded exogenous process disturbance.

Definition 10.1. The system (10.9) is robustly stable if the system's state x remains bounded in presence of bounded disturbances w.

Polytopic time-varying systems (10.9) are systems where the dynamical matrix evolves in a polytope defined by its vertices. Switched systems can be viewed as polytopic systems with the particularity that the allowable values for the dynamical matrix are those corresponding to the vertices of the polytope. Stability analysis results proposed in [2, 3], allow to find a parameter dependent Lyapunov function to check stability of polytopic time varying systems and/or linear switched systems. Nevertheless, finding a quadratic common Lyapunov function ($V := x^T P x$) of the system (10.9) is always more suitable and probably more simple for *a priori* stable matrices A_i, $i = 1, \cdots, N$. We can make use of results presented in [5] to find a quadratic common Lyapunov function. The next lemma allow to find a such Lyapunov function for a certain class of stable LPV systems and for stable arbitrary-switched linear systems.

Lemma 10.1. *The polytopic system (10.9) is robustly stable, in presence of bounded disturbances, if*

$$A_i^T P A_i - P < 0 \tag{10.11}$$

for all $i = 1, \cdots N$.

Then a single matrix P which satisfies the condition given in Lemma 10.1 may be found by the use of now standard efficient LMI tools.

Definition 10.2. (**Robust positive invariance**) The set $\Omega \in \mathbb{R}^n$ is a robustly positively invariant (RPI) set for the polytopic discrete-time system (10.9) with disturbances in Δ, if for any $x \in \mathbb{R}^n$, $k \in \mathbb{N}^+$ and any $w \in \Delta$ it holds that $x^+ \in \Omega$.

Definition 10.3. (**Ultimate boundedness**) We define that the polytopic discrete-time system (10.9) is ultimately bounded (UB) to the set Ω, if for each $x_0 \in \mathbb{R}^n$ there exists a $k^* > 0$ such that any state trajectory of (10.9) with initial condition x_0 (and any arbitrary realization of the disturbance $w : \mathbb{N} \mapsto \Delta$) satisfies $x(k) \in \Omega$ for all $k > k^*$.

10.3 Invariant-Sets Computation

10.3.1 Invariant-Sets for Subsystems

We present below a result that will allow us to compute ultimate bounds for the polytopic system's states. This result extends results presented in [9] and [21] to a class of LPV systems with constant perturbation bounds. In the sequel, $|M|$ denotes the elementwise magnitude of a (possibly complex) matrix M and $x \preceq y$ ($x \prec y$) denotes the set of elementwise (strict) inequalities between the components of the real vectors x and y.

Assumption 10.1. *Considering the matrices A_i, $i = 1, \cdots, N$, describing the polytopic system (10.9). We assume that there exist a common matrix P such that the condition (10.11) holds.*

Theorem 10.2. *Consider the robustly stable polytopic system (10.9) together with Assumption 10.1. Let $V_i D_i V_i^{-1}$ be the Jordan matrix decomposition of each A_i. Assume that, for all $\rho \in \mathbb{P}$, $|w(k)| \prec \bar{w}$ for all $k \geq 0$, where $\bar{w} \in \mathbb{R}^m$, $\bar{w} \succ 0$. In addition, take $\omega_i := |V_i^{-1} B_i \bar{w}|$. For $\varepsilon \in \mathbb{R}^n$, $\varepsilon \geq 0$, define the set*

$$\mathbf{R} \triangleq S_1 \oplus S_2 \oplus \cdots \oplus S_N \tag{10.12}$$

with

$$S_i \triangleq \left\{ x \in \mathbb{R}^n : \left| V_i^{-1} x \right| \prec (I - D_i)^{-1} \omega_i + \varepsilon \right\}. \tag{10.13}$$

for $i = 1, 2, \cdots, N$, and where $\oplus$ denotes the Minkowski sum of sets.
Then:

1. *For any subsystem $x^+ = A_i x + B_i w$, the set S_i is **robustly positively invariant**. That is, if $x(0) \in S_i$, then $x(k) \in S_i$ for all $k \geq 0$.*
2. *The set $\mathbf{R}$ is an **ultimate bound** of trajectories of the polytopic system (10.9). That is, there exists $k^* \geq 0$ such that $x(k) \in \mathbf{R}$ for all $k \geq k^*$.* ∘

Proof. Notice that we can rewrite the original polytopic system (10.9) as follows:

$$x^+ = A(\alpha)x + B(\alpha)w \tag{10.14}$$

$$x^+ = (\alpha_1 A_1 + \alpha_2 A_2 + \cdots + \alpha_N A_N)x + (\alpha_1 B_1 + \alpha_2 B_2 + \cdots + \alpha_N B_N)w \tag{10.15}$$

$$x^+ = \underbrace{(\alpha_1 A_1 x + \alpha_1 B_1 w)}_{\texttt{subsystem 1}} + \underbrace{(\alpha_2 A_2 x + \alpha_2 B_2 w)}_{\texttt{subsystem 2}} + \cdots + \underbrace{(\alpha_N A_N x + \alpha_N B_N w)}_{\texttt{subsystem N}} \tag{10.16}$$

In this way, it is possible to define a family of N independent subsystems by taken $x_i := \alpha_i x$ and $w_i := \alpha_i w$ (with $i = 1,2,\cdots,N$) as follows:

$$x_1^+ = A_1 x_1 + B_1 w_1 \tag{10.17}$$
$$x_2^+ = A_2 x_2 + B_2 w_2 \tag{10.18}$$
$$\vdots \tag{10.19}$$
$$x_N^+ = A_N x_N + B_N w_N \tag{10.20}$$
$$x = x_1 + x_2 + \cdots + x_N \tag{10.21}$$

Remark that $x_1 + x_2 + \cdots + x_N = (\alpha_1 + \alpha_2 + \cdots + \alpha_N)x = x$ because $(\alpha_1 + \alpha_2 + \cdots + \alpha_N) = 1$ and all $\alpha_i \geq 0$, $i = 1,2,\cdots,N$. In addition, $|w_i| = |\alpha_i w| \preceq |w| \preceq \bar{w}$ for a given $\bar{w} > 0$. We assume that the family of systems (10.17)-(10.20) share a common Lyapunov function. If this is not the case we can apply the Lemma 10.1 to assure that an arbitrary switching between subsystems does not affect the stability of the polytopic system.

Let $V_i D_i V_i^{-1}$ be the Jordan matrix decomposition of A_i and taking a vector $\bar{w} \succ 0$ such that $|w_i| \preceq \bar{w}$. Then, any subsystem i, with $i = 1,2,\cdots,N$ verifies:

$$x_i^+ = A_i x_i + B_i w_i \tag{10.22}$$
$$V_i^{-1} x_i^+ = V_i^{-1} A_i x_i + V_i^{-1} B_i w_i \tag{10.23}$$
$$V_i^{-1} x_i^+ = V_i^{-1} V_i D_i V_i^{-1} x_i + V_i^{-1} B_i w_i \tag{10.24}$$
$$V_i^{-1} x_i^+ = D_i V_i^{-1} x_i + V_i^{-1} B_i w_i \tag{10.25}$$
$$|V_i^{-1} x_i^+| \preceq |D_i||V_i^{-1} x_i| + |V_i^{-1} B_i \bar{w}| \tag{10.26}$$

Thus, defining the auxiliary system :

$$\xi^+ \preceq |D_i|\xi + \omega_i \tag{10.27}$$

with $\xi := |V_i^{-1} x_i|$ and $\omega_i := |V_i^{-1} B_i \bar{w}|$. Taking the fact that, by assumption, D_i has all its eigenvalues inside the unit circle, a final value bound of the state ξ (e.g. by using the *final-value theorem* for z-transforms) could be computed as

$$\xi \preceq (I - |D_i|)^{-1} \omega_i \tag{10.28}$$

and therefore, an **invariant set** of the trajectories of x_i for system (10.22) could be obtained as follows:

$$|V_i^{-1} x_i| \preceq (I - |D_i|)^{-1} \omega_i \tag{10.29}$$

Defining the set S_i, for $\varepsilon \in \mathbb{R}^n$, $\varepsilon \geq 0$, such that

$$S_i := \left\{ x_i \in \mathbb{R}^n : \left| V_i^{-1} x_i \right| \preceq (I - |D_i|)^{-1} \omega_i + \varepsilon \right\}, \tag{10.30}$$

and taking the fact that $x = x_1 + x_2 + \cdots + x_M$, an **ultimate bound** of the trajectories of the original system's state x could be obtained as follows:

$$\mathbf{R} = S_1 \oplus S_2 \oplus \cdots \oplus S_N \tag{10.31}$$

where $\oplus$ denotes the Minkowski sum of sets. The sets S_i are, by definition, convex sets and then $\mathbf{R}$ will be a convex set as well. The result then follows. □

Remark 10.1. Part 1 of Theorem 10.2 characterises invariant sets for subsystems in the state space, the smallest being the set S_i obtained by taking $\varepsilon = 0$ in (10.13). Part 2 shows that the state trajectories of the polytopic system asymptotically converge to the ultimate bound R for $\varepsilon \geq 0$ from any initial condition. In addition, for $\varepsilon > 0$, the state trajectories enter R in finite time. ○

Remark 10.2. Using the fact that, for any x, the following is true: $|x| \preceq |V||V^{-1}x|$. Then an ultimate bound for the state x_i, for $i = 1, 2, \cdots, N$, could be computed as

$$|x_i| \preceq |V_i|(I - |D_i|)^{-1}|V_i^{-1}B_i\bar{w}| \tag{10.32}$$

○

10.3.2 Refinements of Obtained Invariant-Sets

A refined invariant-set could be obtained by implementing a sequence of ε-*outer*-approximations of *Robust Positively Invariant* (RPI) sets as proposed in [15], that is, a sequence of sets can be recursively built by considering the Minkowski sum between the image of an RPI set through the linear transformation Λ and the polyhedral set $B\Delta$:

$$\Phi(h+1) = \Lambda\Phi(h) \oplus B\Delta, \quad \Phi(0) = \Psi \tag{10.33}$$

with Λ a stable matrix (all its eigenvalues inside the unit circle) and $B\Delta$ a polyhedral set which includes all the disturbances trajectories. Here $\Psi \in \mathbb{R}^n$ is a polyhedral describing an initial ultimate-bound invariant set estimation of the state trajectories which are computed using (10.13). Hence, [15] states that for any $\varepsilon > 0$ exists $h^* \in \mathbb{N}^+$ such that the following relation is true

$$\Omega \subseteq \Phi(h^*) \subseteq \Psi \tag{10.34}$$

Then, $\Phi \to \Omega$ for $h^* \to \infty$, that is,

$$\Omega \subseteq \Phi(h^*) \subseteq \Omega \oplus \mathbb{B}_p^n(\varepsilon) \tag{10.35}$$

where $\mathbb{B}_p^n(\varepsilon)$ denotes a n-dimensional ball with radius ε respect to the p-norm.

Remark 10.3. The initial set Ψ in the set recursion (10.33) can be in fact any RPI set for the dynamics (10.22). Theorem 10.2 provides a simple and direct way of obtaining the initial condition using RPI sets (10.13), in view of an algorithmic implementation. ○

Remark 10.4. The ultimate bounds of the form (10.29) have polyhedral shape if the eigenvalues of matrix A_i are real and (possibly degenerate) ellipsoidal shape

if these eigenvalues are complex (see [6] for details). For the last case, it is probably more suitable to compute an ε-*inner*-approximation (instead of an ε-*outer*-approximation) of the *Robust Positively Invariant* (RPI) set for obtaining a polyhedral set which approximates the theoretical ellipsoid. ∘

That is,

$$\Phi(h+1) = A\Phi(h) \oplus B\Delta, \quad \Phi(0) = 0 \tag{10.36}$$

and then $\Phi \to \Omega$ for $h^* \to \infty$,

$$\Phi(h^*) \subseteq \Omega \subseteq \Phi(h^*) \oplus \mathbb{B}_p^n(\varepsilon) \tag{10.37}$$

In this case the invariant set-inclusion property (10.35) is not more guaranteed [18]. However, after an important number of iterations (10.36), the obtained invariant-set is in general a good approximation of the theoretical minimal invariant-set Ω. Conditions to suitable stop the recursive equation (10.36) are presented in [17].

10.3.3 Invariant-Set Computation for Polytopic Systems

The next result allow us to compute invariant-sets for polytopic systems by making use of individuals invariant-sets S_i, $i = 1, \cdots, N$. The result allow "shrinking" the ultimate bound computed by using Theorem 10.2, and guarantees that the obtained set is an invariant-set (probably a mRPI set) of the polytopic system (10.9).

Theorem 10.3. *Consider the robustly stable polytopic system (10.9) together with Assumption 10.1. Let S_i be the mRPI sets associated to the subsystem $x^+ = A_i x + B_i w$, for $i = 1, \cdots, N$. Assume that, $w \in \Delta$, with Δ a given convex polytope. Define the set*

$$S \triangleq convex.hull\left\{\bar{S}_1, \bar{S}_2, \cdots \bar{S}_N\right\}, \tag{10.38}$$

with $\bar{S}_i = \bar{S}_i(p)$, for some value of $p \geq 0$, $p \in \mathbb{N}^+$, obtained by implemented the following sequence:

$$\bar{S}_i(p+1) = convex.hull\left\{\bigcup_{j \neq i}^{N} S_j, A_i \bar{S}_i(p) \oplus B_i \Delta\right\}, \tag{10.39}$$

where $\bar{S}_i(0) := \mu_i S_i$ with $\mu_i \geq 1$ a scaling factor (i.e. $\bar{S}_i(0) \supseteq S_i$), such that

$$\bar{S}_i \supseteq \bigcup_{j=1}^{N} S_j. \tag{10.40}$$

Then:

1. *The set S is **robustly positively invariant** set for the state-trajectories of the system (10.9). That is, if $x(0) \in S$, then $x(k) \in S$ for all $k \geq 0$.*

2. *The system (10.9) is* ***ultimately bounded*** *to the set S, i.e. there exists* $k^* \geq 0$ *such that* $x(k) \in S$ *for all* $k \geq k^*$. ○

Proof. By assumption all sets S_j, $j = 1, \cdots, N$, are (convex) invariant sets of state trajectories dictated by the dynamics $x^+ = A_j x + B_j w$. At any time $k^* > 0$, for $i = 1, \cdots, N$, the state trajectories that belong to the set S_j evolves by following a new dynamics dictated by $x^+ = A_i x + B_i w$, then the trajectories starting inside S_j will converge to the ultimate bound S_i, in finite time k_f. Therefore, the whole trajectories of the system from $k = 0$ to $k = k^* + k_f$ belong to both sets S_i and S_j. The whole set, namely $\bar{S}_i$, describes the minimal convex set containing S_i and S_j when the state trajectories evolving with dynamics $x^+ = A_i x + B_i w$. Equation (10.39) allow us to find this minimal set $\bar{S}_i$. The same analysis could be done by state trajectories starting in S_i and going to S_j. Then, the total behavior of the state trajectories can be described by the minimal convex set containing $\bar{S}_i$ and $\bar{S}_j$. Since the polytopic system is a convex combination of N subsystems, i.e. $x^+ = (\alpha_1 A_1 + \cdots + \alpha_N A_N)x + (\alpha_1 B_1 + \cdots + \alpha_N B_N)w$ (for $\sum_i^N \alpha_i = 1$, $\alpha_i \geq 0$, $i = 1, \cdots, N$), it can be shown inductively that, the state trajectories belong to the minimal convex set $S = \text{convex.hull}\left\{\bar{S}_1, \bar{S}_2, \cdots \bar{S}_N\right\}$. The result then follows. □

Remark 10.5. Part 1 of Theorem 10.3 characterises an invariant set for polytopic system (10.9) in the state space. Part 2 shows that the state trajectories asymptotically converge to the invariant set S from any initial condition. In addition, the state trajectories enter S in finite time. ○

Remark 10.6. (**Set Inclusion Condition**) Equation (10.39) characterises an invariant set $\bar{S}_i$ for the dynamics $x^+ = A_i x + B_i w$ which includes all the trajectories starting inside the invariant-set S_j. Condition (10.40). ○

10.4 Application on a Vehicle Lateral Dynamics

The vehicle model under consideration is the well known bicycle system, which dynamics is given by :

$$\begin{bmatrix} \dot{\beta}(t) \\ \ddot{\psi}(t) \end{bmatrix} = \begin{bmatrix} \frac{-(c_{\alpha V} + c_{\alpha H})}{mv(t)} & \frac{l_H c_{\alpha H} - l_v c_{\alpha V}}{mv^2(t)} - 1 \\ \frac{l_H c_{\alpha H} - l_V c_{\alpha V}}{I_z} & \frac{-(l_v^2 c_{\alpha V} + l_H^2 c_{\alpha H})}{I_z} \end{bmatrix} \begin{bmatrix} \beta(t) \\ \dot{\psi}(t) \end{bmatrix} + \begin{bmatrix} \frac{c_{\alpha V}}{mv(t)} \\ \frac{l_V c_{\alpha V}}{I_z} \end{bmatrix} u_L(t) \tag{10.41}$$

where β denotes the side slip angle, $\dot{\psi}$ the yaw rate, u_L the relative steering wheel angle and $v(t)$ the speed of the vehicle. Others symbols in (10.41) represent constant parameters of the model.

Thus, the model is converted to discrete-time according to the rectangular discretisation. Other methods should give even better results in terms of matching

errors. However this method is taken here because it preserves the linearity in the parameters. It yields a discrete time model sampled by the sampling period T_s:

$$x(k+1) = \mathscr{A}x(k) + \mathscr{B}u_L(k) \tag{10.42}$$

with

$$\begin{aligned}\mathscr{A} = &\begin{bmatrix} 1 & -T_s \\ T_s\frac{l_H c_{\alpha H} - l_V c_{\alpha V}}{I_z} & 1 \end{bmatrix} \\ &+ \frac{1}{v(k)}\begin{bmatrix} T_s\frac{-(c_{\alpha V}+c_{\alpha H})}{m} & 0 \\ 0 & -T_s\frac{l_V^2 c_{\alpha V} + l_H^2 c_{\alpha H}}{I_z} \end{bmatrix} \\ &+ \frac{1}{v(k)^2}\begin{bmatrix} 0 & T_s\frac{l_H c_{\alpha H} - l_v c_{\alpha V}}{m} \\ 0 & 0 \end{bmatrix}\end{aligned} \tag{10.43a}$$

$$\mathscr{B} = \begin{bmatrix} 0 \\ T_s\frac{l_V c_{\alpha V}}{I_z} \end{bmatrix} + \frac{1}{v(k)}\begin{bmatrix} T_s\frac{c_{\alpha V}}{m} \\ 0 \end{bmatrix}. \tag{10.43b}$$

This model can be considered as an LPV model by defining $n = 2$ scheduling parameters $\rho_1(k) \triangleq 1/v(k)$ and $\rho_2(k) \triangleq 1/v(k)^2$. Since the vehicle speed is bounded, the scheduling parameters are also bounded : $\rho_1 \in [\underline{\rho}_1 \quad \bar{\rho}_1]$ and $\rho_2 \in [\underline{\rho}_2 \quad \bar{\rho}_2]$.

This LPV model can be turned into a polytopic one by considering the dependency between each parameters ρ_1 and ρ_2. As a consequence, the parameter set, which is for instance initially composed of $2^n = 4$ vertices, can be restricted to 3 vertices as illustrated in figure 10.1. Each vertex coordinates is given by: $\omega_1 := [\underline{\rho}_1 \ \underline{\rho}_2]$; $\omega_2 := [\bar{\rho}_1 \ \underline{\rho}_2]$; $\omega_3 := [\bar{\rho}_1 \ \bar{\rho}_2]$.

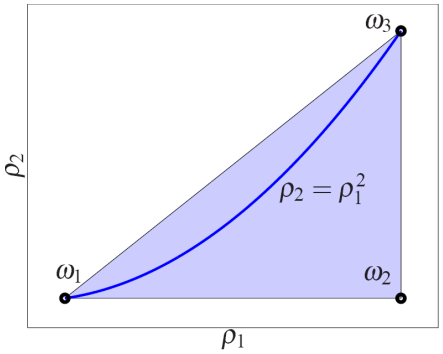

Fig. 10.1 Illustration of the schedule-parameters polytope

The polytopic coordinates could be obtained by solving the following matrix equality :

$$\underbrace{\begin{bmatrix} \underline{\rho}_1 & \bar{\rho}_1 & \bar{\rho}_1 \\ \underline{\rho}_2 & \underline{\rho}_2 & \bar{\rho}_2 \\ 1 & 1 & 1 \end{bmatrix}}_{\mathscr{M}} \begin{bmatrix} \alpha_1(k) \\ \alpha_2(k) \\ \alpha_3(k) \end{bmatrix} = \begin{bmatrix} \rho_1(k) \\ \rho_2(k) \\ 1 \end{bmatrix} \tag{10.44}$$

yielding:

$$\begin{bmatrix}\alpha_1(k)\\ \alpha_2(k)\\ \alpha_3(k)\end{bmatrix} = \mathscr{M}^{-1}\begin{bmatrix}\rho_1(k)\\ \rho_2(k)\\ 1\end{bmatrix} \tag{10.45}$$

Then, polytopic matrices A_i and B_i are obtained by evaluating the LPV matrices at each vertex of the polytope, that is

$$\begin{aligned} A_i &= \mathscr{A}(\omega_i)\\ B_i &= \mathscr{B}(\omega_i)\end{aligned} \tag{10.46}$$

It is then obtained the *polytopic* vehicle model ($T_s = 0.02s$) with matrices:

$$A_1 = \begin{bmatrix}0.9583 & -0.0197\\ 0.5973 & 0.9207\end{bmatrix} \qquad B_1 = \begin{bmatrix}0.0178\\ 0.9803\end{bmatrix}$$

$$A_2 = \begin{bmatrix}0.7914 & -0.0197\\ 0.5973 & 0.6035\end{bmatrix} \qquad B_2 = \begin{bmatrix}0.0891\\ 0.9803\end{bmatrix}$$

$$A_3 = \begin{bmatrix}0.7914 & -0.0125\\ 0.5973 & 0.6035\end{bmatrix} \qquad B_3 = \begin{bmatrix}0.0891\\ 0.9803\end{bmatrix}$$

By solving suitable LMIs, it is obtained that the systems $x^+ = A_i x$ (for $i = 1,2,3$), share a quadratic common Lyapunov function P:

$$P = \begin{bmatrix}262.0896 & 6.2394\\ 6.2394 & 14.8042\end{bmatrix}$$

Thus, the Assumption 10.1 is verified. The figure 10.2 illustrates the obtained **ultimated bound** by applying Theorem 10.2 (with refinements presented in Section) and an **invariant set** by applying Theorem 10.3 (for a normalized disturbance, i.e. $|w(k)| < 1$). In figure 10.2 it is depicted an ultimate bound **R** of the state trajectories, the invariant set S and simulated state trajectories starting at vertices (trajectories inside the set S). The curve **E** that circumscribes the set S, corresponds to a minimum volume ellipsoid around the polytope S.

The obtained polytope S has 42 sides (or faces). In order to reduce the complexity of the obtained invariant sets for real-time applications, for instance, we can make use of more simple shape approximations, as for example ellipsoidal approximations of a polytope. Such approximation could be done by finding a matrix M which solves the following problem:

$$\begin{aligned} &\texttt{maximize}(\log\det(M))\\ &\texttt{subject to } v_i^T M v_i \leq 1\end{aligned} \tag{10.47}$$

where v_i, $i = \{1, \cdots N_v\}$ stand for the N_v vertices of a given polytope S. This is in fact the problem of finding the minimum volume ellipsoid around a given polytope defined by the convex hull of vertices v_i. This ellipsoid could be described as follows:

$$\mathbf{E} \triangleq \{x : x^T M x \leq 1\}$$

Thus, by solving the problem (10.47) it is obtained the following shape matrix M:

$$M = \begin{bmatrix} 0.2821 & 0.0052 \\ 0.0052 & 0.0076 \end{bmatrix}$$

As a final remark, a less conservative invariant-set could be obtained in practice by including the actuator dynamics into the model. This fact will constraint the steering angle dynamics that is taken here as a disturbance, i.e. $w(k) = u_L(k)$ in (10.42).

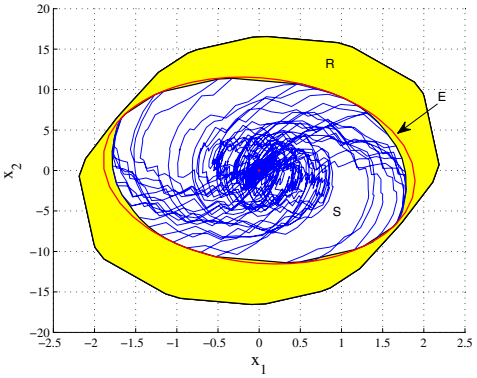

Fig. 10.2 Ultimate bound **R** and invariant set **S** of the polytopic vehicle model system

10.5 Sensor Fault-Detection Principle

Consider a linear parameter varying (LPV) system represented by the following state-space realization:

$$x^+ = A(\rho)x + B(\rho)u \tag{10.48}$$

where $x \in \mathbb{R}^n$ is the state vector and $u \in \mathbb{R}^m$ is the control input. In the above formulation, the time-varying parameter vector $\rho \in \mathbb{P}$ is assumed to be unknown a priori but can be measured or estimated in real-time. We assume that there is a stable reference dynamics that provides the desired references (as proposed in [13] for longitudinal dynamics control), i.e.

$$x_{ref}^+ = A(\rho)x_{ref} + B(\rho)u_{ref} \tag{10.49}$$

Assumption 10.4 ***(Reference bounds).*** *The reference signals u_{ref} and x_{ref} in (10.49) are bounded. In particular, constant vectors $x_{ref}^0 \in \mathbb{R}^n$ and $\bar{x}_{ref} \in \mathbb{R}^n$ are known such that $x_{ref}(k) \in X_{ref} \triangleq \{x_{ref} \in \mathbb{R}^n : |x_{ref} - x_{ref}^0| \leq \bar{x}_{ref}\}$.* ∘

Then, the tracking error dynamics could be obtained as follows

$$\tilde{x}^+ = A(\rho)\tilde{x} + B(\rho)\tilde{u} \tag{10.50}$$

with $\tilde{x} := x - x_{ref}$, $\tilde{u} := u - u_{ref}$.

Consider now a family of M sensors (or M combination of sensors) :

$$y_i = C_i(\rho)x + \eta_i \tag{10.51}$$

with η_i a bounded sensor noise, and with $i \in \{1,\dots,M\}$.

We also assume that the available sensors allow us to estimate the state $\tilde{x}$. That is, the pairs $(A(\rho), C_i(\rho))$ are detectable (see [1] for LPV observer design). Therefore, a healthy sensor will provide

$$\tilde{y}_i = y_i - C_i(\rho)x_{ref} = C_i(\rho)\tilde{x} + \eta_i \tag{10.52}$$

Our fault model is described in the following definition. We consider *abrupt* faults that lead to sensor *outage*.

Definition 10.4. A sensor is *operational* (or "healthy") when its measured output is given by (10.51). When a jth sensor *fails* its measured output during the fault is given by

$$y_j = \eta_F, \tag{10.53}$$

where η_F is a bounded noise and with $j \in \{1,\dots,M\}$. ∘

In the following subsections we shall establish closed-loop stability under sensor fault by providing conditions that guarantee that a switching scheme never selects faulty sensors to implement the control law.

Remark that a failed sensor will provide an output

$$\tilde{y}_F = y_j - C_j(\rho)x_{ref} = -C_F(\rho)x_{ref} + \eta_F \tag{10.54}$$

Consider now a family of M observers

$$\theta_i^+ = A(\rho)\theta_i + B(\rho)\tilde{u} + L_i(\rho)(\tilde{y}_i - C_i(\rho)\theta_i) \tag{10.55}$$

with $i = 1,2,\cdots M$ (where M is the number of sensors and/or combination of sensors). The dynamics of the estimation error for every "healthy" observer will be:

$$\varepsilon_i^+ = [A(\rho) - L_i(\rho)C_i(\rho)]\varepsilon_i + L_i(\rho)\eta_i \tag{10.56}$$

with bounded noise η_i. The observers are designed to assure that the dynamics (10.56) will be stable, i.e. the matrices $A(\rho) - L_i(\rho)C_i(\rho)$ are Schur matrices for all $i \in \{1,\dots,M\}$. Then, from (10.56) and using Theorem 10.2 we can compute an invariant set $\mathbf{E_H}$ for the trajectories of the estimation errors ε_i.

Assumption 10.5 ***(working hypothesis).*** *A switching scheme always selects only healthy sensors whose estimation errors satisfy (10.56).* ○

The feedback controller will then implemented as follows

$$\tilde{u} = -K(\rho)\theta_\sigma \tag{10.57}$$

At each time step, we perform the optimisation

$$\sigma = \arg\min_i \Big\{ J(\theta_i) : \theta_i \in \{\theta_1, \cdots, \theta_M\} \Big\}, \tag{10.58}$$

where the minimization of the cost function J guarantee that only healthy sensors are chosen. This is actually a ***working hypothesis*** that will be assured latter. Thus, up to now we consider that there is an automatic mechanism that assures that only healthy sensors are chosen at each time instant. Remark that if only healthy sensors are chosen the feedback control (10.57) becomes

$$\tilde{u} = -K(\rho)(\tilde{x} - \varepsilon_\sigma) \tag{10.59}$$

where ε_σ stands for the estimation error of the observer using the σ sensor (i.e. $\varepsilon_\sigma = \tilde{x} - \theta_\sigma$). Then, the system (10.50) in closed-loop with (10.57) will gives

$$\tilde{x}^+ = [A(\rho) - B(\rho)K(\rho)]\tilde{x} + B(\rho)K(\rho)\varepsilon_\sigma \tag{10.60}$$

Hence, the trajectories of $\tilde{x}$ belongs to an invariant set $\tilde{\mathbf{X}}$ because the matrix $A(\rho) - B(\rho)K(\rho)$ has all its eigenvalues inside the unit circle for all $\rho \in \mathbb{P}$, and ε_σ is assumed to be bounded. Remark that, under the ***working hypothesis***, any healthy H sensor dynamics will be

$$\theta_H^+ = [A(\rho) - L_H(\rho)C_H(\rho)]\theta_H + \gamma_{\sigma H} \tag{10.61}$$

with $\gamma_{\sigma H} := B(\rho)K(\rho)\varepsilon_\sigma + (-B(\rho)K(\rho) + L_H(\rho)C_H(\rho))\tilde{x} + L_H(\rho)\eta_H$.

Because the matrix $A(\rho) - L_H(\rho)C_H(\rho)$ has all its eigenvalues inside the unit circle for all $\rho \in \mathbb{P}$, an invariant set, namely $\mathbf{S_H}$, could be computed for the trajectories of every healthy sensor H.

10.5.1 Healthy Sensors

Provided only healthy sensors are selected by the switching controller, the closed-loop dynamics of the estimator tracking errors for each of the ith sensors that remain healthy continue to obey (10.61), that is, do not change in the event a jth sensor fails. Moreover, the bounds that define the sets $\mathbf{S_H}$, namely $|\gamma_{\sigma H}| \leq \bar{\gamma}_{\sigma H}$, remain valid while (10.56) holds for the selected sensor. Thus, under Assumption 10.5, if the

trajectories of healthy sensors (10.61) are evolving in the corresponding invariant set $\mathbf{S_H}$, then they remain in this set.

10.5.2 Faulty Sensors

Assuming that the switching mechanism (10.58) only selects healthy sensors $\sigma \in \{1,\cdots,M\}$, $\sigma \neq F$, then using equations (10.54) and (10.55) together with (10.53), we have the following closed-loop estimator tracking error subsystems during the fault:

$$\theta_F^+ = [A(\rho) - L_F(\rho)C_F(\rho)]\theta_F + \gamma_{\sigma F} \tag{10.62}$$

where $\gamma_{\sigma F} := B(\rho)K(\rho)\varepsilon_\sigma - B(\rho)K(\rho)\tilde{x} + L_F(\rho)\eta_F - L_F(\rho)C_F(\rho)x_{ref}$ with $\sigma \in \{1,\ldots,M\}$, $\sigma \neq F$.

Remark that (10.62) could be rewritten, using Assumption 10.4, as follows:

$$\theta_F^+ = [A(\rho) - L_F(\rho)C_F(\rho)]\theta_F + \tilde{\gamma}_{\sigma F} - L_F(\rho)C_F(\rho)x_{ref}^0 \tag{10.63}$$

where $\tilde{\gamma}_{\sigma F} := -B(\rho)K(\rho)\tilde{x} + B(\rho)K(\rho)\varepsilon_\sigma + L_F(\rho)\eta_F - L_F(\rho)C_F(\rho)\tilde{x}_{ref}$ with $\sigma \in \{1,\ldots,M\}$, $\sigma \neq F$.

Comparing (10.63) with (10.61), we observe that some of the inputs to the estimation tracking error subsystems have changed after the fault. However, under Assumption 10.5, the signals $\tilde{x}$, ε_σ, for all operational sensors $\sigma \in \{1,\ldots,M\}$, $\sigma \neq F$, satisfy the same bounds as before the fault. In addition, η_F, for $F \in \{1,\ldots,M\}$, and x_{ref} are bounded by assumption.

Hence, as before, we can use these different bounds to obtain a bound $\bar{\gamma}_{\sigma F}$ such that $|\tilde{\gamma}_{\sigma F}| \leq \bar{\gamma}_{\sigma F}$. Using (10.13) (with $\varepsilon = 0$) we can then compute the "under-fault" set

$$\mathbf{S_F} := \tilde{\mathbf{S}}_\mathbf{F} \oplus \{\theta_F^0\}, \tag{10.64}$$

where $\oplus$ denotes the Minkowski sum of sets, $\tilde{\mathbf{S}}_\mathbf{F}$ is an invariant set for the trajectories (10.63) and where the offset θ_F^0, due to the offset x_{ref}^0 of x_{ref}, is computed as:

$$\theta_F^0 = -(I - A_{L_F}(\rho))^{-1}L_F(\rho)C_F(\rho)x_{ref}^0. \tag{10.65}$$

with $A_{L_F}(\rho) := A(\rho) - L_F(\rho)C_F(\rho)$.

Thus, it follows from Theorem 10.2 and the previous analysis that, under Assumption 10.5, the trajectories of (10.62) remain in $\mathbf{S_F}$ defined in (10.64) if started inside or will asymptotically converge towards $\mathbf{S_F}$ if started outside.

We are now ready to establish conditions to ensure that our working hypothesis (Assumption 10.5) is satisfied.

10.6 Closed-Loop Stability under Sensor Fault

10.6.1 Conditions for Closed-Loop Stability

The analysis of Section 10.5 motivates us to impose the following assumption, which describes the less conservative fault scenario that allows us to obtain fault tolerance guarantees within the proposed framework.

Assumption 10.6 (Fault scenario)

1. *At any time instant, at least one sensor is operational; in addition, all operational sensors have estimation errors (10.56) inside the invariant sets* $\mathbf{E_H}$ *and estimation tracking errors (10.61) inside the invariant sets* $\mathbf{S_H}$.
2. *Any time a jth sensor fails, for any* $j \in \{1,\dots,M\}$, *the states of the corresponding estimator tracking error subsystem (10.62), at the following sampling time, belong to the invariant set* $\mathbf{S_F}$ *(10.64).*

The above fault scenario allows any sequence of persistent sensor faults, including simultaneous faults of several sensors, as long as the first fault occurs after sufficiently long time of operation without fault (such that all variables have entered the corresponding invariant sets) and at least one sensor remains operational.

From (10.60) we can compute, using the techniques described in Section 10.3.1, an invariant set, $\tilde{\mathbf{X}}$, such that $\tilde{x} \in \tilde{\mathbf{X}}$, whenever the chosen sensors are healthy. We can also construct bounding sets, $\mathbf{N_F}$, for the bounded noises, such that $\eta_F \in \mathbf{N_F}$, $F = 1,\dots,M$. Then, assuming that the jth sensor has been healthy for sufficiently long time, so that $\theta_j \in \mathbf{S_F}$, we can see from (10.62) that, the instant *after the occurrence of a fault*, the variable θ_j will be in the following *after fault* transitional set:

$$\mathbf{S_{H\to F}} := A_{L_F}\mathbf{S_F} \oplus (-B(\rho)K(\rho))\tilde{\mathbf{X}} \oplus (B(\rho)K(\rho)) \bigcup_{\sigma=1}^{M} \tilde{\mathbf{S}}_\sigma \oplus L_F\mathbf{N_F} \oplus (-L_FC_F)\mathbf{X_{ref}}. \tag{10.66}$$

for a given $\rho \in \mathbb{P}$. Finally, the following pre-checkable condition guarantees, in combination with Condition 1) of Assumption 10.6, that Condition 2) of Assumption 10.6 is satisfied.

Assumption 10.7. *The sets (10.64) and (10.66) satisfy* $\mathbf{S_{H\to F}} \subseteq \mathbf{S_F}$, *for all* $j = 1,\dots,M$. ∘

The following theorem provides conditions to guarantee closed-loop stability under sensor fault.

Theorem 10.8. *Suppose that bounds on the sensor noises* η_i, *and on the "fault noises"* η_F *for* $i = 1,\dots,M$, *are given in the form* $\eta_i \in \mathbf{N_i}$, *and* $\eta_F \in \mathbf{N_F}$, *respectively, where* $\mathbf{N_i}$ *and* $\mathbf{N_F}$ *are polyhedral sets. Suppose that the following conditions hold for all* $j = 1,\dots,M$:

$$\max_i \{J_i^{max} : i \in \{1,\dots,M\}, i \neq j\} < J_j^{min}, \tag{10.67}$$

where

$$J_i^{max} := \max\left\{(\theta_i)^T P \theta_i : \theta_i \in \mathbf{S_H}\right\} \tag{10.68}$$

$$J_j^{min} := \min\left\{(\theta_j)^T P \theta_j : \theta_j \in \mathbf{S_F}\right\}. \tag{10.69}$$

with P a given real matrix[1].

Then, under the fault scenario of Assumption 10.6, the closed-loop dynamics of the multisensor switching scheme described in Section 10.5 remain stable in the event any sensor fails.

Proof. Suppose that a jth sensor fails. At the sampling instant following the fault, Condition 1) of Assumption 10.6 guarantees that there exists at least one operational σth sensor that has the states of the corresponding estimator tracking error subsystem (10.61) in the invariant set $\mathbf{S}_\sigma$. In addition, Assumption 10.7 guarantees that Condition 2) of Assumption 10.6 is fulfilled at the sampling instant following the time of the fault, i.e., the states of the estimator tracking error subsystem corresponding to the failed sensor are in $\mathbf{S_F}$. Conditions 10.67–10.69 then ensure that the σth sensor has smaller cost than the failed jth sensor and thus the latter cannot be selected by the switching mechanism (10.58). It follows that at the sampling instant following the time of the fault the controller selects any of the available healthy sensors (not necessarily the σth sensor) which, by Condition 1) of Assumption 10.6 have estimation errors inside $\mathbf{S_H}$, hence satisfying the bounds (10.56). Thus Assumption 10.5 holds at the sampling instant following the time of the fault and the analysis of Section 10.5 shows that the states of the estimator tracking error subsystems corresponding to healthy sensors and to the failed jth sensor remain in $\mathbf{S_H}$ and $\mathbf{S_F}$, respectively. The previous argument can be repeated inductively for the duration of the fault, concluding that the switching controller never selects faulty sensors to implement the control law and that the resulting dynamics remain in the respective invariant sets. The result then follows. □

Remark 10.7. Note that Fault Detection and Isolation (FDI), a feature normally needed in fault tolerant control, is performed *implicitly* via the switching mechanism (10.58), through satisfaction of the pre-checkable conditions of Assumption 10.7 and (10.67)–(10.69). (In effect, as was proven in the previous theorem, under those conditions the switching mechanism exclusively selects healthy sensors.) Necessary and sufficient conditions for sensor recovery are presented in [16]. ○

10.6.2 Geometric Interpretation

In this section we give a geometric interpretation of conditions (10.67)–(10.69). We require the following definitions. If $X \subset \mathbb{R}^n$ and $Y \subset \mathbb{R}^n$ are some sets, their *sum* is the set $X + Y = \{z \in \mathbb{R}^n : z = x + y, x \in X, y \in Y\}$. If $T \in \mathbb{R}^{n\times m}$ is a matrix and $X \subset \mathbb{R}^m$ is a set, the set $TX \subset \mathbb{R}^n$ is defined as $TX = \{z \in \mathbb{R}^n : z = Tx, x \in X\}$.

[1] The matrix P could be computed, for instance, using the method described in Section 10.4.

Next, introduce the variable $s_i \triangleq P^{1/2}\theta_i$, where $P^{1/2}$ is the symmetric square root of the switching cost matrix P. Using the sets

$$\mathbf{B_H} \triangleq P^{1/2}\mathbf{S_H}, \tag{10.70}$$

$$\mathbf{B_F} \triangleq P^{1/2}\mathbf{S_F}, \tag{10.71}$$

we have that (10.68) and (10.69) have the equivalent form

$$J_i^{max} = \max\left\{\|s_i\|^2 : s_i \in \mathbf{B_H}\right\}, \tag{10.72}$$

$$J_j^{min} = \min\left\{\|s_j\|^2 : s_j \in \mathbf{B_F}\right\}, \tag{10.73}$$

where $\|\cdot\|$ is the vector 2-norm. Thus, J_i^{max} is the maximum squared-norm over all vectors in $\mathbf{B_H}$ and J_j^{min} is the minimum squared-norm over all vectors in $\mathbf{B_F}$. Clearly, for (10.67) to hold for a particular index i, the sets $\mathbf{B_H}$ and $\mathbf{B_F}$ must be separated by a sphere in $\mathbb{R}^n$ centred at zero. Figure 10.3 shows an illustration of a case where condition (10.67) holds for particular indices i and j.

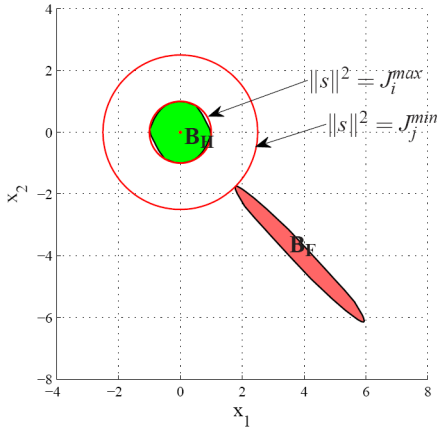

Fig. 10.3 Geometric interpretation of conditions (10.67)–(10.69)

Once the conditions for separation of the sets are fulfilled, then one could, in principle, perform fault detection and isolation using this information. Here we have chosen to achieve faulty sensor detection and isolation "implicitly" by guaranteeing that the switching cost avoids selecting faulty sensors. This feature of the proposed scheme, we believe, departs from other available techniques to achieve fault detection and isolation. Notice also that the proposed switching scheme is motivated by a control performance criterion and has a good performance in the absence of sensor failure. The possibility to provide fault tolerance guarantees with the scheme without any modification comes as a bonus. Moreover, a nice property of the proposed scheme is the simplicity of its on-line implementation, which requires only to compare cost values. On the other hand, the use of the separation of the sets

as a mechanism for fault detection and isolation would result in a relatively more complex scheme requiring more involved on-line tests.

References

1. Blanchini, F., Miani, S.: Stabilization of lpv systems: state feedback, state estimation and duality. In: Proceedings of the 42nd IEEE Conference on Decision and Control, Hawaii, USA (December 2003)
2. Daafouz, J., Bernussou, J.: Parameter dependent lyapunov functions for discrete time systems with time varying parametric uncertainties. Systems & Control Letters 43(5), 355–359 (2001)
3. Daafouz, J., Riedinger, P., Iung, C.: Stability analysis and control synthesis for switched systems: a switched lyapunov function approach. IEEE Transactions on Automatic Control 47(11), 1883–1887 (2002)
4. Dasarathy, B.V.: Sensor fusion potential exploitation–Innovative architectures and illustrative applications. Proceedings of the IEEE 85(1), 24–38 (1997)
5. de Oliveira, M.C., Bernussou, J., Geromel, J.C.: A new discrete-time robust stability condition. Systems & Control Letters 37(4), 261–265 (1999)
6. Haimovich, H., Kofman, E., Seron, M.M.: Analysis and improvements of a systematic componentwise ultimate-bound computation method. In: Proceedings of the 17th IFAC World Congress, Seoul, South Korea (July 2008)
7. Hsiao, T., Tomizuka, M.: Sensor fault detection in vehicle lateral control systems via switching Kalman filtering. In: Proc. of the 2005 American Control Conference, Portland, OR, USA, pp. 5009–5014 (2005)
8. Kalandros, M.K., Trailović, L., Pao, L.Y., Bar-Shalom, Y.: Tutorial on multisensor management and fusion algorithms for target tracking. In: Proc. of the 2004 American Control Conference, Boston, MA, USA, vol. 5, pp. 4734–4748 (June 2004)
9. Kofman, E.J., Haimovich, H., Seron, M.M.: A systematic method to obtain ultimate bounds for perturbed systems. International Journal of Control 80(2), 167–178 (2007)
10. Luo, R.C., Kay, M.G.: Multisensor integration and fusion in intelligent systems. IEEE Trans. on Systems, Man and Cybernetics 19(5), 901–931 (1989)
11. Luo, R.C., Yih, C.-C., Su, K.L.: Multisensor fusion and integration: approaches, applications, and future research directions. IEEE Sensors Journal 2(2), 107–119 (2002)
12. Martínez, J.J., Zhuo, X.W., De Doná, J.A., Seron, M.M.: Multisensor switching strategy for automotive longitudinal control. In: Proc. of the 2006 American Control Conference, Minneapolis, MN, USA (2006)
13. Martinez, J.-J., de Wit, C.C.: A safe longitudinal control for adaptive cruise control and stop-and-go scenarios. IEEE Transactions on Control Systems Technology 15(2), 246–258 (2007)
14. Niemann, H., Stoustrup, J.: An architecture for fault tolerant controllers. International Journal of Control 78(14), 1091–1110 (2005)
15. Olaru, S., De Doná, J.A., Seron, M.M., Stoican, F.: Positive invariant sets for fault tolerant multisensor control schemes. International Journal of Control 83(12), 2622–2640 (2010)
16. Olaru, S., Stoican, F., De Doná, J.A., Seron, M.M.: Necessary and sufficient conditions for sensor recovery in a multisensor control scheme. In: Proceedings of the 7th IFAC Symposium on Fault Detection, Supervision and Safety of Technical Processes, Barcelona, Spain, pp. 977–982 (July 2009)

17. Rakovic, S.V.: Minkowski algebra and banach contraction principle in set invariance for linear discrete time systems. In: 2007 46th IEEE Conference on Decision and Control, pp. 2169–2174 (December 2007)
18. Rakovic, S.V., Kerrigan, E.C., Kouramas, K.I., Mayne, D.Q.: Invariant approximations of the minimal robust positively invariant set. IEEE Transactions on Automatic Control 50(3), 406–410 (2005)
19. Richter, J.H., Heemels, W.P.M.H., van de Wouw, N., Lunze, J.: Reconfigurable control of piecewise affine systems with actuator and sensor faults: Stability and tracking. Automatica 47(4), 678–691 (2011)
20. Seron, M.M., De Doná, J.A., Richter, J.: Fault tolerant control using virtual actuators and set-separation detection principles. International Journal of Robust and Nonlinear Control 22(7), 709–742 (2012)
21. Seron, M.M., Zhuo, X.W., De Dona, J.A., Martinez, J.J.: Multisensor switching control strategy with fault tolerance guarantees. Automatica 44(1), 88–97 (2008)
22. Sun, S.-L., Deng, Z.-L.: Multi-sensor optimal information fusion Kalman filter. Automatica 40(6), 1017–1023 (2004)
23. Vahidi, A., Eskandarian, A.: Research advances in intelligent collision avoidance and adaptive cruise control. IEEE Transactions on Intelligent Transportation Systems 4(3), 143–153 (2003)
24. Varshney, P.K.: Multisensor data fusion. Electronics & Communication Eng. Journal 9(6), 245–253 (1997)
25. Xu, L., Zhang, J.Q., Yan, Y.: A wavelet-based multisensor data fusion algorithm. IEEE Trans. on Instrumentation and Measurement 53(6), 1539–1545 (2004)

Chapter 11
VRFT for LPV Systems: Theory and Braking Control Application

Simone Formentin, Giulio Panzani, and Sergio M. Savaresi

Abstract. This chapter presents the Virtual Reference Feedback Tuning approach for linear parameter-varying (LPV) control system design. The method is a noniterative direct data-driven technique, *i.e* a gain-scheduled fixed order controller can be derived from a finite number of datasets, without need of identifying a model of the plant. Therefore, the closed-loop performance cannot be jeopardized by modeling errors and the design procedure becomes easier and faster, as neither LPV state-space realization and controller reduction are required. The method employs basic instrumental variables and optimal data prefiltering to deal with measurement noise and underparameterization of the controller. As an example in the vehicle dynamics field, the case of braking control system design for two-wheeled vehicles is considered. The approach shows effective, when elementary physical knowledge is used to select the most suited identification experiment, the reference model, the controller structure and the scheduling variable, whereas no model parameters are needed to achieve satisfactory results.

11.1 Introduction and Motivation

One of the most straightforward methods to specify the desired behaviour of a control system is to describe the dynamic relationship between the reference signal and the controlled output. This design approach is usually known as “model-reference control" (MRC) or “model-following control" (MFC) and has been widely studied during the last years, see *e.g.* [20], [13], [29] and references therein. The objective of MRC is to design a feedback controller that, when applied to the real plant, allows the closed-loop system to match the behaviour of a given reference model. The control engineer has actually more than one choice to fulfil this desired task.

Simone Formentin · Giulio Panzani · Sergio M. Savaresi
Dipartimento di Elettronica e Informazione, Politecnico di Milano,
Piazza Leonardo da Vinci 32, Milano, Italy
e-mail: {formentin,panzani,savaresi}@elet.polimi.it

O. Sename et al. (Eds.): *Robust Control and LPV Approaches*, LNCIS 437, pp. 289–309.
DOI: 10.1007/978-3-642-36110-4_11

The first way is to develop a “first-principle" model of the system, by writing the physical laws describing its working principles. Such a model can also be used to evaluate the performance specifications for the feedback loop composed by the feedback controller and the model. The actual performance of the real feedback loop are then strongly dependent on model mismatch, typically due to incomplete knowledge of model parameters, underparameterization of model structure and time/economical constraints that might yield loss of accuracy.

In the last decades, big progress in data collection technology and performance of electronic processing units have provided another way to design suited process models. As witnessed by the huge number of contributions in the control literature, system identification theory, *i.e.* the science of learning models from data, has become more and more important for designing simple and reliable models for control purposes, see *e.g.* [15], [16], [18] and references therein. On the other hand, using “black-box" modeling, information about the plant is completely derived from input/output (I/O) data, therefore appropriate identification experiments and model structures needs to be chosen from some “a-priori" knowledge or data-driven procedures. The final closed-loop performance are then still affected by modeling accuracy depending on these factors.

The problem of undermodeling arises in both the above approaches, as the control design is “model-based", that is the feedback controller is designed using information about the model of the plant to control. However, these are not the only ways to synthesize a control system. When experimental data on the plant are available, a third choice for the control engineer is to resort to “data-to-controller" algorithms. In these techniques, the data are directly used to minimize a control criterion and therefore the modeling step is skipped. Moreover, the overall procedure is much faster than in the standard case, since, quoting [23]:

“it is widely recognized [. . .] that obtaining the process model is the single most time consuming task in the application of model-based control."

The first auto-tuning method dates back to the pioneering work on the design of industrial PID controllers in [34]. Since then, many more techniques started to appear, partly as modifications and extensions of the Ziegler and Nichols method, partly as developments in new directions. All model-reference direct data-driven methods can be classified in three different categories, as illustrated in Table 11.1: on-line, off-line iterative and off-line noniterative methods. Among all, off-line noniterative methods can be seen as control design techniques reformulated as pure identification problems. In other words, both CbT and VRFT approaches are identification methods where the system to identify, starting from one or two datasets, is

Table 11.1 Taxonomy of direct data-driven control design methods

On-line	Off-line iterative	Off-line noniterative
Adaptive control	IFT	CbT
Unfalsified control	ICbT	VRFT

the ideal controller instead of the plant. The big advantage of this formulation is that all the results in identification theory can be directly exploited for control design.

In the vehicle dynamics field, many systems that usually need electronic control systems can be modeled as linear parameter-varying (LPV) systems, see *e.g.* [26], [10], [14], [8]. Therefore, the most suited noniterative method in this framework is the Virtual Reference Feedback Tuning, introduced in [17], fixed in [5] in the linear time-invariant setting and extended in [12] to LPV systems. The LPV version of VRFT can be very useful in practice as, being the controller directly derived from data in input/output (I/O) description, the most tricky phases in LPV fixed-order control system design, *i.e.* state-space realization and controller-reduction, can be avoided.

The other noniterative method, *i.e.* Correlation-based Tuning, cannot be analogously extended since the development of the controller tuning procedure is based on the commutation of systems in the block diagram (see [33]) and this passage would not be allowed in a nonlinear setting.

In this chapter, Virtual Reference Feedback Tuning for noniterative direct design of gain-scheduled controllers is presented and its effectiveness is tested on a typical problem in motorcycle dynamics, *i.e.* rear braking control (see [25]), as braking is recognized to be one of the most critical and sensitive maneuvers by pilots and race-engineers.

The motivation for the interest in this application is that standard methods (see *e.g.* [21, 31]) typically require an accurate knowledge of model parameters of braking dynamics and their identification may be very time-consuming. This requirement constitutes a big issue, especially when some hardware components change or when low-cost products are used, as in these situations the control system should be fast to calibrate and re-tune.

Starting from the observation that the importance of the load transfer effect is the main difference between four and two-wheeled vehicles, a gain-scheduled fixed-order controller can be instead synthesized using the VRFT method in [12], in case the measurement of the rear vertical force is available. The testing platform is the motorcycle multi-body simulator BikeSim^{TM}, a comprehensive and experimentally validated simulator for motorcycles, developed according to the works by Prof. R. Sharp, D. Limebeer and S. Evangelou at the Imperial College of London, see [28].

The remainder of the chapter is as follows. The first part (Sections 11.2 and 11.3) is dedicated to the presentation of the VRFT method for LPV systems, whereas the second part (Section 11.4) is devoted to the application of the method to the rear braking control problem in two-wheeled vehicles. More specifically, Section 11.2 introduces the notation and formally defines the problem, whereas Section 11.3 describes the method in all its features: the main idea is given in the introduction of Section 11.2, the case of noisy data is discussed in Subsection 11.3.1 and the case of underparameterized controllers is analyzed in Subsection 11.3.2. In Section 11.4, the application problem is first formally described from a physical point of view, then the VRFT solution is adapted to the case study in Subsection 11.4.1 and finally the simulation results are illustrated in Subsection 11.4.2. The chapter is ended by some concluding remarks.

11.2 Problem Statement and Notation

In this work SISO LPV systems will be considered and represented by LPV transfer operators, according to the following definition.

Definition 1. An LPV transfer operator $G(q^{-1}, p(t))$, $p(t) \in \Pi \subset \mathbb{R}^{dim(p)}$ is defined as

$$G(q^{-1}, p(t)) = \sum_{k=0}^{\infty} g_k(p(t)) q^{-k} \ , \ p(t) \in \Pi$$

where q^{-1} indicates the backward-shift time operator and $g_k(p(t))$ is the kth impulse response coefficient.

It is important to stress that the foregoing expression for the LPV system corresponds to the standard LTI transfer function operator only in case of constant $p(t)$. Nonetheless, such a notation presents many interesting aspects like reading comfort and it helps with deriving the main results. Therefore it will be employed throughout the whole chapter, together with the following notion of LPV stability, firstly introduced in [3].

Definition 2. An LPV transfer operator $G(q^{-1}, p(t))$, $p(t) \in \Pi \subset \mathbb{R}^{dim(p)}$ is LPV stable if it holds that

$$|g_k(p(t))| \leq \overline{g_k} \ , \ \sum_{k=0}^{\infty} \overline{g_k} < \infty.$$

Consider now that the system to control is the data-generator $G_0(q^{-1}, p(t))$. The output of $G_0(q^{-1}, p(t))$ is denoted by

$$y(t) = G_0(q^{-1}, p(t))u(t) + v(t),$$

where $p(t) \in \Pi \subset \mathbb{R}^{dim(p)}$ is a measurable exogenous parameter vector at time t and $v(t) = H_0(q^{-1}, p(t))e(t)$ is a coloured noise generated by the, possibly LPV, transfer operator $H_0(q^{-1}, p(t))$ from a set of zero-mean random variables $e(t)$.

Assume then that both $G_0(q^{-1}, p(t))$ and $H_0(q^{-1}, p(t))$ are LPV stable for all possible trajectories of p, according to Definition 2.

Consider the case of scalar $p(t)$ for clarity of presentation and let $\mathscr{C}_l$ be the class of linear-in-parameters controllers with an additional LTI component $I(q^{-1})$ (*e.g.* integral action) in input-output description

$$\mathscr{C}_l = \left\{ C_\theta(q^{-1}, p(t)) = I(q^{-1}) \beta^T(q^{-1}, p(t)) \theta \ , \ p(t) \in \Pi \right\},$$

$$\begin{aligned} \beta(q^{-1}, p(t)) = [&\beta_0(q^{-1}), \beta_0(q^{-1})p(t), \ldots, \beta_0(q^{-1})p(t)^{n_p}, \\ &\beta_1(q^{-1}), \beta_1(q^{-1})p(t), \ldots, \beta_1(q^{-1})p(t)^{n_p}, \ldots, \\ &\beta_{n_q}(q^{-1}), \beta_{n_q}(q^{-1})p(t), \ldots, \beta_{n_q}(q^{-1})p(t)^{n_p}]. \end{aligned}$$

The term $\beta_i(q^{-1})$, $i = 0,\ldots,n_q$, can be any kind of orthonormal basis functions, *e.g.* Laguerre or Kautz (see [32]). Without loss of generality, from now on simple backward-shift operators will be employed, that is $\beta_i(q^{-1}) = q^{-i}$, $i = 0,\ldots,n_q$. Further, consider that the subscript θ attributed to a signal indicates that the signal refers to the closed-loop system with the controller $C_\theta(q^{-1},p(t))$ in the loop.

Introduce now the user-defined closed-loop desired behaviour as the LPV reference transfer operator $M(q^{-1},p(t))$. Given $G_0(q^{-1},p(t))$, $\mathscr{C}_l$ and $M(q^{-1},p(t))$, the model-reference control problem for LPV case can be defined as follows, by extending the LTI concept.

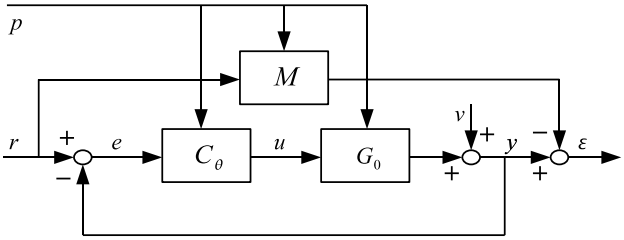

Fig. 11.1 Closed-loop system with controller C_θ and matching error generation

Definition 3. Consider the closed-loop system illustrated in Figure 11.1, where $G_0(q^{-1},p(t))$, $H_0(q^{-1},p(t))$ and $M(q^{-1},p(t))$ are defined as above and $C_\theta(q^{-1},p(t))$ is a fixed-structure gain-scheduled controller parameterized by θ.

The problem of finding the LPV controller $C_\theta(q^{-1},p(t))$ minimizing

$$J_{MR}(\theta) = \lim_{N\to\infty} \frac{1}{N} \sum_{t=1}^{N} \varepsilon_\theta(t)^2, \tag{11.1}$$

$$\varepsilon_\theta(t) = y_\theta(t) - M(q^{-1},p(t))r(t) =$$
$$= G_0(q^{-1},p(t))C_\theta(q^{-1},p(t))(r(t) - y_\theta(t)) - M(q^{-1},p(t))r(t) + v(t),$$

with respect to a specified parameter trajectory $p(\cdot)$, is referred to as **LPV model reference control problem**.

The optimal controller $C^\circ(q^{-1},p(t))$ can now be introduced.

Definition 4. In the LPV model reference control framework, the optimal controller $C^\circ(q^{-1},p(t))$ is the feedback controller such that $v = 0$ implies $J_{MR} = 0$.

Notice that the optimal controller might not exist or cannot belong to the set of available controllers. It might also happen that $C^\circ(q^{-1},p(t))$ depends on future values of the trajectory of $p(t)$. However, this system will become useful for analysis-purpose.

11.3 The VRFT Approach for LPV Control System Design

Consider the model-reference setting described in Section 11.2 and illustrated in Figure 11.1. In a noiseless setting, when the closed-loop system behaves exactly as $M(q^{-1},p(t))$, the reference signal can be expressed by $r_V(t) = M(q^{-1},p(t))^{-1}y(t)$, where the subscript V stands for "Virtual".

Consider now then the data-dependent cost function

$$J_{VR}(\theta) = \lim_{N\to\infty} \frac{1}{N}\sum_{t=1}^{N} \left(u(t) - C_\theta(q^{-1},p(t))\,(r_V(t) - y(t))\right)^2. \tag{11.2}$$

The criterion (11.2) does not require any knowledge of $G(q^{-1},p(t))$, since all information on the plant is included in the dataset. In general, (11.1) and (11.2) are different, however the following proposition holds.

Theorem 11.1. *Assume that $C^\circ(q^{-1},p(t))$ belongs to the class of considered controllers. $C^\circ(q^{-1},p(t))$ is a minimizer of (11.2) for any trajectory of p.*

Proof. See [12].

Corollary to Theorem 11.1. *If (11.2) has a unique minimizer, e.g. if the class of controllers is linearly parameterized, such a minimizer is exactly $C^\circ(q^{-1},p(t))$ and then it guarantees perfect matching.*

The controller parameterization introduced in Section 11.2 is exactly the one considered in the Corollary above, therefore the data-dependent cost criterion (11.2) is quadratic in the unknown θ and its (unique) minimizer can be found via least-squares techniques (see [22]). More specifically, it is possible to compute the minimum of the finite-time approximation of (11.2)

$$J_{VR}^N(\theta) = \frac{1}{N}\sum_{t=1}^{N} \left(u(t) - \varphi^T(t,p(t))\theta\right)^2, \tag{11.3}$$

where the regressor $\varphi(t,p(t))$ is expressed by

$$\varphi(t,p(t)) = I\beta(p(t))(M(p(t))^{-1}y(t) - y(t)),$$

by means of convex optimazion (notice that t and q^{-1} arguments are sometimes omitted for ease of notation). Therefore, the controller parameters θ^N are given by:

$$\theta^N = \arg\min_\theta J_{VR}^N(\theta)$$

As in the LTI case, the VRFT approach converts the design problem into an identification issue, where the knowledge of the process dynamics is no longer necessary.

11.3.1 Dealing with Noisy Data

In order to guarantee consistent results in numerical minimization of (11.3), a different experimental effort is required depending on the Signal-to-Noise Ratio (SNR), even if only the complete-parameterization case is considered. The analysis of this section naturally follows from the (more general) theoretical study in [4] and from some observations reported in [3].

Consider the case where $C^\circ \in \mathscr{C}$ and disturbance v is identically null, for any time instant t. The minimum of (11.3) is given by the Gauss-formula

$$\theta^N = \left[\frac{1}{N}\sum_{t=1}^{N} \varphi(t,p(t))\varphi^T(t,p(t))\right]^{-1} \frac{1}{N}\sum_{t=1}^{N} \varphi(t,p(t))u(t). \tag{11.4}$$

Since $C^\circ \in \mathscr{C}$, the input can be expressed as a function of the regressor and the optimal value of parameters, *i.e.* $u(t) = \varphi(t,p(t))^T\theta^\circ$. Then, by substituting such an expression in the Gauss-formula, it is clear that $\theta^N = \theta^\circ$ only if the persistency of excitation condition

$$\frac{1}{N}\sum_{t=1}^{N} \varphi(t,p(t))\varphi^T(t,p(t)) > 0 \tag{11.5}$$

holds.

Remark. A sufficient condition such that (11.5) is verified for polynomial-type coefficient dependence and ARX noise models is that $u(t)$ is rich enough (as in LTI case) and the trajectory of $p(t)$ visits $n_p + 1$ points infinitely many times (see [1]). As the noise model is expressed by

$$H(q^{-1},p(t)) = H_0(q^{-1},p(t))\left(1 - M(q^{-1},p(t))\right) \tag{11.6}$$

persistency of excitation might not be satisfied when (11.6) cannot be well-described by an ARX model. In this case, more general results on persistency of excitation for LPV identification would be required (this is not a problem due to use of VRFT). It should be said that, in authors' experience, simulations have always shown a good behaviour with conditions expressed in [1], as will be shown later on in the numerical examples.

In any real experimental environment, the measured output is always affected by noise. Moreover, it may happen that also the measurement of the scheduling parameter p is contaminated by additional disturbances. In these situations, one solution is to resort to Instrumental Variable (IV) techniques and repeated-experiment procedures. Consistency results are explained next.

Consider the IV reformulation of (11.4)

$$\theta^N = \left[\frac{1}{N}\sum_{t=1}^{N} \zeta(t,p_\zeta(t))\varphi^T(t,p(t))\right]^{-1} \frac{1}{N}\sum_{t=1}^{N} \zeta(t,p_\zeta(t))u(t), \tag{11.7}$$

where $\zeta(t,p(t))$ is a parameter-varying IV vector. In detail, $\zeta(t,p_\zeta(t))$ is constructed as

$$\zeta(t,p_\zeta(t)) = I(q^{-1})\beta(q^{-1},p_\zeta(t))(M(q^{-1},p(t))^{-1}y_\zeta(t) - y_\zeta(t)),$$

where $y_\zeta(t)$ is the output of a second open-loop experiment performed by employing the same input and parameter sequences of the first dataset and $p_\zeta(t)$ is the parameter sequence with a different realization of noise.

By writing the outputs of the two open-loop experiments as sums of the nominal signal y_{nom} and the $i-$th disturbance realization v_i, namely

$$y(t) = y_{nom}(t) + v_1(t)\ ,\ y_\zeta(t) = y_{nom}(t) + v_2(t),$$

and by applying the same rationale on p, that is

$$p(t) = p_{nom}(t) + d_{p1}(t)\ ,\ p_\zeta(t) = p_{nom}(t) + d_{p2}(t),$$

it is possible to distinguish among four different components inside the regressors, *i.e.*

$$\varphi(t,p(t)) = \psi_{y_{nom}}(t,p_{nom}(t)) + \psi_{v_1}(t,p_{nom}(t)) + \psi_{y_{nom}}(t,d_{p1}(t)) + \psi_{v_1}(t,d_{p1}(t)),$$

$$\zeta(t,p_\zeta(t)) = \psi_{y_{nom}}(t,p_{nom}(t)) + \psi_{v_2}(t,p_{nom}(t)) + \psi_{y_{nom}}(t,d_{p2}(t)) + \psi_{v_2}(t,d_{p2}(t)),$$

where ψ-terms are defined as

$$\begin{aligned}
\psi_{y_{nom}}(p_{nom}) &= I\beta(p_{nom})(M^{-1}y_{nom} - y_{nom}),\\
\psi_{y_{nom}}(d_{p1}) &= I\beta(d_{p1})(M^{-1}y_{nom} - y_{nom}),\\
\psi_{y_{nom}}(d_{p2}) &= I\beta(d_{p2})(M^{-1}y_{nom} - y_{nom}),\\
\psi_{d_1}(p_{nom}) &= I\beta(p_{nom})(M^{-1}v_1 - v_1),\\
\psi_{d_1}(d_{p1}) &= I\beta(d_{p1})(M^{-1}v_1 - v_1),\\
\psi_{d_2}(p_{nom}) &= I\beta(p_{nom})(M^{-1}v_2 - v_2),\\
\psi_{d_2}(d_{p2}) &= I\beta(d_{p2})(M^{-1}v_2 - v_2).
\end{aligned}$$

By noticing that $u(t) = \psi_{y_{nom}}(t,p_{nom}(t))^T\theta^\circ$ with the representation above, the IV version of the Gauss formula (11.4) can be rewritten, after some cumbersome computations, as

$$\theta^N = \theta^\circ - \left[\frac{1}{N}\sum_{t=1}^{N}\zeta(t,p(t))\varphi^T(t,p(t))\right]^{-1}\frac{1}{N}\sum_{t=1}^{N}\zeta(t,p_\zeta(t))\psi_{d_1}(t,p_{nom}(t))\theta^\circ +$$

$$+\zeta(t,p_\zeta(t))\psi_{y_{nom}}(t,d_{p1}(t))\theta^\circ + \zeta(t,p_\zeta(t))\psi_{d_1}(t,d_{p1}(t))\theta^\circ.$$

It can be concluded that for the IV estimate to be consistent it is required that

$$\frac{1}{N}\sum_{t=1}^{N}\zeta(t,p_\zeta(t))\varphi^T(t,p(t))>0$$

and

$$\lim_{N\to\infty}\frac{1}{N}\sum_{t=1}^{N}\zeta(t,p_\zeta(t))\psi_{v_1}(t,p_{nom}(t))+$$
$$+\zeta(t,p_\zeta(t))\psi_{y_{nom}}(t,d_{p1}(t))+\zeta(t,p_\zeta(t))\psi_{v_1}(t,d_{p1}(t))$$

is null, with probability 1.

The first condition is a persistency of excitation condition and can be treated like (11.5).

Concerning the second condition, further reasoning is required. It could be shown that the expected value of cross-products of any ψ-term with ζ is null, as different realizations of output and parameter noises are included in the IV vector. Therefore, the method gives consistent estimate only if ζ and the ψ-terms are ergodic in correlation, *i.e.* if as $N\to\infty$,

$$\left\|\frac{1}{N}\sum_{t=1}^{N}\zeta(t,p_\zeta(t))\psi_i(t)-\mathbb{E}\left[\zeta(t,p_\zeta(t))\psi_i(t)\right]\right\|_F\to 0, \tag{11.8}$$

where $\psi_i(t)$ stands for any ψ-term except for $\psi_{y_{nom}}(p_{nom})$ and $\|\cdot\|_F$ indicates the Frobenius norm.

In [3] and [4], it is proved that (11.8) holds in the *noiseless parameter* case, if

1. the data-generating system is LPV stable;
2. the noise-generating system is LPV stable;
3. trajectories of p and u are bounded.

In the present case, the first requirement is true by hyphotheses and the second one is easily verified by looking at the expression of $H(q^{-1},p(t))$ given in (11.6). Therefore, only the third requirement is really an additional (but reasonable for most of LPV applications) requirement for system working conditions.

If the *scheduling parameter is noisy*, the method also requires that

1. the controller parameterization with respect to p is affine;
2. noises on p and y are uncorrelated.

The latter may constitute a problem in applications where the scheduling parameter is the output itself and for quasi-LPV systems. In these situations, an additional realization of the parameter trajectory, *i.e.* another experiment, is required. This “three-experiment" procedure will be referred to as “double-IV"-identification, whereas the “two-experiment" method for noiseless parameter measurement will be denoted as “IV"-identification.

Remark. It should be recalled that the proposed technique is not statistically optimal, since IV methods eliminate the noise bias by increasing the variance of the parameter estimate. This fact may also compromize the quality of the closed-loop model-matching because the expected value of the model reference cost depends on the weighted covariance of the parameter vector. From a practical point of view, it can then be concluded that the proposed IV method are good and fast way to overcome the problem of noise, provided N is large.

11.3.2 Underparameterized Controllers

In many practical applications, perfect matching is not possible, mainly because of control limitations and uncomplete knowledge of the system structure. In this situation, two critical problems arise:

1. **a control problem:** when $C_\theta(q^{-1},p(t))$ cannot match $M(q^{-1},p(t))$ for any θ, no information is available on stability and performance for different working conditions.
2. **an identification problem:** in the underparameterization case, the result in Theorem 11.1 no longer holds.

The first problem is a general issue of model-reference control of LPV systems where only low-order controllers are available and it is not directly related to VRFT. Therefore, the following discussion will focus on the second problem. Far from being a complete analysis, this Section aims at laying the groundwork of future research, providing a suitable approach and discussing some (so far) open problems.

11.3.2.1 Optimal Data Prefiltering

Consider the case of underparameterized controller structure. Let the complete parameterization of the controller be $\theta^+ = \left[\theta^T \ \tilde{\theta}\right]^T$,

$$C_\theta^+(q^{-1},p(t)) = C_\theta(q^{-1},p(t)) + \tilde{\theta}\Delta C_\theta(q^{-1},p(t)),$$

where $\Delta C_\theta(q^{-1},p(t))$ is the "residual" of the optimal controller. Notice that if $C_\theta^+(p)$ is employed, the perfect matching holds by Definition 3 for any trajectory of $p(t)$. Notice that the full-order optimal controller $C^{\circ+}(q^{-1},p(t))$ is obtained for $\theta^+ = \theta^+_{min} = \left[\theta^{\circ T} \ 1\right]^T$ and the reduced-order optimal controller $C^\circ_\theta(p)$ is given by $\theta^+ = \left[\theta^T_{min} \ 0\right]^T$. Now let the virtual reference cost with filtered data be

$$J_{VR}(\theta,L) = \lim_{N\to\infty} \frac{1}{N}\sum_{t=1}^{N} \left(L(p)u(t) - L(p)C_\theta(p)\left(r_V(t) - y(t)\right)\right)^2. \tag{11.9}$$

where $L(q^{-1},p(t))$ is an LPV prefilter to be chosen to shape the bias effect due to undermodeling. The result presented herein follows the same rationale of [5]

and [6] and it guarantees an analytical relationship between the real and the virtual reference cost functions also in case of undermodeling. Notice that prefiltering and closed-loop behaviour are strictly related to the parameter trajectory of the open-loop experiment.

Theorem 11.2. *If*

$$L(q^{-1},p(t)) = \big(M(q^{-1},p(t)) - 1\big)\, G_0(q^{-1},p(t)), \tag{11.10}$$

then

$$\frac{\partial^2 J_{VR}(\theta,L)}{\partial \theta^{+2}}|_{\theta^+_{min}} = \frac{\partial^2 J_{MR}(\theta)}{\partial \theta^{+2}}|_{\theta^+_{min}} \tag{11.11}$$

Proof. See [12].

Notice that unlike the case of optimal controller (for which the perfect model-following is achieved for any parameter trajectory), with the underparameterized controller guarantees can be provided only for a given $p(\cdot)$, *i.e.* the one corresponding to the identification experiment and employed inside the prefilter. A good practice is then to choose, among all the persistently exciting trajectories of the parameter, the one closest to that required in closed-loop operation.

11.3.2.2 Filter Implementation

The optimal filter (11.10) cannot be directly applied as the process dynamics are unknown. A direct data-driven filter implementation strategy is illustrated next.

First notice that in (11.9) two different terms are required, *i.e.*

$$L(p)u(t), \;\; L(p)C_\theta(p)\,(r_V - y)\,.$$

Considering the first term, it should be noted that, in a noiseless setting,

$$L(p)u(t) = (M(p)-1)\,G_0(p)u(t) = (M(p)-1)\,y(t).$$

On the other hand, the second term can be rewritten as

$$L(p)C_\theta(p)\,(r_V - y) = \theta^T\,(M(p)-1)\,G_0(p)\beta(p)Ie.$$

Since each element of $\beta(p)$ is the composition of a i-step time shift and a j-powered version of the parameter, *i.e.* $p^j(t)q^{-i}$, a data-driven estimation of the quantity above can be inferred from a set of *ad-hoc* experiments by using the time series of $y(t)$ and $p(t)$ that characterize the first dataset. Specifically, $n_{exp} = dim(\theta)$ open-loop experiments are required, where $G_0(p)$ must be fed by the input signal $\tilde{u}_{i,j}(t) = p^j(t)q^{-i}I(q^{-i})e(t)$ during the experiment denoted with the couple (i,j). The output signals $\tilde{y}_{i,j}(t) = G_0(p)p^j(t)q^{-i}(p)I(q^{-i})e(t)$ can then be weighted with θ and filtered off-line by $M(p)-1$ to obtain the desired quantity.

Notice that the data-driven computation of the second term requires an additional experimental effort, *e.g.* a PI controller with affine parameterization in p requires 4 *ad-hoc* experiments. However, the design of experiment procedure is completely defined and model-free. Moreover, the signals in $J_{VR}(\theta)$ are filtered by the real L and not with an approximation, unlike the LTI case (see again [5]).

11.4 Active Braking Control via Load Transfer Scheduling

In this second part, the braking control problem for two-wheeled vehicles will be dealt with from an LPV point of view. More specifically, this note will focus on wheel slip (λ) control, due to the successful application of such a control paradigm, see *e.g.* [27, 31, 30]. In the following, some physical reasoning will be proposed to correctly select the identification experiment, the reference model and the controller structure, whereas the controller parameters will be subsequently derived from I/O data only.

The most widespread dynamic model in literature is the so called *Single Corner Model*: it relates the system input, that is the braking torque T applied to the wheel, to the wheel slip that has to be regulated. Although very simple, this model is capable of capturing some of the main features of braking control issues and its analysis proves useful for a proper comprehension of the braking problem tackled (see also *e.g.* [19, 27] for further details). The Single Corner torque-to-slip linearized transfer function is expressed by

$$\lambda(s) = \frac{R/J\dot{x}}{s + \left[\left(\frac{R^2}{J} + \frac{1}{m_t}\right)\mu'\right]\frac{F_z}{\dot{x}}} T(s) \tag{11.12}$$

According to this model, the dynamics between the braking torque and the wheel slip are expressed as a first order filter and depends on: the wheel radius R, the moment of inertia of the wheel J, the whole vehicle mass m_t, the vehicle speed $\dot{x}$, the vertical load that insists on the wheel center F_z and μ', that is the derivative of the Pacejka friction curve (see [24]) evaluated in the considered equilibrium point, namely

$$\mu' = \left.\frac{\partial \mu(\lambda)}{\partial \lambda}\right|_0 .$$

It is reasonable to consider that vehicle properties such as vehicle mass, wheel radius and its moment of inertia keep constant (at least slight variations occur); conversely, the same assumption cannot be done for the other parameters. The vehicle speed $\dot{x}$ by definition changes as the vehicle decelerates; the Pacejka derivative μ' cannot be considered a constant parameter, as it changes with the considered equilibrium point and mainly when different surfaces are considered (*e.g.* dry asphalt, snow). Finally, the vertical load F_z is another fundamental variable, in particular in two-wheeled vehicles.

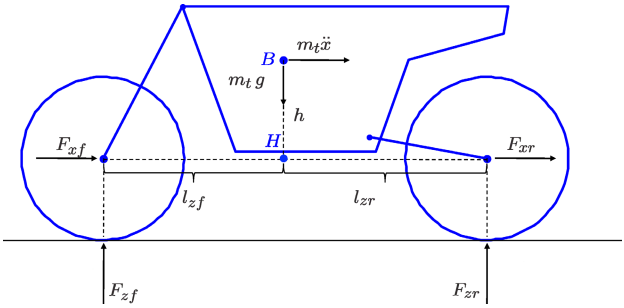

Fig. 11.2 Vehicle pictorial representation

To better understand the latter point, consider Figure 11.2 where a pictorial representation of a motorcycle is provided. For the sake of simplicity, the vehicle is assumed to be rigid, *i.e.* no suspension deflection is considered, and the whole vehicle mass located in the main frame center of gravity (point B). During a deceleration phase, the momentum balance with respect to the point H leads to the following front and rear vertical forces expressions:

$$F_{zf} = m_t\, g \frac{l_{zr}}{l_{zf}+l_{zr}} - m_t \frac{h}{l_{zf}+l_{zr}}\ddot{x} = F_{zf0} - m_t \frac{h}{l_{zf}+l_{zr}}\ddot{x}$$
$$F_{zr} = m_t\, g \frac{l_{zf}}{l_{zf}+l_{zr}} + m_t \frac{h}{l_{zf}+l_{zr}}\ddot{x} = F_{zr0} + m_t \frac{h}{l_{zf}+l_{zr}}\ddot{x}$$

Thus, the vertical load that insists on the wheels changes when the vehicle decelerates: in particular during braking ($\ddot{x} < 0$), the front wheel vertical force increases and the rear wheel vertical force decreases proportionally to the deceleration (acceleration) of the vehicle. The vertical force variation is amplified as the ratio $h/(l_{zf}+l_{zr})$ increases: two-wheeled vehicles are usually characterized by a higher center of gravity (COG) position and a moderate wheelbase, which makes the load transfer phenomena outstanding if compared to four-wheeled vehicles.

The wheel slip control problem herein tackled is specialized only on the rear wheel, since motorcycle brake-by-wire systems are available so far only for the rear wheel (see e.g. [11]), mainly due to safety and reliability issues. Moreover, among the mentioned parameters that modify the torque-to-slip dynamics, only the rear wheel vertical force influence is here taken into account. Actually, the vehicle speed is not a critical parameter and satisfactory closed loop performances can be achieved disregarding its variations (when 1-5Hz) closed loop bandwidth is desired); its influence should be considered in the control system design for very high values ($\dot{x}$ > 300 Km/h). The same reasoning does not hold when dealing with surface (μ') variations; a wheel slip regulation problem that takes into account the mentioned parameter has been studied in [9], with an LPV model-based approach. Beside the

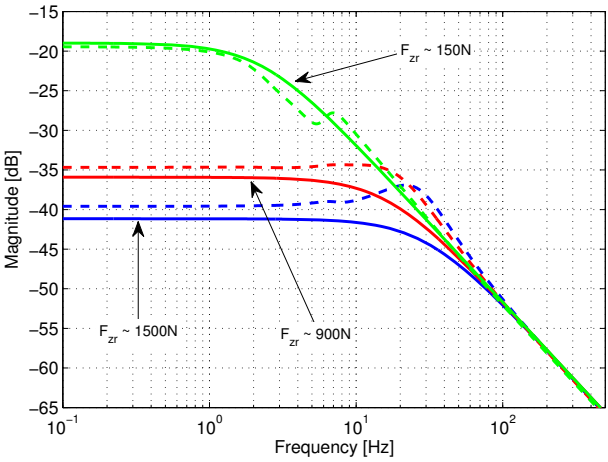

Fig. 11.3 Influence of vertical load on the rear wheel slip transfer function: linearized simulator model (dashed line) and Single Corner (solid line)

theoretical interest, the proposed approach is not suitable for practical implementation, since surface estimation and practical LPV identification of such a system are still open issues.

To better understand the influence of the load transfer in rear wheel slip control design, Figure 11.3 shows the Bode plot respectively for different decelerations, *i.e.* rear vertical forces (a comparison between the Single Corner model and the linearized BikeSim^{TM}transfer function is also depicted). Generally speaking, the Single Corner model provides a reasonable description of slip dynamics in a bandwidth limited around $[0--5]$Hz; considering that the nowadays brake-by-wire actuators are capable of a $[0--10]$Hz bandwidth, the range in which the Single Corner model can be considered valid is satisfactory. Beyond this limit, vehicle dynamics mainly due to suspensions appear in the considered transfer function. It can be seen how a change in the rear vertical force causes an important modification in the DC gain (over 20dB) of the torque-to-slip transfer function, along with a wheel pole frequency slowdown.

To take into account these variations, the torque-to-slip dynamics can be considered as a *linear parameter varying (LPV) system*. It should be here noticed that, practically, direct measurements of F_z are possible thanks to load sensing bearings, see [2], that are becoming an interesting opportunity for on-board force sensing, even though their actual diffusion are limited to test bench ([7]) or vehicle prototypes.

In the following sections, it will be shown how rear slip closed loop performances can be significantly enhanced by designing a control system that explicitly takes into account the variation of the load transfer.

11.4.1 Implementation of the VRFT Strategy

Although direct data-driven methods are sometimes referred to as “model-free", this term might be misleading when dealing with some engineering problems. Strictly speaking, the model parameters do not really need to be identified however some “a-priori" knowledge of the structure of the plant to-be-controlled could significantly guide the selection of the reference model and the controller class. In this section, this kind of reasoning will be proposed for what concerns the braking application for two-wheeled vehicles.

Considering the Single Corner model (11.12) it is clear that the LPV VRFT controller could be in general scheduled on F_z, $\dot{x}$ or μ' (when an accurate measurement is available). Nevertheless, with the proposed VRFT approach the controller can be scheduled only on the vertical load. This is motivated by the requirements for persistency of excitation of the LPV version of VRFT method. According to Subsection 11.3.1, the identification experiment should be designed such that the vehicle speed visits $n_s + 1$ points infinitely many times, where n_s is the maximum power at which the speed appears in the controller parameters. Since during braking the velocity naturally decreases, the maximum n_s allowed is 0, that is the speed must be assumed constant. Similar reasoning holds for μ' that, moreover, cannot be either changed when needed nor easily measured. On the other side, a sinusoidal trajectory for F_z is operable, as F_z can be suitably modulated by means of the front brake, and then no limits are given to the maximum power at which the force appears in the controller parameters.

In this context, it will be assumed that the reference model is achievable with a controller in the considered class and that the measurement devices are such that the noise power is low. It follows that the LPV controller will be tuned only using a single experiment.

As shown in Figure 11.3, the inclusion of the vertical load F_z allows to well describe low-frequency vehicle dynamics: accordingly, it is expected that an LPV controller scheduled only on the vertical force can achieve satisfactory performances for low-frequency (up to 5Hz) bandwidth. It should be said that closed-loop cutoff frequencies of 1-2Hz are not undersized with respect to benchmark control systems (see [27]). At these frequencies, the energy of the measurement noise is typically low, moreover the intrinsic nature of feedback further attenuates its effect on the output during closed-loop operation. Therefore, this topic will be here neglected to focus on the more critical dynamic coupling effect.

Thus, the LPV VRFT controller tuning experiment should follow these guidelines:

- the reference model has a sufficiently low cutoff frequency (*e.g.* $1Hz$ for the model illustrated in Figure 11.3),
- the experiment is performed at low velocities ($\dot{x} < 150$), where the effect of speed on the pole is not visible and the unique time-varying effect is due to load transfer.
- the frequency of excitation of F_z is below the minimum pole frequency.

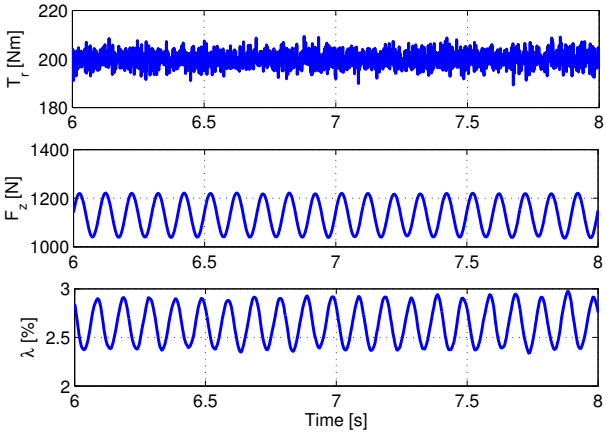

Fig. 11.4 Open-loop experiment on the Multibody Simulator

The latter requirement is due to the fact that, when F_z is at high frequencies, if the vehicle speed is high, the estimate of the system gain is biased, because λ is mitigated by the speed-filtering effect.

Once the range of interesting frequencies is bounded, to select the controller class it is sufficient to observe that the DC-gain of (11.12) linearly depends on the inverse of F_z. Then, an integral controller with the gain linearly depending on F_z allows the gain variations to be compensated and a first order reference model can be achieved; it can be then considered that the integral controller is not underparameterized (with respect to the controller structure that allows to achieve the desired closed loop performances) and thus the use of the optimal prefiltering, discussed in Section 11.3.2.1, is not necessary.

A last remark about the identification experiment is compulsory. Although the scheduling parameter is F_z, the real manipulable variable to vary it during the identification experiment is the front brake, that not only affects F_z, but also directly influences λ as a secondary input, if the whole vehicle dynamics are considered (obviously, this cannot be seen on the Single Corner model). In order to make the effect of the rear torque T visible on the slip, the front braking maneuvers to modulate F_z must be such that the front torque is much lower than the rear one.

An example of a realistic effective experiment is illustrated in Figure 11.4, where a white noise rear torque is generated. The same experiment will be used in the next Subsection to tune the gain-scheduled controller. It should be finally stressed that information about the model was so far only used to design the identification experiment and suitably select the reference model. No information about numerical values of its parameters was instead needed, unlike standard model-based control design.

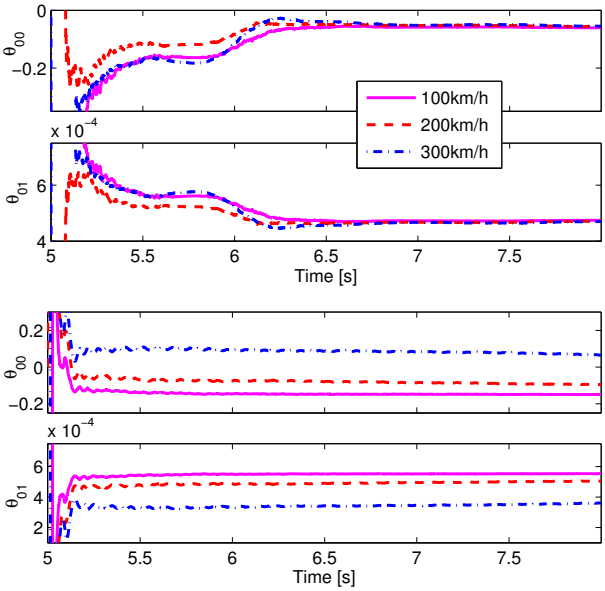

Fig. 11.5 Parameter trajectories at different initial speeds for different frequencies of excitation of F_z: 0.5Hz (top) and 10Hz (bottom)

11.4.2 Simulation Results

The VRFT approach has been applied to the fully nonlinear multi-body simulator Bikesim. The integral controller has been tuned to match a first order reference model with a bandwidth of [0–1]Hz, according to the identification experiment discussed in the previous section. The optimization procedure has led to the following discrete-time control law:

$$u(t) = u(t-1) + (\theta_{00} + \theta_{01} F_z(t))(r(t) - y(t)),$$

where:

$$\theta_{00} = -0.0567, \theta_{01} = 0.000471.$$

The convergence of the controller parameters is illustrated in Figure 11.5, that can be also interpreted as a sensitivity analysis to the length of the dataset. Notice that a biased estimate occurs if the excitation frequency is too high, as explained in the previous Section. Moreover, the bias is bigger when experiments are performed at high speed, since the filtering effect of the system pushes towards lower frequency when speed increases.

The effectiveness of the proposed controller is first showed for different constant F_z values: the rear wheel slip controller is fed with step setpoint for different values of vehicle deceleration. Recalling equation (11.13), vehicle deceleration at steady-state results in a change of the rear wheel vertical force. Figure 11.6 shows a comparison between system response with the LPV controller (top) and a model-based LTI controller (bottom, see [27]) in which the parameter value has kept constant to the nominal value (with zero vehicle deceleration). The LPV controller correctly compensate the increasing DC-gain of the rear slip transfer function allowing to keep the system response always close to the reference one. Indeed, the LTI controller cannot cope with such a change, proving how such a variable should be really taken into account in the design of a rear wheel slip controller.

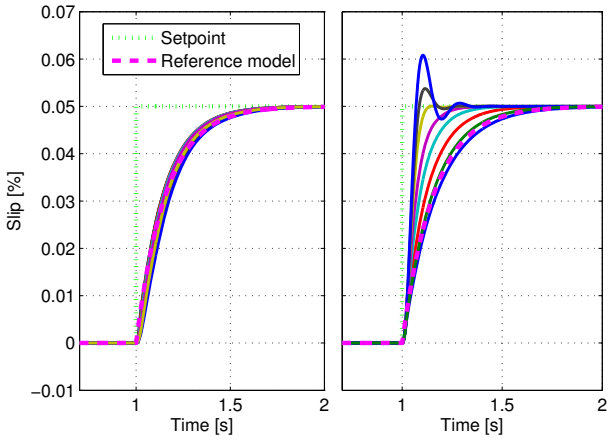

Fig. 11.6 Comparison between slip step-response of the closed-loop system with the LPV controller (left) and a standard model-based LTI controller (right) for different values of the vertical load

To check the proper controller design in a more realistic simulation which involves the complete nonlinear behaviour of the vehicle, two realistic panic brake maneuvers are considered.

First, a front braking torque step is applied and contemporaneously the rear wheel slip loop is fed with a step reference. The comparison between LPV and LTI controller is presented in Figure 11.7. Secondly, another panic braking maneuver is tried: a step reference is applied to the rear slip loop and then a front braking action (that acts as “load disturbance") is performed when the system is at steady-state. Results are shown in Figure 11.8, where, the front braking disturbance rejection proves more effective when the load transfer is measured.

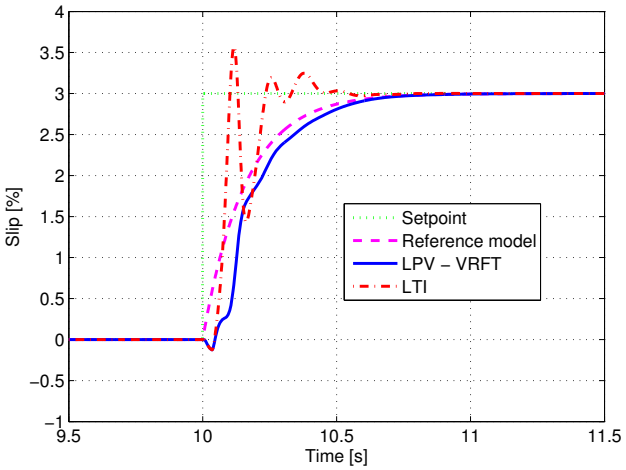

Fig. 11.7 LPV and LTI slip controller during the first panic brake maneuver described in the text

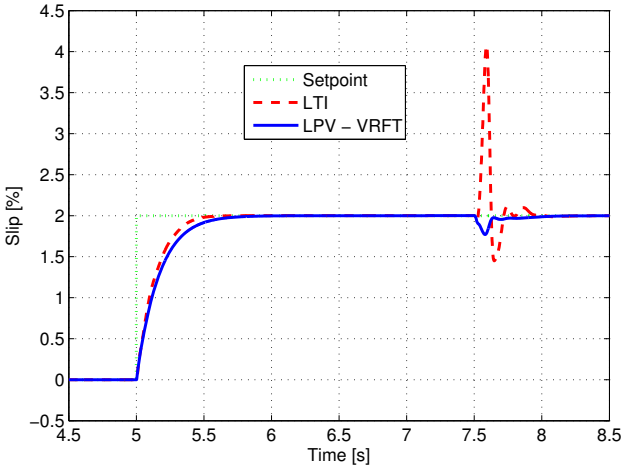

Fig. 11.8 LPV and LTI slip controller during the second panic brake maneuver described in the text

11.5 Concluding Remarks

In this chapter, the Virtual Reference Feedback Tuning approach for gain-scheduling controller design has been presented. The method does not require any model of the plant and it is based on convex optimization techniques, if the controller is suitably parameterized. Moreover, under some hypotheses, it guarantees consistency of the estimate, even in case of both output and parameter noisy measurements.

The approach has been tested on a braking control application for two-wheeled vehicles. Qualitative physics-based information about the dynamical structure of the system can be used to select the scheduling parameter, the reference model and the controller structure, whereas the control parameters are tuned with a single dataset collected on an open-loop experiment. The proposed strategy has been tested on the motorcycle multi-body simulator BikeSim^{TM}, providing satisfactory results also when tried on critical panic maneuvers.

Acknowledgements. This work has been partially supported by the Austrian Center of Competence in Mechatronics (ACCM), the MIUR project “New methods for Identification and Adaptive Control for Industrial Systems" and the FIRB project “Highly innovative motorbikes with ultra-low emission engine, active suspensions, electronic brakes and new materials".

References

1. Bamieh, B., Giarre, L.: Identification of linear parameter varying models. International Journal of Robust and Nonlinear Control 12(9), 841–853 (2002)
2. Bankestrom, J.O.: Load sensing bearing, US Patent 5,503,030 (April 2,1996)
3. Butcher, M., Karimi, A.: Data-driven tuning of linear parameter-varying precompensators. International Journal of Adaptive Control and Signal Processing (2010)
4. Butcher, M., Karimi, A., Longchamp, R.: On the consistency of certain identification methods for linear parameter varying systems. In: Proc. of the 17th IFAC World Congress, pp. 4018–4023 (2008)
5. Campi, M.C., Lecchini, A., Savaresi, S.M.: Virtual reference feedback tuning: a direct method for the design of feedback controllers. Automatica 38(8), 1337–1346 (2002)
6. Campi, M.C., Savaresi, S.M.: Direct nonlinear control design: The virtual reference feedback tuning (vrft) approach. IEEE Transactions on Automatic Control 51(1), 14–27 (2006)
7. Corno, M., Gerard, M., Verhaegen, M., Holweg, E.: Hybrid abs control using force measurement. IEEE Transactions on Control Systems Technology PP(99), 1–13 (2011)
8. Corno, M., Savaresi, S.M., Balas, G.J.: On linear-parameter-varying (LPV) slip-controller design for two-wheeled vehicles. International Journal of Robust and Nonlinear Control 19(12), 1313–1336 (2009)
9. Corno, M., Savaresi, S.M., Balas, G.J.: On linear parameter varying (lpv) slip-controller design for two-wheeled vehicles. International Journal of Robust and Nonlinear Control 19(12), 1313–1336 (2009)
10. Corno, M., Tanelli, M., Savaresi, S.M., Fabbri, L.: Design and validation of a gain-scheduled controller for the electronic throttle body in ride-by-wire racing motorcycles. IEEE Transactions on Control Systems Technology 19(1), 18–30 (2011)
11. Dardanelli, A., Alli, G., Savaresi, S.M.: Modeling and control of an Electro-Mechanical brake-by-wire actuator for a sport motorbike. In: Proc. of the 5th IFAC Symposium on Mechatronic Systems, Cambridge, MA, USA (2010)
12. Formentin, S., Savaresi, S.: Virtual reference feedback tuning for linear parameter-varying systems. In: Proc. of 18th IFAC World Congress, vol. 18, pp. 10219–10224 (2011)

13. Fu, M.: Model reference robust control. In: Robust Control. Springer (1992)
14. Gáspár, P., Szabó, Z., Bokor, J.: Design of reconfigurable and fault-tolerant suspension systems based on lpv methods. In: 47th IEEE Conference on Decision and Control, pp. 5384–5389 (2008)
15. Gevers, M.: Towards a joint design of identification and control? Essays on Control: Perspectives in the Theory and its Applications, 111 (1993)
16. Gevers, M.: Identification for control. Annual Reviews in Control 20, 95–106 (1996)
17. Guardabassi, G.O., Savaresi, S.M.: Approximate feedback linearization of discrete-time non-linear systems using virtual input direct design. Systems & Control Letters 32(2), 63–74 (1997)
18. Hjalmarsson, H.: From experiment design to closed-loop control. Automatica 41, 393–438 (2005)
19. Johansen, T.A., Petersen, I., Kalkkuhl, J., Lüdemann, J.: Gain-scheduled wheel slip control in automotive brake systems. IEEE Transactions on Control Systems Technology 11(6), 799–811 (2003)
20. Landau, Y.D.: Adaptive control: The model reference approach. Control and Systems Theory 8, 426 (1979)
21. Limebeer, D.J.N., Sharp, R.S., Evangelou, S.: The stability of motorcycles under acceleration and braking. Proc. of the Institution of Mechanical Engineers, Part C: Journal of Mechanical Engineering Science 215(9), 1095 (2001)
22. Ljung, L.: System identification: theory for the user, II edn. Prentice-Hall, Englewood Cliffs (1999)
23. Ogunnaike, B.A.: A contemporary industrial perspective on process control theory and practice. Annual Reviews in Control 20, 1–8 (1996)
24. Pacejka, H.B.: Tyre and Vehicle Dynamics. Buttherworth Heinemann, Oxford (2002)
25. Panzani, G., Formentin, S., Savaresi, S.M.: Active motorcycle braking via direct data-driven load transfer scheduling. In: 16th IFAC Symposium on System Identification, Brussels, Belgium (Submitted 2012)
26. Poussot-Vassal, C., Sename, O., Dugard, L., Savaresi, S.M.: Vehicle dynamic stability improvements through gain-scheduled steering and braking control. Vehicle System Dynamics 49(10), 1597–1621 (2011)
27. Savaresi, S.M., Tanelli, M.: Active Braking Control Systems Design for Vehicles. Springer (2010)
28. Sharp, R.S., Evangelou, S., Limebeer, D.J.N.: Multibody aspects of motorcycle modelling with special reference to Autosim. In: Ambrosio, J.A.C. (ed.) Advances in Computational Multibody Systems, pp. 45–68. Springer (2005)
29. Skogestad, S., Postlethwaite, I.: Multivariable Feedback Control. Analysis and Design. John Wiley & Sons (2005)
30. Tanelli, M., Astolfi, A., Savaresi, S.M.: Robust nonlinear output feedback control for brake by wire control systems. Automatica 44(4), 1078–1087 (2008)
31. Tanelli, M., Corno, M., Boniolo, I., Savaresi, S.M.: Active braking control of two-wheeled vehicles on curves. International Journal of Vehicle Autonomous Systems 7(3), 243–269 (2009)
32. Toth, R.: Modeling and Identification of Linear Parameter-Varying Systems, an Orthonormal Basis Function Approach. PhD thesis, Delft University of Technology (2008)
33. van Heusden, K., Karimi, A., Bonvin, D.: Data-driven model reference control with asymptotically guaranteed stability. International Journal of Adaptive Control and Signal Processing (2011)
34. Nichols, N.B., Ziegler, J.G.: Optimum settings for automatic controllers. Transactions of the ASME 64, 759–768 (1942)

Chapter 12
Design of a Hierarchical Controller for Suspension Systems

Péter Gáspár and Zoltán Szabó

Abstract. The chapter proposes the design of a hierarchical controller of an active suspension system for a full-car vehicle. The performance specifications are met by a high-level controller, in which the control input is a demanded virtual force. For the design of the high-level controller linear parameter varying (LPV) methods, in which both the performance specifications and the uncertainties of the model are taken into consideration, are proposed. The generation of the forces is based on the road disturbances and the measured signals. Once the desired forces are provided by the high-level, the actuator must track these reference signals by adjusting its spool valve. The actuator which is designed to carry out force-tracking is modelled as a nonlinear system. Control design in the low-level is based on the backstepping method. The modular design of both the high-level controller for the performance specifications and the low-level controller for the actuator has several advantages: it results in reduced-complexity models for the control design and changes in the actuator level do not affect the design of the high-level controller.

Keywords: backstepping design, LPV control, tracking control, performances, robustness, active suspension.

12.1 Introduction

Suspension systems are used to provide good handling characteristics and improve ride comfort while harmful vibrations caused by road irregularities and on-board excitation sources act upon the vehicle. The performance of suspension systems is

Péter Gáspár · Zoltán Szabó
Computer and Automation Research Institute, Hungarian Academy of Sciences,
Kende u. 13-17, Budapest, H1111 Hungary
e-mail: {gaspar,szaboz}@sztaki.hu

O. Sename et al. (Eds.): *Robust Control and LPV Approaches*, LNCIS 437, pp. 311–328.
DOI: 10.1007/978-3-642-36110-4_12

assessed quantitatively in terms of several parameters: passenger comfort, suspension deflection, tire load variation and energy consumption, see [4, 15]. The suspension problem is analyzed in fundamental papers such as [3, 7, 9].

One of the difficulties in the control design is that the different control goals are usually in conflict and a trade-off must be achieved between them. The variance of the sprung mass acceleration decreases when the variance of suspension or tire deflections increases, thus its minimization implies maximum admissible deflections. The result also indicates that generally the constraints imposed on the suspension deflection limit the tire deflection simultaneously and vice versa, see [6, 8]. Another difficulty in the control design is that the suspension model contains components whose behavior contains uncertainties. The uncertainty is caused by neglected dynamics, high-order modes, inadequate knowledge of components or alteration of their behavior due to changes in operating conditions.

The actuator built in a suspension system might be semi-active or active. An active solution can introduce energy in the system if necessary while a semiactive solution can only dissipate energy. A semi-active actuator works according to the characteristic depicted in Figure 12.1, where the damper force depends on the damping mechanism and the damper velocity. The active suspension system requires control forces independently of the relative velocity. The plot in Figure 12.1(b) contains the force demands provided by an active controller based on the quarter-car model (points). The lines are the graphs of the damper characteristics corresponding to different command values (lines). The modelling of vertical dynamics and the formalization of various performance specifications result in a high-complexity model which contains nonlinear suspension components and actuator dynamics. The hydraulic actuator which generates the suspension force has an inherently nonlinear nature. The direct inclusion of the actuator in the state space description of the suspension dynamics leads to a high-complexity model.

In the chapter a hierarchical design of the suspension system is proposed. In the design of a high-level controller a full-car model containing the suspension dynamics is considered where passenger comfort, road holding and tire deflection are

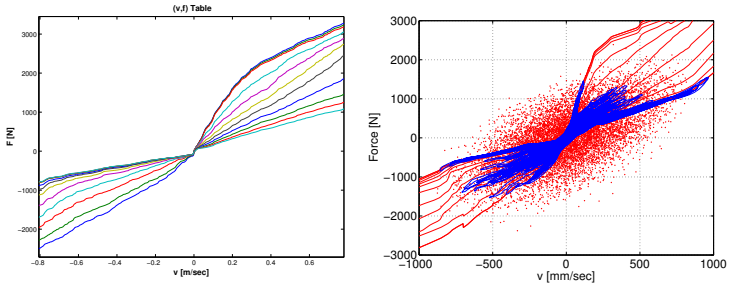

(a) Semi-active actuator characteristic (b) Required and achieved forces

Fig. 12.1 Operation of a semi-active damper

taken into consideration as performance outputs and the control input designed is the control force. In this step the uncertainties of the model are also considered. The designed control force is a required force, which must be created by the hydraulic actuator. The required force is tracked by a low-level controller by setting the valve of the actuator. The backstepping-based nonlinear method is presented for the design of the low-level controller. This approach explores the possibilities of the application of classical nonlinear control techniques for the output tracking control of an actuator subsystem used in active suspensions. Thus, the control design can be divided into two separate steps. The advantage of the hierarchical design is that the actuator dynamics and the suspension dynamics are handled in independent control design steps. The controller allows a modular design. Changes in the design of the actuator level do not affect the design of the upper level controller.

The structure of the chapter is as follows. In Section 12.2 the design of the suspension control from the modeling to the LPV-based control design is presented. The model of the hydraulic actuator used in the suspension system is also shown. In Section 12.3 the design of the actuator control based on the backstepping method is presented. In Section 12.4 the operation of the hierarchical controller is demonstrated through simulation examples. Finally, Section 12.5 contains some concluding remarks.

12.2 Design of the Suspension Control Based on LPV Methods

12.2.1 Modeling of the Suspension Systems

The control design is based on a full-car model of the suspension system. The full-car model, which is shown in Figure 12.2, comprises five parts: the sprung mass and four unsprung masses.

Let the sprung and unsprung masses be denoted by m_s, m_{uf}, and m_{ur}, respectively. All suspensions consist of a spring, a damper and an actuator to generate a pushing force between the body and the axle. The suspension damping force and the suspension spring force and the tire force are denoted by $F_{bij}, F_{kij}, F_{tij}$, respectively. The displacement of the sprung mass at the four suspension points is denoted by x_{1ij}, while the displacement of the unsprung mass is denoted by x_{2ij}. The disturbances w_{ij} are caused by road irregularities. The input signals f_{ij} are generated by the actuators. The system equations correspond to a seven degrees-of-freedom full-car vehicle model. The sprung mass is assumed to be a rigid body and has freedoms of motion in the vertical, pitch and roll directions. The x_1 is the vertical displacement at the center of gravity, θ is the pitch angle and ϕ is the roll angle of the sprung mass, respectively.

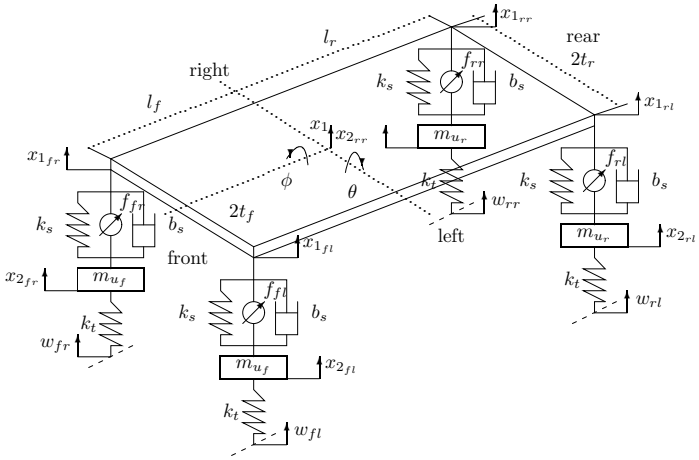

Fig. 12.2 The full car model

$$
\begin{aligned}
m_s\ddot{x}_1 =& F_{kfl}+F_{kfr}+F_{krl}+F_{krr}+F_{bfl}+F_{bfr}+F_{brl}+F_{brr}- \\
&-f_{fl}-f_{fr}-f_{rl}-f_{rr} && (12.1a)\\
I_\theta\ddot{\theta} =& l_fF_{kfl}+l_fF_{kfr}-l_rF_{krl}-l_rF_{krr}+l_fF_{bfl}+l_fF_{bfr}-l_rF_{brl}+l_rF_{brr}- \\
&-l_ff_{fl}-l_ff_{fr}+l_rf_{rl}+l_rf_{rr} && (12.1b)\\
I_\phi\ddot{\phi} =& t_fF_{kfl}-t_fF_{kfr}+t_rF_{krl}-t_rF_{krr}+t_fF_{bfl}-t_fF_{bfr}+t_rF_{brl}-t_rF_{brr}- \\
&-t_ff_{fl}+t_ff_{fr}-t_rf_{rl}+t_rf_{rr} && (12.1c)\\
m_{uf}\ddot{x}_{2_{fl}} =& -F_{kfl}-F_{tfl}-F_{bfl}+f_{fl} && (12.1d)\\
m_{uf}\ddot{x}_{2_{fr}} =& -F_{kfr}-F_{tfr}-F_{bfr}+f_{fr} && (12.1e)\\
m_{ur}\ddot{x}_{2_{rl}} =& -F_{krl}-F_{trl}-F_{brl}+f_{rl} && (12.1f)\\
m_{ur}\ddot{x}_{2_{rr}} =& -F_{krr}-F_{trr}-F_{brr}+f_{rr} && (12.1g)
\end{aligned}
$$

where the following linear approximations are applied: $x_{1_{fl}} = x_1 + l_f\theta + t_f\phi$, $x_{1_{fr}} = x_1 + l_f\theta - t_f\phi$, $x_{1_{rl}} = x_1 - l_r\theta + t_r\phi$, and $x_{1_{rr}} = x_1 - l_r\theta - t_r\phi$.

Figure 12.3 illustrates the nonlinear properties of the suspension spring and damper components. The suspension damping force and the suspension spring force, respectively, are as follows, see [5]:

$$F_{bij} = b_s^l(\dot{x}_{2ij}-\dot{x}_{1ij}) - b_s^{sym}|\dot{x}_{2ij}-\dot{x}_{1ij}| + b_s^{nl}\sqrt{|\dot{x}_{2ij}-\dot{x}_{1ij}|}\,\mathrm{sgn}(\dot{x}_{2ij}-\dot{x}_{1ij}), \tag{12.2a}$$

$$F_{kij} = k_s^l(x_{2ij}-x_{1ij}) + k_s^{nl}(x_{2ij}-x_{1ij})^3, \tag{12.2b}$$

and f_{ij} are the forces of the actuator, where $ij \in \{fl, fr, rl, rr\}$. Here, parts of the nonlinear suspension damper b_s are b_s^l, b_s^{nl} and b_s^{sym}. The b_s^l coefficient affects the

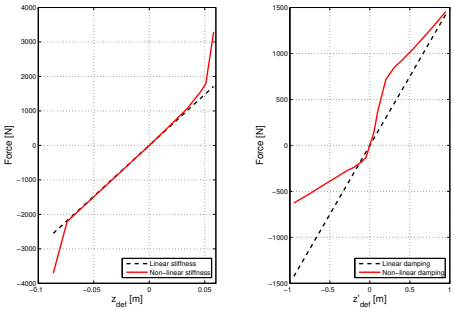

Fig. 12.3 Nonlinear properties of the suspension components

damping force linearly while b_s^{nl} has a nonlinear impact on the damping characteristics. b_s^{sym} describes the asymmetric behavior of the characteristics. Parts of the nonlinear suspension stiffness k_s are a linear coefficient k_s^l and a nonlinear one, k_s^{nl}. The tire force is approximated by a linear model:

$$F_{tij} = k_t(x_{2ij} - w_{ij}). \tag{12.3}$$

Remark 15. *The performance signals of the nonlinear model differ from those in the linear model with respect to their transient behavior. As an example for the front wheel they are tested by using a bump illustrated in Figure 12.4. The overshoots of the heave acceleration are larger by about* 10 % *in the nonlinear case than in the linear one, however, the transient duration in the nonlinear case is shorter than in the linear one. At the same time the values of suspension deflections are smaller in the nonlinear case than in the linear one. These properties are caused by the nonlinear damping characteristics, which are significantly different from the linear characteristics around the equilibrium point.*

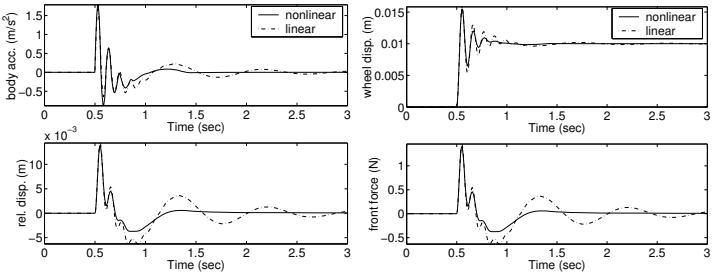

Fig. 12.4 Time responses of the vehicle to a bump

The state vector x is selected as follows: $x = \begin{bmatrix} q^T & x_u^T & \dot{q}^T & \dot{x}_u^T \end{bmatrix}^T$ with $q = \begin{bmatrix} x_1 & \theta & \phi \end{bmatrix}^T$ and $x_u = \begin{bmatrix} x_{2fl} & x_{2fr} & x_{2rl} & x_{2rr} \end{bmatrix}^T$. In the LPV modeling scheduling variables, which are directly measured or can be calculated from the measured signals, must be selected. Variables concerning the front and rear displacement between the sprung mass and the unsprung mass on the left and right side and their velocities are selected as scheduling variables:

$$\rho_{bij} = \dot{x}_{2ij} - \dot{x}_{1ij}, \tag{12.4a}$$

$$\rho_{kij} = x_{2ij} - x_{1ij} \tag{12.4b}$$

with $ij \in \{fl, fr, rl, rr\}$. The scheduling variable ρ_{bij} depends on the relative velocity, while the scheduling variable ρ_{kij} depends on the relative displacement. In practice, the relative displacement is a measured signal. The relative velocity is then determined by numerical differentiation from the measured relative displacement. Thus, in the LPV model of the active suspension system eight parameters are selected as scheduling variables.

The design of the high-level controller is based on the parameter-dependent LPV method. The state space representation of the *LPV* model is as follows:

$$\dot{x} = A(\rho)x + B_1(\rho)w + B_2(\rho)u, \tag{12.5}$$

where $u = \begin{bmatrix} f_{fl} & f_{fr} & f_{rl} & f_{rr} \end{bmatrix}^T$ and $w = \begin{bmatrix} w_{fl} & w_{fr} & w_{rl} & w_{rr} \end{bmatrix}^T$.

12.2.2 Performance Specifications of the Suspension System

The performance of a suspension system can be assessed quantitatively in terms of four parameters: passenger comfort, suspension deflection, tire load variation and energy consumption, see [4]. Vehicle vibrations excited by road irregularities might lead to the fatigue of the driver and passengers, as well as damage to the vehicle and the payload. It is widely accepted that there is a correlation between passenger comfort (or ride comfort) and the heave, pitch and roll accelerations of the sprung mass. The suspension working space, which is defined as the relative displacement between the sprung and unsprung masses and also called suspension deflection, may affect directional stability because of particular suspension geometries. It is required that suspension deflection be minimized. The suspension system must guarantee that the vehicle remains on the track in all maneuvers. The tire load is made up of a static component due to gravity and a dynamic component due to road unevenness. In order to reduce variations of the side force during a vehicle maneuver, it is necessary that the dynamic tire load component be kept as small as possible. The control force limitation is incorporated into the design procedure in order to avoid large control forces.

Consider the closed-loop system in Figure 12.5, which includes the feedback structure of the nominal model G and controller K, and elements associated with the uncertainty models and performance objectives. In the diagram, u is the control

input, which is generated by actuators, y is the measured output, n is the measurement noise. The measured outputs are the front and rear displacement between the sprung mass and the unsprung mass on the left and right side, $y_{ij} = x_{1ij} - x_{2ij}$, with $ij \in \{fl, fr, rl, rr\}$. In the figure, w_{ij} is the disturbance signal, which is caused by road irregularities. z represents the performance outputs: the passenger comfort (heave acceleration) ($z_{aij} = \ddot{x}_{1ij}$), the suspension deflection ($z_{sij} = x_{1ij} - x_{2ij}$) and the wheel relative displacement ($z_{tij} = x_{2ij} - w_{ij}$). The control force limitation is incorporated into the design procedure in order to avoid large control requirements ($z_{uij} = f_{ij}$). The vector of the performance output is the following: $z = \left[z_{aij}\ z_{sij}\ z_{tij}\ z_{uij}\right]^T$.

$$z = C_1(\rho)x + C_{12}(\rho)u, \tag{12.6}$$

The feedback structure also includes the uncertainties caused by neglected dynamics, uncertain components, inadequate knowledge of components, or alteration of their behavior due to changes in operating conditions. In order to maintain the design complexity between bounds in this structure uncertainties are represented by a multiplicative LTI block Δ_m and a weighting function W_r. It is assumed that the transfer function W_r is known, and it reflects the uncertainty bound in the model. Δ_m is assumed to be stable and unknown with the norm condition $\|\Delta_m\|_\infty < 1$.

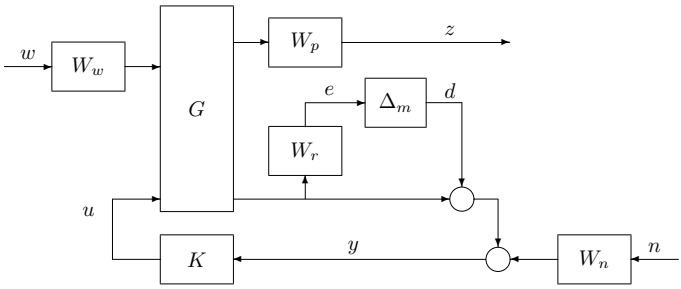

Fig. 12.5 The closed-loop interconnection structure

The aim of the control design is to create four control forces $f = \left[f_{fl}\ f_{fr}\ f_{rl}\ f_{rr}\right]$ in such a way that all the heave accelerations, the suspension deflections, the tire deflections and the control inputs should be as small as possible over the desired operation range.

The purpose of weighting functions $W_{p,az}$, $W_{p,sd}$, $W_{p,td}$ and $W_{p,f}$ is to keep the heave acceleration, suspension deflection, wheel travel, and control input small over the desired operation range. These weighting functions chosen for performance outputs can be considered as penalty functions, i.e., weights should be large in a frequency range where small signals are desired and small where larger performance outputs can be tolerated. Thus, $W_{p,az}$ and $W_{p,sd}$ are selected as

$$W_{p,az} = \gamma_{az} \frac{T_{s1}s+1}{T_{s2}s+1}, \tag{12.7a}$$

$$W_{p,sd} = \gamma_{sd} \frac{T_{s3}s+1}{T_{s4}s+1}. \tag{12.7b}$$

The choice of the actual values of the filter coefficients T_{sk} are chosen based on the engineering knowledge on the problem at hand. The parameter dependence of the gains is characterized by the constants ρ_1 and ρ_2 in the following way:

$$\gamma_{az} = \begin{cases} 1 & \text{if} \quad |\rho_{kij}| < \rho_1, \\ \frac{|\rho_{kij}|-\rho_2}{\rho_1-\rho_2} & \text{if} \quad \rho_1 \le |\rho_{kij}| \le \rho_2, \\ 0 & \text{if} \quad R \ge R_s \text{ or } |\rho_{kij}| > \rho_2. \end{cases}$$

$$\gamma_{sd} = \begin{cases} 0 & \text{if} \quad |\rho_{kij}| < \rho_1, \\ \frac{|\rho_{kij}|-\rho_1}{\rho_2-\rho_1} & \text{if} \quad \rho_1 \le |\rho_{kij}| \le \rho_2, \\ 1 & \text{if} \quad R \ge R_s \text{ or } |\rho_{kij}| > \rho_2. \end{cases}$$

Here, it is assumed that in the low frequency domain disturbances at the heave accelerations of the body should be rejected by a parameter-dependent factor of ρ_{kij} and at the suspension deflection by the same factor. The gains are characterized by the selection of the constants ρ_1 and ρ_2. This corresponds to an LPV controller that minimizes only the vertical acceleration when the suspension travel is less than ρ_1, and which gradually begins focusing on the suspension deflection when the travel is greater than ρ_1. Over ρ_2 it minimizes only the suspension deflection. During the design constant weighting factors are selected for the other performances as $W_{p,tij} = \gamma_3$ and $W_{p,fij} = \gamma_4$. Note that although these weighting functions are formalized in the frequency domain, their state space representation forms are applied in the weighting strategy and in the control design.

The difficulty in formulating the control objectives through the performance signals z is that there is a conflict between the different performance demands: e.g., passengers comfort and suspension deflection cannot be improved simultaneously. Thus a trade-off between them must be achieved by a suitable choice of the performance weights: in (12.7a) and (12.7b) a large gain γ_{az} and a small gain γ_{sd} correspond to a design that emphasizes passenger comfort. On the other hand, choosing γ_{az} small and γ_{sd} large correspond to a design that focuses on suspension deflection. In the *LPV* controller ρ_{kij} is the relative displacement between the sprung and the unsprung masses according to (12.4a), i.e., $\rho_{kij} = x_{1ij} - x_{2ij}$. The scheduling variable ρ_{kij} is used to focus on minimizing either the vertical acceleration or the suspension deflection response, depending on the magnitude of the vertical suspension deflection.

The structure of the augmented plant can be put into the form shown in Figure 12.6 with disturbances $\tilde{w} = \begin{bmatrix} w & n \end{bmatrix}^T$, uncertainty $\Delta = \Delta_m$ and control input $u = f$. The robust control framework is formulated using the closed-loop interconnection structure depicted in Figure 12.6, where $G_{\mathscr{F}_{\mathscr{P}}}$ is the generalized plant containing the nominal plant and all the performance, disturbance and uncertainty weights, $\tilde{w}$

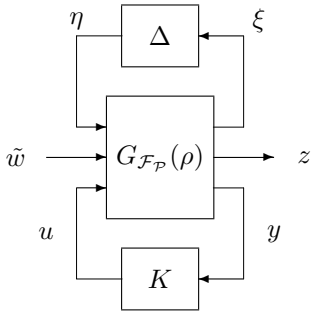

Fig. 12.6 The closed-loop interconnection structure

contains the disturbances while Δ is the possibly structured normalized diagonal uncertainty block, for details, see e.g., [17, 19].

12.2.3 Design of a High-Level Controller Based on an LPV Method

The control design is based on induced $\mathscr{L}_2$-norm of the LPV system $G_{\mathscr{F}_\mathscr{P}}$, with zero initial conditions, defined as

$$\left\|G_{\mathscr{F}_\mathscr{P}}\right\|_\infty = \sup_{\rho\in\mathscr{F}_\mathscr{P}} \sup_{\|\Delta\|_\infty<1} \sup_{\|\tilde{w}\|_2\neq 0,\tilde{w}\in\mathscr{L}_2} \frac{\|z\|_2}{\|\tilde{w}\|_2}. \tag{12.8}$$

The $\mathscr{L}_2$-norm level $\gamma = \left\|G_{\mathscr{F}_\mathscr{P}}\right\|_\infty$ for an LPV system represents the largest ratio of disturbance norm to performance norm over the set of all causal linear operators described by the LPV system, hence it is the final performance index of the design. For an appropriate selection of the performance and disturbance weights a successful design means $\gamma < 1$. It is noted that the weighting functions must be selected according to the control goals.

The solution of an LPV problem is based on the set of LMIs being satisfied for all $\rho \in \mathscr{F}_\mathscr{P}$. In practice, this problem is set up by gridding the parameter space and solving the set of LMIs that hold on the subset of $\mathscr{F}_\mathscr{P}$. Weighting functions are defined in all of the grid points. For details, see [2, 12, 18]. With respect to the robustness requirement, the same frequency weighting functions are applied in the whole parameter space and the effect of the scheduling variable is neglected. It is a reasonable engineering assumption, since unmodelled dynamics does not depend on the gridding parameters. The required force designed by the high-level controller must be tracked by a low-level controller by setting the valve of the actuator.

12.3 Design of the Actuator Control

12.3.1 Modeling of the Actuator Dynamics

The force of the actuator is expressed in the following way:

$$f_{ij} = A_P P_{Lij}, \tag{12.9}$$

where A_P is the area of the piston and P_{Lij} $(i \in f,r,\ j \in l,r)$ is the pressure drop across the piston, see [11]. The derivative of P_{Lij} is given by

$$\dot{P}_{Lij} = -\beta P_{Lij} + \alpha A_P z_{ij} + \gamma Q_{ij}, \tag{12.10}$$

in which Q_{ij} is the hydraulic load flow, $z_{ij} = \dot{x}_{2ij} - \dot{x}_{1ij}$ is the the damper velocity and α, β, γ are constants. The hydraulic load flow can be expressed

$$Q_{ij} = sgn\left[P_S - sgn(x_{vij})P_{Lij}\right] Q_{0ij} x_{vij}, \tag{12.11}$$

where

$$Q_{0ij} = \sqrt{|P_S - \mathrm{sign}(x_{vij})P_{Lij}|}, \tag{12.12}$$

$$\mathrm{sign}(x_{vij}) = \begin{cases} 1, & x_{vij} > 0 \\ 0, & x_{vij} = 0 \\ -1, & x_{vij} < 0 \end{cases}, \tag{12.13}$$

with the supply pressure P_S and the displacement of the spool valve x_{vij}. The damper velocity acts as a coupling from the position output of the cylinder to the pressure differential across the piston. It is considered a feedback term, which has been analyzed by [1]. It is assumed that during the operation $P_S > P_{Lij}$. Using the assumption (12.11) reads $Q_{ij} = Q_{0ij} x_{vij}$, which defines a state-dependent bimodal switching system for the actuator dynamics. Moreover, in order to avoid the technical difficulties caused by the non-smoothness of the sign function the $\mathrm{sign}(x) \approx \tanh(x/\sigma)$ – with a very small σ – will be used.

The displacement of the spool valve is controlled by the input to the servo-valve u_{ij}:

$$\dot{x}_{vij} = \frac{1}{\tau_{ij}} \left(-x_{vij} + u_{ij}\right). \tag{12.14}$$

where τ_{ij} is a time constant.

Each of the four actuator models are formalized separately based on the generic model which is used for the design of the low-level control as

$$\dot{\xi}_1 = -\beta \xi_1 + \gamma Q_0(\xi_1, \xi_2)\xi_2 + \alpha A_P z, \tag{12.15a}$$

$$\dot{\xi}_2 = -\frac{1}{\tau}\xi_2 + \frac{1}{\tau}u. \tag{12.15b}$$

for the ij^{th} actuator with ξ_1 and ξ_2 denote P_{Lij} and x_{vij}, respectively, while $Q_0 = Q_{0ij}$, $z = z_{ij}$ and $\tau = \tau_{ij}$. The component $Q_0(\xi_1, \xi_2)$ is expressed in form (12.12).

12.3.2 Design of a Low-Level Controller Based on Backstepping Method

For the control system this requires that the actuators provide the demanded virtual inputs given by the high-level controllers. For the application example of this chapter this means that once the desired forces in the front and the rear on the right-hand and the left-hand sides of the vehicle are provided by the supervisory level, the actuator must track these reference signals by adjusting its valve. The starting point is that a force requirement, which is designed by the LPV controller, is given, thus a demand of a pressure drop $P_{L,dem}$ is given.

The force required by the upper level control ($\xi_{1,dem}$) must be generated by the low-level control. The purpose of the tracking control is to follow the force demand, i.e., the difference between the pressure demand and the actual pressure must be minimal:

$$\xi_1 \rightarrow \xi_{1,dem} \tag{12.16}$$

The pressure demand required by the high-level control will be denoted by $\xi_{1,dem}$ while $\xi_{2,dem}$ denotes the demand of the spool valve displacement $x_{v,dem}$. The actual value of the displacement of the spool valve (x_v) is denoted by ξ_2. It is assumed that both ξ_1 and ξ_2 are available for the measurement. It is assumed that the required value of the pressure $\xi_{1,dem}$ is at least two times differentiable.

In order to show the principle of the backstepping method the notations of [13, 14] are used. It is assumed that the high level system is modelled by an LPV system augmented by the four actuator dynamics leading to the cascaded system:

$$\dot{\zeta} = A(\zeta)\zeta + B(\zeta)[\xi_1^{ij}], \tag{12.17a}$$

$$\dot{\xi}_1^{ij} = a_1(\zeta, \xi_1^{ij}) + b_1(\xi_1^{ij}, \xi_2^{ij})\xi_2^{ij}, \tag{12.17b}$$

$$\dot{\xi}_2^{ij} = a_2(\xi_2^{ij}) + b_2 u^{ij}, \tag{12.17c}$$

that can be put in the strict feedback form, see chapter 6. of [14],

$$\dot{\zeta} = A(\zeta)\zeta + B(\zeta)[\xi_1^{ij}], \tag{12.18a}$$

$$\dot{\xi}_1^{ij} = a_1(\zeta, \xi_1^{ij}) + \tilde{\xi}_2^{ij}, \tag{12.18b}$$

$$\dot{\tilde{\xi}}_2^{ij} = \tilde{a}_2(\xi_1^{ij}, \tilde{\xi}_2^{ij}) + \tilde{b}_2(\xi_1^{ij}, \tilde{\xi}_2^{ij})u^{ij}, \tag{12.18c}$$

by using the state transform $\tilde{\xi}_2^{ij} = b_1(\xi_1^{ij}, \xi_2^{ij})\xi_2^{ij}$. Since the nominal system (12.18a) is globally asymptotically stable by construction the resulting closed–loop system containing the tracking controllers will be stable, see, e.g., chapter 5 in [13]. Note that the state transform that leads to the strict feedback form is needed only to

relate the original system to the already developed passivity based framework of cascaded systems and the actual computations can be done on the individual actuator subsystems.

The backstepping design for the actuator subsystem can be performed in two steps. In the first step, let us consider $\xi_{2,dem}$ as a virtual input and $e_1 = \xi_1 - \xi_{1,dem}$ the realized tracking error. The errors between the pressure demand and the actual value of the pressure and its dynamics are $e_1 = \xi_1 - \xi_{1,dem}$ and $\dot{e}_1 = \dot{\xi}_1 - \dot{\xi}_{1,dem}$. The aim is to construct a feedback that guarantees the tracking of the pressure demand required by the upper level control. A feedback control that guarantees an exponential tracking of $\xi_{1,dem}$ is constructed. The feedback component k_1 is chosen such that the error dynamics tends to zero exponentially $\dot{e}_1 = -k_1 e_1$, $k_1 > 0$. The dynamics of the pressure is

$$\dot{\xi}_1 = \dot{\xi}_{1,dem} - k_1(\xi_1 - \xi_{1,dem}). \tag{12.19}$$

Since ξ_1 is not a manipulable input, the aim is to construct the demand of the displacement of the spool valve $\xi_{2,dem}$ as a virtual input. Using the equation

$$\dot{\xi}_1 = -\beta\xi_1 + \gamma Q_0(\xi_1, \xi_{2,dem})\xi_{2,dem} + \alpha A_P z, \tag{12.20}$$

the displacement demand of the spool valve

$$\xi_{2,dem} = \frac{\dot{\xi}_{1,dem} - k_1(\xi_1 - \xi_{1,dem}) + \beta\xi_1 - \alpha A_P z}{\gamma Q_0(\xi_1, \xi_{2,dem})} \tag{12.21}$$

Note that $Q_0(\xi_1, \xi_{2,dem}) = \sqrt{|P_S - \text{sign}(\xi_{2,dem})\xi_1|}$. It is assumed that $\text{sign}(\xi_{2,dem}) = \text{sign}(\xi_2)$. A non-smoothness of the sign function is provided by the following approximation $\text{sign}(\xi_2) = \tanh(\xi_2/\sigma)$ with a very small σ. Consequently, $\xi_{2,dem}$ can be calculated.

The error between the displacement of the spool valve and the the actual value of the displacement and its dynamics are $e_2 = \xi_2 - \xi_{2,dem}$, $\dot{e}_2 = \dot{\xi}_2 - \dot{\xi}_{2,dem}$. In the second step, the aim is to construct a feedback that guarantees the tracking of the displacement demand of the spool valve. The feedback component k_2 is chosen such that the error dynamics tends to zero exponentially $\dot{e}_2 = -k_2 e_2$, $k_2 > 0$. The dynamics of the displacement demand is

$$\dot{\xi}_2 = \dot{\xi}_{2,dem} - k_2(\xi_2 - \xi_{2,dem}). \tag{12.22}$$

Finally, based on the expression $u_{dem} = \tau\dot{\xi}_2 + \xi_2$ the physical manipulable actuator input u can be expressed as follows

$$u_{dem} = \tau\dot{\xi}_{2,dem} - \tau k_2(\xi_2 - \xi_{2,dem}) + \xi_2. \tag{12.23}$$

In the calculation of u_{dem} both $\xi_{2,dem}$ and $\dot{\xi}_{2,dem}$ are required.

$$\xi_{2,dem} = \frac{\psi}{\gamma Q_0(\xi_1, \xi_{2,dem})}, \tag{12.24}$$

$$\dot{\xi}_{2,dem} = \frac{\dot{\psi}}{\gamma Q_0(\xi_1, \xi_{2,dem})} - \frac{\xi_{2,dem}\dot{Q}_0(\xi_1, \xi_{2,dem})}{Q_0(\xi_1, \xi_{2,dem})}, \tag{12.25}$$

where $\psi = \dot{\xi}_{1,dem} - k_1(\xi_1 - \xi_{1,dem}) + \beta\xi_1 - \alpha A_P z$. Using

$$\dot{Q}_0 = -\frac{\dot{\xi}_{2,dem}\xi_1}{2\xi_{2,dem}Q_0}\frac{\xi_{2,dem}/\sigma}{\cosh^2(\xi_{2,dem}/\sigma)} - \frac{\dot{\xi}_1 \tanh(\xi_{2,dem}/\sigma)\xi_{2,dem}}{2\xi_{2,dem}Q_0}$$

the signal $\dot{\xi}_{2,dem}$ can be computed

$$\dot{\xi}_{2,dem} = \frac{1}{\gamma Q_0}\left(\dot{\Psi} + \xi_{2,dem}\gamma\frac{\dot{\xi}_1 \text{sign}(\xi_{2,dem})}{2Q_0}\right). \tag{12.26}$$

The algorithm of the backstepping method is illustrated in Figure 12.7.

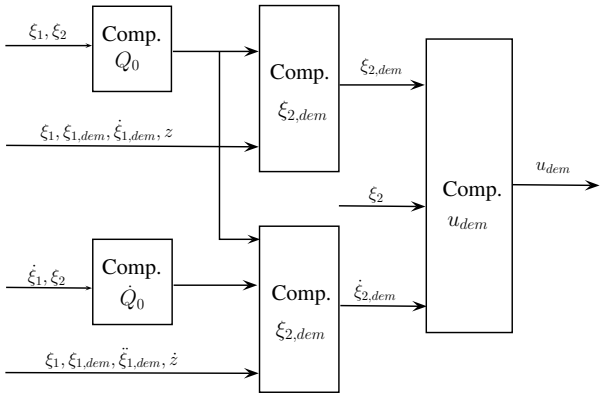

Fig. 12.7 Illustration of the backstepping method

The measured signals required by the algorithm are $\xi = P_L$, $x_2 = x_v$ and z. The implementation of the backstepping method requires the computation of the time derivatives of $\dot{\xi}_1 = \dot{P}_L$, $\ddot{\xi}_1 = \ddot{P}_L$, $\xi_{1,dem} = P_{L,dem}$ and $\dot{z}$ which can be done in a number of ways depending on the measurement noise conditions and the required precision. In this method the controller parameters k_1 and k_2 determine the convergence speed of the tracking errors e_1 and e_2, respectively. As a conclusion in the backstepping method two parameters, k_1 and k_2 are chosen to handle the dynamics of the tracking. By selecting suitable parameters the accuracy of tracking can be improved but the physical limits of the actuator must be taken into consideration. Failing to do so may result in discrepancy between the planned and the realized forces, i.e., tracking error. Possible strategies for numerical differentiation are contained in [10, 16].

Remark 16. *Note that the control design in the actuator level can also be performed by using LPV methods. In order to reduce the complexity of the control design the actuator dynamics is built into the quarter-car model, illustrated in Figure 12.8. The equations of the quarter-car model are:*

$$m_s\ddot{x}_1 = F_{kf} + F_{bf} - f_f \tag{12.27a}$$
$$m_u\ddot{x}_2 = -F_{kf} - F_{bf} - F_{tf} + f_f \tag{12.27b}$$
$$\dot{P}_L = -\beta P_L + \alpha A_P(\dot{x}_2 - \dot{x}_1) + \gamma Q \tag{12.27c}$$
$$\dot{x}_v = -\frac{1}{\tau}x_v + \frac{1}{\tau}u. \tag{12.27d}$$

where $f_f = A_P P_L$, $Q = sgn(P_S - sgn(x_v)P_L)Q_0 x_v$.

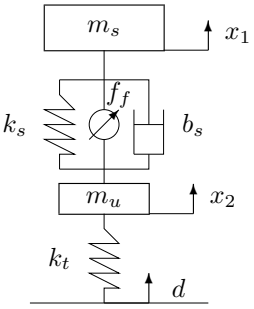

Fig. 12.8 Quarter-car model

The state space representation of vertical dynamics:

$$\dot{x} = A(\rho_s)x + B(\rho_s)u, \tag{12.28}$$

The components of the state vector are the vertical displacement of the sprung mass x_1*, the vertical displacement of the unsprung mass* x_2*, their derivatives* $x_3 = \dot{x}_1$*,* $x_4 = \dot{x}_2$*, the pressure drop* $x_5(= P_L)$*, and the servo valve displacement* $x_6(= x_v)$*. The input signal is the input to the servo valve. The scheduling vector is selected as* $\rho_s = \begin{bmatrix}\rho_Q & \rho_b & \rho_k\end{bmatrix}$ *where the scheduling variables are assumed to be available:*

$$\rho_Q = sgn(P_S - sgn(x_v)P_L)Q_0,$$
$$\rho_b = \dot{x}_2 - \dot{x}_1,$$
$$\rho_k = x_2 - x_1.$$

The advantages of this approach are that in the control-oriented model the nonlinear behavior of suspension components, the actuator dynamics and the performance specifications are taken into consideration. Moreover, the control design is based on LPV methods. However, the disadvantage is that the solution does not provide modularity in the design. The details can be seen in [5].

12.4 Simulation Examples

In the simulation example the operation of the hierarchical controller is illustrated. The nominal parameters of the vehicle model are listed in Table 12.1.

Table 12.1 Parameters of the suspension system

Parameters	Value	Unit
m_s	1400	kg
I_θ	2100	$kg.m^2$
I_ϕ	460	$kg.m^2$
m_{uf}, m_{ur}	40, 40	kg
k_s^l	$235 \cdot 10^2$	N/m
k_s^{nl}	$235 \cdot 10^4$	N/m^3
k_t	$190 \cdot 10^3$	N/m
b_s^l, b_s^{sym}	200, 400	Ns/m
b_s^{nl}	400	$N\sqrt{s}/\sqrt{m}$
α, β, γ,	$4.515 \cdot 10^{13}$, 1, $4.969 \cdot 10^{12}$	
A_P	$3.35 \cdot 10^{-4}$	m^2
P_s	10342500	Pa
τ	$1/30$	s

The purpose of the weighting functions is to meet performance specification. They are chosen $W_{p,aij} = 0.5\,\gamma_{az}\,\frac{s/350+1}{s/10+1}$ and $W_{p,sij} = \gamma_{sd}\,\frac{s/350+1}{s/10+1}$. It is assumed that in the low frequency domain disturbances on the heave acceleration should be rejected by a factor of 2 and on the suspension deflection by a factor of 1. The parameter-dependent gains are characterized by the selection of the constant $\rho_1 = 0.05$ and $\rho_2 = 0.07$. The weights for the wheel travel, i.e., $W_{p,tij} = 1$ and for the control input $W_{p,fij} = 10^{-3}$, are selected in order to avoid actuator saturation. The uncertainty is modelled as a complex full block with multiplicative uncertainty at the plant output. The weighting function of the unmodelled dynamics is set at $W_r = 0.1\,\frac{s/20+1}{s/450+1}$, reflecting a 10% uncertainty level in the low frequency domain. The upper-level control is designed by the LPV method.

The suspension systems are tested on a fictitious bad-quality road, on which different bumps disturb the motion of the vehicle, see Figure 12.9(a). Between the bumps there are velocity-dependent stochastic road excitations. The time responses of the performance signals to the road disturbances depicted in Figure 12.9 show the superiority of the LPV controller in terms of decay rate and overshoots. Figure 12.9(c) illustrates the force required by the upper level controller.

In the low-level the required force must be realized by the backstepping method. The parameters of the backstepping method are selected as $k_1 = 20$ and $k_2 = 20$. In the simulation example the sampling time of the measured signals is selected $T_s = 0.01$ *sec*, which corresponds to practice. The time responses of the low-level controller are illustrated in Figure 12.10. The illustrated signals are the pressure

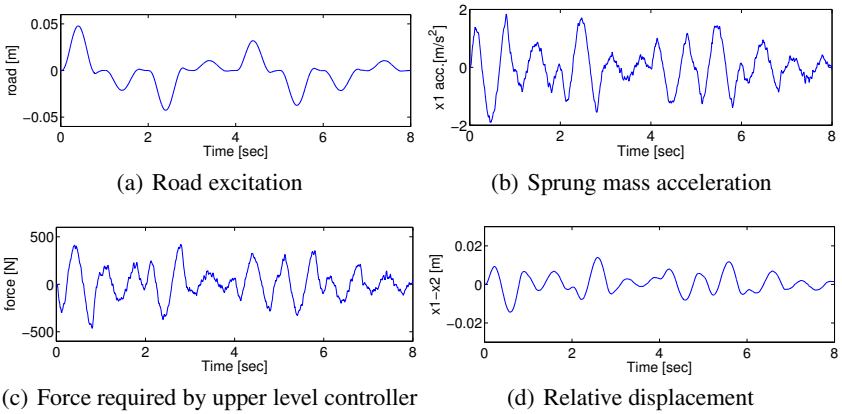

(a) Road excitation (b) Sprung mass acceleration

(c) Force required by upper level controller (d) Relative displacement

Fig. 12.9 Time responses of the controlled system using an upper-level controller

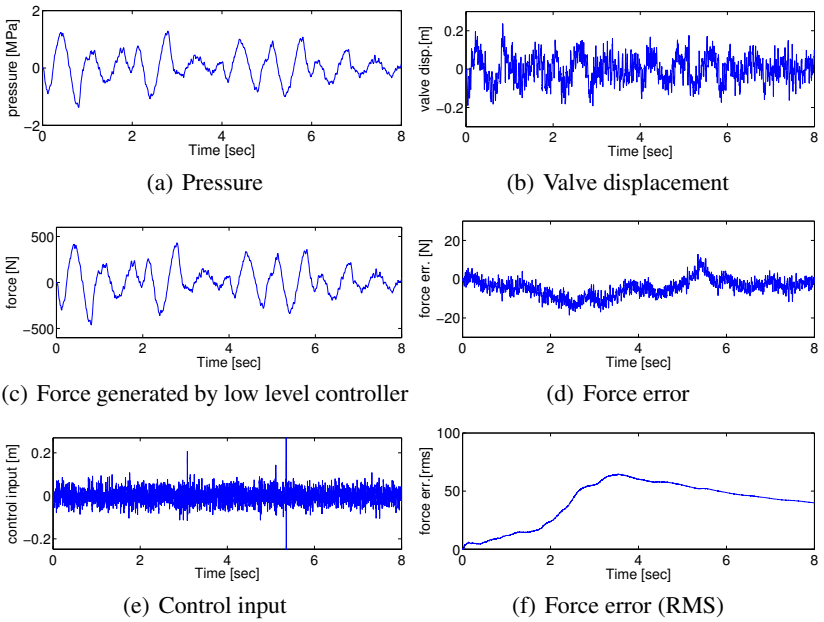

(a) Pressure (b) Valve displacement

(c) Force generated by low level controller (d) Force error

(e) Control input (f) Force error (RMS)

Fig. 12.10 Time responses of the controlled system using a low-level controller

drop across the piston, the displacement of the spool valve, the control input, the achieved force and the force error. The force generated by the actuator follows the required force with high precision. It is illustrated by the force error and its RMS values, see Figure 12.10(d) and Figure 12.10(f).

12.5 Conclusions

In the chapter a hierarchical controller has been proposed for the design of active suspension systems: one level for the suspension and another for the actuator. An LPV-based controller is used to compute the required input force, which is tracked using a nonlinear controller for the actuator subsystem. The performance requirements guaranteed by the controller in the upper level can be achieved by solving the tracking task with the low-level controller. For the actuator level a backstepping controller has been designed.

This method is advantageous for several reasons. The main advantage of the proposed solution is its ability to meet complex control performance criteria together with the handling of the nonlinear actuator dynamics. An additional advantage is that changes in the actuator level do not affect the design of the high-level controller.

References

1. Alleyne, A., Liu, R.: A simplified approach to force control for electro-hydraulic systems. Control Engineering Practice 8, 1347–1356 (2000)
2. Balas, G., Fialho, I., Lee, L., Nalbantoglu, V., Packard, A., Tan, W., Wolodkin, G., Wu, F.: Theory and application of linear parameter varying control techniques. In: Proc. of the American Control Conference (1997)
3. Crolla, D.: Active suspension control algorithms for a four-wheel vehicle model. International Journal of Vehicle Design 13(2), 144–158 (1992)
4. Gillespie, T.: Fundamentals of vehicle dynamics. Society of Automotive Engineers Inc. (1992)
5. Gáspár, P., Szászi, I., Bokor, J.: Active suspension design using linear parameter varying control. International Journal of Vehicle Autonomous Systems 1, 206–221 (2003)
6. Hac, A.: Adaptive control of vehicle suspension. Vehicle System Dynamics 16, 57–74 (1987)
7. Hedrick, J., Butsuen, T.: Invariant properties of automotive suspensions. Proc. of the Institution of Mechanical Engineers 204, 21–27 (1990)
8. Hrovat, D.: Optimal active suspension structures for quarter car vehicle models. Automatica 26(5), 845–860 (1990)
9. Hrovat, D.: Survey of advanced suspension developments and related optimal control applications. Automatica 33, 1781–1817 (1997)
10. Levant, A.: Higher-order sliding modes, differentiation and output feedback control. International Journal of Control 76(9/10), 924–941 (2003)
11. Merritt, H.: Hydraulic control systems. Wiley and Sons (1967)
12. Rough, W., Shamma, J.: Research on gain scheduling. Automatica 36, 1401–1425 (2000)
13. van der Schaft, A.J.: L2-Gain and Passivity Techniques in Nonlinear Control. Springer, Berlin (2000)
14. Sepulchre, R., Jankovic, M., Kokotovic, P.: Constructive Nonlinear Control. Springer (1997)
15. Sharp, R., Crolla, D.: Road vehicle suspension system design: A review. Vehicle System Dynamics 16, 167–192 (1987)

16. Vasiljevic, L.K., Khalil, H.: Differentiation with high-gain oservers the presence of measurement noise. In: Proceedings of the 45th IEEE Conference on Decision and Control, San Diego, CA, USA, pp. 4717–4722 (2006)
17. Wu, F.: A generalized LPV system analysis and control synthesis framework. International Journal of Control 74, 745–759 (2001)
18. Wu, F., Yang, X., Packard, A., Becker, G.: Induced $\mathscr{L}_2$ norm controller for LPV systems with bounded parameter variation rates. International Journal of Robust and Nonlinear Control 6, 983–988 (1996)
19. Zhou, K., Doyle, J., Glover, K.: Robust and Optimal Control. Prentice Hall (1996)

Part III
Some Cases of LPV Methods for Railway, Aerospace and Underwater Applications

Chapter 13
Observer-Based Brake Control for Railways

Péter Gáspár and Zoltán Szabó

Abstract. Since in a braking operation the shortest possible brake distance is required at all times an efficient and robust slip prevention control must be developed. The aim of this chapter is to present a control strategy based on an estimation method for the actual wheel–rail friction coefficient. A logic-based scheme that estimates a set point that prevents wheel slip is proposed. Having this estimation a conventional control algorithm maintains the system at the prescribed set point. If the external environment changes a new set point corresponding to the current condition is estimated. The estimation method is based on an adaptive observer design. The proposed control procedure does not rely on measured values of the slip ratio. The control algorithm is tested through simulation examples.

13.1 Introduction

During braking, the wheels of the train exert a frictional force on the track, which reduces the speed of the train. However, if the braking force at the point of contact between the wheel and the track is too large, the wheels may lock and wheel-skidding occurs. This has a detrimental effect over time because the friction and heat produced can damage both the wheels and the track. Flat surfaces on the wheels caused by skidding will lead to higher vibration and audible noise. In addition, the lifespan of the wheels and the track will be reduced. Nevertheless, reducing the brake force to low levels does not efficiently solve the problem of wheel skidding. This is because the shortest possible brake distance is desired at all times, and thus the maximum possible braking force is required. The requirement of maximum braking force is particularly important when the track is slippery.

Péter Gáspár · Zoltán Szabó
Computer and Automation Research Institute, Hungarian Academy of Sciences,
Kende u. 13-17, Budapest, H1111 Hungary
e-mail: {gaspar,szaboz}@sztaki.hu

O. Sename et al. (Eds.): *Robust Control and LPV Approaches*, LNCIS 437, pp. 331–346.
DOI: 10.1007/978-3-642-36110-4_13

Adhesion is the amount of force available between the rail and the wheel as a result of the frictional forces. The adhesive force is given by $F_a = \mu F_n = \mu m_a g$, where μ is the wheel-rail adhesion coefficient, F_n is the normal load, m_a is the adhesive mass of the vehicle and g is the gravitational constant. Railway rolling stock wheel skidding commonly occurs when the adhesion coefficient μ has decreased on a rail.

There are several factors that can affect the value of the wheel-rail adhesion coefficient which is a highly nonlinear, time varying and complex function, and has characteristics that can vary widely during the operation of the train. This is because the coefficient of friction depends on the actual value of the wheel skid λ and on several other factors including weather conditions, material used in the railway track and wheels, the condition of the contact point between the wheel and the track (e.g. the presence of oil, grease, mud) and slope variations of the rail track. It is very difficult to accurately quantify and measure the effect on μ of all of the above factors. The slip ratio (wheel skid) λ is defined as $\lambda = (R\omega - v)/v$, where v is the velocity of the train carriage, ω is the angular wheel velocity, i.e., $R\omega$ is the velocity of the wheel. During braking $\lambda \leq 0$ and its magnitude $|\lambda|$ can take values between 0 (no braking) and 1 (blocking).

Extended studies have clarified that the tracks and structures on the way-side such as turnouts, grade crossings, and rail lubricators, as well as fallen leaves in thickly wooded areas and needles from coniferous trees can cause large, localized decreases in μ, and that rain, snow, etc., that wet the rails can cause decreases in μ over wide areas. Concerning velocity, in general it can be said that the adhesive force is reduced with increasing vehicle velocity.

Normally only the effect on the coefficient of friction corresponding to the weather conditions and the magnitude of wheel skid are taken into account, for a given type of track and wheel material. A simplified adhesion characteristic $\mu(\lambda)$ measured for a given track surface condition is plotted in Figure 13.1, see [3]. Measurements have shown that on the slip curve the magnitude $|\mu|$ of adhesion coefficient has a peak $|\mu_0|$ at a certain slip λ_0 and that the maximum value at this peak decreases with increasing vehicle velocity. Let us denote by μ_∞ the adhesion coefficient realized when the wheel is blocked. In this model the different characteristics are determined by the values of the parameters $\lambda_0, \mu_0, \mu_\infty$ and all the tribological conditions are modeled through these parameters. The effect of the velocity and of the external conditions are modeled through the variation of these parameters during operational time.

The role of the ideal antiskid controller is to prevent the wheels from locking whilst providing the maximum possible braking force under all conditions. The brake torque should be applied in such a manner that the adhesion characteristic is near its peak μ_0, but the actual skid value λ is less than the point of maximum adhesion λ_0. Antiskid control, however, is a difficult problem. It becomes obvious if one examines the differential equation describing the motion of the train axle wheels together with the function describing wheel skid.

Several papers on antiskid controller design propose strategies that use comparison of measured signals with predefined thresholds in order to prevent skidding.

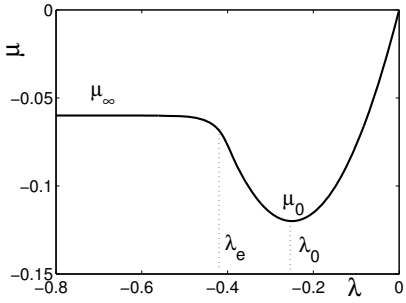

Fig. 13.1 A generic adherence-slack dependence

These algorithms are concerned with the situation when the adhesion characteristic is unchanged, i.e., the point of maximum adhesion λ_0 is unchanged, which is the major drawback of the approach. An other branch of papers assume that the values of the slip ratio can be measured. Based on this assumption robust schemes are proposed using sliding mode controllers or adaptive extremum seeking controllers. In practice, however, it is hard to know the actual velocity of a railway vehicle moreover when slip occurs the estimation of the forward velocity is extremely inaccurate. A further problem is that these methods assume ideal actuators while in reality there is a considerable delay in the actuation determined by the sampling period and the time constant of the actuator which is comparable with the time in which slipping occurs. Therefore the applicability of these theoretically appealing methods in practice are questionable.

Starting from a suitable parametrization of the adhesion curve in [26] and [25] an adaptive observer scheme is proposed to provide a near optimal braking control scheme. While the shape depicted in Figure 13.1 reflects the main characteristics of the adhesion curve, for rail applications considerably less information is available on the nature of this curve. Compared to road vehicle applications where the performance degradation in terms of the magnitude of the friction coefficient is less than 20% this value is usually greater than 50% for rails. Moreover the peak values for rail applications are significantly smaller than those for road vehicles. It is clear that the achievable estimation performance provided by these direct adaptive schemes is not satisfactory in our framework.

The aim of this chapter is to present a method for the estimation of a safe set point that ensures acceptable performance during operation. Then a control is applied that maintains the system at the estimated set point while possible changes in the external conditions are continuously monitored. If significant changes occur in the external conditions, i.e., in the adhesion characteristic, the set point is re–evaluated.

In the proposed method the actual wheel-rail friction coefficient μ is estimated using an adaptive observer scheme starting from the values of the measured signals: the angular velocity of the wheel, the moment generated by the braking force

(braking pressure) and the moment generated by the wheel load. If a slip occurs the value of the actual wheel-rail friction coefficient μ does not change or even decreases considerably whilst the braking pressure remains unchanged or even increases, and there is a large change in the deceleration of ω. This fact makes possible the detection of the slip without measuring the actual values of the slip ratio. Using the estimated wheel-rail friction coefficients μ and the corresponding values of the measured braking pressure p we give an estimate for a suitable set point that makes antislip braking possible by applying a set point control.

The structure of the chapter is the following: in Section 13.2 a short overview of previous results is given. Section 13.3 presents a sketch of a model for a railway vehicle. Section 13.4 gives a comprehensive presentation of the adaptive parameter estimation scheme used for the wheel–rail friction coefficient estimation. The control scheme is presented in Section 13.5. The efficiency of the proposed method is demonstrated in Section 13.6 through a simulation example, followed by the concluding remarks in Section 13.7.

13.2 Overview of Current Approaches

Many of the slip control strategies focus on detecting the adhesive force or the adhesion coefficient. Diagnostic algorithms are often combined with observers of various kinds or with consistency relations, which provide information about how the system is expected to behave according to known physical relations. The advantages of adhesion observers are that they have a simple structure and are robust against disturbances and parameter variation.

With this information at hand simple controllers can be derived based on the partial derivative of the adhesion coefficient, $\partial_t \mu$ together with a PI-controller, by choosing a reference slip and using this as a control signal, see [14]. Another way of using the adhesion observer is to use the time differential of both the adhesion coefficient and the slip, $(\partial_t \mu, \partial_t \lambda)$, combined with some adaptive identification algorithm. Theoretically this enables an on-line estimation of the current slope of the slip curve, [17], and an extremum–seeking control strategy, [4], [7]. A hybrid approach that also uses conventional methods based on speed difference and vehicle deceleration compared to a specific threshold shows remarkably better results, [15].

There are several papers that are concerned with the situation, in which the adhesion characteristic is unchanged, i.e., the point of maximum adhesion λ_0 is unchanged, moreover it is assumed that the values of the slip ratio can be measured, [20], [22]. In practice it is hard to know the actual velocity of a railway vehicle. The conventional method to compute the velocity of a vehicle v is to multiply the angular velocity ω of a non-driven wheel with the wheel radius R. However, since in most railway motor cars all wheels are driven, the use of this method is not reliable. Therefore, a direct measurement of the velocity v - hence of the slip ratio λ - is usually not available.

Consider the following one–wheel model, [25], which is often used in this type of applications, see Figure 13.2. Using the force and torque balance equations the following expressions are formalized:

$$\dot{\omega} = -\alpha_1 F_n \mu - \alpha_2 p, \tag{13.1}$$

$$\dot{\mathrm{v}} = \alpha_3 F_n \mu, \tag{13.2}$$

where p is the braking pressure, F_n is the normal load while α_i's are constants depending on the geometry of the wheel and the braking mechanism. It is assumed that the braking force F_b is proportional with the braking pressure p.

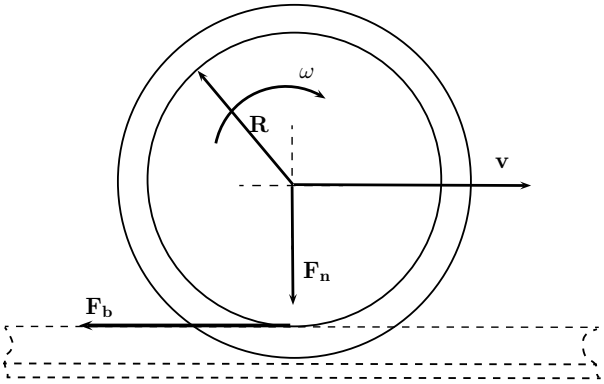

Fig. 13.2 One-wheel model

If the acceleration $a = \dot{\mathrm{v}}$ is measured, one has

$$\dot{\omega} = -\frac{\alpha_1}{\alpha_3} a - \alpha_2 p. \tag{13.3}$$

It is apparent that the system is not observable for ω as a measured input. Usually an estimation of the forward velocity is obtained by "integrating" the forward acceleration. Since this integration is not a numerically stable technique some "black art" is needed to obtain reliable values for the estimate, see e.g. [10]. Assuming a specific additional aerodynamical resistance term an estimation algorithm was proposed in [1]. Computing the relative error of the slip ratio one has the following bound:

$$\left|\frac{\Delta\lambda}{\lambda}\right| \leq \left|1 + \frac{1}{\lambda}\right| \left(\left|\frac{\Delta\omega}{\omega}\right| + \left|\frac{\Delta \mathrm{v}}{\mathrm{v}}\right|\right). \tag{13.4}$$

Since at the desired operational point $\lambda \sim -0.1$, the respective values for the estimated velocity and slip ratio might be affected by considerable "measurement" errors that make their application in a control algorithm rather questionable. However, if the external conditions change, the preset value of λ^* cannot prevent wheel slipping.

To overcome this problem usually a slip velocity $v_s = \omega R - v_{ref}$ is computed where v_{ref} is estimated from the minimum of the angular wheel velocities, ω_{min}, see [24]. One of the drawbacks of the method is that if the surface provides low friction for a long time, or if all wheels slip too much simultaneously, this will not be detected. It may cause uncontrolled slip that may lead to brake locking, which will cause massive wheel deformation. Therefore, it is important to have an acceleration criterion that reduces the torque when this happens. The acceleration criterion is triggered when an acceleration threshold determined by the vehicle's maximum acceleration is exceeded. Hence conventional antislip braking controllers adjust a pressure control valve using logics based on the comparison of the actual wheel slip velocity v_s and the deceleration of the wheel with predefined threshold values, see [9], [18], [19].

There are several other non-classical methodologies like neural networks and evolutionary algorithms. The disadvantage with these methods is that they rely on numeric or measured data to form system models, however, the fuzzy algorithms can include experienced human experts linguistic rules, describing how to design the slip control system that can be important when the access to measured data is limited. These rules can be translated into "if–then" rules and in this form be included in the fuzzy logic algorithm, [6].

A key to a successful optimizing slip control is to be able to tell were the peak of the slip curve is in order to be on the stable linear side of the slip curve. From the characteristics of the slip curve it is easy to observe that different slip, depending on the rail condition, implies different optimums of the adhesive force since the adhesion coefficient differs between dry, wet and icy rail. Therefore a PID-controller cannot be used alone.

A further observation is that the performance criterion, i.e., to reduce the braking distance, imposes conditions on the values of the wheel-rail friction coefficient μ rather than on the slip ratio λ. Therefore it is much more reasonable to set as a control objective to track a fairly large fixed value of μ^* rather than to try to maintain a prescribed λ^* during the operational time.

As a conclusion of this overview antislip braking algorithms might fail or might have a reduced performance due to inaccurate estimations of the slip ratio λ and due to the lack of adaptation to the variation in the external parameters, i.e., the different optimums of the adhesive force.

13.3 The Modeling of a Railway Vehicle

In this chapter the estimation of the wheel-rail friction coefficient is based on the individual wheels. For the purposes of this chapter it is assumed that the angular velocity ω of the wheel, the normal load F_n and the braking pressure p_b are measured. It is assumed that the braking force is proportional with the braking pressure.

The controller design is based on the following one–wheel model (13.1) and (13.2). Note that the sign of μ is negative during braking. From

$$\frac{d}{dt}\left(\frac{\omega}{\mathrm{v}}\right) = \frac{\omega}{\mathrm{v}}\left(\frac{\dot{\omega}}{\omega} - \frac{\omega}{\mathrm{v}}\frac{\dot{\mathrm{v}}}{\omega}\right) \tag{13.5}$$

it follows that

$$\dot{\lambda} = -\varphi(\mathrm{v})\left[p + \left(1 + (\lambda+1)c_2\right)c_1\mu\right], \tag{13.6}$$

where $\varphi(\mathrm{v}) = \frac{R\alpha_2}{\mathrm{v}}$, $c_1 = \frac{\alpha_1 F_n}{\alpha_2}$ and $c_2 = \frac{\alpha_3}{R\alpha_1}$.

Let us suppose that $\mu = \mu(\lambda, t)$, i.e., $\dot{\mu} = \partial_\lambda \mu \dot{\lambda} + \partial_t \mu$. We assume that the term $\partial_t \mu$ can be considered as a disturbance with prescribed norm bound ε_μ and that for every fixed t the shape of this function is as in Figure 13.1, i.e., considering the left half plane (braking situation) it has a single minimum, $(\lambda_0(t), \mu_0(t))$. On the stable side of the μ/λ curve, i.e., if $\lambda > \lambda_0$ one has $\partial_\lambda \mu \geq 0$, moreover, for $\lambda \geq \bar{\lambda} > \lambda_0$ the value of $\partial_\lambda \mu$ is bounded from below by a constant $c > 0$. The function $\varphi(\mathrm{v})$ is a nondecreasing positive function which is bounded in the validity region of the model, i.e., $\mathrm{v} \geq \mathrm{v}_l > 0$.

From the equation

$$\dot{\mu} = -\partial_\lambda \mu \varphi(\mathrm{v})\left[p + \left(1 + (\lambda+1)c_2\right)c_1\mu\right] + \partial_t \mu. \tag{13.7}$$

follows, that in a stationary point (λ_s, μ_s) one has

$$p_s = -\left(1 + (\lambda_s+1)c_2\right)c_1\mu_s + \frac{\mathrm{v}\partial_t \mu|_{\lambda_s}}{\alpha_2 R \partial_\lambda \mu|_{\lambda_s}}, \tag{13.8}$$

the last term being bounded by $\mathrm{v}\frac{\varepsilon_\mu}{cR}$. Let us denote by $\bar{p}_s$ the pressure defined by (13.8) assuming $\partial_t \mu = 0$.

Figure 13.3 shows the values $\bar{p}_s$ for different μ/λ curves. For a given pressure value one might have a single (stable) stationary point, two stationary points (one stable and one unstable), or no stationary points. A stable stationary point (λ_s, p_s) is indicated for a pressure level of $0.3p_{max}$. If $|\lambda_s| > |\lambda_0|$ then the corresponding stationary point is unstable. A pressure value is "admissible" for a given curve if it has stationary points, i.e., a pressure admissible in given circumstances might not be admissible for another adhesion characteristics. For example: the pressure level $0.6p_{max}$ is admissible for the dashed curves while it is not admissible for the continuous characteristics.

Applying the control pressure $\bar{p}_s$ to (13.1) one has

$$\dot{\omega}_s = (\lambda_s+1)\alpha_2 c_1 c_2 \mu_s - \frac{\mathrm{v}\partial_t \mu|_{\lambda_s}}{R\partial_\lambda \mu|_{\lambda_s}},$$

i.e., $|\dot{\omega}_s| \leq \alpha_2 c_1 c_2 |\mu_s|$ provided that $\partial_t \mu = 0$. Let us denote by

$$\eta = -\frac{\dot{\omega}}{\alpha_2 c_1 c_2}, \tag{13.9}$$

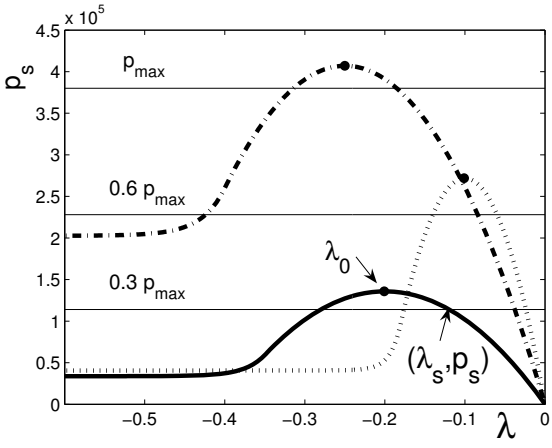

Fig. 13.3 Admissible pressures

the normalized wheel deceleration then on the set of admissible equilibrium points its values are

$$\eta_a = -(\lambda_s + 1)\mu_s + \frac{\mathrm{v}}{\alpha_2 R c_1 c_2} \frac{\partial_t \mu|_{\lambda_s}}{\partial_\lambda \mu|_{\lambda_s}}. \tag{13.10}$$

It follows that if the actual values of μ were available one could control μ directly instead of trying to manipulate it through the values of λ. It follows that it is possible to "measure" μ, i.e., to obtain its estimation with an acceptable accuracy. Moreover, it is possible to construct a controller that does not need the knowledge of the actual values of λ. Another advantage of the method is that using a direct estimation of the μ values it is not necessary to know the actual nonlinear function $\mu(\lambda, t)$.

13.4 The Estimation of the Wheel-Rail Friction Coefficient

The equation that governs the evolution of the dynamics of the angular velocity for a single wheel can be put in the form

$$\dot{\omega} = \mu R F_n + \alpha F_b, \tag{13.11}$$

see (13.1), which is a linear system if μ is considered as a given exogenous signal. For this system an adaptive observer of the form:

$$\dot{\hat{\omega}} = \alpha F_b + R F_n \hat{\mu} + \kappa(\omega - \hat{\omega}) \tag{13.12}$$

$$\dot{\hat{\mu}} = -\gamma(\omega - \hat{\omega}). \tag{13.13}$$

is constructed. Note that the nonlinearity, uncertainty and time dependence of the model are hidden within the parameter μ. This parameter is estimated all the time by using an on-line adaptive observer. The aim of this estimation is that the controller exploits the value of the estimated friction coefficient during its operation.

Adaptive state estimation, i.e., the simultaneous estimation of state and some unknown parameters, has several known solutions for linear time invariant (LTI) systems with the so-called adaptive observers, see [13]. There is not any particular difficulty in the state estimation problem for multi-input-multi-output (MIMO) systems, but it is not the case for adaptive state estimation. For linear time varying (LTV) systems an adaptive scheme was proposed in [27]. For some specific classes of nonlinear systems adaptive observers with global convergence were proposed in [8, 11, 12]. For an overview of the problem in the nonlinear context see [2]. It is also possible to apply extended Kalman filters (EKF) to joint state and parameter estimation of the resulting nonlinear system by extending the state vector with the unknown parameters, but in general only local convergence is expected, see [5, 16].

For road vehicles where the tire/road dynamical friction is given by a LuGre model observer–based estimation was proposed for the adhesion coefficient in [25] and [21]. The estimation method proposed by this work is based on the approach presented in [27] and [12], which provides a globally exponentially convergent adaptive observer scheme in a linear time varying context.

By a suitable choice of κ and γ the scheme is convergent, moreover, since $F_n > 0$, it is globally exponentially convergent. If the measurements are corrupted by noise or bounded disturbance, i.e., $\bar{\omega} = \omega + w$, where $||w|| < c_w$, a slightly modified adaptive observer can be used to ensure global robust adaptivity, for details see [11]. The performance properties of the observer depend heavily on the choice of the gain κ and the parameter γ, however there has been no theoretically justified method for their choice yet.

13.5 The Design of an Antislip Braking Control Algorithm

The signals available for measurement are: the angular velocity of the wheel, the moment generated by the braking force (braking pressure p) and the moment generated by the wheel load (wheel load F_n). A maximal value of the admissible slip $\bar{\lambda}$ is fixed such that it cannot be exceeded during normal operational time without slipping.

The designed controller performs the following steps:

s_1: Estimates a *target operational point* (λ^*, μ^*) on the stable side of the current μ/λ adhesion characteristic curve.

s_2: Sets the braking force that corresponds to the estimated set point. If the *current operational point* (λ, μ) leaves a predefined region centered at (λ^*, μ^*), then

s_3: Reruns the s_1 cycle.

The detailed logical scheme is depicted in Figure 13.4.

The heart of the algorithm is the estimation procedure s_1, which consists of the following elements:

Step e_1: Increase the brake pressure until slip is detected. In each sampling period the value (p_m, μ_m) that corresponds to the maximal values of the adhesion coefficient until the current time is memorized.

Step e_2: If slip is detected reduce the brake pressure until the current operational point is securely placed on the stable side of the μ/λ curve. This is ensured by the condition $|\mu| < |\mu_{inf}|$, where $\mu_{inf} = \gamma_2 \mu_m$, with $\gamma_2 \ll 1$, e.g., for practical purposes the value $\gamma_2 = 0.2$ is satisfactory.

Step e_3: Set the target set point to $\mu^* = \gamma_3 \mu_m$, with $\gamma_3 < 1$. In practice a value $\gamma_3 = 0.8$ is satisfactory. One reason for this choice of γ_3 is given by the presence of uncertainties in the adhesion curve. On the other hand, it is not known where the maximum of the actual curve is attended nor is the exact value of λ^*. Therefore the maximum admissible value p^* of the braking pressure that would maintain the system in the point (λ^*, μ^*) is not known. The value p_m corresponding to μ_m, which can be measured in the s_1 step, is only an upper bound for it. By using (13.8) a lower bound for p^* is given by $\underline{p}^* = -(1 + (\bar{\lambda} + 1)c_2)c_1\mu^*$ while its upper bound is $\bar{p}^* = -(1 + c_2)c_1\mu^*$. Therefore in the setting stage the brake pressure is increased gradually not exceeding the value $\tilde{p}^* = \gamma_4 \bar{p}^*$, with $0.7 \leq \gamma_4 \leq 0.9$.

Slip is detected by monitoring the normalized wheel deceleration η, (13.9). When slip occurs the actual values of η increase considerably, i.e., $\eta > -\gamma_1 \mu$, see (13.10) with $\bar{\eta}_a = -(\lambda_s + 1)\mu_s$.

Remark 17. *Since the value of the desired pressure set by the controller is constant during a sampling period (quantization effect) an unacceptable increase in the actual pressure during the sampling period may occur. In practice, such an unwanted increase in the pressure may drive the system to the unstable side, causing a chattering effect preventing the controller from setting a stable operational point. Therefore one has to choose the parameters γ_i of the algorithm carefully. The choice of these parameters depends on the actuator dynamics, the sampling time and the worst-case bound of the estimation error of the adhesion coefficient.*

The holding step s_2 of the controller is defined as follows:

Step h_1: Monitor the values of μ. If the actual value of μ leaves a prescribed neighborhood of the desired set point, i.e., $|\mu| \notin [\gamma_5|\mu^*|, \gamma_6|\mu^*|] = N_{\mu^*}$, then either a slip occurs or a significant (possibly favorable) change occurs in the external conditions. In both situations we choose to rerun the s_1 cycle. Otherwise we run a set point controller algorithm h_2.

Step h_2: Set the braking force that corresponds to the given point μ^*. To do that the desired control pressure will be set at the value

$$p_c = p^* - \gamma_c(\mu^* - \mu) \tag{13.14}$$

where the value of γ_c is determined by using a set point control based on a simplified (one–wheel) model.

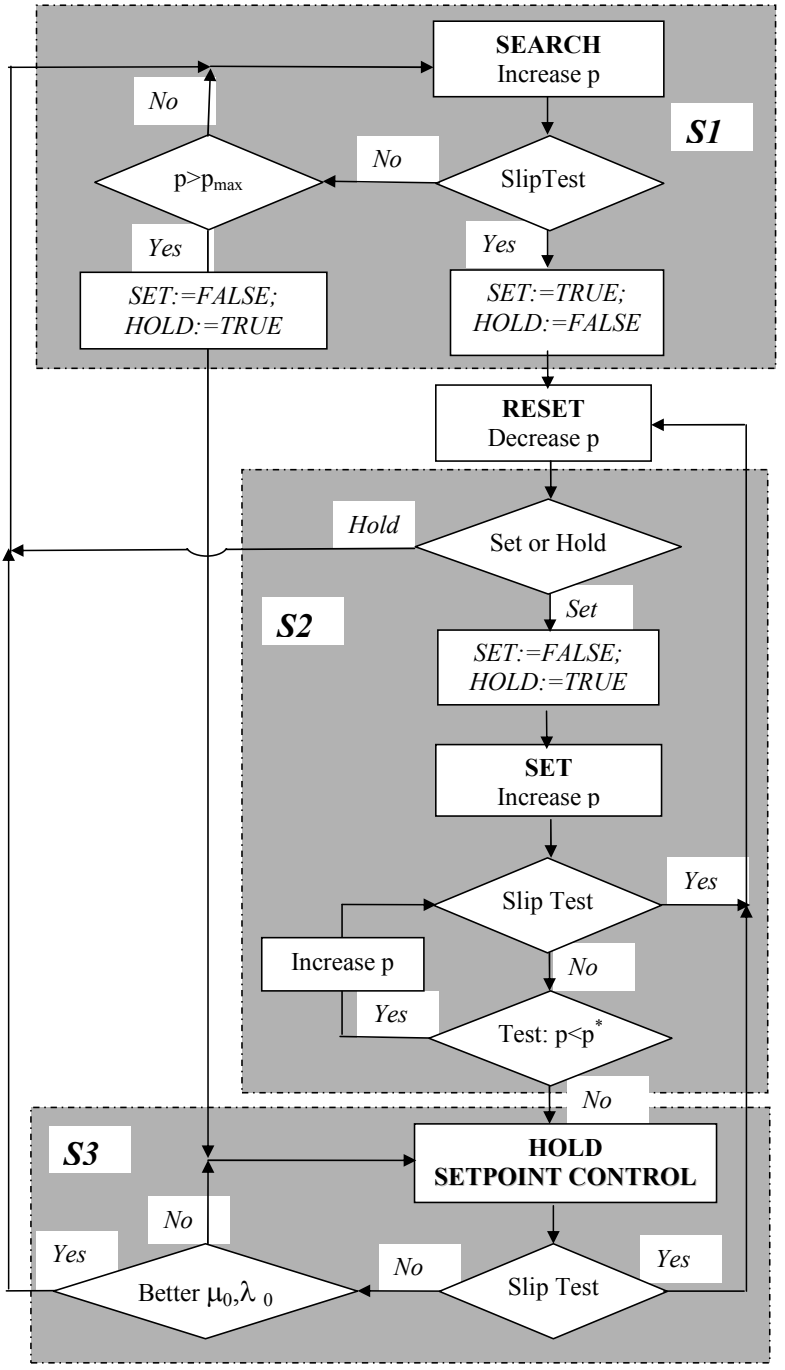

Fig. 13.4 Logical scheme of the antislip braking control algorithm

The local stability of the holding scheme – in the neighborhood N_{μ^*} – can be proved similarly as the convergence of the adaptive observers. Let $V(e_\mu) := \frac{1}{2}e_\mu^2$ with $e_\mu = \mu^* - \mu$. From (13.14) one has $p_c - p^* = -\gamma_c e_\mu$. Applying (13.7) and (13.8) with $\partial_t \mu^* = 0$ it follows that

$$\dot{e}_\mu = -\partial_\lambda \mu \varphi(\mathrm{v}) \left[\gamma_c + \left(1 + (\lambda+1)c_2\right) c_1\right] e_\mu + \\ + \partial_\lambda \mu \varphi(\mathrm{v})(\lambda - \bar{\lambda}) c_2 c_1 \mu^* - \partial_t \mu. \tag{13.15}$$

Then in the nominal case ($\partial_t \mu = 0$, $\bar{\lambda} = \lambda^*$) one has

$$\dot{V}(e_\mu) = -\partial_\lambda \mu \varphi(\mathrm{v}) \left[\gamma_c + \left(1 + (\lambda+1)c_2\right) c_1\right] e_\mu^2 + \\ + \partial_\lambda \mu \varphi(\mathrm{v})(\lambda - \bar{\lambda}) c_2 c_1 \mu^* e_\mu. \tag{13.16}$$

By using the arguments of [11] it follows that for a suitable choice of γ_c one has local stability, i.e., $lim_{t\to\infty} e_\mu = 0$, moreover the tracking error remains between acceptable bounds if $\partial_t \mu < \varepsilon_\mu$ and if the measurements of μ are "noisy".

Remark 18. *In the holding step h_2 it is possible to apply more elaborate control schemes if an acceptable estimate of the slip λ is available. Then the theoretically appealing methods proposed in [7], [9], [18] are applicable. However for very noisy estimations of the slip the theoretical background and the practical applicability of these methods vanish.*

Remark 19. *At low speeds the relative errors of the μ estimation may be unacceptably high. Moreover the modeling error also increases in this domain. Therefore in practice an auxiliary control logic must be applied to achieve a complete stop.*

13.6 Simulation Examples

In this section the operation of the braking control that is able to adapt to the changes in set points to prevent wheel slip and provide a suitable control is presented. The essence of this test is to analyze how the controllers handle different types of slip curves and sudden changes between these curves. Its objective is to test the adaptability of the controller under unknown rail conditions assuming that the reality is not what it is expected to be.

The $\mu(\lambda)$ curve used during the simulation is approximated as:

$$\mu = \begin{cases} sign(\lambda)\left(4\mu_0 \frac{|\lambda|}{2\lambda_0}\left(1 - \frac{|\lambda|}{2\lambda_0}\right)\right) & \text{if } |\lambda| < \lambda_e \\ sign(\lambda)\left(\eta e^{-\chi(|\lambda| - \lambda_e)} + \mu_\infty\right) & \text{if } |\lambda| \geq \lambda_e \end{cases} \tag{13.17}$$

where $\eta = 4\mu_0 \frac{\lambda_e}{2\lambda_0}\left(1 - \frac{\lambda_e}{2\lambda_0}\right) - \mu_\infty$ and $\chi = -\frac{2\mu_0}{\lambda_0 \eta}\left(1 - \frac{\lambda_e}{\lambda_0}\right)$, see [23].

In our simulation example the initial values of the tribological parameters of the rail are set at the values $\lambda_0 = 0.25, \lambda_e = 0.4, \mu_0 = 0.12, \mu_\infty = 0.06$. These values are changed to $\lambda_0 = 0.2, \lambda_e = 0.35, \mu_0 = 0.04, \mu_\infty = 0.01$ at 3 sec and at 8 sec their values are reset at $\lambda_0 = 0.1, \lambda_e = 0.18, \mu_0 = 0.06, \mu_\infty = 0.012$.

The actual $\mu = f(\lambda)$ plot in Figure 13.5 reveals that in the first part of the simulation the vehicle can be maintained at the point π_1 till changes in the tribological parameters result in a slip of the wheel. As a consequence the operational conditions change from curve A to curve B. Moreover the actual operational point will move to the uncontrollable, sliding part of the curve B_2. When the braking force is reduced the actual operational point moves to the controllable, sliding part of the curve B_1, where it is possible to maintain a new set point π_2. When the tribological parameters are reset at their final values in part C, a further slip occurs due to the delay in the actuator dynamics and the quantization generated by the sampling effect in step s_1 of the control algorithm. The final set point will be π_3.

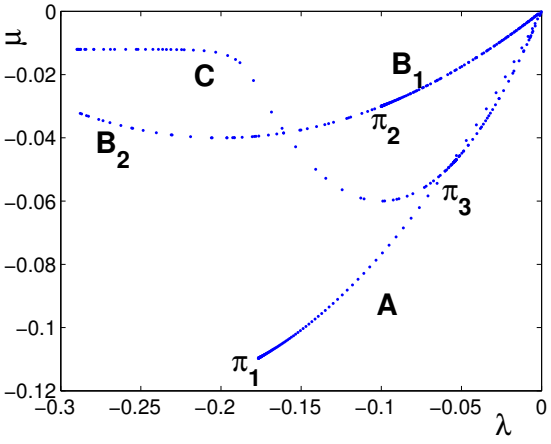

Fig. 13.5 The relation between λ and μ

During this operation a braking control determined by the control algorithm described in Section 13.5 and (13.14) is applied. For the actuators a realistic behavior is assumed, i.e., the change of the cylinder pressure is governed by first-order dynamics with different time constants for air compression and decompression.

The acquired angular wheel velocity ω is shown in Figure 13.6*a*. Using the estimated wheel-rail friction coefficient μ, depicted in Figure 13.6*b* by the solid line, and the corresponding values of the slip ratio λ (available in the simulation environment) it is possible to obtain the adherence slack dependence ($\mu(\lambda)$ curve) in the operational time. It can be seen that the proposed observer-based method approximates sufficiently the changes that occur in the values of the real μ shown by the dotted lines. The applied braking pressure and the achieved velocity v are depicted in Figure 13.6*c* and Figure 13.6*d*.

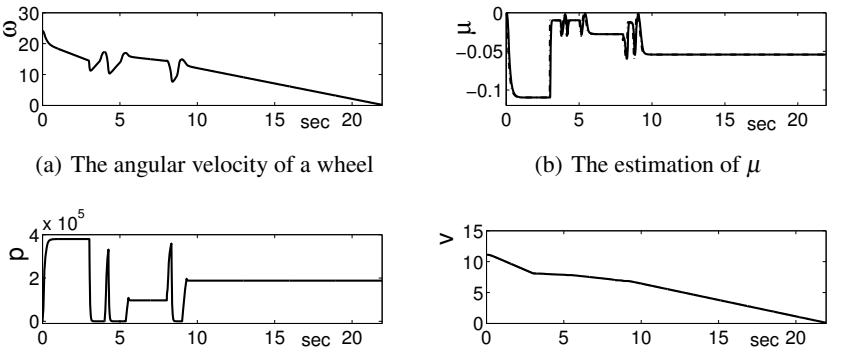

(a) The angular velocity of a wheel (b) The estimation of μ

(c) The control pressure applied (d) Velocity of the vehicle during braking

Fig. 13.6 Simulation results

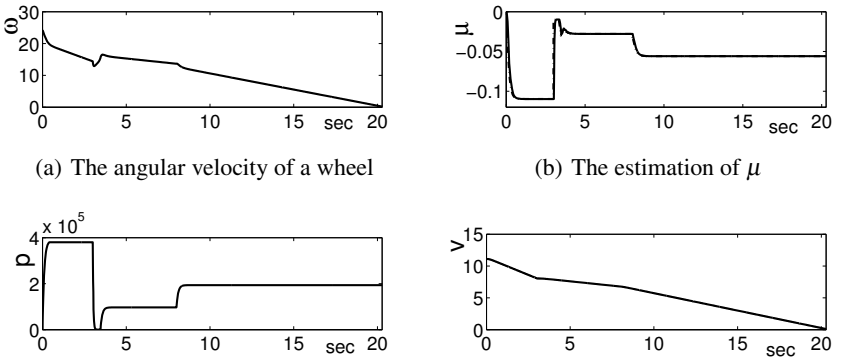

(a) The angular velocity of a wheel (b) The estimation of μ

(c) The control pressure applied (d) Velocity of the vehicle during braking

Fig. 13.7 Simulation results using the ideal control

In an ideal situation, i.e., with full knowledge of the curve $\mu(\lambda)$ and of the actual parameters $(\lambda_0(t), \mu_0(t))$ and with ideal actuators the optimal control would be a piecewise constant function with pressure values that correspond to the maximum points of the curves depicted in Figure 13.3. In Figure 13.7 the simulation results are depicted corresponding to the unrealistic situation when the actual parameters $(\lambda_0(t), \mu_0(t))$ are known. The dynamics of the actuators is the same as in the previous case. The achievable set point was chosen to be at the level $\mu^* = 0.95\mu_0$. Even in an idealistic situation it is unrealistic to assume the knowledge of the changes in tribological parameters in advance. Therefore in the scenario used in our simulation a slip will also occur, see Figure 13.6.*b*.

As there are practical limitations it is not possible to obtain this optimum, however comparing Figure 13.6.*d* with the applied braking pressure in Figure 13.7.*d* one

can see that the controller finds acceptable set points, hence, realizes reliable braking distances, performing much better than conventional controllers that use preset threshold values and(or) only set point controls.

13.7 Conclusions

This chapter proposes a logic-based (hybrid) antislip control strategy that aims to achieve the shortest possible brake distance using an estimation method for the actual wheel-rail friction coefficient. Using an observer-based estimation of friction coefficient μ the proposed scheme estimates a set point that prevents wheel slip and provides suitable control to maintain the system at the prescribed set point without using measured values of the slip ratio. If external conditions change a new set point is estimated corresponding to the current situation. The applicability of the proposed control algorithm was demonstrated through simulations examples.

References

1. Alvarez, L., Yi, J., Horowitz, R., Olmos, L.: Dynamic friction model-based tire-road friction estimation and emergency braking control. ASME Journal of Dynamic Systems Measurement and Control 127(1), 22–32 (2005)
2. Besancon, G.: Remarks on nonlinear adaptive observer design. Systems and Control Letters 41(4), 271–280 (2000)
3. Boiteux, M.: Le probléme de l'adhérence en freinage, Revue générale des chemins de fer (1986)
4. Drakunov, S., Özgüner, Ü., Dix, P., Ashrafi, B.: ABS control using optimum search via sliding modes. IEEE Transactions on Control Systems Technology 3, 79–85 (1995)
5. Emicke, G.A., White, L.B.: Robust extended Kalman filtering. IEEE Transactions on Signal Processing 47(9), 2596–2599 (1999)
6. Garcia-Riviera, M., Sanz, R., Perez-Rodriguez, J.: An anti-slipping fuzzy logic controller for a railway traction system. In: Proc. of the 6th IEEE International Conference on Fuzzy Systems, vol. (1), pp. 119–124 (1997)
7. Guay, M., Zhang, T.: Adaptive extremum seeking control of nonlinear dynamic systems with parametric uncertainties. Automatica 39, 1283–1293 (2003)
8. Haessig, D., Friedland, B.: A method for simultaneous state and parameter estimation in nonlinear systems. In: Proc. of the American Control Conference, Albuquerque, New Mexico, pp. 947–951 (1997)
9. Huh, K., Hong, D., Yoon, P., Kang, H., Hwang, I.: Robust wheel slip control for brake-by-wire systems. In: SAE World Congress, Detroit, pp. 01–1584 (2005)
10. Jiang, F., Gao, Z.: An adaptive nonlinear filter approach to the vehicle velocity estimation for ABS. In: Proc. of the Int. Conference on Control Applications, Anchorage (2000)
11. Marino, R., Santosuosso, G.L.: Robust adaptive observers for nonlinear systems with bounded disturbances. In: Proc. of the 38th IEEE Conference on CDC, Phoenix, Arizona, pp. 5200–5205 (1999)

12. Marino, R., Tomei, P.: Adaptive observers with arbitrary exponential rate of convergence for nonlinear systems. IEEE Transactions on Automatic Control 40(7), 1300–1304 (1995)
13. Narendra, K.S., Annaswamy, A.: Stable Adaptive Systems. Prentice-Hall, Englewood Cliffs (1989)
14. Ohishi, K., Ogawa, Y., Miyashita, I., Yasukawa, S.: Anti-slip re-adhesion control of electric motor coach based on force control using disturbance observer. In: IEEE Industry Applications Conference, pp. 1001–1007 (2000)
15. Park, D., Kim, M., Hwang, D., Kim, Y., Lee, J.: Hybrid re-adhesion control method for traction system of high-speed railway. In: Proc. of the 5th Int. Conference on Electrical Machines and Systems, pp. 739–742 (2001)
16. Reif, K., Unbehauen, R.: The extended Kalman filter as an exponential observer for nonlinear systems. IEEE Transactions on Signal Processing 47(8), 2324–2328 (1999)
17. Sado, H., Sakai, S., Hori, Y.: Road condition estimation for traction control in electric vehicle. In: Proc. of the IEEE International Symposium on Industrial Electronics, pp. 973–978 (1999)
18. Savaresi, S., Tanelli, M., Cantoni, C.: Mixed slip-deceleration control in automotive braking systems. ASME Journal of Dynamic Systems, Measurement, and Control 129, 20–31 (2007)
19. Szabó, Z., Gáspár, P., Bokor, J.: Tracking design for wiener systems based on dynamic inversion. In: Proc. of the Conference on Control and Applications, CCA, Munich, Germany (2006)
20. Tanelli, M., Astolfi, A., Savaresi, S.: Non-local extremum seeking control for active braking control systems. In: Proc. of the Conference on Control and Applications, CCA, Munich, Germany (2006)
21. de Wit, C.C., Horowitz, R.: Observers for tire/road contact friction using only wheel angular velocity information. In: Proc. of the 42th IEEE Conference on Decision and Control, Maui, Hawaii, pp. 2246–2251 (2003)
22. Yamazaki, H., Karino, Y., Nagai, M., Kamada, T.: Wheel slip prevention control by sliding mode control for railway vehicles. In: Proc. of the International Conference on Advanced Intelligent Mechatronics, pp. 271–276 (2005)
23. Yamazaki, H., Nagai, M., Kamada, T.: A study of adhesion force model for wheel slip prevention control. JSME International Journal, Series C 47, 496–501 (2004)
24. Yasuoka, I., Henmi, T., Nakazawa, Y., Aoyama, I.: Improvement of re-adhesion for commuter trains with vector control traction inverter. In: Proc. of the IEEE Power Conversion Conference, vol. (1), pp. 51–56 (1997)
25. Yi, J., Alvarez, L., Claeys, C., Horowitz, R.: Emergency braking control with an observer-based dynamic tire/road friction model and wheel angular velocity measurement. Vehicle System Dynamics 39(2), 81–97 (2003)
26. Yi, J., Alvarez, L., Horowitz, R.: Adaptive emergency braking control with underestimation of friction coefficient. IEEE Transactions on Control Systems Technology 10(3), 381–392 (2002)
27. Zhang, Q.: Adaptive observer for multiple-input-multiple-output (MIMO) linear time-varying systems. IEEE Transactions on Automatic Control 47(3), 525–529 (2002)

Chapter 14
Linear Parameter-Varying Control Strategies for Aerospace Applications

Jean-Marc Biannic

Abstract. As is already emphasized in previous chapters of this book, Linear Parameter Varying (LPV) control techniques have known a large success over the past 15 years. This is easily explained by the convex nature of standard LPV control problems together with recent progress in convex optimization technique and the emergence of efficient Linear Matrix Inequalities (LMI) solvers. However, for a large majority of aerospace systems, controllers have to be scheduled as a function of many parameters, part of which are slowly varying. In this context, basic (and convex) LPV control techniques are often too conservative, while more recent algorithms (taking into account bounds on the rate-of-variations of the parameters) become numerically intractable as soon as the number of parameters increases. Alternative strategies are then discussed in this chapter to cope with such difficulties and two aerospace control problems (missile and fighter aircraft) are presented.

14.1 Introduction

The design of feedback controllers for aerospace systems still remains today a challenging and time-consuming task since, in most cases, a large operating domain is to be considered. These controllers are often designed at various flight conditions using linearized models and are then scheduled as a function of several parameters such as the Mach number, the velocity, the aerodynamic configuration, *etc*... Part of these parameters are time-varying, while others (such as the configuration for example) are fixed. Various methods can be used for controller scheduling, among which, the most popular approach – still widely used by control engineers from the aerospace community – is the linear interpolation of static gains. The resulting controllers are

Jean-Marc Biannic
Onera – The French Aerospace Lab
F-31055, Toulouse, France
e-mail: biannic@onera.fr

O. Sename et al. (Eds.): *Robust Control and LPV Approaches*, LNCIS 437, pp. 347–373.
DOI: 10.1007/978-3-642-36110-4_14

easily implemented but unfortunately no guarantee can be obtained in case of rapid changes in the scheduling variables [1, 2]. This weakness was the main motivation for initial research on LPV control techniques in the 1990's [3, 4, 5, 6, 7, 8, 9, 10]. More recently, during the past decade, many efforts were devoted to various improvements in order to reduce the conservatism of standard LPV design approaches [11, 12, 13, 14, 15, 16, 17]. Unfortunately, most of the proposed extensions introduce many additional variables and lead to (possibly non-convex) optimization problems which rapidly become intractable beyond three parameters. This certainly explains why more standard gain-scheduling design approaches are still experiencing a large success in the aerospace industry today. This has also been a strong motivation for many researchers who explored connections between LPV control and gain-scheduling methods [2, 18] or provided frameworks [19, 1, 20] thanks to which the latter can be theoretically justified. Based on such frameworks, the development of specific implementation strategies for gain-scheduled controllers was made possible. A possible strategy uses the concept of velocity-based linearization [21, 22, 23] but the most popular ones, which will further be discussed in Section 14.3 are certainly stability preserving interpolation methods [24, 25, 26, 27, 28]. In the specific context of aerospace applications, for which analytical models are often available, LPV or gain-scheduled control laws can be interestingly replaced by nonlinear dynamic-inversion (NDI) based controllers. Moreover, as is clarified in [29, 30, 31] strong links can be established between LPV and NDI control. These links offer interesting ways to study the stability of nonlinear closed-loop systems with NDI controllers. They also provide new possibilities for improving the design of robust NDI controllers as is further clarified in Section 14.5.

The outline of the chapter is as follows. In Section 14.2, the most standard LPV control technique is applied to a modified design model in order to take into account bounds on the rate-of-variations of the parameters. The proposed strategy is applied to a missile autopilot design problem. An alternative scheme is then presented in Section 14.3. It is based on the interpolation of locally robust controllers. This method has been applied to the design of subsonic flight control laws for a fighter aircraft. A similar application is finally considered in Section 14.4 which combines the LPV framework with dynamic-inversion (DI) based techniques. Brief conclusions are given in Section 14.5.

14.2 Missile Autopilot Design via a Modified LPV Approach

As is emphasized in the introduction, one of the most critical issues in LPV control design consists in introducing bounds on the rate-of-variations of the parameters while limiting the numerical complexity. Standard approaches are based on the use of parameter-dependent Lyapunov functions [16]. These methods are theoretically sound, but they unfortunately introduce numerous decision variables in the LMI problems to be solved. An alternative solution is proposed in this section. The central idea [32, 33] consists in filtering the parameters via low-pass weighting functions.

14.2.1 Technical Backgrounds on Standard LPV Control Techniques

Consider an LPV interconnection plant $P(s,\theta)$:

$$\begin{cases} \dot{x} = A(\theta)x + B_1(\theta)w + B_2(\theta)u \\ z = C_1(\theta)x + D_{11}(\theta)w + D_{12}(\theta)u \\ y = C_2(\theta)x + D_{21}(\theta)w + D_{22}(\theta)u \end{cases} \tag{14.1}$$

where θ is a time-varying vector of parameters. Then, the most standard LPV control problem consists of finding the best LPV controller $K(s,\theta)$:

$$\begin{cases} \dot{x}_K = A_K(\theta)x_K + B_K(\theta)y \\ u = C_K(\theta)x_K + D_K(\theta)y \end{cases} \tag{14.2}$$

such that the closed-loop LPV plant which is illustrated in the center of Figure 14.1 remains stable for any admissible trajectory $\theta(t)$ and for which the induced $\mathscr{L}_2$ norm of the transfer from the exogenous input w to the exogenous output z is minimized. Many approaches have been developed over the past 15 years to solve this problem and can be classified according to the chosen representation of the LPV plant. Two of these are illustrated on Figure 14.1: the polytopic description and the Linear Fractional Representation (LFR or LFT). In case of affine parametric dependency, both descriptions are equivalent. When possible, the use of a polytopic description should be preferred since it leads to a simpler characterization of the LPV controller.

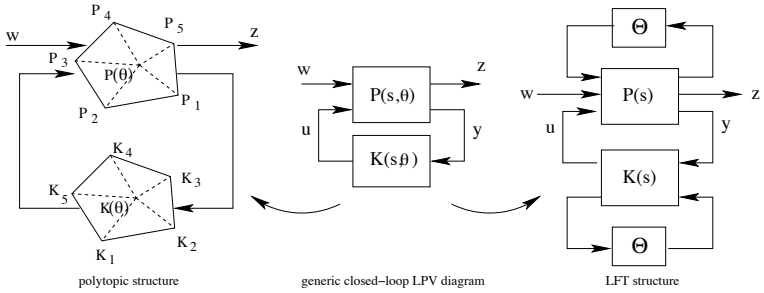

Fig. 14.1 H_∞ Synthesis Structure for LPV systems

Assuming that the LPV interconnection (14.1) can be described by the following polytope, as illustrated by the left diagram in Figure 14.1:

$$P(s,\theta) \in Co\left\{ \begin{pmatrix} A_i & B_{1i} & B_2 \\ C_{1i} & D_{11i} & D_{12} \\ C_2 & D_{21} & 0 \end{pmatrix}, i = 1,\ldots,r \right\} \tag{14.3}$$

then a polytopic controller can be computed if the existence conditions of Theorem 14.1 are satisfied.

Theorem 14.1 (Existence Conditions for a polytopic LPV controller). *[6]*
Let $\mathbb{N}_R$ and $\mathbb{N}_S$ denote bases of the null spaces of $\left(B_2^T, D_{12}^T\right)$ and (C_2, D_{21}), respectively and define $\tilde{\mathbb{N}}_R = diag(\mathbb{N}_R, \mathbf{0})$, $\tilde{\mathbb{N}}_S = diag(\mathbb{N}_S, \mathbf{0})$. There exists a polytopic LPV controller ensuring the stability of the polytopic closed-loop such that the $\mathscr{L}_2$ gain of the transfer from w to z is bounded by γ iff there exist two symmetric matrices (R,S) in $\mathbb{R}^{n\times n}$ satisfying the following set of LMIs:

$$\tilde{\mathbb{N}_R}^T \left(\begin{array}{cc|c} A_iR + RA_i^T & RC_{1i}^T & B_{1i} \\ C_{1i}R & -\gamma I & D_{11i} \\ \hline B_{1i}^T & D_{11i}^T & -\gamma I \end{array}\right) \tilde{\mathbb{N}_R} < 0 \ , \ i = 1, \ldots, r \tag{14.4}$$

$$\tilde{\mathbb{N}_S}^T \left(\begin{array}{cc|c} A_i^TS + SA_i & SB_{1i} & C_{1i}^T \\ B_{1i}^TS & -\gamma I & D_{11i}^T \\ \hline C_{1i} & D_{11i} & -\gamma I \end{array}\right) \tilde{\mathbb{N}_S} < 0 \ , \ i = 1, \ldots, r \tag{14.5}$$

$$\begin{pmatrix} R & I \\ I & S \end{pmatrix} \geq 0 \tag{14.6}$$

This theorem is of high practical interest since it describes a convex characterization of the controllers which still can be solved efficiently for rather high order plants (up to 20 or 30 states). Note that the controller is easily derived from a solution (R,S,γ) of (14.4)-(14.5)-(14.6) by an algebraic approach [5]. Unfortunately, this simple result may often lead to infeasible characterizations since no possibility is given here to limit the rate-of-variations of the parameters. This can be easily explained by the fact that Theorem 14.4 is based on the notion of quadratic stability. Its proof indeed relies on the use of quadratic Lyapunov functions.

14.2.2 On Bounding the Parameters Rate-of-Variations

A standard approach to relax the aforementioned conservatism consists of using parameter-dependent Lyapunov functions, but this often leads to numerically intractable conditions when the number of states gets higher than 10. The alternative below is based on filtering the parameters. For this approach, the LFT description is used. Let us define a low-pass function:

$$F(s) = \frac{I_q}{1+\tau s} \tag{14.7}$$

where q matches the size of $\Theta(t)$ in the LFT description, and the time constant τ is chosen small enough so that the dynamics of the filter will not interact with those of the controlled plant. As shown on Figure 14.2, the filter is placed after the parametric block $\Theta(t)$ in order to avoid non physical rapid changes in the signal w_θ which could be induced by arbitrarily fast variations of $\Theta(t)$. Thus, with the notation of Figure 14.2, the filtered signal $\tilde{w}_\theta$ verifies the approximation $\tilde{w}_\theta \approx \tilde{w}_{\theta_F}$, which

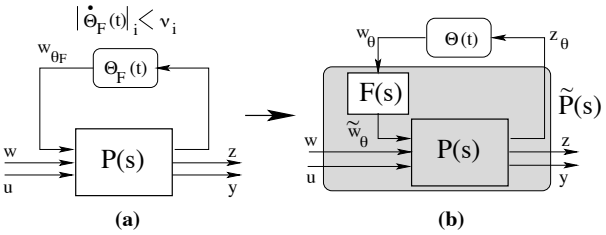

Fig. 14.2 Introduction of a low-pass filter on the parametric block $\Theta(t)$

means that the modified interconnection $\tilde{P}(s)$ gives rise to a possible formulation of a standard LPV control problem in which constraints on the rate-of-variations of the parameters are included.

Remark 14.1. Since the filter $F(s)$ is a strictly proper function, any potential feedthrough term in the upper-left block of $P(s)$ is removed so that the upper LFT interconnection $\mathscr{F}_u(\tilde{P}(s),\Theta(t))$ **affinely** depends on Θ. As a result, an equivalent **polytopic** description can be obtained.

Remark 14.2. The order $\tilde{n}$ of $\tilde{P}(s)$ is obviously higher than the order n of the initial plant ($\tilde{n} = n+q$), which makes the numerical resolution of the control problem more demanding when the size of Θ increases.

14.2.3 Application to a Pitch-Axis Missile Autopilot Design

Let us now apply and detail the above strategy to the design of a pitch-axis missile autopilot. A tail-controlled missile over a large flight envelope detailed in [34] is considered. The objective is to track the vertical acceleration a_z of the missile which admits a quasi-LPV description as follows:

$$\begin{cases} \begin{bmatrix} \dot{\alpha} \\ \dot{q} \end{bmatrix} = \begin{bmatrix} z_\alpha(M,\alpha) & 1 \\ m_\alpha(M,\alpha) & 0 \end{bmatrix} \begin{bmatrix} \alpha \\ q \end{bmatrix} + \begin{bmatrix} z_\delta(M,\alpha) \\ m_\delta(M,\alpha) \end{bmatrix} \delta \\ a_z = n_\alpha(M,\alpha)\,\alpha + n_\delta(M,\alpha)\,\delta \end{cases} \tag{14.8}$$

where α, q and δ respectively denote the angle-of-attack, the pitch rate and the control deflection. From the above equations, a standard LPV model can be obtained by considering the Mach number $M \in [2\ 4]$ and the angle-of-attack $\alpha \in [-20^o, 20^o]$) (which is also a state here) as external time-varying parameters. But, as is detailed in [6], a simpler model is derived by choosing $\theta = m_\alpha$ as a **unique** parameter and observing that the other coefficients can be expressed as functions of m_α. The LFT model of the open-loop plant exhibits the structure of Figure 14.3.

As discussed in subsection 14.2.2, the varying parameter θ is filtered so as to remove arbitrarily fast variations. The modified LFT model is then inserted in the standard design diagram of Figure 14.4.a for which, as emphasized in Remark 14.1, an

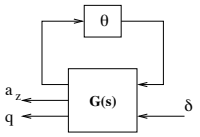

Fig. 14.3 LFT model of the open-loop plant

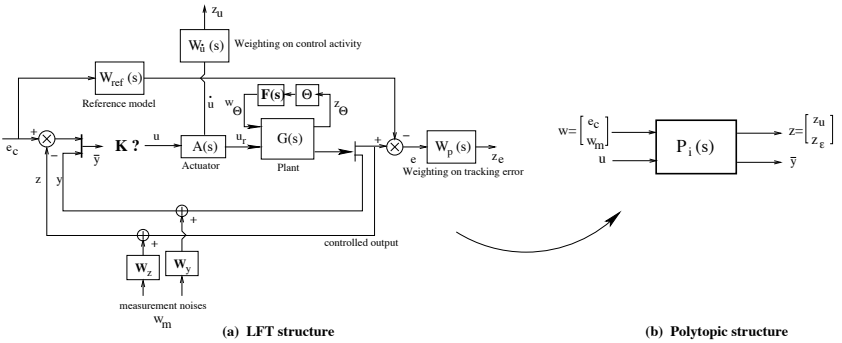

Fig. 14.4 Design diagram

equivalent polytopic model can be derived. The latter, visualized on Figure 14.4.b, is in the appropriate format of equation (14.3) for a direct application of the results stated by Theorem 14.1.

For this application, the filter time constant is fixed at a maximum value of 0.35 above which the modified model would no longer be representative because of interactions with the dynamics of the plant. A reference model $W_{ref}(s)$ is used to force

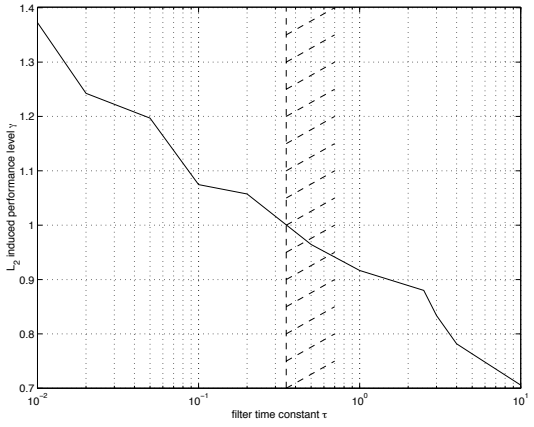

Fig. 14.5 Performance index as a function of τ

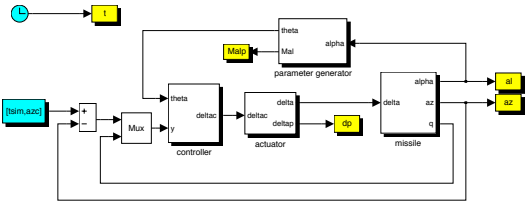

Fig. 14.6 Nonlinear simulation diagram

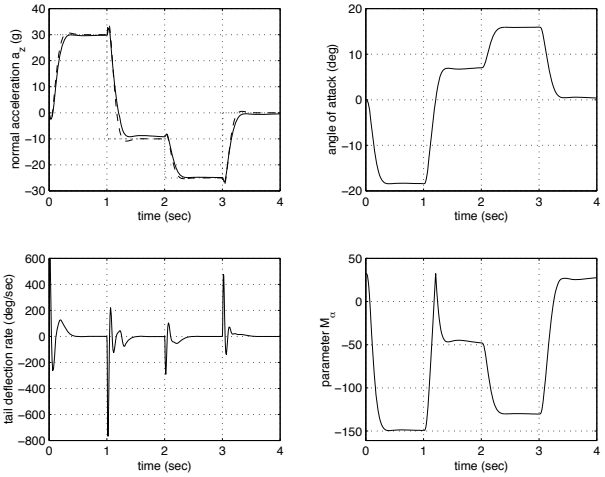

Fig. 14.7 Nonlinear simulation results

a second-order behavior on the acceleration to be tracked. As is usual in H_∞ design approaches, weighting functions $W_p(s)$ and $W_{\dot{\delta}}(s)$ are tuned so that the output matches that of the reference model with a limited control activity. Further details on the selection of such filters can be found in [6]. The LMIs of Theorem 14.1 are solved for different values of the time constant τ for which the performance index γ is minimized. As expected and visualized by Figure 14.5, the latter is a decreasing function of τ.

Note that the LPV controllers which have been obtained for $\tau > 0.35$ are not realistic since for such cases the modified plant is no longer representative of the initial one. In the following, we selected the controller obtained for $\tau = 0.35$, for which $\gamma = 1$. This means that the specifications imposed via the weighting functions are satisfied and that this controller should fulfill all the requirements. The latter is finally implemented in a nonlinear simulation. The SIMULINK^{TM} diagram is visualized on Figure 14.6. Nonlinear simulation results are presented on Figure 14.7.

During this nonlinear simulation, a first step command is applied on the vertical acceleration from 0 to $30\,g$. After $1s$ a new step is applied to drive it back to $-10\,g$, then to $-25\,g$ and finally back to 0. During this operations, it can be observed that the angle-of-attack nearly covers the flight domain of interest. Moreover, as shown

on Figure 14.8, the Mach number is reduced from 4 to 2. On the lower-left plot of Figure 14.7 one observes that the control activity is compatible with actuators constraints. The lower-right plot shows the variations of the coefficient m_α which is also here the scheduling parameter.

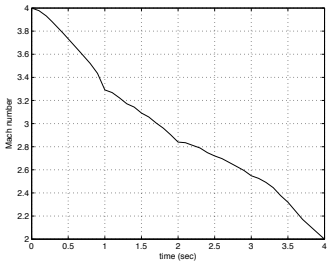

Fig. 14.8 Mach number profile

14.2.4 Conclusion

In this section, a first LPV control strategy has been proposed to cope with limitations on the rate-of-variations of the parameters, without considering parameter-dependent Lyapunov functions. Interestingly the method is based on the use of standard design results for polytopic LPV plants and is then applicable to systems of medium sizes. However, when the number of parameters increases, such an approach might fail (see remark 14.2).

14.3 Parameter-Varying Aircraft Control Design

As observed above, the design of control laws for parameter-varying systems with several scheduling variables remains a challenge for standard LMI-based LPV control techniques. In such a case, gain-scheduling methods are still a widely used alternative. In the context of aerospace applications, a short discussion on these techniques is given next and a specific approach is presented with its application to flight control laws design.

14.3.1 Gain-Scheduling Methods

In the aerospace industry, the preferred approach for designing gain-scheduled controllers consists of interpolating static gains which are computed by standard linear techniques for various flight conditions. A two-dimensional illustration of this

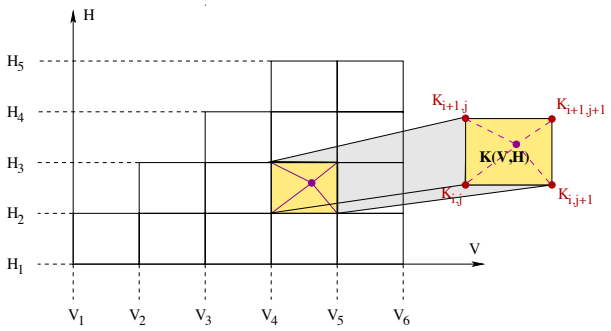

Fig. 14.9 Illustration of a static interpolation in (V,H) flight domain

approach is visible on Figure 14.9 where static gains have been obtained as functions of the airspeed (V) and altitude (H) and are then linearly interpolated on-line.

This approach, validated many times in practice, raises several theoretical issues among which stability properties between interpolation points throughout the flight domain have received a specific attention. For example, in the case of full-order dynamic controllers, a specific interpolation formulae has been developed in [24, 25] with which, stability is preserved throughout the whole operating domain. This requires however, that "neighboring" controllers partially overlap so that a controller $K_i(s)$ which nominally stabilizes a point P_i will also stabilize its neighbors. In the case of a single parameter, this principle is illustrated by Figure 14.10. Interestingly, the interpolation formulae of [24] is based on the existence of Lyapunov functions which can be computed off-line. However, its implementation remains numerically demanding and requires powerful on-board computers, more specifically when local controllers are not sufficiently robust. A possible approach to alleviate on-line computations consists in designing robust local controllers with guaranteed stability domains such that, along predefined trajectories, transitions from one controller to the next are proved to be stable. Since those domains are computed off-line, the implementation of such a strategy will remain rather cheap. Its efficiency will increase with the size of the stability domains. An illustration of this strategy [28] is given on Figure 14.11.

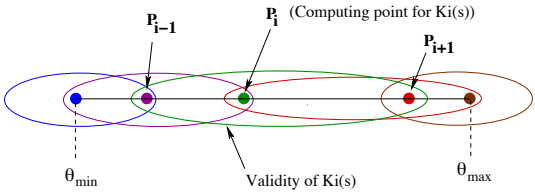

Fig. 14.10 Non uniform grid with guaranteed overlap

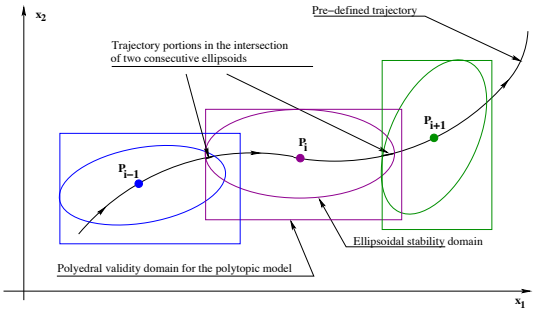

Fig. 14.11 Intersection of ellipsoidal stability domains along a predefined trajectory

14.3.2 Design and Interpolation of Locally Robust Controllers

Based on the above ideas, our proposed strategy consists in computing a family of locally robust controllers by a polytopic design approach. A family of polytopes is then generated so as to cover the flight domain of interest with overlaps as shown on Figure 14.12. Next, polytopic design models are defined for each polytope. This step is illustrated by Figure 14.13. A PID-like structure with a reference model is proposed here and a full access to the states of the augmented plant is assumed. In the context of aerospace applications, this last assumption is not so restrictive since most of the states are generally available for feedback. When necessary, reliable estimations can be obtained.

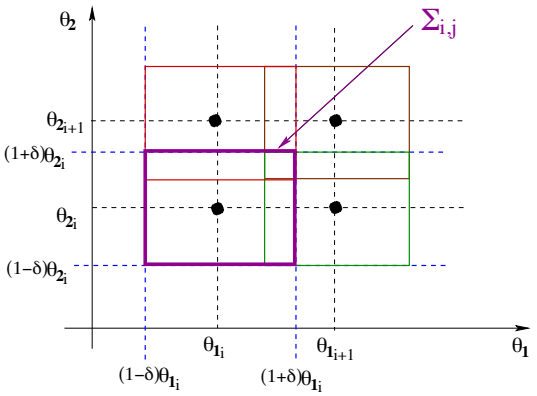

Fig. 14.12 Illustration of a 2D parametric grid

Assuming that the augmented design plant around point (j,k), denoted by $P_{jk}(s,\delta)$ on Figure 14.13, admits the polytopic description of equation 14.3, then a robust state-feedback controller K is easily computed thanks to the following proposition adapted from [35]:

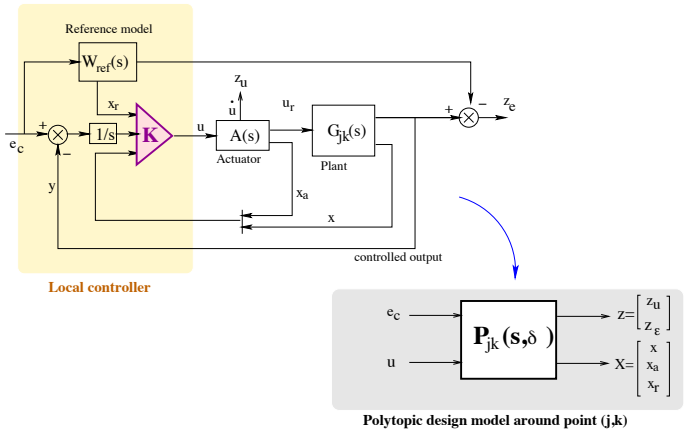

Fig. 14.13 A polytopic design model for the synthesis of locally robust controllers

Proposition 14.1. *Consider a polytopic system $P(s,\delta)$ as defined by (14.3) and assume that there exist a positive definite matrix X, and any matrix W of appropriate dimensions, such that:*

$$\forall i = 1 \ldots N, \begin{cases} \begin{pmatrix} A_iX + B_{2i}W & B_{1i} & 0 \\ 0 & -\frac{\gamma}{2}I & 0 \\ C_{1i}X + D_{12i}W & D_{11i} & -\frac{\gamma}{2}I \end{pmatrix} + (\star) < 0 \\ A_iX + B_{2i}W + \lambda X + (\star) < 0 \\ \begin{pmatrix} -\rho X & A_iX + B_{2i}W \\ (A_iX + B_{2i}W)' & -\rho X \end{pmatrix} < 0 \\ \begin{pmatrix} sin\alpha\,(A_iX + B_{2i}W) & -cos\alpha\,(A_iX + B_{2i}W) \\ cos\alpha\,(A_iX + B_{2i}W) & sin\alpha\,(A_iX + B_{2i}W) \end{pmatrix} + (\star) < 0 \end{cases} \tag{14.9}$$

then, every closed-loop LTI system inside the polytope $G(s) = C(sI - A)^{-1}B + D = F_l(P(s,\delta), K)$ with $K = WX^{-1}$ exhibits the following properties :

(i) $\|G(s)\|_\infty < \gamma$
(ii) $spec\,(A) \subset \mathscr{S}(\lambda, \rho, \alpha)$

where $\mathscr{S}(\lambda,\rho,\alpha)$ denotes the truncated sector of complex numbers z such that $\mathbb{R}(z) \leq -\lambda$, $|z| \leq \rho$ and $\Im(e^{-j\alpha}z) \leq 0$.

The first property is used to specify performance and disturbances attenuation, while the second is very useful to constrain the closed-loop poles so as to make sure for example that no interactions will appear with high frequency non modeled dynamics. These constraints can also be interestingly considered if the actuator model $A(s)$ is omitted in the design model. In such a case, the state feedback controller K will only use the aircraft outputs and will thus be more easily implemented.

14.3.3 Design Procedure and Implementation Issues

Thanks to the above proposition, locally robust controllers are easily computed on a grid of the flight domain. In a next step, a standard linear interpolation can be implemented to generate the global parameter-varying control laws. This step, illustrated by Figure 14.14 is made simple here thanks to the choice of a static state-feedback structure for each local controller. Note that the reference model can also be easily tuned as a function of the flight condition. A common practice consists in using faster models for high speed flight conditions.

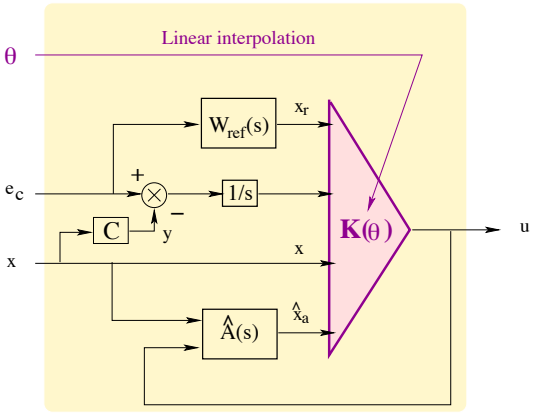

Fig. 14.14 Implementation diagram

Remark 14.3. On Figure 14.14, the LTI operator $\hat{A}(s)$ denotes an estimator of the actuator $A(s)$ which states are not systematically available for feedback.

14.3.4 Application to Flight Control Design

Let us now apply the above strategy to a flight control design problem for a generic fighter aircraft along the longitudinal axis. The nonlinear model is described with more details in Section 14.4. As is visible on Figure 14.15, a large operating domain is considered. This domain is gridded as shown on the same figure and for each point of this $2D$ grid, the aircraft is linearized about different values of the angle-of-attack, such that the load factor remains in the interval $[-3g\ \ 9g]$. A set of linearized models on a $3D$ grid of the whole subsonic operating range of the aircraft is thus obtained:

$$\begin{bmatrix}\dot{\alpha}\\ \dot{q}\end{bmatrix} = \begin{bmatrix}Z_\alpha(\alpha_i,V_i,H_i) & Z_q((\alpha_i,V_i,H_i)\\ M_\alpha(\alpha_i,V_i,H_i) & M_q(\alpha_i,V_i,H_i)\end{bmatrix}\begin{bmatrix}\alpha\\ q\end{bmatrix} + \begin{bmatrix}Z_\delta(\alpha_i,V_i,H_i)\\ M_\delta(\alpha_i,V_i,H_i)\end{bmatrix}\delta_m \qquad (14.10)$$

Following the above procedure, polytopic models are then determined around each triplet (α_i,V_i,H_i) such that a 20% overlap (as illustrated on Figure 14.12) is

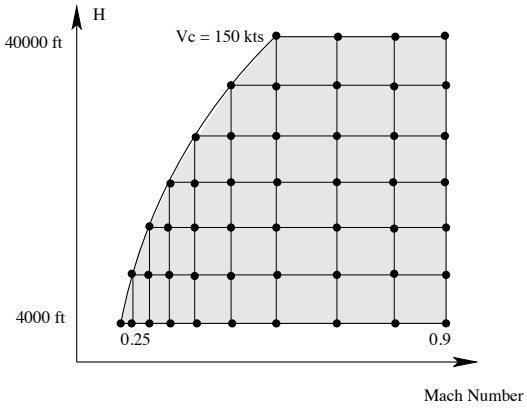

Fig. 14.15 Operating range in (M,H) plane with a lower bound constraint on V_c

guaranteed. Finally, design models are defined according to the structure of Figure 14.13 and the results of Proposition 14.1 are applied to compute a set of static gains $K_i = K(\alpha_i, V_i, H_i)$. The latter are finally implemented as discussed already. The general scheme of Figure 14.14 is adapted to the aircraft application as shown on Figure 14.16. For the reference model, a second-order transfer function has been considered with a fixed damping ratio $\xi_r = 0.7$ and a varying pulsation $\omega_r = \omega_r(V_c) \in [4, 10]$ as a linear function of the calibrated airspeed.

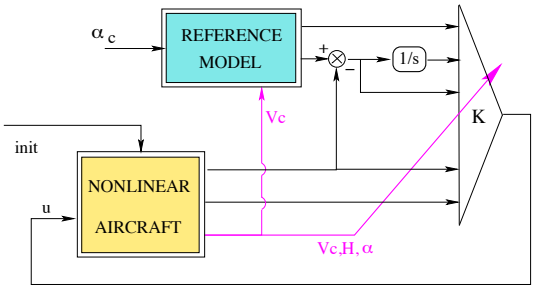

Fig. 14.16 Implementation of the parameter-varying controller

The above controller is finally implemented in a nonlinear simulation diagram which also implements a complete and realistic nonlinear representation of the aircraft along the longitudinal axis. Further details can be found in [35]. A preliminary frozen-time analysis is performed by checking the poles of the linearized closed-loop plants throughout the flight envelope. The results are displayed on Figure 14.17. Then, step responses are also realized throughout the flight envelope. The plots of Figure 14.18 reveal that the reference model is correctly followed whatever the mass and center-of-gravity location.

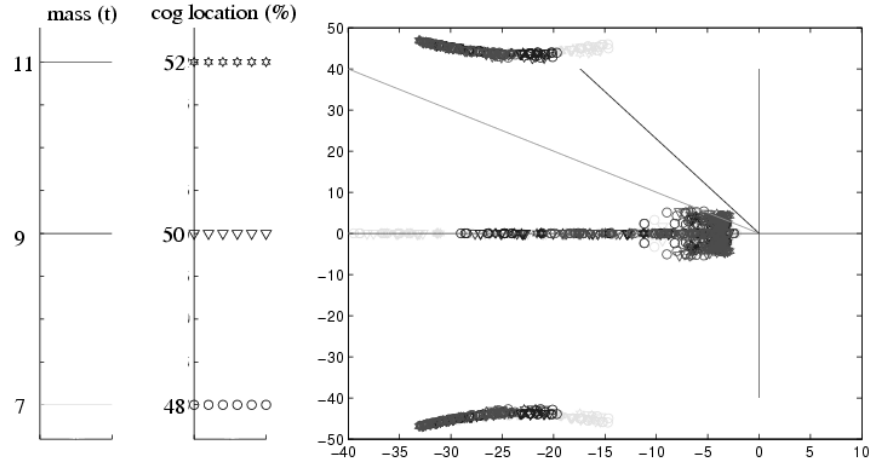

Fig. 14.17 Poles map throughout the flight envelope

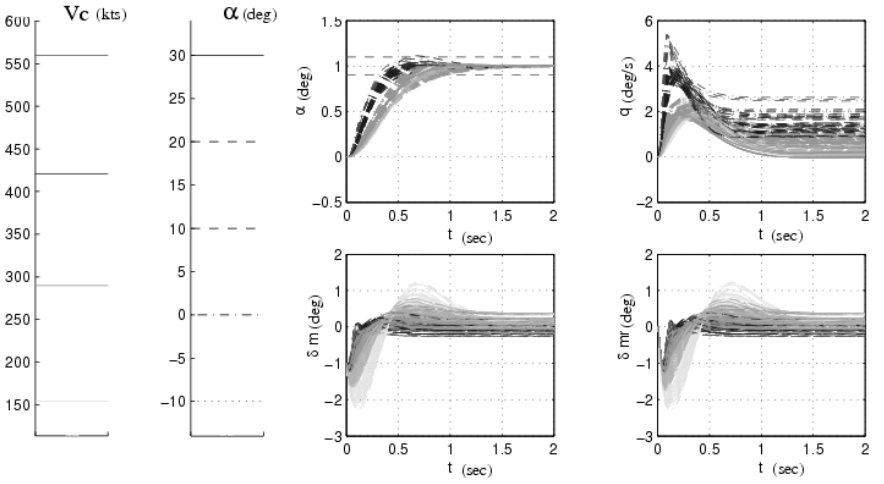

Fig. 14.18 Step responses throughout the flight envelope

14.3.5 Conclusion

As illustrated by the proposed application, the LPV control strategy of this section has permitted to take into account three parameters without any specific difficulty. The main drawback of this methodology is a lack of formal guarantee *a priori* regarding the closed-loop stability. As is further discussed in subsection 14.4.6, this property must be checked *a posteriori*. One other weak point of the method may also appear if the number of scheduling variables gets larger than 3. This is a standard

limitation of gain-scheduling techniques. In such cases indeed, numerous designs must be performed and it rapidly becomes very time-consuming. Moreover, the on-line interpolation becomes tricky and might exceed the capacity of the on-board computers. A third approach is considered in the next section, for which the notion of scheduling is viewed differently.

14.4 Dynamic-Inversion Based LPV Control

Since the early 1990s, nonlinear dynamic-inversion (NDI) based (or feedback linearization) control techniques have received considerable attention in the literature regarding their application to the design of flight control systems for missiles and aircraft. Given a possibly time-varying nonlinear plant:

$$\dot{x} = f(x,\theta) + g(x,\theta)u \tag{14.11}$$

a control law that achieves the desired response characteristics may be formulated as follows

$$u = g(x,\theta)^{-1}\left(v - f(x,\theta)\right) \tag{14.12}$$

where v specifies the desired response and is generally produced as the output of a linear controller, remarking that – in the ideal case – the closed-loop system now simply reads:

$$\dot{x} = v \tag{14.13}$$

Interestingly, when an accurate model is available, the control structure (14.12) compensates not only the nonlinearities of the plant but also its parametric variations as is further clarified below. Unfortunately, an exact compensation is never achieved in practice because of uncertainties in the model, because of noises on the measurements, because part of the states might not be available and finally because of control saturations. For these reasons, the elaboration of the desired response v needs a special attention. In this section, a strategy is proposed and illustrated by the design of flight control laws for the same aircraft as the one of Section 14.3.

14.4.1 NDI Control for LPV Systems

Assume that the nonlinear differential equation (14.11) can be rewritten as:

$$\begin{cases} \dot{x} = A(\theta)x + B(\theta)u \\ z = Lx \end{cases} \tag{14.14}$$

where z denotes the signal to be tracked and $B(\theta)$ is square and non singular matrix throughout the operating domain of the plant. Then, the "linearizing" control law (14.12) is adapted as follows:

$$u = B(\theta)^{-1}\left(B_0 v - (A(\theta) - A_0)x\right) \tag{14.15}$$

so that the LPV plant now becomes LTI:

$$\begin{cases} \dot{x} = A_0 x + B_0 v \\ z = Lx \end{cases} \tag{14.16}$$

for which the new control input v in the following format:

$$v = H(s)z_c + K(s)x \tag{14.17}$$

is easily designed by any standard approach. It is easily verified that the combination of equations (14.15) and (14.17) defines a standard LPV control law:

$$u = B(\theta)^{-1}\left[B_0 H(s)z_c + (B_0 K(s) + A_0 - A(\theta))x\right] \tag{14.18}$$

It is very interesting here to point out that any difficulty related to the size of θ has been removed. Note that the selection of the "central" matrices A_0 and B_0 is completely free. A standard choice consists in setting $A_0 = A(\bar{\theta})$ and $B_0 = B(\bar{\theta})$ where $\bar{\theta}$ denotes a mean value of the varying parameter. But in some cases, it might no be the best. Rather than considering mean values of the parameters, an interesting alternative, consists in focusing on worst case combinations for which the instability degree of A_0 for example is maximized, or for which the control efficiency is minimized. The central idea is that the LTI system (14.16) should not necessarily capture the mean behavior of the LPV plant but a worst case behavior. Unfortunately, there still exits no general rules for the selection of the "central" model. This is still an open issue and it seems that the best choice will highly depend on the application. Another difficulty of the proposed approach is related to the assumption on the matrix $B(\theta)$ which must be square and invertible. In practice, these two requirements are rarely met. But, in the context of aerospace systems, a time scale separation technique can be used to bypass such difficulties [29]. This point is clarified next.

14.4.2 Back to the Aircraft Control Problem

Let us consider again the longitudinal aircraft control problem which was introduced in Section 14.3. Using standard notation, the nonlinear short-term dynamics of the aircraft along its longitudinal axis are given by:

$$\begin{cases} \dot{\alpha} = q + w_\alpha(\theta_p) \\ J_{yy}\dot{q} = w_q(\theta_p) + \lambda(\theta_p)\delta_m \end{cases} \tag{14.19}$$

with:

$$\begin{cases} w_\alpha(\theta_p) = \frac{g}{V\cos\beta}(\cos\alpha\cos\theta\cos\phi + \sin\alpha\sin\theta + \tilde{a}_z\cos\alpha - \tilde{a}_x\sin\alpha) - p_t\tan\beta \\ w_q(\theta_p) = q_d SL(C_{M_\alpha}(M_a)\alpha + qLC_{M_q}/V) + (J_{zz} - J_{xx})pr + J_{xz}(r^2 - p^2) \\ \lambda(\theta_p) = q_d SLC_{M_\delta}(M_a) \end{cases} \tag{14.20}$$

and:

$$\begin{cases} p_i = p\cos\alpha + r\sin\alpha \\ \tilde{a}_x = ga_{x_m} + L_a g(q^2 + r^2) \\ \tilde{a}_z = ga_{z_m} + L_a g(\dot{q} - pr) \end{cases} \tag{14.21}$$

In the above representation, to avoid any confusion with a pitch angle θ, the notation θ_p is used to capture all parametric variations of the system (mainly induced by the variations of velocity). The longitudinal short-term motion of the aircraft is essentially controlled through the second equation in (14.19) via the control input δ_m denoting the elevator deflection. The latter also impacts the first equation through a small effect on the accelerations $\tilde{a}_x$ and $\tilde{a}_z$. But this one is small enough to be neglected.

Interestingly, the expressions of the nonlinear inputs (w_α and w_q) and of the control efficiency ($\lambda(\theta_p)$) given in (14.20) depend on known and on-line measurable data. Consequently, these three parameter-varying terms can be used by the controller. Observing that the control efficiency verifies $\lambda(\theta_p) < 0$ (and is then invertible) throughout the whole flight envelope, a standard NDI approach consists in inverting the moment equation so as to control the pitch rate. Assuming that the actuators dynamics are much faster than the desired response on q, they are temporarily neglected. It is then readily verified that the following control law:

$$\delta_c = \lambda(\theta_p)^{-1}(J_{yy}\tau_q^{-1}(q_c - q) - w_q) \tag{14.22}$$

yields:

$$\dot{q} \approx \tau_q^{-1}(q_c - q) \tag{14.23}$$

Since the pitch rate evolves much faster than the angle-of-attack, (this also can be enforced by choosing τ_q small enough) one further considers that $q \approx q_c$, so that the first equation in (14.19) is now controlled via q_c and the following choice for the commanded pitch rate:

$$q_c = \omega_r^2 \int_0^t (\alpha_c - \alpha) d\tau - 2\xi_r \omega_r \alpha - w_\alpha \tag{14.24}$$

enforces a second-order behavior on the angle-of-attack:

$$\frac{\alpha}{\alpha_c}(s) \approx \frac{\omega_r^2}{s^2 + 2\xi_r\omega_r s + \omega_r^2} \tag{14.25}$$

where the desired closed-loop pulsation ω_r is chosen as a function of the calibrated airspeed. Combining the above equations, one observes that the nonlinear parameter-varying control law may be summarized as:

$$u_c = \lambda(\theta_p)\delta_c = H(s)[\alpha_c \;\; w_\alpha \;\; w_q]' + K(s)[\alpha \;\; q]' \tag{14.26}$$

with

$$H(s) = \begin{bmatrix} \dfrac{J_{yy}\,\omega_r^2}{\tau_q s} & -\dfrac{J_{yy}}{\tau_q} & -1 \end{bmatrix}, \quad K(s) = -\dfrac{J_{yy}}{\tau_q}\begin{bmatrix} \dfrac{\omega_r^2}{s} + 2\xi_r\omega_r & 1 \end{bmatrix} \tag{14.27}$$

Note that equation (14.26) can be viewed as an alternative formulation of (14.18). With this approach, rather sophisticated parameter-varying control laws covering the whole flight domain of interest are then easily obtained after a very short design process. However, the efficiency of such control laws relies strongly on the availability of the nonlinear inputs w_α and w_q. In practice, uncertainties affect these two signals and the control efficiency $\lambda(\theta_p)$ is not precisely known. Moreover, because of the actuators dynamics, the actual deflection δ_m may differ sometimes significantly from the commanded variable δ_c. In the context of dynamic inversion, several techniques have been proposed to cope with these limitations by improving the robustness of the controller [29]. The central idea of these techniques consists of mixing the concept of dynamic inversion with robust control theory. Based on this idea, in the design procedure which is detailed next, a multi-objective H_∞ framework is proposed to generalize the above control structure and better optimize the gains $K(s)$ and $H(s)$.

14.4.3 Towards a New Design Procedure

As mentioned above, the desired elevator deflection is not produced instantaneously but is delivered by an actuator of limited capacity. In our context, its dynamics are accurately described by a linear second-order transfer function. Here, to further simplify the following discussion, let us temporarily reduce it to a first-order system so that $\dot{\delta}_m = \tau^{-1}(\delta_c - \delta_m)$ and let us define the new variable $u = \lambda(\theta_p)\delta_m$. Then, one obtains:

$$\dot{u} = \lambda(\theta_p)\dot{\delta}_m + \dot{\lambda}(\theta_p)\delta_m = \lambda(\theta_p)\dot{\delta}_m + w_u = \tau^{-1}(u_c - u) + w_u \tag{14.28}$$

where the commanded input u_c is defined in (14.26) and the perturbation term w_u may further be characterized as:

$$w_u = \frac{\dot{\lambda}(\theta_p)}{\lambda(\theta_p)}u = \mu(\theta_p)u \tag{14.29}$$

Hence, the nonlinear aircraft model of equation (14.19) including the actuator can be drawn as shown on Figure 14.19 where the state-space data of the linear system $G(s) = C_G(sI - A_G)^{-1}B_G$ are initially given by:

$$A_G = \begin{bmatrix} 0 & 1 \\ 0 & 0 \end{bmatrix}, \; B_G = \begin{bmatrix} 1 & 0 & 0 \\ 0 & J_{yy}^{-1} & J_{yy}^{-1} \end{bmatrix}, \; C_G = \begin{bmatrix} 1 & 0 \\ 0 & 1 \end{bmatrix} \tag{14.30}$$

Remark 14.4. As already discussed in subsection 14.4.1, the linear system $G(s)$ should at least locally capture a realistic behavior of the aircraft, which is definitely

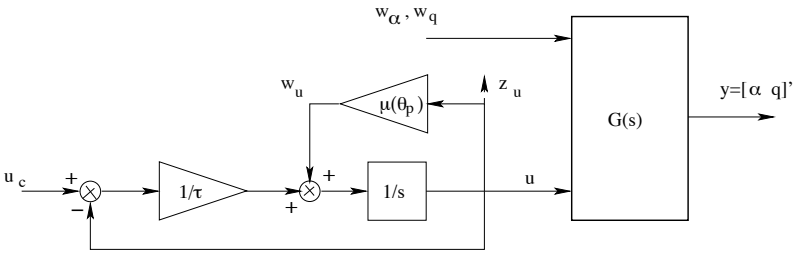

Fig. 14.19 Description of a nonlinear plant as a linear system with nonlinear inputs

not the case in (14.30) which corresponds to a double-integrator. For given values $\bar{\theta}_p$ of the varying parameters, a linearization technique yields:

$$\begin{cases} w_\alpha = \frac{\partial w_\alpha}{\partial \alpha}(\bar{\theta}_p).\alpha + \frac{\partial w_\alpha}{\partial q}(\bar{\theta}_p).q + \tilde{w}_\alpha \\ w_q = \frac{\partial w_q}{\partial \alpha}(\bar{\theta}_p).\alpha + \frac{\partial w_q}{\partial q}(\bar{\theta}_p).q + \tilde{w}_q \end{cases} \tag{14.31}$$

Then, the nonlinear inputs of $G(s)$ become $\tilde{w}_\alpha$ and $\tilde{w}_q$ and its A_G matrix is updated as follows:

$$A_G(\bar{\theta}_p) = \begin{bmatrix} \frac{\partial w_\alpha}{\partial \alpha}(\bar{\theta}_p) & 1 + \frac{\partial w_\alpha}{\partial q}(\bar{\theta}_p) \\ \frac{\partial w_q}{\partial \alpha}(\bar{\theta}_p) & \frac{\partial w_q}{\partial q}(\bar{\theta}_p) \end{bmatrix} \tag{14.32}$$

14.4.3.1 Formulation as a Multi-channel $\mathscr{H}_\infty$ Design Problem

Merging the above actuator description and $G(s)$, an augmented linear interconnection model $M(s)$ can be obtained and used to define an H_∞ design diagram as proposed on Figure 14.20.

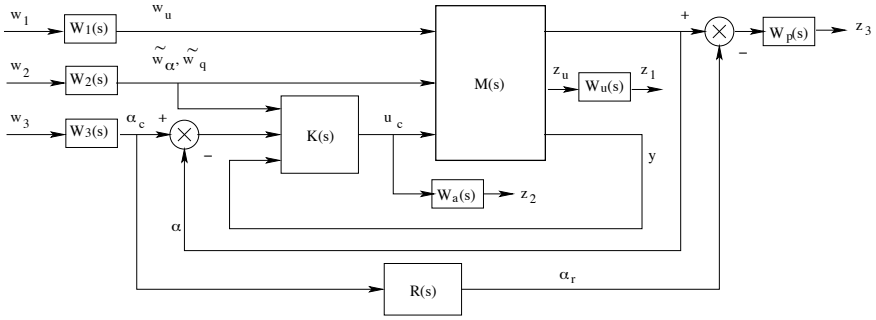

Fig. 14.20 Design model

Basically, the general idea consists of computing the best controller $K(s)$ such that each weighted transfer from w_i to z_i is minimized. More precisely, the transfer from w_3 to z_3 can be associated to the nominal performance since w_3 corresponds to a control input on the angle-of-attack while z_3 denotes the error between the actual output and that of the reference model $R(s)$. Then the problem to be solved take the form of the following multi-channel $\mathscr{H}_\infty$ optimization program:

$$\min_{K(s)} \|\mathscr{T}_{w_3\to z_3}(s)\|_\infty \quad \text{with} \quad \begin{cases} \|\mathscr{T}_{w_1\to z_1}(s)\|_\infty \le c_{11} \\ \|\mathscr{T}_{w_2\to z_3}(s)\|_\infty \le c_{23} \\ \|\mathscr{T}_{w_3\to z_2}(s)\|_\infty \le c_{32} \\ \|\mathscr{T}_{w_2\to z_2}(s)\|_\infty \le c_{22} \end{cases} \tag{14.33}$$

where constant terms c_{ij} can be tuned to quantify various robustness levels:

- c_{11}: stability robustness against the neglected term $w_u = \mu(\theta)u$
- c_{23}: performance robustness against perturbations $\tilde{w}_\alpha$ and $\tilde{w}_q$
- c_{32}: bound on the nominal control activity
- c_{22}: bound on the "perturbed" (by $\tilde{w}_\alpha$ and $\tilde{w}_q$) control activity

14.4.4 Interpretation and Controller Structure

As is visible on the diagram of Figure 14.20 and from (14.33), the nonlinear control design problem has been re-formulated as a rejection problem of on-line estimated nonlinear input perturbations. Assume that a controller $K(s)$ has been computed, then the control law to be implemented will read:

$$\delta_c = \frac{1}{\lambda(\theta_p)} K(s)[\tilde{w}_\alpha, \tilde{w}_q, \alpha_c - \alpha, y]' \tag{14.34}$$

The above expression generalizes (14.26). Here, the unique compensator $K(s)$ includes both the feedforward (previously denoted $H(s)$) and feedback (previously denoted $K(s)$) paths. Note that the signal w_u is not used by the controller, since its estimation might be very poor (because of possibly fast variations). Moreover, it has been observed in practice that this signal is often very small. As is clear from (14.29), its magnitude is directly related to the rate-of-change in the varying parameters.

14.4.4.1 Weighting Functions Tuning Procedure

In $\mathscr{H}_\infty$ design approaches, the most challenging task, once the controller structure has been defined consists of tuning correctly the weighting functions. This step is often very tricky. Fortunately, the situation is here quite favorable since an initial solution can be obtained by a standard dynamic inversion approach (see equations (14.26) and (14.27)). As a result, the weighting functions can be tuned by a frequency-domain analysis of the design model in feedback loop with this standard

solution. Then, there only remains to iterate from this starting point to improve the standard controller.

14.4.4.2 Dealing with Saturations

A key improvement axis in the above procedure consists of minimizing the control activity by "playing" on the weighting function $W_a(s)$ for example. It is then hoped that magnitude and rate limits will no longer induce loss of performance or stability. In a next step, further improvements can be obtained by plugging an anti-windup compensator $J(s)$ which can also be optimized by $\mathscr{H}_\infty$ norm minimization together with the previous feedback gain $K(s)$. Further details on such an approach can be found in [36] and [37].

14.4.4.3 About the Resolution

Last but not least, the resolution of the multi-channel $\mathscr{H}_\infty$ optimization problem (14.33) deserves a few comments. Unlike standard full-order $\mathscr{H}_\infty$ design problems the latter is non-convex because of the multi-channel aspect. Moreover, as shown by Figure 14.20, numerous weighting functions have been introduced in the design model which contributes to a significant increase of its number of states. As a result, the optimization of a full-order controller would certainly result in non-implementable control laws. It is then strongly recommended here to search for **fixed-order** and structured controllers which is a second source of non-convexity. Until recently, these problems were very hard to solve, which certainly explains why formulations as those stated by (14.33) have rarely been considered. But, during the last few years, thanks to very recent progress on non-smooth optimization techniques [38, 39, 40], new efficient tools dedicated to the local optimization of fixed-order and fixed structure $\mathscr{H}_\infty$ controllers have appeared. Let us first cite the public domain software **HIFOO** [41, 42, 43] for use with MATLAB, which is backed up by the theoretical advances described in [40]. Then appeared the the routine **HINFSTRUCT** whose theoretical foundations are described in [38]. The latter has been directly integrated to MATLAB by the *Mathworks Inc.* and is available with the Robust Control Toolbox [44].

14.4.5 Results on the Flight Control Problem

The above strategy is now applied to the flight control problem of section 14.3 but here both the longitudinal and the lateral axes are considered. Baseline controllers are preliminarily designed for each axis along the lines of subsection 14.4.2. Next both controllers are plugged into design models as shown on Figure 14.20, where all weighting functions are first set to identity. A singular value analysis is then performed in order to initialize the weighting functions and the fixed-order multi-channel $\mathscr{H}_\infty$ (14.33) is preliminarily solved for each axis. In each case, the initial

set of weighting functions is chosen so that all constraints c_{ij} are normalized. The best achieved $\mathscr{H}_\infty$ norm of the main transfer associated to the nominal performance also verifies: $\|\mathscr{T}_{w_3 \to z_3}(s)\|_\infty < 1$. Then, an iterative procedure is applied to decrease the constants c_{ij} while preserving the nominal performance constraint. During this procedure, one essentially tries to minimize c_{23} which reflects the capacity of the controllers to reject the nonlinear input signals thus extending their operating domains. For each axis, this value is approximately divided by 3.

Both longitudinal and lateral controllers are then implemented in a nonlinear SIMULINK diagram including a complete description of the aircraft which remains valid on the whole subsonic flight domain. Ten simulations are then performed to evaluate both the longitudinal and lateral controllers throughout the flight domain in which 5 points are selected (see Table 14.1).

Table 14.1 Test points in the flight domain

Point #	Mach number	Altitude (ft)
1	0.25	5000
2	0.5	20000
3	0.7	10000
4	0.9	36000
5	0.9	5000

For each of these points, the aircraft is preliminarily trimmed and two maneuvers are performed:

- **Longitudinal maneuver:** this sequence consists of two steps on the angle-of-attack. The first one is applied after $1\,s$. Its magnitude is tuned according to the flight point so that the vertical load factor does not exceed the maximum value of $9\,g$. Next, after $6\,s$ a new step is applied so that the final angle-of-attack is now between 0 and $-10\,deg$. Here again, the magnitude is adapted as a function of the flight point so that the vertical load factor remains above its minimum value which is fixed to $-3\,g$. The total length of this maneuver is $10\,s$. The simulations results are visible on Figure 14.21.
- **Lateral maneuver:** during this sequence, the lateral behavior of the aircraft control laws is evaluated through their capacity of tracking roll-rate commands. To this purpose, a series of roll-rate steps is applied as shown on Figure 14.22. During these steps, the objective is to maintain the sideslip angle around 0.

14.4.6 Concluding Remarks

In this section an original control design methodology combining the concepts of dynamic inversion and LPV control techniques has been described. The proposed strategy which essentially consists of revisiting NDI control as a linear control problem with measured (or estimated) nonlinear disturbing inputs is particularly

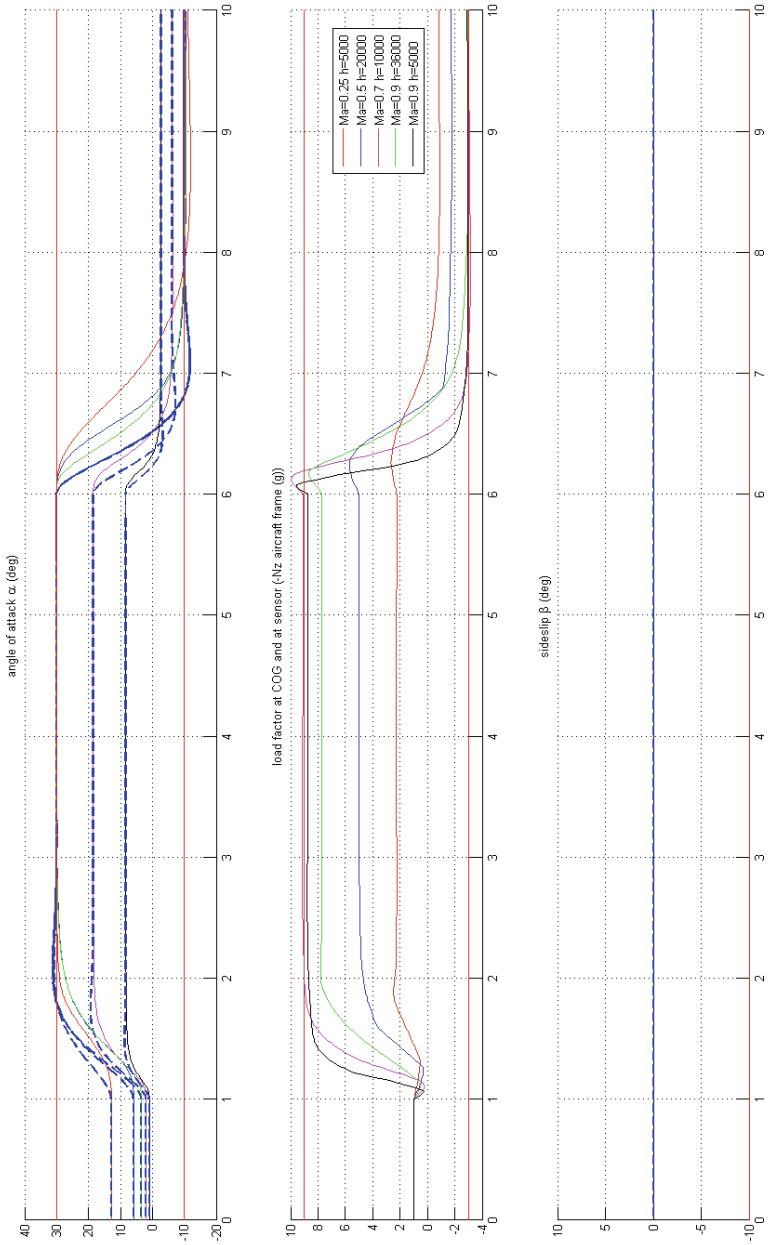

Fig. 14.21 Nonlinear simulations for various flight conditions: Longitudinal axis

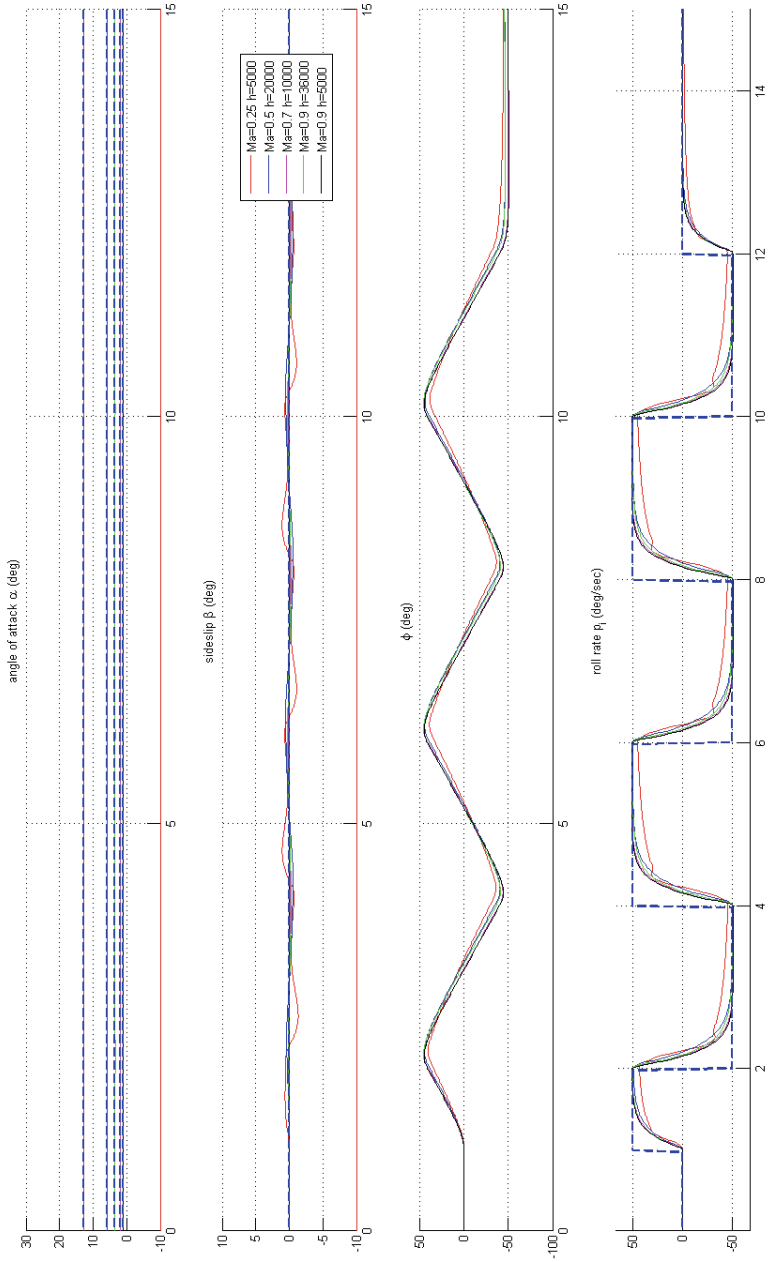

Fig. 14.22 Nonlinear simulations for various flight conditions: Lateral axis

well-suited to aerospace applications. The proposed design approach has been validated on a realistic and complete aircraft control problem throughout a large flight envelope. A key advantage of this last parameter-varying control strategy resides in its capacity of handling many parameters without critical impact during the design process.

However, when the nonlinear input signals – which in most cases have to be estimated on-line – differ significantly from the reality, it becomes difficult to predict wether the closed-loop properties will be guaranteed or not. A controller validation phase is then required, as this was also the case with the previous two methodologies which were developed in Sections 14.2 and 14.3. Such validations generally consist of extensive nonlinear simulations for many flight conditions, many parametric configurations, many different types of maneuvers. This unavoidable process takes a lot of time. This is why many efforts have been recently devoted to the development of numerically cheaper validation techniques for parameter-varying flight control laws. The interested reader may consult the book [45] and the references therein.

14.5 General Conclusion

In this chapter, a brief overview of LPV control strategies for aerospace systems has been presented. A special interest has been paid to specific methods for better managing the difficult tradeoff between conservatism and numerical complexity which rapidly increases with the number of scheduling parameters. In the context of aerospace systems, the combination of dynamic-inversion methods with the LPV framework appears to be a good compromise. Unlike more standard LPV control techniques essentially based on the use of parameter-dependent Lyapunov functions, the control strategies of this chapter generate controllers requiring a post-design validation process. This weak point is unfortunately the price to pay for numerically cheaper techniques.

References

1. Shamma, J.S., Athans, M.: Analysis of gain scheduled control for nonlinear plants. IEEE Transactions on Automatic Control 35(8), 898–907 (1990)
2. Shamma, J.S., Athans, M.: Guaranteed properties of gain scheduled control for linear parameter-varying plants. IEEE Transactions on Automatic Control 27(3), 559–564 (1991)
3. Packard, A.: Gain scheduling via linear fractional transformations. Systems and Control Letters 22(2), 79–92 (1994)
4. Becker, G., Packard, A.: Robust performance of linear parametrically varying systems using parametrically-dependent linear feedback. Systems and Control Letters 23(3), 205–215 (1994)
5. Apkarian, P., Gahinet, P.: A convex characterization of gain-scheduled H_∞ controllers. IEEE Transactions on Automatic Control 40(5), 853–864 (1995)

6. Apkarian, P., Biannic, J.-M.: Self-scheduled H_∞ control of missiles via Linear Matrix Inequalities. Journal of Guidance Control and Dynamics 18(3), 532–538 (1995)
7. Wu, F., Packard, A., Balas, G.J.: LPV control design for pitch-axis missile autopilots. In: Proceedings of the IEEE CDC, New Orleans, LA, USA (December 1995)
8. Biannic, J.-M., Apkarian, P., Garrard, W.: Parameter-varying control of a high performance aircraft. Journal of Guidance Control and Dynamics 20(2), 225–231 (1997)
9. Helmersson, A.: μ Synthesis and LFT gain scheduling with real uncertainties. International Journal of Robust and Nonlinear Control 8(7), 631–642 (1998)
10. Köse, I.E., Jabbari, F.: Control of LPV systems with partly measured parameters. IEEE Transactions on Automatic Control 44(3), 658–663 (1999)
11. Scorletti, G., El Ghaoui, L.: Improved LMI conditions for gain scheduling and related control problems. International Journal of Robust and Nonlinear Control 8(10), 845–877 (1998)
12. Apkarian, P., Adams, R.: Advanced gain scheduling techniques for uncertain systems. IEEE Transactions on Control Systems Technology 6(1), 21–32 (1998)
13. Wu, F.: A generalized LPV system analysis and control synthesis framework. International Journal of Control 74(7), 745–759 (2001)
14. Scherer, C.W.: LPV control and full block multipliers. Automatica 37(3), 361–375 (2001)
15. Wang, F., Balakrishnan, V.: Improved stability analysis and gain-scheduled controller synthesis for parameter-dependent systems. IEEE Transactions on Automatic Control 47(5), 720–734 (2002)
16. Wu, F., Dong, K.: Gain scheduling control of LFT systems using parameter-dependent Lyapunov functions. Automatica 42(1), 39–50 (2006)
17. Scherer, C.W., Köse, I.E.: Gain-scheduling synthesis with dynamic D-scalings. In: Proceedings of the IEEE CDC, New Orleans, LA, USA (December 2007)
18. Rugh, W.J., Shamma, J.S.: Research on gain scheduling. Automatica 36(10), 1401–1425 (2000)
19. Rugh, W.J.: Analytical framework for gain scheduling. IEEE Control System Magazine 11(1), 79–84 (1991)
20. Fromion, V., Scorletti, G.: A theoretical framework for gain scheduling. International Journal of Robust and Nonlinear Control 13(10), 951–982 (2003)
21. Kaminer, I., Pascoal, A.M., Khargonekar, P., Coleman, E.E.: A velocity algorithm for the implementation of gain-scheduled controllers. Automatica 31(8), 1185–1191 (1995)
22. Leith, D.J., Leithad, W.E.: Gain scheduled & nonlinear systems: Dynamic analysis by velocity-based linearisation families. International Journal of Control 70(2), 289–317 (1998)
23. Jones, C.D.C., Lowenberg, M.H., Richardson, T.S.: Tailored dynamic gain-scheduled control. Journal of Guidance Control and Dynamics 29(16), 1271–1281 (2006)
24. Stilwell, D.J., Rugh, W.J.: Interpolation of observer state feedback controllers for gain scheduling. IEEE Transactions on Automatic Control 44(6), 1225–1229 (1999)
25. Stilwell, D.J., Rugh, W.J.: Stability preserving interpolation methods for the synthesis of gain scheduled controllers. Automatica 36(5), 665–671 (2000)
26. Pellanda, P.C., Apkarian, P., Alazard, D.: Gain-scheduling through continuation of observer-based realizations - Applications to H_∞ and μ controllers. In: Proceedings of the IEEE CDC, Sidney, Australia (December 2000)
27. Stilwell, D.J., Rugh, W.J.: Stability and L_2 gain properties of LPV systems. Automatica 36(9), 1601–1606 (2002)
28. Teppa, P., Bernussou, J., Garcia, G., Khansah, H.: Scheduling of local robust control laws for nonlinear systems. Studies in Informatics and Control 16(2) (February 2007)

29. Reiner, J., Balas, G.J., Garrard, W.: Flight control design using robust dynamic inversion and time-scale separation. Automatica 32(11), 1493–1504 (1996)
30. Reigelsperger, W.C., Hammett, K.D., Banda, S.S.: Robust control law design for lateral-directional modes of an f-16/matv using μ-synthesis and dynamic inversion. International Journal of Robust and Nonlinear Control 7(8), 777–795 (1997)
31. Papageorgiou, G., Hyde, R.A.: Analyzing the stability of NDI-based flight controllers with LPV methods. In: Proceedings of the AIAA GNC Conference, Monreal, Canada (August 2001)
32. Biannic, J.-M., Apkarian, P.: Missile autopilot design via a modified LPV synthesis technique. Journal of Aerospace Science and Technology 3(3), 153–160 (1999)
33. Masubuchi, I., Kurata, I.: Gain-scheduled control synthesis by using filtered scheduling parameters. In: Proceedings of the IEEE CDC, Shangai, China (December 2009)
34. Reichert, R.T.: Robust autopilot design using μ-synthesis. In: Proceedings of the ACC, San Diego, CA, pp. 2368–2373 (May 1990)
35. Biannic, J.-M., Roos, C., Knauf, A.: Design and analysis of fighter aircraft flight control laws. European Journal of Control 12(1), 71–85 (2006)
36. Biannic, J.-M., Apkarian, P.: Anti-windup design via nonsmooth multi-objective H_∞ optimization. In: Proceedings of the ACC, San Francisco, CA, USA (June 2011)
37. Biannic, J.-M., Burlion, L., Tarbouriech, S., Garcia, G.: On dynamic inversion with rate saturations. In: Proceedings of the ACC, Montreal (June 2012)
38. Apkarian, P., Noll, D.: Nonsmooth H_∞ Synthesis. IEEE Transactions on Automatic Control 51(1), 71–86 (2006)
39. Apkarian, P., Noll, D.: Nonsmooth Optimization for Multidisk H_∞ Synthesis. European Journal of Control 12(3), 229–244 (2006)
40. Burke, J.V., Henrion, D., Lewis, A.S., Overton, M.L.: Stabilization via nonsmooth nonconvex optimization. IEEE Transactions on Automatic Control 51(11), 1760–1769 (2006)
41. Gumussoy, S., Millstone, M., Overton, M.L.: H_∞ strong stabilization via HIFOO, a package for fixed-order controller design. In: Proceedings of the IEEE CDC, Cancun, Mexico, pp. 4135–4140 (2008)
42. Gumussoy, S., Overton, M.L.: Fixed-Order H_∞ Controller Design via HIFOO, a Specialized Nonsmooth Optimization Package. In: Proceedings of the ACC, Seattle, USA (June 2008)
43. Gumussoy, S., Henrion, D., Millstone, M., Overton, M.L.: Multi-objective Robust Control with HIFOO 2.0. In: Proceedings of the IFAC Symposium on Robust Control Design, Haifa, Israël (July 2009)
44. MathWorks. Matlab R2010b, Robust Control Toolbox (September 2010), http://www.mathworks.com/help/toolbox/robust/ref/hinfstruct.html
45. Varga, A., Hansson, A., Puyou, G. (eds.): Optimization Based Clearance of Flight Control Laws. LNCIS, vol. 416. Springer, Heidelberg (2012)

Chapter 15
LPV Approaches for Varying Sampling Control Design: Application to Autonomous Underwater Vehicles

Emilie Roche, Olivier Sename, and Daniel Simon

Abstract. This chapter deals with the robust control of an Autonomous Underwater Vehicle (AUV) subject to computation or communication constraints. The aim is the design of a gain-scheduled varying sampling controller using non periodic measurements, where the varying sampling rate is considered as a known parameter. First a Linear Parameter Varying (LPV) model of the AUV is developed to keep some non-linearities of the plant in the model, thus enlarging the model's domain of validity around nominal conditions. The weighting templates are also made bandwidth dependent to take into account the dependencies between the achievable control performances and the sampling interval. From this model a LPV controller is synthesized in continuous time and then discretized over the range of predefined sampling rates. The approach is applied to the altitude control of an AUV, where depth measurements are asynchronously supplied by acoustic sensors.

15.1 Introduction

In the context of network-controlled systems the idea of using varying control intervals naturally arises when the available computing power devoted to feedback control is limited, e.g. in embedded systems. It can be easily shown, e.g. [27], that decreasing the control frequency directly decreases the amount of computations needed for control. In that case a feedback scheduler is assumed to compute on-line new control intervals according to the CPU load and system's state. Another case is

Emilie Roche · Daniel Simon
INRIA RA, 655 avenue de l'Europe - Montbonnot 38334 Saint Ismier Cedex
e-mail: emilie.roche@inrialpes.fr, Daniel.Simon@inria.fr

Olivier Sename
GIPSA-Lab, 11 rue des Mathématiques Grenoble Campus BP 46 F - 38402 SAINT MARTIN D'HERES
e-mail: olivier.sename@gipsa-lab.grenoble-inp.fr

O. Sename et al. (Eds.): *Robust Control and LPV Approaches*, LNCIS 437, pp. 375–395.
DOI: 10.1007/978-3-642-36110-4_15

when sensing cannot be done at any time. For example, underwater vehicles mainly sense their environment using acoustic sensors. Due to the slow propagation of the acoustic signals, measurements are subject to delays increasing with the distance to the target. Also, to avoid cross-talking between acoustic sensors working in a narrow area, these sensors must be scheduled, so that some of the sensors used in the control laws are triggered only at instants determined by an external manager, e.g. using a TDMA (Time division multiple access) scheduler [14]. In all these cases the control intervals are not equidistant, nevertheless they can be accurately measured by the internal clock of the controller when the control computation is started.

The problem of varying sampling control design have already been study for LTI systems in [18, 19, 10], where the sampling interval is considered as the unique varying (and known) parameter of a discrete-time Linear Parameter Varying (LPV) system under the polytopic representation. Another approach has been presented in [20, 21] to design sampling varying gain-scheduled discrete-time controller for LPV systems, based on the Linear Fractional Representation (LFR). The idea here is to extend the former approach for more complex LPV models accounting for some non-linearities of the plant.

Indeed LPV systems are increasingly used to deal with the robust control of non-linear systems. In particular they allow to represent some non-linearities of the plant as varying parameters, assuming that some knowledge of these parameters is available from modeling and internal measurements ([6],[3],[13],[26]). From the LPV model it is then possible to synthesize a gain-scheduled controller according to some performance criteria. The theoretical background has been often developed in association with robust control theory, e.g. as in [18], [1], [2], [23], [9], [3] and [4]. It is able to handle a wide variety of non-linear plants as in [24] for electrostatic devices, for the control of road vehicles in [7, 16], for the control of Diesel engines in [30], or for the control of semi-active suspensions as in [17].

This chapter extends these works bringing the design of a robust controller parametrized both by varying parameters of the plant and by the varying sampling interval. The method proposed here is based on the LPV polytopic representation of the plant, as already used in [19] to control discrete-time LTI systems with varying sampling intervals, where it led to low complexity models and easy control synthesis. However, combining both the plant's non-linearities and sampling intervals as varying parameters in the polytopic discrete-time model leads to far more larger model size, and control synthesis becomes difficult. Therefore it is chosen here to first synthesize the plant's parameter dependent controller in continuous time, and to discretize it for various values of the sampling interval inside predefined bounds.

The proposed LPV approach is applied to the altitude control of an Autonomous Underwater Vehicle (AUV). The control of AUVs is an active research field since twenty years, due to their large use for the exploration of the sea and for collecting data. The $\mathscr{H}_\infty$framework has already been used for the control of this kind of vehicle, in [5] for example where a reduced order $\mathscr{H}_\infty$controller is developed. The control of an AUV in the vertical plane is considered in [25], using a non-linear gain-scheduling approach (where the cruising speed of the vehicle is the scheduling parameter). The same approach is applied in [26] for the depth control of the AUV.

Other control approaches have been developers, as for example sliding mode in [8], or a PID structure and an anti-windup scheme in [13].

The next section 15.2 presents different models of the AUV, and section 15.3 gives the hierarchical control structure chosen for the altitude control in the vertical plan, as well as the LPV control-oriented model. Then the polytopic approach to design a controller, scheduled by both systems parameters and the variation of the sampling interval, is presented in section 15.4. In section 15.5 simulations results running on the non-linear model of the AUV show the feasibility of the proposed approach.

15.2 Underwater Vehicles Models

The Autonomous Underwater Vehicle (AUV) considered in this study is the $Aster^X$, presented on Figure 15.1, designed and operated by IFREMER[1] (French Research Institute for Exploitation of the Sea).

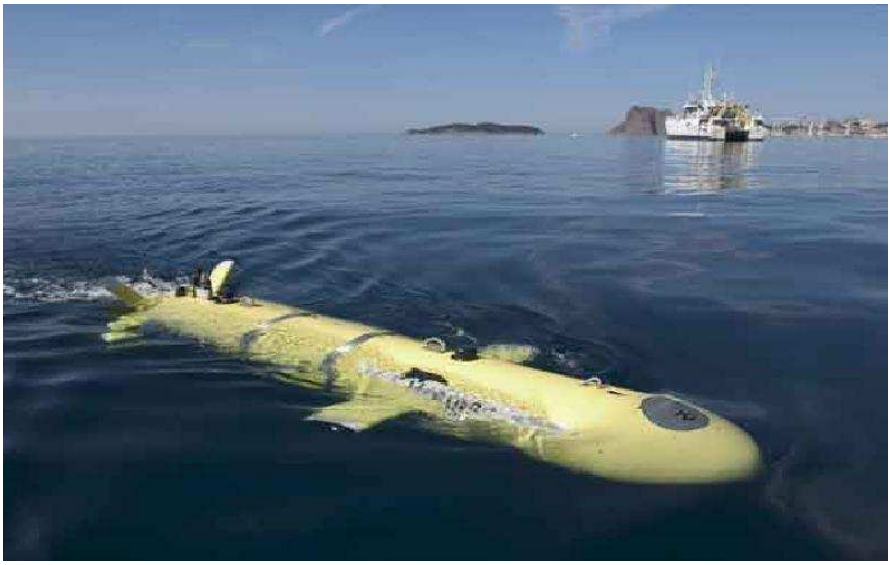

Fig. 15.1 The $Aster^X$ AUV operated by Ifremer

The complete modeling of this kind of AUV is a classical problem already studied, e.g. in [6, 22]. In this section the objective is first to give a global non-linear model of the AUV (used in the sequel for realistic simulations) and then a simplified model under polytopic formulation, in view of control design and synthesis.

[1] http://www.ifremer.fr/fleet/r&dprojets.htm

15.2.1 Non-linear Model

The motions of the autonomous underwater vehicle (AUV) are referenced in two frames :

- $\mathscr{R}(C,X,Y,Z)$ is the frame linked to the vehicle, whose origin C is the hull's center of buoyancy;
- $\mathscr{R}_0(O,X_0,Y_0,Z_0)$ is the inertial referential, it is considered linked to the earth in the case of an AUV moving at slow speed.

For the description of the vehicle behavior, we consider a 12 dimensional state vector : $X = \begin{bmatrix}\eta & \nu\end{bmatrix}^T$.

- $\eta \in \mathbb{R}^6$ is the pose of the vehicle in the inertial referential $\mathscr{R}_0$, made of the position vector η_1 and the angular position η_2: $\eta = \begin{bmatrix}\eta_1 & \eta_2\end{bmatrix}^T$ with $\eta_1 = \begin{bmatrix}x & y & z\end{bmatrix}^T$ and $\eta_2 = \begin{bmatrix}\phi & \theta & \psi\end{bmatrix}^T$ where x, y and z are the positions of the vehicle in $\mathscr{R}_0$, and ϕ, and θ and ψ are respectively the roll, pitch and yaw angles.
- $\nu \in \mathbb{R}^6$ is the velocity vector expressed in the local referential $\mathscr{R}$, it describes the linear and angular velocities (first derivative of the positions) through the change of frame (given by eq. (15.2)) : $\nu = \begin{bmatrix}\nu_1 & \nu_2\end{bmatrix}^T$ with $\nu_1 = \begin{bmatrix}u & v & w\end{bmatrix}^T$ and $\nu_2 = \begin{bmatrix}p & q & r\end{bmatrix}^T$

The dynamics of the vehicle is deduced from the 2^{nd} Newton law as modeled by the following equations:

$$M\dot{\nu} = G(\nu)\nu + D(\nu)\nu + \Gamma_g + \Gamma_p + \Gamma_u \tag{15.1}$$

$$\dot{\eta} = J_c(\eta_2)\nu \tag{15.2}$$

where:

- M is the inertia matrix, it represents the real mass of the vehicle augmented by the "water-added-mass" part,
- $G(\nu)$ represents the action of Coriolis and centrifugal forces,
- $D(\nu)$ is the matrix of hydrodynamics damping coefficients,
- Γ_g correspond to the gravity and hydrostatic forces,
- Γ_p represents disturbing forces and moments (e.g. due to waves, ocean currents...)
- $J_c(\eta_2)$ is the matrix for the change of frame from $\mathscr{R}(C,xyz)$ to $\mathscr{R}_0(O,X_0Y_0Z_0)$,
- Γ_u represent the forces and moments applied by the vehicle's actuators. The considered AUV has a screw propeller for velocity control in the Ox direction (providing a forward force Q_c) and 5 control surfaces:
  - a pair of 2 horizontals fins ("lifting canard") in the front part of the vehicle, controlled with angles β_1 and β_1';
  - 1 vertical fin at the tail of the vehicle, controlled with angle δ_1

– a pair of 2 tilted fins (with angle $\pm\pi/3$ w.r.t the vertical axis of the hull) at the tail, controlled with angles β_2 and β_2'.

Due to mechanical constraints, the control surfaces have their tilt angle limited to $0.5rad$. Note that an allocation module could be used to map the forces/torques screw components computed by the controllers on the available actuators, to make the controller adaptive w.r.t. various control surfaces layouts.

The model is non-linear with 12 state variables and 6 controls inputs (β_1, β_1', δ_1, β_2, β_2' and Q_c). To avoid some unnecessary complexity, a hierarchical control approach will be used, allowing to reduce the dimension of the control-oriented model, as presented on figure 15.2 and explained below.

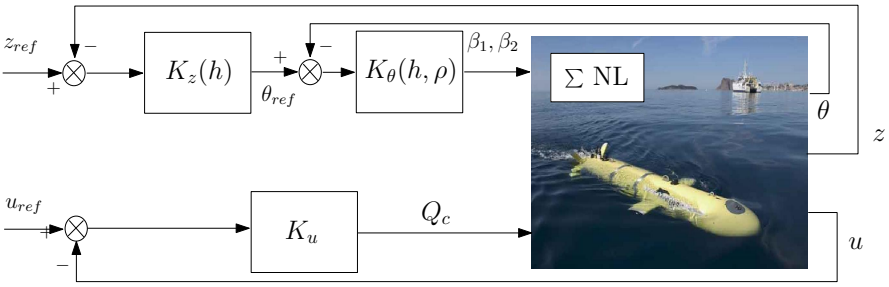

Fig. 15.2 Global control structure

15.2.2 Model Partition and Reduction

The full non-linear model of the vehicle involves coupled dynamics between the translation and rotation motions through many uncertain parameters. Moreover the system is under-actuated, due to the nature, the limited number and the location of the actuators. Rather than trying to handle all the degrees of freedom and motion axis in a single controller, the usual solution is to separate the global model into different sub-models with reduced size. This allows for a decoupled control synthesis for the motions in the horizontal and vertical plans and for the forward velocity control.

To control the altitude z, the model is reduced to 4 state variables : z, θ and the corresponding velocity w and q. For the actuation, only 4 control surfaces are needed : the 2 horizontal fins in the front part of the vehicle (with angles β_1 and β_1') and the 2 tilted fins at the tail (with angles β_2 and β_2'). Since only motions of the AUV in the vertical plan are considered, both fins in a pair are actuated with the same angle (as if they were mechanically linked) so the control variables are chosen such as: $\beta_1 = \beta_1'$ and $\beta_2 = \beta_2'$.

We focus on the control of the altitude z with adaptation to the sampling period, where the main goal is bottom referenced altitude control. In this scenario the forward speed u is controlled using a separated traditional (i.e. constant sampling) $\mathscr{H}_\infty$controller to keep the forward velocity constant as detailed in [20]).

15.3 Depth Cascade Control Structure

Assuming a forward velocity fast enough to provide effective lift forces, the motions in the vertical plane are controlled by the pairs of front and rear control surfaces through their angles β_1 and β_2. Thanks to this set of actuators, a torque around the pitch axis and a lift force along the z vehicle axis can be theoretically generated independently, and motions along the vertical axis and around the pitch axis can be decoupled, e.g. allowing for vertical motions while keeping the vehicle body horizontal.

However this kind of trajectory generates a lot of drag due to the angle of incidence between the main body and the fluid. As on-board energy storage is a crucial and limited resource for an AUV, the angle of incidence between the vehicle's body and the forward trajectory must be kept as small as possible. In consequence the lift efforts due to the front and rear tilted fins must be coordinated to keep the vehicle tangent to its trajectory to minimize the drag forces.

Obviously the AUV's altitude variations are strongly related to the pitch angle, and the cost effective way to climb a slope is to keep the AUV parallel to the slope by using the pitch angle as the control variable of the altitude controller. Therefore a cascaded control structure is considered, as depicted in Figure 15.3. The altitude controller K_z computes a reference of pitch angle from the comparison between the actual altitude and the desired one, then this reference is used by the pitch controller K_θ to compute the control actions (i.e. fins angles) to be applied to the AUV.

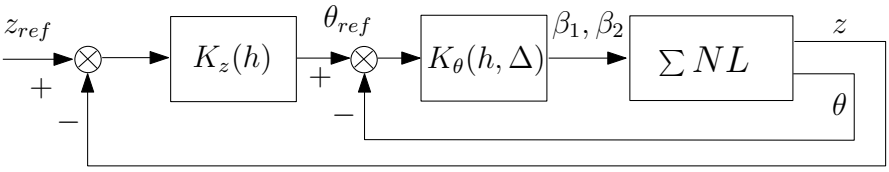

Fig. 15.3 Cascade control configuration for altitude control

Note that the maximum slope that can be tracked by the AUV depends on the combination between its hydrostatic stability, where the return torque is a function of the metacentric height (i.e. the distance between the body's center of buoyancy and the center of mass), and the maximum lift forces on the control surface which increases with the square of the forward velocity. Therefore the input of the altitude controller, which is primitively built from the observed distance to bottom, must be filtered to generate only physically feasible trajectories.

Similar cascade structures has been already described, e.g. in [11] where the PD/PI cascaded control structure is assumed to provide a good disturbances rejection. In this chapter the $\mathscr{H}_\infty$framework is used for the controller computation, since it can be naturally associated with LPV models to ensure performances of the closed loop system.

Two controllers, each of them being scheduled by varying parameters, are involved in this cascade control structure : the altitude controller $K_z(h)$ only depends on the sampling interval h and the pitch angle controller $K_\theta(h,\Delta)$ also depends on some non-linearities Δ of the model.

15.3.1 The Altitude Control-Oriented Model

Using the geometrical relation between the altitude variations and the pitch angle (Figure 15.4), it appears that the the pitch angle, combined with the forward velocity, is in some sense the "actuator" to be used to generate altitude variations with low drag. Therefore the altitude controller computes the pitch angle set-point needed to follow the desired path.

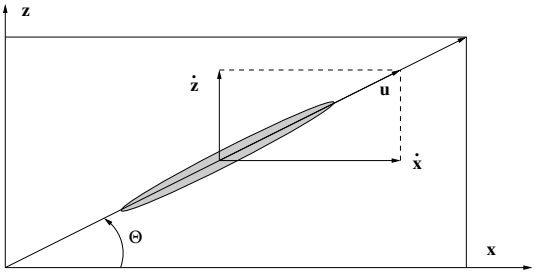

Fig. 15.4 Projection of velocities in the fixed frame

Projecting the body velocities in the fixed frame lead to this simple model :

$$\dot{z} = u \sin\theta \tag{15.3}$$

A Taylor expansion at order 1 of the *sinus* function is valid for the moderate pitch angles which are feasible by the AUV, it provides a linearized relation :

$$\dot{z} = u_0 \theta \tag{15.4}$$

leading to the transfer function :

$$G_z(s) = \frac{z}{\theta} = \frac{u_0}{s} \tag{15.5}$$

where u_0 is the desired cruising speed used for linearization. The internal loop of the cascade control structure is therefore approximated by a simple integrator.

Remark 15.1. Connected to parameter dependent weighting functions, a LPV generalized plant will be considered in the H_∞ framework. A LPV controller, considering the sampling interval as varying parameter will then be obtained, as shown in section 15.4.

15.3.2 LPV Polytopic Model for the Pitch Control

In the case of the altitude control of an AUV, where only motions in the vertical plane are considered using the cascade control structure presented before, one of the most important remaining variable of the system is the pitch angle θ which strongly influences the return torque acting on the hull and corresponding drag forces. However this variable appears in the non-linear model through trigonometric functions. A linear parameter-varying model, depending on a set of parameters inherited from the non-linearities, is here derived from the physical model. Indeed, to keep the control design and analysis in the framework of linear systems, the model is chosen to be linearized around a variable equilibrium point θ_{eq} such that the pitch angle θ is kept in the LPV model as a varying and known parameter.

From the 12 state variables of the original AUV model only 2 of them are needed here, namely the pitch angle θ and the pitch velocity q. Considering a constant forward velocity u_0, the non-linear equations describing the behavior of the AUV around the pitch axis are extracted from the full original model :

$$\begin{aligned} \dot{\theta} =& cos(\phi)q - sin(\phi)r \\ M_{55}\dot{q} =& -pr(I_x - I_z) - m[Z_g(qw - rv)] - (Z_q m - Z_f \mu V)gsin(\theta) \\ & - (X_q m - X_f \mu V)gcos(\theta)cos(\phi) + M_{wq}w|q| + M_{qq}q|q| + F_{fins} \end{aligned} \tag{15.6}$$

where M_{55} is a diagonal element of the mass matrix (including water-added mass), m is the mass of the vehicle, V the volume of the hull and μ the density of the fluid. $I_x, I_z, Z_g, Z_q, Z_f, X_q, X_f, M_{wq}$ are inertial and hydrodynamics scalar coefficients. F_{fins} is the torque induced by the lift and drag actions on the control surfaces. Note that for a constant forward velocity the lift forces are considered as approximately proportional to the angle of incidence, while this angle is far enough from stall angles.

The pitch angle is kept as a parameter in the LPV model after linearization around the equilibrium point: $X_{eq} = [.\ u_0\ .\ 0\ .\ 0\ 0\ 0\ \theta_{eq}\ 0\ 0\ 0]$ for which all velocities are assumed equal to zero except the cruising speed equal to u_0 and the pitch angle equal to θ_{eq}. No particular value is assigned to θ_{eq}, as it is a variable parameter of the model measured in real-time during the controller execution.

Finally a LPV representation is derived :

$$G_\theta : \begin{cases} \dot{\tilde{\theta}} = \tilde{q} \\ M_{55}\dot{\tilde{q}} = [-(Z_g m - Z_f \mu V)gcos(\theta_{eq}) + (X_g m - X_f \mu V)gsin(\theta_{eq})]\tilde{\theta} + F_{fins} \end{cases} \tag{15.7}$$

where the new state variables $\tilde{\theta}$ and $\tilde{q}$ are the variations of θ and q around the equilibrium point.

From these equations a polytopic model is carried out using the 2 parameters $\rho_1 = cos(\theta_{eq})$ and $\rho_2 = sin(\theta_{eq})$. Considering the physicals limits of the AUV (due

to the hydrostatic equilibrium) the angle θ is bounded by $[-30°, 30°]$ leading to the followings bounds for the 2 parameters: $\rho_1 \in [0.86, 1]$ and $\rho_2 \in [-0.5, 0.5]$.

Equations (15.7) are affine w.r.t the 2 parameters, and the vector formed by these 2 parameters evolves inside the polytope (rectangle) defined by the four vertices of coordinates: $\underline{\rho_1}\underline{\rho_2}$, $\underline{\rho_1}\overline{\rho_2}$, $\overline{\rho_1}\underline{\rho_2}$, $\overline{\rho_1}\overline{\rho_2}$.

The polytopic representation of the system is defined by equations (15.7) computed at each vertex of the polytope.

Remark: Note that the dependency of the 2 parameters on a single variable θ_{eq} may induce some conservatism. Moreover, as $\rho_1 = f(\rho_2)$ is a circle, considering the variations of $\theta \in [-30°, +30°]$ the admissible set of variation for the parameters is an arc of a circle. Enveloping this arc of a circle by a rectangle leads to some conservatism, but allows to express the polytope in a simple way.

15.4 A Polytopic LPV Control Approach for Sampling Dependent Systems

This section presents the methodology considered to get discrete-time LPV controller for the control structure 15.3, depending on the sampling interval, as well as on some system parameters, from the LPV models presented before.

Among possible LPV representations, the polytopic approach can be used when the dependency of the plant model matrices w.r.t. the parameters is affine. Each parameter ρ_i is assumed to belong to an interval $\rho_i \in [\underline{\rho_i}, \overline{\rho_i}]$, so that the vector of n varying parameters remains inside a polytope P of vertices ω_j defined as $\omega_j = [\nu_{j1}, \ldots, \nu_{jn}]^T$ with ν_{ji} taking the extreme values of parameter ρ_i, i.e. $\nu_{ji} \in \{\underline{\rho_i}, \overline{\rho_i}\}$.

At each instant t, the current value of the parameter vector $\rho(t)$ is given by the convex combination of the N vertices of the polytope ($N = 2^n$ in the hyper-cubic case n being the number of varying parameters):

$$\rho(t) = \sum_{i=1}^{N} \alpha_i(t) \times \omega_i, \text{ with } \alpha_i(t) \geq 0, \sum_{i=1}^{N} \alpha_i(t) = 1 \tag{15.8}$$

where $\alpha_i(t)$ are the polytopic coordinates of the parameters which can be computed on-line at low cost, e.g. [15]. Then the matrices of the LPV system are given by the convex combination of the N vertices matrix (state space matrices taken at each vertex of the polytope) as:

$$\begin{pmatrix} A(\rho(t)) & B(\rho(t)) \\ C(\rho(t)) & D(\rho(t)) \end{pmatrix} = \sum_{i=1}^{N} \alpha_i(t) \begin{pmatrix} A(\omega_i) & B(\omega_i) \\ C(\omega_i) & D(\omega_i) \end{pmatrix} \tag{15.9}$$

Under mild conditions (as derived in chapter 13.7) a gain-scheduled controller $K(\rho)$ is computed as the convex combination of controllers synthesized at each vertex([2]):

$$K(\rho):\begin{pmatrix} A_K(\rho) & B_K(\rho) \\ C_K(\rho) & D_K(\rho) \end{pmatrix} = \sum_{i=1}^{N} \alpha_i(t) \begin{pmatrix} A_K(\omega_i) & B_K(\omega_i) \\ C_K(\omega_i) & D_K(\omega_i) \end{pmatrix} \tag{15.10}$$

$$\text{with } \alpha_i(t) \text{ such that } \sum_{i=1}^{N} \alpha_i(t) = 1 \tag{15.11}$$

The main advantage of this representation is its simplicity which allows for using convex optimization at the controller design step. However, while the control design methodology uses $(2+1)$ Linear Matrix Inequalities in the LTI case, the synthesis of a polytopic controller relying on the polytopic model needs to solve $(2N+1)$ LMIs (with the same Lyapunov function for all LMIs). Thus the number of parameters n is a limiting factor, and this method is usually used only for a small set of parameters.

On the other hand, this chapter aims at obtaining a discrete-time LPV controller scheduled by the set of parameters $\rho(.)$ and by the sampling interval h. Indeed the first idea would be using h as a varying parameter as previously done in [19]. However, this approach would require the discretization of the LPV model containing the plant's varying parameters. As shown in [29], the discretization of an LPV model is not straightforward and the affine dependence on the parameters could not be longer guaranteed. In particular, when the sampling interval is kept as a parameter, the use of a Taylor approximation often leads to a polynomial model, vanishing the affine dependence carried out for the LTI plants. Finally considering both the plant's parameters and approximations of the sampling interval as varying parameters in a polytopic model leads to drastically increase the number n of parameters, and subsequent vertices and LMIs number, potentially involving numerical difficulties.

A simple way to overcome this problem is to design a continuous-time polytopic controller, dependent on some varying parameters of the continuous plant, and then to discretize it on-line for the current value of the sampling interval.

The chosen design methodology relies on the $\mathscr{H}_\infty$ framework. The problem considered is the classical mixed sensitivity problem, as depicted on Figure 15.5, where two weighting functions W_e and W_u are used to specify the desired closed-loop performances.

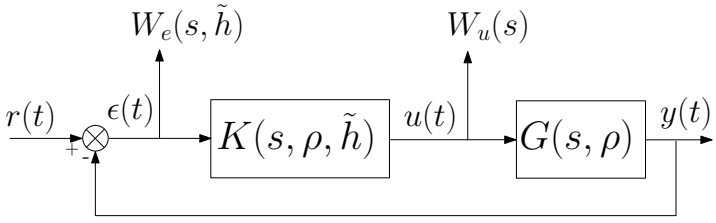

Fig. 15.5 Mixed sensitivity problem

The continuous-time polytopic synthesis is presented on the following steps:

Step 1: Performance specification. The required closed-loop performances are specified using some weighting functions. The weighting functions used for loop shaping are defined in continuous-time. To take into account that the control

performance usually degrades when the sampling rate becomes slower, they are made dependent on a parameter $\tilde{h}$ which represent the sampling interval further used for discretization. This parameter makes possible the performance adaptation with respect to the expected sampling interval value, even if the controller is synthesized in continuous time, as proposed in [19].

For example a first order weighting function depending on parameter $\tilde{h}$ can be defined as:

$$W(\tilde{h}) = \frac{\frac{s}{M_s} + w_b\tilde{h}}{s + w_b\tilde{h}\varepsilon} \tag{15.12}$$

where M_s is the desired module margin, $w_b\tilde{h}$ the bandwidth and ε the tracking error.

For the mixed sensitivity problem considered here, two weighting functions must be defined. The weight W_u takes into account the actuators saturation. The weight W_e on the tracking error is used to specify the closed-loop performances, with a variable bandwidth depending on $\tilde{h}$ following equation (15.12).

Step 2: Connection of the system and the weighting function. The interconnection of the LPV polytopic model (depending on the plant's parameters) and the weighting functions leads to a continuous-time polytopic model depending on both the plant's parameters and on the future sampling interval $\tilde{h}$.

For each vertex of the first polytope $\omega_i = [v_{i1}, \ldots, v_{in}]$, 2 new vertices are created following :

$$\omega_i' = [v_{i1}, \ldots, v_{in}, \underline{\tilde{h}}] \text{ and } \omega_i'' = [v_{i1}, \ldots, v_{in}, \overline{\tilde{h}}] \tag{15.13}$$

Step 3: Continuous-time controller synthesis. An LPV continuous-time polytopic controller is computed using the methodology presented in [2]. The result is a set of controllers synthesized at the vertices of the polytope. Considering the current value of the parameters, a convex combination of the N vertices controllers leads to the continuous-time controller:

$$\begin{pmatrix} A_K(\rho,\tilde{h}) & B_K(\rho,\tilde{h}) \\ C_K(\rho,\tilde{h}) & D_K(\rho,\tilde{h}) \end{pmatrix} = \sum_{i=1}^{N} \alpha_i(t) \begin{pmatrix} A_K(\omega_i) & B_K(\omega_i) \\ C_K(\omega_i) & D_K(\omega_i) \end{pmatrix} \tag{15.14}$$

Step 4: Discretization of the LPV polytopic controller. During this step, the parameter $\tilde{h}$, who was until now not related to any real variable, is considered identical to the sampling period h. From the continuous time-controller, computed on-line as in (15.14), a discrete-time controller is obtained using any usual numerical method, e.g. using the exact exponential of a matrix.

$M = \begin{pmatrix} A_K & B_K \\ 0 & 0 \end{pmatrix}$ as:

$$\begin{cases} x_{K_{k+1}} = A_{K_d} x_{K_k} + B_{K_d} u_k \\ y_K = C_{K_d} x_{K_k} + D_{K_d} u_k \end{cases} \tag{15.15}$$

$$\begin{pmatrix} A_{K_d} & B_{K_d} \\ 0 & I \end{pmatrix} := exp\left(\begin{pmatrix} A_K & B_K \\ 0 & 0 \end{pmatrix} h \right) \tag{15.16}$$

where A_K and B_K are defined in (15.14).

Finally this controller is a LPV discrete-time one which depends both on the plant's parameters and on the varying sampling interval. The main drawback in this case remains in the on-line computation of the exponential of a state matrix (to get the exact representation), which may be too costly to be computed in real-time for an embedded processor with limited computing power.

To be real-time effective it is possible to approximate the matrix exponential by a Taylor series of order l as:

$$A_\delta \approx I + \sum_{i=1}^{l} \frac{A^i}{i!}\,\delta^i \tag{15.17}$$

where δ is the deviation of the sampling interval h w.r.t. its central value h_0, given by $h = h_0 + \delta$ with $h_{min} - h_0 \leq \delta \leq h_{max} - h_0$. It has been shown in [19] that the approximation error, measured by

$$J_N = \max_{h_{min}<h<h_{max}} \| G_{d_e}(h) - G_d(h) \|_\infty$$

where G_{d_e} and G_d are the discrete-time models using the exact and the approximated methods, are negligible for $l \geq 2$ for useful sampling rates variations, e.g. $h_{max} = 3.h_{min}$.

Other ways to approximate the exact form of the discrete matrices can be found in [29]. Anyway remind that it is not possible to compute a discretization of the vertices matrix and then build a convex combination since the convexity is lost during the discretization step.

15.5 LPV Control of the AUV

The methodology presented in section 15.4 is now applied to the altitude control of the AUV, considering the cascade structure presented in section 15.3. The design configuration and frequency-domain analysis is first presented. Then some simulation results, obtained on the full non linear AUV model, are provided.

15.5.1 Design Method and Analysis

Let us recall that, according to the structure 15.3, two controllers are designed following the steps given in section 15.4. It is worth noting that to get the solution of the control problems the YALMIP parser [12] and SeDuMi solver [28] have been used.

15.5.1.1 Altitude Controller

The altitude controller is designed using the geometrical model (15.5) of section 15.3. The continuous-time altitude model does not depend on any varying parameter (this model is LTI). However the controller depends only on the sampling period h.

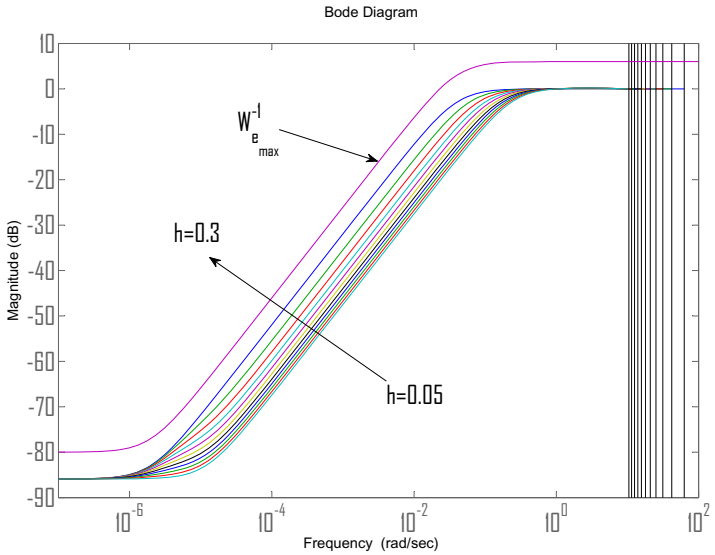

Fig. 15.6 S sensitivity function - altitude controller

The mixed sensitivity problem is stated as in section 15.4 using the two following weighting functions :

- $W_e(\tilde{h}) = \frac{\frac{s}{M_s}+w_b\tilde{h}}{s+w_b\tilde{h}\varepsilon}$ with $M_s = 2$, $w_b = 10 rad/s$ and $\varepsilon = 10^{-4}$
- $W_u = \frac{1}{M_{s_u}}$ with $M_{s_u} = 5$.

The continuous-time polytopic approach is then applied to the altitude controller synthesis, which in this case is reduced to a two-vertices polytope (since the varying parameter is the sampling interval only). The sensitivity function obtained is presented on Figure 15.6. The S function shows that the bandwidth varies w.r.t. the sampling interval according to the performances specifications defined by the weighting function W_e. The KS sensitivity function (Figure 15.7) show limited variations of the gain w.r.t. the sampling interval, and that the W_u weighting function is respected everywhere.

15.5.1.2 Pitch Angle Controller

The method described in section 15.4 is applied to the polytopic model obtained in subsection 15.3.2.

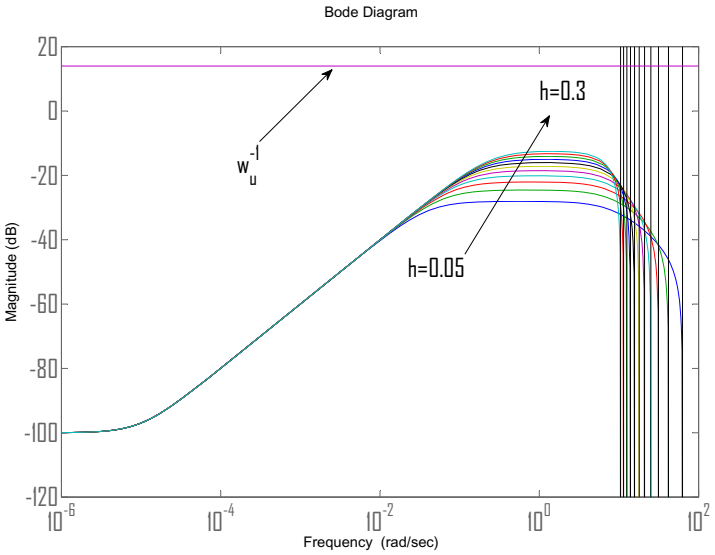

Fig. 15.7 KS sensitivity function - altitude controller

The mixed sensitivity problem is again considered with the two following weighting functions :

- $W_e(\tilde{h}) = \frac{\frac{s}{M_s}+w_b\tilde{h}}{s+w_b\tilde{h}\varepsilon}$ with $M_s = 2$, $w_b = 0.4rad/s$ and $\varepsilon = 10^{-4}$
- $W_{\theta_u} = \begin{bmatrix} 0.75 & 0 \\ 0 & 1.5 \end{bmatrix}$.

By the connection of the polytopic model of the system and the weighting function, a new continuous-time LPV polytopic model is built, depending both on the parameters ρ_1 and ρ_2 inherited from the non-linear system and on $\tilde{h}$, the sampling interval afterward used for discretization. Finally a LPV polytopic model with 8 vertices is achieved :

$$\underline{\rho_1\rho_2}\underline{\tilde{h}},\ \underline{\rho_1\rho_2}\overline{\tilde{h}},\ \underline{\rho_1}\overline{\rho_2}\underline{\tilde{h}},\ \underline{\rho_1}\overline{\rho_2}\overline{\tilde{h}},\ \overline{\rho_1}\underline{\rho_2}\underline{\tilde{h}},\ \overline{\rho_1}\underline{\rho_2}\overline{\tilde{h}},\ \overline{\rho_1}\overline{\rho_2}\underline{\tilde{h}},\ \overline{\rho_1}\overline{\rho_2}\overline{\tilde{h}} \tag{15.18}$$

This model $G_\theta(\rho_1,\rho_2,\tilde{h})$ can be directly used to compute a LPV polytopic controller. The continuous-time controller synthesis is applied on the polytopic model build for the pitch angle controller (15.10) over polytope (15.18), depending on the sampling interval and the two parameters $\cos(\theta)$ and $\sin(\theta)$. The resulting S sensitivity function is presented on Figure 15.8, which emphasizes again the performance adaptation w.r.t the sampling interval.

Remark: The cascade structure in this chapter uses different bandwidth for the two loops (altitude and pitch) which therefore are uncoupled, see the values given to w_b

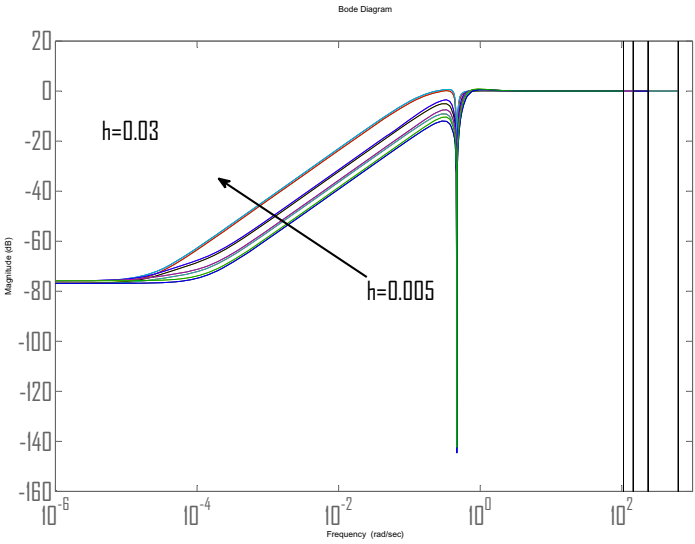

Fig. 15.8 S sensitivity function - pitch angle controller

for the two controllers. However successful simulations have been also carried out using the same sampling range for the two controllers.

Remark: The geometric model for the altitude controller uses a Taylor expansion around $\theta = 0$ while the pitch controller uses $\theta_{eq} \neq 0$ as varying parameter, which seems conflicting. Indeed, for $\theta_{max} = 0.5$ rads, the linearization error on the integration gain used for altitude control is about 4%. This is negligible considering others modeling uncertainties, and it is handled by the robustness of the controller. On the other hand, a $\theta_{max} = 0.5$ pitch angle induces a return torque around the pitch axis close to the maximum lift capabilities of the control surfaces. Hence using θ_{eq} in the pitch control design allows for an effective trim of the fins control angle w.r.t. the current pitch angle.

15.5.2 Simulation Scenario

Let us recall that the full (12 state variables) non-linear model of the AUV is used for the simulations.

The mission considered here is the sea bottom following at a constant altitude while keeping constant the forward speed. The global control structure used for the simulations is presented in Figure 15.9.

To implement the AUV mission three controllers are designed and implemented. A discrete-time $\mathscr{H}_\infty$controller K_u with a constant sampling period of $0.1s$ is used for the control of the longitudinal speed $u_0 = 1m/sec$. The forward velocity must be

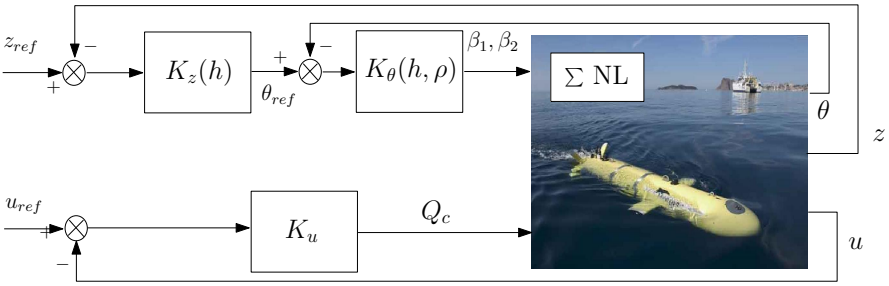

Fig. 15.9 Global control structure

large enough to provide lift on the actuators. Moreover most payloads, e.g. side-scan acoustic sensors used to build maps, actually require a constant forward velocity. The design of this controller is not detailed here (see in [21]).

Both gain-scheduled feedback loops are now $K_z(h)$ and $K_\theta(\rho_1,\rho_2,h)$. The altitude controller $K_z(h)$ (computed from the model $G_z(\tilde{h})$) gives the reference pitch angle θ_{ref}, which is used by the pitch angle controller $K_\theta(\rho_1,\rho_2,h)$ using the model $G_\theta(\rho_1,\rho_2,\tilde{h})$ to compute the actions applied to the AUV.

Remark: The continuous models, based on the expected sampling interval $\tilde{h}$, are discretized on the fly for the actual value of h

The pitch angle polytopic controller $K_\theta(\rho_1,\rho_2,h)$ is a discrete-time controller, scheduled by the sampling period h and the two parameters inherited from the LPV model $cos(\theta_{eq})$ and $sin(\theta_{eq})$. The measure of the pitch angle θ is used for the computation of the 2 parameters.

For evaluation purpose, the non equidistant control intervals are generated as a sinusoidal signal ranging between $0.005s$ and $0.03s$ (Figure 15.10). The current value of the parameters is then used to compute the controller matrices at the working point, the variations of the parameters are depicted by Figure 15.14.

The design of the altitude controller $K_z(h)$, which depends only on the sampling interval h), is achieved using the methodology presented in section 15.4 for a parameter $\tilde{h} = h$ (sampling interval) varying inside the interval $[\tilde{h}_{min};\tilde{h}_{max}] = [0.05;0.3]s$

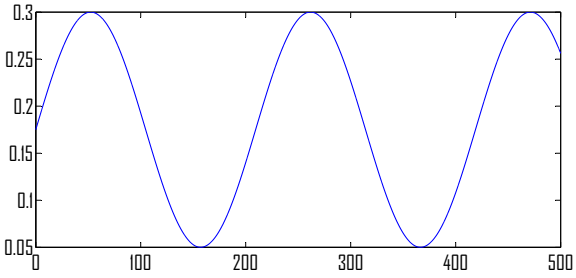

Fig. 15.10 Reference of sampling interval h

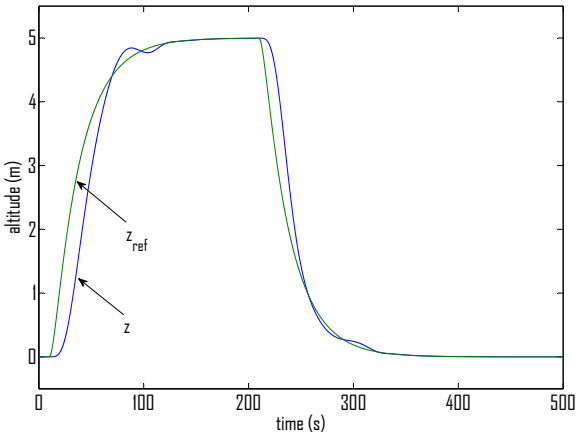

Fig. 15.11 Reference and measure of the altitude z

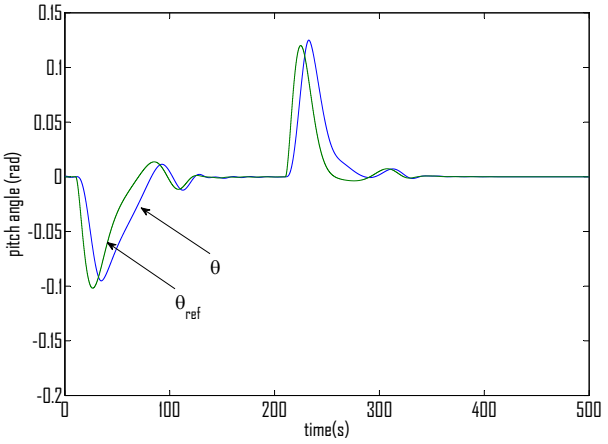

Fig. 15.12 Reference and measure of the pitch angle θ

To track feasible trajectories, the desired altitude is given through a second order filter whose tuning avoids excessive solicitations of the control surfaces.

It is worth noting that both other parameters (ρ_1, ρ_2) depends on the output θ of the system and therefore change during the simulation. The maximum value of the pitch angle is here $0.5rad$ which corresponds with the maximum return torque that can be achieved by the actuators at the chosen forward velocity. The speed of variation of the reference θ_{ref} is also close to the limits of the vehicle capabilities.

15.5.3 Simulation Results

Simulations results using Matlab/Simulink are presented on Figures 15.11 to 15.15. These results show the effective adaptivity of the controller w.r.t. the variations of the parameters which were considered in the LPV model.

The main achievement is that the stability of the control loops is preserved despite the variations of the sampling rate during control execution. When controlled by a classical $\mathscr{H}_\infty$regulator designed for the nominal sampling period, the same plant rapidly becomes unstable when variations of the sampling interval are applied [20].

Compared with a previous approach where the only varying parameter in the LPV model was the sampling rate ([21]), the tracking of the altitude reference (Figure 15.11) and of the pitch reference (Figure 15.12) are achieved with better performances when the non-linearities involving θ are kept in the LPV model. Indeed accounting for the value of the actual pitch angle in the controller allows for efficiently increase the control actions to counterbalance the return torque due to the hydrostatic stability of the hull.

Figure 15.13 shows that the angles applied to the control surfaces are far from the angle limitations (set at $0.5rad$ for all actuators), as only 30% of the available range is used. It is worth noting that the results presented use the best tuning tested for this control configuration. Considering the under use of the actuators, it should be physically possible to improve the performances (e.g settling time) but numerical problem rapidly arise when trying to tune the weighting function in that direction.

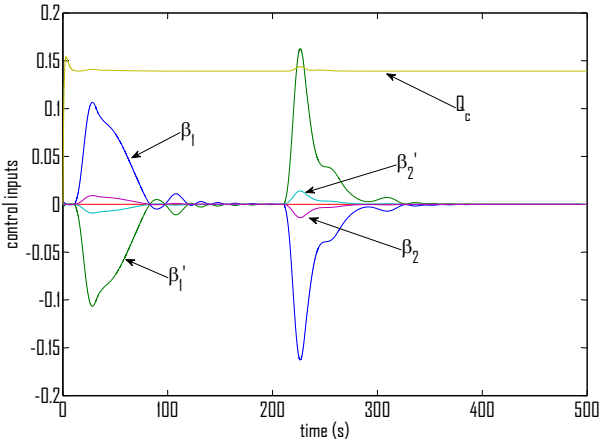

Fig. 15.13 Actions applied to the vehicle

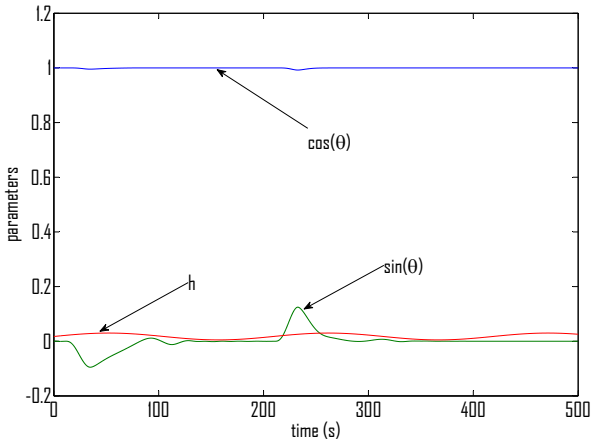

Fig. 15.14 Evolution of the parameters during the simulation

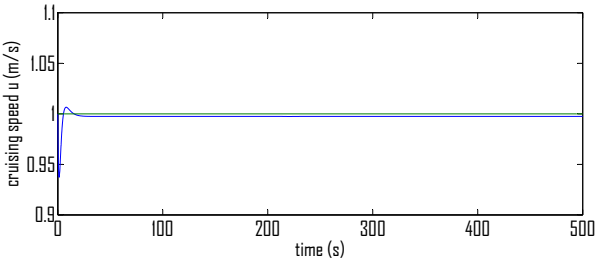

Fig. 15.15 Reference and measure of the cruising speed u

15.6 Conclusion

In this chapter the altitude control of an AUV is addressed, considering the varying sampling control of a LPV system. A continuous-time polytopic approach is proposed to avoid, in the control design step, the non straightforward discretization of an LPV representation.

Simulation results presented in this chapter show the feasibility of the proposed approach. Thanks to the adaptation of the controller w.r.t. the current value of the varying parameters, the polytopic controller leads to good results, considering the fact that simulations are running on the full (12 state variables) non-linear model of the AUV, while the controllers design is made considering a reduced-order LPV model.

The proposed cascade control structure takes into account the strong link existing between the altitude and the pitch angle, and enables to achieve cost-effective

control objectives in the vertical plan, since the altitude controler computes the suitable pitch angle reference to minimize drag.

Moreover the methodology proposed in this chapter, considering as varying parameter the sampling interval and parameters inherited from the non-linear model ($\cos(\theta_{eq})$ and $\sin(\theta_{eq})$) allows to improve the close loop performances compared to the previously studied case where only the sampling rate was considered as a parameter.

Note that other representations of LPV systems can be used for solving this problem. For example, the Linear Fractional Representation (LFR) considers the varying parameters (including uncertainties and non-linearities) as additional inputs of a nominal LTI plant. Indeed this approach is appealing since it allows for considering both the system's varying parameters and the sampling rate in an unified framework. Some results are under development following these ideas.

References

1. Apkarian, P., Gahinet, P.: A convex characterisation of gain-scheduled $\mathscr{H}_\infty$ controllers. IEEE Transaction on Automatic Control 40, 853–864 (1995)
2. Apkarian, P., Gahinet, P., Becker, G.: Self-scheduled $\mathscr{H}_\infty$ control of linear parameter-varying systems: a design example. Automatica 31(9), 1251–1261 (1995)
3. Bokor, J., Balas, G.: Detection filter design for LPV systems–a geometric approach. Automatica 40(3), 511–518 (2004)
4. Briat, C., Sename, O., Lafay, J.F.: Memory-resilient gain-scheduled state-feedback control of uncertain LTI/LPV systems with time-varying delays. Systems and Control Letters 59(8), 451–459 (2010)
5. Feng, Z., Allen, R.: Reduced order $\mathscr{H}_\infty$control of an autonomous underwater vehicle. Control Engineering Practice 12, 1511–1520 (2004)
6. Fossen, T.I.: Guidance and Control of Ocean Vehicles. John Wiley & Sons (1994)
7. Gaspar, P., Szabo, Z., Bokor, J.: LPV design of fault-tolerant control for road vehicles. In: 2010 Conference on Control and Fault-Tolerant Systems (SysTol), pp. 807–812 (October 2010)
8. Healey, A.J., Lienard, D.: Multivariable sliding mode control for autonomous diving and steering of unmanned underwater vehicles. Oceanic Engineering 18(3), 327–339 (1993)
9. Heemels, W.P.M.H., Daafouz, J., Millerioux, G.: Observer-based control of discrete-time LPV systems with uncertain parameters. IEEE Transactions on Automatic Control 55(9), 2130–2135 (2010)
10. Hetel, L., Kruszewski, A., Perruquetti, W., Richard, J.-P.: Discrete and intersample analysis of systems with aperiodic sampling. IEEE Transactions on Automatic Control 56(7), 1696–1701 (2011)
11. Leveille, E.A.: Analysis, redesign and verification of the iver2 autonomous underwater vehicle motion controller. Master's thesis, University of Massachusetts Dartmouth (2007)
12. Lofberg, J.: YALMIP: A toolbox for modeling and optimization in MATLAB. In: Proceedings of the CACSD Conference, Taipei, Taiwan (2004)

13. Miyamaoto, S., Aoki, T., Maeda, T., Hirokawa, K., Ichikawa, T., Saitou, T., Kobayashi, H., Kobayashi, E., Iwasaki, S.: Maneuvering control system design for autonomous underwater vehicle. In: MTS/IEEE Conference and Exhibition, vol. 1, pp. 482–489 (November 2001)
14. Opderbecke, J.: Description of the scientific mission scenario(s) to be investigated for the marine application. deliverable D08.01, FeedNetBack project (2009), http://feednetback.eu/public-deliverables/public-deliverables-pdf/ploneexfile.2009-12-09.1317343148/
15. Pellanda, P.C., Apkarian, P., Tuan, H.D., Alazard, D.: Missile autopilot design via a multi-channel LFT/LPV control method. In: 15th IFAC World Congress, Barcelona, Spain (2002)
16. Poussot-Vassal, C., Sename, O., Dugard, L., Gáspár, P., Szabó, Z., Bokor, J.: Attitude and handling improvements through gain-scheduled suspensions and brakes control. Control Engineering Practice 19(3), 252–263 (2011)
17. Poussot-Vassal, C., Sename, O., Dugard, L., Gáspár, P., Szabó, Z., Bokor, J.: A new semi-active suspension control strategy through LPV technique. Control Engineering Practice 16(12), 1519–1534 (2008)
18. Robert, D.: Contribution à l'interconnection commande / ordonnancement. PhD thesis, Institut National Polytechnique de Grenoble (2007)
19. Robert, D., Sename, O., Simon, D.: An h_∞ LPV design for sampling varying controllers: experimentation with at inverted pendulum. IEEE Transactions on Control Systems Technology 18(3), 741–749 (2010)
20. Roche, E., Sename, O., Simon, D.: LPV / $\mathscr{H}_\infty$ varying sampling control for autonomous underwater vehicles. In: Proceedings of the IFAC SSSC, Ancona, Italy (2010)
21. Roche, E., Sename, O., Simon, D.: A hierarchical varying sampling $\mathscr{H}_\infty$ control of an AUV. In: Proceedings of the IFAC World Congress, Milano, Italy (2011)
22. Santos, A.S.: Contribution à la conception des sous-marins autonomes: architecture des capteurs d'altitude, et commande référencées capteurs. PhD thesis, Ecole nationale supérieure des Mines de Paris (1995) (in French)
23. Scherer, C.W.: LPV control and full block multipliers. Automatica 37(3), 361–375 (2001)
24. Shirazi, F.A., Mohammadpour Velni, J., Grigoriadis, K.M.: An LPV design approach for voltage control of an electrostatic MEMS actuator. Journal of Microelectromechanical Systems 20(1), 302–311 (2011)
25. Silvestre, C., Pascoal, A.: Control of the INFANTE AUV using gain scheduled static output feedback. Control Engineering Practice 12(12), 1501–1509 (2004)
26. Silvestre, C., Pascoal, A.: Depth control of the INFANTE AUV using gain-scheduled reduced order output feedback. Control Engineering Practice 15(7), 883–895 (2007)
27. Simon, D., Robert, D., Sename, O.: Robust control/scheduling co-design: application to robot control. In: 11th IEEE Real Time and Embedded Technology and Applications Symposium, RTAS 2005, pp. 118–127 (March 2005)
28. Sturm, J.F.: Using SeDuMi 1.02, a MATLAB toolbox for optimization over symmetric cones. Optim. Methods Softw. 11/12(1-4), 625–653 (1999), Interior point methods
29. Tóth, R., Heuberger, P.S.C., Van den Hof, P.M.J.: Discretisation of linear parameter-varying state-space representations. IET Control Theory and Applications 4(10), 2082–2096 (2010)
30. Wei, X., del Re, L.: Gain scheduled $\mathscr{H}_\infty$ control for air path systems of diesel engines using LPV techniques. IEEE Transactions on Control Systems Technology 15(3), 406–415 (2007)

Author Index